Theory of excitons in cuprous oxide

Von der Fakultät Mathematik und Physik der Universität Stuttgart
zur Erlangung der Würde eines Doktors der Naturwissenschaften
(Dr. rer. nat.) genehmigte Abhandlung

Vorgelegt von

Frank Stefan Schweiner

aus Böblingen

Hauptberichter:	Prof. Dr. Jörg Main
Mitberichter:	Prof. Dr. Maria Daghofer Prof. Dr. Manfred Bayer
Tag der mündlichen Prüfung:	14. Dezember 2017

Universität Stuttgart

1. Institut für Theoretische Physik

2017

Inhaltsangabe

Exzitonen sind die elementaren Anregungen des elektronischen Systems eines Halbleiters und stellen damit fundamentale Quasiteilchen in der Festkörperphysik dar. Sie setzen sich aus einem negativ geladenen Elektron im Leitungsband und einem positiv geladenen Loch im Valenzband zusammen, zwischen denen eine abgeschirmte Coulomb-Wechselwirkung besteht. Aufgrund dieser Tatsache werden Exzitonen oft als das Wasserstoff-Analogon der Festkörperphysik angesehen. Hierbei sind Exzitonen in Kupferoxydul ($\mathrm{Cu_2O}$) von besonderem Interesse, da sie eine vergleichsweise hohe Rydberg-Energie aufweisen. Erst vor drei Jahren ist es T. Kazimierczuk *et al.* [Nature **514**, 343 (2014)] gelungen, ein nahezu perfektes Wasserstoffspektrum für die gelbe Exzitonserie in $\mathrm{Cu_2O}$ bis zu einer Hauptquantenzahl von $n = 25$ zu beobachten. Dieses herausragende Experiment eröffnete das Forschungsgebiet der Rydberg-Exzitonen.

In der vorliegenden Arbeit wird die Theorie der Exzitonen in $\mathrm{Cu_2O}$ eingehend untersucht, wobei Abweichungen vom Wasserstoffmodell, Spektren in äußeren Magnetfeldern sowie die Wechselwirkung der Exzitonen mit anderen Quasiteilchen die Schwerpunkte darstellen.

Die Beobachtung von Exzitonzuständen mit einem Drehimpuls $L \geq 2$ in Einphotonen- und Zweiphotonen-Absorptionsspektren von $\mathrm{Cu_2O}$ zeigen, dass es zwingend erforderlich ist, die vollständige kubische Valenzbandstruktur in einer quantitativen Theorie der Exzitonen zu berücksichtigen. Der Einfluss der Valenzbandstruktur auf das Exzitonspektrum wird untersucht und die Luttinger Parameter, welche die Krümmung der Valenzbänder beschreiben, werden bestimmt. Zur Lösung der zugehörigen Schrödingergleichung wird eine vollständige Basis eingeführt, die auf den Coulomb-Sturmschen Basisfunktionen beruht. Diese Lösungsmethode erlaubt nicht nur die Bestimmung der Exzitonenergien sondern auch der Dipol- und Quadrupoloszillatorstärken. Es wird weiterhin gezeigt, dass die Valenzbandstruktur Ursache einer richtungsabhängigen Dispersion der Exzitonen ist und zu einer Aufspaltung des Exziton-Grundzustandes in Abhängigkeit des Schwerpunktimpulses $\hbar K$ führt. Beiträge einer K-abhängigen Austauschwechselwirkung werden im Detail diskutiert, letztendlich jedoch aufgrund ihrer geringen Größe als weitere Ursache der experimentell beobachteten Aufspaltung ausgeschlossen. Unter der Berücksichtung weiterer Korrekturen zum Wasserstoffmodell der Exzitonen wie etwa der K-unabhängigen analytischen Austauschwechselwirkung und der sogenannten „Central-Cell Corrections“ oder „Zentralzellen-Korrekturen“, welche aufgrund des winzigen Radius des Exziton-Grundzustandes notwendig werden, wird ein konsistentes theoretisches Modell für die gesamte gelbe und grüne Exzitonserie in $\mathrm{Cu_2O}$ aufgestellt. Die sehr gute Übereinstimmung zwischen Theorie und Experiment sowohl bezüglich der Energien als auch der Oszillatorstärken ist ein überzeugender Beweis für die Gültigkeit dieser Theorie.

Zu den in der vorliegenden Arbeit diskutierten Quasiteilchen-Wechselwirkungen gehören die Exziton-Phonon- und die Exziton-Photon-Wechselwirkung. Die erstgenannte ist verantwortlich für eine Verschiebung und eine Verbreiterung der Linien in Absorptionsspektren. Mithilfe der von Y. Toyozawa entwickelten Theorie können die experimentell beobachteten Linienbreiten innerhalb derselben Größenordnung berechent werden. Weitere Effekte, welche den verbleibenden Unterschied zwischen Theorie und Experiment erklären können, werden im Detail diskutiert. Da aufgrund der Exziton-Photon-Wechselwirkung nie „reine Exzitonen" in Halbleitern vorliegen, sondern Exzitonen und Photonen immer zu Polaritonen gekoppelt werden, stellt sich unausweichlich die Frage, inwiefern ein Multi-Polariton-Konzept zur korrekten theoretischen Beschreibung dieser Quasiteilchen nötig ist. Aus diesem Grunde wird die Theorie der Exziton-Polaritonen in Cu_2O präsentiert und die sehr komplizierte Polariton-Dispersion berechnet, wobei auf die starke Durchmischung der Exzitonzustände aufgrund der Exziton-Photon-Wechselwirkung hingewiesen wird. Speziell für den Exziton-Grundzustand wird ein 5×5 Matrixmodell aufgestellt, welches die Berechnung der Dispersion für beliebige Richtungen des Schwerpunktimpulses ermöglicht. Die Vergleiche der theoretischen Ergebnisse mit experimentellen Resultaten für die Gruppengeschwindigkeit und die Quadrupoloszillatorstärke sowie mit Transmissionsspektren zeigen eine gute Übereinstimmung. Mithilfe von Kriterien zur Beobachtbarkeit von Polaritoneffekten kann gezeigt werden, dass diese für alle Exzitonzustände mit Ausnahme des Grundzustandes bei der Behandlung von Absorptionsspektren vernachlässigt werden können.

Die Effekte der kubischen Valenzbandstruktur sind im Falle von Magnetoexzitonen, d.h. von Exzitonen in äußeren Magnetfeldern, noch erheblich stärker ausgeprägt. Nach der Diskussion der Theorie der Magnetoexzitonen in Cu_2O wird zunächst die extrem komplizierte Aufspaltung der Exzitonlinien untersucht. Ein Vergleich mit experimentellen Spektren ermöglicht die Bestimmung des vierten Luttinger-Parameters. Im Gegensatz zum Wasserstoffatom in äußeren Feldern wird eine Abhängigkeit der Spektren von der Orientierung des Magnetfeldes beobachtet. In jenen Fällen, in denen das Magnetfeld nicht einer der Symmetrieflächen des kubischen Gitters von Cu_2O liegt, werden alle antiunitären Symmetrien gebrochen. Folglich wird der erste theoretische Beweis für ein räumlich homogenes System erbracht, welches alle antiunitären Symmetrien bricht. Die Entstehung von Quantenchaos oder das Auftreten der Gaußschen unitären Statistik werden sowohl analytisch als auch numerisch nachgewiesen. Durch die Änderung bestimmter Systemparameter können weiterhin Übergänge zwischen der Poisson-Statistik sowie der Gaußschen orthogonalen und Gaußschen unitären Statistik untersucht werden. Es wird weiterhin gezeigt, dass die Exziton-Phonon-Wechselwirkung einen Bewegungs-Stark-Effekt hervorruft, durch den auch für jene Fälle, in denen das Magnetfeld in einer der Symmetrieflächen des kubischen Gitters von Cu_2O liegt, alle antiunitären Symmetrien gebrochen werden. Folglich kann in Übereinstimmung mit experimentellen Ergebnissen das Auftreten der Gaußschen unitären Statistik für alle Magnetfeldrichtungen nachgewiesen werden.

Abstract

Excitons are the elementary excitations of the electronic system of a semiconductor and, hence, fundamental quasi-particles in solid state theory. Consisting of a negatively charged electron in the conduction band and a positively charged hole in the valence band, which interact via a screened Coulomb interaction, excitons are often regarded as the hydrogen analog of the solid state. Excitons in cuprous oxide (Cu_2O) are of particular interest due to their high Rydberg energy. Only three years ago an almost perfect hydrogen-like absorption series up to a principal quantum number of $n = 25$ has been observed in Cu_2O by T. Kazimierczuk *et al.* [Nature **514**, 343, (2014)]. This outstanding experiment has opened the field of research of giant Rydberg excitons.

In this thesis the theory of excitons in Cu_2O is presented with particular emphasis on the deviations from the hydrogen-like model, on the spectra of excitons in external magnetic fields, and on the interaction of excitons with other quasi particles.

The observation of excitons with an angular momenta $L \geq 2$ in one-photon and two-photon absorption spectra has given evidence that it is mandatory to include the complete cubic valence band structure of Cu_2O in a quantitative theory. The impact of the valence band structure on the exciton spectrum is investigated and the Luttinger parameters, which describe the curvature of the valence bands, are determined. To solve the corresponding Schrödinger equation a complete basis set based on the Coulomb-Sturmian functions is introduced. This method of solving the problem allows not only for the calculation of the exciton energies but also for the calculation of dipole and quadrupole oscillator strengths. It is furthermore shown that the valence band structure the cause for a direction-dependent dispersion of the exciton and for a splitting of the exciton ground state depending on the momentum $\hbar K$ of its center of mass. A K-dependent exchange interaction is discussed in detail but, due to its negligible size, can be ruled out as another cause for the experimentally observed splitting. Considering further corrections like the momentum-independent exchange interaction and the central-cell corrections, which account for the very small radius of the exciton ground state, we set up a consistent theoretical model for the complete yellow and green exciton spectrum of Cu_2O. The consistency between theory and experiment with respect to energies and oscillator strengths is a convincing proof for the validity of the applied theory.

The inter-particle interactions considered in this thesis are the exciton-phonon and the exciton-photon interaction. The former is responsible for a shift and a broadening of the exciton lines in absorption spectra. Applying the theory of Y. Toyozawa, the experimentally observed line widths are calculated within the same order of magnitude. Further effects explaining the remaining discrepancy are discussed in detail. Since there are no bare excitons in the semiconductor due to

the exciton-photon interaction but since excitons and photons are always coupled to polaritons, inevitably the question arises whether a multi-polariton concept is needed for a correct theoretical description of these quasi particles. Hence, the theory of exciton-polaritons in Cu_2O is presented. Having calculated the very complex polariton dispersions, it is pointed out that a strong mixing of exciton states occurs. For the exciton ground state a 5×5 matrix model is set up, which allows for the calculation of the polariton dispersion for any direction of the momentum of the center of mass. A comparison with experimental results like the group velocity, the quadrupole oscillator strength and transmission spectra show a good agreement. Using criteria for the observability of polariton effects, it is shown that these effects can be neglected for all exciton states but the ground state as regards absorption experiments.

The effects of the cubic valence band structure are significantly stronger in the case of magnetoexcitons, i.e., excitons in external magnetic fields. Having discussed the theory of magnetoexcitons in Cu_2O, at first the extremely complex splitting pattern of exciton states is evaluated. A comparison with experimental spectra allows for the determination of the fourth Luttinger parameter. In contrast to the hydrogen-atom in external fields a dependence of the spectra on the direction of the external field is observed. If the magnetic field is not oriented in one of the symmetry planes of the cubic lattice of Cu_2O, all antiunitary symmetries are broken. Hence, the first theoretical evidence for a spatially homogeneous system breaking all antiunitary symmetries is given. The emergence of quantum chaos or the appearance of the statistics of a Gaussian unitary ensemble are proven analytically and numerically. By changing certain parameters of the system, also transitions between Poissonian statistics, the statistics of a Gaussian orthogonal ensemble and the statistics of a Gaussian unitary ensemble are investigated. It is shown that the exciton-phonon interaction leads to a motional Stark effect by which all antiunitary symmetries are broken even for those cases in which the magnetic field is oriented in one symmetry plane of the lattice. Hence, the appearance of the statistics of a Gaussian unitary ensemble is proven for all orientations of the external field in agreement with experimental results.

Contents

List of abbreviations

bcc	body-centered cubic
BZ	Brillouin zone
CB	conduction band
CCC	central-cell corrections
cf.	compare
e	electron
e.g.	for example
exc	exciton
fcc	face-centered cubic
Fig.	figure
GOE	Gaussian orthogonal ensemble
GSE	Gaussian symplectic ensemble
GUE	Gaussian unitary ensemble
h	hole
HRS	hyper-Raman scattering
i.e.	that is
IR	infrared (radiation)
LA	longitudinal acoustic
LO	longitudinal optical
LPB	lower polariton branch

LT	longitudinal transverse
MW	microwave (radiation)
NA	nonanalytic
NNS	nearest-neighbor spacing
OPA	one-photon absorption
Sec.	section
so	spin-orbit
TA	transversal acoustic
TO	transversal optical
TPA	two-photon absorption
uc	unit cell
UPB	upper polariton branch
UV	ultraviolet (radiation)
VB	valence band
VIS	visible (light/radiation)
viz.	namely
WSC	Wigner-Seitz cell

1 Introduction

1.1 Motivation

Ever since the first formulation of their concept by Frenkel [1–3], Peierls [4], and Wannier [5] in the 1930s; and their experimental discovery in Cu_2O by Gross and Karryjew in 1952 [6], excitons are of large physical interest since they are the quanta of the fundamental optical excitations in both insulators and semiconductors in the visible and ultraviolet spectrum of light. The uniqueness of excitons to solids demonstrates itself in the fact that they represent bound states, which can be spatially extended over a giant number of unit cells but can nevertheless migrate coherently through the crystal [7]. The extensive field of excitons promises, amongst others, possible applications in communication and information technologies as well as in optoelectronics [8].

Excitons consist of a positively charged hole in the valence band and a negatively charged electron in the conduction band of a crystal solid. One distinguishes further between Frenkel and (Mott-)Wannier excitons [5, 9] according to the spatial distance between electron and hole. In the case of Frenkel excitons the binding between electron and hole is strong ($\sim 1\,\mathrm{eV}$) and both quasi-particles are confined to one atom in the solid. On the other hand, Wannier excitons extend over many unit cells of the crystal, have a smaller binding energy ($\sim 1 - 100\,\mathrm{meV}$) and can be treated within a very simple approach as an analogue of the hydrogen atom. The corresponding Schrödinger equation, which describes these excitons, is the so-called Wannier equation [7, 10, 11]. We will limit ourselves in this thesis to Wannier excitons since they are the typical excitons in semiconductors. Frenkel excitons, on the other hand, can be found in insulators and organic crystals. Although one is confronted with a huge number of particles ($\sim 10^{23}$) in condensed matter, it is often possible to assign particle character to elementary excitations of the whole solid. As regards the electronic system the electron and the hole of an exciton are treated in a single particle picture, where the influence of other electrons is considered by introducing effective masses and screening the Coulomb interaction. For this reason they are called quasi-particles.

The field of excitonic research covers, e.g., excitons in reduced dimensionality [12], biexcitons [13–17], trions [18], polyexcitons [19], bound exciton complexes [20] or exciton-exciton scattering [12], polariton lasers [21–24] and excitonic Bose-Einstein condensation [25–29].

Very recently, new attention has been drawn to the field of excitons by an experimental observation of the yellow exciton series in Cu_2O up to a large principal quantum number of $n = 25$ [30].

This discovery has opened up the research field of giant Rydberg excitons and led to a variety of new experimental and theoretical investigations [30–57].

By moving Rydberg excitons precisely in the crystal using microscopic potential landscapes and monitoring their interaction with other excitations in the solid, one expects to gain novel insights into condensed matter physics [30]. Rydberg atoms themselves show a lot of interesting properties like strong dipolar interactions and long lifetimes of the excited states, which may be used for quantum information technologies [58]. Based on the fact that a single Rydberg atom could recently be coupled to a Bose-Einstein condensate [59], accordant couplings may also be possible in solids with Rydberg excitons [25, 30]. In the publication on Rydberg excitons [30] also a dipole blockade effect has been reported, which prevents the excitation of an exciton in the vicinity of another exciton with a high quantum number. This effect may be used to construct mesoscopic single-photon logic devices and nonlocal all-optical switches [60]. By applying external magnetic and electric fields the blockade effect, the excitonic interaction in general and the stability of excitons are assumed to be controllable. Against this background it is inevitable to completely understand the theory of excitons in semiconductors like Cu_2O.

The main features, which make Cu_2O one of the most investigated semiconductors relating to excitons, are the large excitonic binding energy of $R_{\mathrm{exc}} \approx 86\,\mathrm{meV}$ [37] and the non-degeneracy of its uppermost valence band often justifying the simple-band model with a hydrogen-like exciton spectrum. Even though the spectrum of Rydberg excitons in Cu_2O can be described quite well in a first approximation by the hydrogen-like model of Wannier, one must keep in mind that excitons are complex many-body states of the solid and, hence, that there are significant limitations to this model or to the atom-like description of these quasi-particles [61]. After a completion of the Wannier model by Elliot [62] and Dresselhaus [63], enabled by experimental work of Nikitine [64, 65], Gross [66–68], Ueta [69], and McLean [70] on ionic crystals and covalent solids, more extensive corrections of the hydrogen-like exciton model were introduced in the following years to describe the experimentally observed spectra (see, e.g., Refs. [7, 12, 71, 72] and further references therein). Furthermore, interactions of excitons with other excitations of the solid - such as phonons - cannot be ignored and have to be considered, as well [73–75].

In this thesis, we investigate the corrections to the simple hydrogen-like model of Wannier excitons which are necessary to describe the experimental spectra of excitons in cuprous oxide without and with external fields applied.

The absorption spectrum of giant Rydberg excitons observed in Ref. [30] shows characteristic peaks of asymmetric Lorentzian shape. The main cause for an asymmetric broadening and shifting of the excitonic lines is, besides the effect of impurities in the crystal, the exciton-phonon interaction [7], for which the general theory has been developed by Toyozawa in the late 1950s and early 1960s [73–76]. We present a theoretical calculation of the absorption spectrum of cuprous oxide based on the general theory developed by Y. Toyozawa. An inclusion not only of acoustic phonons but also of optical phonons and of specific properties of the excitons in Cu_2O like the central-cell corrections for the $1S$-exciton allows us to calculate the experimentally observed line widths [30] within the same order of magnitude, which demonstrates a clear improvement in comparison to earlier work on this topic. We also discuss a variety of further effects, which explain the still observable discrepancy between theory and experiment but which can hardly be included in theoretical calculations.

One of the most important corrections to the hydrogen-like model when treating excitons in cuprous oxide is the consideration of the complete cubic valence band structure. Only after Altarelli, Baldereschi, and Lipari had developed the theory of excitons in semiconductors with degenerate valence bands in the 1970s [77–81], a controversy regarding the correct assignment of the exciton states for Cu_2O could be settled by Ch. Uihlein *et al.* in 1981 [72], i.e., almost 30 years after the first experimental discovery of excitons in Cu_2O by Gross and Karryjew [6]. After the observation of Rydberg excitons, the complex valence band structure of Cu_2O has also moved into the focus once again [36, 37]. Within this regard two of the most striking experimental findings when investigating exciton spectra in cuprous oxide using high-resolution spectroscopy are the observability and the fine structure splitting of F excitons reported by J. Thewes *et al.* [36].

We present a method to calculate the excitonic spectra of all direct semiconductors with a complex valence band structure. The Schrödinger equation is solved using a complete basis set with Coulomb Sturmian functions, which also allows for the computation of oscillator strengths. The results obtained for Cu_2O differ from those of J. Thewes *et al.* [36], which can be, however, explained by the fact that the evaluation of all three Luttinger parameters is not uniquely possible. In contrast to Ref. [36] our results are consistent with band structure calculations. Considering also a finite momentum $\hbar K$ of the center of mass, we show that the large K-dependent line splitting observed for the $1S$ exciton state by G. Dasbach *et al.* [82–84] is not related to an exchange interaction but rather to the complex valence band structure of Cu_2O.

When treating the exchange interaction of Wannier excitons, usually only the leading terms of the analytic and the nonanalytic exchange interaction are considered. However, higher order terms can lead to a splitting of exciton states, for which reason a splitting of the $1S$ exciton in cuprous oxide depending on its total momentum $\hbar K$ has originally been attributed to a K dependent analytic exchange interaction by Dasbach *et al.* [82]. Going beyond the common treatment of the exchange interaction, we derive the correct expressions for these K dependent higher order terms using $\boldsymbol{k}\cdot\boldsymbol{p}$ perturbation theory. We prove that the appearance of a K dependent exchange interaction is inseparably connected with a K independent exchange interaction of P and D excitons. We estimate the magnitude of these terms for Cu_2O from microscopic calculations and show that they are far too small to explain the observed K dependent splitting. Instead, this splitting has to be treated in terms of the dispersion of the excitons. Furthermore, we prove the occurence of a coupling between longitudinal and transverse excitons in Cu_2O due to the K dependent nonanalytic exchange interaction.

In Cu_2O parity is a good quantum number and thus the exciton spectrum falls into two parts: The dipole-active exciton states of negative parity and odd angular momentum, which can be observed in one-photon absorption (Γ_4^- symmetry), and the exciton states of positive parity and even angular momentum, which can be observed in two-photon absorption (Γ_5^+ symmetry). The unexpected observation of D excitons in two-photon absorption has given first evidence that the dispersion properties of the Γ_5^+ orbital valence band is giving rise to a coupling of the yellow and green exciton series. However, a first theoretical treatment by Ch. Uihlein *et al.* [72] was based on a simplified spherical model. The observation of F excitons in one-photon absorption is a further proof of a coupling between yellow and green exciton states. We show that the even and odd parity exciton system can be consistently described within the same theoretical approach. However, the Hamiltonian of the even parity system needs, in comparison to the odd exciton case, modifications to account for the very small radius of the yellow and green $1S$ exciton. In the presented treatment we take special care of the central-cell corrections, which comprise a reduced screening of the Coulomb potential at distances comparable to the polaron radius, the exchange interaction being responsible for the exciton splitting into ortho and para states, and the inclusion of terms in the fourth power of p in the kinetic energy being consistent with O_h symmetry. Since the yellow $1S$ exciton state is coupled to all other states of positive parity, we show that the central-cell corrections affect the whole even exciton series. The close resonance of the $1S$ green exciton with states of the yellow exciton series has a strong impact on the energies and oscillator strengths of all implied states.

The consistency between theory and experiment in comparisons of the energies and the oscillator strengths of the even and the odd exciton system in Cu_2O is a convincing proof for the validity of the applied theory.

The inclusion of the complex valence band structure and the cubic symmetry of the solid in the theory of excitons is all the more important for magnetoexcitons, where the external magnetic field reduces the symmetry of the system even further. Due to the specific material parameters in Cu_2O, the exciton radius is much larger than the Bohr radius known from atomic physics. This makes excitons attractive for investigations in external fields since the region of "high magnetic fields" can be reached within several Tesla, in contrast to the hydrogen atom, where this region begins above several hundreds of Tesla [35, 71]. We present the theory of excitons in Cu_2O in an external magnetic field and especially discuss the dependence of the spectra on the direction of the external magnetic field, which cannot be understood from a simple hydrogen-like model. The theoretical results are in excellent agreement with experimental spectra obtained for cuprous oxide in Faraday configuration using high-resolution spectroscopy. Furthermore, the comparison of the spectra allows for the determination of the fourth Luttinger parameter κ of this semiconductor.

Recent experimental investigations by M. Aßmann *et al.* [31, 32] on the spectrum of magnetoexcitons in cuprous oxide revealed the statistics of a Gaussian unitary ensemble (GUE). We show analytically and numerically that the application of an external magnetic field to highly excited Rydberg excitons breaks all antiunitary symmetries in the system. Only by considering the complete valence band structure of a direct band gap cubic semiconductor, the Hamiltonian of excitons leads to the statistics of a Gaussian unitary ensemble (GUE) without the need for interactions with other quasi-particles like phonons. Hence, we give theoretical evidence for a spatially homogeneous system breaking all antiunitary symmetries.

As the nearest neighbor spacing distribution of magnetoexcitons can exhibit Poissonian statistics, the statistics of a Gaussian orthogonal ensemble (GOE) or a Gaussian unitary ensemble (GUE) depending on the system parameters, magnetoexcitons are an ideal system to investigate the transitions between these statistics. Hence, we also investigate the transitions between GOE and GUE statistics and between Poissonian and GUE statistics by changing the angle of the magnetic field with respect to the crystal lattice and by changing the scaled energy known from the hydrogen atom in external fields. Comparing our results with analytical formulae for these transitions derived with random matrix theory, we obtain a very good agreement and thus confirm the Wigner surmise for the exciton system.

The model, which includes the complete cubic valence band structure of the solid, can explain the appearance of GUE statistics if the magnetic field is not oriented in one of the symmetry planes of the cubic lattice. However, it cannot explain the experimental observation of GUE statistics for all orientations of the field. Hence, it is then necessary to investigate the effect of quasi-particle interactions or especially the exciton-phonon interaction on the level statistics of magnetoexcitons. We show that the motional Stark field induced by the exciton-phonon interaction leads to the occurrence of GUE statistics for arbitrary orientations of the magnetic field in agreement with experimental observations. Importantly, the breaking of all antiunitary symmetries can be explained only by considering both the exciton-phonon interaction *and* the cubic crystal lattice but not by the exction-phonon interaction alone as supposed in Refs. [31, 32].

The observation of giant Rydberg excitons in cuprous oxide also inevitably raises the question whether these quasi-particles must be described within a multi-polariton framework since excitons and photons are always coupled in the solid. We present the theory of exciton-polaritons in Cu_2O, accounting for the complete valence band structure, the exchange interaction, and the central-cell corrections. To this end we extend the Hamiltonian which includes all these effects, for finite values of the exciton momentum $\hbar K$. Having discussed the theory of exciton-polaritons, we discuss at first the main effects of the exciton-photon interaction on the giant Rydberg exciton states within the simple hydrogen-like model of excitons and show that a strong mixing of exciton states occurs. For the exciton states with small principal quantum numbers $n \leq 4$ all the corrections mentioned above need to be considered. Hence, very complex polariton spectra for the three orientations of $\boldsymbol{K}$ along the axes [001], [110], and [111] of high symmetry are obtained. Using criteria for spatial or temporal coherence concerning the observability of polariton effects, we show that these effects can be neglected for $n \geq 2$ as regards transmission or absorption experiments in Cu_2O. The dispersion of the $1S$ ortho exciton, for which pronounced polariton effects have been measured in experiments, is discussed in detail. We set up a 5×5 matrix model which allows us to treat its dispersion for any direction of $\boldsymbol{K}$. We compare our results with experimental transmission spectra as well as with values of the K-dependent splitting and the group velocity and obtain good agreements.

1.2 Outline

Chapter 2 gives an introduction to the basic concepts of solid state theory paying special attention to semiconductors and excitons. Having presented the structure and the Hamiltonian of solids, the lattice dynamics and the electron dynamics are discussed. After a short section on light-matter interaction in solids, we give a detailed introduction to the theory of excitons. The semiconductor cuprous oxide, for which all calculations will be performed in this thesis, is presented at last.

The theoretical description of the electron-phonon interaction and consequently the exciton-phonon interaction will be given in Chapter 3. This Chapter is mainly concerned with the application of the theory of Y. Toyozawa to the absorption spectrum of excitons in cuprous oxide. In Chapter 4 we present the cubic valence band structure as the first important correction to the simple hydrogen-like model of excitons. Here we also describe the complete basis set used to solve the Schrödinger equation and derive formulas to calculate dipole and quadrupole oscillator strengths, which will be used throughout the rest of this thesis. The observability and the splitting of F excitons as well as the K-dependent splitting of the $1S$ ortho exciton state are investigated. The analytic and nonanalytic exchange interaction, which have originally been assigned as the cause for the K-dependent splitting, are discussed in detail in Chapter 5. Having considered only the exciton states with odd parity so far, the focus will be on the exciton states with even parity in Chapter 6. Here the central-cell corrections, which affect not only the exciton ground state but the whole even exciton series, are investigated.

Chapters 7 and 8 are concerned with the spectra of magnetoexcitons. In Chapter 7 we describe the Hamiltonian of magnetoexcitons and prove a very good agreement between theoretical results with experimental absorption spectra as regards not only the energies but also the oscillator strengths of the excitons. The breaking of all antiunitary symmetries for magnetoexcitons due to the cubic valence band structure and the exciton-phonon interaction is the topic of Chapter 8. The appearance of Poissonian, GOE and GUE statistics also allows us to investigate transitions between these statistics. In Chapter 9 we present the concept of exciton-polaritons. The dispersion of these quasi-particles, which have to be introduced due to the exciton-photon interaction, is discussed. We especially investigate the properties of the $1S$ ortho-exciton polariton and also show that polariton effects can be neglected for all other exciton states with a principal quantum number $n \geq 2$. Finally, we give a summary and outlook in Chapter 10.

Essential parts of the Chapters 3-9 have been published:

- *Linewidths in excitonic absorption spectra of cuprous oxide*,
  F. Schweiner, J. Main, G. Wunner,
  Phys. Rev. B **93**, 085203 (2016)

- *Impact of the valence band structure of* Cu_2O *on excitonic spectra*,
  F. Schweiner, J. Main, M. Feldmaier, G. Wunner, Ch. Uihlein,
  Phys. Rev. B **93**, 195203 (2016)

- K*-dependent exchange interaction of the* $1S$ *exciton in* Cu_2O,
  F. Schweiner, J. Main, G. Wunner, Ch. Uihlein,
  Phys. Rev. B **94**, 115201 (2016)

- *Magnetoexcitons in cuprous oxide*,
  F. Schweiner, J. Main, G. Wunner, M. Freitag, J. Heckötter,
  Ch. Uihlein, M. Aßmann, D. Fröhlich, M. Bayer,
  Phys. Rev. B **95**, 035202 (2017)

- *Magnetoexcitons break antiunitary symmetries*,
  F. Schweiner, J. Main, G. Wunner,
  Phys. Rev. Lett. **118**, 046401 (2017)

- *The even exciton series in* Cu_2O,
  F. Schweiner, J. Main, G. Wunner, Ch. Uihlein,
  Phys. Rev. B **95**, 195201 (2017)

- *GOE-GUE-Poisson transitions in the nearest neighbor*
  spacing distribution of magnetoexcitons,
  F. Schweiner, J. Main, G. Wunner,
  Phys. Rev. E **95**, 062205 (2017)

- *Exciton-phonon interaction breaking all*
  antiunitary symmetries in external magnetic fields,
  F. Schweiner, P. Rommel, J. Main, G. Wunner,
  Phys. Rev. B **96**, 035207 (2017)

- *Exciton-polaritons in cuprous oxide: Theory and comparison with experiment*,
  F. Schweiner, J. Ertl, J. Main, G. Wunner, Ch. Uihlein,
  Phys. Rev. B **96**, 245202 (2017)

2 Foundations of solid state theory

In this chapter we give a brief overview of solid state theory including phonons, electronic band structure and excitons. In several cases a larger stress will be laid on the specific properties of semiconductors. At last, we discuss the semiconductor cuprous oxide (Cu_2O), for which all calculations in this thesis are performed.

This introductory chapter is mainly based on (and partly parallels sections of) the books *Theory of excitons* by Robert S. Knox [7], *Solid State Theory* by U. Rössler [85], *Semiconductor Optics* by Claus F. Klingshirn [12], and *Festkörperphysik* by S. Hunklinger [86] as well as the Ph.D. thesis by M. Jörger [87] and the article *Giant Rydberg Excitons in Couprous Oxide* by the group of M. Bayer and D. Fröhlich [30].

Readers acquainted with solid state theory can skip this Chapter. The new results of this thesis are presented in Chapters 3-9.

2.1 Structure and Hamiltonian of solids

In this Section we discuss the structure of solids and introduce the most important quantities connected with crystal lattices. Furthermore, the Hamiltonian of solids is introduced and the Born-Oppenheimer approximation, which describes the decoupling of the electronic system and the lattice vibrations, is explained.

2.1.1 Structure of solids

Crystalline solids can be understood as built up from a periodic repetition of so-called unit cells, which consist of a finite numbers of atoms at different positions and represent the building blocks of the crystal. Due to the resulting long-range order, sharp Bragg peaks appear in diffraction experiments, which can be used to determine the structure of the solid. This structure is described in three dimensions by a set of lattice vectors

$$\boldsymbol{R}_{\boldsymbol{n}} = \sum_{i=1}^{3} n_i \boldsymbol{a}_i,\ n_i \in \mathbb{Z}, \tag{2.1}$$

defining a point lattice. The vectors $\boldsymbol{a}_i$, the primitive lattice vectors, are linearly independent and span a parallelepiped: the primitive unit cell (uc) with a volume of

$$V_{\mathrm{uc}} = \boldsymbol{a}_1 \cdot (\boldsymbol{a}_2 \times \boldsymbol{a}_3). \tag{2.2}$$

A unit cell is called primitive, if it is of minimum possible volume. The absolute values of the primitive lattice vectors are the lattice constants $a_i = |\boldsymbol{a}_i|$. By linear combination of the vectors $\boldsymbol{a}_i$, every point of the lattice can be reached. However, instead of the unit cell one often uses the so-called Wigner-Seitz cell, which is obtained by the following construction: One chooses a point of the lattice as the origin, draws lines to the nearest and next-nearest neighbors and constructs the planes[1] bisecting these lines perpendicularly at the half-distance between each two lattice points. The resulting minimal volume enclosed by these planes around the origin is the Wigner-Seitz cell [12].

Crystal lattices with only one atom per unit cell are called Bravais lattices. In three dimensions there are 14 different Bravais lattices[2] [88], which can be graded into 7 crystal systems [86]. In any other case one speaks of a lattice with basis. The unit cells then contain several atoms and the vectors

$$\boldsymbol{R}_{\boldsymbol{n}\boldsymbol{\tau}} = \boldsymbol{R}_{\boldsymbol{n}} + \boldsymbol{\tau} \tag{2.3}$$

describe the crystal structure. By $\boldsymbol{\tau}$ the position of the atoms within the unit cell or the basis is denoted. Additionally one can define a reciprocal lattice by the vectors

$$\boldsymbol{G}_{\boldsymbol{m}} = \sum_{i=1}^{3} m_i \boldsymbol{b}_i,\ m_i \in \mathbb{Z}, \tag{2.4}$$

where the primitive reciprocal translations $\boldsymbol{b}_i$ are perpendicular to the planes spanned by each two of the vectors $\boldsymbol{a}_j$, respectively:

$$\boldsymbol{b}_i \ = \ \frac{2\pi}{V_{\mathrm{uc}}} \sum_{j,k=1}^{3} \varepsilon_{ijk} (\boldsymbol{a}_j \times \boldsymbol{a}_k) \quad \Rightarrow \quad \boldsymbol{b}_i \cdot \boldsymbol{a}_j = 2\pi\delta_{ij},\ i,j \in \{1,2,3\}\,. \tag{2.5}$$

The Wigner-Seitz cell constructed in reciprocal space is called the first Brillouin zone (BZ). Due to the high symmetry of the point lattice, the BZ can be invariant under inversions, rotations and reflections. The amount of these operations leaving the BZ invariant form the so-called point group. In the special case of semiconductors the three most important point groups are the cubic group O_{h} for diamond-type structures, the group T_{d} for zincblende-type structures and $C_{6\mathrm{v}}$ for wurtzite-type structures [12]. Appending translations to the point group one obtains the space group, which contains all symmetry operations of the crystal structure. These operations can be used to classify quantum-mechanical eigenstates of the crystal exploiting methods of group theory [12, 85, 89–92]. Specific points and symmetry lines of the BZ are denoted by letters as shown in Fig. 2.1. The energies or frequencies of lattices vibrations and electrons are often shown along these symmetry lines displaying their dependency on the momenta of particles.

Due to the periodicity of the crystal, all of the relevant properties of the solid show the same periodicity. Every periodic function $f(\boldsymbol{r}) = f(\boldsymbol{r} + \boldsymbol{R}_{\boldsymbol{n}})$ can be expanded in a Fourier series, where the sum leads over all reciprocal lattice vectors:

$$f(\boldsymbol{r}) = \sum_{\boldsymbol{G}} f_{\boldsymbol{G}} e^{i\boldsymbol{G}\boldsymbol{r}}, \quad f_{\boldsymbol{G}} = \frac{1}{V_{\mathrm{uc}}} \int_{\mathrm{uc}} \mathrm{d}\boldsymbol{r}\, f(\boldsymbol{r}) e^{-i\boldsymbol{G}\boldsymbol{r}}. \tag{2.6}$$

---

[1] Planes in the crystal are normally specified by Miller indices. A determination of these indices is, e.g., given in [86].

[2] The most important are face-centered cubic (fcc), body-centered cubic (bcc), hexagonal close-packed and tetragonal.

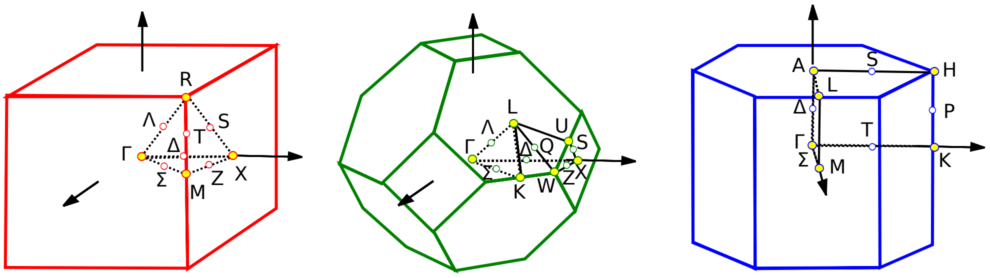

Figure 2.1.: First Brillouin zones of a simple cubic lattice (red), a diamond-type or zincblende-type structure (green; point groups O_h or T_d), and a hexagonal wurtzite-type structure (blue; point group $C_{6\mathrm{v}}$). Adapted from [12].

All effects occuring in the solid can therefore be described in reciprocal space or in real space. The changeover between these spaces is given by a Fourier series.

As we will see, the appropriate space for the momenta $\hbar\boldsymbol{k}$ of particles is the reciprocal space. Since there is no symmetry with respect to infinitesimal translations in the crystal, the momentum conservation following from Noether's theorem has to modified. The momentum is only conserved within integer multiples of the primitive reciprocal translations $\boldsymbol{b}_i$. For this reason, one can always add a reciprocal lattice vector $\boldsymbol{G}$ to a given $\boldsymbol{k}$-vector,

$$\boldsymbol{k} \leftrightarrows \boldsymbol{k} + \boldsymbol{G}, \tag{2.7}$$

without changing the physical meaning. It is therefore possible to restrict oneself to the first BZ. Due to this ambiguity of the momentum in a crystal, one prefers to speak of a quasi-momentum [93]. The momentum conservation in a crystal reads

$$\sum_i \hbar\boldsymbol{k}_i = \sum_j \hbar\boldsymbol{k}_j + \hbar\boldsymbol{G} \tag{2.8}$$

with all $\boldsymbol{k}_i$, $\boldsymbol{k}_j$ being in the first BZ. The term $\hbar\boldsymbol{G}$ in (2.8) can be understood as a Bragg reflection[3] taking place simultaneously, where the additional momentum is transferred to the crystal [86].

There is one further important consequence from the fact that all of the relevant properties of the solid show the same periodicity. If we define a translation operator $T_{\boldsymbol{R_n}}$, the different potentials V which enter the Hamiltonian of the solid obey

$$T_{\boldsymbol{R_n}} V(\boldsymbol{r}) = V(\boldsymbol{r} + \boldsymbol{R_n}) = V(\boldsymbol{r}) \tag{2.9}$$

with an arbitrary lattice vector $\boldsymbol{R_n}$. Therefore the Hamiltonian commutes with the operator[4] $T_{\boldsymbol{R_n}}$,

$$[H, T_{\boldsymbol{R_n}}] = 0, \tag{2.10}$$

---

[3] The Bragg condition of reflection is a condition for constructive interference when light is scattered by the atoms of a crystal structure. It involves the wave vector $\boldsymbol{k}$ of light and an arbitrary reciprocal vector $\boldsymbol{G}$. In the most general form it reads $\boldsymbol{k} \cdot \boldsymbol{G}/2 = (\boldsymbol{G}/2)^2$.

[4] Sometimes one can find $T_{\boldsymbol{R_n}} = e^{-\frac{i}{\hbar}\boldsymbol{p}\boldsymbol{R_n}}$ as a representation of $T_{\boldsymbol{R_n}}$, where $\boldsymbol{p}$ denotes the momentum operator.

so that eigenfunctions of H are also eigenfunctions of $T_{\boldsymbol{R_n}}$. If we choose a plane wave expansion for the wave functions, i.e.,

$$\phi(\boldsymbol{r}) = \sum_{\boldsymbol{k}} c_{\boldsymbol{k}} e^{i\boldsymbol{kr}} \tag{2.11}$$

and use the Fourier series

$$V(\boldsymbol{r}) = \sum_{\boldsymbol{G}} V_{\boldsymbol{G}} e^{i\boldsymbol{Gr}} \tag{2.12}$$

of the potential V in the Schrödinger equation

$$\frac{\boldsymbol{p}^2}{2m}\phi + V\phi = E\phi, \tag{2.13}$$

we obtain [86]

$$\sum_{\boldsymbol{k}} e^{i\boldsymbol{kr}} \left[\left(\frac{\hbar^2 k^2}{2m} - E \right) c_{\boldsymbol{k}} + \sum_{\boldsymbol{G}} V_{\boldsymbol{G}} c_{\boldsymbol{k}-\boldsymbol{G}} \right] = 0, \tag{2.14}$$

which must hold for all values of $\boldsymbol{r}$. Therefore, the term in brackets must vanish for every value of $\boldsymbol{k}$. Since the last term in brackets only couples coefficients $c_{\boldsymbol{k}}$ differing by reciprocal lattice vectors, we can write

$$\phi_{\boldsymbol{k}}(\boldsymbol{r}) = \sum_{\boldsymbol{G}} c_{\boldsymbol{k}-\boldsymbol{G}} e^{i(\boldsymbol{k}-\boldsymbol{G})\boldsymbol{r}} = e^{i\boldsymbol{kr}} u_{\boldsymbol{k}}(\boldsymbol{r}). \tag{2.15}$$

This is known as Bloch's theorem [85]: Wave functions of the solid can always be written as a product of a plane wave and a lattice periodic part

$$u_{\boldsymbol{k}}(\boldsymbol{r} + \boldsymbol{R_n}) = u_{\boldsymbol{k}}(\boldsymbol{r}). \tag{2.16}$$

We now see that

$$T_{\boldsymbol{R_n}} \phi_{\boldsymbol{k}}(\boldsymbol{r}) = e^{-i\boldsymbol{k}\boldsymbol{R_n}} \phi_{\boldsymbol{k}}(\boldsymbol{r}) \tag{2.17}$$

holds. This also results from

$$T_{\boldsymbol{R_n}} \phi(\boldsymbol{r}) = \phi(\boldsymbol{r} - \boldsymbol{R_n}) = \lambda \phi(\boldsymbol{r}) \quad \text{and} \quad \|T_{\boldsymbol{R_n}} \phi(\boldsymbol{r})\| = \|\phi(\boldsymbol{r})\| = |\lambda| = 1 \tag{2.18}$$

since $T_{\boldsymbol{R_n}}$ is a unitary operator.

2.1.2 Hamiltonian of solids

When treating the solid mathematically it is not convenient to treat all the nuclei and the electrons independently. Comparing the distance between neighboring atoms in a lattice to the wave functions of different electrons, one can see that electrons in the inner shells of one atom are not affected by other atoms. This is shown schematically in Fig. 2.2. Only the valence electrons rearrange in a solid and establish chemical bindings. Hence, the solid is seen as a composition of ions (closed electron shells and nuclei) and valence electrons. Different types of chemical bindings are, e.g., the metallic binding, the ionic or heteropolar binding, the covalent or homopolar binding and the binding due to van-der-Waals interaction. The type of binding established depends on the overlap of the wave functions of the valence electrons. The arrangement of the atoms due to these interactions results in the configuration of minimum energy, which defines the ground state of the many-body system.

The Hamiltonian can be written as

$$H_0 = H_{\text{ion}} + H_{\text{el}} + H_{\text{el-ion}} + H_{\text{S}} \tag{2.19}$$

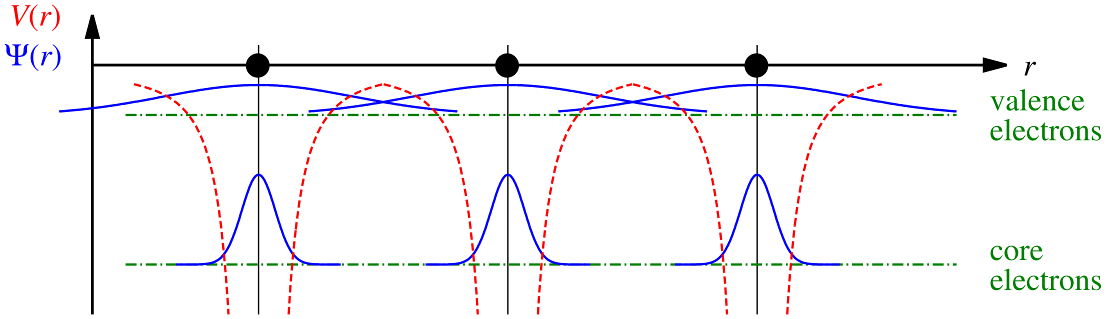

Figure 2.2.: The wave functions of core electrons are not affected by the potential of neighboring atoms, whereas an overlap of the wave functions of the valence electrons will lead to chemical binding. The dashed line depicts the periodic potential of the solid as a superposition of atomic potentials. Adapted from [85].

with the ionic part

$$H_{\text{ion}} = \sum_{i=1}^{N_I} \frac{\boldsymbol{P}_i^2}{2M_i} + \frac{1}{2} \sum_{i,j=1,\, i\neq j}^{N_I} V(\boldsymbol{R}_i - \boldsymbol{R}_j), \tag{2.20}$$

the electronic part

$$H_{\text{el}} = \sum_{l=1}^{N_e} \frac{\boldsymbol{p}_l^2}{2m_0} + \frac{1}{2} \sum_{k,l=1,\, k\neq l}^{N_e} \frac{e^2}{4\pi\varepsilon_0 \left|\boldsymbol{r}_l - \boldsymbol{r}_k\right|}, \tag{2.21}$$

an interaction term

$$H_{\text{el}-\text{ion}} = \sum_{i=1}^{N_I} \sum_{l=1}^{N_e} v(\boldsymbol{r}_l - \boldsymbol{R}_i), \tag{2.22}$$

and a spin-dependent part H_{S}, which contains, e.g., the spin-orbit intercation. N_I (N_e) denotes the number of ions (electrons) and $V(\boldsymbol{R}_i - \boldsymbol{R}_j)$, $v(\boldsymbol{r}_l - \boldsymbol{R}_i)$ represent general interaction potentials[5]. The term H_{S} will be neglected at present.

In macroscopic crystals the number of electrons and ions is very high (N_I, $N_e \sim 10^{23}$) and the physical properties do not depend on these numbers, but only on the densities N/V. One can consider these properties within the thermodynamic limit

$$N \to \infty, \quad \frac{N}{V} = \text{const.} \tag{2.23}$$

where V denotes the crystal volume. In a more general approach one could use instead of the kinetic terms in Eqs. (2.20) and (2.21) the relativistic Dirac operator to account for nuclear spins [85].

In a crystal lattice the actual positions of the ions are

$$\boldsymbol{R}_{\boldsymbol{n}\boldsymbol{\tau}} = \boldsymbol{R}_{\boldsymbol{n}\boldsymbol{\tau}}^0 + \boldsymbol{u}_{\boldsymbol{n}\boldsymbol{\tau}} \tag{2.24}$$

with the equilibrium positions $\boldsymbol{R}_{\boldsymbol{n}\boldsymbol{\tau}}^0$ given by Eqs. (2.1) and (2.3) and the (time-dependent) displacements $\boldsymbol{u}_{\boldsymbol{n}\boldsymbol{\tau}}$ describing the motion of the ions. Compared to the lattice constant these displacements

---

[5] In the case of point-like ions V and v are Coulomb interaction potentials.

are assumed to be small, for which reason we are allowed to perform a Taylor expansion of the potentials in Eqs. (2.20) and (2.22):

$$\begin{aligned} V(\boldsymbol{R}_{\boldsymbol{n\tau}}-\boldsymbol{R}_{\boldsymbol{m\sigma}}) &= V(\boldsymbol{R}^0_{\boldsymbol{n\tau}}-\boldsymbol{R}^0_{\boldsymbol{m\sigma}})+\delta V(\boldsymbol{R}_{\boldsymbol{n\tau}}-\boldsymbol{R}_{\boldsymbol{m\sigma}}), \qquad (2.25a)\\ v(\boldsymbol{r}_l-\boldsymbol{R}_{\boldsymbol{n\tau}}) &= v(\boldsymbol{r}_l-\boldsymbol{R}^0_{\boldsymbol{n\tau}})+\delta v(\boldsymbol{r}_l-\boldsymbol{R}_{\boldsymbol{n\tau}}). \qquad (2.25b)\end{aligned}$$

The complete (non-relativistic) Hamiltonian now reads

$$\begin{aligned} H_0 &= \sum_{\boldsymbol{n\tau}}\frac{\boldsymbol{P}^2_{\boldsymbol{n\tau}}}{2M_{\boldsymbol{\tau}}}+\frac{1}{2}\sum_{\boldsymbol{n\tau}\neq\boldsymbol{m\sigma}}\delta V(\boldsymbol{R}_{\boldsymbol{n\tau}}-\boldsymbol{R}_{\boldsymbol{m\sigma}})+\sum_l\frac{\boldsymbol{p}_l^2}{2m_0}+\frac{1}{2}\sum_{k\neq l}\frac{e^2}{4\pi\varepsilon_0|\boldsymbol{r}_l-\boldsymbol{r}_k|}\\ &+ \sum_{\boldsymbol{n\tau}l}v(\boldsymbol{r}_l-\boldsymbol{R}^0_{\boldsymbol{n\tau}})+\frac{1}{2}\sum_{\boldsymbol{n\tau}\neq\boldsymbol{m\sigma}}V(\boldsymbol{R}^0_{\boldsymbol{n\tau}}-\boldsymbol{R}^0_{\boldsymbol{m\sigma}})+\sum_{\boldsymbol{n\tau}l}\delta v(\boldsymbol{r}_l-\boldsymbol{R}_{\boldsymbol{n\tau}}). \qquad (2.26)\end{aligned}$$

The first five terms of Eq. (2.26) describe the lattice dynamics and the electronic system within a static lattice potential. The last two terms describe the constant ionic interaction energy in equilibrium and the coupling of the dynamics of the electronic and the ionic system, respectively.

The different physical properties of solids are related to one of these terms like specific heat, sound propagation, thermal expansion and elastic properties (lattice dynamics), electric conductivity and magnetic properties (electronic system), relaxation phenomena in transport and superconductivity (coupling term) or to several terms like optical properties and heat conduction.

2.1.3 Born-Oppenheimer approximation

A complete description of the solid can be obtained solving the Schrödinger equation

$$H_0\Psi = i\hbar\frac{\partial}{\partial t}\Psi \qquad (2.27)$$

with the Hamilton operator H_0 of Eq. (2.26) and a wave function Ψ depending on all coordinates of the electrons and the ions. From a thermodynamic point of view, one can consider an electronic system and an ionic system, which are in contact. In thermal equilibrium both systems have the same temperature and the average thermal energy per degree of freedom is the same for all particles. This can be expressed by

$$\left\langle\frac{\boldsymbol{p}_l^2}{2m_0}\right\rangle = \left\langle\frac{\boldsymbol{P}^2_{\boldsymbol{n\tau}}}{2M_{\boldsymbol{\tau}}}\right\rangle. \qquad (2.28)$$

Since the mass of the electrons is much smaller than that of the ions, the electronic motion is much faster then the ionic one.

This statement can also be obtained by a model with oscillators [12]: By assuming the force constants describing the binding of the valence electrons to the ions to be of the same value as those, which describe the binding between neighboring ions, one can see that the highest resonance frequencies Ω of the ions are much smaller than those of the electrons:

$$\Omega \approx \sqrt{\frac{\beta}{M_{\boldsymbol{\tau}}}} \ll \omega = \sqrt{\frac{\beta}{m_0}}. \qquad (2.29)$$

As a consequence, the electrons can adjust instantaneously to an arbitrary configuration of the ions. A quantitative calculation based on the fact that $m_0/M \ll 1$ holds, leads to a separation of the motion of electrons and ions and can be found in [85]. This is the so-called Born-Oppenheimer or adiabatic approximation since the electrons follow the ions without changing their eigenstate, i.e., adiabatically. The Schrödinger equations for the separated systems read

$$[H_{\text{ion}} + E_{\text{el},\alpha}]\,\Phi_\alpha = \left[\sum_{\boldsymbol{n\tau}} \frac{\boldsymbol{P}_{\boldsymbol{n\tau}}^2}{2M_{\boldsymbol{\tau}}} + U_\alpha(\{\boldsymbol{R}_{\boldsymbol{n\tau}}\})\right]\Phi_\alpha = i\hbar\frac{\partial}{\partial t}\Phi_\alpha \tag{2.30}$$

and

$$[H_{\text{el}} + H_{\text{el}-\text{ion}}]\,\Psi_\alpha = E_{\text{el},\alpha}\Psi_\alpha. \tag{2.31}$$

The ions notice the adiabatic potential

$$U_\alpha(\{\boldsymbol{R}_{\boldsymbol{n\tau}}\}) = E_{\text{el},\alpha}(\{\boldsymbol{R}_{\boldsymbol{n\tau}}\}) + \frac{1}{2}\sum_{\boldsymbol{n\tau}\neq\boldsymbol{m\sigma}} V(\boldsymbol{R}_{\boldsymbol{n\tau}} - \boldsymbol{R}_{\boldsymbol{m\sigma}}), \tag{2.32}$$

which depends not only on the interaction between the ions, but also on the eigenenergy of the electronic system in the eigenstate α. Given the ion configuration the stationary problem of Eq. (2.31) for the electron system can be solved. In a simpler approach the ion positions $\boldsymbol{R}_{\boldsymbol{n\tau}}$ in Eq. (2.31) can be replaced by their equilibrium positions $\boldsymbol{R}^0_{\boldsymbol{n\tau}}$.

2.2 Lattice dynamics and phonons

The lattice dynamics of a solid in the Born-Oppenheimer approximation is described by the Schrödinger equation (2.30). We will solve the problem of the lattice dynamics in this Section applying some further approximations and then introduce the concept of phonons.

2.2.1 Harmonic approximation

At first we assume that the electron system is in its ground state[6], which allows us to drop the index α in $U_\alpha(\{\boldsymbol{R}_{\boldsymbol{n\tau}}\})$. The positions of the ions are

$$\boldsymbol{R}_{\boldsymbol{n\tau}}(t) = \boldsymbol{R}^0_{\boldsymbol{n\tau}} + \boldsymbol{u}_{\boldsymbol{n\tau}}(t) \tag{2.33}$$

with a time-dependent displacement $\boldsymbol{u}_{\boldsymbol{n\tau}}(t)$ being much smaller[7] than the lattice constant a. Therefore $U(\{\boldsymbol{R}_{\boldsymbol{n\tau}}\})$ can be written as a Taylor series[8] around $\boldsymbol{R}^0_{\boldsymbol{n\tau}}$. The term being linear in $\boldsymbol{u}_{\boldsymbol{n\tau}}(t)$ vanishes since the energy is at its minimum when all ions are located at the positions $\boldsymbol{R}^0_{\boldsymbol{n\tau}}$. Neglecting terms of third and higher order, one arrives at the harmonic approximation

$$H_{\text{ion}} = \sum_{\boldsymbol{n\tau}} \frac{\boldsymbol{P}_{\boldsymbol{n\tau}}^2}{2M_{\boldsymbol{\tau}}} + \frac{1}{2}\sum_{\boldsymbol{n\tau}i\boldsymbol{m\sigma}j} \Phi_{\boldsymbol{n\tau}i\boldsymbol{m\sigma}j}\, u_{\boldsymbol{n\tau}i}\, u_{\boldsymbol{m\sigma}j} \tag{2.34}$$

with

$$\Phi_{\boldsymbol{n\tau}i\boldsymbol{m\sigma}j} = \left.\frac{\partial^2 U}{\partial u_{\boldsymbol{n\tau}i}\partial u_{\boldsymbol{m\sigma}j}}\right|_{\{\boldsymbol{R}^0_{\boldsymbol{n\tau}}\}}. \tag{2.35}$$

---

[6] If there are not too many excited electrons, the dynamical matrix $\Phi_{\boldsymbol{n\tau}i\boldsymbol{m\sigma}j}$ will also be primarily determined by the ground state of the electron system [7].

[7] The case of $|\boldsymbol{u}_{\boldsymbol{n\tau}}| \approx a$ would describe the destruction of the solid and melting.

[8] The complete potential between neighboring atoms can be described in analytic approximations. Their results are known as, e.g., the Lennard-Jones or the Born-Mayer potential [12].

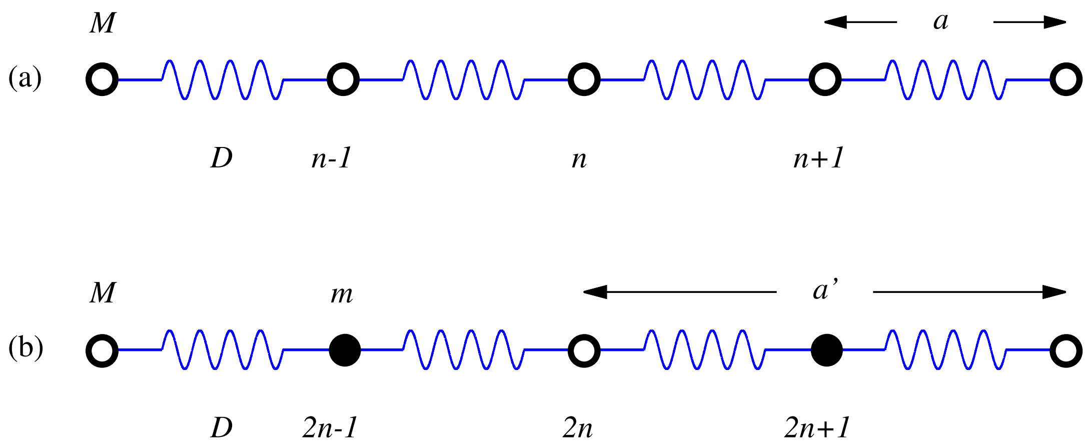

Figure 2.3.: Model of a one-dimensional solid with (a) one and (b) two ions in the unit cell. The lattice constants are denoted by a and a', respectively. Adapted from [12].

The resulting equations of motion for the displacements $\boldsymbol{u}_{\boldsymbol{n\tau}}$ and the conjugate momenta $\boldsymbol{P}_{\boldsymbol{n\tau}}$ are those of coupled harmonic oscillators with force constants $\Phi_{\boldsymbol{n\tau}i\boldsymbol{m\sigma}j}$. Via

$$\dot{P}_{\boldsymbol{n\tau}i} = -\frac{\partial H_{\text{ion}}}{\partial u_{\boldsymbol{n\tau}i}}, \quad \dot{u}_{\boldsymbol{n\tau}i} = \frac{\partial H_{\text{ion}}}{\partial P_{\boldsymbol{n\tau}i}}, \tag{2.36}$$

we obtain

$$M_{\boldsymbol{\tau}}\, \ddot{u}_{\boldsymbol{n\tau}i} = -\sum_{\boldsymbol{m\sigma}j} \Phi_{\boldsymbol{n\tau}i\boldsymbol{m\sigma}j}\, u_{\boldsymbol{m\sigma}j}. \tag{2.37}$$

Instead of solving the general problem we will treat a one-dimensional model at first.

2.2.2 1D chain

To obtain a first understanding of the lattice dynamics we will solve the lattice equation of motion for a one-dimensional solid. To this aim we assume the solid as being built up of identical atoms with mass M, which are connected to the nearest neighbors by springs with identical force constants D as shown in Fig. 2.3(a). The distance between two atoms in equilibrium is given by the lattice constant a. With the displacements u_n the equation of motion reads

$$M\frac{\partial^2 u_n}{\partial t^2} = D\left[(u_{n+1} - u_n) - (u_n - u_{n-1})\right]. \tag{2.38}$$

The solution of Eq. (2.38) is a plane wave with identical amplitudes for the different atoms:

$$u_n = Ae^{i(qna-\omega t)}. \tag{2.39}$$

Inserting Eq. (2.39) into (2.38) and solving for ω yields the dispertion relation, i.e., the dependence of ω on the wave vector q,

$$\omega(q) = \sqrt{\frac{4D}{M}}\left|\sin\frac{qa}{2}\right|, \tag{2.40}$$

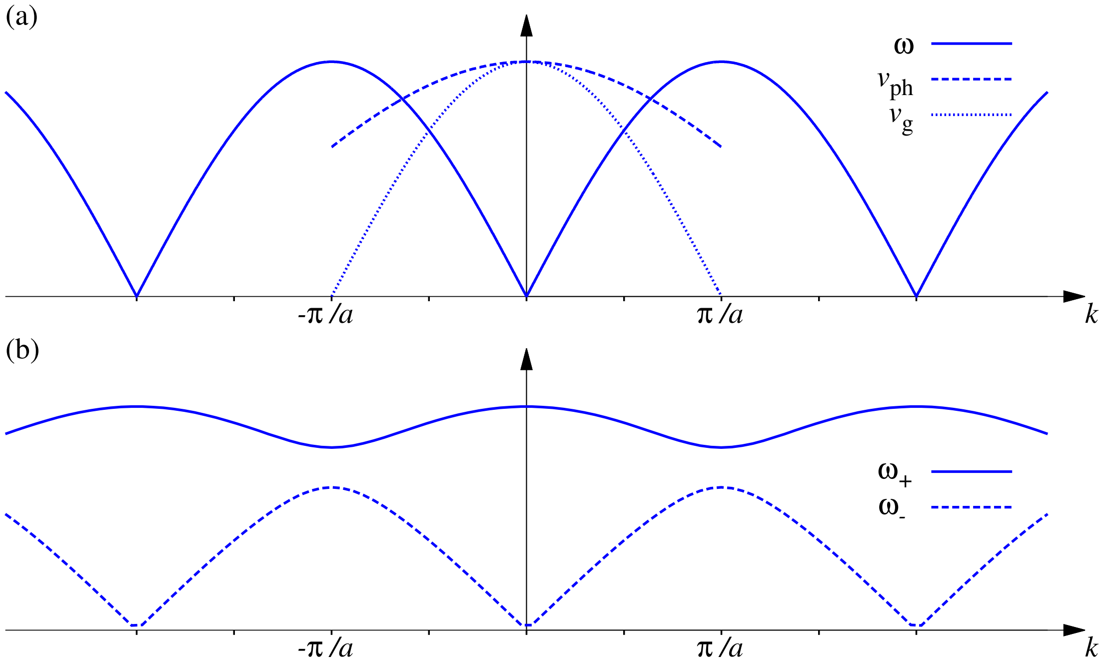

Figure 2.4.: (a) Dispersion relation of the 1D chain model depicted in Fig. 2.3(a). The dashed and dotted lines display the phase and group velocity, respectively. (b) Dispersion relation of the 1D chain model depicted in Fig. 2.3(b). Due to the diatomic basis two branches are obtained. The upper one is called the optical branch and the lower one is called the acoustic branch. Adapted from [12].

which is shown in Fig. 2.4(a). It can be seen that the dispersion relation is periodic with a periodicity given by the reciprocal lattice vector $G = 2\pi/a$. As it has already been outlined at the end of Sec. 2.1.1, we can restrict ourselves to the first BZ with $-\pi/a \leq q \leq \pi/a$. This can also be understood by considering Fig. 2.5: The shortest meaningful wavelength is given by $\lambda_{\mathrm{min}} = 2a$, which leads to

$$q_{\mathrm{max}} = \frac{2\pi}{\lambda_{\mathrm{min}}} = \frac{\pi}{a}. \tag{2.41}$$

Waves of shorter wavelength cannot be depicted in an unique way. A wave with $q = 3\pi/a$ corresponds, e.g., to a wave within the first BZ with $q = \pi/a$.

If we finally introduce periodic boundary conditions

$$u_n = u_{n+L} = u_{n+Na}, \tag{2.42}$$

in which N and L denote the length of the chain and the number of atoms[9] along the chain, respectively, the values of q become discrete with

$$q = \frac{2\pi m}{Na}, \quad m \in \mathbb{Z}. \tag{2.43}$$

---

[9] We assume N to be an even number.

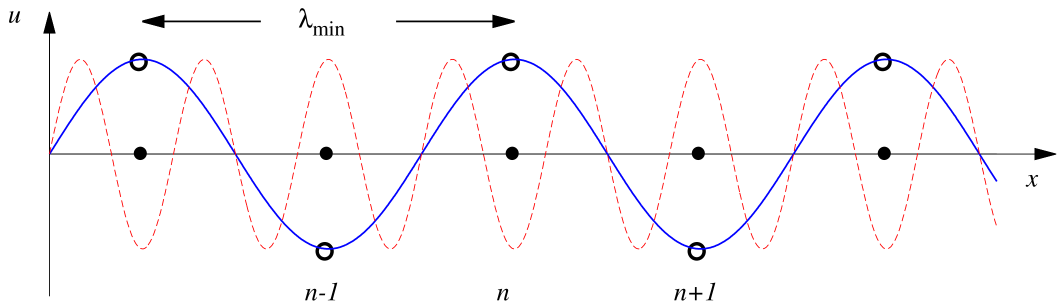

Figure 2.5.: Plane waves with a wavelength of $\lambda < \lambda_{\text{min}}$ cannot be reproduced unambiguously by lattice vibrations. Adapted from [12]

As a result of the restriction of q being within the first BZ there are N different values (N different natural oscillations), where it is important to note that the special cases of $m = \pm N/2$ describe only one solution due to $e^{i\pi} = e^{-i\pi}$ [cf. Eq. (2.39)]. For very large values of N the range of permitted q-values becomes quasi-continuous [86].

We will now take a look at a one-dimensional solid with a diatomic basis as shown in Fig. 2.3(b). The lattice constant is $a' = 2a$, where a denotes the distance between the two atoms with masses m and M. The equations of motion,

$$M\frac{\partial^2 u_{2n}}{\partial t^2} = D\left[(u_{2n+1} - u_{2n}) - (u_{2n} - u_{2n-1})\right], \tag{2.44a}$$

$$m\frac{\partial^2 u_{2n+1}}{\partial t^2} = D\left[(u_{2n+2} - u_{2n+1}) - (u_{2n+1} - u_{2n})\right], \tag{2.44b}$$

can be solved by the ansatz

$$u_{2n} = A_M e^{i(2naq-\omega t)}, \tag{2.45a}$$

$$u_{2n+1} = A_m e^{i((2n+1)aq-\omega t)}, \tag{2.45b}$$

yielding

$$\begin{pmatrix} 2D - \omega^2 M & -2D\cos(qa) \\ -2D\cos(qa) & 2D - \omega^2 m \end{pmatrix} \begin{pmatrix} A_M \\ A_m \end{pmatrix} = \begin{pmatrix} 0 \\ 0 \end{pmatrix}. \tag{2.46}$$

A non-trivial solution can be obtained only if the determinant of the coefficient matrix vanishes. The resulting secular problem can be solved for ω to give the dispersion relation

$$\omega_\pm(q) = \left(\frac{D}{\mu} \pm \sqrt{\left(\frac{D}{\mu}\right)^2 - \frac{4D^2}{Mm}\sin^2\left(\frac{qa'}{2}\right)}\right)^{\frac{1}{2}}, \tag{2.47}$$

with the reduced mass $\mu = mM/(m+M)$. The dispertion relation consists of two branches as shown in Fig. 2.4(b), which are called the optical branch (ω_+) and the acoustic branch (ω_-). A treatment of the ratio A_M/A_m in dependence of q shows that the two atoms are always displaced in phase in case of the acoustic branch and displaced in anti-phase in case of the optical branch (see Fig. 2.6). This explains the terms *acoustic* and *optical*: On the one hand, sound waves propagate always according to the modes of the acoustic branch. On the other hand, if the two atoms are differently

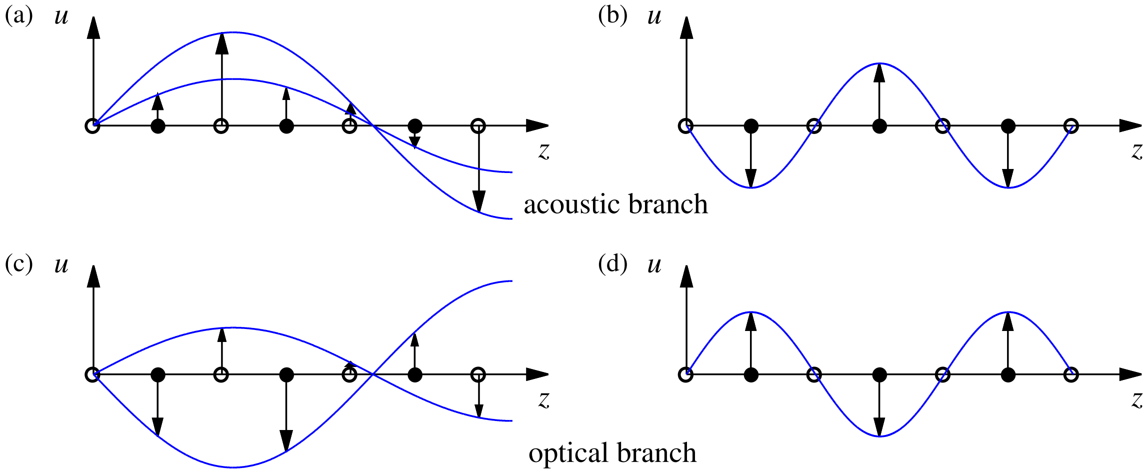

Figure 2.6.: In the case of an acoustic mode the two atoms of the basis are always displaced in phase (a,b), whereas they are displaced in anti-phase in the case of an optical mode (c,d). The panels (b) and (d) show the special case of $k = k_{\max}$. Adapted from [12].

charged, an oscillation with the atoms being displaced in anti-phase results in an oscillating electric dipole, which can couple to the electric field of light, thus justifying the term optical branch.

The dispersion relations are generally horizontal at the border of the BZ and the group velocity

$$v_{\mathrm{g}} = \frac{\partial \omega(q)}{\partial q} \tag{2.48}$$

is zero. This can be understood by the fact that the Bragg condition of reflection is fulfilled for these values of q. The reflected and the incident wave interfere to yield a standing wave with $v_{\mathrm{g}} = 0$ (see also Sec. 2.1.1).

In the limit of long wavelengths or small wave vectors $|q| \ll \pi/a$, the dispersions of the branches can be simplified to

$$\omega_{+} = \omega_{\mathrm{opt}} = \mathrm{const.} \tag{2.49}$$

for the optical branch and

$$\omega_{-} = \omega_{\mathrm{ac}} = v_{\mathrm{s}} q \tag{2.50}$$

for the acoustic branch, where v_{s} denotes the sound velocity. Due to the small thermal energy $k_{\mathrm{B}}T$ at low temperatures in comparison with the energy of phonons, only the acoustic branch in the vicinity of $q = 0$ can be excited thermally. Therefore Eq. (2.50) is the initial point of the so-called Debye model.

2.2.3 General solution and normal coordinates

We will now treat the three-dimensional problem[10]. Via Newton's third axiom, symmetry considerations as well as nearest and next-nearest neighbor approximation one can drastically reduce the number of independent force constants in Eq. (2.37) [85].

---

[10] For a detailed analysis of three-dimensional dispersion relations see [12, 85, 86] and references therein. Dispersion relations can be investigated experimentally by scattering with light (cf. also Sec. 2.4.1) or thermal neutrons [86].

We follow the descriptions in [85, 94] to set up the secular equation for the problem. This is done using a complex ansatz for $\boldsymbol{u}_{\boldsymbol{n\tau}}$. Knowing that there are only linear operations in the following calculation, we can afterwards treat real superpositions of the $\boldsymbol{u}_{\boldsymbol{n\tau}}$ as the true physical results[11]. At first, we separate the time dependency via

$$\boldsymbol{u}_{\boldsymbol{n\tau}}(t) = \frac{1}{\sqrt{M_{\boldsymbol{\tau}}}} \tilde{\boldsymbol{u}}_{\boldsymbol{n\tau}} e^{-i\omega t}. \tag{2.51}$$

Then we use Bloch's theorem (2.17) to write

$$\tilde{u}_{\boldsymbol{n}+\boldsymbol{m}\boldsymbol{\tau}i}(\boldsymbol{q}) = \tilde{u}_{\boldsymbol{n\tau}i}(\boldsymbol{q}) e^{i\boldsymbol{q}\cdot\boldsymbol{R}^0_{\boldsymbol{m}}} = \tilde{u}_{\boldsymbol{0\tau}i}(\boldsymbol{q}) e^{i\boldsymbol{q}\cdot(\boldsymbol{R}^0_{\boldsymbol{n}}+\boldsymbol{R}^0_{\boldsymbol{m}})}. \tag{2.52}$$

If we finally assume periodic boundary conditions, which results in discrete values for $\boldsymbol{q}$,

$$q_i = \frac{2\pi}{N_i a_i} n_i, \qquad n_i = -\frac{N_i}{2}, \ldots, \frac{N_i}{2} - 1, \qquad i \in \{1, 2, 3\}, \tag{2.53}$$

we obtain

$$\omega^2 \tilde{u}_{\boldsymbol{0\tau}i}(\boldsymbol{q}) = \sum_{\boldsymbol{\sigma}j} D_{\boldsymbol{\tau}i,\boldsymbol{\sigma}j}(\boldsymbol{q}) \tilde{u}_{\boldsymbol{0\sigma}j}(\boldsymbol{q}), \tag{2.54}$$

where the dynamical matrix[12]

$$\begin{aligned} D_{\boldsymbol{\tau}i,\boldsymbol{\sigma}j}(\boldsymbol{q}) &= \sum_{\boldsymbol{m}} \frac{1}{\sqrt{M_{\boldsymbol{\tau}} M_{\boldsymbol{\sigma}}}} \Phi_{\boldsymbol{n\tau}i\boldsymbol{m\sigma}j} e^{i\boldsymbol{q}\cdot(\boldsymbol{R}^0_{\boldsymbol{m}}-\boldsymbol{R}^0_{\boldsymbol{n}})} \\ &= \sum_{\boldsymbol{m}} \frac{1}{\sqrt{M_{\boldsymbol{\tau}} M_{\boldsymbol{\sigma}}}} \Phi_{\boldsymbol{n}-\boldsymbol{m\tau}i\boldsymbol{0\sigma}j} e^{i\boldsymbol{q}\cdot(\boldsymbol{R}^0_{\boldsymbol{m}}-\boldsymbol{R}^0_{\boldsymbol{n}})} \\ &= \sum_{\boldsymbol{v}} \frac{1}{\sqrt{M_{\boldsymbol{\tau}} M_{\boldsymbol{\sigma}}}} \Phi_{\boldsymbol{v\tau}i\boldsymbol{0\sigma}j} e^{-i\boldsymbol{q}\cdot\boldsymbol{R}^0_{\boldsymbol{v}}} \end{aligned} \tag{2.55}$$

is independent of $\boldsymbol{n}$ and fulfills $D_{\boldsymbol{\tau}i,\boldsymbol{\tau}'j}(\boldsymbol{q}) = D_{\boldsymbol{\tau}i,\boldsymbol{\tau}'j}(-\boldsymbol{q})$. For each of the $N = N_1 N_2 N_3$ values of $\boldsymbol{q}$ there is a secular problem

$$\left\| D_{\boldsymbol{\tau}i,\boldsymbol{\sigma}j}(\boldsymbol{q}) - \omega^2 \delta_{\boldsymbol{\tau\sigma}} \delta_{ij} \right\| = 0 \tag{2.56}$$

with $3r$ solutions

$$\omega_s(\boldsymbol{q}) = \omega_s(-\boldsymbol{q}), \qquad s \in \{1,\, 2,\, \ldots,\, 3r\}, \tag{2.57}$$

where r denotes the number of atoms in the basis.

The solution for the three-dimensional case is now a simple generalization of that for the one-dimensional case. In three dimensions there are only a few facts to be considered:

- The waves can propagate in arbitrary directions and one has to calculate with a wave *vector* $\boldsymbol{q}$. The dispersion relations becomes directional.
- The first BZ is a complicated three-dimensional body.
- There are three degrees of freedom of ionic motion, which cause two transversal modes and one longitudinal mode. If $\boldsymbol{q}$ is oriented in a direction of high symmetry of the BZ, the transversal modes are often degenerated.

---

[11] This is a procedure known from electrodynamics. Compare, e.g., Ref. [95].

[12] The identity $\Phi_{\boldsymbol{n\tau}i\boldsymbol{m\sigma}j} = \Phi_{\boldsymbol{n}-\boldsymbol{m\tau}i\boldsymbol{0\sigma}j}$ is due to the translational symmetry of the lattice.

- There are 3 acoustic and $3r-3$ optical branches.
- Applying periodic boundary conditions, there are $3rN$ solutions. This equals the total number of degrees of freedom since $N = N_1N_2N_3$ is the number of lattice or unit cells.

The general solutions describe collective modes, i.e., the time dependency of the motion is the same for all ions but they move phase-shifted with respect to each other. The motion of an ion at $\boldsymbol{R}_{\boldsymbol{n\tau}}$ with mass $M_{\boldsymbol{\tau}}$ in the mode $s\boldsymbol{q}$ is described by

$$\boldsymbol{u}^s_{\boldsymbol{n\tau}}(\boldsymbol{q},\,t) \sim \frac{1}{\sqrt{M_{\boldsymbol{\tau}}}}\boldsymbol{e}^s_{\boldsymbol{\tau}}(\boldsymbol{q})e^{i(\boldsymbol{q}\,\cdot\,\boldsymbol{R}^0_{\boldsymbol{n}}-\omega_s(\boldsymbol{q})t)} \tag{2.58}$$

with $\boldsymbol{e}^s_{\boldsymbol{\tau}}(\boldsymbol{q})$ denoting the ortho-normalized eigenvectors for each mode s, i.e.,

$$\sum_{\boldsymbol{\sigma}j} D_{\boldsymbol{\tau}i,\boldsymbol{\sigma}j}(\boldsymbol{q})e^s_{\boldsymbol{\sigma}j}(\boldsymbol{q}) = [\omega_s(\boldsymbol{q})]^2\,e^s_{\boldsymbol{\tau}i}(\boldsymbol{q}) \tag{2.59}$$

and [94]

$$\sum_{\boldsymbol{\tau}i} e^{s*}_{\boldsymbol{\tau}i}(\boldsymbol{q})e^{s'}_{\boldsymbol{\tau}i}(\boldsymbol{q}) = \delta_{ss'}. \tag{2.60}$$

Any arbitrary motion of an ion can be expressed using the eigenmodes as a basis since they form a complete set of solutions. We write

$$u_{\boldsymbol{n\tau}i}(t) = \frac{1}{\sqrt{NM_{\boldsymbol{\tau}}}}\sum_{s\boldsymbol{q}} Q_s(\boldsymbol{q},\,t)e^s_{\boldsymbol{\tau}i}(\boldsymbol{q})e^{i\boldsymbol{q}\,\cdot\,\boldsymbol{R}^0_{\boldsymbol{n}}}, \tag{2.61}$$

where we defined the normal coordinate for the mode $s\boldsymbol{q}$ by[13]

$$Q_s(\boldsymbol{q},\,t) = f_s(\boldsymbol{q})e^{-i\omega_s(\boldsymbol{q})t} + f^*_s(-\boldsymbol{q})e^{i\omega_s(\boldsymbol{q})t}. \tag{2.62}$$

The $\boldsymbol{u}_{\boldsymbol{n\tau}}$ have to be real [96], which results in

$$\boldsymbol{e}^s_{\boldsymbol{\tau}}(-\boldsymbol{q}) = \boldsymbol{e}^{s*}_{\boldsymbol{\tau}i}(\boldsymbol{q}), \quad Q_s(-\boldsymbol{q},\,t) = Q^*_s(\boldsymbol{q},\,t). \tag{2.63}$$

By introducing normal coordinates, it is possible to write the Hamiltonian in a form which describes a set of $3rN$ uncoupled oscillators. The intended normal-coordinate transformation can be at the best expressed by the following scheme [85]:

$$\begin{array}{ccc}
\text{coupled motion} & \Rightarrow & \text{uncoupled collective motion} \\
\text{localized} & & \text{delocalized} \\
u_{\boldsymbol{n\tau}i}(t) & \rightarrow & Q_s(\boldsymbol{q},\,t) \\
H(\boldsymbol{u}_{\boldsymbol{n\tau}},\,\boldsymbol{P}_{\boldsymbol{n\tau}}) & \rightarrow & H(Q_s(\boldsymbol{q},\,t),\,P_s(\boldsymbol{q},\,t))
\end{array}$$

The dispersion relations $\omega_s(\boldsymbol{q})$ are not influenced by this transformation. At first, we take a look at the Lagrangian which corresponds to H_{ion} in Eq. (2.34). Using

$$\dot{u}_{\boldsymbol{n\tau}i} = \frac{\partial H_{\text{ion}}}{\partial P_{\boldsymbol{n\tau}i}} \rightarrow P_{\boldsymbol{n\tau}i} = M_{\boldsymbol{\tau}}\dot{u}_{\boldsymbol{n\tau}i} = \sqrt{\frac{M_{\boldsymbol{\tau}}}{N}}\sum_{s\boldsymbol{q}}\dot{Q}_s(\boldsymbol{q},\,t)e^s_{\boldsymbol{\tau}i}(\boldsymbol{q})e^{i\boldsymbol{q}\,\cdot\,\boldsymbol{R}^0_{\boldsymbol{n}}}, \tag{2.64}$$

---

[13] Note that the expression for the normal coordinate is wrong in Ref. [85]. The normal coordinate has to be defined in the form of Eq. (2.62) so that the relation (2.63) holds. The equation of motion (2.71) is then still fulfilled.

we obtain

$$\begin{aligned} L &= \sum_{\boldsymbol{n}\boldsymbol{\tau}} \frac{\boldsymbol{P}^2_{\boldsymbol{n}\boldsymbol{\tau}}}{2M_{\boldsymbol{\tau}}} - \frac{1}{2} \sum_{\boldsymbol{n}\boldsymbol{\tau} i \boldsymbol{m}\boldsymbol{\sigma} j} \Phi_{\boldsymbol{n}\boldsymbol{\tau} i \boldsymbol{m}\boldsymbol{\sigma} j}\, u_{\boldsymbol{n}\boldsymbol{\tau} i}\, u_{\boldsymbol{m}\boldsymbol{\sigma} j} \\ &= \frac{1}{2N} \left(\sum_{\boldsymbol{n}\boldsymbol{\tau} i} \sum_{s\boldsymbol{q}} \sum_{s'\boldsymbol{q}'} \dot{Q}_s(\boldsymbol{q},\, t) \dot{Q}_{s'}(\boldsymbol{q}',\, t) e^s_{\boldsymbol{\tau} i}(\boldsymbol{q}) e^{s'}_{\boldsymbol{\tau} i}(\boldsymbol{q}') e^{i(\boldsymbol{q}+\boldsymbol{q}')\cdot \boldsymbol{R}^0_{\boldsymbol{n}}} \right. \\ & \qquad \left. - \sum_{\boldsymbol{n}\boldsymbol{\tau} i} \sum_{\boldsymbol{\sigma} j} \sum_{s\boldsymbol{q}} \sum_{s'\boldsymbol{q}'} D_{\boldsymbol{\tau} i, \boldsymbol{\sigma} j}(\boldsymbol{q}') Q_s(\boldsymbol{q},\, t) Q_{s'}(\boldsymbol{q}',\, t) e^s_{\boldsymbol{\tau} i}(\boldsymbol{q}) e^{s'}_{\boldsymbol{\sigma} j}(\boldsymbol{q}') e^{i(\boldsymbol{q}+\boldsymbol{q}')\cdot \boldsymbol{R}^0_{\boldsymbol{n}}} \right) . \end{aligned} \tag{2.65}$$

We can now perform the sum over $\boldsymbol{n}$ considering that $\boldsymbol{q}$ and $\boldsymbol{q}'$ lie already within the first BZ:

$$\sum_{\boldsymbol{n}} e^{i(\boldsymbol{q}+\boldsymbol{q}')\cdot \boldsymbol{R}^0_{\boldsymbol{n}}} = N \sum_{\boldsymbol{G}} \delta_{\boldsymbol{q}, -\boldsymbol{q}'+\boldsymbol{G}} = N \delta_{\boldsymbol{q}, -\boldsymbol{q}'}. \tag{2.66}$$

Exploiting Eq. (2.63), it is

$$\begin{aligned} L &= \frac{1}{2} \left(\sum_{\boldsymbol{\tau} i} \sum_{ss'\boldsymbol{q}} \dot{Q}_s(\boldsymbol{q},\, t) \dot{Q}^*_{s'}(\boldsymbol{q},\, t) e^s_{\boldsymbol{\tau} i}(\boldsymbol{q}) e^{s'*}_{\boldsymbol{\tau} i}(\boldsymbol{q}) \right. \\ & \qquad \left. - \sum_{\boldsymbol{\tau} i} \sum_{\boldsymbol{\sigma} j} \sum_{ss'\boldsymbol{q}} Q_s(\boldsymbol{q},\, t) Q^*_{s'}(\boldsymbol{q},\, t) e^s_{\boldsymbol{\tau} i}(\boldsymbol{q}) \sum_{\boldsymbol{\sigma} j} D_{\boldsymbol{\tau} i, \boldsymbol{\sigma} j}(-\boldsymbol{q}) e^{s'*}_{\boldsymbol{\sigma} j}(\boldsymbol{q}) \right) . \end{aligned} \tag{2.67}$$

Defining the conjugate momenta

$$P_s(\boldsymbol{q},\, t) = \frac{\partial L}{\dot{Q}_s(\boldsymbol{q},\, t)} = \dot{Q}^*_s(\boldsymbol{q},\, t) \tag{2.68}$$

and using Eq. (2.59), one finally arrives at the Hamiltonian [85]

$$H(Q_s(\boldsymbol{q},\, t),\, P_s(\boldsymbol{q},\, t)) = \sum_{s\boldsymbol{q}} \left[P^*_s(\boldsymbol{q},\, t) P_s(\boldsymbol{q},\, t) + \omega^2_s(\boldsymbol{q}) Q^*_s(\boldsymbol{q},\, t) Q_s(\boldsymbol{q},\, t) \right] . \tag{2.69}$$

For each mode $s\boldsymbol{q}$ the equation of motion then reads

$$\dot{P}_s(\boldsymbol{q},\, t) = -\frac{\partial H}{Q_s(\boldsymbol{q},\, t)}, \quad \dot{Q}_s(\boldsymbol{q},\, t) = -\frac{\partial H}{P_s(\boldsymbol{q},\, t)} \tag{2.70}$$

or

$$\ddot{Q}_s(\boldsymbol{q},\, t) = -\left[\omega_s(\boldsymbol{q})\right]^2 Q_s(\boldsymbol{q},\, t). \tag{2.71}$$

If we used higher order terms in the approximation (2.34), the Hamiltonian would describe nonlinear lattice dynamics. In this situation a decoupling of the motions is no longer possible. The nonlinear lattice dynamics are necessary to describe, e.g., phonon-phonon interaction, thermal lattice expansion and the phononic part of heat transport. For more general models than the presented rigid-ion model with massive spheres and springs see [85] and references therein.

2.2.4 Phonons

Up to now the system has been discussed in terms of classical mechanics. We can now treat $P_s(\boldsymbol{q})$ and $Q_s(\boldsymbol{q})$ as quantum-mechanical operators obeying the commutation relations

$$\begin{aligned} \big[Q_s(\boldsymbol{q}),\, P_{s'}(\boldsymbol{q}')\big] &= i\hbar\delta_{ss'}\delta_{\boldsymbol{q}\boldsymbol{q}'}, && (2.72\text{a}) \\ \big[Q_s(\boldsymbol{q}),\, Q_{s'}(\boldsymbol{q}')\big] = \big[P_s(\boldsymbol{q}),\, P_{s'}(\boldsymbol{q}')\big] &= 0, && (2.72\text{b}) \end{aligned}$$

and introduce creation and annihilation operators for each mode,

$$\begin{aligned} a_s^\dagger(\boldsymbol{q}) &= \frac{1}{\sqrt{2\hbar\omega_s(\boldsymbol{q})}}\left[\omega_s(\boldsymbol{q})Q_s(-\boldsymbol{q}) - iP_s(\boldsymbol{q})\right], && (2.73\text{a}) \\ a_s(\boldsymbol{q}) &= \frac{1}{\sqrt{2\hbar\omega_s(\boldsymbol{q})}}\left[\omega_s(\boldsymbol{q})Q_s(\boldsymbol{q}) + iP_s(-\boldsymbol{q})\right], && (2.73\text{b}) \end{aligned}$$

with

$$\begin{aligned} \left[a_s(\boldsymbol{q}),\, a_{s'}^\dagger(\boldsymbol{q}')\right] &= \delta_{ss'}\delta_{\boldsymbol{q}\boldsymbol{q}'}, && (2.74\text{a}) \\ \big[a_s(\boldsymbol{q}),\, a_{s'}(\boldsymbol{q}')\big] = \left[a_s^\dagger(\boldsymbol{q}),\, a_{s'}^\dagger(\boldsymbol{q}')\right] &= 0, && (2.74\text{b}) \end{aligned}$$

to write the Hamiltonian (2.69) using these operators as

$$H = \sum_{s\boldsymbol{q}} \hbar\omega_s(\boldsymbol{q}) \left(a_s^\dagger(\boldsymbol{q})a_s(\boldsymbol{q}) + \frac{1}{2}\right). \tag{2.75}$$

The ground state $|\Psi_0\rangle = |\{0\}\rangle = |0,\ldots,0,\,\text{for all}\, s\boldsymbol{q}\rangle$ obeys $a_s(\boldsymbol{q})\,|\Psi_0\rangle = 0$ and is called the phonon vacuum. Every excitation out of this state is then called a phonon, where the phonon energy and the phonon momentum are given by $\hbar\omega_s(\boldsymbol{q})$ and $\hbar\boldsymbol{q}$, respectively[14]. Based on the fact that a phonon cannot exist outside of the solid and that its momentum is only a quasi-momentum (cf. Sec. 2.1.1), it is considered as a quasi-particle. The energy

$$E_0 = \sum_{s\boldsymbol{q}} \frac{1}{2}\hbar\omega_s(\boldsymbol{q}) \tag{2.76}$$

of the ground state is due to the uncertainity principle and describes the zero-point motion of the ions. The eigenstates of H or of the occupation number operator $\hat{n}_s(\boldsymbol{q}) = a_s^\dagger(\boldsymbol{q})a_s(\boldsymbol{q})$ can be written in occupation number representation as

$$|\{n_s(\boldsymbol{q})\}\rangle = \prod_{s\boldsymbol{q}} \frac{1}{\sqrt{n_s(\boldsymbol{q})!}} \left[a_s^\dagger(\boldsymbol{q})\right]^{n_s(\boldsymbol{q})} |\{0\}\rangle \tag{2.77}$$

with the number $n_s(\boldsymbol{q})$ of phonons in the mode $s\boldsymbol{q}$.

It is not possible to prepare a certain eigenstate in the solid. Instead, the system takes on a thermodynamic state, which is definded by the temperature T. The average occupation of the modes is given by

$$\langle\hat{n}_s(\boldsymbol{q})\rangle = \frac{1}{Z_G}\mathrm{Tr}\left(\hat{n}_s(\boldsymbol{q})e^{-(H-\mu N)/k_\mathrm{B}T}\right) \tag{2.78}$$

---

[14] Note that a phonon interacts with other particle as if it had the momentum $\hbar\boldsymbol{q}$. However, it has no real physical momentum since there is no mass transport [86].

with the grand-canonical partition function Z_G and $N = \sum_{s\boldsymbol{q}} \hat{n}_s(\boldsymbol{q})$. The chemical potential μ is zero since there is no conservation of the number of phonons. The final result,

$$n_s(\omega_s(\boldsymbol{q}), T) = \langle \hat{n}_s(\boldsymbol{q}) \rangle = \frac{1}{e^{\hbar\omega_s(\boldsymbol{q})/k_\mathrm{B}T} - 1}, \tag{2.79}$$

shows that phonons obey Bose-Einstein statistics. At last we will introduce the density of states,

$$D(\omega) = \sum_{s\boldsymbol{q}} \delta(\omega - \omega_s(\boldsymbol{q})), \tag{2.80}$$

which sums over all branches in the first BZ and thereby counts the number of modes at a given frequency ω. Since every state takes a volume of $(2\pi)^3/V$ in $\boldsymbol{q}$ space, it is possible to write Eq. (2.80) as an integral:

$$D(\omega) = \frac{V}{(2\pi)^3} \sum_s \int_{BZ} \delta(\omega - \omega_s(\boldsymbol{q})). \tag{2.81}$$

Performing the integration over the δ function, one is left with a two-dimensional integral over the surface $S_{\boldsymbol{q}}$ in $\boldsymbol{q}$ space, for which $\omega = \omega_s(\boldsymbol{q})$ holds [85, 86]:

$$D(\omega) = \sum_s D_s(\omega) = \frac{V}{(2\pi)^3} \sum_s \int_{S_{\boldsymbol{q}}} \frac{\mathrm{d}S_{\boldsymbol{q}}}{|\nabla_{\boldsymbol{q}}\omega_s(\boldsymbol{q})|}. \tag{2.82}$$

Realistic densities of states can be found, e.g., in [97].

2.3 Electron dynamics

Having treated the lattice dynamics of the solid, we will now describe the electron dynamics. According to the considerations of the Secs. 2.1.2 and 2.1.3, only the valence electrons of the atoms in a solid are of importance. The corresponding Hamiltonian within the Born-Oppenheimer approximation reads

$$H = \sum_l \frac{\boldsymbol{p}_l^2}{2m_0} + \frac{1}{2} \sum_{k \neq l} \frac{e^2}{4\pi\varepsilon_0 |\boldsymbol{r}_l - \boldsymbol{r}_k|} + \sum_{\boldsymbol{n}\tau l} v(\boldsymbol{r}_l - \boldsymbol{R}^0_{\boldsymbol{n}\tau}) + \frac{1}{2} \sum_{\boldsymbol{n}\tau \neq \boldsymbol{m}\sigma} V(\boldsymbol{R}^0_{\boldsymbol{n}\tau} - \boldsymbol{R}^0_{\boldsymbol{m}\sigma}), \tag{2.83}$$

where the ions are assumed to be in equilibrium positions.

At first, we will describe the simplified model of free electrons in Sec. 2.3.1. One can then treat corrections due to the periodic potential of the ions, which will be done in the subsequent Secs. 2.3.1-2.3.6. In Sec. 2.3.7 we describe the effective-mass approximation before excited states of the electronic system are treated in Sec. 2.3.8.

2.3.1 Free electron gas

In a first approximation one can consider the simple case of a homogeneous electron gas, in which structural aspects are neglected and the ions are replaced by a homogeneous background charge H_+. This is the so-called jellium model [85] with the Hamiltonian

$$H = \sum_{l=1}^{N_e} \frac{\boldsymbol{p}_l^2}{2m_0} + \frac{1}{2} \sum_{k,l=1,\, k \neq l}^{N_e} \frac{e^2}{4\pi\varepsilon_0 |\boldsymbol{r}_l - \boldsymbol{r}_k|} + H_+. \tag{2.84}$$

Neglecting supplementary the Coulomb interaction, one arrives at the model of free electrons without interaction. Hence, we initially consider the Hamiltonian

$$H = \sum_{l=1}^{N_e} \frac{\boldsymbol{p}_l^2}{2m_0}. \tag{2.85}$$

The corresponding Schrödinger equation can be solved by the following ansatz for the many-particle wave function, which is a product of single-particle wave functions:

$$\Psi(\{\boldsymbol{r}_l\}) = \prod_{l=1}^{N_e} \psi(\boldsymbol{r}_l). \tag{2.86}$$

The resulting single-particle problem

$$H_l \psi(\boldsymbol{r}_l) = \frac{\boldsymbol{p}_l^2}{2m_0} \psi(\boldsymbol{r}_l) = E_l \psi(\boldsymbol{r}_l) \tag{2.87}$$

has the solutions

$$\psi_{\boldsymbol{k}}(\boldsymbol{r}) = \frac{1}{\sqrt{V}} e^{i\boldsymbol{k}\cdot\boldsymbol{r}}, \quad E(\boldsymbol{k}) = \frac{\hbar^2 \boldsymbol{k}^2}{2m_0}. \tag{2.88}$$

The electronic states are solely characterized by the wave vector $\boldsymbol{k}$ when neglecting the spin degree of freedom. Assuming periodic boundary conditions for a solid being of the form of a cuboid with volume $V = L_1 L_2 L_3$, the wave vectors $\boldsymbol{k}$ become discrete,

$$k_i = \frac{2\pi}{L_i} n_i, \quad n_i \in \mathbb{Z}, \quad i \in \{1, 2, 3\}, \tag{2.89}$$

and each state takes a volume $(2\pi)^3/V$ in $\boldsymbol{k}$-space. These boundary conditions are introduced as a trick, allowing to obtain countable discrete states. However, the only relevant physical quantity entering into the physical observables is the single particle density $n = N_e/V$ with $n =$ const. in the limit $V \to \infty$.

The ground state at $T = 0\,\mathrm{K}$ is obtained by placing the electrons in the states with lowest energy bearing in mind Pauli's principle. The energy of the ground state can then be evaluated using the density of states

$$D(k) = 2 \frac{V}{(2\pi)^3} 4\pi k^2, \tag{2.90}$$

where the factor 2 accounts for the spin degeneracy. Since $E(\boldsymbol{k}) \sim \boldsymbol{k}^2$ holds, the filled states form a sphere in $\boldsymbol{k}$-space around $\boldsymbol{k} = 0$ with a radius k_F depending on the density n:

$$n = \frac{N}{V} = \frac{1}{V} \int_0^{k_F} D(k)\,\mathrm{d}k = \frac{1}{4\pi^2} k_F^3. \tag{2.91}$$

This sphere is called the Fermi sphere. The electrons with $k = k_F$ have the highest energy[15] at $T = 0\,\mathrm{K}$, which is the so-called Fermi energy

$$E_F = \frac{\hbar^2 k_F^2}{2m_0}. \tag{2.92}$$

---

[15] The electrons in the vicinity of the Fermi energy are the relevant ones if magnetic or optical properties as well as the electronic contributions to electric and heat conductivity of metals at finite temperatures are examined [86].

We now find the expressions for the ground state energy at this temperature,

$$E_0 = \int_0^{k_F} E(k)D(k)\,\mathrm{d}k = \frac{3}{5}NE_F, \tag{2.93}$$

and the average energy per particle

$$\epsilon_0 = \frac{E_0}{N} = \frac{3}{5}\frac{\hbar^2}{2m_0}(3\pi^2 n)^{\frac{2}{3}}, \tag{2.94}$$

depending only on the density n. At last we give the density of states in dependence on the energy E, which is obtained by

$$D(E)\mathrm{d}E = D(k)\frac{\mathrm{d}k}{\mathrm{d}E}\mathrm{d}E \quad \text{or} \quad D(E) = 2\sum_{\boldsymbol{k}}\delta(E - E(\boldsymbol{k})) \tag{2.95}$$

and using Eqs. (2.88) and (2.90):[16]

$$D(E) = \frac{V}{2\pi^2}\left(\frac{2m_0}{\hbar^2}\right)^{\frac{3}{2}}\sqrt{E}. \tag{2.96}$$

The density of states can then be used to determine the energy at finite temperatures:

$$E_0(T) = \int_0^{\infty} ED(E)f(E,\,\mu,\,T)\,\mathrm{d}E. \tag{2.97}$$

$f(E,\,\mu,\,T)$ is the Fermi-Dirac distribution function

$$f(E,\,\mu,\,T) = \frac{1}{e^{(E-\mu)/k_{\mathrm{B}}T} + 1}, \tag{2.98}$$

in which the chemical potential μ is identified by the condition of a fixed particle density[17]:

$$n = \int_0^{\infty} D(E)f(E,\,\mu,\,T)\,\mathrm{d}E. \tag{2.99}$$

The ansatz (2.86) for the many-particle wave function of the free electron gas did not consider an important fact when dealing with fermions: This wave function should be antisymmetric when two particles are interchanged. Therefore, it is appropriate to use the formalism of second quantization, which is shortly explained in Appendix A.2.

With the single-particle solutions $\psi_{\boldsymbol{k}_i\sigma_i}(x_i)$ the many-particle wave function reads

$$|\Psi\rangle = |\{n_{\boldsymbol{k}\sigma}\}\rangle = c^{\dagger}_{\boldsymbol{k}_1\sigma_1}c^{\dagger}_{\boldsymbol{k}_2\sigma_2}\dots c^{\dagger}_{\boldsymbol{k}_N\sigma_N}|\{0\}\rangle\,, \tag{2.100}$$

where we use creation and annihilation operators $c^{\dagger}_{\boldsymbol{k}_i\sigma_i}$ and $c_{\boldsymbol{k}_i\sigma_i}$. We can then express the Hamiltonian of the jellium model (2.84) in terms of electron creation and annihilation operators $c^{\dagger}_{\boldsymbol{k}\sigma}$, $c_{\boldsymbol{k}\sigma}$ using the single-particle wave functions

$$\psi_{\boldsymbol{k}\sigma} = \frac{1}{\sqrt{V}}e^{i\boldsymbol{k}\cdot\boldsymbol{r}}\chi_{\sigma}(s). \tag{2.101}$$

---

[16] The resulting expression for the density of states is generally used for metals. Expressions respecting the specific conditions of semiconductors can be found, e.g., in [12, 86].

[17] The meaning of this equation is simple to understand: The density of particles equals the integral over the product of the probability of a state being occupied and the density of states [12].

The function $\chi_\sigma(s)$ describes the state of the electron spin. One finds

$$H = \sum_{\boldsymbol{k}\sigma} \frac{\hbar^2 \boldsymbol{k}^2}{2m_0} c^\dagger_{\boldsymbol{k}\sigma} c_{\boldsymbol{k}\sigma} + \frac{1}{2} \sum_{\boldsymbol{pqk}\sigma\sigma'} v_{\boldsymbol{k}} c^\dagger_{\boldsymbol{p}+\boldsymbol{k}\sigma} c^\dagger_{\boldsymbol{q}-\boldsymbol{k}\sigma'} c_{\boldsymbol{q}\sigma'} c_{\boldsymbol{p}\sigma} - \frac{1}{2} v_{\boldsymbol{0}} N^2 \tag{2.102}$$

with the Fourier transform of the Coulomb potential $v_{\boldsymbol{k}} = e^2/\varepsilon_0 V \boldsymbol{k}^2$. This Hamiltonian applies to electron systems in vacuum as well as to electron systems in matter. In the latter case only two corrections are necessary: The effective mass m^* replaces the free electron mass and the Coulomb interaction is screened, i.e., it is multiplied by $1/\varepsilon$, where ε denotes the dielectric constant of the solid. These corrections will be discused further in Secs. 2.3.7 and 2.5.1.

2.3.2 Electrons in a periodic potential

At the beginning of this section we presented the Hamiltonian of the electron system in the potential of fixed ions [cf. Eq. (2.83)]. This periodic potential will now be incorporated in the Hamiltonian (2.84) but we will use a more simple notation, where we do not refer to the ion positions:

$$H = \sum_{l=1}^{N_e} \left(\frac{\boldsymbol{p}_l^2}{2m_0} + V(\boldsymbol{r}_l) \right) + \frac{1}{2} \sum_{k,l=1,\, k\neq l}^{N_e} \frac{e^2}{4\pi\varepsilon_0 \left|\boldsymbol{r}_l - \boldsymbol{r}_k\right|} . \tag{2.103}$$

Due to the simultaneous presence of the electron-electron interation and the periodic lattice potential, the problem is highly complex and a rigorous solution aiming to find the ground-state energy is hardly possible [7, 85, 98, 99]. Even for the best known solutions of the problem – the Hartree-Fock solutions – the Hartree-Fock energy differs from the true value of the ground-state energy due to the one-electron approximation [7]. The correction to this energy obtained via perturbation theory is called correlation energy. An example for the correlation energy is the electron-hole interaction, i.e., the energy difference when one electron is (optically) excited and an exciton is formed.

To simplify the problem the Coulomb and the lattice term are often replaced by an effective single-particle potential, which incorporates the interaction between the particles [100–103]:

$$H = \sum_{l=1}^{N_e} \left(\frac{\boldsymbol{p}_l^2}{2m_0} + V_{\text{eff}}(\boldsymbol{r}_l) \right) . \tag{2.104}$$

In this case H is said to describe quasi-particles. A definition of this potential as well as a justification of this approach[18] can be obtained using density functional theory [85, 104, 106–112]. We will not follow this discussion but concentrate on the effects of a periodic potential on the free electron gas leading to the band structure of electrons in a solid. An examination of the band structures of real semiconductors[19] can be found, e.g., in [12].

2.3.3 Bloch functions and band structure

Starting from the Hamiltonian (2.104) we want to find solutions of the corresponding Schrödinger equation by exploiting the symmetry of the problem. Due to Bloch's theorem, which has been described in Sec. 2.1.1, one can write the common eigenfunctions of H and $T_{\boldsymbol{R}^0_{\boldsymbol{n}}}$ [cf. Eq. (2.9)] as

---

[18] The interaction between the electrons can play a crucial role in heavy Fermion systems or in the Hubbard model. These special cases are treated, for example, in [85, 104, 105].

[19] The band structure of Si will be shown in Fig. 2.11.

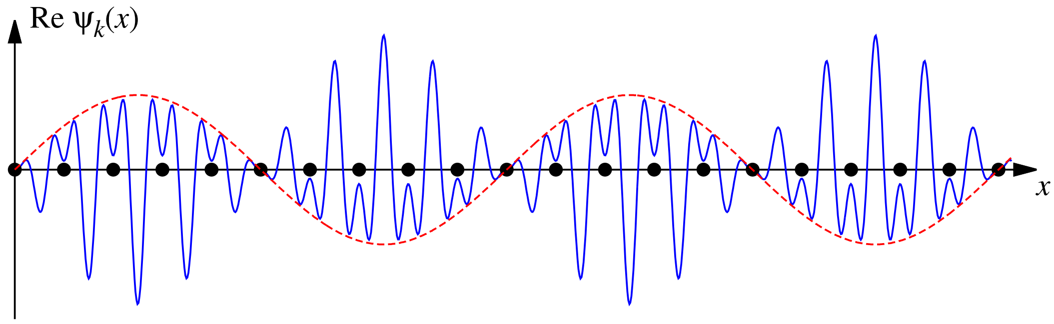

Figure 2.7.: One-dimensional Bloch function. Black dots mark the positions of ions. Adapted from [86].

a product of a lattice periodic function and an exponential function, i.e., as a Bloch function (see Fig. 2.7)

$$\psi_{\boldsymbol{k}}(\boldsymbol{r}) = \sum_{\boldsymbol{G}} c_{\boldsymbol{k}-\boldsymbol{G}} e^{i(\boldsymbol{k}-\boldsymbol{G})\cdot\boldsymbol{r}} = e^{i\boldsymbol{k}\cdot\boldsymbol{r}} u_{\boldsymbol{k}}(\boldsymbol{r}), \tag{2.105}$$

which is characterized by the wave vector $\boldsymbol{k}$. Since $\hbar\boldsymbol{k}$ enters the conservation laws of momentum, it is the momentum of the electron [86]. The characterization of the state of an electron is unique only for all $\boldsymbol{k}$ within the first BZ since two wave vectors within the first BZ do not differ by a reciprocal lattice vector. If we replace $\boldsymbol{k}$ by $\boldsymbol{k}+\boldsymbol{G}$ in the Bloch function (2.105) and change the index of summation ($\boldsymbol{G}-\boldsymbol{G}' \to \boldsymbol{G}''$), we see that $\psi_{\boldsymbol{k}}$ is periodic in reciprocal space [86]:

$$\psi_{\boldsymbol{k}+\boldsymbol{G}'}(\boldsymbol{r}) = \sum_{\boldsymbol{G}} c_{\boldsymbol{k}+\boldsymbol{G}'-\boldsymbol{G}} e^{i(\boldsymbol{k}+\boldsymbol{G}'-\boldsymbol{G})\cdot\boldsymbol{r}} = \sum_{\boldsymbol{G}''} c_{\boldsymbol{k}-\boldsymbol{G}''} e^{i(\boldsymbol{k}-\boldsymbol{G}'')\cdot\boldsymbol{r}} = \psi_{\boldsymbol{k}}(\boldsymbol{r}). \tag{2.106}$$

Therefore, $\hbar\boldsymbol{k}$ is more generally called quasi-momentum because it is only unique up to a reciprocal lattice vector $\boldsymbol{G}$ (cf. also Sec. 2.1.1).

For each value of $\boldsymbol{k}$ the eigenvalue problem

$$\left(-\frac{\hbar^2}{2m_0}\triangle + V_{\mathrm{eff}}(\boldsymbol{r})\right)\psi_\alpha = E_\alpha\psi_\alpha \tag{2.107}$$

provides an infinite number of independent solutions. These solutions are distinguished by introducing a new quantum number, the so-called band index n. The complete set of quantum numbers is therefore $\alpha = (n, \boldsymbol{k})$ (neglecting spin) and the energy band structure is defined by the energy eigenvalues $E_n(\boldsymbol{k})$ with n and $\boldsymbol{k}$ from the first BZ. Using periodic boundary conditions each band can accomodate $2N$ electrons, since there are N different $\boldsymbol{k}$-values in the first BZ[20]. The energy eigenvalues exhibit several symmetries [85]:

1. Translation symmetry: $E_n(\boldsymbol{k}) = E_n(\boldsymbol{k}+\boldsymbol{G})$. This results from

$$H\psi_{n\boldsymbol{k}} = H\psi_{n\boldsymbol{k}+\boldsymbol{G}} = E_n(\boldsymbol{k})\psi_{n\boldsymbol{k}} = E_n(\boldsymbol{k}+\boldsymbol{G})\psi_{n\boldsymbol{k}+\boldsymbol{G}} = E_n(\boldsymbol{k}+\boldsymbol{G})\psi_{n\boldsymbol{k}}. \tag{2.108}$$

2. Symmetry under operations S of the point group:

$$\{E_n(S\boldsymbol{k}),\, \mathrm{all}\, n\} = \{E_n(\boldsymbol{k}),\, \mathrm{all}\, n\}\,. \tag{2.109}$$

---

[20] This means that each unit cell contributes one independent value of $\boldsymbol{k}$ to each energy band.

3. Spin degeneracy due to 2. and time reversal symmetry:

$$\{E_{n\uparrow}(\boldsymbol{k}),\,\mathrm{all}\,n\} = \{E_{n\downarrow}(\boldsymbol{k}),\,\mathrm{all}\,n\}\,. \tag{2.110}$$

By finally introducing creation and annihilation operators for each band and $\boldsymbol{k}$-value one can formulate the many-particle Hamiltonian in an approximate way in second quantization:

$$H = \sum_{n\boldsymbol{k}} E_n(\boldsymbol{k}) c^{\dagger}_{n\boldsymbol{k}} c_{n\boldsymbol{k}}. \tag{2.111}$$

2.3.4 Almost free electrons

The aim is now to find solutions of the Schrödinger equation

$$\left(-\frac{\hbar^2}{2m_0}\triangle + V_{\mathrm{eff}}(\boldsymbol{r})\right)\psi_{n\boldsymbol{k}} = E_n(\boldsymbol{k})\psi_{n\boldsymbol{k}} \tag{2.112}$$

with the Bloch functions

$$\psi_{n\boldsymbol{k}}(\boldsymbol{r}) = e^{i\boldsymbol{k}\boldsymbol{r}} u_{n\boldsymbol{k}}(\boldsymbol{r}) = \sum_{\boldsymbol{G}} c_{n\boldsymbol{k}-\boldsymbol{G}} e^{i(\boldsymbol{k}-\boldsymbol{G})\cdot\boldsymbol{r}}. \tag{2.113}$$

Inserting Eq. (2.113) in (2.112), multiplying with $e^{i(\boldsymbol{k}+\boldsymbol{G}')\cdot\boldsymbol{r}}$ and integrating over the volume V of the crystal one obtains a set of coupled linear equations for the coefficients $c_{n\boldsymbol{k}-\boldsymbol{G}}$,

$$\sum_{\boldsymbol{G}}\left\{\left(\frac{\hbar^2}{2m_0}(\boldsymbol{k}+\boldsymbol{G})^2 - E\right)\delta_{\boldsymbol{G}\boldsymbol{G}'} + V(\boldsymbol{G}-\boldsymbol{G}')\right\} c_{n\boldsymbol{k}-\boldsymbol{G}} = 0, \tag{2.114}$$

with the Fourier transform of the effective potential

$$V(\boldsymbol{G}-\boldsymbol{G}') = \frac{1}{V}\int V_{\mathrm{eff}}(\boldsymbol{r}) e^{i(\boldsymbol{G}-\boldsymbol{G}')\cdot\boldsymbol{r}}\,\mathrm{d}\boldsymbol{r}. \tag{2.115}$$

A non-trivial solution can be obtained if

$$\left\|\left(\frac{\hbar^2}{2m_0}(\boldsymbol{k}+\boldsymbol{G})^2 - E\right)\delta_{\boldsymbol{G}\boldsymbol{G}'} + V(\boldsymbol{G}-\boldsymbol{G}')\right\| = 0 \tag{2.116}$$

holds. This yields the energy eigenvalues.

The concept derived here can only be employed if the effective potential affects the free electron states as a *small* perturbation, i.e., if the expansion (2.113) converges rapidly and if the Fourier components of the effective potential are small. In this case the kinetic or diagonal terms in (2.116) are the dominating ones. The secular problem (2.116) can then be solved using different pseudopotentials [113–116].

We will take a look at the specific case, in which the dispersion is that of free electrons but with the symmetries of the energies taken into account. Fig. 2.8 shows the dispersion for the one-dimensional solid with the boundaries of the first BZ located at $\pm\pi/a$. Due to the periodicity we can limit ourselves to the first BZ, which leads to the reduced zone scheme[21]. At the boundaries

---

[21] This is in analogy to the limitation in the case of phonons (see Sec. 2.2.2). However, it is important to mention that the limitation to the first BZ in the case of the phonons is due to the impossibility to depict waves of too small wavelengths since ions do not fill the whole crystal. This is not true for the electrons. The limitation for these (quasi-)particles is due to the symmetry of the periodic potential.

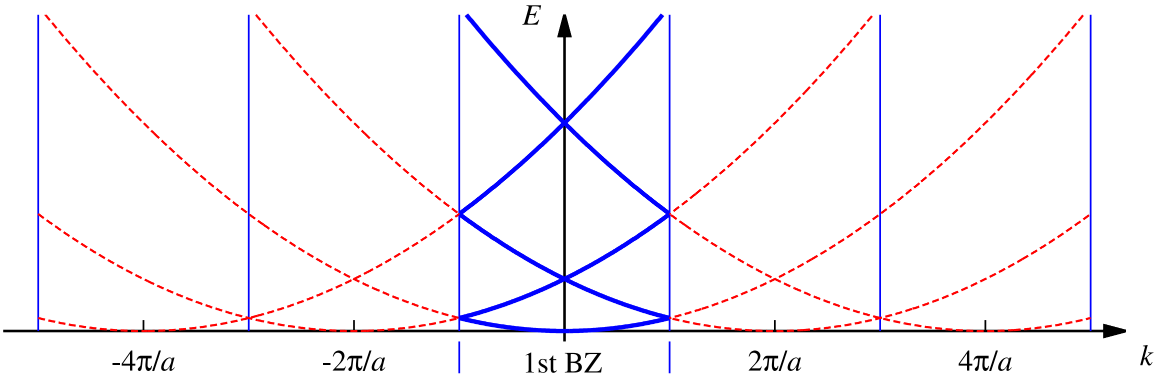

Figure 2.8.: Extended and reduced zone scheme. Adapted from [85].

and in the center of the first BZ degeneracies of the dispersion appear. These degeneracies can be investigated by writing (2.116) for the corresponding states:

$$\left\| \begin{matrix} E(k) - E & V(G) \\ V(G) & E(k-G) - E \end{matrix} \right\| = 0, \quad G = \frac{2\pi}{a}. \tag{2.117}$$

With $k = \pi/a$ and $E(k) = E(k-G) = \hbar^2/2m_0(\pi/a)^2$ one obtains two different solutions,

$$E = \frac{\hbar^2}{2m_0}\left(\frac{\pi}{a}\right)^2 \pm \left|V\left(\frac{2\pi}{a}\right)\right|, \tag{2.118}$$

indicating that the periodic potential removes the degeneracies. At the positions of the former degeneracies band gaps or energy gaps appear (see Fig. 2.9). These energy gaps can be understood when taking a look at the wave functions. At $k = \pm\pi/a$ the Bragg condition for reflection of plane waves is fulfilled (cf. also Sec. 2.1.1) [86]. The initial and reflected waves interfere to form standing waves:

$$\psi(x) \sim \sin\left(\frac{\pi x}{a}\right) \quad \text{and} \quad \psi(x) \sim \cos\left(\frac{\pi x}{a}\right). \tag{2.119}$$

According to these functions the charge density of the electrons is maximal or minimal at the positions of the atoms. Therefore, the energy of the two states is raised or lowered compared to the free electron case, which causes the band gap. Since the group velocity of standing waves is zero, the dispersion relation is horizontal at the border of the BZ.

The electrons are now filled in the different states. If the Fermi sphere exceeds the boundaries of the first BZ it has to be folded back to obtain the reduced zone scheme [85, 86]. Additionally, the Fermi sphere is distorted close to the BZ boundaries due to the formation of band gaps[22]. The electrons within the first BZ fill the lowest energy band completely while the electrons of the back-folded states occupy higher energy bands. If at least one band is only partially filled or if a partial overlap of bands occurs, the system will be characterized as a metal [117]. On the other hand, if the Fermi energy is within the gap, there are only empty or completely filled bands[23] leading to insulators or semiconductors [118]. Semiconductors and insulators are distinguished by the size of the energy gap E_g. If $E_\mathrm{g} \lesssim 4\,\mathrm{eV}$ holds, electrons can be thermally excited at room temperature

---

[22] Different experimental methods to determine the shape of the Fermi surface in real solids can be found, e.g., in [86].

[23] In this case an electrical current flow cannot be evoked by an external electric field since a continuous change of the total momentum of electrons is not possible if all accessible states are occupied [86].

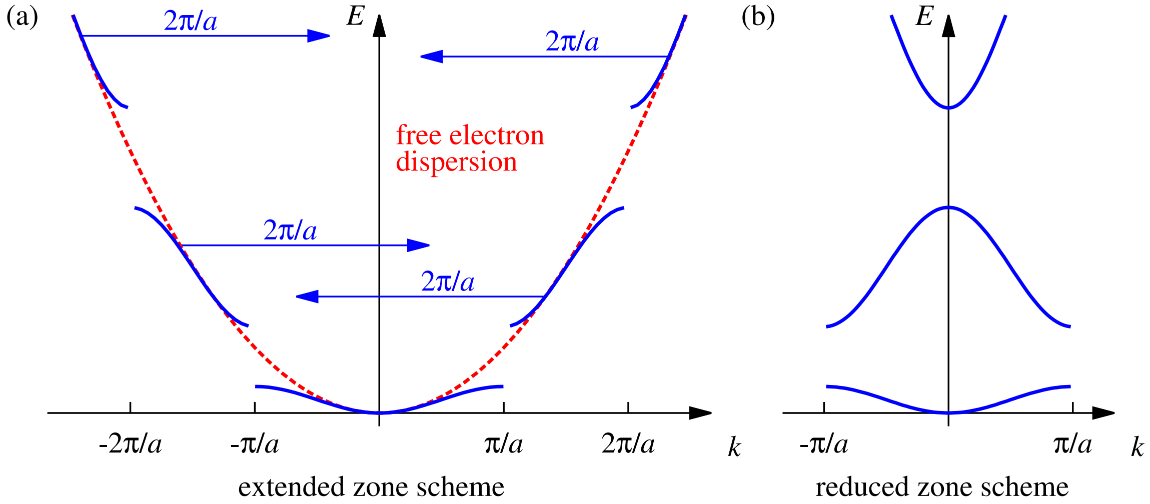

Figure 2.9.: (a) Opening of energy gaps and (b) reduced zone scheme showing the electronic energy bands. Adapted from [12].

and contribute to electrical transport. This is the case for a semiconductor. The band structure of a solid and the electronic density of states can be determined experimentally by, e.g., angular resolved photo-electron spectroscopy (ARPES) [86].

2.3.5 LCAO and tight-binding approximation

A different approach to calculate the electronic band structure is the one of tightly bound electrons, for which the approximation of almost free electrons is not valid. It starts from isolated atoms described by the Schrödinger equation

$$\left(-\frac{\hbar^2}{2m_0}\triangle + v_{\text{at}}(\boldsymbol{r}-\boldsymbol{R}_{\boldsymbol{n}}^0)\right)\phi_\nu(\boldsymbol{r}-\boldsymbol{R}_{\boldsymbol{n}}^0) = E_\nu\phi_\nu(\boldsymbol{r}-\boldsymbol{R}_{\boldsymbol{n}}^0), \tag{2.120}$$

with the atomic potential $v_{\text{at}}(\boldsymbol{r}-\boldsymbol{R}_{\boldsymbol{n}}^0)$ centered at the position $\boldsymbol{R}_{\boldsymbol{n}}^0$ and the index ν denoting a set of atomic quantum numbers. We will use the notation $\phi_{\nu\boldsymbol{R}_{\boldsymbol{n}}^0}(\boldsymbol{r}) = \phi_\nu(\boldsymbol{r}-\boldsymbol{R}_{\boldsymbol{n}}^0)$ according to Ref. [7] in the following. The effective potential of the solid can then be expressed as a superposition of the atomic potentials:

$$V_{\text{eff}}(\boldsymbol{r}) = \sum_{\boldsymbol{n}} v_{\text{at}}(\boldsymbol{r}-\boldsymbol{R}_{\boldsymbol{n}}^0). \tag{2.121}$$

The atomic orbitals overlap and form Bloch functions

$$\psi_{\nu\boldsymbol{k}}(\boldsymbol{r}) = \frac{1}{\sqrt{N}}\sum_{\boldsymbol{n}} e^{i\boldsymbol{k}\cdot\boldsymbol{R}_{\boldsymbol{n}}^0}\phi_{\nu\boldsymbol{R}_{\boldsymbol{n}}^0}(\boldsymbol{r}), \tag{2.122}$$

which are a complete basis set. Hence, they can be used for expansions

$$\psi_{n\boldsymbol{k}}(\boldsymbol{r}) = \sum_\nu C_{n\nu}\psi_{\nu\boldsymbol{k}}(\boldsymbol{r}). \tag{2.123}$$

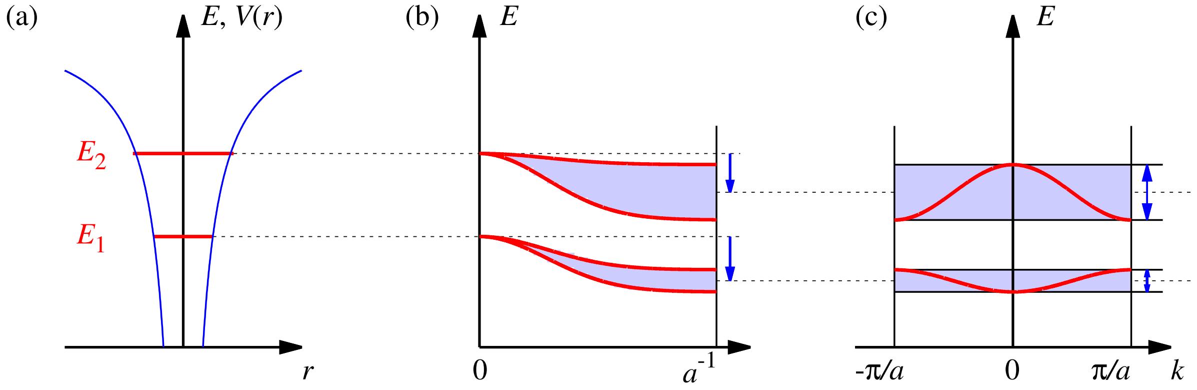

Figure 2.10.: Due to the interaction between different atoms in the solid the discrete atomic levels (a) are energetically lowered and a splitting occurs (b) in dependence on the interatomic distance a. The final dispersion is shown in (c). Adapted from [86].

This shows that the wave functions of the solid can be written as linear combinations of atomic orbitals (LCAO). The calculation of the coefficients $C_{n\nu}$ leads to a secular problem [85], which will not be treated here.

The result is shown in Fig. 2.10: Due to the interation between the atoms a splitting of the atomic levels occurs. At last there are as many states as there are different atoms in the solid. This can be compared to the coupling between two classical oscillators, which results in two close-lying eigenfrequencies. According to the large number of atoms ($\sim 10^{23}$) the spacing between the levels is so small that one can assume continuous energy bands. Due to the lower energy of the electrons in the combined potential of the atom to which they originally belonged and the neighboring atoms, the energy bands are lowered with respect to the position of the former atomic energy levels. The magnitude of the splitting of the energy levels depends on the number of nearest neighbors, i.e., on the crystal structure, and on the overlap of the atomic potentials [86]. Since the overlap is smaller for energetically lower atomic states, their splitting is likewise smaller. The appearance of band gaps can be understood from this model simply as a result of a too small splitting of (lower) energy levels. At higher energies it is possible that overlaps between different bands occur.

2.3.6 Ground state energy and Wannier functions

Provided that we know the Bloch functions $\psi_{n\boldsymbol{k}}$ by solving Eq. (2.112) or the functions $\phi_{\nu\boldsymbol{R}_{\boldsymbol{n}}^0}$ by solving Eq. (2.120), we can write the ground state of N electrons (including spin) as

$$\Phi_0 = \mathcal{A}\psi_{n\boldsymbol{k}_1\alpha}(\boldsymbol{r}_1)\psi_{n\boldsymbol{k}_1\beta}(\boldsymbol{r}_2)\psi_{n\boldsymbol{k}_2\alpha}(\boldsymbol{r}_3)\ldots\psi_{n\boldsymbol{k}_{N/2}\beta}(\boldsymbol{r}_N), \tag{2.124a}$$

$$\Phi_0 = \mathcal{A}\phi_{\nu\boldsymbol{R}_{\boldsymbol{n}_1}^0\alpha}(\boldsymbol{r}_1)\phi_{\nu\boldsymbol{R}_{\boldsymbol{n}_1}^0\beta}(\boldsymbol{r}_2)\phi_{\nu\boldsymbol{R}_{\boldsymbol{n}_2}^0\alpha}(\boldsymbol{r}_3)\ldots\phi_{\nu\boldsymbol{R}_{\boldsymbol{n}_{N/2}}^0\beta}(\boldsymbol{r}_N), \tag{2.124b}$$

with spin quantum numbers α, β and $\mathcal{A}$ denoting the antisymmetric mapping. These two states can be seen as approximations to a similar ansatz with Hartree-Fock functions. The ground-state energy (in first order) of the Hamiltonian (2.103) is then given by[24] $E_0^{(1)} = \langle\Phi_0\,|H|\,\Phi_0\rangle$. It is also possible to create an ansatz using the Bloch functions of Eq. (2.122) instead of $\phi_{\nu\boldsymbol{R}_{\boldsymbol{n}}^0\alpha}$ and it can be proven that the resulting ansatz is mathematically identical to the one of Eq. (2.124b) [7].

---

[24] The complete expressions for $E_0^{(1)}$ can be found in [7].

Even though the different assumptions are at the base of the method of almost free electrons or the tight-binding approximation, one can always describe the ground state of the solid via Bloch functions, which comprise both approaches: the almost free electrons are described by the plane wave part and via the lattice periodic part $u_{n\boldsymbol{k}}$ the wave functions of the isolated atoms are remembered.

However, the assumptions of the tight-binding model are often not appropriate and a description of the bands using Eq. (2.122) is inaccurate [7]. Contrariwise, it is often desirable to work with spatially localized functions comparable to the $\phi_{\nu\boldsymbol{R}_{\boldsymbol{n}}^0}$. A possible resort are the Wannier functions $a_{n\boldsymbol{R}_{\boldsymbol{n}}^0}$: If it is possible to obtain Bloch functions $\psi_{n\boldsymbol{k}}$ by a precise method, the Wannier functions are defined likewise to the inverse of Eq. (2.122) as wave packets, i.e., as a superposition of Bloch waves [5, 7]

$$a_{n\boldsymbol{R}_{\boldsymbol{n}}^0}(\boldsymbol{r}) = \frac{1}{\sqrt{N}} \sum_{\boldsymbol{k}} e^{-i\boldsymbol{k}\cdot\boldsymbol{R}_{\boldsymbol{n}}^0} \psi_{n\boldsymbol{k}}(\boldsymbol{r}) \,. \tag{2.125}$$

Due to the remarks given above, it is evident that the ground state of the solid can also be written in terms of Wannier functions:

$$\Phi_0 = \mathcal{A} a_{\nu\boldsymbol{R}_{\boldsymbol{n}_1}^0}\alpha(\boldsymbol{r}_1) a_{\nu\boldsymbol{R}_{\boldsymbol{n}_1}^0}\beta(\boldsymbol{r}_2) a_{\nu\boldsymbol{R}_{\boldsymbol{n}_2}^0}\alpha(\boldsymbol{r}_3) \ldots a_{\nu\boldsymbol{R}_{\boldsymbol{n}_{N/2}}^0}\beta(\boldsymbol{r}_N). \tag{2.126}$$

However, one has to stress that Wannier functions are generally not atomic functions $\phi_{\nu\boldsymbol{R}_{\boldsymbol{n}}^0}$ [7].

2.3.7 Effective-mass approximation

In this section we derive the effective-mass approximation for semiconductors. Semiconductors behave like insulators at very low temperatures since the electrons in completely filled energy bands (valence bands, VB) cannot react to external electric fields. Raising the temperature, the Fermi distribution function (2.98) smeares out and some of the states in the previously empty conduction bands (CB) are populated by electrons. In a description of the electronic system it is common to treat the occuring empty VB states as quasi-particles instead of treating the much larger number of remaining electrons. These new quasi-particles with positive charge are called holes [86] and their properties are listed in Table 2.1. Instead of thermal excitation it is also possible to create free electrons in the CB by doping or via optical excitation with photon energies $\hbar\omega \geq E_\mathrm{g}$. The electrons in the CB and the holes in the VB then determine the electric properties of the semiconductor. Due to the small number of excited electrons, only states at the minimum of the lowest CB and at the maximum of the uppermost VB are occupied by electrons and holes.

According to the relative position of VB maximum and CB minimum one distinguishes between direct and indirect semiconductors. In the first case, the extrema are located at the same position (normally the center) of the first BZ and electrons can be excited directly form the VB to the CB by the absorption of a photon[25] with $\hbar\omega \geq E_\mathrm{g}$ (direct process). In the latter case, the positions differ. In indirect semiconductors like Ge or Si the VB maximum is normally located at the center of the BZ – the so-called Γ-point – while the CB minimum is located along one of the high symmetry lines of the BZ. An excitation of electrons simply by optical absorption is not possible since the wave vector of the photon is too small in comparison to the extension of the BZ (cf. Sec. 2.4.1). The excitation is rendered possible only with the additional contribution of a phonon, by which momentum conservation is satisfied (indirect process). The probability of an excitation is smaller in this situation due to the required additional coupling to a phonon [86].

---

[25] The absorption of a photon with $\hbar\omega = E_\mathrm{g}$ is called fundamental absorption [86].

Table 2.1.: Comparison of the properties of a hole with those of the removed electron [12, 86]. The negative sign of the energy dispersion means that the energy of a hole increases when it is moved to deeper lying states in the VB.

Property	Hole	Removed electron
wave vector	$\boldsymbol{k}_\mathrm{h}$	$= -\boldsymbol{k}_\mathrm{e}$
energy dispersion	$E_\mathrm{h}(\boldsymbol{k}_\mathrm{h})$	$= -E_\mathrm{e}(\boldsymbol{k}_\mathrm{e})$
group velocity	$\boldsymbol{v}_\mathrm{h}(\boldsymbol{k}_\mathrm{h})$	$= \boldsymbol{v}_\mathrm{e}(\boldsymbol{k}_\mathrm{e})$
effective mass	m_h	$= -m_\mathrm{e} > 0$
electric charge	q_h	$= -q_\mathrm{e}$
spin	σ_h	$= -\sigma_\mathrm{e}$

Effective-mass tensor

When describing the motion of a hole or an electron in an external field, one generally uses wave packets, i.e., Wannier functions, instead of infinitely extended Bloch waves [12]. The $\boldsymbol{k}$-vector is reasonably well-definded if the wave function extends over more than one unit cell since the uncertainity of $\boldsymbol{k}$ in reciprocal space is then much smaller than the extension of the first BZ. On the other hand, the wave packet will react to an external field as a compact particle if the wave length of the external field is much larger than the extension of the wave packet [86]. The energy of a wave packet under the influence of an external force changes according to

$$\frac{\mathrm{d}E(\boldsymbol{k})}{\mathrm{d}t} = \boldsymbol{F} \cdot \boldsymbol{v}_\mathrm{g} \tag{2.127}$$

with the group velocity

$$\boldsymbol{v}_\mathrm{g} = \frac{1}{\hbar}\nabla_{\boldsymbol{k}} E(\boldsymbol{k}). \tag{2.128}$$

Combining Eqs. (2.127) and (2.128) yields Newton's equation of motion for quasi-momenta $\hbar\boldsymbol{k}$:

$$\hbar\frac{\mathrm{d}\boldsymbol{k}}{\mathrm{d}t} = \boldsymbol{F}. \tag{2.129}$$

The wave packet is accelerated with an acceleration of

$$a_i = \frac{\mathrm{d}v_{\mathrm{g},i}}{\mathrm{d}t} = \frac{1}{\hbar}\frac{\mathrm{d}}{\mathrm{d}t}\left[\nabla_{\boldsymbol{k}} E(\boldsymbol{k})\right]_i = \frac{1}{\hbar}\sum_j \frac{\partial^2 E(\boldsymbol{k})}{\partial k_i \partial k_j}\frac{\mathrm{d}k_j}{\mathrm{d}t} = \frac{1}{\hbar^2}\sum_j \frac{\partial^2 E(\boldsymbol{k})}{\partial k_i \partial k_j} F_j. \tag{2.130}$$

By comparison of Eq. (2.130) with the trivial case $\boldsymbol{F} = m\boldsymbol{a}$ the effective mass tensor m^* with

$$\left(\frac{1}{m^*}\right)_{ij} = \frac{1}{\hbar^2}\frac{\partial^2 E(\boldsymbol{k})}{\partial k_i \partial k_j} \tag{2.131}$$

is obtained, which describes the reaction of a quasi-particle to an external field. If the energy band is parabolic in the vicinity of a given wave vector $\boldsymbol{k}_0$, the effective mass will be constant and isotropic. The effective mass takes into account the effective interaction with other electrons in the single-particle approximation and can be determined experimentally using, e.g., cyclotron resonance spectroscopy [86]. Owing to its relation to the band curvature (2.131), the following scheme can be deduced[26] [12]:

---

[26] Compare Sec. 2.3.5.

High effective mass ⟷ small band curvature ⟷ small band width

⟷ weak coupling between neighboring atoms and vice versa.

Finally, we can state that the effective masses of quasi-particles in semiconductors with a wide band gap tend to be larger since the bands are smaller in this case.

$\boldsymbol{k}\cdot\boldsymbol{p}$–perturbation theory

Since the main properties of semiconductors[27] are determined by the band structure in the vicinity of the extrema of the bands, we will now outline a method describing the energy dispersion around a given point $\boldsymbol{k}_0$ [85, 120–123]. It is based on an expansion around $\boldsymbol{k}_0$, usually under the constraint $|\boldsymbol{k}-\boldsymbol{k}_0| \ll 2\pi/a$.

We assume that the Schrödinger equation has been solved for $\boldsymbol{k}_0$:

$$H\psi_{n\boldsymbol{k}_0}(\boldsymbol{r}) = E_n(\boldsymbol{k}_0)\psi_{n\boldsymbol{k}_0}(\boldsymbol{r}). \tag{2.132}$$

With the Bloch function

$$\psi_{n\boldsymbol{k}}(\boldsymbol{r}) = e^{i(\boldsymbol{k}-\boldsymbol{k}_0)\cdot\boldsymbol{r}} e^{i\boldsymbol{k}_0\cdot\boldsymbol{r}} u_{n\boldsymbol{k}}(\boldsymbol{r}) \tag{2.133}$$

the Schrödinger equation for an arbitrary $\boldsymbol{k}$-vector reads

$$\left[-\frac{\hbar^2}{2m_0}\triangle + V_{\mathrm{eff}}(\boldsymbol{r}) + \frac{\hbar^2}{2m_0}(\boldsymbol{k}-\boldsymbol{k}_0)^2 + \frac{\hbar}{m_0}(\boldsymbol{k}-\boldsymbol{k}_0)\cdot\boldsymbol{p}\right] e^{i\boldsymbol{k}_0\cdot\boldsymbol{r}} u_{n\boldsymbol{k}}(\boldsymbol{r}) = E_n(\boldsymbol{k}) e^{i\boldsymbol{k}_0\cdot\boldsymbol{r}} u_{n\boldsymbol{k}}(\boldsymbol{r}). \tag{2.134}$$

The functions $u_{n\boldsymbol{k}_0}(\boldsymbol{r})$ ($\boldsymbol{k}_0$ fixed, all n) form a complete set of lattice periodic functions, which can be used to write

$$u_{n\boldsymbol{k}}(\boldsymbol{r}) = \sum_{n'} c_{nn'}(\boldsymbol{k}-\boldsymbol{k}_0) u_{n'\boldsymbol{k}_0}(\boldsymbol{r}). \tag{2.135}$$

Inserting this expansion in Eq. (2.134) and writing $E = E_n(\boldsymbol{k})$, one obtains

$$\sum_{n'} c_{nn'}(\boldsymbol{k}-\boldsymbol{k}_0)\left\{E_{n'}(\boldsymbol{k}_0) + \frac{\hbar^2}{2m_0}(\boldsymbol{k}-\boldsymbol{k}_0)^2 - E + \frac{\hbar}{m_0}(\boldsymbol{k}-\boldsymbol{k}_0)\cdot\boldsymbol{p}\right\} e^{i\boldsymbol{k}_0\cdot\boldsymbol{r}} u_{n'\boldsymbol{k}_0}(\boldsymbol{r}) = 0, \tag{2.136}$$

leading to set of coupled equations after a multiplication from the left with $\psi^*_{n\boldsymbol{k}_0}(\boldsymbol{r})$ and an integration over V:

$$\sum_{n'} c_{nn'}(\boldsymbol{k}-\boldsymbol{k}_0)\left\{\left(E_{n'}(\boldsymbol{k}_0) + \frac{\hbar^2}{2m_0}(\boldsymbol{k}-\boldsymbol{k}_0)^2 - E\right)\delta_{nn'} + \frac{\hbar}{m_0}(\boldsymbol{k}-\boldsymbol{k}_0)\cdot\boldsymbol{p}_{nn'}(\boldsymbol{k}_0)\right\} = 0. \tag{2.137}$$

The derived concept is called $\boldsymbol{k}\cdot\boldsymbol{p}$–perturbation theory because the term $\hbar(\boldsymbol{k}-\boldsymbol{k}_0)\cdot\boldsymbol{p}/m_0$ is treated as a perturbation. Via the matrix elements

$$\boldsymbol{p}_{nn'}(\boldsymbol{k}_0) = \int u^*_{n\boldsymbol{k}_0}(\boldsymbol{r})\boldsymbol{p}u_{n'\boldsymbol{k}_0}(\boldsymbol{r})\,\mathrm{d}^3\boldsymbol{r} \tag{2.138}$$

a coupling between different bands is established. The dispersion relations $E_n(\boldsymbol{k})$ are finally obtained as the solutions of the secular problem

$$\left\|\left(E_{n'}(\boldsymbol{k}_0) + \frac{\hbar^2}{2m_0}(\boldsymbol{k}-\boldsymbol{k}_0)^2 - E\right)\delta_{nn'} + \frac{\hbar}{m_0}(\boldsymbol{k}-\boldsymbol{k}_0)\cdot\boldsymbol{p}_{nn'}(\boldsymbol{k}_0)\right\| = 0. \tag{2.139}$$

The solutions of this problem will be given in the following for the normal cases of semiconductors with a CB minimum resulting from s anti-bonding orbitals and a VB-maximum resulting from p bonding orbitals.

---

[27] An according treatment for metals can be found in Refs. [119].

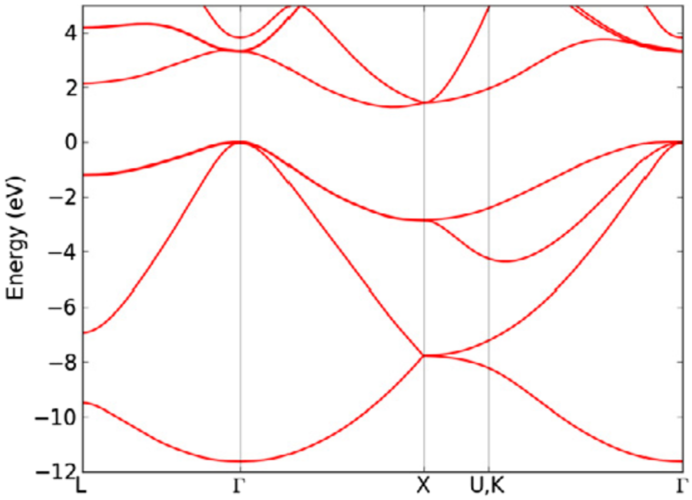

Figure 2.11.: Band structure of Silicon. The energy of the VB-maximum at the Γ-point is chosen to be zero. The CB-minimum can be found along the Γ-X-line, i.e., the Δ-axis. The energy gap amounts to $E_\mathrm{g} = 1.27\,\mathrm{eV}$. Taken from [124].

Conduction band minimum at $\boldsymbol{k}_0 = \boldsymbol{0}$ For the case of a CB minimum at $\boldsymbol{k}_0 = \boldsymbol{0}$, which normally occurs in direct semiconductors, one obtains the second order perturbation expression

$$E_c(\boldsymbol{k}) = E_c(\boldsymbol{0}) + \frac{\hbar^2 \boldsymbol{k}^2}{2m_0}\left(1 + \frac{2}{m_0}\sum_{n'(p)} \frac{|\langle S\,|p_x|\,X_{n'}\rangle|^2}{E_c(\boldsymbol{0}) - E_{n'}(\boldsymbol{0})}\right), \tag{2.140}$$

where $|S\rangle$ denotes the s anti-bonding state of the CB with $n = c$ and $|X_{n'}\rangle$ denotes the p bonding states with band indices n'. Using Eq. (2.131) we can deduce from Eq. (2.140) the effective mass m^*:

$$\frac{1}{m^*} = \frac{1}{m_0} + \frac{2}{m_0^2}\sum_{n'(p)} \frac{|\langle S\,|p_x|\,X_{n'}\rangle|^2}{E_c(\boldsymbol{0}) - E_{n'}(\boldsymbol{0})}. \tag{2.141}$$

From the denominator of Eq. (2.141) we conclude that the effective mass becomes smaller with a decreasing band gap, as it was already stated above. If higher order terms are taken into account, the anisotropy and flattening of the band becomes noticeable and the effective mass shows anisotropy as well as an energy dependence.

Conduction band minimum at $\boldsymbol{k}_0 = k_0\hat{\boldsymbol{e}}_z;\ k_0 \neq 0$ This case normally occurs in indirect semiconductors like, e.g., silicon. In Si the CB minimum is located on the Γ-X-axis (or Δ-axis; see Fig. 2.11). The reduced symmetry of the problem leads to an anisotropy of the reduced mass and to the dispersion relation

$$E_c(\boldsymbol{k}) = E_c(\boldsymbol{0}) + \frac{\hbar^2}{2}\left(\frac{k_x^2 + k_y^2}{m_\perp^*} + \frac{(k_z - k_0)^2}{m_\parallel^*}\right), \tag{2.142}$$

in which $m_\perp^*$ and $m_\parallel^*$ denote the effective masses perpendicular and parallel to the Δ-axis. Since the BZ of Si has cubic symmetry, there are altogether six CB minima, which are equally populated.

Valence band maximum at $\boldsymbol{k}_0 = \mathbf{0}$ In semiconductors with zincblende-type or diamond-type structure the VB-maximum is threefold degenerate (neglecting spin) and derives from p bonding orbitals. Due to spin-orbit coupling[28] this VB splits into a deeper lying band and a two-fold degenerate band at $\boldsymbol{k} = \mathbf{0}$, which furthermore splits into two bands of different curvature for $\boldsymbol{k} \neq \mathbf{0}$. In the case of large spin-orbit coupling, the lower lying band can be neglected in the calculation and one obtains

$$E_{v\pm}(\boldsymbol{k}) = E_v(\mathbf{0}) + \frac{\hbar^2}{2m_0}\left[\gamma_1 \boldsymbol{k}^2 \pm 2\sqrt{\gamma_2(k_x^4 + k_y^4 + k_z^4) + 3(\gamma_3^2 - \gamma_2^2)(k_x^2 k_y^2 + k_x^2 k_z^2 + k_y^2 k_z^2)}\,\right] \tag{2.143}$$

with the so-called Luttinger parameters γ_i [126]. The parameter γ_1 is the inverse of the average effective mass, whereas γ_2 and γ_3 describe the splitting of the band and a warping[29] of the surface of constant energy via the term $3(\gamma_3^2 - \gamma_2^2)$. The two bands resulting from the splitting are called light-hole (lh) and heavy-hole (hh) band and the according effective masses read in the case of negligible warping

$$m^*_{\mathrm{lh}} = \frac{m_0}{\gamma_1 - 2\gamma_2}, \quad m^*_{\mathrm{hh}} = \frac{m_0}{\gamma_1 + 2\gamma_2}. \tag{2.144}$$

2.3.8 Excited electronic states

After the introduction of holes as new quasi-particles in the previous section 2.3.7, we will now present the rigorous treatment of excited states following the descriptions of Ref. [7]. To begin with, we assume one electron with momentum $\hbar\boldsymbol{k}_{\mathrm{e}}$ and spin τ to be in a Bloch state of the conduction band and $N-1$ electrons to be in Bloch states of the valence bands. A justification for this assumption is given in [7]. We denote the excited states in zero-order perturbation theory by

$$|vc\,\boldsymbol{k}_{\mathrm{h}}\boldsymbol{k}_{\mathrm{e}}\rangle \equiv \Phi^{\sigma\tau}_{vc}(\boldsymbol{k}_{\mathrm{h}},\,\boldsymbol{k}_{\mathrm{e}}) = \mathcal{A}\psi_{v\boldsymbol{k}_1\alpha}\psi_{v\boldsymbol{k}_1\beta}\ldots\psi_{v\boldsymbol{k}_{\mathrm{h}}\sigma}\psi_{c\boldsymbol{k}_{\mathrm{e}}\tau}\ldots\psi_{v\boldsymbol{k}_{N/2}\beta} \tag{2.145}$$

and remark that the valence band state with momentum $\hbar\boldsymbol{k}_{\mathrm{h}}$ and spin $-\sigma$ is unoccupied. The total momentum $\hbar\boldsymbol{K} = \hbar\boldsymbol{k}_{\mathrm{e}} - \hbar\boldsymbol{k}_{\mathrm{h}}$ determines the behavior of the state under translational symmetry operations. In the simple case with the Schrödinger equation (2.112), the energy difference between the excited state and the ground state would be simply $E_c(\boldsymbol{k}_{\mathrm{e}}) - E_v(\boldsymbol{k}_{\mathrm{h}})$. On the other hand, it is also possible to take the Hamiltonian of Eq. (2.103) to obtain a better value for the energy:

$$\begin{aligned}\left\langle vc\,\boldsymbol{k}_{\mathrm{h}}\boldsymbol{k}_{\mathrm{e}}\left|H\right|vc\,\boldsymbol{k}'_{\mathrm{h}}\boldsymbol{k}'_{\mathrm{e}}\right\rangle &= \delta_{\sigma\sigma'}\delta_{\tau\tau'}\delta_{\boldsymbol{k}_{\mathrm{h}},\boldsymbol{k}'_{\mathrm{h}}}\delta_{\boldsymbol{k}_{\mathrm{e}},\boldsymbol{k}'_{\mathrm{e}}}\left[E_0^{(1)} + W_c(\boldsymbol{k}_{\mathrm{e}}) - W_v(\boldsymbol{k}_{\mathrm{h}})\right] \\ &+ \delta_{\boldsymbol{k}_{\mathrm{e}}-\boldsymbol{k}_{\mathrm{h}},\boldsymbol{k}'_{\mathrm{e}}-\boldsymbol{k}'_{\mathrm{h}}}\left[-\delta_{\sigma\sigma'}\delta_{\tau\tau'}\left\langle c\boldsymbol{k}_{\mathrm{e}}v\boldsymbol{k}'_{\mathrm{h}}\left|V_{\mathrm{C}}\right|c\boldsymbol{k}'_{\mathrm{e}}v\boldsymbol{k}_{\mathrm{h}}\right\rangle\right. \\ &\left.+\delta_{\sigma\tau}\delta_{\sigma'\tau'}\left\langle c\boldsymbol{k}_{\mathrm{e}}v\boldsymbol{k}'_{\mathrm{h}}\left|V_{\mathrm{C}}\right|v\boldsymbol{k}_{\mathrm{h}}c\boldsymbol{k}'_{\mathrm{e}}\right\rangle\right].\end{aligned} \tag{2.146}$$

This expression contains the ground-state energy $E_0^{(1)}$, the energy $W_c(\boldsymbol{k})$ of one electron in the conduction band interacting via exchange and Coulomb interaction with the electrons in the valence band

$$W_c(\boldsymbol{k}) = E_c(\boldsymbol{k}) + \langle c\boldsymbol{k}\left|V - V_{\mathrm{eff}}\right|c\boldsymbol{k}\rangle + \sum_{\boldsymbol{k}}\left[2\left\langle c\boldsymbol{k}v\boldsymbol{k}'\left|V_{\mathrm{C}}\right|c\boldsymbol{k}v\boldsymbol{k}'\right\rangle - \left\langle c\boldsymbol{k}v\boldsymbol{k}'\left|V_{\mathrm{C}}\right|v\boldsymbol{k}'c\boldsymbol{k}\right\rangle\right], \tag{2.147}$$

---

[28] The spin-orbit coupling arises when treating the electrons in the solid in a relativistic way using the Dirac equation [10, 125].

[29] This means that the curvature of the bands depend on the direction of $\boldsymbol{k}$.

the according energy $W_v(\boldsymbol{k})$ of one electron in the valence band

$$W_v(\boldsymbol{k}) \;=\; E_v(\boldsymbol{k}) + \langle v\boldsymbol{k}\,|V - V_{\mathrm{eff}}|\,v\boldsymbol{k}\rangle + \sum_{\boldsymbol{k}'}\left[2\left\langle v\boldsymbol{k}v\boldsymbol{k}'\,|V_{\mathrm{C}}|\,v\boldsymbol{k}v\boldsymbol{k}'\right\rangle - \left\langle v\boldsymbol{k}v\boldsymbol{k}'\,|V_{\mathrm{C}}|\,v\boldsymbol{k}'v\boldsymbol{k}\right\rangle\right], \quad (2.148)$$

the Coulomb potential $V_{\mathrm{C}} = e^2/(4\pi\varepsilon_0\,|\boldsymbol{r}_1 - \boldsymbol{r}_2|)$, and the definition

$$\left\langle v\boldsymbol{k}c\boldsymbol{k}'\,|V_{\mathrm{C}}|\,v\boldsymbol{k}''c\boldsymbol{k}'''\right\rangle = \int \mathrm{d}\boldsymbol{r}_1 \int \mathrm{d}\boldsymbol{r}_2\;\; \psi^*_{v\boldsymbol{k}}(\boldsymbol{r}_1)\psi^*_{c\boldsymbol{k}'}(\boldsymbol{r}_2)V_{\mathrm{C}}\psi_{v\boldsymbol{k}''}(\boldsymbol{r}_1)\psi_{c\boldsymbol{k}'''}(\boldsymbol{r}_2). \quad (2.149)$$

One can identify the first term of Eq. (2.146) as being the approximative energy of the excited state. The second and the third term are further corrections to the first term and describe (for $\boldsymbol{k}_{\mathrm{h}} = \boldsymbol{k}'_{\mathrm{h}}$ and $\boldsymbol{k}_{\mathrm{e}} = \boldsymbol{k}'_{\mathrm{e}}$) the Coulomb and exchange interaction between hole and electron, respectively. Note that the exchange interaction includes the term $\delta_{\sigma\tau}\delta_{\sigma'\tau'}$. One could also introduce the total spin $S = \tau - \sigma$ considering that the hole describes a removed electron and that its spin is $-\sigma$. The singlet and triplet states of the form $|S, M\rangle$ are then given by [127]

$$|1,1\rangle \;=\; -\,|\uparrow\downarrow\rangle\,, \quad (2.150a)$$
$$|1,0\rangle \;=\; (|\uparrow\uparrow\rangle - |\downarrow\downarrow\rangle)/\sqrt{2}, \quad (2.150b)$$
$$|1,-1\rangle \;=\; |\downarrow\uparrow\rangle\,, \quad (2.150c)$$
$$|0,0\rangle \;=\; (|\uparrow\uparrow\rangle + |\downarrow\downarrow\rangle)/\sqrt{2}. \quad (2.150d)$$

Using these states, the term $\delta_{\sigma\tau}\delta_{\sigma'\tau'}$ takes the form $2\delta_{S,0}$ [7, 127].

Since we have already pointed out that a description of electrons and holes generally includes Wannier functions, we will now treat a different ansatz instead of diagonlizing H and finding the excited states in the above representation within first order perturbation theory. The ansatz[30]

$$|vc\,\boldsymbol{R}_i\boldsymbol{R}_j\rangle \equiv \Phi^{\sigma\tau}_{vc}(\boldsymbol{R}_i,\,\boldsymbol{R}_j) = \mathcal{A}a_{v\boldsymbol{R}_1\alpha}a_{v\boldsymbol{R}_1\beta}\ldots a_{v\boldsymbol{R}_i\sigma}a_{c\boldsymbol{R}_j\tau}\ldots a_{v\boldsymbol{R}_{N/2}\beta} \quad (2.151)$$

for the excited state is not identical to Eq. (2.145), but

$$\Phi^{\sigma\tau}_{vc}(\boldsymbol{k}_{\mathrm{h}},\,\boldsymbol{k}_{\mathrm{e}}) = \frac{1}{N}\sum_{i,j} e^{i(\boldsymbol{k}_{\mathrm{e}}\,\cdot\,\boldsymbol{R}_j - \boldsymbol{k}_{\mathrm{h}}\,\cdot\,\boldsymbol{R}_i)}\Phi^{\sigma\tau}_{vc}(\boldsymbol{R}_i,\,\boldsymbol{R}_j) \quad (2.152)$$

holds. The expression $\langle vc\,\boldsymbol{R}_i\boldsymbol{R}_j|H|vc\,\boldsymbol{R}'_i\boldsymbol{R}'_j\rangle$ is by far more complicated than that of Eq. (2.146). With $\boldsymbol{R}_j = \boldsymbol{R}_i + \boldsymbol{\beta}$ and $\boldsymbol{R}'_j = \boldsymbol{R}'_i + \boldsymbol{\beta}'$ one can, however, make use of the translational symmetry to find that this expression depends only on $\boldsymbol{R}'_i - \boldsymbol{R}_i$, $\boldsymbol{\beta}$, and $\boldsymbol{\beta}'$:

$$\left\langle vc\,\boldsymbol{R}_i\boldsymbol{R}_j\,|H|\,vc\,\boldsymbol{R}'_i\boldsymbol{R}'_j\right\rangle = f(\boldsymbol{R}'_i - \boldsymbol{R}_j,\,\boldsymbol{\beta},\,\boldsymbol{\beta}'). \quad (2.153)$$

We see that neither the first attempt with Bloch functions nor the second attempt with Wannier functions is suitable to obtain a useful Hamiltonian matrix [7]. A useful ansatz for the true excited state should explicitly contain the total momentum $\hbar\boldsymbol{K}$ of the hole-electron pair *and* the resulting matrix elements should then explicitly depend on the hole-electron separation[31] $\boldsymbol{\beta}$. Both demands are satisfied by the so-called "exciton representation" of Wannier:

$$\Phi^{\sigma\tau}_{vc}(\boldsymbol{K},\,\boldsymbol{\beta}) \;=\; \frac{1}{\sqrt{N}}\sum_{\boldsymbol{k}} e^{-i\boldsymbol{k}\,\cdot\,\boldsymbol{\beta}}\Phi^{\sigma\tau}_{vc}(\boldsymbol{k} - \boldsymbol{K},\,\boldsymbol{k}) \quad (2.154a)$$
$$\;=\; \frac{1}{\sqrt{N}}\sum_{j} e^{i\boldsymbol{K}\,\cdot\,\boldsymbol{R}_j}\Phi^{\sigma\tau}_{vc}(\boldsymbol{R}_j,\,\boldsymbol{R}_j + \boldsymbol{\beta}). \quad (2.154b)$$

---

[30] In this section we will use $\boldsymbol{R}_i$ instead of $\boldsymbol{R}^0_{\boldsymbol{n}_i}$ for reasons of simplicity.

[31] Note that $\boldsymbol{\beta}$ can take – similar to $\boldsymbol{R}_j$ – only discrete values.

The summand in the last expression (2.154b) can be understood as the wave function of an electron located at $\boldsymbol{R}_j + \boldsymbol{\beta}$ and a hole located at $\boldsymbol{R}_j$. The total momentum $\hbar\boldsymbol{K}$ describes the motion of the two particles. Considering that $\boldsymbol{K}$ is a good quantum number, the matrix element now reads

$$\begin{aligned}\left\langle vc\boldsymbol{K}\boldsymbol{\beta}\left|H\right|vc\boldsymbol{K}\boldsymbol{\beta}'\right\rangle &= \delta_{\sigma\sigma'}\delta_{\tau\tau'}\left[\delta_{\boldsymbol{\beta},\boldsymbol{\beta}'}E_0^{(1)} + W(c\boldsymbol{\beta},\, c\boldsymbol{\beta}') - e^{i\boldsymbol{K}\cdot(\boldsymbol{\beta}-\boldsymbol{\beta}')}W(v\boldsymbol{0}, v\boldsymbol{\beta}-\boldsymbol{\beta}')\right] \\ &\quad + \sum_{\boldsymbol{R}_j} e^{i\boldsymbol{K}\cdot\boldsymbol{R}_j}\left[-\delta_{\sigma\sigma'}\delta_{\tau\tau'}\left\langle c\boldsymbol{\beta}v\boldsymbol{R}_j\left|V_\mathrm{C}\right|c\boldsymbol{R}_j+\boldsymbol{\beta}'v\boldsymbol{0}\right\rangle\right. \\ &\quad \left. +\delta_{\sigma\tau}\delta_{\sigma'\tau'}\left\langle c\boldsymbol{\beta}v\boldsymbol{R}_j\left|V_\mathrm{C}\right|v\boldsymbol{0}c\boldsymbol{R}_j+\boldsymbol{\beta}'\right\rangle\right] \end{aligned} \tag{2.155}$$

with the arbitrarily chosen origin $\boldsymbol{R} = \boldsymbol{0}$. The second and third term describe how the hole and the electron contribute to the energy of the excited state. They can be expressed using the functions of Eqs. (2.147) and (2.148):

$$\begin{aligned} & W(c\boldsymbol{\beta},\, c\boldsymbol{\beta}') - e^{i\boldsymbol{K}\cdot(\boldsymbol{\beta}-\boldsymbol{\beta}')}W(v\boldsymbol{0}, v\boldsymbol{\beta}-\boldsymbol{\beta}') \\ =\ & \frac{1}{N}\sum_{\boldsymbol{k}} e^{i\boldsymbol{k}\cdot(\boldsymbol{\beta}-\boldsymbol{\beta}')}\left[W_c(\boldsymbol{k}) - W_v(\boldsymbol{k}-\boldsymbol{K})\right] \\ =\ & \frac{1}{N}e^{i\boldsymbol{K}\cdot(\boldsymbol{\beta}-\boldsymbol{\beta}')/2}\sum_{\boldsymbol{k}} e^{i\boldsymbol{k}\cdot(\boldsymbol{\beta}-\boldsymbol{\beta}')}\left[W_c(\boldsymbol{k}+\frac{1}{2}\boldsymbol{K}) - W_v(\boldsymbol{k}-\frac{1}{2}\boldsymbol{K})\right]. \end{aligned} \tag{2.156}$$

The fourth and fifth term of Eq. (2.155) contain the Coulomb interaction and the exchange interaction between the electron and the hole [128].

The remaining problem is now to diagonalize the matrix with the elements $\langle vc\boldsymbol{K}\boldsymbol{\beta}\left|H\right|vc\boldsymbol{K}\boldsymbol{\beta}'\rangle$. As a consequence of the relation (2.153), the matrix elements of H between the states $\Phi_{vc}(\boldsymbol{R}_j,\, \boldsymbol{R}_j - \boldsymbol{\beta})$ would be independent of $\boldsymbol{R}$ and an N-fold degeneracy would appear. Due to the specific form of the sum in the Wannier function (2.154b), this degeneracy is lifted. The diagonalization can now be achieved by finding an appropriate linear combination of Wannier functions,

$$\Psi^{\sigma\tau}_{vc\nu\boldsymbol{K}} = \sum_{\boldsymbol{\beta}} U_{vc\nu\boldsymbol{K}}(\boldsymbol{\beta})\Phi^{\sigma\tau}_{vc}(\boldsymbol{K},\, \boldsymbol{\beta}), \tag{2.157}$$

where the coefficients $U_{vc\nu\boldsymbol{K}}(\boldsymbol{\beta})$ are determined from

$$\sum_{\boldsymbol{\beta}'}\left\langle vc\boldsymbol{K}\boldsymbol{\beta}\left|H\right|vc\boldsymbol{K}\boldsymbol{\beta}'\right\rangle U_{vc\nu\boldsymbol{K}}(\boldsymbol{\beta}') = EU_{vc\nu\boldsymbol{K}}(\boldsymbol{\beta}) \tag{2.158}$$

with the secular equation

$$\left\|\left\langle vc\boldsymbol{K}\boldsymbol{\beta}\left|H\right|vc\boldsymbol{K}\boldsymbol{\beta}'\right\rangle - E\delta_{\boldsymbol{\beta},\boldsymbol{\beta}'}\right\| = 0. \tag{2.159}$$

Up to now we assumed that the electron and the hole are located in two particular bands. The above treatment may therefore be generalized to more than two bands especially in the case of band degeneracies. The according value of $\langle mn\,\boldsymbol{K}\boldsymbol{\beta}\,|H|\,m'n'\,\boldsymbol{K}\boldsymbol{\beta}'\rangle$ is

$$\begin{aligned}\left\langle mn\,\boldsymbol{K}\boldsymbol{\beta}\,|H|\,m'n'\,\boldsymbol{K}\boldsymbol{\beta}'\right\rangle &= \delta_{\sigma\sigma'}\delta_{\tau\tau'}\Big[\delta_{n,n'}\delta_{m,m'}\delta_{\boldsymbol{\beta},\boldsymbol{\beta}'}E_0^{(1)} \\ &+ \delta_{m,m'}W(n\boldsymbol{\beta},\,n'\boldsymbol{\beta}') - \delta_{n,n'}e^{i\boldsymbol{K}\cdot(\boldsymbol{\beta}-\boldsymbol{\beta}')}W(m\boldsymbol{0},m'\boldsymbol{\beta}-\boldsymbol{\beta}')\Big] \\ &+ \sum_{\boldsymbol{R}_j} e^{i\boldsymbol{K}\cdot\boldsymbol{R}_j}\left[-\delta_{\sigma\sigma'}\delta_{\tau\tau'}\left\langle n\boldsymbol{\beta}m'\boldsymbol{R}_j\,|V_{\mathrm{C}}|\,n'\boldsymbol{R}_j+\boldsymbol{\beta}'m\boldsymbol{0}\right\rangle\right. \\ &\left.\qquad +\delta_{\sigma\tau}\delta_{\sigma'\tau'}\left\langle n\boldsymbol{\beta}m'\boldsymbol{R}_j\,|V_{\mathrm{C}}|\,m\boldsymbol{0}n'\boldsymbol{R}_j+\boldsymbol{\beta}'\right\rangle\right] \qquad (2.160)\end{aligned}$$

with $m' \neq n$ and $n' \neq m$. On the other hand - without band degeneracies - it is possible to account for the other bands by introducing a dielectric constant since the medium can be polarized by the electron and the hole if higher states are included in the calculation.

We neglected spin-orbit interaction, which contributes one energy term to the hole and one to the electron. However, since the according matrix elements depend on the relative spin of the quasi-particles and the symmetry of their wave functions, a general expression cannot be given.

At last we have to mention that all of the calculations have been done assuming “LS coupling”, i.e., that the total spin S is a good quantum number. If the spin and the space parts of the valence and the conduction band states are already coupled when the excited state is constructed (“jj coupling”), the matrix elements have to be transformed accordingly [7].

2.4 Light-matter interaction

The most common methods to investigate structural, electronic, and phononic properties of a solid exploit its interaction with light. The different experimental methods involve, e.g., light-scattering, Raman- and Brillouin scattering, photoemission spectroscopy, two- and three-photon absorption, high-excitation spectroscopy, and photo-luminescence [12, 86, 94, 101, 129–131]. In turn, the solid itself can serve as a source of light in, e.g., LEDs and solid-state lasers. In this section we discuss the light-matter interaction in a theoretical way.

2.4.1 Interaction mechanisms

Here we give an overview over different interaction mechanisms of light with an atom (see also Fig. 2.12). For reasons of simplicity we assume the atom to have two energy levels, which can be occupied by the single electron of the atom. The two-level system can be regarded as, e.g., a simplification of the band model of a solid.

If the atom is in its ground state, a photon can be annihilated and the electron is excited in the state of higher energy E_{ex}. The energy of the photon has to equal exactly the difference of the energies of the excited and the ground state E_{g}:

$$\hbar\omega = E_{\mathrm{ex}} - E_{\mathrm{g}}. \qquad (2.161)$$

The process is called absorption if the energy of the annihilated photon is afterwards converted into other forms of energy and if coherence with the incident light field is destroyed [12]. This can

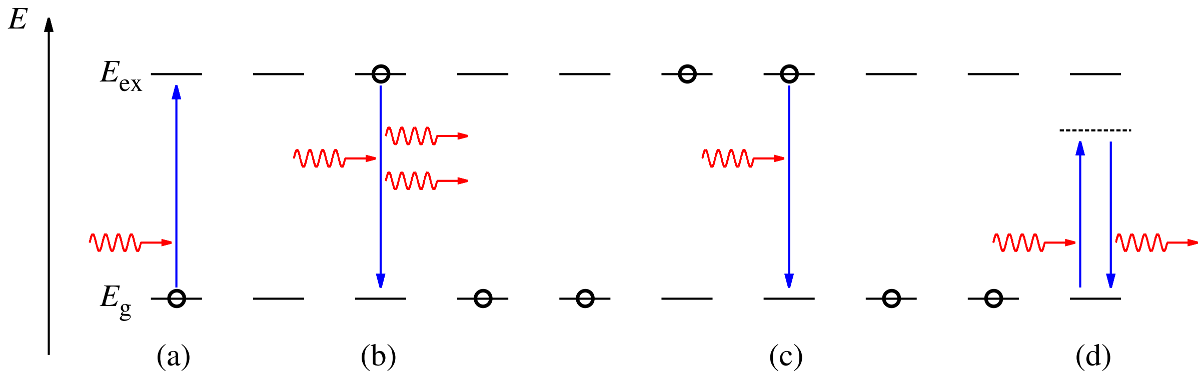

Figure 2.12.: Schematic representations of different light-matter interaction processes: (a) absorption, (b) stimulated emission, (c) spontaneous emission, and (d) virtual excitation. Adapted from [12].

be achieved, e.g., by relaxation of the electron with a simultaneous emission of photons, which are not coherent with the annihilated one, or of phonons.

On the other hand, an incident photon can also cause a dis-excitation of the atom. In this case the electron reenters the ground state emitting a second photon of identical energy, momentum, polarization and phase. This stimulated emission therefore amplifies the photon field. Even without an incident photon, the electron can undergo a transition to the ground state emitting a photon. The spontaneous radiative recombination or spontaneous emission can be understood as being introduced by the zero-point vibrations[32] or vacuum fluctuations of the electromagnetic field.

The last important process is virtual excitation, which is possible due to the quantum-mechanical uncertainty principle for energy and time:

$$\Delta E \Delta t \geq \frac{\hbar}{2}. \tag{2.162}$$

In virtual excitation a state is created, the energy of which differs from that of the excited state but the wave function of which is the same. The electron can be excited to this state by a photon with the energy $\hbar\omega'$ for a maximum time of

$$\Delta t \approx \hbar \left| E_{\mathrm{ex}} - E_{\mathrm{g}} - \hbar\omega' \right|^{-1}. \tag{2.163}$$

During this time interval the virtual state collapses, the electron reenters the ground state and a photon of the same energy is emitted. Due to a phase delay between the incident and the emitted photon, the phase-velocity of light is lowered in a solid, which can be described by the refractive index $n(\omega)$ in a phenomenological way. The better the photon energy fulfills the resonance condition (2.161), the more deviates the wave propagation in the solid from that in vacuum and the stronger become the deviations of $n(\omega)$ from the value $n(\omega) = 1$. If the emitted photon propagates in a direction different from that of the incident photon, the process is called scattering.

An inelastic scattering process, in which not only a photon is emitted but also a phonon (or phonon-polariton [12]) is created or absorbed, is called Brillouin scattering or Raman scattering

---

[32] These zero-point vibrations are described by the term $\sum_{\lambda\boldsymbol{\kappa}} \hbar\omega(\boldsymbol{\kappa})/2$ in Eq. (2.191).

process[33]. In the first case the phonon is an acoustic one, in the latter case it is an optical one. The energy of the emitted photon is then given by

$$\hbar\omega_{\mathrm{e}} = \hbar\omega' \pm \hbar\Omega_{\mathrm{phonon}}, \tag{2.164}$$

where "+" and "−" denote the anti-Stokes and Stokes process, respectively. Due to the very small wave vector $|\boldsymbol{k}| = 2\pi/\lambda \approx \pi/1000a$ of (visible) light in comparison with the extension $|\boldsymbol{k}| = \pi/a$ of the first BZ, only phonons in the vicinity of the center of the first BZ participate in the interaction with light. A detailed treatment of Raman and Brillouin scattering can be found in [12].

2.4.2 Hamiltonian

For simplicity we restrict ourselves to the case of fixed ions. The Hamiltonian H_N which describes the interacting system of the electrons and the electromagnetic field must be chosen in a way that the time-dependent Schrödinger equation

$$H_N \Psi_N = i\hbar \frac{\partial}{\partial t} \Psi_N \tag{2.165}$$

is invariant under an arbitrary gauge transformation

$$\boldsymbol{A} \to \boldsymbol{A} + \nabla\chi, \quad \phi \to \phi - \frac{\partial\chi}{\partial t} \tag{2.166}$$

of the vector potential $\boldsymbol{A}$ and the electric potential ϕ, under which the N-electron wave function is simultaneously transformed according to

$$\Psi_N(\boldsymbol{r}_1, \ldots, \boldsymbol{r}_N, t) \to e^{-i\frac{e}{\hbar}(\chi(\boldsymbol{r}_1,t)+\ldots+\chi(\boldsymbol{r}_N,t))} \Psi_N(\boldsymbol{r}_1, \ldots, \boldsymbol{r}_N, t). \tag{2.167}$$

This is generally achieved by the so-called minimal substitution of the momenta and the energy:

$$\boldsymbol{p}_l \to \boldsymbol{p}_l - q\boldsymbol{A}(\boldsymbol{r}_l, t), \quad E \to E + q\sum_l \phi(\boldsymbol{r}_l, t). \tag{2.168}$$

In the case of the radiation field of a laser, we use radiation gauge[34] [132],

$$\phi = 0, \quad \nabla\boldsymbol{A} = 0, \tag{2.169}$$

and the Hamiltonian reads [85]

$$\begin{aligned} H_N &= \sum_l \frac{1}{2m_0}(\boldsymbol{p}_l + e\boldsymbol{A}(\boldsymbol{r}_l))^2 + \frac{1}{2}\sum_{k\neq l} \frac{e^2}{4\pi\varepsilon_0\,|\boldsymbol{r}_l - \boldsymbol{r}_k|} + \sum_{\boldsymbol{n\tau}l} v(\boldsymbol{r}_l - \boldsymbol{R}^0_{\boldsymbol{n\tau}}) \\ &+ \frac{1}{2}\sum_{\boldsymbol{n\tau}\neq\boldsymbol{m\sigma}} V(\boldsymbol{R}^0_{\boldsymbol{n\tau}} - \boldsymbol{R}^0_{\boldsymbol{m\sigma}}) + \frac{\varepsilon_0}{2}\int \mathrm{d}^3\boldsymbol{r}\,(\boldsymbol{E}^2 + c^2\boldsymbol{B}^2). \end{aligned} \tag{2.170}$$

---

[33] In the case of Raman scattering the phonon mode has to be Raman active, i.e., the phonons should modulate the polarizability of the solid [12, 86]. The complete absorption of a photon with the simultaneous creation of a phonon is obtained in infrared (or obsolete ultrared) spectroscopy, for which $\omega' = \Omega_{\mathrm{phonon}}$ holds (in contrast to $\omega' \gg \Omega_{\mathrm{phonon}}$ for Raman and Brillouin scattering) [86].

[34] In Coulomb gauge one demands $\nabla\boldsymbol{A} = 0$. The scalar potential additionally vanishes in regions which are far from electric charge. Radiation gauge is, e.g., used to quantize electromagnetic radiation.

The last term describes the energy of the radiation field and is referred to by H_{rad}. Separating H_N into three parts describing the uncoupled systems and the interaction part, respectively, yields

$$H_N = H_0 + H_{\mathrm{rad}} + H_{\mathrm{el-rad}} \tag{2.171}$$

with the Hamiltonian H_0 of the electron system [cf. Eq. (2.83)] and the interaction term

$$H_{\mathrm{el-rad}} = \sum_{l=1}^{N_e} \left(\frac{e}{m_0} \boldsymbol{A}(\boldsymbol{r}_l,\, t)\boldsymbol{p}_l + \frac{e^2}{2m_0} [\boldsymbol{A}(\boldsymbol{r}_l,\, t)]^2 \right). \tag{2.172}$$

2.4.3 Single-particle approximation

In Sec. 2.3.2 we introduced the single-particle approximation, in which the electron system is described by single electrons moving in an effective potential V_{eff}. Making use of this approximation and disregarding H_{rad} as a constant, we arrive at the single-particle Hamiltonian

$$H = -\frac{\hbar^2}{2m_0} \triangle + V_{\mathrm{eff}}(\boldsymbol{r}) + \frac{e}{m_0} \boldsymbol{A} \cdot \boldsymbol{p} + \frac{e^2}{2m_0} \boldsymbol{A}^2. \tag{2.173}$$

The second-last and last term can be regarded as perturbations of first and second order, respectively, if the radiation field is sufficiently weak. The interaction with light causes transitions of the electrons between different states. If we assume monochromatic light[35]

$$\boldsymbol{A}(\boldsymbol{r},\, t) = A_0 \hat{\boldsymbol{e}} e^{i(\boldsymbol{\kappa} \cdot \boldsymbol{r} - \omega t)} + \text{c.c.}, \tag{2.174}$$

with the polarization vector $\hat{\boldsymbol{e}}$ and use Fermi's Golden Rule, since the perturbation is periodic in time, the transition rate in first order perturbation theory for the absorption of a photon [94] is given by

$$W_{n\boldsymbol{k},n'\boldsymbol{k}'} = \frac{2\pi}{\hbar} \left| \left\langle n\boldsymbol{k} \left| H' \right| n'\boldsymbol{k}' \right\rangle \right|^2 \delta(E_n(\boldsymbol{k}) - E_{n'}(\boldsymbol{k}') - \hbar\omega) \tag{2.175}$$

with

$$H' = \frac{e}{m_0} A_0 e^{i\boldsymbol{\kappa} \cdot \boldsymbol{r}} \hat{\boldsymbol{e}} \cdot \boldsymbol{p}. \tag{2.176}$$

The δ-function demonstrates energy conservation and since we deal with absorption processes it is $E_n(\boldsymbol{k}) > E_{n'}(\boldsymbol{k}')$. We can now rewrite the matrix element

$$\left\langle n\boldsymbol{k} \left| H' \right| n'\boldsymbol{k}' \right\rangle = \int_V \mathrm{d}\boldsymbol{r} \;\; \psi^*_{n\boldsymbol{k}}(\boldsymbol{r}) \left(\frac{e}{m_0} A_0 e^{i\boldsymbol{\kappa} \cdot \boldsymbol{r}} \hat{\boldsymbol{e}} \cdot \boldsymbol{p} \right) \psi_{n'\boldsymbol{k}'}(\boldsymbol{r}) \tag{2.177}$$

as an integral over one Wigner-Seitz cell making use of the property (2.105) of the Bloch functions under translations. The extracted phase factors lead to a term representing momentum conservation:

$$\left\langle n\boldsymbol{k} \left| H' \right| n'\boldsymbol{k}' \right\rangle \;=\; \int_{\mathrm{WSC}} \ldots \cdot \sum_{\boldsymbol{n}} e^{i(\boldsymbol{\kappa}+\boldsymbol{k}'-\boldsymbol{k}) \cdot \boldsymbol{R}^0_{\boldsymbol{n}}} = \int_{\mathrm{WSC}} \ldots \cdot \delta_{\boldsymbol{k},\, \boldsymbol{k}'+\boldsymbol{\kappa}}. \tag{2.178}$$

---

[35] We also assume the frequency to be sufficiently high so that phonons cannot be excited [7]. Additionally, the crystal shall be small enough so that any damping of the field within the crystal can be neglected, i.e., the wave vector $\boldsymbol{\kappa}$ is real.

Since the wavelength of light is much larger than the diameter of the Wigner-Seitz cell, we make use of the dipole approximation[36]

$$e^{i\boldsymbol{\kappa}\cdot\boldsymbol{r}} = 1 + i\boldsymbol{\kappa}\cdot\boldsymbol{r} + \ldots \approx 1 \tag{2.179}$$

to obtain

$$W_{n\boldsymbol{k},n'\boldsymbol{k}} = \frac{2\pi}{\hbar}\frac{e^2A_0^2}{m_0^2}\left|\left\langle n\boldsymbol{k}\left|\hat{\boldsymbol{e}}\cdot\boldsymbol{p}\right|n'\boldsymbol{k}\right\rangle\right|^2\delta(E_n(\boldsymbol{k})-E_{n'}(\boldsymbol{k})-\hbar\omega). \tag{2.180}$$

The matrix element can finally be rewritten using

$$\boldsymbol{p} = \frac{im_0}{\hbar}\left[H_0,\,\boldsymbol{r}\right], \quad H_0 = -\frac{\hbar^2}{2m_0}\triangle + V_{\text{eff}}(\boldsymbol{r}), \tag{2.181}$$

and the δ-function, which finally provides

$$W_{n\boldsymbol{k},n'\boldsymbol{k}} = \frac{2\pi}{\hbar}\omega^2A_0^2\left|\hat{\boldsymbol{e}}\cdot\left\langle n\boldsymbol{k}\left|H^D\right|n'\boldsymbol{k}\right\rangle\right|^2\delta(E_n(\boldsymbol{k})-E_{n'}(\boldsymbol{k})-\hbar\omega). \tag{2.182}$$

At this point we introduced the dipole operator

$$H^D = -e\boldsymbol{r} \tag{2.183}$$

and we will generally call

$$\left|H_{if}^D\right|^2 = \left|\hat{\boldsymbol{e}}\cdot\left\langle f\left|H^D\right|i\right\rangle\right|^2 \tag{2.184}$$

the dipole matrix element or dipole transition probability between two states $|i\rangle$ and $|f\rangle$.

The rate (2.182) depends on A_0^2 and is therefore proportional to the light intensity or, in the view of second quantization, to the density of photons in a specific mode (see Sec. 2.4.4). It has a non-vanishing value only for direct transitions, i.e., transitions without a change of the wave vector of the Bloch state. If the energy of the light or the photons is high enough, photoemission takes place and the excited electron leaves the solid as a free particle. Due to energy and momentum conservation, one can recalculate the dispersion relation of electrons in the solid after detecting the energy and momentum of the photo-emitted electrons in angular resolved photoemission spectroscopy (ARPES) [85, 86].

Owing to the absorption of photons, the intensity of light behind a solid of thickness d is smaller according to

$$I = I_0e^{-\alpha(\omega)d}. \tag{2.185}$$

The absorption coefficient[37] $\alpha(\omega)$ is proportional to the imaginary part k of the complex index of refraction and can also be expressed using Eq. (2.180) [94]:

$$\alpha(\omega) = \frac{2\omega k}{c} = \frac{2\hbar}{\varepsilon_0 nc\,\omega A_0^2V}\sum_{nn'\boldsymbol{k}\sigma}W_{n\boldsymbol{k},n'\boldsymbol{k}}(\omega) = \frac{2\hbar}{\varepsilon_0 nc\,\omega A_0^2}\sum_{nn'}\frac{2}{(2\pi)^3}\int \mathrm{d}\boldsymbol{k}\,W_{n\boldsymbol{k},n'\boldsymbol{k}}(\omega). \tag{2.186}$$

The second term results for the case that the crystal volume V is very large and that $\boldsymbol{k}$ can be treated as a continuous variable. The imaginary part of the dielectric function is simply

$$\varepsilon_2(\omega) = \frac{\alpha nc}{\omega} = \frac{4\pi e^2}{\varepsilon_0\omega^2m_0^2V}\sum_{nn'\boldsymbol{k}\sigma}\left|\left\langle n\boldsymbol{k}\left|\hat{\boldsymbol{e}}\cdot\boldsymbol{p}\right|n'\boldsymbol{k}\right\rangle\right|^2\delta(E_n(\boldsymbol{k})-E_{n'}(\boldsymbol{k})-\hbar\omega), \tag{2.187}$$

---

[36] If higher terms are used in the given Taylor expansion, one speaks of quadrupole, octopole or transitions of higher-order [12].

[37] In a more general way, $\alpha(\omega)$ is the extinction coefficient. The attenuation of light, which is described by Eq. (2.185), is normally caused by absorption *and* scattering. Hence, it is generally $\alpha_{\text{ext}}(\omega) = \alpha_{\text{abs}}(\omega) + \alpha_{\text{scat}}(\omega)$ [12].

and the real part can then be obtained using Kramers-Kronig relations [12, 85, 97, 129, 133, 134],

$$\varepsilon_1(\omega) = 1 + \frac{4e^2}{\varepsilon_0 m_0 V} \sum_{nn'\boldsymbol{k}\sigma} \frac{f_{nn'}(\boldsymbol{k})}{[\omega_{nn'}(\boldsymbol{k})]^2 - \omega^2}, \tag{2.188}$$

with the oscillator strength being given by

$$f_{nn'}(\boldsymbol{k}) = \frac{2\left|\langle n\boldsymbol{k}\left|\hat{\boldsymbol{e}}\cdot\boldsymbol{p}\right|n'\boldsymbol{k}\rangle\right|^2}{m_0\hbar\omega_{nn'}(\boldsymbol{k})} \tag{2.189}$$

and the energy difference

$$\hbar\omega_{nn'}(\boldsymbol{k}) = E_n(\boldsymbol{k}) - E_{n'}(\boldsymbol{k}). \tag{2.190}$$

2.4.4 Photons

We have already seen that energy exchange between matter and light is possible only in terms of quanta $\hbar\omega$. To conclude this chapter on light-matter interaction, we therefore give the quantized form of the electromagnetic field, which describes light as being composed of photons. Detailed derivations of the following formulas can be found, e.g., in Refs. [135–138].

The Hamiltonian of the radiation field takes a similar form to that of phonons in Eq. (2.75):

$$H_{\text{rad}} = \sum_{\xi\boldsymbol{\kappa}} \hbar\omega_{\xi\boldsymbol{\kappa}} \left(a^\dagger_{\xi\boldsymbol{\kappa}} a_{\xi\boldsymbol{\kappa}} + \frac{1}{2} \right). \tag{2.191}$$

The quanta of the electromagnetic field, which are created by the operators $a^\dagger_{\xi\boldsymbol{\kappa}}$, are called photons. The energy of a photon in the mode $\xi\boldsymbol{\kappa}$ with the polarization ξ and the wave vector $\boldsymbol{\kappa}$ is given by $\hbar\omega_{\xi\boldsymbol{\kappa}} = \hbar c\kappa$ in vacuum. Its momentum reads $\boldsymbol{p} = \hbar\boldsymbol{\kappa}$. The operators $a_{\xi\boldsymbol{\kappa}}$ and $a^\dagger_{\xi\boldsymbol{\kappa}}$ obey Bose commutation relations

$$\begin{aligned} \left[a_{\xi\boldsymbol{\kappa}}, a^\dagger_{\xi'\boldsymbol{\kappa}'}\right] &= \delta_{n,n'}\delta_{\boldsymbol{k},\boldsymbol{k}'}, && (2.192\text{a}) \\ \left[a_{\xi\boldsymbol{\kappa}}, a_{\xi'\boldsymbol{\kappa}'}\right] = \left[a^\dagger_{\xi\boldsymbol{\kappa}}, a^\dagger_{\xi'\boldsymbol{\kappa}'}\right] &= 0, && (2.192\text{b}) \end{aligned}$$

which results in the following action on the states of the photon field in occupation number representation:

$$\begin{aligned} a_{\xi\boldsymbol{\kappa}} \left|\ldots, n_{\xi\boldsymbol{\kappa}}, \ldots\right\rangle &= \sqrt{n_{\xi\boldsymbol{\kappa}}} \left|\ldots, n_{\xi\boldsymbol{\kappa}} - 1, \ldots\right\rangle, && (2.193\text{a}) \\ a^\dagger_{\xi\boldsymbol{\kappa}} \left|\ldots, n_{\xi\boldsymbol{\kappa}}, \ldots\right\rangle &= \sqrt{n_{\xi\boldsymbol{\kappa}} + 1} \left|\ldots, n_{\xi\boldsymbol{\kappa}} + 1, \ldots\right\rangle. && (2.193\text{b}) \end{aligned}$$

Due to the use of the Coulomb gauge in the process of quantization, the vector potential $\boldsymbol{A}$ is transverse. It reads

$$\boldsymbol{A}(\boldsymbol{r}) = \sum_{\xi\boldsymbol{k}} \left(\frac{\hbar}{2\varepsilon_0\omega_{\xi\boldsymbol{\kappa}}V} \right)^{\frac{1}{2}} \hat{\boldsymbol{e}}_{\xi\boldsymbol{\kappa}} \left(a_{\xi\boldsymbol{\kappa}} + a^\dagger_{\xi-\boldsymbol{\kappa}} \right) e^{i\boldsymbol{\kappa}\cdot\boldsymbol{r}} \tag{2.194}$$

with the transverse polarization vectors $\hat{\boldsymbol{e}}_{\xi\boldsymbol{\kappa}}$ ($\hat{\boldsymbol{e}}_{\xi\boldsymbol{\kappa}} \cdot \boldsymbol{\kappa} = 0$) for each of the two polarizations ξ. Taking a look at the angular momentum[38] of a photon parallel to $\boldsymbol{\kappa}$ (the quantization axis), $s_\parallel = \pm\hbar$, one

---

[38] Since there are no longitudinal electromagnetic waves in vacuum, the third possibility $s_\parallel = 0$ for a particle of spin one is forbidden.

can see that photons must be bosons and therefore obey Bose-Einstein statistics in thermodynamic equilibrium. Consequently their distribution function reads[39]

$$f(E,\, \mu,\, T) = \frac{1}{e^{(E-\mu)/k_\mathrm{B}T} - 1} \tag{2.195}$$

with $E = \hbar\omega_{\boldsymbol{\kappa}}$. The chemical potential μ is zero since there is no conservation of the number of photons.

We can finally write the Hamiltonian (2.172) of light-matter interaction in second quantization using Eq. (2.194). In first order perturbation theory only the term linear in $\boldsymbol{A}$ is of relevance. Hence, the Hamiltonian

$$H_\mathrm{Ap} = \sum_{n\boldsymbol{k}n'\boldsymbol{k}'\xi\boldsymbol{\kappa}} \frac{e}{m_0} \left(\frac{\hbar}{2\varepsilon_0 \omega_{\xi\boldsymbol{\kappa}} V} \right)^{\frac{1}{2}} \left\langle n\boldsymbol{k} \left| e^{i\boldsymbol{\kappa}\cdot\boldsymbol{r}} \hat{\boldsymbol{e}}_{\xi\boldsymbol{\kappa}} \cdot \boldsymbol{p} \right| n'\boldsymbol{k}' \right\rangle \left(a_{\xi\boldsymbol{\kappa}} + a^\dagger_{\xi-\boldsymbol{\kappa}} \right) c^\dagger_{n\boldsymbol{k}} c_{n'\boldsymbol{k}'} \tag{2.196}$$

is the starting point of a treatment of light-matter interaction in second quantization.

2.5 Excitons

Excitons are the fundamental excitations in semiconductors in the visible and ultraviolet range of light. In the following we will introduce the simple hydrogen-like description of Wannier excitons. Most of the corrections to this model as well as the interaction of excitons with other quasi-particles will be discussed in the Chapters 3 to 9.

2.5.1 The simple exciton model

In the ground state of a semiconductor the valence bands are completely filled while there are no electrons in the conduction bands. The electron system can be described by the Hamiltonian (2.104), in which the effective potential V_eff is the same for all electrons independently of the energy band. Due to the interaction with light it is possible to excite one electron into the conduction band[40]. Treating the missing electron in the conduction band as a hole (cf. Sec. 2.3.7) and the now missing contribution to V_eff as a Coulomb interaction between electron and hole, one obtains the Hamiltonian

$$H_\mathrm{e-h} = E_\mathrm{g} + \frac{\boldsymbol{p}_\mathrm{e}^2}{2m_\mathrm{e}} + \frac{\boldsymbol{p}_\mathrm{h}^2}{2m_\mathrm{h}} - \frac{e^2}{4\pi\varepsilon_0\varepsilon\, |\boldsymbol{r}_\mathrm{e} - \boldsymbol{r}_\mathrm{h}|} \tag{2.197}$$

for the two-particle problem in effective-mass approximation[41]. We assume non-degenerate, parabolic bands and band extrema being located at $\boldsymbol{k} = \boldsymbol{0}$. Since there are more than only two bands (one CB and one VB), the description of the problem has to include all other bands via a dielectric constant ε (see Sec. 2.3.8). This constant is typically isotropic in crystals with cubic symmetry [37].

---

[39] Compare Eqs. (2.79) and (2.98).

[40] It is also possible that one or more electrons are thermally excited. The formation of an exciton is likely if $k_\mathrm{B}T$ is much smaller than the exciton binding energy and if the excess energy of the band-to-band transition can be dissipated shortly by phonon emission. In the other case, i.e., if $k_\mathrm{B}T$ is larger than or equal to the exciton binding energy, a thermal ionization of excitons will take place [12].

[41] In the following we will drop the star in m^*, which indicates the effective masses.

The Hamiltonian (2.197) is of the same form as that of the hydrogen atom. It can be separated into a part describing the relative motion of the electron and the hole and another part describing the motion of the center of mass. To this aim, we introduce relative and center-of-mass coordinates and momenta,

$$\boldsymbol{r} = \boldsymbol{r}_{\mathrm{e}} - \boldsymbol{r}_{\mathrm{h}}, \qquad \boldsymbol{R} = \left(m_{\mathrm{e}}\boldsymbol{r}_{\mathrm{e}} + m_{\mathrm{h}}\boldsymbol{r}_{\mathrm{h}}\right) / \left(m_{\mathrm{e}} + m_{\mathrm{h}}\right), \tag{2.198a}$$

$$\boldsymbol{p} = \left(m_{\mathrm{h}}\boldsymbol{p}_{\mathrm{e}} - m_{\mathrm{e}}\boldsymbol{p}_{\mathrm{h}}\right) / \left(m_{\mathrm{e}} + m_{\mathrm{h}}\right), \qquad \boldsymbol{P} = \boldsymbol{p}_{\mathrm{e}} + \boldsymbol{p}_{\mathrm{h}}, \tag{2.198b}$$

giving

$$H_{\mathrm{e-h}} = E_{\mathrm{g}} + \frac{\boldsymbol{p}^2}{2\mu} - \frac{e^2}{4\pi\varepsilon_0\varepsilon r} + \frac{\boldsymbol{P}^2}{2M} \tag{2.199}$$

with the total mass $M = m_{\mathrm{e}} + m_{\mathrm{h}}$, the reduced mass $\mu = m_{\mathrm{e}}m_{\mathrm{h}}/(m_{\mathrm{e}} + m_{\mathrm{h}})$ and the momentum operators for the relative motion $\boldsymbol{p}$ and the motion of the center of mass $\boldsymbol{P}$. The solutions[42] of the corresponding time-independent Schrödinger equation [139]

$$\psi_{\nu\boldsymbol{K}}(\boldsymbol{r},\, \boldsymbol{R}) = e^{i\boldsymbol{K}\cdot\boldsymbol{R}}F_{\nu}(\boldsymbol{r}) \tag{2.200}$$

describe a new quasi-particle, the so-called exciton. The exciton wave vector is denoted by $\boldsymbol{K} = \boldsymbol{k}_e - \boldsymbol{k}_h$ and $F_{\nu}(\boldsymbol{r})$ denotes the solutions of the relative movement. In general one would write $F_{nLM}(\boldsymbol{r})$, but we abbreviate the principal quantum number n, the angular quantum number L and the magnetic quantum number M by ν for reasons of simplicity. These quantum numbers can be used in the same way as for the hydrogen atom unless angular momentum is not a good quantum number in the case that the deviations from the simple $1/r$-behavior of the Coulomb potential are too large [12]. Deviations are, e.g., due to the crystal structure, non-parabolicity of the bands and electron-phonon interaction.

At this point we want to mention that sometimes relative and average coordinates,

$$\boldsymbol{r} = \boldsymbol{r}_{\mathrm{e}} - \boldsymbol{r}_{\mathrm{h}}, \quad \tilde{\boldsymbol{R}} = \frac{1}{2}(\boldsymbol{r}_{\mathrm{e}} + \boldsymbol{r}_{\mathrm{h}}), \tag{2.201}$$

are used in literature [7]. These coordinates lead to the Schrödinger equation

$$\left[-\frac{\hbar^2}{2\mu}\nabla_{\boldsymbol{r}}^2 - \frac{\hbar^2}{2}\left(\frac{1}{m_{\mathrm{h}}} - \frac{1}{m_{\mathrm{e}}}\right)\nabla_{\boldsymbol{r}}\cdot\nabla_{\boldsymbol{R}} + \frac{\hbar^2}{2M}\nabla_{\boldsymbol{R}}^2 - \frac{e^2}{4\pi\varepsilon_0}\frac{1}{r}\right]\psi = E\psi, \tag{2.202}$$

which can be solved by

$$\psi_{\nu\boldsymbol{K}}(\boldsymbol{r},\, \boldsymbol{R}) = e^{i\boldsymbol{K}\cdot(\tilde{\boldsymbol{R}}+\alpha'\boldsymbol{r})}F_{\nu}(\boldsymbol{r}). \tag{2.203}$$

With the constant $\alpha' = (m_{\mathrm{e}} - m_{\mathrm{h}})/2(m_{\mathrm{e}} + m_{\mathrm{h}})$ one can then identify

$$\tilde{\boldsymbol{R}} + \alpha'\boldsymbol{r} = \boldsymbol{R}. \tag{2.204}$$

The eigenenergies of the exciton

$$E_{\nu\boldsymbol{K}} = E_{\mathrm{g}} - \frac{R_{\mathrm{exc}}}{n^2} + \frac{\hbar^2\boldsymbol{K}^2}{2M} \tag{2.205}$$

yield a series of bound states with the quantum number $n \in \mathbb{N}$ and $\boldsymbol{K}$ ranging over the whole first BZ. Since the resulting “exciton bands” represent excited states of the whole crystal, it has to

---

[42] Note that our conventions to write specific parameters sometimes differ from Ref. [85]. In this case we use notations of Refs. [7, 86, 139].

be stated that these bands should not be placed in diagrams showing the band structure of one electron in order to avoid confusion [7]. Above the bound states a continuum of electron-hole pair states or a continuum of band-to-band excitations can be found.

The Rydberg energy Ry and the Bohr radius a_0 of the hydrogen atom are scaled in the case of the exciton:

$$R_{\text{exc}} = Ry\frac{\mu}{m_0\varepsilon^2}, \quad a_{\text{exc}} = a_0\frac{m_0\varepsilon}{\mu}. \tag{2.206}$$

Since the Bohr radius of the exciton is much larger than the lattice constant a, the orbits of hole and electron extend over many unit cells. Thus, the continuum approximation, which assumes a homogeneous dielectric and effective masses, is *a posteriori* justified. Inserting typical material parameters one finds [12]

$$1\,\text{meV} \leq R_{\text{exc}} \leq 200\,\text{meV} \ll E_{\text{g}} \tag{2.207}$$

and

$$50\,\text{nm} \gtrsim a_{\text{exc}} \geq 1\,\text{nm} > a. \tag{2.208}$$

To avoid a spatial separation of electron and hole it is important that their group velocities are equal [12, 86]. Therefore, excitons in direct gap semiconductors form preferentially in the vicinity of the direct gap. A treatment of excitons in indirect gap semiconductors can be found in Ref. [129].

At the end of this section we would like to note that the excitons treated so far are called Wannier or Mott-Wannier excitons [5]. There is another type of excitons, the so-called Frenkel excitons [2], which can be found in insulators and organic crystals and which describe electrons and holes located at the same lattice site. A description of these excitons in effective-mass approximation is not possible since the extension of the wave function is smaller than the diameter of one unit cell[43]. A detailed treatment of Frenkel excitons can be found in Ref. [7].

2.5.2 Wannier equation and exciton wave function

In this section we extend the calculations of Sec. 2.3.8 to present the accurate treatment of excitons with their complete wave function and to derive the simple hydrogen-like exciton model[44]. At first, we separate the matrix element of Eq. (2.155) as[45]:

$$\left\langle vc\,\boldsymbol{K}\boldsymbol{\beta}\,|H|\,vc\,\boldsymbol{K}\boldsymbol{\beta}'\right\rangle = H_{\boldsymbol{\beta}\boldsymbol{\beta}'}(\boldsymbol{K}) + J_{\boldsymbol{\beta}\boldsymbol{\beta}'}(\boldsymbol{K}) \tag{2.209}$$

with

$$\begin{aligned}
H_{\boldsymbol{\beta}\boldsymbol{\beta}'}(\boldsymbol{K}) &= \delta_{\boldsymbol{\beta},\boldsymbol{\beta}'}E_0^{(1)} - \delta_{\boldsymbol{\beta},\boldsymbol{\beta}'}\frac{e^2}{4\pi\varepsilon_0}\frac{1}{\beta} \\
&+ \frac{1}{\sqrt{N}}e^{i\boldsymbol{K}\cdot(\boldsymbol{\beta}-\boldsymbol{\beta}')/2}\sum_{\boldsymbol{k}} e^{i\boldsymbol{k}\cdot(\boldsymbol{\beta}-\boldsymbol{\beta}')}\left[W_c\left(\boldsymbol{k}+\frac{1}{2}\boldsymbol{K}\right) - W_v\left(\boldsymbol{k}-\frac{1}{2}\boldsymbol{K}\right)\right], \\
J_{\boldsymbol{\beta}\boldsymbol{\beta}'}(\boldsymbol{K}) &= \delta_{\boldsymbol{\beta},\boldsymbol{\beta}'}\frac{e^2}{4\pi\varepsilon_0}\frac{1}{\beta} - \sum_{\boldsymbol{R}_j} e^{i\boldsymbol{K}\cdot\boldsymbol{R}_j}\left\langle c\boldsymbol{\beta}v\boldsymbol{R}\,|V_{\text{C}}|\,c\boldsymbol{R}+\boldsymbol{\beta}'v\boldsymbol{0}\right\rangle \\
&+ 2\delta_{S,0}\sum_{\boldsymbol{R}_j} e^{i\boldsymbol{K}\cdot\boldsymbol{R}_j}\left\langle c\boldsymbol{\beta}v\boldsymbol{R}\,|V_{\text{C}}|\,v\boldsymbol{0}c\boldsymbol{R}+\boldsymbol{\beta}'\right\rangle.
\end{aligned} \tag{2.210a}$$

---

[43] In this case an exciton can be regarded as an excited state of one ion in the solid [86].

[44] In this section we will again follow the descriptions in Ref. [7].

[45] Note that $\boldsymbol{R}_j$ describes a lattice vector and not a center-of-mass coordinate.

We insert only $H_{\boldsymbol{\beta}\boldsymbol{\beta}'}(\boldsymbol{K})$ in the eigenvalue equation (2.158) and will treat $J_{\boldsymbol{\beta}\boldsymbol{\beta}'}(\boldsymbol{K})$ later as a perturbation. Setting

$$\tilde{U}_{\nu\boldsymbol{K}}(\boldsymbol{\beta}) = e^{-i\boldsymbol{K}\cdot\boldsymbol{\beta}/2} U_{\nu\boldsymbol{K}}(\boldsymbol{\beta}) \tag{2.211}$$

we obtain

$$\begin{aligned}\left[E_0^{(1)} - \frac{e^2}{4\pi\varepsilon_0}\frac{1}{\beta}\right]\tilde{U}_{\nu\boldsymbol{K}}(\boldsymbol{\beta}) + \frac{1}{N}\sum_{\boldsymbol{\beta}'}\sum_{\boldsymbol{k}} e^{i\boldsymbol{k}\cdot(\boldsymbol{\beta}-\boldsymbol{\beta}')} & \\ \times\left[W_c\left(\boldsymbol{k}+\frac{1}{2}\boldsymbol{K}\right) - W_v\left(\boldsymbol{k}-\frac{1}{2}\boldsymbol{K}\right)\right]\tilde{U}_{\nu\boldsymbol{K}}(\boldsymbol{\beta}') &= E\tilde{U}_{\nu\boldsymbol{K}}(\boldsymbol{\beta}),\end{aligned} \tag{2.212}$$

We can simplify the double sum using

$$\begin{aligned}\frac{1}{N}\sum_{\boldsymbol{\beta}'}\sum_{\boldsymbol{k}} e^{i\boldsymbol{k}\cdot(\boldsymbol{\beta}-\boldsymbol{\beta}')} f(\boldsymbol{k}) g(\boldsymbol{\beta}') &= \frac{1}{N}\sum_{\boldsymbol{\beta}'}\sum_{\boldsymbol{k}} e^{i\boldsymbol{k}\cdot(\boldsymbol{\beta}-\boldsymbol{\beta}')} f(\boldsymbol{k})\left[\frac{1}{\sqrt{N}}\sum_{\boldsymbol{x}} e^{-i\boldsymbol{x}\cdot\boldsymbol{\beta}'}G(\boldsymbol{x})\right] \\ &= \frac{1}{\sqrt{N}^3}\sum_{\boldsymbol{k}}\sum_{\boldsymbol{x}} e^{i\boldsymbol{k}\cdot\boldsymbol{\beta}} f(\boldsymbol{k})G(\boldsymbol{x})\sum_{\boldsymbol{\beta}'} e^{-i(\boldsymbol{k}+\boldsymbol{x})\cdot\boldsymbol{\beta}'} \\ &= \frac{1}{\sqrt{N}^3}\sum_{\boldsymbol{k}}\sum_{\boldsymbol{x}} e^{i\boldsymbol{k}\cdot\boldsymbol{\beta}} f(\boldsymbol{k})G(\boldsymbol{x})\,N\delta(\boldsymbol{k}+\boldsymbol{x}) \\ &= \frac{1}{\sqrt{N}}\sum_{\boldsymbol{k}} e^{i\boldsymbol{k}\cdot\boldsymbol{\beta}} f(\boldsymbol{k})G(-\boldsymbol{k}) \\ &= f(-i\nabla_{\boldsymbol{\beta}})g(\boldsymbol{\beta}),\end{aligned} \tag{2.213}$$

to arrive at

$$\left[W_c\left(-i\nabla+\frac{1}{2}\boldsymbol{K}\right) - W_v\left(-i\nabla-\frac{1}{2}\boldsymbol{K}\right) - \frac{e^2}{4\pi\varepsilon_0}\frac{1}{\beta}\right]\tilde{U} = \left[E - E_0^{(1)}\right]\tilde{U}. \tag{2.214}$$

In effective mass approximation we make the following assumption[46]:

$$W_c(\boldsymbol{k}) = E_c + \frac{\hbar^2 k^2}{2m_\mathrm{e}}, \quad W_v(\boldsymbol{k}) = E_v - \frac{\hbar^2 k^2}{2m_\mathrm{h}}. \tag{2.215}$$

With the energy E_g of the band gap the definition $\tilde{E} = E - E_0^{(1)}$ and the reduced mass μ, the eigenvalue equation now reads

$$\left[-\frac{\hbar^2}{2\mu}\triangle - \frac{e^2}{4\pi\varepsilon_0}\frac{1}{\beta} - \frac{\hbar^2}{2i}\left(\frac{1}{m_\mathrm{h}} - \frac{1}{m_\mathrm{e}}\right)\boldsymbol{K}\cdot\nabla\right]\tilde{U} = \left[\tilde{E} - E_\mathrm{g} - \frac{\hbar^2 K^2}{8\mu}\right]\tilde{U}. \tag{2.216}$$

This is the same differential equation as in the previous section 2.5.1 if relative and average coordinates are used [cf. Eq. (2.202)]. Setting

$$\tilde{U}(\boldsymbol{\beta}) = e^{i\alpha'\boldsymbol{K}\cdot\boldsymbol{\beta}}F(\boldsymbol{\beta}), \tag{2.217}$$

---

[46] A treatment of bands with maxima at $\boldsymbol{k} \neq 0$ and effective mass tensors of more general form can be found in [7].

we obtain the hydrogen-like Schrödinger equation[47]

$$\left[-\frac{\hbar^2}{2\mu}\triangle-\frac{e^2}{4\pi\varepsilon_0}\frac{1}{\beta}\right]F=\left[\tilde{E}-E_{\mathrm{g}}-\frac{\hbar^2K^2}{2M}\right]F. \tag{2.218}$$

with the eigenenergies[48]:

$$E^{(0)}_{\nu\boldsymbol{K}}=E^{(1)}_0+E_{\mathrm{g}}+\frac{\hbar^2K^2}{2M}-\frac{\mu e^4}{(4\pi\varepsilon_0)^2\hbar^2}\frac{1}{n^2} \tag{2.219}$$

According to the calculation above the *full* exciton wave function is

$$\Psi_{vc\nu\boldsymbol{K}}=\sum_{\boldsymbol{\beta}}U_{vc\nu\boldsymbol{K}}(\boldsymbol{\beta})\Phi_{vc}(\boldsymbol{K},\,\boldsymbol{\beta})=\sum_{\boldsymbol{\beta}}e^{i\alpha\boldsymbol{K}\cdot\boldsymbol{\beta}}F_\nu(\boldsymbol{\beta})\Phi_{vc}(\boldsymbol{K},\,\boldsymbol{\beta}), \tag{2.220}$$

with $\alpha=1/2+\alpha'$. $|F_\nu|^2$ can be interpreted as the probability to find the electron at the position $\boldsymbol{\beta}'$ and the hole at the origin, i.e., as the probability for the system to be in the state $\Phi_{vc}(\boldsymbol{K},\,\boldsymbol{\beta})$. Although $\boldsymbol{\beta}'$ can take only discrete values (see Sec. 2.3.8), $F_\nu(\boldsymbol{\beta})$ can be considered as a continuous hydrogenic function if the crystal is considerably larger than the exciton radius. If the properties of $F_\nu(\boldsymbol{\beta})$ as a point function become important, $F_\nu(\boldsymbol{\beta})$ has to be defined as *the average value of the hydrogenic wave function in the unit cell containing* $\boldsymbol{\beta}$ [7] multiplied by $V_{\mathrm{uc}}^{1/2}$ in order to fulfill the normalization condition

$$\sum_{\boldsymbol{\beta}}|F_\nu(\boldsymbol{\beta})|^2=1. \tag{2.221}$$

We will now take a look at the matrix elements of the complete Hamiltonian in the basis (2.220):

$$\begin{aligned}\left\langle vc\,\nu\boldsymbol{K}\left|H\right|vc\,\nu'\boldsymbol{K}\right\rangle &= \sum_{\boldsymbol{\beta},\boldsymbol{\beta}'}U^*_{vc\nu\boldsymbol{K}}(\boldsymbol{\beta})U_{vc\nu'\boldsymbol{K}}(\boldsymbol{\beta}')\left[H_{\boldsymbol{\beta}\boldsymbol{\beta}'}(\boldsymbol{K})+J_{\boldsymbol{\beta}\boldsymbol{\beta}'}(\boldsymbol{K})\right]\\ &= \delta_{\nu,\nu'}E^{(0)}_{\nu\boldsymbol{K}}-\left[\left\langle\nu\mathbf{0}v\mathbf{0}\left|V_{\mathrm{C}}\right|\nu'\mathbf{0}'v\mathbf{0}\right\rangle-\sum_{\boldsymbol{\beta}}\frac{e^2}{4\pi\varepsilon_0}\frac{1}{r}F^*_\nu(\boldsymbol{\beta})F_{\nu'}(\boldsymbol{\beta})\right]\\ &+ 2\delta_{S,0}\sum_{\boldsymbol{R}_j}e^{i\boldsymbol{K}\cdot\boldsymbol{R}_j}\left\langle\nu\boldsymbol{R}_jv\mathbf{0}\left|V_{\mathrm{C}}\right|v\boldsymbol{R}_j\nu'\mathbf{0}\right\rangle\\ &- \sum_{\boldsymbol{R}_j\neq\mathbf{0}}e^{i\boldsymbol{K}\cdot\boldsymbol{R}_j}\left\langle\nu\boldsymbol{R}_jv\mathbf{0}\left|V_{\mathrm{C}}\right|\nu'\mathbf{0}v\boldsymbol{R}_j\right\rangle.\end{aligned} \tag{2.222}$$

The abbreviation $\nu\boldsymbol{R}$ in the matrix elements denotes functions of the form

$$\phi_{c\nu\boldsymbol{R}}(\boldsymbol{x})=\sum_{\boldsymbol{\beta}}e^{i\alpha'\boldsymbol{K}\cdot\boldsymbol{\beta}}F_\nu(\boldsymbol{\beta})a_{c(\boldsymbol{R}+\boldsymbol{\beta})}(\boldsymbol{x}), \tag{2.223}$$

which *act as molecular orbitals for the excited electron in the crystal* [7].

The terms in square brackets describe corrections of the Coulomb interaction caused by the finite size (of the Wannier functions) of electron and hole as well as the correction due to the symmetry

---

[47] The Coulomb interaction is not scaled by a dielectric constant since this constant is a result of higher-order effects [7]. See also Sec. 2.3.8 and Chapter 6.

[48] The upper index (0) denotes that these energies are the zero-order energies according to perturbation theory if $J_{\boldsymbol{\beta}\boldsymbol{\beta}'}(\boldsymbol{K})$ is treated as a perturbation.

of the crystal. These terms cancel each other for large values of $|\boldsymbol{\beta}|$, where electron and hole can be approximated as point charges. The fourth term is the exchange interaction between electron and hole. This interaction will be discussed in Chapter 5. The last term in Eq. (2.222) describes a Coulomb interaction between two charge clouds, whose effective charges decrease exponentially with increasing $\boldsymbol{R}$.

2.5.3 Excitons in second quantization

In the many-particle picture or in second quantization excitons can be considered as particles which are created by creation operators $B^\dagger_{\nu\boldsymbol{K}}$ applied to the ground state $|0\rangle$,

$$B^\dagger_{\nu\boldsymbol{K}}\,|0\rangle = (|\nu\boldsymbol{K}\rangle\,\langle 0|)\,|0\rangle = |\nu\boldsymbol{K}\rangle\,. \tag{2.224}$$

The Hamiltonian then[49] reads

$$H_{\mathrm{exc}} = \sum_{\nu\boldsymbol{K}} E_{\nu\boldsymbol{K}}\left(B^\dagger_{\nu\boldsymbol{K}}B_{\nu\boldsymbol{K}} + \frac{1}{2}\right). \tag{2.225}$$

Before we can express the operator $B^\dagger_{\nu\boldsymbol{K}}$ in terms of electron and hole creation operators, we have to describe the excited electronic states (see Sec. 2.3.8) in second quantization[50]. The ground state (2.124a) reads according to the descriptions in Appendix A.2

$$|\Phi_0\rangle = c^\dagger_{v\boldsymbol{k}_1\alpha}c^\dagger_{v\boldsymbol{k}_1\beta}c^\dagger_{v\boldsymbol{k}_2\beta}\cdots c^\dagger_{v\boldsymbol{k}_{N/2}\beta}\,|\{0\}\rangle\,. \tag{2.226}$$

The operator $c^\dagger_{n\boldsymbol{k}\sigma}$ creates an electron or destroys a hole with momentum $\boldsymbol{k}$ and spin σ in the band n. The creation operator of a hole or annihilation operator of an electron is consequently denoted by $c_{n\boldsymbol{k}\sigma}$. As both quasi-particles are fermions, the operators obey anti-commutation relations

$$\begin{aligned} \left\{c_{n\boldsymbol{k}\sigma},\, c^\dagger_{n'\boldsymbol{k}'\sigma'}\right\} &= \delta_{n,n'}\delta_{\boldsymbol{k},\boldsymbol{k}'}\delta_{\sigma,\sigma'}, && (2.227\text{a})\\ \left\{c_{n\boldsymbol{k}\sigma},\, c_{n'\boldsymbol{k}'\sigma'}\right\} = \left\{c^\dagger_{n\boldsymbol{k}\sigma},\, c^\dagger_{n'\boldsymbol{k}'\sigma'}\right\} &= 0. && (2.227\text{b}) \end{aligned}$$

Using the relation (2.125), we can also define creation and annihilation operators for Wannier states,

$$c_{n\boldsymbol{R}_j\sigma} = \frac{1}{\sqrt{N}}\sum_{\boldsymbol{k}} e^{i\boldsymbol{k}\cdot\boldsymbol{R}_j}c_{n\boldsymbol{k}\sigma}, \qquad c^\dagger_{n\boldsymbol{R}_j\sigma} = \frac{1}{\sqrt{N}}\sum_{\boldsymbol{k}} e^{-i\boldsymbol{k}\cdot\boldsymbol{R}_j}c^\dagger_{n\boldsymbol{k}\sigma}, \tag{2.228}$$

which also obey anti-commutation relations.

We can now treat the excited states $\Phi^{\sigma\sigma'}_{vc}(\boldsymbol{k}_{\mathrm{h}},\,\boldsymbol{k}_{\mathrm{e}})$ and $\Phi^{\sigma\sigma'}_{vc}(\boldsymbol{R}_i,\,\boldsymbol{R}_j)$ of Eqs. (2.145) and (2.151). These states have a very simple form:

$$|vc\boldsymbol{k}_{\mathrm{h}}\boldsymbol{k}_{\mathrm{e}}\rangle = c^\dagger_{c\boldsymbol{k}_{\mathrm{e}}\sigma'}c_{v\boldsymbol{k}_{\mathrm{h}}\sigma}\,|\Phi_0\rangle\,, \qquad |vc\boldsymbol{R}_i\boldsymbol{R}_j\rangle = c^\dagger_{c\boldsymbol{R}_j\sigma'}c_{v\boldsymbol{R}_i\sigma}\,|\Phi_0\rangle\,. \tag{2.229}$$

The comparison with Eq. (2.154b) now supplies the correct expression of the operator $B^\dagger_{\nu\boldsymbol{K}}$ in terms of electron and hole creation operators. With the operator

$$b^\dagger_{\boldsymbol{\beta}\boldsymbol{K}} = \frac{1}{\sqrt{N}}\sum_{\boldsymbol{k}} e^{-i\boldsymbol{k}\cdot\boldsymbol{\beta}}c^\dagger_{c\boldsymbol{k}}c_{v\boldsymbol{k}-\boldsymbol{K}} = \frac{1}{\sqrt{N}}\sum_{j} e^{i\boldsymbol{K}\cdot\boldsymbol{R}_j}c^\dagger_{c\boldsymbol{R}_j+\boldsymbol{\beta}}c_{v\boldsymbol{R}} \tag{2.230}$$

---

[49] Compare, e.g., Refs. [140, 141].

[50] An alternative derivation leading to the same expression can be found in Ref. [139].

we finally obtain

$$B^{\dagger}_{\nu\boldsymbol{K}} = \sum_{\boldsymbol{\beta}} U_{vc\nu\boldsymbol{K}}(\boldsymbol{\beta}) b^{\dagger}_{\boldsymbol{\beta K}}. \tag{2.231}$$

In the limit of low excitation densitites the excitons can be treated as bosons. This can be shown by [7, 139, 142]

$$\left[B_{\nu\boldsymbol{K}},\, B^{\dagger}_{\nu'\boldsymbol{K}'}\right] = \delta_{\nu,\nu'}\delta_{\boldsymbol{K},\boldsymbol{K}'} + \mathcal{O}(N_{\mathrm{exc}}/N). \tag{2.232}$$

The deviation from the value 1 is given by the number of excitons N_{exc}. The additional term results from the impossibility to excite one lattice site more than once and thus represents an interference effect between the excitons. Only if $N_{\mathrm{exc}} \ll N$ holds, the number operator $B^{\dagger}_{\nu\boldsymbol{K}}B_{\nu\boldsymbol{K}}$ in Eq. (2.225) has the eigenvalues 0, 1, 2, ... [7].

In the case of higher excitation densities the individual parts of the exciton, i.e. the hole and the electron, become more relevant [143–145]. This leads to several phenomena like exciton molecules or electron-hole plasmas [85] and makes it difficult to create Bose-Einstein condensates of excitons [12, 146].

2.5.4 Excitation process and channels of decay

In this section we shortly discuss the excitation process of excitons and possible channels for its decay. A mathematical description of the excitation process will be given in Sec. 4.4. The excitation of electrons from the ground state of a semiconductor into the lowest CB by a applying a short laser pulse normally ends in the continuum states of excitons. The excess energy is then transferred to other degrees of freedom by different scattering processes including [12]

- scattering with acoustic and optical phonons, which becomes more relevant with increasing temperature,
- scattering with different electronic excitations like electron-exciton scattering or exciton-exciton scattering, which is of importance in the case of doping or high optical excitation,
- and scattering at lattice defects [147] or impurities [148–151], if present.

Having run through some scattering processes, the excitons reach the energetically lowest states in less than $t = 1\,\mathrm{ps}$ [152]. A thermal distribution, which can usually be described by Boltzmann statistics, is reached after $t \approx 100\,\mathrm{ps}$ [7, 153]. The thermal velocity $\sqrt{3k_{\mathrm{B}}T/M} \approx 4 \times 10^4\,\mathrm{m/s}$ of the excitons is then much larger than their initial velocity $\hbar\kappa/M \approx 500\,\mathrm{m/s}$, which is determined by the wave vector κ of light. The excitons finally deacy after some time. The most likely channels for the decay of excitons are [7]

- radiative decay into a photon (and a phonon) [76, 154],
- dissociation into a electron-hole pair, which can be detected as photoconductivity, by phonon or defect scattering, collision of two excitons, field ionization, and collision ionization,
- self-trapping, i.e., the excitation becomes localized at some definite site due to a large exciton-phonon coupling, and subsequent luminescence, radiationless decay with a burst of phonons [155], or jump to another lattice site,
- trapping by defects and subsequent decay of the excited state of the defect.

In the case of radiative decay one distinguishes between direct and indirect transitions. Indirect exciton decay is the inverse of indirect absorption and represents a single-phonon process. For indirect exciton decay the lifetime of excitons has been estimated to be of the order of $1\,\mu$s [76]. Direct exciton decay is more complicated since the polariton properties need to be considered (see Chapter 9). If one assumes that excitons or polaritons thermalize on the lower polariton branch (LPB) (cf. Fig. 9.1) at large values of κ, scattering with acoustic phonons must take place so that the polaritons reach the steep part of the LPB where their photon component becomes large enough to emit a photon [7, 76]. In this context, the inflection region of the LPB is called "bottleneck" since the transit time of about $10^{-9}\,$s through this region is 1000 times longer than the typical thermalization time [7]. This behavior is due to weak exciton-phonon coupling and a low density of exciton states at small values of the wave vector κ. The lifetime of the exciton as regards direct transitions is basically determined by the transition time and amounts to about $10^{-9}\,\mathrm{s} - 10^{-8}\,\mathrm{s}$ [76]. For a further discussion of exciton decay see Refs. [7, 12] and further references therein.

2.6 Cuprous oxide Cu_2O

Since all of the theoretical calculations in this thesis are performed for cuprous oxide (Cu_2O), we will now give a short introduction to this semiconductor. Cuprous oxide is a red-colored solid crystalizing in a cubic lattice with space group O_h [30]. Although there are some growth techniques for Cu_2O [156, 157], crystals of natural origin have a much better quality[51]. Especially crystals with little strain and little defects are preferred for experiments.

The crystal unit cell of Cu_2O is shown in Fig. 2.13. The oxygen ions are arranged in a bcc sublattice while the copper ions are arranged in a fcc sublattice. The basis in Cu_2O consits of six ions, for which reasons 3 acoustic and 15 optical phonon branches can be found. Due to degeneracies only 8 different optical frequencies at $\boldsymbol{k} = \boldsymbol{0}$ remain[52] and only two of the transverse modes are infrared active, i.e., they can couple to an external electric field [161, 162].

While Cu_2O is of little interest for technical applications because of difficulties in its fabrication and its poor conductance [163], it is the semiconductor in which excitons have been discovered experimentally for the first time [6, 164]. Ever since this discovery by Hayashi and Katsuki in 1950 [165, 166] as well as by Gross and Karryjew in 1952 [6, 164], cuprous oxide has attained a lot of interest in the last 65 years for basic research on excitons (see Refs. [12, 30, 71, 167] and further references therein).

In Fig. 2.14 we show the band structure of Cu_2O. Cuprous oxide is a direct semiconductor, where the different bands stem from O $2p$ electrons (Γ_4^--CB), Cu $4s$ electrons (Γ_1^+-CB) and Cu $3d$ electrons (Γ_3^+ and Γ_5^+-VBs) [168]. The symmetry of the bands is assigned by the irreducible representations[53] $\Gamma_i^\pm$ of the group O_h. Due to the crystal field, the degeneracy between the Γ_3^+-VB and the Γ_5^+-VB is lifted. Since the uppermost VB and the lowest CB stem from electrons of the same atom, the creation of the according exciton by a photon takes place at the same atom. This is atypical for a direct semiconductor. Including the electron spin (symmetry Γ_6^+), the Γ_5^+-VB is split due to the spin-orbit interaction [125, 171]. By considering all possible excitations from the

---

[51] The natural crystals used by the group of M. Bayer and D. Fröhlich were found in the Tsumeb mine in Namibia. From these crystals samples with different orientation were cut [30], whereby the crystal orientation was determined via X-ray scattering.

[52] All optical phonon energies can be found in Refs. [97, 158–160].

[53] An introduction to the group theory of crystals and sets of tables can be found, e.g., in [12, 90, 169, 170].

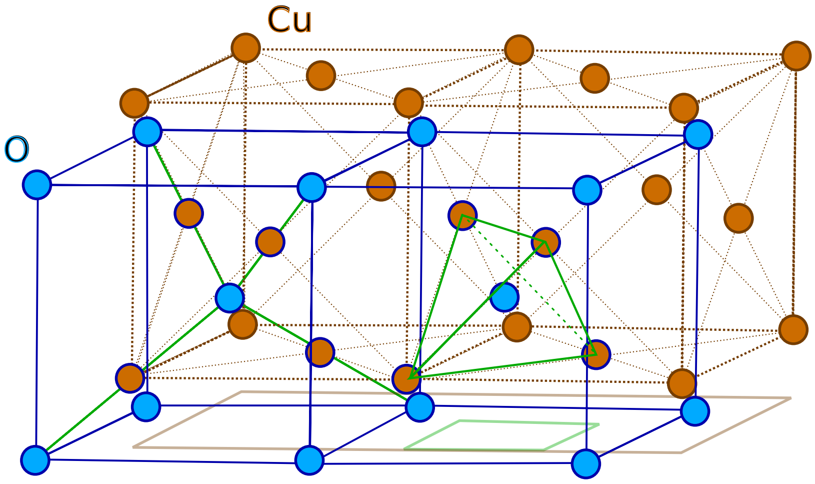

Figure 2.13.: The crystal structure of Cu_2O can be regarded as built up of an fcc lattice of copper ions and a bcc lattice of oxygen atoms, which are shifted against each other by 1/4 of the space diagonal. Adapted from [87].

valence bands to the conduction bands shown in Fig. 2.14, four exciton series are obtained, which are named after the color of the light needed for these excitations [30]: the yellow, the green, the blue, and the violet series. In the literature the yellow exciton series is of special interest. In contrast to other semiconductors like GaAs, the exciton Rydberg energy in Cu_2O is with about 90 meV comparatively high. This facilitates the observation of excitons in cuprous oxide. Already in early years excitons with principal quantum numbers of $n = 9$ have been observed [6, 67].

Very recently, new attention has been drawn to the field of excitons by an experimental observation of the yellow exciton series in Cu_2O up to a large principal quantum number of $n = 25$ [30]. This discovery has opened up the research field of giant Rydberg excitons and led to a variety of new experimental and theoretical investigations [30, 31, 33–49, 51–55]. In Ref. [30] the size of the excitons with $n = 25$ has been calculated using the formula [174]

$$\langle r \rangle = \frac{1}{2} a_{\mathrm{exc}} \left[3n^2 - L(L+1) \right] \tag{2.233}$$

for the average radius. This yielded $\langle r \rangle = 1.04\,\mu\mathrm{m}$ with the Bohr radius $a_{\mathrm{exc}} = 1.11\,\mathrm{nm}$ for P excitons ($L = 1$). Hence, the wave function of the exciton is ten times larger than the wave length of yellow light and spans an area comprising more than 10^9 unit cells!

In Cu_2O parity is a good quantum number and thus the exciton spectrum falls into two parts: The dipole-active exciton states of negative parity and odd angular momentum, which can be observed in one-photon absorption (Γ_4^- symmetry) and the exciton states of positive parity and even angular momentum, which can be observed in two-photon absorption (Γ_5^+ symmetry). As was already menitoned, the parities of the lowest CB and the uppermost VB are identical, for which reason the direct excitation of excitons is parity-forbidden in Cu_2O (cf. Refs. [7, 62] and Sec. 4.4). Hence, only excitons of negative parity or especially P excitons are dipole allowed.

In Fig. 2.15 the absorption spectrum of the P excitons is shown [30]. The absorption peaks

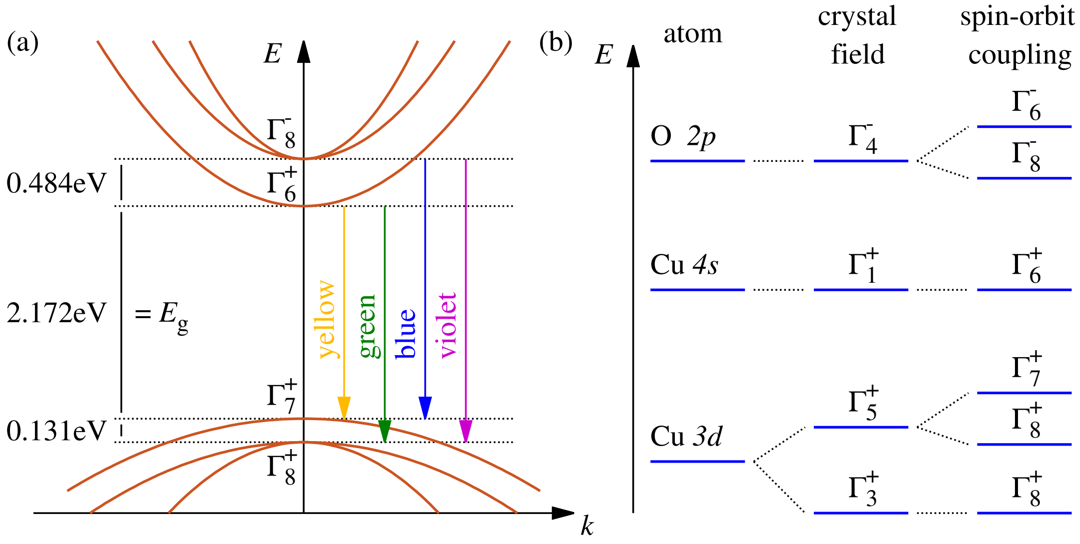

Figure 2.14.: (a) Schematic band structure of Cu_2O around the center of the first BZ. The terms of the form $\Gamma_i^\pm$ denote the symmetry of the wave functions in the different energy bands (cf. Refs. [12, 90, 169]). Different electronic excitations lead to a total of four exciton series. The yellow and green series are parity forbidden whereas the blue and violet series are allowed [30, 172]. Adapted from [30]. (b) The lowest conduction bands and uppermost valence bands stem from the $3d$ and $4s$ orbitals of the Cu atoms and from the $2p$ orbital of the O atoms. Adapted from [173]. Note that there are different results regarding the origin of the Γ_8^- conduction band in the literature [30, 51, 168].

take the form of asymmetric Lorentzians for $n \lesssim 10$ and become Gaussian for very large values of n, both indicating the interactions with phonons [73, 74]. The theoretical calculation of the line widths of the peaks due to the exciton-phonon interaction will be topic of Chapter 3.

By fitting asymmetric Lorentzians to the experimental spectrum and neglecting the phonon background, the resonance energies E_n could be obtained in Ref. [30]. A comparison with Eq. (2.205) yielded $E_g = 2.17208\,\mathrm{eV}$ and $R_{\mathrm{exc}} = 92\,\mathrm{meV}$. A deviation of the peak areas from the predicted $(n^2-1)/n^5$-law [7, 171] for $n > 17$ was attributed to a dipole blockade effect preventing the excitation of an exciton in the vicinity of another exciton with a high quantum number. Other effects like ionization of the exciton due to thermal excitation or an invalidity of the dipole approximation due to the large exciton radius, which would also lead to such a deviation, were excluded since the line widths of the absorption peaks were much smaller than the energy separation between the observed states and the ionization continuum and since it was found that the blockade effect depends on the laser intensity.

At finite temperatures the density of states with its square root dependence on the energy appears in the absorption spectrum due to LO-phonon assisted processes [cf. also Eq. (2.96)]. The exciton states are then superimposed on this absorption band. Additionally, the exciton resonances are shifted towards lower energies in absorption spectra due to a decrease of the band gap with increasing temperature. In Fig. 2.16 we show the actual absorption spectrum of Cu_2O, where the phonon background has not been removed.

As can be seen from Fig. 2.14, the yellow and green exciton series share the same threefold degenerate Γ_5^+ orbital valence band state, which is split due to spin-orbit interaction into an upper

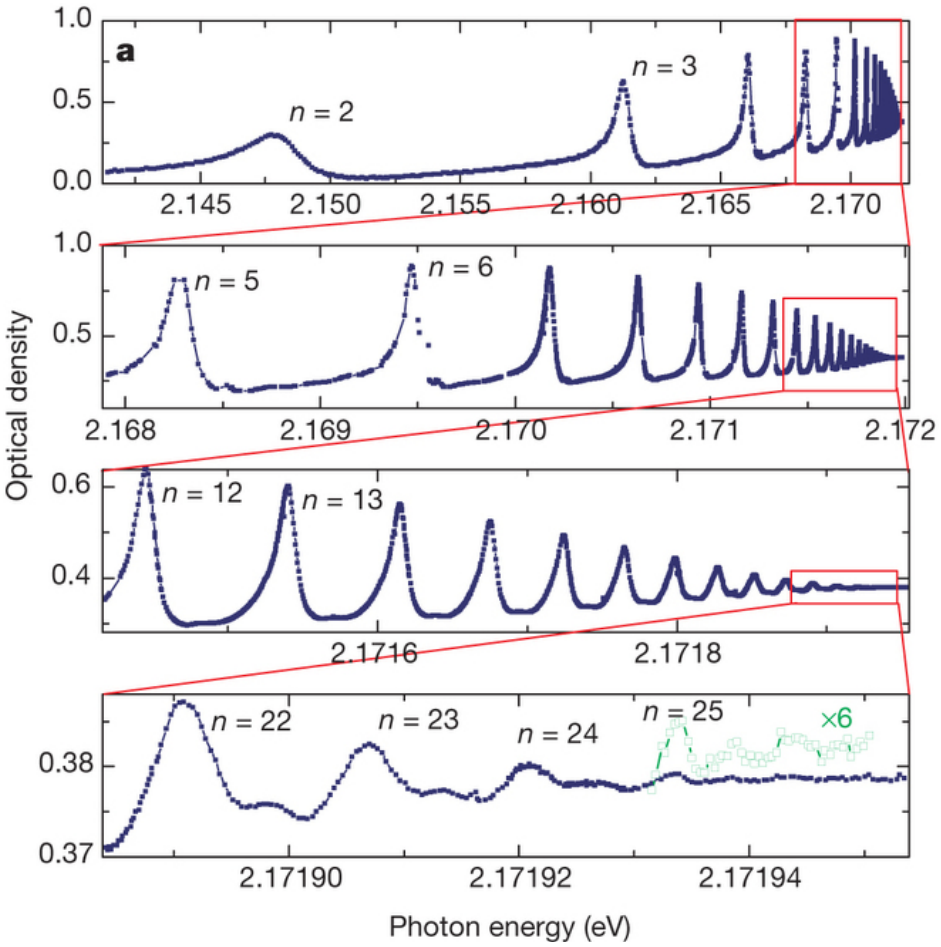

Figure 2.15.: Absorption spectrum of the yellow P exciton series at $T = 1.2\,\mathrm{K}$. Taken from [30].

twofold degenerate Γ_7^+ valence band (yellow series) and a lower fourfold degenerate Γ_8^+ valence band (green series). The band structure of both bands is essentially determined by the anisotropic dispersion properties of the orbital state. The threefold degeneracy of the orbital state is lifted as soon as a non-zero $\boldsymbol{k}$ vector gets involved, with new eigenvectors depending on the orientation of $\boldsymbol{k}$. A consequence of the splitting of the orbital state is a partial quenching of the spin-orbit interaction. This $\boldsymbol{k}$ dependent quenching is not only responsible for a remarkable non-parabolicity of the two top valence bands but leads likewise to a $\boldsymbol{k}$ dependent mixing of the Γ_7^+ and Γ_8^+ Bloch states and can thus cause a mixing of the yellow and green exciton series. The mixing of both series is favored by the large Rydberg energy of approximately 90 meV, a corresponding large exciton extension in k space and the small spin-orbit splitting of only 130 meV. We will present a thorough discussion of the effects of the non-parabolic valence band structure and the coupling of the yellow and green series in Chapters 4 and 6.

The ground states ($n = 1$) of the different exciton series do not match a hydrogen series. Due to their small radii, these excitons are intermediate excitons between a Frenkel and a Wannier exciton. To describe these states theoretically, the so-called central-cell corrections have to be introduced, which will be discussed in detail in Chapter 6.

The total symmetry of an exciton is determined not only by the symmetry of the bands but also

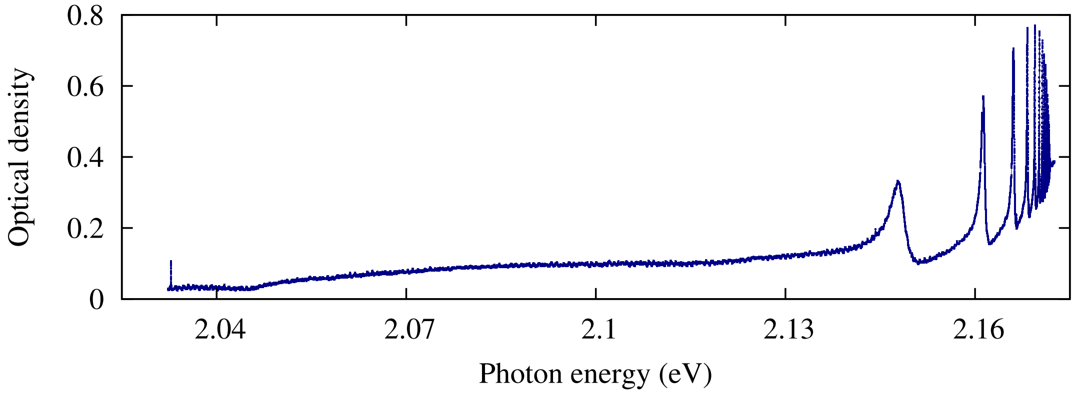

Figure 2.16.: Absorption spectrum of the yellow exciton series at $T = 1.2\,\mathrm{K}$ without subtracting the phonon background. One can furthermore see the weakly quadrupole-allowed $1S$ exciton as a very narrow line at $E \approx 2.032\,\mathrm{eV}$. Plotted with experimental data taken by the group of M. Bayer and D. Fröhlich.

by the symmetry of its envelope function [30, 90]:

$$\Gamma_{\mathrm{exc}} = \Gamma_{\mathrm{v}}(\mathrm{hole}) \otimes \Gamma_{\mathrm{c}}(\mathrm{electron}) \otimes \Gamma_{\nu}(\mathrm{envelope}) = \sum_{\alpha} c_\alpha \Gamma_\alpha . \tag{2.234}$$

Especially for the yellow exciton series with $\Gamma_{\mathrm{v}} = \Gamma_7^+$ and $\Gamma_{\mathrm{c}} = \Gamma_6^+$ it is

$$\Gamma_{\mathrm{exc}} = \Gamma_7^+ \otimes \Gamma_6^+ \otimes \Gamma_\nu = (\Gamma_5^+ \oplus \Gamma_2^+) \otimes \Gamma_\nu , \tag{2.235}$$

and we obtain for S excitons, i.e., excitons with zero angular momentum:

$$\Gamma_{\mathrm{exc}} = (\Gamma_5^+ \oplus \Gamma_2^+) \otimes \Gamma_1^+ = \Gamma_5^+ \oplus \Gamma_2^+ . \tag{2.236}$$

The S excitons of symmetry Γ_2^+ are called para-excitons as they do not have a spin-singlet component. The excitons of symmetry Γ_5^+ are called ortho-excitons. Due to the exchange interaction between the electron and the hole, the ortho-exciton is located 12 meV above the para-exciton [175, 176]. In several publications an additional splitting of the yellow $1S$ ortho-exciton has been reported and discussed in terms of an exchange interaction, which depends on the momentum $\hbar K$ of the exciton center of mass [82–84]. We will discuss the exchange interaction in Chapter 5 and show that the K-dependent terms are negligible small in $\mathrm{Cu_2O}$. Instead, the observed splitting has to be explained in terms of the cubic valence band structure as we will show in Chapter 4.

The impact of the valence band structure on the exciton spectrum is significantly stronger in external fields. Very recently, it has been shown for the yellow excitons in $\mathrm{Cu_2O}$ that a transition to quantum chaos takes place and that all antiunitary symmetries are broken when increasing the field strengths [31, 32]. This effect cannot be explained with a simple hydrogen-like model. We investigate in Chapter 7 at first the exciton spectra in an external magnetic field before we explain breaking of all antiunitary symmetries in Chapter 8.

Since the $1S$ exciton is dipole-forbidden in $\mathrm{Cu_2O}$, its lifetime is very long. However, an excitation of the ortho-exciton in quadrupole approximation is possible since the quadrupole operator has the symmetry $\Gamma_3^+ \oplus \Gamma_5^+$. One can weakly see an absorption peak for the $1S$ ortho-exciton in one-photon transition in Fig. 2.16. Although the quadrupole oscillator strength and thus the

Rabi energy [177] are small, the polariton effect for the $1S$ exciton exists and can be measured experimentally [178–180]. The small Rabi energy leads only to weak radiate broadening and an extremely sharp resonance in experiments [163, 178]. The polariton effects of the excitons in Cu_2O and especially of the $1S$ ortho-exciton will be discussed in Chapter 9.

As has been stated above, the para-exciton is spin-flip forbidden and cannot be excited optically [175]. Hence, its binding energy as well as its lifetime have to be deduced by a more difficult procedure [181–184]. The $1S$ para-exciton and $1S$ ortho-exciton states are coupled via an interconversion process, i.e., an exchange of particles between both states is enabled by acoustic phonons [185], which can be described by rate equations [87]. However, these conversion processes are temperature-dependent and can be neglected at very small temperatures ($T < 4\,\mathrm{K}$) [186, 187].

Excitons are generally treated in the low density regime. In the high density regime inter-particle interactions become important. This interaction leads to the formation of biexcitons [188] or of an electron-hole liquid [88]. However, both effects are inhibited in Cu_2O due to the electron-hole exchange interaction, which countervails the attractive interaction between two excitons. Therefore, Cu_2O is an interesting semiconductor regarding the investigation of excitons in the high density regime (see Ref. [163] and further references therein). Due to its long lifetime and its small radius, the para-exciton in Cu_2O is a promising candidate for excitonic Bose-Einstein condensation [28, 74, 189–191]. Although there were many attempts to verify the existence of such a condensate [192–196], there was no unambiguous proof of it [197]. More recent attempts to create an excitonic Bose-Einstein condensate in Cu_2O use harmonic strain traps [198, 199], which are inspired by the ion traps used for alkali ions [200]. Excitonic Bose-Einstein condensates are also investigated in microcavities [201, 202] and coupled quantum wells [203] of other semiconductors.

Intraexcitonic transitions, i.e., the equivalent of the hydrogen Lyman series, obey the known selection rules of atomic physics and have already been observed for Cu_2O [87]. The transition energies are located in the mean infrared range of light ($100 - 200\,\mathrm{meV}$). Interexcitonic transitions to other (green, blue, violet) exciton series are treated in Ref. [87], but have not been found experimentally.

Further topics in exciton spectroscopy on Cu_2O include, e.g.,

- direction-dependent and differing effective masses of para- and ortho-excitons [82–84, 179],
- phonoritons [204],
- the investigation of absolute luminescence in dependence on temperature [186, 205],
- and superfluid exciton transport as well as Bose-Einstein condensation (see Refs. [12, 74, 189] and further references therein).

All relevant material parameters of cuprous oxide, which will be needed in the numerical calculations of the subsequent Chapters 3 to 9, are listed in Table 2.2.

Table 2.2.: Material parameters used in the calculations of Chapters 3 to 9 unless otherwise stated.

band gap energy	$E_{\mathrm{g}} = 2.17208\,\mathrm{eV}$	[30]
electron mass	$m_{\mathrm{e}} = 0.99\,m_0$	[206]
hole mass	$m_{\mathrm{h}} = 0.58\,m_0$	[206]
spin-orbit coupling	$\Delta = 0.131\,\mathrm{eV}$	[37]
valence band parameters	$\gamma_1 = 1.76$	[37]
	$\gamma_2 = 0.7532$	[37]
	$\gamma_3 = -0.3668$	[37]
	$\eta_1 = -0.020$	[37]
	$\eta_2 = -0.0037$	[37]
	$\eta_3 = -0.0337$	[37]
fourth Luttinger parameter	$\kappa = -0.5$	Sec. 7.4
g-factor of conduction band	$g_{\mathrm{c}} = 2.1$	[207]
lattice constant	$a = 0.42696\,\mathrm{nm}$	[208]
dielectric constants	$\varepsilon_{\mathrm{s1}} = 7.5$	[97]
	$\varepsilon_{\mathrm{b1}} = \varepsilon_{\mathrm{s2}} = 7.11$	[97]
	$\varepsilon_{\mathrm{b2}} = 6.46$	[97]
exchange energy	$J_0 = 0.792\,\mathrm{eV}$	Sec. 6.2
central-cell correction	$V_0 = 0.539\,\mathrm{eV}$	Sec. 6.2
energy of Γ_4^--LO phonons	$\hbar\omega_{\mathrm{LO1}} = 18.7\,\mathrm{meV}$	[162]
	$\hbar\omega_{\mathrm{LO2}} = 87\,\mathrm{meV}$	[162]
Deformation potentials	$D_{\mathrm{e}} = 2.4\,\mathrm{eV}$	[209]
	$D_{\mathrm{h}} = 2.2\,\mathrm{eV}$	[209]
Mass density	$\rho = 6.09\,\frac{\mathrm{g}}{\mathrm{cm}^3}$	[97]
Sound wave velocity	$c_{\mathrm{LA}} = 4.5405 \times 10^3\,\frac{\mathrm{m}}{\mathrm{s}}$	[97]

3 Linewidths in excitonic absorption spectra of cuprous oxide

The main features, which make Cu_2O one of the most investigated semiconductors relating to excitons, are the large excitonic binding energy of $R_{\mathrm{exc}} \approx 86\,\mathrm{meV}$ [37] and the non-degeneracy of its uppermost valence band justifying the simple-band model with a hydrogen-like exciton spectrumgiven in Eq. (2.205). Beyond the simple-band model, one often has to account for a variety of further effects of the solid. Possible corrections of this model include, e.g., central-cell corrections [162], a coupling of the uppermost valence band to other valence bands [36, 72], and especially the interaction with phonons, which are the quasi-particles of lattice vibrations. This interaction is, besides the effect of impurities in the crystal, the main cause for an asymmetric broadening and shifting of the excitonic lines observed in absorption spectra [7]. The general theory for the effect of phonons on excitonic spectra has been developed by Toyozawa in the late 1950s and early 1960s [73–76].

When taking a look at the experimental hydrogen-like series of Cu_2O in Fig. 2.15, the asymmetric broadening due to phonons is clearly visible. However, the line widths differ from earlier theoretical calculations on this topic [74], which leads us to a new investigation of the main parameters describing the shape of the excitonic absorption lines.

In this chapter we present a theoretical calculation of the absorption spectrum of cuprous oxide based on the general theory developed by Y. Toyozawa. Having presented the basic theory of the electron-phonon and the exciton-phonon interaction in detail in Sec. 3.1, we discuss the main results of Toyozawa in Sec. 3.2. An inclusion not only of acoustic phonons but also of optical phonons and of specific properties of the excitons in Cu_2O like the central-cell corrections for the $1S$-exciton allows us in Sec. 3.3.1 to calculate the experimentally observed line widths. within the same order of magnitude. This demonstrates a clear improvement in comparison to earlier work on this topic. In contrast to these works, we perform calculations including all exciton states and make no approximations as regards the phonon wave vector [74, 210]. We also discuss in Sec. 3.3.2 a variety of further effects, which explain the still observable discrepancy between theory and experiment but which can hardly be included in theoretical calculations. Essential parts of this Chapter have been published in Ref. [33].

3.1 Electron-phonon interaction

In Chapter 2 the electron system and the ion system have been treated independently using the Born-Oppenheimer approximation of Sec. 2.1.3. If one allows the systems to exchange energy, a variety of effects can be observed[1] like [85]

- finite lifetimes of electrons in their single-particle states as they can emit phonons to get rid of their excess energy,
- a temperature-dependent electric conductivity due to scattering of electrons with phonons,
- the creation of a new quasi-particle, the so-called "electronic polaron" [220], which can be described as an electron sorrounded by a polarization cloud being due to polar electron-phonon coupling,
- the exchange of virtual phonons, which describes the fact that one electron can absorb the phonon emitted by another one, leading to an attractive electron-electron interaction, the formation of Cooper pairs and superconductivity.

In the Hamiltonian of the solid (2.26) the electron-ion interaction reads

$$H_{\mathrm{el-ion}} = \sum_{l\boldsymbol{n}\boldsymbol{\tau}} v(\boldsymbol{r}_l - \boldsymbol{R}_{\boldsymbol{n}\boldsymbol{\tau}}). \tag{3.1}$$

The movement of the ions is described by Eq. (2.33) with displacements $\boldsymbol{u}_{\boldsymbol{n}\boldsymbol{\tau}}$ being much smaller than the lattice constant. This allows us to perform a Taylor expansion of the interaction Hamiltonian:

$$H_{\mathrm{el-ion}} = \sum_{l\boldsymbol{n}\boldsymbol{\tau}} v(\boldsymbol{r}_l - \boldsymbol{R}^0_{\boldsymbol{n}\boldsymbol{\tau}}) - \sum_{l\boldsymbol{n}\boldsymbol{\tau}} \nabla_l v(\boldsymbol{r}_l - \boldsymbol{R}_{\boldsymbol{n}\boldsymbol{\tau}})|_{\boldsymbol{R}^0_{\boldsymbol{n}\boldsymbol{\tau}}} \cdot \boldsymbol{u}_{\boldsymbol{n}\boldsymbol{\tau}} + \dots . \tag{3.2}$$

The first term already appeared in the effective single-particle potential of the electrons. Neglecting terms of higher order, one arrives at the linear electron-phonon coupling

$$H_{\mathrm{el-ph}} = -\sum_{l\boldsymbol{n}\boldsymbol{\tau}} \nabla_l v(\boldsymbol{r}_l - \boldsymbol{R}_{\boldsymbol{n}\boldsymbol{\tau}})|_{\boldsymbol{R}^0_{\boldsymbol{n}\boldsymbol{\tau}}} \cdot \boldsymbol{u}_{\boldsymbol{n}\boldsymbol{\tau}}. \tag{3.3}$$

An expression for the lattice displacements in terms of annihilation and creation operators can be derived using Eqs. (2.61), (2.62), (2.73a) and (2.73b):

$$\boldsymbol{u}_{\boldsymbol{n}\boldsymbol{\tau}} = \frac{1}{\sqrt{NM_{\boldsymbol{\tau}}}} \sum_{s\boldsymbol{q}} \boldsymbol{e}^s_{\boldsymbol{\tau}}(\boldsymbol{q}) e^{i\boldsymbol{q}\cdot\boldsymbol{R}^0_{\boldsymbol{n}}} Q_s(\boldsymbol{q}) \tag{3.4a}$$

$$= \frac{1}{\sqrt{NM_{\boldsymbol{\tau}}}} \sum_{s\boldsymbol{q}} \boldsymbol{e}^s_{\boldsymbol{\tau}}(\boldsymbol{q}) e^{i\boldsymbol{q}\cdot\boldsymbol{R}^0_{\boldsymbol{n}}} \sqrt{\frac{\hbar}{2\omega_s(\boldsymbol{q})}} \left[a^\dagger_s(-\boldsymbol{q}) + a_s(\boldsymbol{q})\right]. \tag{3.4b}$$

The gradient of the potential v will be written as a Fourier series:

$$\sum_l \nabla_l v(\boldsymbol{r}_l - \boldsymbol{R}_{\boldsymbol{n}\boldsymbol{\tau}})|_{\boldsymbol{R}^0_{\boldsymbol{n}\boldsymbol{\tau}}} = \sum_{l\boldsymbol{\kappa}} i\boldsymbol{\kappa} v_{\boldsymbol{\kappa}} e^{i\boldsymbol{\kappa}\cdot(\boldsymbol{r}_l - \boldsymbol{R}^0_{\boldsymbol{n}\boldsymbol{\tau}})}. \tag{3.5}$$

---

[1] See also Refs. [94, 102, 129, 130, 211–219]

We now express the interaction in second quantization using Bloch states $|n\boldsymbol{k}\rangle$ [see Eq. (2.113)]:

$$\begin{aligned} H_{\text{el-ph}} &= \sum_{nn'\boldsymbol{k}\boldsymbol{k}'} \sum_{s\boldsymbol{q}} \sum_{\boldsymbol{\kappa}} \sum_{\boldsymbol{\tau}} \left[\sum_{\boldsymbol{n}} e^{i(\boldsymbol{q}-\boldsymbol{\kappa})\cdot \boldsymbol{R}^0_{\boldsymbol{n}\boldsymbol{\tau}}} \right] \langle n\boldsymbol{k}|\, e^{i\boldsymbol{\kappa}\cdot\boldsymbol{r}}\, |n'\boldsymbol{k}'\rangle \\ &\times \frac{1}{\sqrt{NM_{\boldsymbol{\tau}}}} \left[i v_{\boldsymbol{\kappa}} \boldsymbol{\kappa}\cdot \boldsymbol{e}^s_{\boldsymbol{\tau}}(\boldsymbol{q}) \right] \sqrt{\frac{\hbar}{2\omega_s(\boldsymbol{q})}} \left[a^\dagger_s(-\boldsymbol{q}) + a_s(\boldsymbol{q}) \right] c^\dagger_{n\boldsymbol{k}} c_{n'\boldsymbol{k}'}. \end{aligned} \tag{3.6}$$

Using Eq. (2.3) and performing the sum over $\boldsymbol{n}$ with

$$\sum_{\boldsymbol{n}} e^{i(\boldsymbol{q}-\boldsymbol{\kappa})\cdot\boldsymbol{R}^0_{\boldsymbol{n}}} = N \sum_{\boldsymbol{G}} \delta_{\boldsymbol{q}-\boldsymbol{\kappa},\,\boldsymbol{G}} \tag{3.7}$$

yields

$$\begin{aligned} H_{\text{el-ph}} &= \sum_{nn'\boldsymbol{k}\boldsymbol{k}'} \sum_{s\boldsymbol{q}} \sum_{\boldsymbol{G}} \sum_{\boldsymbol{\tau}} \left[\int \mathrm{d}^3\boldsymbol{r}\, \frac{1}{V} e^{-i\boldsymbol{k}\cdots\cdot\boldsymbol{r}} e^{i\boldsymbol{k}'\cdot\boldsymbol{r}} e^{i(\boldsymbol{q}-\boldsymbol{G})\cdot\boldsymbol{r}} u^*_{n\boldsymbol{k}}(\boldsymbol{r}) u_{n'\boldsymbol{k}'}(\boldsymbol{r}) \right] e^{-i(\boldsymbol{q}-\boldsymbol{G})\cdot\boldsymbol{\tau}} \\ &\times \left[i v_{\boldsymbol{q}-\boldsymbol{G}} (\boldsymbol{q}-\boldsymbol{G})\cdot \boldsymbol{e}^s_{\boldsymbol{\tau}}(\boldsymbol{q}) \right] \sqrt{\frac{\hbar N}{2M_{\boldsymbol{\tau}}\omega_s(\boldsymbol{q})}} \left[a^\dagger_s(-\boldsymbol{q}) + a_s(\boldsymbol{q}) \right] c^\dagger_{n\boldsymbol{k}} c_{n'\boldsymbol{k}'}. \end{aligned} \tag{3.8}$$

The integral contains apart from $e^{i(\boldsymbol{k}'-\boldsymbol{k}+\boldsymbol{q}-\boldsymbol{G})\cdot\boldsymbol{r}}$ only the lattice periodic term $u^*_{n\boldsymbol{k}}(\boldsymbol{r})u_{n'\boldsymbol{k}'}(\boldsymbol{r})$ and therefore vanishes unless $\boldsymbol{k}'-\boldsymbol{k}+\boldsymbol{q}-\boldsymbol{G}=\boldsymbol{0}$ holds [94]. We set

$$\int \mathrm{d}^3\boldsymbol{r}\, \frac{1}{V} e^{i(\boldsymbol{k}'-\boldsymbol{k}+\boldsymbol{q}-\boldsymbol{G})\cdot\boldsymbol{r}} u^*_{n\boldsymbol{k}}(\boldsymbol{r}) u_{n'\boldsymbol{k}'}(\boldsymbol{r}) = M_{\boldsymbol{k},\boldsymbol{q}-\boldsymbol{G}} \delta_{\boldsymbol{k}',\,\boldsymbol{k}-\boldsymbol{q}+\boldsymbol{G}} \tag{3.9}$$

and obtain

$$\begin{aligned} H_{\text{el-ph}} &= \sum_{nn'\boldsymbol{k}} \sum_{s\boldsymbol{q}} \sum_{\boldsymbol{G}} \sum_{\boldsymbol{\tau}} M_{\boldsymbol{k},\boldsymbol{q}-\boldsymbol{G}} \left[i v_{\boldsymbol{q}-\boldsymbol{G}} (\boldsymbol{q}-\boldsymbol{G})\cdot \boldsymbol{e}^s_{\boldsymbol{\tau}}(\boldsymbol{q}) \right] e^{-i(\boldsymbol{q}-\boldsymbol{G})\cdot\boldsymbol{\tau}} \\ &\times \sqrt{\frac{\hbar N}{2M_{\boldsymbol{\tau}}\omega_s(\boldsymbol{q})}} \left[a^\dagger_s(-\boldsymbol{q}) + a_s(\boldsymbol{q}) \right] c^\dagger_{n\boldsymbol{k}} c_{n'\boldsymbol{k}-\boldsymbol{q}+\boldsymbol{G}}. \end{aligned} \tag{3.10}$$

The linear electron-phonon interaction can finally be written in the form

$$H_{\text{el-ph}} = \sum_{nn'\boldsymbol{k}} \sum_{s\boldsymbol{q}} \sum_{\boldsymbol{G}} V_{s,\boldsymbol{k},\boldsymbol{q}-\boldsymbol{G}} \left[a^\dagger_s(-\boldsymbol{q}) + a_s(\boldsymbol{q}) \right] c^\dagger_{n\boldsymbol{k}} c_{n'\boldsymbol{k}-\boldsymbol{q}+\boldsymbol{G}} \tag{3.11}$$

Since $H_{\text{el-ph}}$ is linearly dependent on the phonon operators[2] and contains two electron operators, it describes a process, in which the scattering of an electron between two Bloch states takes place with the simultaneous absorption or emission of a phonon. The indices of the operators show that the total momentum is conserved. Depending on the momenta, there are two processes to be distinguished:

- Normal process: $\boldsymbol{k}'$ and $\boldsymbol{k}'+\boldsymbol{q}$ are within the first BZ. In this case the initial and final momentum do not differ much and are almost parallel.

---

[2] Due to its linear dependence on phonon operators, this Hamiltonian may be inappropriate for describing extremely strong coupling [7].

- Umklapp process: If $\boldsymbol{k}' + \boldsymbol{q}$ is outside the first BZ, it has to be brought back into the first BZ by adding a suitable reciprocal lattice vector $\boldsymbol{G}$. The final momentum of the electron is then almost antiparallel to the initial one. The Umklapp process plays an important role regarding the electric transport properties of a solid [HUN,SST]. Umklapp processes are more probable at higher temperatures due to the higher number of thermally excited phonons with large wave vectors.

One may note that energy conservation is not explicitly included in the Hamiltonian (3.10). This is due to the fact that we chose the Schrödinger picture[3] for our calculations and that the state vectors therefore contain the full time dependence [7].

3.1.1 Coupling mechanisms

We now want to calculate the coupling matrix elements $V_{s,\boldsymbol{k},\boldsymbol{q}-\boldsymbol{G}}$ for the interaction of electrons with different kinds of phonons.

Deformation potential coupling (acoustic phonons) Acoustic phonons of long wavelentgh cause a compression or dilation of the lattice leading to a local relative volume change

$$\Delta(\boldsymbol{r}) = \left.\frac{\Delta V}{V}\right|_{\boldsymbol{r}} . \tag{3.12}$$

Since the electronic band structure depends on the periodicity of the effective potential V_{eff} and thus on the periodicity of the lattice, a change in the volume will change the single-particle energies of the electrons. For reasons of simplicity, we assume the electron to be in a nondegenerate band deriving from atomic s orbitals. The local potential seen by the electrons and causing the electron-phonon interation then reads

$$H_{\mathrm{el-ph}}^{\mathrm{D}} = -D \sum_{l} \Delta(\boldsymbol{r}_l) \tag{3.13}$$

with the so-called deformation potential D, which is a constant on the order of a few eV. The change ΔV in the volume caused by the phonons can be expressed by the flux of the displacement field $\boldsymbol{u}(\boldsymbol{r})$ through the surface enlosing the volume V:

$$\Delta V = \oint \boldsymbol{u} \cdot \mathrm{d}\boldsymbol{A} = \int_V \nabla \cdot \boldsymbol{u}\, \mathrm{d}V. \tag{3.14}$$

In the limit of long wavelengths $\boldsymbol{u}(\boldsymbol{r})$ can be obtained from the displacement $\boldsymbol{u}_{\boldsymbol{n}\boldsymbol{\tau}}$ (3.4a) using an appropriate expression for $\boldsymbol{e}_{\boldsymbol{\tau}}^{s}(\boldsymbol{q})$ and replacing $\boldsymbol{R}_{\boldsymbol{n}}^{0}$ by $\boldsymbol{r}$ [85]. This leads to a description of acoustic phonon waves in a continuous form. The volume V is assumed to be small compared to the wavelength of the acoustic phonon and we can set $\Delta V = V\, \nabla \cdot \boldsymbol{u}$. We now write

$$H_{\mathrm{el-ph}}^{\mathrm{D}} = \sum_{l} H_{\mathrm{el-ph}}^{D(1)}(\boldsymbol{r}_l) \tag{3.15}$$

---

[3] In the Heisenberg picture the phonon creation and annihilation operators would read $a_s^{\dagger}(\boldsymbol{q},\, t) = a_s(\boldsymbol{q}) e^{i\omega_s(\boldsymbol{q})t}$ and $a_s(\boldsymbol{q},\, t) = a_s(\boldsymbol{q}) e^{-i\omega_s(\boldsymbol{q})t}$.

with

$$\begin{aligned} H^{\mathrm{D}(1)}_{\mathrm{el-ph}}(\boldsymbol{r}) &= -D\nabla\cdot\boldsymbol{u}(\boldsymbol{r}) \\ &= -D\frac{1}{\sqrt{NM_{\boldsymbol{\tau}}}}\sum_{s\boldsymbol{q}} Q_s(\boldsymbol{q},\,t)i\left[\boldsymbol{q}\cdot\boldsymbol{e}^{s}_{\boldsymbol{\tau}}(\boldsymbol{q})\right]e^{i\boldsymbol{q}\cdot\boldsymbol{r}} \\ &= -D\frac{1}{\sqrt{NM_{\boldsymbol{\tau}}}}\sum_{s\boldsymbol{q}}\sqrt{\frac{\hbar}{2\omega_s(\boldsymbol{q})}}i\left[\boldsymbol{q}\cdot\boldsymbol{e}^{s}_{\boldsymbol{\tau}}(\boldsymbol{q})\right]e^{i\boldsymbol{q}\cdot\boldsymbol{r}}\left[a_s(\boldsymbol{q})+a^\dagger_s(-\boldsymbol{q})\right] \end{aligned} \tag{3.16}$$

and s denoting only acoustic modes. On the one hand, if we use Eq. (2.63), we obtain a result that can be compared to, e.g., the corresponding equations in Refs. [96, 221]:

$$H^{\mathrm{D}(1)}_{\mathrm{el-ph}}(\boldsymbol{r}) = -D\frac{1}{\sqrt{NM_{\boldsymbol{\tau}}}}\sum_{\boldsymbol{q}}\sqrt{\frac{\hbar}{2\omega_{\mathrm{LA}}(\boldsymbol{q})}}\,i\boldsymbol{q}\cdot\left[\boldsymbol{e}^{s}_{\boldsymbol{\tau}}(\boldsymbol{q})a_{\mathrm{LA}}(\boldsymbol{q})e^{i\boldsymbol{q}\cdot\boldsymbol{r}} - \boldsymbol{e}^{s*}_{\boldsymbol{\tau}}(\boldsymbol{q})a^\dagger_{\mathrm{LA}}(\boldsymbol{q})e^{-i\boldsymbol{q}\cdot\boldsymbol{r}}\right]. \tag{3.17}$$

On the other hand, we can use the relations [85, 94]

$$\boldsymbol{e}^{\mathrm{LA}}_{\boldsymbol{\tau}}(\boldsymbol{q}) \parallel \boldsymbol{q}, \qquad \boldsymbol{e}^{\mathrm{TA}}_{\boldsymbol{\tau}}(\boldsymbol{q}) \perp \boldsymbol{q} \tag{3.18}$$

for longitudinal (LA) and transversal acoustic phonons (TA). Due to the scalar product $\boldsymbol{q}\cdot\boldsymbol{e}^{s}_{\boldsymbol{\tau}}(\boldsymbol{q})$, only LA phonons contribute to the interaction. With the expression[4] $\boldsymbol{e}^{\mathrm{LA}}_{\boldsymbol{\tau}}(\boldsymbol{q}) = i\sqrt{M_{\boldsymbol{\tau}}/M}\,\boldsymbol{q}/q$ and $M=\sum_{\boldsymbol{\tau}}M_{\boldsymbol{\tau}}$, it is

$$H^{\mathrm{D}(1)}_{\mathrm{el-ph}}(\boldsymbol{r}) = D\sum_{s\boldsymbol{q}}\sqrt{\frac{\hbar}{2NM\omega_{\mathrm{LA}}(\boldsymbol{q})}}\,q\,e^{i\boldsymbol{q}\cdot\boldsymbol{r}}\left[a_s(\boldsymbol{q})+a^\dagger_{\mathrm{LA}}(-\boldsymbol{q})\right]. \tag{3.19}$$

With the descriptions of Appendix A.2 and the electronic ground state (2.124a) we can write the Hamiltonian in second quantization. In effective-mass approximation, we may write the Bloch functions as [141]

$$\psi_{\boldsymbol{k}}(\boldsymbol{r}) = e^{i\boldsymbol{k}\cdot\boldsymbol{r}}u_{\boldsymbol{k}}(\boldsymbol{r}) \approx \frac{1}{\sqrt{V}}e^{i\boldsymbol{k}\cdot\boldsymbol{r}} \tag{3.20}$$

and obtain[5] due to Eq. (A.10):

$$\sum_{l} e^{i\boldsymbol{q}\cdot\boldsymbol{r}_l} \to \sum_{\boldsymbol{k}\boldsymbol{k}'}\left\langle\boldsymbol{k}\left|e^{i\boldsymbol{q}\cdot\boldsymbol{r}}\right|\boldsymbol{k}'\right\rangle c^\dagger_{\boldsymbol{k}}c_{\boldsymbol{k}'} \approx \sum_{\boldsymbol{k}\boldsymbol{k}'\boldsymbol{G}}\delta_{\boldsymbol{k}',\boldsymbol{k}-\boldsymbol{q}+\boldsymbol{G}}c^\dagger_{\boldsymbol{k}}c_{\boldsymbol{k}'} = \sum_{\boldsymbol{k}\boldsymbol{G}}c^\dagger_{\boldsymbol{k}}c_{\boldsymbol{k}-\boldsymbol{q}+\boldsymbol{G}}. \tag{3.21}$$

Finally, the deformation potential coupling reads

$$H^{\mathrm{D}}_{\mathrm{el-ph}} = \sum_{\boldsymbol{k}\boldsymbol{q}\boldsymbol{G}}V_{\mathrm{LA}}(\boldsymbol{q})\left[a_{\mathrm{LA}}(\boldsymbol{q})+a^\dagger_{\mathrm{LA}}(-\boldsymbol{q})\right]c^\dagger_{\boldsymbol{k}}c_{\boldsymbol{k}-\boldsymbol{q}+\boldsymbol{G}} \tag{3.22}$$

in second quantization with the coupling matrix element[6]

$$V_{\mathrm{LA}}(\boldsymbol{q}) = D\sqrt{\frac{\hbar}{2NM\omega_{\mathrm{LA}}(\boldsymbol{q})}}\,q = D\sqrt{\frac{\hbar}{2\rho V\omega_{\mathrm{LA}}(\boldsymbol{q})}}\,q = D\sqrt{\frac{\hbar}{2\rho Vc_{\mathrm{LA}}}}\,q^{\frac{1}{2}}. \tag{3.23}$$

---

[4] The expression $\boldsymbol{e}^{\mathrm{LA}}_{\boldsymbol{\tau}}(\boldsymbol{q}) = \sqrt{M_{\boldsymbol{\tau}}/M}\,\boldsymbol{q}/q$ in Ref. [85] cannot be correct due to Eq. (2.63). With Eqs. (2.60) and (2.63) the correct expression must read $\boldsymbol{e}^{\mathrm{LA}}_{\boldsymbol{\tau}}(\boldsymbol{q}) = i\sqrt{M_{\boldsymbol{\tau}}/M}\,\boldsymbol{q}/q$ in order to obtain the results in Refs. [7, 73].

[5] Note that we are dealing with electrons being in the same band. Hence, we neglect the band index n.

[6] We can use the expressions $V = Na^3$ and $\rho = M/a^3$ for the volume of the solid and the mass density, respectively, to replace NM by ρV.

The dispersion relation $\omega_{\mathrm{LA}}(\boldsymbol{q})$ has been chosen to be $\omega_{\mathrm{LA}}(\boldsymbol{q}) = c_{\mathrm{LA}}q$. This is valid for wave vectors being small compared to the extension of the first BZ (see Sec. 2.2.2). If the electrons considered are in energy bands originating from p or d atomic orbitals, one has to account for degeneracies resulting from the higher angular momentum. In this case $H^{D}_{\mathrm{el-ph}}$ becomes a matrix and coupling to transverse optical phonons becomes possible. Additionally, coupling between different bands also needs to be considered.

The general expression[7] of the deformation potential coupling for nondegenerate bands n, n' can be found in Ref. [7]:

$$H^{\mathrm{D}}_{\mathrm{el-ph}} = \sum_{nn'\boldsymbol{k}\boldsymbol{k}'} \Xi^{\mathrm{D}}_{nn'}(\boldsymbol{k},\, \boldsymbol{k}')c^{\dagger}_{n\boldsymbol{k}}c_{n'\boldsymbol{k}'} = \sum_{nn'\boldsymbol{k}\boldsymbol{k}'} \Xi^{\mathrm{D}}_{nn'}(\boldsymbol{k}-\boldsymbol{k}')c^{\dagger}_{n\boldsymbol{k}}c_{n'\boldsymbol{k}'} \tag{3.24}$$

with

$$\begin{aligned} \Xi^{\mathrm{D}}_{nn'}(\boldsymbol{k},\, \boldsymbol{k}') &= \int \mathrm{d}\boldsymbol{r}\, \psi^{*}_{n\boldsymbol{k}}(\boldsymbol{r})H^{\mathrm{D}(1)}_{\mathrm{el-ph}}(\boldsymbol{r})\psi_{n'\boldsymbol{k}'}(\boldsymbol{r}) \\ &= \sum_{\boldsymbol{q}\boldsymbol{G}} \sqrt{\frac{\hbar}{2\rho V \omega_{\mathrm{LA}}(\boldsymbol{q})}} D_{nn'}\, q\, \delta_{\boldsymbol{k}',\boldsymbol{k}-\boldsymbol{q}+\boldsymbol{G}} \left[a_{\mathrm{LA}}(\boldsymbol{q}) + a^{\dagger}_{\mathrm{LA}}(-\boldsymbol{q})\right]. \end{aligned} \tag{3.25}$$

The term $D_{nn'}$ denotes the respective deformation potential.

Fröhlich coupling (polar coupling with optical phonons) Longitudinal optical phonons crystals with differently charged constituents cause a polarization or a macroscopic polarization field

$$\boldsymbol{P}(\boldsymbol{r}) = \frac{\boldsymbol{M}(\boldsymbol{r})}{V}, \tag{3.26}$$

where $\boldsymbol{M}(\boldsymbol{r})$ denotes the electric dipole field. The electron, for reasons of simplicity assumed to be in one energy band, interacts with this polarization. In general, the interaction energy of a charge density $\rho(\boldsymbol{r})$ in a polarization field reads

$$E_{\mathrm{int}} = -\int \mathrm{d}\boldsymbol{r}\ \boldsymbol{P}(\boldsymbol{r}) \cdot \boldsymbol{E}(\boldsymbol{r}) \tag{3.27}$$

with

$$\boldsymbol{E}(\boldsymbol{r}) = -\nabla \int \mathrm{d}\boldsymbol{r}\ \frac{\rho(\boldsymbol{r}')}{4\pi\varepsilon_0\varepsilon_{\mathrm{b}}\left|\boldsymbol{r}-\boldsymbol{r}'\right|}. \tag{3.28}$$

Since the electrons are in the solid, the electric field (3.28) is scaled by the dielectric constant ε_{b} of the material at high frequencies. We perform a partial integration in (3.27) to write

$$E_{\mathrm{int}} = -\int \mathrm{d}\boldsymbol{r}\ \nabla\boldsymbol{P}(\boldsymbol{r}) \int \mathrm{d}\boldsymbol{r}'\ \frac{\rho(\boldsymbol{r}')}{4\pi\varepsilon_0\varepsilon_{\mathrm{b}}\left|\boldsymbol{r}-\boldsymbol{r}'\right|}. \tag{3.29}$$

The macroscopic dipole moment caused by longitudinal optical phonons in a crystal with a Wigner-Seitz cell consisting of two ions reads

$$\boldsymbol{M} = \sum_{\boldsymbol{n}\boldsymbol{\tau}} \eta_{\boldsymbol{\tau}}\boldsymbol{u}_{\boldsymbol{n}\boldsymbol{\tau}} \tag{3.30}$$

---

[7] Note that the notations and definitions for phonons in Ref. [7] differ from those in Ref. [85]. Therefore, the given expression has been obtained by comparing the notations of both references and adapting the formula of Ref. [7] to the derivations described above and to the results in Ref. [73].

with the dynamical effective charges of the moving ions determined within linear response theory [85]:

$$\eta_1 = -\eta_2 = \eta = \sqrt{\frac{\mu V \varepsilon_0}{N}\left(\frac{1}{\varepsilon_\mathrm{b}} - \frac{1}{\varepsilon_\mathrm{s}}\right)}\,\varepsilon_\mathrm{b}\omega_\mathrm{LO}. \tag{3.31}$$

The frequency ω_LO can be treated as a constant factor in the case of small phonon wave vectors or in the limit of long wavelengths. We denote by $\mu = (1/M_1 + 1/M_2)^{-1}$ the reduced mass of the two ions while ε_s and ε_b denote the values of the dielectric function $\varepsilon(\omega)$ for $\omega \ll \omega_\mathrm{LO}$ and $\omega \gg \omega_\mathrm{LO}$, respectively. The displacement $\boldsymbol{u_{n\tau}}$ (3.4a) reads

$$\boldsymbol{u_{n\tau}} = \frac{1}{\sqrt{NM_{\boldsymbol{\tau}}}} \sum_{s\boldsymbol{q}} \boldsymbol{e}_{\boldsymbol{\tau}}^\mathrm{LO}(\boldsymbol{q}) Q_\mathrm{LO}(\boldsymbol{q}) e^{i\boldsymbol{q}\cdot\boldsymbol{R}_{\boldsymbol{n}}^0} \tag{3.32}$$

with the eigenvectors

$$\boldsymbol{e}_1^\mathrm{LO}(\boldsymbol{q}) = -i\sqrt{\frac{M_2}{M}}\frac{\boldsymbol{q}}{q} \quad \text{and} \quad \boldsymbol{e}_2^\mathrm{LO}(\boldsymbol{q}) = i\sqrt{\frac{M_1}{M}}\frac{\boldsymbol{q}}{q}. \tag{3.33}$$

Replacing $\boldsymbol{R}_{\boldsymbol{n}}^0$ by $\boldsymbol{r}$ and the sum over $\boldsymbol{n}$ by N, we obtain

$$\nabla\boldsymbol{P}(\boldsymbol{r}) = \frac{\eta}{V}\sum_{\boldsymbol{q}}\sqrt{\frac{N}{\mu}}\,q\,Q_\mathrm{LO}(\boldsymbol{q})e^{i\boldsymbol{q}\cdot\boldsymbol{r}}. \tag{3.34}$$

The charge density of the electrons reads

$$\rho(\boldsymbol{r}) = -\frac{e}{V}\sum_{l\boldsymbol{q}'} e^{i\boldsymbol{q}'\cdot(\boldsymbol{r}-\boldsymbol{r}_l)} \to -\frac{e}{V}\sum_{\boldsymbol{q}'} e^{i\boldsymbol{q}'\cdot\boldsymbol{r}} \sum_{\boldsymbol{kG}} c_{\boldsymbol{k}}^\dagger c_{\boldsymbol{k}+\boldsymbol{q}'+\boldsymbol{G}}. \tag{3.35}$$

We insert Eqs. (3.34) and (3.35) into Eq. (3.29) and perform the integrations,

$$\frac{1}{V}\int \mathrm{d}\boldsymbol{r}\int \mathrm{d}\boldsymbol{r}'\, e^{i\boldsymbol{q}\cdot\boldsymbol{r}} e^{i\boldsymbol{q}'\cdot\boldsymbol{r}'} \frac{1}{|\boldsymbol{r}-\boldsymbol{r}'|} = \frac{4\pi}{q^2}\delta_{\boldsymbol{q},-\boldsymbol{q}'}, \tag{3.36}$$

in order to write E_int as the Hamiltonian of the Fröhlich coupling [222, 223] in second quantization,

$$H_\mathrm{el-ph}^\mathrm{F} = \sum_{\boldsymbol{kqG}} V_\mathrm{LO}(\boldsymbol{q}) \left[a_\mathrm{LO}(\boldsymbol{q}) + a_\mathrm{LO}^\dagger(-\boldsymbol{q})\right] c_{\boldsymbol{k}}^\dagger c_{\boldsymbol{k}-\boldsymbol{q}+\boldsymbol{G}} \tag{3.37}$$

with the coupling matrix element

$$V_\mathrm{LO}(\boldsymbol{q}) = \sqrt{\frac{e^2\hbar\omega_\mathrm{LO}}{2V\varepsilon_0}\left(\frac{1}{\varepsilon_\mathrm{b}} - \frac{1}{\varepsilon_\mathrm{s}}\right)}\,\frac{1}{q}. \tag{3.38}$$

One can now define the Fröhlich coupling constant

$$\alpha^\mathrm{F} = \frac{e^2}{8\pi\varepsilon_0\hbar\omega_\mathrm{LO}}\sqrt{\frac{2m^*\omega_\mathrm{LO}}{\hbar}}\left(\frac{1}{\varepsilon_\mathrm{b}} - \frac{1}{\varepsilon_\mathrm{s}}\right), \tag{3.39}$$

which quantifies the strength of the interaction and depends on ω_LO, the effective mass m^* of the electrons and the polarity entering via $(1/\varepsilon_\mathrm{b} - 1/\varepsilon_\mathrm{s})$. Depending on the size of α^F, one distinguishes between the weak couling regime ($\alpha^{\mathrm{F}} < 1$) and the strong coupling regime ($\alpha^{\mathrm{F}} > 1$). In the first case the interaction can be treated using perturbation theory. This leads to a new quasi-particle, the so-called polaron[8], which represents an electron plus a sorrounding phonon cloud. Its energy dispersion reads

$$E^{\mathrm{P}}(\boldsymbol{k}) = -\alpha^{\mathrm{F}}\hbar\omega_{\mathrm{LO}} + \frac{\hbar^2\boldsymbol{k}^2}{2m^*}\left(1 - \frac{\alpha^{\mathrm{F}}}{6}\right) \tag{3.40}$$

in first order perturturbation theory. The polaron mass and its radius are given by

$$m^{\mathrm{P}} = m^*\left(1 - \frac{\alpha^{\mathrm{F}}}{6}\right)^{-1} \tag{3.41}$$

and

$$a^{\mathrm{P}} = \sqrt{\frac{\hbar}{2m^*\omega_{\mathrm{LO}}}}, \tag{3.42}$$

respectively. In the latter case of the strong coupling regime special concepts have been developed, which are described, e.g., in Ref. [227].

The general expression of the Fröhlich coupling for nondegenerate bands n, n' reads according to Ref. [7]

$$H^{\mathrm{D}}_{\mathrm{el-ph}} = \sum_{nn'\boldsymbol{k}\boldsymbol{k}'} \Xi_{nn'}(\boldsymbol{k},\,\boldsymbol{k}')c^\dagger_{n\boldsymbol{k}}c_{n'\boldsymbol{k}'} = \sum_{nn'\boldsymbol{k}\boldsymbol{k}'} \Xi_{nn'}(\boldsymbol{k}-\boldsymbol{k}')c^\dagger_{n\boldsymbol{k}}c_{n'\boldsymbol{k}'} \tag{3.43}$$

with

$$\begin{aligned}\Xi^{\mathrm{F}}_{nn'}(\boldsymbol{k},\,\boldsymbol{k}') &= \int \mathrm{d}\boldsymbol{r}\,\psi^*_{n\boldsymbol{k}}(\boldsymbol{r})H^{\mathrm{F}(1)}_{\mathrm{el-ph}}(\boldsymbol{r})\psi_{n'\boldsymbol{k}'}(\boldsymbol{r}) \\ &= \sum_{\boldsymbol{q}\boldsymbol{G}}\sqrt{\frac{e^2\hbar\omega_{\mathrm{LO}}(\boldsymbol{q})}{2V\varepsilon_0}\left(\frac{1}{\varepsilon_{\mathrm{b}}} - \frac{1}{\varepsilon_{\mathrm{s}}}\right)}\,\frac{1}{q}\,\delta_{\boldsymbol{k}',\boldsymbol{k}-\boldsymbol{q}+\boldsymbol{G}}\left[a_s(\boldsymbol{q}) + a^\dagger_s(-\boldsymbol{q})\right].\end{aligned} \tag{3.44}$$

Piezoelectric coupling (acoustic phonons) If the lattice of the solid does not show inversion symmetry, a third coupling mechanism between electrons and phonons occurs: the piezoelectric coupling. In this case an externally applied homogeneous strain will cause a dielectric polarization

$$P_i = \sum_{i,j} e_{ijk}\epsilon_{jk}, \tag{3.45}$$

which is determined by the product of the piezoelectric tensor (e_{ijk}) and the strain tensor (ϵ_{jk}). Expressing the strain tensor via the displacement fields and assuming for simplicity a zincblende structure with[9] $e_{ijk} = e_{14}\,|\varepsilon_{ijk}|$, one can derive the Hamiltonian [85]

$$H^{\mathrm{P}}_{\mathrm{el-ph}} = \sum_{s\boldsymbol{k}\boldsymbol{q}\boldsymbol{G}} V_s(\boldsymbol{q})\left[a_s(\boldsymbol{q}) + a^\dagger_s(-\boldsymbol{q})\right]c^\dagger_{\boldsymbol{k}}c_{\boldsymbol{k}-\boldsymbol{q}+\boldsymbol{G}}, \tag{3.46}$$

which describes the piezoelectric coupling of acoustic phonons and electrons. The coupling matrix element reads

$$V_s(\boldsymbol{q}) = -\frac{2ee_{14}}{\varepsilon_0\varepsilon_\infty}\sqrt{\frac{\hbar N}{2Mv_s}}\,q^{-\frac{1}{2}}\left(\frac{q_xq_ye^s_z(\boldsymbol{q}) + q_zq_xe^s_y(\boldsymbol{q}) + q_yq_ze^s_x(\boldsymbol{q})}{q^2}\right) \tag{3.47}$$

with the sound velocities v_s of the different phonon branches s.

---

[8] For more information see, in particular, Refs. [85, 94, 224–226] and further references therein.

[9] The piezoelectric constant is given in Voigt notation. ε_{ijk} denotes the complete antisymmetric tensor or Levi-Civita symbol.

3.1.2 Lifetime

As it was already mentioned, the interaction between electrons and phonons leads to a finite lifetime of an electron in a single-particle state. In the limit of weak coupling one can treat this interaction as a perturbation. In the interaction picture the phonon operators are time-dependent:

$$a_s(\boldsymbol{q},\, t) = e^{iH_0 t/\hbar} a_s(\boldsymbol{q},\, 0) e^{-iH_0 t/\hbar} = a_s(\boldsymbol{q},\, 0) e^{-i\omega_s(\boldsymbol{q})t}. \tag{3.48}$$

The operator $H_{\mathrm{el-ph}}$ then describes a timely periodic interaction and one can use Fermi's Golden Rule (cf. Sec. 2.4.3), giving the scattering rate

$$r_{n\boldsymbol{k},n'\boldsymbol{k}'} = \frac{2\pi}{\hbar} \left|\left\langle n\boldsymbol{k} \left| H_{\mathrm{el-ph}} \right| n'\boldsymbol{k}' \right\rangle\right|^2 \delta(E_n(\boldsymbol{k}) - E_{n'}(\boldsymbol{k}') - \Delta E) \tag{3.49}$$

between the two Bloch states $|n\boldsymbol{k}\rangle$, $|n'\boldsymbol{k}'\rangle$ with energies $E_n(\boldsymbol{k})$, $E_{n'}(\boldsymbol{k}')$. ΔE represents the energy change if the scattering is inelastic. Considering the scattering from the state $|n\boldsymbol{k}\rangle$ to all other possible states $|n'\boldsymbol{k}'\rangle$ the single-particle lifetime $\tau_{n\boldsymbol{k}}$ is given by

$$\frac{1}{\tau_{n\boldsymbol{k}}} = \sum_{n'\boldsymbol{k}'} r_{n\boldsymbol{k},n'\boldsymbol{k}'} \left[1 - f(n'\boldsymbol{k}')\right] \tag{3.50}$$

with the distribution function $f(n'\boldsymbol{k}')$. In the special case of one electron being in an otherwise empty band $f(n'\boldsymbol{k}') = 0$ holds. The finite lifetime leads to a level broadening of the single-particle energy levels.

We now make use of the one-band approximation of Sec. 3.1.1 and restrict ourselves to normal processes. Calculating the matrix element in (3.49) and expressing the number of phonons in the mode $s\boldsymbol{q}$ by $n_s(\boldsymbol{q})$, the inverse lifetime is given by [85]

$$\frac{1}{\tau_{\boldsymbol{k}}} = \frac{2\pi}{\hbar} \sum_{s,\boldsymbol{q}} |V_s(\boldsymbol{q})|^2 \left[1 - f(\boldsymbol{k}+\boldsymbol{q})\right] \tag{3.51}$$

$$\left[n_s(\boldsymbol{q}) + \frac{1}{2} \mp \frac{1}{2}\right] \delta(E(\boldsymbol{k}) - E(\boldsymbol{k}+\boldsymbol{q}) \mp \hbar\omega_s(\boldsymbol{q})). \tag{3.52}$$

In the case of phonon absorption (emission) the upper (lower) sign applies. Since it is $\omega_{\mathrm{LA/TA}} \ll \omega_{\mathrm{LO/TO}}$, the scattering with optical phonons leads to a considerable change in the electron energy while the scattering with acoustic phonons can be regarded as almost elastic as long as $E(\boldsymbol{k}) \gg \hbar\omega_s(\boldsymbol{q})$ holds. There are two important processes caused by electron-phonon interaction, which are further treated in literature:

- energy relaxation of an optically excited electron in the conduction band [130, 228–231],
- scattering of electrons in electric transport, which is described by the Boltzmann equation and leads to an expression for the electric conductivity of a material [85, 86, 232–235].

3.1.3 Exciton-phonon interaction

The interaction between excitons and phonons will lead to a shift and an inhomogeneous broadening of absorption lines. The line broadening is caused by the fact that the momentum conservation $\boldsymbol{\kappa} = \boldsymbol{K} + \boldsymbol{G}$ is replaced by $\boldsymbol{\kappa} \pm \boldsymbol{q} = \boldsymbol{K} + \boldsymbol{G}$ with an arbitrary phonon wave vector $\boldsymbol{q}$ (see Fig. 3.1). In this section we derive the Hamiltonain of the exciton-phonon interaction in second quantization.

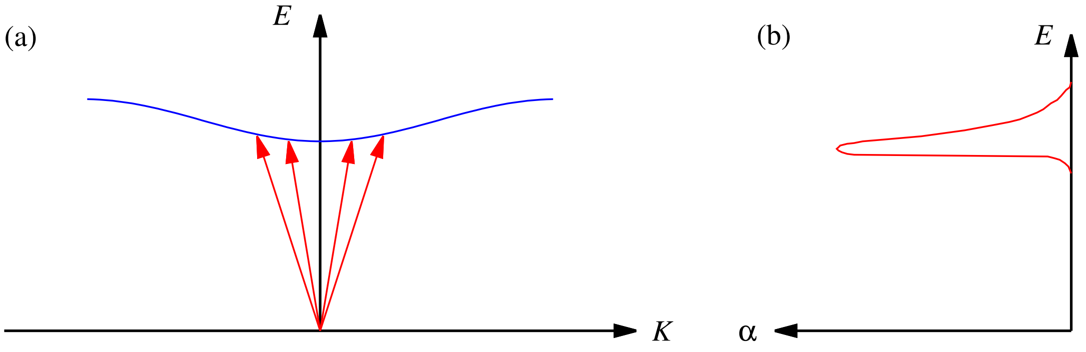

Figure 3.1.: The change of the momentum conservation rule from $\boldsymbol{\kappa} = \boldsymbol{K} + \boldsymbol{G}$ to $\boldsymbol{\kappa} \pm \boldsymbol{q} = \boldsymbol{K} + \boldsymbol{G}$ when accounting for phonons leads to an inhomogeneous line broadening. μ denotes the absorption coefficient. Adapted from [7].

The influence of phonons on absorption spectra will then be discussed in the subsequent sections of this Chapter.

At first, we will use Eqs. (3.3) and (3.4a) to write the electron-phonon Hamiltonian in a more simple form:

$$H_{\mathrm{el-ph}} = \sum_{s\boldsymbol{q}} \tilde{H}_s(\boldsymbol{q})\, Q_s(\boldsymbol{q}). \tag{3.53}$$

It can be shown that the term $\tilde{H}_s(\boldsymbol{q})$ is not completely symmetric under lattice translations $\boldsymbol{R} \to \boldsymbol{R} + \boldsymbol{a}$ but acquires a phase of $e^{-i\boldsymbol{q}\boldsymbol{a}}$ [7]. This is the reason why it couples electronic states $|n\boldsymbol{k}\rangle$ and $|n'\boldsymbol{k}'\rangle$ with wave vectors fulfilling[10] $\boldsymbol{k} = \boldsymbol{k}' + \boldsymbol{q} - \boldsymbol{G}$. Now the same conclusion will also hold for excitonic states. Therefore, we write the exciton phonon Hamiltonian in the following form:

$$\begin{aligned} H_{\mathrm{exc-ph}} &= \sum_{s\boldsymbol{q}\boldsymbol{G}} \sum_{\nu\boldsymbol{K}} \sum_{\nu'\boldsymbol{K}'} \left\langle \Psi_{\nu\boldsymbol{K}} \middle| \tilde{H}_s(\boldsymbol{q}) \middle| \Psi_{\nu'\boldsymbol{K}'} \right\rangle Q_s(\boldsymbol{q}) B^{\dagger}_{\nu\boldsymbol{K}} B_{\nu'\boldsymbol{K}'} \\ &= \sum_{s\boldsymbol{q}\boldsymbol{G}} \sum_{\nu\boldsymbol{K}} \sum_{\nu'\boldsymbol{K}'} \delta_{\boldsymbol{q},\boldsymbol{K}-\boldsymbol{K}'+\boldsymbol{G}} G_{\sigma\boldsymbol{q}}(\nu\boldsymbol{K},\, \nu'\boldsymbol{K}') \left(\frac{2\omega_s(\boldsymbol{q})}{\hbar}\right)^{\frac{1}{2}} Q_s(\boldsymbol{q}) B^{\dagger}_{\nu\boldsymbol{K}} B_{\nu'\boldsymbol{K}'} \\ &= \sum_{s\boldsymbol{q}\boldsymbol{G}} \sum_{\nu\boldsymbol{K}} \sum_{\nu'\boldsymbol{K}'} \delta_{\boldsymbol{q},\boldsymbol{K}-\boldsymbol{K}'+\boldsymbol{G}} G_{\sigma\boldsymbol{q}}(\nu\boldsymbol{K},\, \nu'\boldsymbol{K}') \left[a^{\dagger}_s(-\boldsymbol{q}) + a_s(\boldsymbol{q})\right] B^{\dagger}_{\nu\boldsymbol{K}} B_{\nu'\boldsymbol{K}'}. \end{aligned} \tag{3.54}$$

In the last step we made use of the relations (2.73a) and (2.73b). We intentionally left out matrix elements of the form $\langle \Psi_{\nu\boldsymbol{K}} | \tilde{H}_s(\boldsymbol{q}) | \Phi_0 \rangle$, i.e., those including the electronic ground state[11], since the energy of phonons is too small to excite an exciton out of the ground state.

To determine the coupling constant $G_{\sigma\boldsymbol{q}}(\nu\boldsymbol{K},\, \nu'\boldsymbol{K}')$, we write the Hamiltonian (3.53) as a sum over one-electron Hamiltonians:

$$H_{\mathrm{el-ph}} = \sum_{l} H^{(1)}_{\mathrm{el-ph}}(\boldsymbol{r}_l). \tag{3.55}$$

---

[10] This has been shown in Sec. 3.1 in connection with Eqs. (3.8) and (3.9).

[11] Compare also the explanations in connection with Eq. (7.2b).

Via the relations (2.145), (2.154a) and (2.157), we obtain an expression for the interaction matrix element, which allows us to use the results of Sec. 3.1.1:

$$\begin{aligned}\sum_{s\boldsymbol{q}} \left\langle \Psi_{\nu\boldsymbol{K}} \left| \tilde{H}_s(\boldsymbol{q}) \right| \Psi_{\nu'\boldsymbol{K}'} \right\rangle Q_s(\boldsymbol{q}) &= \sum_{\boldsymbol{\beta},\boldsymbol{\beta}'} U^*_{mn\,\nu\boldsymbol{K}}(\boldsymbol{\beta}) U_{m'n'\,\nu'\boldsymbol{K}'}(\boldsymbol{\beta}') \\ &\times \left(\frac{1}{N} \sum_{\boldsymbol{k}} e^{i(\boldsymbol{\beta}-\boldsymbol{\beta}')\cdot\boldsymbol{k}+i\boldsymbol{\beta}'\cdot(\boldsymbol{K}-\boldsymbol{K}')}\, \Xi_{nn'}(\boldsymbol{k},\boldsymbol{k}-\boldsymbol{K}+\boldsymbol{K}') \right. \\ &\left. -\frac{1}{N} \sum_{\boldsymbol{k}} e^{i(\boldsymbol{\beta}-\boldsymbol{\beta}')\cdot\boldsymbol{k}}\, \Xi_{mm'}(\boldsymbol{k}-\boldsymbol{K}',\boldsymbol{k}-\boldsymbol{K}) \right) \qquad (3.56)\end{aligned}$$

with the scattering matrix elements

$$\Xi_{nn'}(\boldsymbol{k},\,\boldsymbol{k}') = \int \mathrm{d}\boldsymbol{r}\, \psi^*_{n\boldsymbol{k}}(\boldsymbol{r}) H^{(1)}_{\text{el-ph}}(\boldsymbol{r}) \psi_{n'\boldsymbol{k}'}(\boldsymbol{r}). \qquad (3.57)$$

These matrix elements can be replaced by the results for the deformation potential coupling or the Fröhlich coupling[12]. Since

$$\Xi_{nn'}(\boldsymbol{k},\,\boldsymbol{k}') = \Xi_{nn'}(\boldsymbol{k}-\boldsymbol{k}') \qquad (3.58)$$

holds for both interactions, we can write

$$\begin{aligned}H_{\text{exc-ph}} &= \sum_{\nu\boldsymbol{K}} \sum_{\nu'\boldsymbol{K}'} \left[q_{\text{e}}(mn\,\nu\boldsymbol{K},\, m'n'\,\nu'\boldsymbol{K}') \Xi_{nn'}(\boldsymbol{K}-\boldsymbol{K}') \right. \\ &\left. -q_h(mn\,\nu\boldsymbol{K},\, m'n'\,\nu'\boldsymbol{K}') \Xi_{mm'}(\boldsymbol{K}-\boldsymbol{K}') \right] B^\dagger_{\nu\boldsymbol{K}} B_{\nu'\boldsymbol{K}'} \qquad (3.59)\end{aligned}$$

with the *effective charges* of Ref. [73]

$$q_{\text{h}} = \sum_{\boldsymbol{\beta}} U^*_{mn\,\nu\boldsymbol{K}}(\boldsymbol{\beta}) U_{m'n'\,\nu'\boldsymbol{K}'}(\boldsymbol{\beta}), \qquad (3.60a)$$

$$q_{\text{e}} = \sum_{\boldsymbol{\beta}} U^*_{mn\,\nu\boldsymbol{K}}(\boldsymbol{\beta}) U_{m'n'\,\nu'\boldsymbol{K}'}(\boldsymbol{\beta}) e^{i(\boldsymbol{K}-\boldsymbol{K}')\cdot\boldsymbol{\beta}}. \qquad (3.60b)$$

If we now assume that scattering takes place only between excitons which are built from the same valence and conduction band ($n = n' = c$, $m = m' = v$), these expressions simply represent Fourier transforms of $F^*_\nu(\boldsymbol{\beta})F_\nu(\boldsymbol{\beta})$, i.e., of a kind of charge distribution, and describe the effective charge of the hole or electron noticed by a phonon. This can escpecially be seen from momentum conservation: In the case of normal processes ($\boldsymbol{G} = \boldsymbol{0}$), we can replace $\boldsymbol{K}-\boldsymbol{K}'$ by $\boldsymbol{q}$. Then the effective charges become very small if $\lambda = 2\pi/q < a_{\text{exc}}$ holds for the wavelength λ of the phonon.

Under the assumption that $n = n' = c$, $m = m' = v$ holds, our final result for the exciton-phonon interaction taking into consideration the deformation potential coupling and the Fröhlich coupling reads

$$H_{\text{exc-ph}} = \sum_{s\boldsymbol{q}\boldsymbol{G}} \sum_{\nu\boldsymbol{K}} \sum_{\nu'\boldsymbol{K}'} \delta_{\boldsymbol{q},\boldsymbol{K}-\boldsymbol{K}'+\boldsymbol{G}} G_{s\boldsymbol{q}}(\nu\boldsymbol{K},\,\nu'\boldsymbol{K}') \left[a^\dagger_s(-\boldsymbol{q}) + a_s(\boldsymbol{q}) \right] B^\dagger_{\nu\boldsymbol{K}} B_{\nu'\boldsymbol{K}'} \qquad (3.61)$$

with

$$\begin{aligned}G_{s\boldsymbol{q}}(\nu\boldsymbol{K},\,\nu'\boldsymbol{K}') &= \delta_{s,\text{LA}} \left(V_{\text{LA}}(\boldsymbol{q}) \left[q_{\text{e}}(\boldsymbol{K}-\boldsymbol{K}',\,\nu\nu') D_{cc} - q_{\text{h}}(\boldsymbol{K}-\boldsymbol{K}',\,\nu\nu') D_{vv} \right] \right) \\ &+ \delta_{s,\text{LO}} \left(V_{\text{LO}}(\boldsymbol{q}) \left[q_{\text{e}}(\boldsymbol{K}-\boldsymbol{K}',\,\nu\nu') - q_{\text{h}}(\boldsymbol{K}-\boldsymbol{K}',\,\nu\nu') \right] \right), \qquad (3.62)\end{aligned}$$

---

[12] See Eqs. (3.25) and (3.44).

the effective charges

$$q_{\mathrm{h}} = \sum_{\boldsymbol{\beta}} e^{-i\frac{m_{\mathrm{e}}}{M}(\boldsymbol{K}-\boldsymbol{K}')\cdot\boldsymbol{\beta}} F_{\nu}^{*}(\boldsymbol{\beta}) F_{\nu'}(\boldsymbol{\beta}), \qquad q_{\mathrm{e}} = \sum_{\boldsymbol{\beta}} e^{+i\frac{m_{\mathrm{h}}}{M}(\boldsymbol{K}-\boldsymbol{K}')\cdot\boldsymbol{\beta}} F_{\nu}^{*}(\boldsymbol{\beta}) F_{\nu'}(\boldsymbol{\beta}) \tag{3.63}$$

and the coupling matrix elements $V_{\mathrm{LA}}(\boldsymbol{q})$ and $V_{\mathrm{LO}}(\boldsymbol{q})$ [cf. Eqs. (3.23) and (3.38)].

3.1.4 Absorption spectra of excitons

The spectra of excitons or exciton-polaritons can be investigated in reflection, absorption and luminescence. A comparison of experimental results with theoretical models is often complicated since the surface of the solid has to be considered, in particular as regards reflection spectra. Hence, assumptions like an exciton-free layer have to be made and special boundary conditions for the components of electric and magnetic field of light at the surface of the solid are required [12]. By a complicated analysis of the line-shape one could determine all relevant parameters of the exciton-polariton like transverse and longitudinal eigenenergy, effective mass, oscillator strength and damping[13].

The luminescence from exciton-polaritons, i.e., the spontaneous emission of light as a consequence of electron–hole recombination, is also rather difficult to investigate [12]. Therefore, we will concentrate in the following on absorption spectra of exciton-polaritons in real solids.

Figure 3.2 shows as an example the absorption spectrum of gallium arsenide (GaAs). Absorption spectra of exciton-polariton resonances with small quantum numbers n are often difficult to measure due to a large absorption coefficient α in the region of the exciton resonance. The stray light of the spectrometer is often larger than the transmitted light intensity making an analysis of $\alpha(\omega)$ impossible for sample thicknesses of $d \gtrsim 1\,\mu\mathrm{m}$ [12]. On the other hand, the absorption can be measured easier for semiconductors with lower oscillator strengths as it is the case, e.g., for GaAs. In Fig. 3.2 one can clearly see the absorption peaks resulting from the $n = 1$, 2 and 3 levels with $L = 0$, which show the dependence $f \sim 1/n^3$ of the oscillator strength qualitatively (cf. Sec. 4.4.2).

Absorption spectrum neglecting phonons Neglecting the phononic part and surface effects, the excitonic absorption spectrum of allowed excitons can be calculated giving Elliot's formula [139],

$$\alpha(\omega) = \alpha_0^{(3)} \frac{2\hbar\omega}{R_{\mathrm{exc}}} \left[\sum_{n=1}^{\infty} \frac{4\pi}{n^3} \delta\left(\Delta + \frac{1}{n^2}\right) + \Theta(\Delta) \frac{\pi e^{\pi/\sqrt{\Delta}}}{\sinh(\pi/\sqrt{\Delta})} \right], \tag{3.64}$$

with the Heaviside step function $\Theta(\Delta)$ and the the dimensionless parameters $\Delta = (\hbar\omega - E_{\mathrm{g}})/R_{\mathrm{exc}}$ and $\alpha_0^{(3)}$. The first part of the absorption coefficient (3.64) describes the absorption due to the different exciton bound states and represents a number of δ-peaks with decreasing oscillator strength. The formula for the oscillator strength will be derived in Sec. 4.4.2. The second part is the continuum part, which can also be written as

$$\alpha_{\mathrm{cont}} = \alpha_{\mathrm{free}} C(\omega) \tag{3.65}$$

---

[13] Since the quantitative analysis of experimental reflection data is rather difficult, there are several other methods by which the dispersion relation of exciton polaritons can be measured more directly like, e.g., hyper-Raman scattering (HRS) and two-photon absorption (TPA) [12, 15, 17, 236–238]. Further methods can be found, e.g., in Ref. [12].

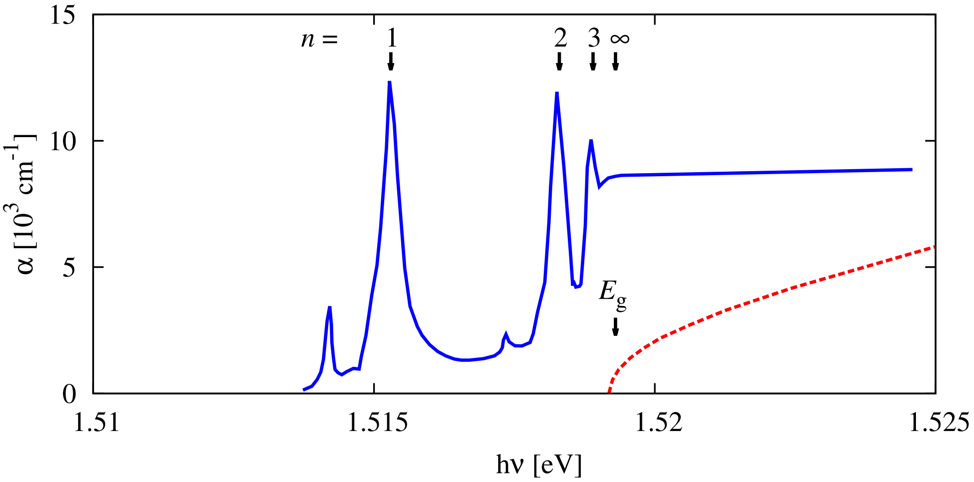

Figure 3.2.: Absorption spectrum of GaAs. The Coulomb interaction between electron and hole also affects the absorption above the band gap and clear deviations from the absorption calculated in single-particle approximation (dashed curve) can be observed. Adapted from [239].

with the absorption α_{free} of free carriers, i.e., of uncoupled electrons and holes, and the Sommerfeld enhancement factor

$$C(\omega) = \frac{\pi}{\sqrt{\Delta}} \frac{e^{\pi/\sqrt{\Delta}}}{\sinh(\pi/\sqrt{\Delta})}, \tag{3.66}$$

which describes the influence of the Coulomb interaction on the ionization continuum. At the band gap ($\hbar\omega = E_{\text{g}}$) the continuum absorption is independent of ω since

$$C(\omega) \to \frac{2\pi}{\sqrt{\Delta}} \quad \text{holds for} \quad \Delta \to 0. \tag{3.67}$$

This can be seen in Fig. 3.2. Hence, due to the Coulomb interaction there is a significant deviation from the square-root-like behavior expected from the density of states (2.96).

Absorption spectrum including phonons - Perturbation approach A complete theory for the absorption coefficient has to treat photons, excitons *and* phonons. The phonons will cause a shift and broadening[14] of the energy peaks described by Elliott's formula. This leads to the problem that higher exciton states cannot be resolved in absorption spectra but merge with the continuum if the temperature is too high, i.e., if too many phonons are thermally excited.

We start with the complete Hamiltonian

$$H_{\text{tot}} = H_{\text{exc}} + H_{\text{ph}} + H_{\text{rad}} + H_{\text{exc-rad}} + H_{\text{exc-ph}}, \tag{3.68}$$

which includes the exciton Hamiltonian H_{exc} given in Eq. (2.225), the phonon Hamiltonian H_{ph} given in Eq. (2.75), the photon Hamiltonian H_{rad} given in Eq. (2.191), the exciton-phonon interaction Hamiltonian $H_{\text{exc-ph}}$ given in Eq. (3.61), and the exciton-photon interaction Hamiltonian

---

[14] A large number of impurities or defects in a crystal cause an additional broadening.

$$H_{\mathrm{exc-rad}} = \sum_{\nu\boldsymbol{K}\,\xi\boldsymbol{\kappa}} \sum_{\boldsymbol{G}} \delta_{\boldsymbol{\kappa},\boldsymbol{K}+\boldsymbol{G}} C_{\xi\,\nu\boldsymbol{K}} \left[a^{\dagger}_{\xi\boldsymbol{\kappa}} B_{\nu\boldsymbol{K}} + a_{\xi\boldsymbol{\kappa}} B^{\dagger}_{\nu\boldsymbol{K}} \right], \tag{3.69}$$

which will be discussed in Chapter 9. We neglect the zero-point energies in the following and disregard Umklapp processes, i.e., we set $\boldsymbol{G} = \boldsymbol{0}$.

To obtain some first qualitative results and insights into the coupled system, we will treat both interactions as perturbations here [7] and consider transitions of the form

$$\begin{aligned} & |\ldots,\, m_{\xi\boldsymbol{\kappa}},\, \ldots;\ldots,\, 0_{\nu\boldsymbol{K}},\, \ldots;\ldots,\, n_{s\boldsymbol{q}},\, \ldots\rangle \\ \rightarrow\ & |\ldots,\, m_{\xi\boldsymbol{\kappa}} - 1,\, \ldots;\ldots,\, 1_{\nu\boldsymbol{K}},\, \ldots;\ldots,\, \tilde{n}_{s\boldsymbol{q}},\, \ldots\rangle\,, \end{aligned} \tag{3.70}$$

in which a photon in the mode $\xi\boldsymbol{\kappa}$ is absorbed and an exciton in the mode $\nu\boldsymbol{K}$ created with a simultaneous annihilation or creation of one phonon in the mode $s\boldsymbol{q}$. Note that all other exciton modes are unoccupied.

The perturbation $H_{\mathrm{exc-ph}}$ affects only those states, in which one electron is excited. In first-order time-independent perturbation theory various other states are admixed to one zero-order state[15]:

$$\begin{aligned} & |m_{\xi\boldsymbol{\kappa}} - 1; 1_{\nu\boldsymbol{K}}; \tilde{n}_{s\boldsymbol{q}}\rangle_1 = \\ & |m_{\xi\boldsymbol{\kappa}} - 1; 1_{\nu\boldsymbol{K}}; \tilde{n}_{s\boldsymbol{q}}\rangle_0 + \textstyle\sum_{s'\nu'\boldsymbol{K}'} G_{s'\boldsymbol{K}'-\boldsymbol{K}}(\nu'\boldsymbol{K}',\, \nu\boldsymbol{K}) \\ & \times \left[\tfrac{\sqrt{n_{s'\boldsymbol{K}'-\boldsymbol{K}}}}{E_{\nu\boldsymbol{K}} - E_{\nu'\boldsymbol{K}'} + \hbar\omega_{s'}(\boldsymbol{K}'-\boldsymbol{K})} \, |m_{\xi\boldsymbol{\kappa}} - 1; 1_{\nu'\boldsymbol{K}'}; \tilde{n}_{s'\boldsymbol{K}'-\boldsymbol{K}} - 1\rangle_0 \right. \\ & \left. + \tfrac{\sqrt{n_{s'\boldsymbol{K}-\boldsymbol{K}'}+1}}{E_{\nu\boldsymbol{K}} - E_{\nu'\boldsymbol{K}'} - \hbar\omega_{s'}(\boldsymbol{K}-\boldsymbol{K}')} \, |m_{\xi\boldsymbol{\kappa}} - 1; 1_{\nu'\boldsymbol{K}'}; \tilde{n}_{s'\boldsymbol{K}-\boldsymbol{K}'} + 1\rangle_0 \right]. \end{aligned} \tag{3.71}$$

We may now express the state $|m_{\xi\boldsymbol{\kappa}} - 1; 1_{\nu\boldsymbol{K}}; \tilde{n}_{s\boldsymbol{q}}\rangle_0$ by the states $|m_{\xi\boldsymbol{\kappa}} - 1; 1_{\nu\boldsymbol{K}}; \tilde{n}_{s\boldsymbol{q}}\rangle_1$ and insert it into the transition probability

$$W = \frac{2\pi}{\hbar} \sum_{f} \left| \langle m_{\xi\boldsymbol{\kappa}}; 0_{\nu\boldsymbol{K}}; n_{s\boldsymbol{q}} \left| H_{\mathrm{exc-rad}} \right| m_{\xi\boldsymbol{\kappa}} - 1; 1_{\nu\boldsymbol{K}}; \tilde{n}_{s\boldsymbol{q}}\rangle_0 \right|^2 \delta(\hbar\omega_{\boldsymbol{\kappa}} - E_{\nu\boldsymbol{K}} \pm \hbar\omega_s(\boldsymbol{q})), \tag{3.72}$$

in first order time-dependent perturbation theory for the transition given above. Leaving out the term without changes in the phonon occupation, we arrive at

$$W(\omega) = \frac{2\pi}{\hbar} \frac{1}{\omega} \sum_{\nu\boldsymbol{K}} \sum_{s,\pm} \left| \sum_{\nu'} \frac{\tilde{C}_{\xi\,\nu'\boldsymbol{K}} \tilde{G}^{\pm}_{s\boldsymbol{\kappa}-\boldsymbol{K}}(\nu'\boldsymbol{\kappa},\, \nu\boldsymbol{K})}{\hbar\omega - E_{\nu'\boldsymbol{\kappa}}} \right|^2 \delta(\hbar\omega - E_{\nu\boldsymbol{K}} \mp \hbar\omega_s\,(\pm[\boldsymbol{\kappa} - \boldsymbol{K}])) \tag{3.73}$$

with

$$\begin{aligned} \tilde{C}_{\xi\,\nu'\boldsymbol{K}} &= \sqrt{m_{\xi\boldsymbol{\kappa}}\omega}\, C_{\xi\,\nu'\boldsymbol{K}}, && (3.74\mathrm{a}) \\ \tilde{G}^{+}_{s\boldsymbol{\kappa}-\boldsymbol{K}}(\nu'\boldsymbol{\kappa},\, \nu\boldsymbol{K}) &= \sqrt{n_{s\boldsymbol{\kappa}-\boldsymbol{K}} + 1}\, G_{s\boldsymbol{\kappa}-\boldsymbol{K}}(\nu'\boldsymbol{\kappa},\, \nu\boldsymbol{K}), && (3.74\mathrm{b}) \\ \tilde{G}^{-}_{s\boldsymbol{\kappa}-\boldsymbol{K}}(\nu'\boldsymbol{\kappa},\, \nu\boldsymbol{K}) &= \sqrt{n_{s\boldsymbol{K}-\boldsymbol{\kappa}}}\, G_{s\boldsymbol{K}-\boldsymbol{\kappa}}(\nu'\boldsymbol{\kappa},\, \nu\boldsymbol{K}). && (3.74\mathrm{c}) \end{aligned}$$

---

[15] We leave out the dots for reasons of simplicity.

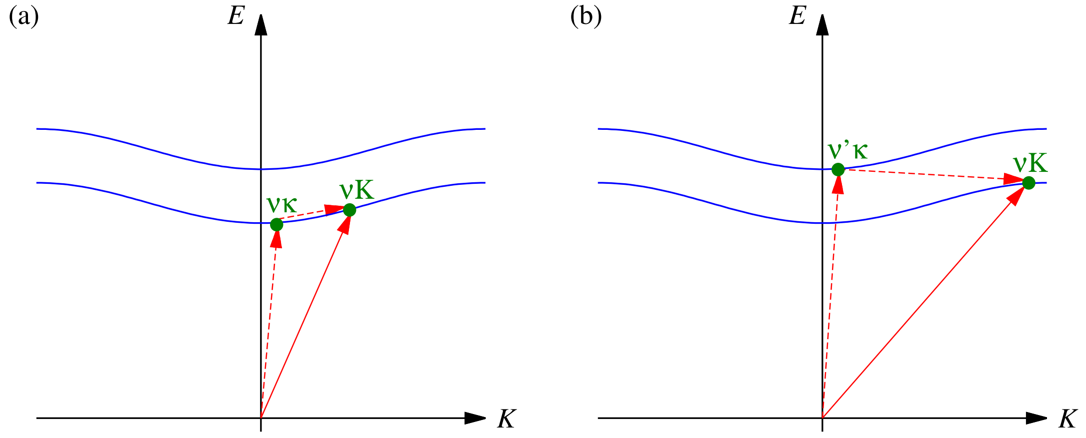

Figure 3.3.: (a) Intraband and (b) interband transition. For further information see text. Adapted from [7].

From this expression we conclude that in an absorption spectrum a large number of smaller lines will appear in the vicinity of the respective central lines. These smaller lines will be almost continuously distributed, for which reason broadened absorption peaks will appear close to the energies $E_{\nu \boldsymbol{K}}$ [7].

Depending on the value of ν' one distinguishes between intraband ($\nu = \nu'$) and interband ($\nu \neq \nu'$) scattering. These two processes are depicted in Fig. 3.3. If we separate the complete transition process (solid arrow) into two sub-processes (dotted arrows), we see that in an intraband transition an intermediate state $\nu\boldsymbol{\kappa}$ lies on the same excitonic energy band as the final state $\nu\boldsymbol{K}$. This process describes the broadening of the absorption peak corresponding to the band ν in the case of small phonon wave vectors. In an interband transition intermediate states $\nu'\boldsymbol{\kappa}$ of other excitonic energy bands are coupled to the state $\nu\boldsymbol{K}$. This process leads to additional broadenings of the absorption peaks corresponding to the bands ν'. For both transition processes the smallness of the denominator in Eq. (3.73) is of importance.

3.2 General theory of Toyozawa

After this introductory part on the exciton-phonon interaction and absorption spectra, we will now present the results of the general theory of Toyozawa, which has been developed[16] in the late 1950's and early 1960's [73–76]. Using a generalized form of the damping theory of van Hove [240] and assuming that the energy shift and broadening of the excitons lines are small in comparison to the energy separation of the exciton states, Toyozawa derived a general expression for the absorption coefficient, which considers the effect of $H_{\mathrm{exc-ph}}$ up to infinite order of perturbation theory.[17]

As has been discussed in Secs. 3.1.1 and 3.1.3, the exciton couples to two different kinds of phonons: to longitudinal acoustic phonons (LA) via deformation potential coupling [221] and to longitudinal optical phonons (LO) via Fröhlich coupling [242]. For both interactions the interaction

---

[16] Note the remark in Ref. [75] that the theory presented in Ref. [73] contains an indefensible assumption. Consequently, we present the results of the general theory of Ref. [74].

[17] A recent investigation on the exciton-phonon interaction using the theory of master equations yielded the same results [241].

Hamiltonian is of the same form in second quantization

$$H_{\mathrm{exc-ph}} \;=\; i\sum_{\boldsymbol{q}}\sum_{\nu\nu'\boldsymbol{K}} \lambda_s(\boldsymbol{q},\,\nu\nu')\left[a_s(\boldsymbol{q}) - a_s^\dagger(-\boldsymbol{q})\right] B^\dagger_{\nu\boldsymbol{K}} B_{\nu'\boldsymbol{K}-\boldsymbol{q}}. \tag{3.75}$$

By $a_s^{(\dagger)}(\boldsymbol{q})$ we denote the operators annihilating (creating) a phonon in the mode $s\boldsymbol{q}$. The operators $B^{(\dagger)}_{\nu\boldsymbol{K}}$ annihilate (create) excitons with momentum $\hbar\boldsymbol{K}$ in the state $|\nu\rangle = |nLM\rangle$. Since we make use of the simple hydrogen-like model, we treat the quantum numbers n, L and M as known from atomic physics as good quantum numbers; even though this is generally not the case due to the cubic symmetry of the solid [36, 37]. We will discuss this problem in Sec. 3.3.2. The coupling matrix elements are given by

$$\lambda_{\mathrm{LA}}(\boldsymbol{q},\,\nu\nu') \;=\; V_{\mathrm{LA}}(q)\left[D_{\mathrm{e}}q_{\mathrm{e}}(\boldsymbol{q},\,\nu\nu') - D_{\mathrm{h}}q_{\mathrm{h}}(\boldsymbol{q},\,\nu\nu')\right], \tag{3.76a}$$

$$\lambda_{\mathrm{LO}}(\boldsymbol{q},\,\nu\nu') \;=\; V_{\mathrm{LO}}(q)\left[q_{\mathrm{e}}(\boldsymbol{q},\,\nu\nu') - q_{\mathrm{h}}(\boldsymbol{q},\,\nu\nu')\right], \tag{3.76b}$$

and the coupling matrix elements $V_{\mathrm{LA}}(q)$ of Eq. (3.23) (with $D = 1$) and $V_{\mathrm{LO}}(q)$ of Eq. (3.39). Here $D_{\mathrm{e/h}}$ denotes the deformation coupling potential of the conduction/valence band. The effective charges read

$$q_{\mathrm{e}}(\boldsymbol{q},\,\nu\nu') \;=\; \int \mathrm{d}\boldsymbol{r}\,\psi^*_\nu(\boldsymbol{r})\psi_{\nu'}(\boldsymbol{r})e^{i\frac{m_{\mathrm{h}}}{M}\boldsymbol{q}\boldsymbol{r}}, \tag{3.77a}$$

$$q_{\mathrm{h}}(\boldsymbol{q},\,\nu\nu') \;=\; \int \mathrm{d}\boldsymbol{r}\,\psi^*_\nu(\boldsymbol{r})\psi_{\nu'}(\boldsymbol{r})e^{-i\frac{m_{\mathrm{e}}}{M}\boldsymbol{q}\boldsymbol{r}}, \tag{3.77b}$$

as defined by Toyozawa [73] with the hydrogen-like exciton wave functions $\psi_\nu(\boldsymbol{r})$. By $m_{\mathrm{e/h}}$ we denote the effective masses of electron and hole.

The interaction with phonons leads to peaks of asymmetric Loretzian shape in the absorption spectrum. The absorption coefficient depending on the frequency of light is given by [73, 74]

$$\alpha(\omega) = \sum_\nu \frac{\alpha_0}{\omega}\tilde{F}_\nu(\omega)\frac{\hbar\tilde{\Gamma}_{\nu\boldsymbol{0}}(\omega) + 2\tilde{A}_\nu(\omega)\left[\hbar\omega - \tilde{E}_{\nu\boldsymbol{0}}(\omega)\right]}{\left[\hbar\omega - \tilde{E}_{\nu\boldsymbol{0}}(\omega)\right]^2 + \left[\hbar\tilde{\Gamma}_{\nu\boldsymbol{0}}(\omega)\right]^2} \tag{3.78}$$

with the energy shift

$$\tilde{\Delta}_{\nu\boldsymbol{0}}(\omega) = \tilde{E}_{\nu\boldsymbol{0}}(\omega) - E_{\nu\boldsymbol{0}} = \Delta_{\nu\nu\boldsymbol{0}}(\omega) + \sum_{\nu'\neq\nu}\frac{|\Delta_{\nu\nu'\boldsymbol{0}}(\omega)|^2 - |\Gamma_{\nu\nu'\boldsymbol{0}}(\omega)|^2}{E_{\nu\boldsymbol{0}} - E_{\nu'\boldsymbol{0}}}, \tag{3.79}$$

the line broadening

$$\tilde{\Gamma}_{\nu\boldsymbol{0}}(\omega) = \Gamma_{\nu\nu\boldsymbol{0}}(\omega) + \sum_{\nu'\neq\nu} 2\,\mathrm{Re}\left(\frac{\Delta_{\nu\nu'\boldsymbol{0}}(\omega)\Gamma_{\nu'\nu\boldsymbol{0}}(\omega)}{E_{\nu\boldsymbol{0}} - E_{\nu'\boldsymbol{0}}}\right), \tag{3.80}$$

the function

$$\begin{aligned}\tilde{F}_\nu(\omega) \;&=\; |M_{\nu g}|^2 + \sum_{\nu'\neq\nu} 2\,\mathrm{Re}\left(\frac{M^*_{\nu g}\Delta_{\nu\nu'\boldsymbol{0}}(\omega)M_{\nu' g}}{E_{\nu\boldsymbol{0}} - E_{\nu'\boldsymbol{0}}}\right)\\ &+\; \sum_{\nu'\neq\nu}\sum_{\nu''\neq\nu} 2\,\mathrm{Re}\left(\frac{M^*_{\nu g}\left[\Delta_{\nu\nu''\boldsymbol{0}}(\omega)\Delta_{\nu''\nu'\boldsymbol{0}}(\omega) - \Gamma_{\nu\nu''\boldsymbol{0}}(\omega)\Gamma_{\nu''\nu'\boldsymbol{0}}(\omega)\right]M_{\nu' g}}{(E_{\nu\boldsymbol{0}} - E_{\nu'\boldsymbol{0}})(E_{\nu\boldsymbol{0}} - E_{\nu''\boldsymbol{0}})}\right)\\ &+\; \sum_{\nu'\neq\nu}\sum_{\nu''\neq\nu} \mathrm{Re}\left(\frac{M^*_{\nu' g}\left[\Delta_{\nu'\nu\boldsymbol{0}}(\omega)\Delta_{\nu\nu''\boldsymbol{0}}(\omega) - \Gamma_{\nu'\nu\boldsymbol{0}}(\omega)\Gamma_{\nu\nu''\boldsymbol{0}}(\omega)\right]M_{\nu'' g}}{(E_{\nu\boldsymbol{0}} - E_{\nu'\boldsymbol{0}})(E_{\nu\boldsymbol{0}} - E_{\nu''\boldsymbol{0}})}\right),\end{aligned} \tag{3.81}$$

and the asymmetry $\tilde{A}_\nu(\omega)$, which can be calculated from

$$\begin{aligned}\tilde{A}_\nu(\omega)\tilde{F}_\nu(\omega) &= \sum_{\nu'\neq\nu}\mathrm{Re}\left(\frac{M^*_{\nu g}\Gamma_{\nu\nu'\mathbf{0}}(\omega)M_{\nu' g}}{E_{\nu\mathbf{0}}-E_{\nu'\mathbf{0}}}\right)\\ &+ \sum_{\nu'\neq\nu}\sum_{\nu''\neq\nu} 2\,\mathrm{Re}\left(\frac{M^*_{\nu g}\left[\Delta_{\nu\nu''\mathbf{0}}(\omega)\Gamma_{\nu''\nu'\mathbf{0}}(\omega)+\Gamma_{\nu\nu''\mathbf{0}}(\omega)\Delta_{\nu''\nu'\mathbf{0}}(\omega)\right]M_{\nu' g}}{(E_{\nu\mathbf{0}}-E_{\nu'\mathbf{0}})(E_{\nu\mathbf{0}}-E_{\nu''\mathbf{0}})}\right)\\ &+ \sum_{\nu'\neq\nu}\sum_{\nu''\neq\nu}\mathrm{Re}\left(\frac{M^*_{\nu' g}\left[\Delta_{\nu'\nu\mathbf{0}}(\omega)\Gamma_{\nu\nu''\mathbf{0}}(\omega)-\Gamma_{\nu'\nu\mathbf{0}}(\omega)\Delta_{\nu\nu''\mathbf{0}}(\omega)\right]M_{\nu'' g}}{(E_{\nu\mathbf{0}}-E_{\nu'\mathbf{0}})(E_{\nu\mathbf{0}}-E_{\nu''\mathbf{0}})}\right). \qquad (3.82)\end{aligned}$$

The quantity $M_{\nu g}$ denotes the transition matrix element between the ground state $|0\rangle$ of the solid and the exciton state $|\nu\rangle$ with $\boldsymbol{K}=0$ due to the electron-photon interaction. In cuprous oxide the transition is parity-forbidden, which results in (cf. Sec. 4.4.2)

$$M_{\nu g} = c\,\frac{n^2-1}{n^5}\delta_{L,1}\delta_{M,0}. \qquad (3.83)$$

Since in both equations (3.81) and (3.82) $M_{\nu g}$ appears quadratically, the asymmetry $\tilde{A}_\nu(\omega)$ will be independent of the proportionality constant c.

The main difficulty in the implementation of the formulas given above is the calculation of the quantities [73, 74]

$$\begin{aligned}\Gamma_{\nu_2\nu_1\mathbf{0}}(\omega) &= \sum_{s\boldsymbol{q}}\sum_{\nu_3}\frac{\pi}{\hbar}\lambda^*_s(\boldsymbol{q},\,\nu_3\nu_2)\lambda_s(\boldsymbol{q},\,\nu_3\nu_1)\left[(n_s(\omega_s(\boldsymbol{q}),\,T)+1)\,\delta(E_{\nu_3\boldsymbol{q}}+\hbar\omega_s(\boldsymbol{q})-\hbar\omega)\right.\\ &\quad\left.+n_s(\omega_s(\boldsymbol{q}),\,T)\,\delta(E_{\nu_3\boldsymbol{q}}-\hbar\omega_s(\boldsymbol{q})-\hbar\omega)\right], \qquad (3.84)\end{aligned}$$

and

$$\begin{aligned}\Delta_{\nu_2\nu_1\mathbf{0}}(\omega) &= \sum_{s\boldsymbol{q}}\sum_{\nu_3}\lambda^*_s(\boldsymbol{q},\,\nu_3\nu_2)\lambda_s(\boldsymbol{q},\,\nu_3\nu_1)\left[(n_s(\omega_s(\boldsymbol{q}),\,T)+1)\,\mathcal{P}\left(\frac{1}{\hbar\omega-E_{\nu_3\boldsymbol{q}}-\hbar\omega_s(\boldsymbol{q})}\right)\right.\\ &\quad\left.+n_s(\omega_s(\boldsymbol{q}),\,T)\,\mathcal{P}\left(\frac{1}{\hbar\omega-E_{\nu_3\boldsymbol{q}}+\hbar\omega_s(\boldsymbol{q})}\right)\right]. \qquad (3.85)\end{aligned}$$

The symbol $\mathcal{P}$ denotes the principal value. We can write

$$\mathcal{P}\left(\frac{1}{x}\right) = \mathcal{P}\int \mathrm{d}E\,\frac{1}{E}\delta(E-x) = \lim_{\epsilon\to 0^+}\left(\int_{-\infty}^{-\epsilon}\mathrm{d}E\,\frac{1}{E}\delta(E-x)+\int_{\epsilon}^{\infty}\mathrm{d}E\,\frac{1}{E}\delta(E-x)\right). \qquad (3.86)$$

The average thermal occupation $n_s(\omega_s(\boldsymbol{q}),\,T)$ of phononic states at a temperature T is given by Eq. (2.79). The numerical evaluation of the functions $\Gamma_{\nu_2\nu_1\mathbf{0}}(\omega)$ and $\Delta_{\nu_2\nu_1\mathbf{0}}(\omega)$ will be presented in the next section 3.2.1.

Toyozawa already proved the correctness of his formulas comparing them to experimental results for, e.g., KI, RbBr and AgCl. In 1969 it was proven that the peaks of the yellow exciton series of Cu_2O for $n=1,2,3$ agree fairly well with the predicted asymmetric Lorentzian shape at different temperatures [243]. However, the experimental values were only fitted by the formula (3.78). A general overview of the form of absorption peaks including a comparison to the Urbach rule[18], the case of strong photon-exciton-phonon interaction and radiative annihilation as well as dissociation and recombination can be found in Ref. [76].

---

[18] The Urbach rule is the empirical formula $\alpha=\alpha_0\exp\left[\sigma(\hbar\omega-\hbar\omega_0)/k_{\mathrm{B}}T\right]$ describing the dependence of α on crystal

3.2.1 Numerical evaluation of line width and energy shift

We will now discuss the numerical evaluation of the functions $\Gamma_{\nu_2\nu_1\boldsymbol{0}}(\omega)$ and $\Delta_{\nu_2\nu_1\boldsymbol{0}}(\omega)$ of Eqs. (3.84) and (3.85).

Due to periodic boundary conditions, the values of the phononic wave vector $\boldsymbol{q}$ are generally discrete [85]. If we apply the continuum approximation, in which the number of atoms N of the solid goes to infinity and the lattice constant a between the atoms goes to zero while the ratio $Na^3 = V$ is kept constant, we can treat $\boldsymbol{q}$ as a continuous quantity and replace the corresponding sums by integrals:

$$\sum_{\boldsymbol{q}} \to \frac{V}{(2\pi)^3} \int \mathrm{d}\boldsymbol{q} \tag{3.87a}$$

with

$$\int \mathrm{d}\boldsymbol{q} = \int_0^{q_\mathrm{D}} \mathrm{d}q\, q^2 \int_0^{\pi} \mathrm{d}q_\vartheta\, \sin q_\vartheta \int_0^{2\pi} \mathrm{d}q_\varphi \tag{3.87b}$$

in spherical coordinates. The upper boundary q_D of the q-integral is given by the boundary of the first Brillouin zone (BZ) and can be calculated from the Debye model [85]. We now write

$$\begin{aligned}\Gamma_{\nu_2\nu_1\boldsymbol{0}}(\omega) &= \frac{V}{(2\pi)^3} \sum_{s,\nu_3} \int_0^{\mathrm{BZ}} \mathrm{d}q\, q^2 \left[f_s(q)\right]^2 \Lambda_s(q,\nu_3\nu_2\nu_1) \\ &\times \left[(n_s(\omega_s(\boldsymbol{q}),\, T) + 1)\, \delta(E_{\nu_3\boldsymbol{q}} + \hbar\omega_s(\boldsymbol{q}) - \hbar\omega) \right.\\ &\left.+\, n_s(\omega_s(\boldsymbol{q}),\, T)\, \delta(E_{\nu_3\boldsymbol{q}} - \hbar\omega_s(\boldsymbol{q}) - \hbar\omega)\right]\end{aligned} \tag{3.88}$$

and

$$\begin{aligned}\Delta_{\nu_2\nu_1\boldsymbol{0}}(\omega) &= \frac{V}{(2\pi)^3} \sum_{s,\nu_3} \int_0^{\mathrm{BZ}} \mathrm{d}q\, q^2 \left[f_s(q)\right]^2 \Lambda_s(q,\nu_3\nu_2\nu_1) \\ &\times \left[(n_s(\omega_s(\boldsymbol{q}),\, T) + 1)\, \mathcal{P}\left(\frac{1}{\hbar\omega - E_{\nu_3\boldsymbol{q}} - \hbar\omega_s(\boldsymbol{q})}\right)\right.\\ &\left.+\, n_s(\omega_s(\boldsymbol{q}),\, T)\, \mathcal{P}\left(\frac{1}{\hbar\omega - E_{\nu_3\boldsymbol{q}} + \hbar\omega_s(\boldsymbol{q})}\right)\right]\end{aligned} \tag{3.89}$$

with

$$\begin{aligned}\Lambda_s(q,\nu_3\nu_2\nu_1) &= \int_0^{\pi} \mathrm{d}q_\vartheta\, \sin q_\vartheta \int_0^{2\pi} \mathrm{d}q_\varphi \left[D_\mathrm{e}^s q_\mathrm{e}^*(\boldsymbol{q},\, \nu_3\nu_2) - D_\mathrm{h}^s q_\mathrm{h}^*(\boldsymbol{q},\, \nu_3\nu_2)\right] \\ &\qquad \times \left[D_\mathrm{e}^s q_\mathrm{e}(\boldsymbol{q},\, \nu_3\nu_1) - D_\mathrm{h}^s q_\mathrm{h}(\boldsymbol{q},\, \nu_3\nu_1)\right].\end{aligned} \tag{3.90}$$

The quantities $D_{\mathrm{e/h}}^s$ are the deformation potentials if $s = \mathrm{LA}$; otherwise they are equal to one.

To evaluate the integral over $\boldsymbol{q}$, the dependence of the effective charges on the angles q_ϑ and q_φ has to be determined. To this end we substitute the variable $\boldsymbol{r}$ in the integrals of Eqs. (3.77a)

---

temperature and photon energy for the *long wavelength tail parts of fundamental absorption* [76] in insulators and semiconductors [244]. It was first discovered for silver halides and is applicable to a large number of solids [7]. There are several explanation attempts for the physical cause of such behavior (see Refs. [7, 12, 245, 246] and further references therein).

and (3.77b) by $\boldsymbol{u} = \boldsymbol{A}^{\mathrm{T}}\boldsymbol{r}$ with a rotation matrix $\boldsymbol{A}$, for which $\boldsymbol{A}^{\mathrm{T}}\boldsymbol{q} = q\hat{\boldsymbol{e}}_z$ holds. By $\hat{\boldsymbol{e}}_z$ we denote the unit vector in z-direction. If we define $\boldsymbol{R}_{\hat{\boldsymbol{n}}\varphi}$ as the rotation matrix describing the rotation about an axis $\hat{\boldsymbol{n}}$ by an angle φ, we can express $\boldsymbol{A}$ as

$$\boldsymbol{A} = \boldsymbol{R}_{\hat{\boldsymbol{e}}_z(-q_\alpha)}\boldsymbol{R}_{\hat{\boldsymbol{e}}_y(-q_\vartheta)}\boldsymbol{R}_{\hat{\boldsymbol{e}}_z(-q_\varphi)} \tag{3.91}$$

with an arbitrary angle q_α. The hydrogen-like wave functions ψ_ν of the exciton read

$$\psi_\nu(\boldsymbol{r}) = R_{nL}(r)Y_{LM}(\vartheta,\, \varphi) \tag{3.92}$$

with the spherical harmonics $Y_{LM}(\vartheta,\, \varphi)$. For the radial part $R_{nL}(r)$ we take the well-known functions of the hydrogen atom [247] but replace the Bohr radius a_0 with the excitonic Bohr radius a_{exc}, which is given by [85]

$$a_{\mathrm{exc}} = a_0 \frac{\mathrm{Ry}}{\varepsilon_{\mathrm{s1}} R_{\mathrm{exc}}} \approx 1.116\,\mathrm{nm}, \tag{3.93}$$

with the Rydberg energy Ry and the dielectric constant $\varepsilon_{\mathrm{s1}}$. These parameters and all other material parameters of $\mathrm{Cu_2O}$ are listed in Table 2.2.

After the substitution, we make use of the special properties of the spherical harmonics under rotations [248]:

$$\begin{aligned} \psi_\nu(\boldsymbol{A}\boldsymbol{u}) &= e^{-\frac{i}{\hbar}q_\alpha\hat{\boldsymbol{e}}_z\cdot\boldsymbol{L}} e^{-\frac{i}{\hbar}q_\vartheta\hat{\boldsymbol{e}}_y\cdot\boldsymbol{L}} e^{-\frac{i}{\hbar}q_\varphi\hat{\boldsymbol{e}}_z\cdot\boldsymbol{L}}\, \psi_\nu(\boldsymbol{u}) = \mathcal{D}(q_\alpha,\, q_\vartheta,\, q_\varphi)\, \psi_\nu(\boldsymbol{u}) \\ &= R_{nL}(u) \sum_{M'=-L}^{L} Y_{LM'}(u_\vartheta,\, u_\varphi)\, D^L_{M'M}(q_\alpha,\, q_\vartheta,\, q_\varphi). \end{aligned} \tag{3.94}$$

The complex factors $D^L_{M'M}(q_\alpha,\, q_\vartheta,\, q_\varphi)$ are the matrix elements of the operator $\mathcal{D}(q_\alpha,\, q_\vartheta,\, q_\varphi)$ corresponding to the spherical harmonics, i.e.,

$$D^L_{M'M}(q_\alpha,\, q_\vartheta,\, q_\varphi) = \left\langle LM' \left| \mathcal{D}(q_\alpha,\, q_\vartheta,\, q_\varphi) \right| LM \right\rangle. \tag{3.95}$$

Since the final expressions do not depend on q_α, it is possible to include an additional integral $1/(2\pi)\int \mathrm{d}q_\alpha$. Making use of the properties of the matrices $D^L_{M'M}$ [7], we can easily evaluate the integrals over q_ϑ and q_φ.

$$\begin{aligned} \Lambda_s(q, \nu_3\nu_2\nu_1) &= \sum_{F=\max(|L_3-L_2|,|L_3-L_1|)}^{\min(L_3+L_2,L_3+L_1)} \; \sum_{G=-\min(L_3,L_2)}^{\max(L_3,L_2)} \; \sum_{H=-\min(L_3,L_1)}^{\max(L_3,L_1)} 4\pi(2F+1)\delta_{M_1M_2} \\ &\times \begin{pmatrix} L_3 & L_1 & F \\ G & H & -G-H \end{pmatrix} \begin{pmatrix} L_3 & L_2 & F \\ H & G & -H-G \end{pmatrix} \\ &\times \begin{pmatrix} L_3 & L_1 & F \\ M_3 & M_1 & -M_3-M_1 \end{pmatrix} \begin{pmatrix} L_3 & L_2 & F \\ M_3 & M_1 & -M_3-M_1 \end{pmatrix} \\ &\times \left(D^s_{\mathrm{e}} \left\langle n_2L_2G \left| e^{-i\frac{m_{\mathrm{h}}}{M}qz} \right| n_3L_3G \right\rangle - D^s_{\mathrm{h}} \left\langle n_2L_2G \left| e^{i\frac{m_{\mathrm{e}}}{M}qz} \right| n_3L_3G \right\rangle \right) \\ &\times \left(D^s_{\mathrm{e}} \left\langle n_1L_1H \left| e^{-i\frac{m_{\mathrm{h}}}{M}qz} \right| n_3L_3H \right\rangle - D^s_{\mathrm{h}} \left\langle n_1L_1H \left| e^{i\frac{m_{\mathrm{e}}}{M}qz} \right| n_3L_3H \right\rangle \right)^{*}. \end{aligned} \tag{3.96}$$

The matrix elements of the form

$$\left\langle nLM \left| e^{iaz} \right| n'L'M \right\rangle = \int \mathrm{d}\boldsymbol{r}\, R_{nL}(r)R_{n'L'}(r)e^{iar\cos\vartheta}Y^*_{LM}(\vartheta,\, \varphi)Y_{L'M}(\vartheta,\, \varphi) \tag{3.97}$$

are calculated using MATHEMATICA.

The evaluation of the integral over q is straightforward. At first, we interchange the integral over q with the integral belonging to the principal value in Eq. (3.89). Then we treat the arguments of the delta functions in Eqs. (3.84) and (3.85) as functions of q and use the relation

$$\delta(f(q)) = \sum_i \left| \left.\frac{\partial f}{\partial q}\right|_{q=q_i} \right|^{-1} \delta(q-q_i), \tag{3.98}$$

where the sum is over all roots q_i of $f(q)$.

The final task is the evaluation of the integral with the pricipal value in $\Delta_{\nu\nu'\mathbf{0}}(\omega)$. This will be done numerically using Hartree units (see Appendix B). One can read from the delta functions obtained by using Eq. (3.98) for which energies E there will be a contribution to the integral. According to the values of the material parameters of $\mathrm{Cu_2O}$ the maximum and minimum value of E are given by

$$E_{\mathrm{max}} = R_{\mathrm{exc}} + \hbar\omega_{\mathrm{LO,\,max}} > 0, \tag{3.99a}$$
$$E_{\mathrm{min}} = -E_{\mathrm{max}} - \hbar^2 q_{\mathrm{max}}^2/(2M) < 0, \tag{3.99b}$$

where $\hbar\omega_{\mathrm{LO,\,max}}$ denotes the energy of the LO-phonon mode of highest energy. Since $|E_{\mathrm{min}}| > E_{\mathrm{max}}$ holds, we can replace the upper value of the integral by $-E_{\mathrm{min}}$ and rewrite the principal value integral as an improper integral

$$\mathcal{P}\int_{E_{\mathrm{min}}}^{-E_{\mathrm{min}}} \mathrm{d}E\, f(E) = \lim_{\epsilon\to 0}\int_{\epsilon}^{-E_{\mathrm{min}}} \mathrm{d}E\,(f(E)+f(-E)), \tag{3.100}$$

which is then evaluated using Gaussian quadrature and a standard algorithm for improper integrals.

3.3 Results and discussion

3.3.1 Contributions to the line widths

In the following we will discuss the different contributions to the line widths $\tilde{\Gamma}_{\nu\mathbf{0}}(\omega)$ in Eq. (3.80) for $\mathrm{Cu_2O}$ at the very low temperature of $T = 1.2\,\mathrm{K}$ [30]. The relevant material parameters are listed in Table 2.2. Although the unit cell of $\mathrm{Cu_2O}$ comprises 6 atoms, which amounts in 15 optical phonon modes, there are only two LO-phonon modes with Γ_4^--symmetry contributing to the Fröhlich interaction [162].

For our discussion we will especially consider the line parameters of the $2P$-exciton since it has always been wondered which effects lead to the large broadening of this line [73, 249–251]. We discuss the contributions to these parameters in several steps.

Step 1: We start with the most simple case, in which we neglect the optical phonons, set the frequency ω to $E_{\nu\mathbf{0}}/\hbar$ and neglect the so-called intraband-contributions [73], i.e., we only include those parts of Eqs. (3.79)-(3.82), which do not contain sums over ν'. The approximation of setting $\omega \approx E_{\nu\mathbf{0}}/\hbar$ is justified since $\tilde{\Gamma}_{\nu\mathbf{0}}(\omega)$ is a slowly varying function with ω [74, 249]. The formula (3.84) includes a sum over all excitonic states. In order to calculate the quantity $\Gamma_{\nu_2\nu_1\mathbf{0}}(\omega)$ within reasonable time, we have to restrict the infinite sum to a finite one via

$$\sum_{\nu_3} \to \sum_{n_3=1}^{n_{\mathrm{max}}} \sum_{L_3=0}^{n_3-1} \sum_{M_3=-L_3}^{L_3} \tag{3.101}$$

with $n_{\max} \leq 7$. As it has also been done by Toyozawa [73], one may at first include only states having the same principal quantum number as the one considered. This means for the $2P$-exciton that the sum reads

$$\sum_{\nu_3} \rightarrow \sum_{n_3=2}^{2} \sum_{L_3=0}^{1} \sum_{M_3=-L_3}^{L_3} . \tag{3.102}$$

This yields very small values for the line width and the energy shift

$$\tilde{\Gamma}_{210\,\mathbf{0}}(E_{210\,\mathbf{0}}/\hbar) \approx 1.70 \times 10^{-9}\,\mathrm{eV}, \tag{3.103a}$$
$$\tilde{\Delta}_{210\,\mathbf{0}}(E_{210\,\mathbf{0}}/\hbar) \approx -9.72 \times 10^{-6}\,\mathrm{eV}. \tag{3.103b}$$

With increasing temperature the band gap energy E_{g} decreases and the absorption edge is shifted towards lower energies. This is first of all unexpected since a raising of the temperature generally increases the lattice constant leading to narrowing of the conduction and valence bands and thus an increasing band gap energy [7]. However, the one-electron states and especially those in the vicinity of the band edges are shifted and broadened owing to the interaction with phonons [252, 253]. Since this effect predominates, the value of E_{g} decreases with increasing T. As the energy of the exciton states directly depends on E_{g}, the exciton states are shifted towards lower energies, as well[19]. This is reflected by a negative value of $\Delta_{\nu_2\nu_1\mathbf{0}}(\omega)$.

Step 2: An obviously better approach is to evaluate the complete sum (3.101) with different $n_{\max}$ and extrapolate the values obtained for $\tilde{\Gamma}_{210\,\mathbf{0}}$ and $\tilde{\Delta}_{210\,\mathbf{0}}$ to the final value for $n_{\max} \rightarrow \infty$. To this aim we fit a function of the form $f(n_{\max}) = a/n_{\max}^2 + b$ to our values. We depict this procedure in Fig. 3.4. This approach yields

$$\tilde{\Gamma}_{210\,\mathbf{0}}(E_{210\,\mathbf{0}}/\hbar) \approx 9.87 \times 10^{-7}\,\mathrm{eV}, \tag{3.104a}$$
$$\tilde{\Delta}_{210\,\mathbf{0}}(E_{210\,\mathbf{0}}/\hbar) \approx -2.32 \times 10^{-5}\,\mathrm{eV}. \tag{3.104b}$$

This already shows that the $1S$-exciton state has a large influence on the line width of the $2P$-state.

Step 3: At very low temperatures only few LA phonons are thermally excited. We therefore expect the optical phonons to increase the line width considerably; especially since the energy of one of these phonons ($\hbar\omega_{\mathrm{LO},1} = 18.7\,\mathrm{meV}$) is of the same magnitude as the energetic difference between two exciton states ($E_{210\,\mathbf{0}} - E_{410\,\mathbf{0}} \approx 17.25\,\mathrm{meV}$). Including optical phonons, we obtain

$$\tilde{\Gamma}_{210\,\mathbf{0}}(E_{210\,\mathbf{0}}/\hbar) \approx 3.45 \times 10^{-5}\,\mathrm{eV}, \tag{3.105a}$$
$$\tilde{\Delta}_{210\,\mathbf{0}}(E_{210\,\mathbf{0}}/\hbar) \approx -8.39 \times 10^{-3}\,\mathrm{eV}. \tag{3.105b}$$

Step 4: Up to now we have assumed that the line width $\tilde{\Gamma}_{210\,\mathbf{0}}(\omega)$ is a slowly varying function of the frequency of light. For this reason we have set $\omega \approx E_{\nu\mathbf{0}}/\hbar$. In the literature it has been discussed that it is necessary to account for the frequency dependence in order to describe the asymmetry of the lines correctly [249]. On the other hand, Toyozawa already stated in Ref. [74] that the line shape would not be of asymmetric Lorentzian shape if $\tilde{\Gamma}_{210\,\mathbf{0}}(\omega)$ varied strongly with

---

[19] Note that from temperature behavior of the yellow exciton series in $\mathrm{Cu_2O}$ the empirical formula

$$E_{\mathrm{g}}(T) = 2.171\,\mathrm{eV} \times \left(1 - 1.87 \times 10^{-5}\frac{1}{\mathrm{K}}T - 3.5 \times 10^{-7}\frac{1}{\mathrm{K}^2}T^2\right)$$

has been deduced [254] for the temperature range $4.2\,\mathrm{K} \leq T \leq 77\,\mathrm{K}$. Hence, the true position of the exciton states at high temperatures are generally not consistent with theoretical predictions when neglecting phonons and assuming a temperature-independent band gap energy.

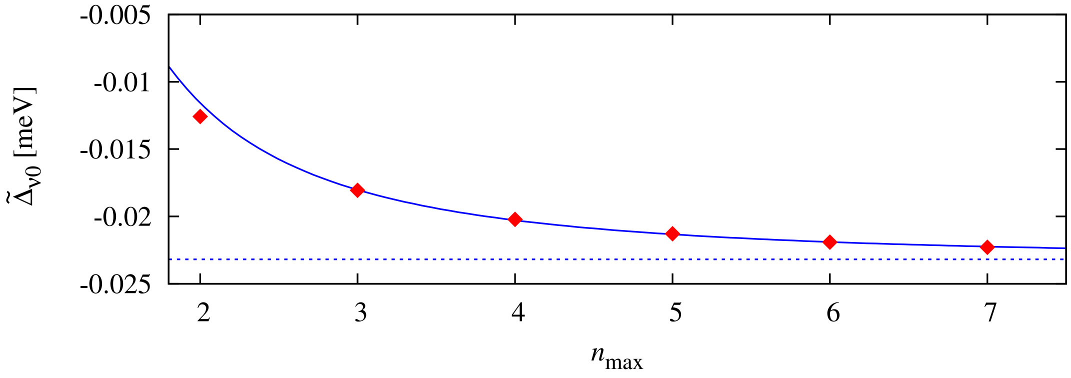

Figure 3.4.: To evaluate the quantities $\Gamma_{\nu_2\nu_1\mathbf{0}}(\omega)$ and $\Delta_{\nu_2\nu_1\mathbf{0}}(\omega)$, one has to cut the infinite sums over ν in the formulas at a finite value $n_{\max}$ of the principal quantum number n [cf. Eq. (3.101)]. Here we show the values obtained for $\tilde{\Delta}_{210\,\mathbf{0}}$ in dependence on $n_{\max}$ for *Step 2*. The final value $\tilde{\Delta}_{210\,\mathbf{0}} = -2.32 \times 10^{-5}\,\mathrm{eV}$ (dashed line) is then calculated from an extrapolation. We used $f(n_{\max}) = a/n_{\max}^2 + b$ as a fit function for $n_{\max} \geq 3$ (solid line).

ω. We see that the energy shift $\tilde{\Delta}_{210\,\mathbf{0}}$ is several meV large. Since the absorption peak is centered around $\tilde{E}_{\nu\mathbf{0}}(\omega)$, we evaluate the line parameters within the range $\omega_{\min} \leq \omega \leq \omega_{\max}$ with

$$\hbar\omega_{\min} = E_{210\,\mathbf{0}} - 2\left|\tilde{\Delta}_{210\,\mathbf{0}}(E_{210\,\mathbf{0}}/\hbar)\right|, \qquad \hbar\omega_{\max} = E_{210\,\mathbf{0}}, \tag{3.106}$$

to determine their frequency dependence. It is found that $\tilde{\Gamma}_{210\,\mathbf{0}}(\omega)$ increases slowly with ω while $\tilde{\Delta}_{210\,\mathbf{0}}(\omega)$ decreases strongly :

$$\tilde{\Gamma}_{210\,\mathbf{0}}(\omega_{\min}) \approx 3.30 \times 10^{-5}\,\mathrm{eV}, \tag{3.107a}$$
$$\tilde{\Gamma}_{210\,\mathbf{0}}(\omega_{\max}) \approx 3.45 \times 10^{-5}\,\mathrm{eV}, \tag{3.107b}$$
$$\tilde{\Delta}_{210\,\mathbf{0}}(\omega_{\min}) \approx -6.97 \times 10^{-3}\,\mathrm{eV}, \tag{3.107c}$$
$$\tilde{\Delta}_{210\,\mathbf{0}}(\omega_{\max}) \approx -8.39 \times 10^{-3}\,\mathrm{eV}. \tag{3.107d}$$

The effect on the line width may be more important in external fields, which would mix different excitonic states [73, 255].

Step 5: An important effect concerns the $1S$-exciton of the yellow series of $\mathrm{Cu_2O}$. The mean distance between electron and hole is so small that this exciton can hardly be treated as a Wannier exciton. The corrections that have to be made due to this small distance are known as the central-cell corrections. They lead to a higher mass of the $1S$-exciton of $\tilde{M} \approx 3m_0$ and to a smaller excitonic Bohr radius of $\tilde{a}_{\mathrm{exc}} \approx 0.53\,\mathrm{nm}$ [162]. These corrections are now included in the excitonic wave function ψ_{100} and in the excitonic energies

$$E_{100\,\boldsymbol{K}} = E_{\mathrm{g}} - \tilde{R}_{\mathrm{exc}} + \frac{\hbar^2\boldsymbol{K}^2}{2\tilde{M}}. \tag{3.108}$$

The binding energy $\tilde{R}_{\mathrm{exc}} \approx 153\,\mathrm{meV}$ of the $1S$-exciton differs much from the excitonic Rydberg constant of the rest of the yellow exciton series. The central-cell corrections have a significant

Table 3.1.: The final values for the line widths $\tilde{\Gamma}_{\nu\mathbf{0}}$, the energy shifts $\tilde{\Delta}_{\nu\mathbf{0}}$ including all of the corrections discussed in Sec. 3.3.1. The values are given at $\hbar\omega = E_{n10\,\mathbf{0}} - \tilde{\Delta}_{n10\,\mathbf{0}}(E_{n10\,\mathbf{0}}/\hbar)$ (cf. *Step 4* of Sec. 3.3.1). In the last column the experimental line widths are listed [30].

ν	$\tilde{\Gamma}_{\nu\mathbf{0}}$ [meV]	$\tilde{\Delta}_{\nu\mathbf{0}}$ [meV]	$\tilde{\Gamma}_{\nu\mathbf{0}}(\text{exp})$ [meV]
210	0.453	−7.737	1.581
310	0.201	−7.574	0.511
410	0.144	−6.551	0.237
510	0.108	−6.560	0.142

influence on the line width and increase it by a factor of about 17 to

$$\begin{aligned}
\tilde{\Gamma}_{210\,\mathbf{0}}(\omega_{\min}) &\approx 6.12\times 10^{-4}\,\text{eV}, && (3.109\text{a})\\
\tilde{\Gamma}_{210\,\mathbf{0}}(\omega_{\max}) &\approx 5.53\times 10^{-4}\,\text{eV}, && (3.109\text{b})\\
\tilde{\Delta}_{210\,\mathbf{0}}(\omega_{\min}) &\approx -6.98\times 10^{-3}\,\text{eV}, && (3.109\text{c})\\
\tilde{\Delta}_{210\,\mathbf{0}}(\omega_{\max}) &\approx -8.18\times 10^{-3}\,\text{eV}. && (3.109\text{d})
\end{aligned}$$

Step 6: We now investigate the influence of intraband scattering. Therefore, we also consider the sums of the form $\sum_{\nu'\neq\nu}$ in Eqs. (3.79)-(3.82), where we also cut these sums at the same value of $n_{\max}$. In contrast to the expectation of Toyozawa [74], the effect of this type of scattering on the line width is quite small. We obtain

$$\begin{aligned}
\tilde{\Gamma}_{210\,\mathbf{0}}(\omega_{\min}) &\approx 4.04\times 10^{-4}\,\text{eV}, && (3.110\text{a})\\
\tilde{\Gamma}_{210\,\mathbf{0}}(\omega_{\max}) &\approx 4.94\times 10^{-4}\,\text{eV}, && (3.110\text{b})\\
\tilde{\Delta}_{210\,\mathbf{0}}(\omega_{\min}) &\approx -7.14\times 10^{-3}\,\text{eV}, && (3.110\text{c})\\
\tilde{\Delta}_{210\,\mathbf{0}}(\omega_{\max}) &\approx -8.57\times 10^{-3}\,\text{eV}. && (3.110\text{d})
\end{aligned}$$

Nevertheless, the asymmetry of the lines can be explained only by intraband scattering. The value of

$$\begin{aligned}
\tilde{A}_{210}(\omega_{\min}) &\approx -3.67\times 10^{-2}, && (3.110\text{e})\\
\tilde{A}_{210}(\omega_{\max}) &\approx -3.69\times 10^{-2}, && (3.110\text{f})
\end{aligned}$$

is, however, very small in comparison with the large asymmetry of the lines observed in Ref. [30]. We will discuss this discrepancy in Sec. 3.3.2.

Step 7: In the literature a large asymmetry has also been assigned to a coupling of the bound exciton states to the continuum states [62, 249, 256, 257], whose energies are given by

$$E_{\boldsymbol{k}\boldsymbol{K}} = E_{\text{g}} + \frac{\hbar^2\boldsymbol{k}^2}{2\mu} + \frac{\hbar^2\boldsymbol{K}^2}{2M} \tag{3.111}$$

in analogy to the hydrogen atom. However, an effect of the continuum states can be excluded via a simple calculation: For the average occupation of the phonon modes one obtains $n_{\text{LO},1}(\omega_s(\boldsymbol{q}),T) = 0$ for $T \lesssim 25\,\text{K}$ and $n_{\text{LO},2}(\omega_s(\boldsymbol{q}),T) = 0$ for $T \lesssim 100\,\text{K}$, i.e., only scattering processes with the emission of phonons can take place at $T = 1.2\,\text{K}$. Furthermore, the emission process can only take

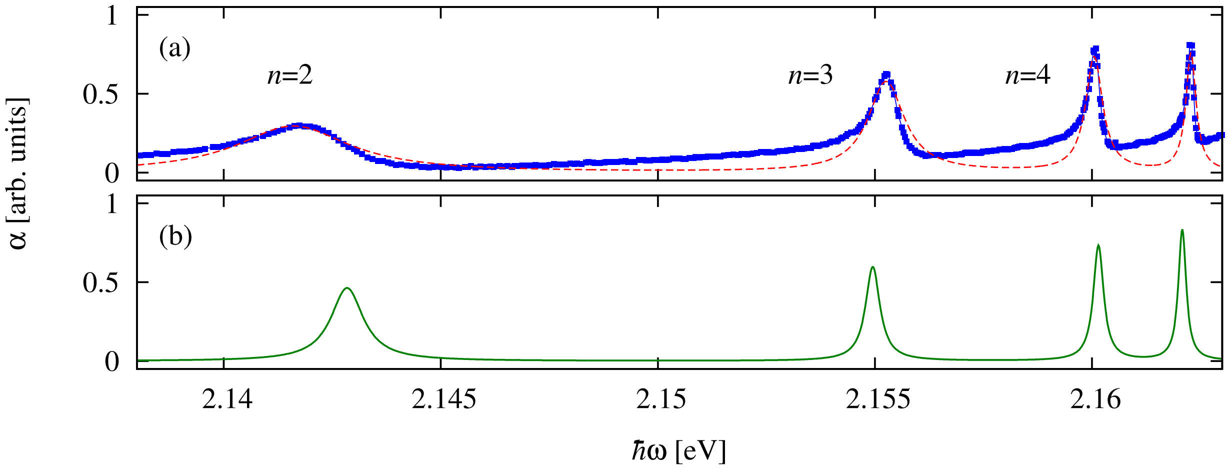

Figure 3.5.: Comparison of (a) the experimental spectrum of Fig. 2.15 with (b) the calculated line shapes using Eq. (3.78) and the values listed in Table 3.1. Since we do not know the proportionality constant c in Eq. (3.83), we chose arbitrary values for the amplitudes $\tilde{F}_\nu(\omega)$. We shifted the experimental values by an amount of -6 meV for a better comparison. The experimental values were fitted by Lorentzians to obtain the experimental line widths (red dashed line).

place if the arguments of the δ-functions in Eqs. (3.84) and (3.85) are positive. This means for acoustic phonons

$$\frac{\hbar^2 \boldsymbol{k}^2}{2\mu} < \frac{1}{2} M c_{\mathrm{LA}}^2 - \frac{R_{\mathrm{exc}}}{n^2} \tag{3.112a}$$

and for optical phonons

$$\frac{\hbar^2 \boldsymbol{k}^2}{2\mu} < -\hbar\omega_{\mathrm{LO}} - \frac{R_{\mathrm{exc}}}{n^2}. \tag{3.112b}$$

Therefore, only LA phonons play a role and only for the line shapes of excitons with $n > 32$. Consequently, a contribution of the continuum states is impossible.

The final results including all of the corrections discussed above are listed in Table 3.1. We also list the experimental line widths, which have been obtained by fitting Lorentzians or Elliotts formula to the experimental absorption spectrum (cf. Fig. 3.5). It can be seen that we obtain the correct behavior of the line parameters with increasing principal quantum number: The line widths decrease with increasing quantum number.

In Fig. 3.5 we compare the predicted line shapes with the measured ones. It is obvious that our calculation cannot reproduce quantitatively the large asymmetry. However, the line widths differ only by a factor of ~ 3.5 or even ~ 1.3, which means that they are of the same order of magnitude. The observable difference in the position of the lines can be explained on the one hand by small inaccuracies of the material constants used, on the other hand in terms of the complex valence band structure of $\mathrm{Cu_2O}$. These facts and further possible reasons for deviations from the experimental spectrum will be discussed in Sec. 3.3.2.

A quantitative comparison of the calculated line widths with the results of previous works is not possible. In Ref. [73] it is reported that the calculated line width of the $2P$-exciton is several times smaller than the experimentally observed one but no value is given. In Ref. [210] the calculated line widths are several times larger than the experimental ones indicating the inappropriateness of the many approximations in that publication.

3.3.2 Further discussion

In the above calculation we made some assumptions, which are discussed in the following. We also discuss possible causes for a further broadening of the lines, which may be difficult to be considered in theory.

We have assumed that the dispersion of LA phonons is linear according to $\omega_{\mathrm{LA}} = c_{\mathrm{LA}}q$ and that the dispersion of LO phonons is constant. If we perform the q-integration according to Eq. (3.87b) only up to a value of $q_{\mathrm{max}} < q_{\mathrm{D}}$, our results do not change for $q_{\mathrm{D}}/2 < q_{\mathrm{max}} < q_{\mathrm{D}}$, i.e., we can always set the upper boundary of the integral to $q_{\mathrm{D}}/2$. Since the assumption of the LA dispersion relation to be linear in q holds for $q < q_{\mathrm{D}}/2$ [258–261], its use is retroactively justified. Furthermore, the change of the energy of the LO phonons within this limit is very small [262].

We have treated L and M as good quantum numbers in the above calculations. This is in general not the case due to the cubic symmetry of the crystal. Nevertheless, since $\mathrm{O_h}$ is the point group with the highest symmetry, it may be justified to treat L approximatively as a good quantum number [36, 37]. However, one would still have to calculate the correct linear combinations of states with different M quantum number, which then transform according to the irreducible representations of the cubic group $\mathrm{O_h}$ [36]. This has not been done since we expect no effect from this rearrangement of states.

The asymmetry of the lines calculated in *Step 6* are considerably smaller than the experimental values. The large asymmetries can be explained in terms of Fano resonances and phonon replicas. Phonon replicas describe, in particular for luminescence, the scattering of a polariton from the exciton-like branch of its dispersion relation to the photon-like branch with the simultaneous emission of LO phonons, or more simply the decay of an exciton with the emission of one photon and LO phonons. In luminescence spectra the line shape then shows a square-root-like energy dependence due to the exciton density of states. While LO-phonon replicas appear on the low-energy side in luminescence spectra, they can also appear on the high-energy side in absorption spectra [12]. In the case of $\mathrm{Cu_2O}$ the Γ_3^- LO phonon assists the $1S$ exciton formation and causes the square-root-like frequency dependence of the absorption coefficient, on which then absorption of the other exciton resonances is superimposed (see, e.g., Refs. [167, 205, 210] and Fig. 2.16). Since the transition amplitudes interfere destructively or constructively on the lower or higher energy side of the resonance with the continuum of the Γ_3^- LO phonon, one obtains asymmetric line shapes of the exciton resonances in accordance with the theory of Fano resonances [263]. Since the formulas of Sec. 3.2 do not account for the phononic background, we could not determine correct asymmetries of the lines. Note that the phononic background has been subtracted from the results of Ref. [30] (cf. Figs. 2.15 and 2.16). For further information on this topic, see also Refs. [12, 264] and further references therein.

The Rydberg energies R_{exc} of excitonic spectra are generally obtained from fits to experimental results. Therefore, the value of R_{exc} for the yellow series of $\mathrm{Cu_2O}$ varies between 86 meV [37] and 97.2 meV [265] in the literature. The same argument holds for the band gap energy E_{g}. One reason for the deviations in the line positions in Fig. 3.5 is thus the uncertainity in these constants.

We have also assumed that the simple band model holds. Indeed, the results in Ref. [30] show that this approximation is reasonable; but one could also include the complete valence band structure in the theory [36, 72]. This makes an investigation of line widths very difficult since the energies $E_{\nu\boldsymbol{K}}$ have to be determined first of all, and a separation of relative motion and the motion of the center of mass is not possible (see Refs. [266, 267] and Chapter 9). The calculations in Ref. [266] on the line widths of the $1S$-exciton states of different semiconductors already show the main problems if one would have to extend the theory to principal quantum numbers of $n \geq 2$. On the other hand, an inclusion of the complete valence band structure results in a coupling of the yellow and green exciton series, especially to the green $1S$-exciton state [72]. Since we found out that the yellow $1S$-exciton state has a significant influence on the line width of the $2P$-exciton state, we expect that the coupling to the green $1S$-exciton state will lead to a further broadening of this line. The coupling to the (energetically higher located) green series may also be a reason for the large degree of asymmetry of the lines.

The complex valence band structure is sometimes treated in a simple approach in terms of quantum defects [30, 37]. However, the results of Ref. [37] show that this approach works well only at high quantum numbers ($n \geq 7$). Therefore, we did not consider quantum defects in our calculations.

The complex valence band structure also facilitates a coupling of excitons to TA phonons [85, 266, 268]. However, the effect of TA phonons is reported to be half as large as the effect of LA phonons [258, 269], which is already very small in our case. The coupling to TA phonons may be more important if external strains are applied to the crystal [270].

Impurities, especially point defects, in the crystal can lead to a broadening of exciton line widths [71]. The effect of an increase in the defect concentration has, according to Toyozawa [73], the same effect as a raising of the temperature. However, it has been discussed in the literature that a large concentration of impurities will lead to a more Gaussian or Voigt line shape [266, 271, 272]. This cannot be seen in the line spectrum measured in Ref. [30], for which reason we have to assume that the concentration of defects is low. Furthermore, the effect of a movement of defects being caused by phonons is said to be negligible [266].

The Fröhlich coupling constant was defined in Eq. (3.39). For $\mathrm{Cu_2O}$ we obtain $\alpha_1^{\mathrm{F}} \approx 0.24$ and $\alpha_2^{\mathrm{F}} \approx 0.20$. Since these values are clearly smaller than 1, we can neglect polaron corrections to the energy and the mass of the excitons [85, 255].

In the unit cell of $\mathrm{Cu_2O}$ there are always four copper atoms arranged in tetragonal symmetry [273], but only in every second tetragon an oxygen atom is located at its center. Since the oxygen atoms are very small, there is a chance that there are sometimes more than two oxygen atom in one unit cell. The excess atoms will then occupy the free positions in the lattice and act as acceptors. This results in small charges and in small internal electric fields, which will influence the exciton and lead to a line broadening. However, it is hard to account for these fields in theory.

The coupling between excitons and phonons is linear, i.e., there is always only one phonon being involved in a scattering process. In the literature, multi-phonon processes are said to be important in connection with piezoelectric coupling [249]. Sometimes, they are said to be negligible [271]. Since piezoelectric coupling is symmetry-forbidden in $\mathrm{Cu_2O}$, we do not consider multi-phonon processes.

The theory of Toyozawa accounts for the effect of $H_{\mathrm{exc-rad}}$ only within first order perturbation theory. If the coupling between excitons and photons is strong, one has to consider the specific properties of polaritons [7]. In other materials than $\mathrm{Cu_2O}$ the excitonic $1S$-ground state is often dipole allowed. The resulting large polariton coupling mainly changes the contribution of LA phonons to the line widths but the contribution of the LO phonons only weakly (see Ref. [255] and further references therein). Since the LA-phononic contribution is small for $\mathrm{Cu_2O}$, we expect that the polariton effect will not change our results significantly, so that it can even be neglected [258]. The related calculations and further corrections on the result of Toyozawa can be found, e.g., in Refs. [255, 266, 274] and further references therein.

We have shown that the central-cell corrections have a major influence on the line width of the $2P$-exciton state. Besides the central-cell corrections, which lead to an increase in the mass of the $1S$-exciton, there exists also a direction-dependent exciton dispersion, which results in a $\boldsymbol{K}$-dependent effective mass $\tilde{M}(\boldsymbol{K})$ of this exciton [82–84]. We expect the influence of the $\boldsymbol{K}$-dependency of the mass $\tilde{M}$ to be small for the following reason: We have proven that the effect of interband coupling on the line width is unimportant. For this reason the main contribution to the line widths comes from the region with $\boldsymbol{K} \approx \mathbf{0}$ and it is sufficient to take the value $\tilde{M}(\mathbf{0})$ (cf. the illustrations of intraband and interband scattering in Ref. [7]).

4 Impact of the valence band structure of Cu_2O on excitonic spectra

The simple band model of excitons assumes that both the valence band and the conduction band are parabolic, isotropic and nondegenerate. However, in all crystals with zinc-blende and diamond structure the valence band is degenerate at the center of the first Brillouin zone [80, 275]. Consequently, an interpretation of experimental spectra in terms of the hydrogen-like description of excitons is often not possible [276]. This is also true for cuprous oxide (Cu_2O). Only after Altarelli, Baldereschi and Lipari had developed the theory of excitons in semiconductors with degenerate valence bands in the 1970s [77–81], a controversy regarding the correct assignment of the exciton states for Cu_2O could be settled by Ch. Uihlein *et al.* in 1981 [72], i.e., almost 30 years after the experimental discovery of excitons in Cu_2O by Gross and Karryjew [6]. In connection with the experimental observation of the yellow exciton series in Cu_2O up to the principal quantum number of $n = 25$ [30], the complex valence band structure of Cu_2O has also moved into the focus once again [36, 37].

In this Chapter we describe at first in Sec. 4.1 the valence band structure of Cu_2O and already discuss its impact on the exciton series qualitatively. Having introduced the Hamiltonian of the exciton in Sec. 4.2, we present in Sec. 4.3 a method to solve the corresponding Schrödinger equation in a complete basis, which is based on the Coulomb-Sturmian functions. This method is not limited to certain quantum numbers as in previous works and also allows for the direct calculation of oscillator strengths [36, 80]. Furthermore, our method is of general applicability for all direct semiconductors with a complex valence band structure like, e.g., GaAs [81], CuBr [277], and other compounds [77]. Only the values of the material parameters used have to be replaced. In Sec. 4.4 we derive the formulas to caluclate the dipole and quadrupole oscillator strengths of exciton states in Cu_2O.

Having presented the theory, we reinvestigate the calculations of Ref. [36] in Sec. 4.5.1 in connection with the values of the three Luttinger parameters of Cu_2O. Deviations from previous results are observed and discussed. Furthermore, we show in Sec. 4.5.2 that a finite momentum $\hbar K$ of the center of mass leads to terms in the Hamiltonian, which were initially assigned to the exchange interaction [82–84]. These terms are of the correct order of magnitude to describe the experimentally observed K-dependent line splitting of the $1S$ exciton [82–84]. Essential parts of this Chapter have been published in Refs. [38, 278].

4.1 Valence band structure and the yellow exciton series in Cu_2O

Concerning its hydrogen-like spectrum up to a principal quantum number of $n = 25$ [30], the yellow exciton in Cu_2O seems to be a perfect example of a Wannier exciton. However, a more precise investigation of this spectrum shows clear deviations from the simple model with spherical effective masses [36, 72]. These deviations can be explained in terms of the complex valence band structure of Cu_2O.

Without spin-orbit coupling the valence band in Cu_2O has the symmetry Γ_5^+ and is threefold degenerate at the Γ-point or the center of the Brillouin zone. This degeneracy can be accounted for by a quasi-spin $I = 1$, which is a convenient abstraction to denote the three orbital Bloch functions xy, yz, and zx, which transform according to Γ_5^+. Since Cu_2O has cubic symmetry, the symmetry of the bands can be assigned by the irreducible representations $\Gamma_i^\pm$ of the cubic group O_h, where the superscript ± denotes the parity[1]. Considering the spin-orbit coupling between the quasi-spin I and the spin S_h of a hole in the valence band, this sixfold degenerate band (now including the hole spin) splits into a lower lying fourfold-degenerate band (Γ_8^+) and a higher lying twofold-degenerate band (Γ_7^+) by an amount of Δ, which is the spin-orbit coupling constant (see Fig. 2.14). The presence of the nonspherical symmetry of the solid as well as interband interactions cause these bands to be nonparabolic but deformed.

Neglecting these effects at first, one arrives at the simple-band model and can distinguish between four exciton series depending on the valence band and the conduction band involved (see Fig. 2.14). Within this model the wave function of an exciton consists of the so-called envelope function, which describes the relative movement of the electron and the hole, and the Bloch functions of the bands involved (cf. Sec. 2.5.2) [7].

Due to the spins of electron and hole, e.g., the yellow exciton series is fourfold degenerate. The presence of an exchange interaction between the spins of the electron and the hole lifts this degeneracy and leads to ortho- and para-excitons [12, 30]. While the threefold degenerate ortho-excitons can be observed in absorption spectra, the non-degenerate para-excitons are spin-flip-forbidden [12].

Going now beyond the simple-band model, the anisotropic dispersion of the valence band has a significant influence on the excitons of the yellow series. The anisotropic dispersion leads to a coupling between the relative motion of the electron and the hole and the orbital Bloch functions xy, yz, and zx [169] of the original Γ_5^+-band. This will be described mathematically by the so-called H_d-term in Sec. 4.3.

As can be seen from Fig. 2.14, the yellow exciton series is connected with the Γ_7^+-valence band. Due to symmetry considerations, the amplitudes which describe the magnitude of the contribution of the orbital Bloch functions xy, yz and zx to this band must have the same absolute value. Thus, the anisotropy of the Γ_5^+-Bloch functions is compensated in the Γ_7^+-band. The same statement now also holds for all non-degenerate exciton states: for reasons of symmetry, the wave function of para-excitons contains the orbital Bloch functions with amplitudes having the same absolute value. Thus, the dispersion of the para-exciton can be described by an isotropic exciton mass.

As regards the threefold degenerate ortho-exciton, the situation is different: each of the three exciton states can have a larger contribution of one of the orbital Bloch functions, respectively,

---

[1] An introduction to the group theory of crystals and sets of tables can be found, e.g., in [12, 90, 169, 170].

without a violation of symmetry. The disparity in the orbital Bloch components of the ortho-exciton is caused by an admixture of the Γ_8^+-valence band via the H_{d}-term. This disparity has then an impact on the relative motion of electron and hole. As a consequence, the envelope function of the ortho-exciton has no further spherical or cubic symmetry but $D_{4\mathrm{h}}$-symmetry. Since $D_{4\mathrm{h}}$ is a subgroup of O_{h}, it contains all symmetry operations, which leave a given Γ_5^+-component of the ortho-exciton invariant. For instance, in the case of the xy-component the symmetry axis of the according subgroup $D_{4\mathrm{h}}$ is the z-axis of the crystal. So the reduction of the symmetry of the envelope function reflects the anisotropic dispersion of the orbital Bloch functions. Due to the H_{d}-term the cubic symmetry O_{h} holds no further for the Bloch functions and the relative motion separately but only for the combined function.

The lower symmetry of the envelope function allows for a smaller mean distance between electron and hole in a specific direction, which leads to a gain of energy due to the Coulomb interaction. This effect may be compared to the Jahn-Teller effect, where a reduction of symmetry in connection with degeneracies leads to a gain of energy in the system.

As can be seen, there is a close connection between degeneracy and symmetry reduction of the envelope function. This fact explains one of the most striking features of excitonic spectra in $\mathrm{Cu_2O}$: the visibility of D and F exciton states, i.e., exciton states with angular momentum $L = 2$ and $L = 3$ [36, 72]. The visibility arises due to the admixture of quadrupole or dipole-allowed S- and P-exciton states.

In the following sections 4.2 and 4.3 we will now introduce the problem of excitons in $\mathrm{Cu_2O}$ from a more mathematical point of view.

4.2 Hamiltonian

Via $\boldsymbol{k}\cdot\boldsymbol{p}$-perturbation theory and symmetry considerations one can derive the Hamiltonian or the kinetic energy of an electron within the valence band structure described in Sec. 4.1 [12, 37, 126]:

$$\begin{aligned} H_{\mathrm{vb}}(\boldsymbol{k}) \;=\;& -H_{\mathrm{so}} + (1/2m_0)\left\{\boldsymbol{k}^2\left[\hbar^2 A_1 + 2B_1(\boldsymbol{I}\cdot\boldsymbol{S}_{\mathrm{h}})\right]\right. \\ & +A_2\left[k_1^2(\boldsymbol{I}_1^2 - \boldsymbol{I}^2/3) + \mathrm{c.p.}\right] + B_2\left[2k_1^2(\boldsymbol{I}_1\boldsymbol{S}_{\mathrm{h}1} - \boldsymbol{I}\boldsymbol{S}_{\mathrm{h}}/3) + \mathrm{c.p.}\right] \\ & \left. +A_3\left[2\left\{k_1,\,k_2\right\}\left\{\boldsymbol{I}_1,\,\boldsymbol{I}_2\right\} + \mathrm{c.p.}\right] + B_3\left[2\left\{k_1,\,k_2\right\}(\boldsymbol{I}_1\boldsymbol{S}_{\mathrm{h}2} + \boldsymbol{I}_2\boldsymbol{S}_{\mathrm{h}1}) + \mathrm{c.p.}\right]\right\} \end{aligned} \tag{4.1}$$

with $\{a,b\} = \frac{1}{2}(ab+ba)$, the free electron mass m_0, and c.p. denoting cyclic permutation. The spin-orbit coupling reads [36, 72]

$$H_{\mathrm{so}} = \frac{2}{3}\Delta\left(1 + \frac{1}{\hbar^2}\boldsymbol{I}\cdot\boldsymbol{S}_{\mathrm{h}}\right). \tag{4.2}$$

Note that we use, in contrast to Ref. [37], the energy shift of $2\Delta/3$, by which the energy of the Γ_7^+-band is set to zero at the Γ-point. Furthermore, we use the spin matrices of spin 1/2 for the hole spin instead of the Pauli matrices. The matrices of the quasi-spin $I = 1$ are defined as in Ref. [126],

$$\boldsymbol{I}_k = \sum_{lm} -i\hbar\varepsilon_{klm}(\hat{\boldsymbol{e}}_l \otimes \hat{\boldsymbol{e}}_m), \tag{4.3}$$

with the unit vectors $\hat{\boldsymbol{e}}_i$ and the Levi-Civita symbol ε_{klm}.

Very recently, the parameters A_i and B_i in Eq. (4.1) have been obtained [37] by fitting the Hamiltonian to results of band structure calculations [279]:

$$A_1 = -1.76, \quad A_2 = 4.519, \quad A_3 = -2.201, \tag{4.4a}$$

$$B_1 = 0.02, \quad B_2 = -0.022, \quad B_3 = -0.202. \tag{4.4b}$$

In the case of an exciton one generally treats the missing electron in the valence band as a hole, i.e., a quasi-particle with an energy being opposite to the energy of the other electrons in the valence band. Using the definition of the three Luttinger parameters,

$$\gamma_1 = -A_1, \quad \gamma_2 = A_2/6, \quad \gamma_3 = A_3/6, \tag{4.5a}$$

and defining by analogy

$$\eta_1 = -B_1, \quad \eta_2 = B_2/6, \quad \eta_3 = B_3/6, \tag{4.5b}$$

the Hamiltonian of the hole reads [12, 36, 85, 280]

$$\begin{aligned} H_\mathrm{h}(\boldsymbol{p}_\mathrm{h}) = {} & H_\mathrm{so} + (1/2\hbar^2 m_0)\left\{\hbar^2(\gamma_1 + 4\gamma_2)\boldsymbol{p}_\mathrm{h}^2\right. \\ & +2(\eta_1 + 2\eta_2)\boldsymbol{p}_\mathrm{h}^2(\boldsymbol{I}\cdot\boldsymbol{S}_\mathrm{h}) - 6\gamma_2\left[p_\mathrm{h1}^2\boldsymbol{I}_1^2 + \mathrm{c.p.}\right] - 12\eta_2\left[p_\mathrm{h1}^2\boldsymbol{I}_1\boldsymbol{S}_\mathrm{h1} + \mathrm{c.p.}\right] \\ & \left. -12\gamma_3\left[\{p_\mathrm{h1}, p_\mathrm{h2}\}\{\boldsymbol{I}_1, \boldsymbol{I}_2\} + \mathrm{c.p.}\right] - 12\eta_3\left[\{p_\mathrm{h1}, p_\mathrm{h2}\}(\boldsymbol{I}_1\boldsymbol{S}_\mathrm{h2} + \boldsymbol{I}_2\boldsymbol{S}_\mathrm{h1}) + \mathrm{c.p.}\right]\right\}. \end{aligned} \tag{4.6}$$

The parameters in Eq. (4.6) describe the dispersion of the hole in the vicinity of the Γ-point: γ_1 and η_1 determine the average effective mass of the hole while the other parameters describe the splitting of the bands in the vicinity of the Γ-point and the so-called band warping or the nonspherical symmetry of the bands [12].

The Hamiltonian of the exciton is then given by [72, 80]

$$H = E_\mathrm{g} + H_\mathrm{e}(\boldsymbol{p}_\mathrm{e}) + H_\mathrm{h}(\boldsymbol{p}_\mathrm{h}) + V + H_\mathrm{exch} + V_\mathrm{CCC} \tag{4.7}$$

with the energy E_g of the band gap and the kinetic energy of the electron,

$$H_\mathrm{e}(\boldsymbol{p}_\mathrm{e}) = \frac{\boldsymbol{p}_\mathrm{e}^2}{2m_\mathrm{e}}. \tag{4.8}$$

Here m_e denotes the effective mass of the electron. The Coulomb interaction, which is screened by the dielectric constant ε, reads

$$V(\boldsymbol{r}_e - \boldsymbol{r}_h) = -\frac{e^2}{4\pi\varepsilon_0\varepsilon_\mathrm{s1}}\frac{1}{|\boldsymbol{r}_e - \boldsymbol{r}_h|}. \tag{4.9}$$

The last two terms of Eq. (4.7) denote the exchange interaction and the central-cell corrections, which will be discussed in detail in Chapters 5 and 6. If no external fields are present, the different terms of the Hamiltonian couple only basis states with even or with odd values of L. We restrict ourselves to odd values of L in this chapter, as the corresponding exciton states are dipole-allowed. Hence, the exchange interaction and the central-cell corrections can be neglected as they affect exciton states with an $L = 0$-component.

For subsequent calculations it is appropriate to write the Hamiltonian (4.7) in terms of irreducible tensors [79, 248, 281], where we additionally set the position and the momentum of the center of mass to zero:

$$\begin{aligned} H = {} & E_{\mathrm{g}} - \frac{e^2}{4\pi\varepsilon_0\varepsilon}\frac{1}{r} + \frac{2}{3}\Delta\left(1+\frac{1}{\hbar^2}I^{(1)}\cdot S_{\mathrm{h}}^{(1)}\right) \\ & + \frac{\gamma_1'}{2\hbar^2 m_0}\left[\hbar^2 p^2 - \frac{\mu'}{3}\left(P^{(2)}\cdot I^{(2)}\right)\right. \\ & \qquad \left. + \frac{\delta'}{3}\left(\sum_{k=\pm4}\left[P^{(2)}\times I^{(2)}\right]^{(4)}_k + \frac{\sqrt{70}}{5}\left[P^{(2)}\times I^{(2)}\right]^{(4)}_0\right)\right] \\ & + \frac{3\eta_1}{\hbar^2 m_0}\left[\frac{1}{3}p^2\left(I^{(1)}\cdot S_{\mathrm{h}}^{(1)}\right) - \frac{\nu}{3}\left(P^{(2)}\cdot D^{(2)}\right)\right. \\ & \qquad \left. + \frac{\tau}{3}\left(\sum_{k=\pm4}\left[P^{(2)}\times D^{(2)}\right]^{(4)}_k + \frac{\sqrt{70}}{5}\left[P^{(2)}\times D^{(2)}\right]^{(4)}_0\right)\right] . \end{aligned} \tag{4.10}$$

The first-order and second-order tensor operators correspond, as in Ref. [281], to the vector operators $\boldsymbol{r}$, $\boldsymbol{I}$, $\boldsymbol{S}_{\mathrm{e/h}}$, and to the second-rank Cartesian operators

$$I_{mn} = 3\left\{I_m,\, I_n\right\} - \delta_{mn}I^2, \tag{4.11a}$$

$$P_{mn} = 3\left\{p_m,\, p_n\right\} - \delta_{mn}p^2, \tag{4.11b}$$

respectively. We also use the abbreviation

$$D_k^{(2)} = \left[I^{(1)}\times S_{\mathrm{h}}^{(1)}\right]^{(2)}_k . \tag{4.12}$$

The coefficients γ_1', μ', and δ' are given by [72, 79]

$$\gamma_1' = \gamma_1 + \frac{m_0}{m_{\mathrm{e}}}, \quad \mu' = \frac{6\gamma_3+4\gamma_2}{5\gamma_1'}, \quad \delta' = \frac{\gamma_3-\gamma_2}{\gamma_1'} \tag{4.13a}$$

and we define by analogy

$$\nu = \frac{6\eta_3+4\eta_2}{5\eta_1}, \quad \tau = \frac{\eta_3-\eta_2}{\eta_1}. \tag{4.13b}$$

Since $\eta_i \ll \gamma_i$ holds in Eq. (4.6), we neglect the corresponding terms of the Hamiltonian (4.10) in the following and use them only for the calculations at the end of Sec. 4.5.1. The material parameters used in our calculations are listed in Table 2.2.

In Ref. [72] the parameters $\gamma_1' = 2.78$ and $\mu' = 0.47$ have been obtained as fit parameters to excitonic spectra using the spherical model, in which the cubic terms in the Hamiltonian, i.e., the δ'-dependent terms, are neglected. Recent calculations on the band structure of $\mathrm{Cu_2O}$ [279] yielded different values for the corresponding material parameters [37]: $\gamma_1' = 2.77$, $\mu' = 0.0586$, and $\delta' = -0.404$. This shows that the spherical model by which $\mu' = 0.47$ had been obtained may be inappropriate since $|\delta'| \gg |\mu'|$ holds.

Note that by setting the total momentum to zero, we neglect polariton effects, even though in experiments the polaritonic part is always present. However, when considering the experimental results of Refs. [82–84], the polariton effect on the $1S$ exciton is on the order of tens of μeV and, hence, much smaller than the energy shifts considered here. Furthermore, in Ref. [282] criteria for the experimental observability of polariton effects are given. Inserting the material parameters of Cu_2O and the experimental linewidths of the exciton states observed in Refs. [30, 36], it can be shown that polariton effects are not observable for the exciton states of $n \geq 2$. We will discuss this in greater detail in Chapter 9.

4.3 Complete basis set

To find an appropriate basis set to solve the Schrödinger equation, we have to discuss the different terms of the Hamiltonian (4.10) as in Ref. [72]. The Hamiltonian

$$H_{\mathrm{sb}} = E_{\mathrm{g}} - \frac{e^2}{4\pi\varepsilon_0\varepsilon_{\mathrm{s1}}}\frac{1}{r} + H_s + V_{\mathrm{CCC}} \tag{4.14}$$

with the spherically symmetric part of the kinetic energy

$$H_s = \frac{\gamma_1' p^2}{2m_0} \tag{4.15}$$

is the hydrogen-like Hamiltonian of the simple-band model. Without the central-cell corrections V_{CCC}, which here account for the deviations of the exciton ground state from the hydrogen-like series, the solutions of H_{sb} are given by

$$E_n = E_{\mathrm{g}} - \frac{R_{\mathrm{exc}}}{n^2} \tag{4.16}$$

with the principal quantum number n and the excitonic Rydberg energy R_{exc} [12]. The eigenfunctions are the well-known solutions of the Schrödinger equation of the hydrogen atom, where only the Bohr radius a_0 is to be replaced by the excitonic radius $a_{\mathrm{exc}} = \varepsilon\gamma_1' a_0$ [12].

The spin-orbit interaction H_{so} couples the quasi-spin $I = 1$ and the hole spin $S_{\mathrm{h}} = 1/2$ to the effective hole spin $J = I + S_{\mathrm{h}}$, where $J = 1/2$ corresponds to the Γ_7^+ valence band and $J = 3/2$ corresponds to the Γ_8^+ valence bands. The value of J therefore distinguishes between the yellow ($J = 1/2$) and the green ($J = 3/2$) exciton series (see Fig. 2.14). Within this approximation, these are two noninteracting hydrogen-like exciton series.

The remaining parts of H without the exchange interaction form the so-called H_d term:

$$H_d = \frac{\gamma_1'}{2\hbar^2 m_0}\left\{-\frac{\mu'}{3}P^{(2)}\cdot I^{(2)} + \frac{\delta'}{3}\left(\sum_{k=\pm 4}\left[P^{(2)}\times I^{(2)}\right]^{(4)}_k + \frac{\sqrt{70}}{5}\left[P^{(2)}\times I^{(2)}\right]^{(4)}_0\right)\right\}. \tag{4.17}$$

This term mixes the two exciton series as discussed in Sec. 4.1. In the spherical approximation ($\delta' = 0$), in which the Hamiltonian has still spherical symmetry, the momentum $F = L + J$ and its z-component M_F are good quantum numbers, while $\boldsymbol{L}$ and $\boldsymbol{J}$ do not commute with H_d. This leads to a fine-structure splitting of the eigenstates of the Hamiltonian, which is discussed, e.g., in Refs. [72, 79, 80] for several semiconductors. The angular momentum part of an appropriate basis set reads

$$|L;\, (I,\, S_{\mathrm{h}}),\, J;\, F,\, M_F\rangle\, |S_{\mathrm{e}},\, M_{S_{\mathrm{e}}}\rangle\,, \tag{4.18}$$

where the z-component $M_{S_{\mathrm{e}}}$ of the electron spin $S_{\mathrm{e}} = 1/2$ is also a good quantum number.

The other parts of H_d with the coefficient δ' have cubic symmetry. For this reason neither F nor M_F are good quantum numbers anymore [78]. The eigenstates of the Hamiltonian transform according to the irreducible representations $\Gamma_i^{\pm}$ of the cubic group O_{h} instead of those of the full rotation group.

In the case in which the value of an arbitrary (integral or half-integral valued) momentum A is less than or equal to four, it is possible to form linear combinations of the states $|A,\, M_A\rangle$ that transform according to the irreducible representations of O_{h} [36, 169]. For example, the state $(|3,\, 2\rangle - |3,\, -2\rangle)/\sqrt{2}$ transforms according to the irreducible representation Γ_2^- of O_{h}. These states are often denoted by $|A,\, \Gamma_i\rangle$ [78]. However, this procedure is not uniquely possible for $A > 4$ due to arising degeneracies [169]. Therefore, it is reasonable to describe the angular-momentum part by Eq. (4.18) even if $\delta' \neq 0$ holds.

The effect of H_d on the eigenstates of the Hamiltonian decreases with increasing principal quantum number n since the wave functions extend over more unit cells and the cubic symmetry of the solid becomes less important [36]. An approach to treat the effects of H_d on exciton states with high values of n in a simple way can be found in Ref. [37].

The exchange interaction H_{exch} couples the spins of electron and hole and leads to a splitting of S excitons, i.e., excitons with $L = 0$, into ortho- and para-excitons [72]. The coupling of the spins leads to a total momentum $F_t = F + S_{\mathrm{e}}$ and we finally obtain

$$|L;\, (I,\, S_{\mathrm{h}}),\, J;\, F,\, S_{\mathrm{e}};\, F_t,\, M_{F_t}\rangle \tag{4.19}$$

for the angular momentum part of an appropriate basis set.

In the literature the radial part of the basis is often not specified. A typical ansatz for the wavefunction of the exciton is

$$\Psi = \sum_{\beta} g_{\beta}(r)\, |L;\, (I,\, S_{\mathrm{h}}),\, J;\, F,\, S_{\mathrm{e}};\, F_t,\, M_{F_t}\rangle\,, \tag{4.20}$$

where β denotes the quantum numbers L, J, F, F_t, and M_{F_t}. The radial functions $g_{\beta}(r)$ are often determined using finite-element methods [72, 277] or variational methods [78–81, 266]. Unfortunately, these methods lead to a huge number of coupled differential equations for the functions $g_{\beta}(r)$.

In contrast to earlier works, we use a complete basis for the radial functions. Since the eigenfunctions of the hydrogen atom do not represent a complete basis without the continuum states, we use the so-called Coulomb-Sturmian functions as described, e.g., in Ref. [283]. The radial functions of this basis read

$$U_{NL}(r) = N_{NL}(2\rho)^L e^{-\rho} L_N^{2L+1}(2\rho) \tag{4.21}$$

with $\rho = r/\alpha$, a normalization factor N_{NL}, the associated Laguerre polynomials $L_n^m(x)$, and an arbitrary scaling parameter α. Note that we use the radial quantum number N, which is related to the principal quantum number n via $n = N + L + 1$. Various recursion relations of these functions, which are needed for our calculations, are given in Appendix E.

Our basis set finally reads

$$|\Pi\rangle \;=\; |N,\, L;\, (I,\, S_{\mathrm{h}}),\, J;\, F,\, S_{\mathrm{e}};\, F_t,\, M_{F_t}\rangle \tag{4.22}$$

and we make the ansatz

$$|\Psi\rangle = \sum_{NLJFF_tM_{F_t}} c_{NLJFF_tM_{F_t}}\, |\Pi\rangle \tag{4.23}$$

for the exciton wave function with real coefficients[2] c. Since the functions $U_{NL}(r)$ actually depend on the coordinate $\rho = r/\alpha$, we substitute $r \to \rho\alpha$ in the Hamiltonian (4.10) and multiply the corresponding Schrödinger equation $H\left|\Psi\right\rangle = E\left|\Psi\right\rangle$ by α^2. Multiplying from the left with another basis state $\left\langle\Pi'\right|$, we obtain a generalized eigenvalue problem of the form

$$\boldsymbol{D}\boldsymbol{c} = E\boldsymbol{M}\boldsymbol{c}, \tag{4.24}$$

which is solved in atomic units using an appropriate Lapack routine [284]. The matrix elements which enter the symmetric matrices $\boldsymbol{D}$ and $\boldsymbol{M}$ are given in Appendix F. The vector $\boldsymbol{c}$ contains the coefficients of the ansatz (4.23).

Since the basis cannot be infinitely large, the values of the quantum numbers are chosen in the following way: For each value of $n = N + L + 1 \leq n_{\max}$ we use

$$\begin{aligned} L &= 0, \ldots, n-1, \\ J &= 1/2,\, 3/2, \\ F &= \left|L-J\right|, \ldots, \min(L+J,\, F_{\max}), \\ F_t &= F-1/2,\, F+1/2, \\ M_{F_t} &= -F_t, \ldots, F_t. \end{aligned} \tag{4.25}$$

The value $F_{\max}$ and the maximum value $n_{\max}$ of n are chosen appropriately large so that the eigenvalues converge. Additionally, we can use the scaling parameter α to enhance convergence. In particular, if the eigenvalues of excitonic states with principal quantum number n are calculated, we set $\alpha = n a_{\mathrm{exc}}$ according to Ref. [283].

The total symmetry of the exciton is given by the symmetry of envelope function and the symmetries of the bands:

$$\Gamma_{\mathrm{exc}} = \Gamma_{\mathrm{env}} \otimes \Gamma_{\mathrm{c}} \otimes \Gamma_{\mathrm{v}}, \tag{4.26}$$

Since we consider the symmetry of the valence band via the spins I and S_{h} as well as the symmetry of the conduction band via the spin S_{e} in our basis, the total symmetry of the exciton can immediately be obtained by an examination of the solutions of the Schrödinger equation in the complete basis set of Eq. (4.22). Three important points have to be considered in this examination:

We already stated in Sec. 4.3 that it is possible to combine the different states $\left|A,\, M_A\right\rangle$ of an arbitrary momentum $A \leq 4$ to the states $\left|A,\, \Gamma_i\right\rangle$. Solving the eigenvalue problem (4.24), we obtain the coefficients c of the basis functions according to Eq. (4.23). We can now compare the coefficients of those basis functions with a fixed value of $F_t \leq 4$ to the coefficients of the functions $\left|A,\, \Gamma_i\right\rangle$ given in Ref. [169] to obtain the symmetry of the eigenstates.

If an eigenvalue is p-fold degenerate, one has to form appropriate linear combinations of the p eigenvectors $\boldsymbol{c}$ at first, before a comparison with the coefficients of the states $\left|A,\, \Gamma_i\right\rangle$ is possible.

The quasi-spin I transforms according to Γ_5^+ whereas a normal spin one transforms according to Γ_4^+. Since $\Gamma_5^+ = \Gamma_2^+ \otimes \Gamma_4^+$ holds for the cubic group O_{h} [169], one has to multiply the symmetries Γ_i obtained via the above comparison by Γ_2^+ [36].

The decisive advantage of the method of solving the Schrödinger equation in a complete basis is the fact that it can also be used for the theoretical investigation of exciton spectra in external magnetic and electric fields, where the effects of the complex valence band structure are much

---

[2] In the treatments with an external magnetic field $\boldsymbol{B}$ in Chapter 8 or with a finite momentum of the center of mass $\hbar\boldsymbol{K}$ in Chapter 9 the coefficients c are complex and also depend on $\boldsymbol{B}$ or $\boldsymbol{K}$. For the latter case we will write $\left|\Psi_{\nu\boldsymbol{K}}\right\rangle = \sum_{NLJFF_tM_{F_t}} c_{NLJFF_tM_{F_t}}^{\nu\boldsymbol{K}} \left|\Pi\right\rangle$, where the index ν denotes the different exciton states.

more evident [276] and where other methods with a restricted amount of quantum numbers [36, 81] may be too imprecise or too complex due to the strong mixing of different exciton states. The investigation of excitonic spectra in an external magnetic field is presented in Chapters 7 and 8.

4.4 Oscillator strengths

Having solved the generalized eigenvalue problem (4.24), one can determine relative oscillator strengths. For reasons of completeness, we derive here the formulas for the dipole *and* the quadrupole oscillator strength but note that for the quadrupole oscillator strength the complete $\boldsymbol{K}$-dependent Hamiltonian of Chapter 9 needs to be solved.

For the derivation of the formulas we will assume that the states of the system are separable, i.e., that there are *true* exciton, photon and phonon states. By this means we can treat the exciton-photon interaction as a perturbation and calculate transition probabilities for the simple excitations of excitons by a photons since they generally determine the strengths of the absorption lines measured [7]. The exciton excited is in this case simply assumed to decay to another unspecified state.

We start with the results of Section 2.4.3. In analogy to[3] Eq. (2.175), the transition rate in first order perturbation theory from the crystal ground state Φ_0 to an exciton state $\Psi^{\sigma\tau}_{vc,\,\nu\boldsymbol{K}}$ is given by

$$W_{\nu\boldsymbol{K},0}=\frac{2\pi}{\hbar}\left|\int\Psi^{\sigma\tau*}_{vc,\,\nu\boldsymbol{K}}\left[\frac{-e}{m_0}\boldsymbol{A}_0(\boldsymbol{\kappa},\xi)\sum_{l=1}^{N}e^{i\boldsymbol{\kappa}\cdot\boldsymbol{r}_l}\boldsymbol{p}_l\right]\Phi_0\,\mathrm{d}\boldsymbol{r}_1\cdots\mathrm{d}\boldsymbol{r}_N\right|^2\delta(E^{(0)}_{\nu\boldsymbol{K}}-E^{(1)}_0-\hbar\omega).\quad(4.27)$$

Here $\boldsymbol{A}_0(\boldsymbol{\kappa},\xi)$ denotes the amplitude of the vector potential of the radiation field with the wave vector $\boldsymbol{\kappa}$ and the polarization ξ. N denotes the number of electrons with the coordinates $\boldsymbol{r}_l$. Since Φ_0 is invariant under all the operations of the space group [7], $\Psi^{\sigma\tau}_{vc,\,\nu\boldsymbol{K}}$ and the operator in square brackets must have at least one common symmetry type. On the one hand, this means $\boldsymbol{\kappa}=\boldsymbol{K}+\boldsymbol{G}$ with a reciprocal lattice vector $\boldsymbol{G}$, which is generally zero. On the other hand, one has to take a look at the symmetries of the perturbation, i.e., discuss the different summands when performing a Taylor expansion in terms of irreducible representations. This will be done later on. Furthermore, the state $\Psi_{\nu\boldsymbol{K}}$ most contain a pure spin singlet component since the perturbation does not act on spin terms. Since typical values of $\boldsymbol{\kappa}$ for visible and ultraviolett light are very small compared to the extension of the first BZ, excitons are generally created in the vicinity of $\boldsymbol{K}=\boldsymbol{0}$.

According to Eq. (4.27) the probability per unit time for a transition from the ground state Φ_0 of the semiconductor to an exciton state $\Psi^{\sigma\tau}_{vc,\,\nu\boldsymbol{K}}$ is proportional to $|M|^2$ with

$$M=\int\Psi^{\sigma\tau*}_{vc,\,\nu\boldsymbol{K}}\left[\frac{-e}{m_0}\boldsymbol{A}_0(\boldsymbol{\kappa},\xi)\sum_{l=1}^{N}e^{i\boldsymbol{\kappa}\cdot\boldsymbol{r}_l}\boldsymbol{p}_l\right]\Phi_0\,\mathrm{d}\boldsymbol{r}_1\cdots\mathrm{d}\boldsymbol{r}_N.\quad(4.28)$$

Within the scope of the simple band model the wave function of an exciton is given by

$$\Psi^{\sigma\tau}_{vc,\,\nu\boldsymbol{K}}\;=\;\sum_{\boldsymbol{q}}f_{vc\,\nu}(\boldsymbol{q})\,\Phi^{\sigma\tau}_{vc}(\boldsymbol{q}-\gamma\boldsymbol{K},\,\boldsymbol{q}+\alpha\boldsymbol{K}),\quad(4.29)$$

---

[3] Note that we do not use the single-particle approximation but instead the Hamiltonian (2.172) neglecting terms of quadratic order in $\boldsymbol{A}$.

where τ and $-\sigma$ denote the spins of the electron and the hole, respectively. As we will discuss below, the spin orbit splitting in Cu_2O does not have a perceptible effect on the oscillator strength. Hence, we will keep the derivation of the formula for the oscillator strength more simple by assuming a threefold degenerate Γ_5^+ valence band and treating the electron and hole spin separately.

The envelope function $f_{vc\,\nu}(\boldsymbol{q})$ in Eq. (4.29) is the Fourier transform of the solution $F_{vc\,\nu}(\boldsymbol{\beta})$ of the Wannier equation (see Sec. 2.5.2 and Refs. [5, 7]),

$$f_{vc\,\nu}(\boldsymbol{q}) = \frac{1}{\sqrt{N}} \sum_{\boldsymbol{\beta}} F_{vc\,\nu}(\boldsymbol{\beta}) e^{-i\boldsymbol{q}\cdot\boldsymbol{\beta}}, \tag{4.30}$$

with ν denoting the different exciton states. Note that the coordinate $\boldsymbol{\beta}$ is a lattice vector which in general takes only discrete values [162]. This coordinate is identical to the relative coordinate $\boldsymbol{r}$ in the continuum approximation. The constant factors $\alpha = m_{\mathrm{e}}/(m_{\mathrm{e}} + m_{\mathrm{h}})$ and $\gamma = 1 - \alpha$ depend on the effective masses of the electron and the hole.

The wave function (4.29) also contains the state $\Phi_{vc}^{\sigma\tau}$ of Eq. (2.145). With the ground state Φ_0 (2.124a) of the semiconductor, we can express the exciton state (4.29) as

$$\left|\Psi_{vc,\,\nu\boldsymbol{K}}^{\sigma\tau}\right\rangle = \sum_{\boldsymbol{q}} f_{vc\,\nu}(\boldsymbol{q}) c^{\dagger}_{c(\boldsymbol{q}+\alpha\boldsymbol{K})\tau} c_{v(\boldsymbol{q}-\gamma\boldsymbol{K})\sigma} \left|\Phi_0\right\rangle, \tag{4.31}$$

using creation and annihilation operators. The operator in square brackets in Eq. (4.28) can be written in second quantization as

$$\sum_{nn'} \sum_{\boldsymbol{k}\boldsymbol{k}'} \sum_{\sigma'\tau'} -\frac{e}{m_0} \boldsymbol{A}_0(\boldsymbol{\kappa}, \xi) \cdot \left\langle \psi_{n'\boldsymbol{k}'\tau'} \left| e^{i\boldsymbol{\kappa}\cdot\boldsymbol{r}} \boldsymbol{p} \right| \psi_{n\boldsymbol{k}\sigma'} \right\rangle c^{\dagger}_{n'\boldsymbol{k}'\tau'} c_{n\boldsymbol{k}\sigma'}. \tag{4.32}$$

The matrix element (4.28) then reads

$$\begin{aligned} M \;=\; & -\frac{e}{m_0} \boldsymbol{A}_0(\boldsymbol{\kappa}, \xi) \cdot \sum_{\boldsymbol{q}} \sum_{nn'} \sum_{\boldsymbol{k}\boldsymbol{k}'} \sum_{\sigma'\tau'} f^{*}_{vc\,\nu}(\boldsymbol{q}) \left\langle \psi_{n'\boldsymbol{k}'\tau'} \left| e^{i\boldsymbol{\kappa}\cdot\boldsymbol{r}} \boldsymbol{p} \right| \psi_{n\boldsymbol{k}\sigma'} \right\rangle \\ & \times \left\langle \Phi_0 \right| c^{\dagger}_{v(\boldsymbol{q}-\gamma\boldsymbol{K})\sigma} c_{c(\boldsymbol{q}+\alpha\boldsymbol{K})\tau} c^{\dagger}_{n'\boldsymbol{k}'\tau'} c_{n\boldsymbol{k}\sigma'} \left|\Phi_0\right\rangle. \end{aligned} \tag{4.33}$$

The second part is nonzero only if $n'\boldsymbol{k}'\tau' = c(\boldsymbol{q} + \alpha\boldsymbol{K})\tau$ and $n\boldsymbol{k}\sigma' = v(\boldsymbol{q} - \gamma\boldsymbol{K})\sigma$ holds. Due to the anticommutation relations for the operators c and $c^{\dagger}$, we obtain

$$M = -\frac{e}{m_0} \boldsymbol{A}_0(\boldsymbol{\kappa}, \xi) \cdot \sum_{\boldsymbol{q}} f^{*}_{vc\,\nu}(\boldsymbol{q}) \int \mathrm{d}\boldsymbol{r}\, \psi^{*}_{c(\boldsymbol{q}+\alpha\boldsymbol{K})\tau}(\boldsymbol{r}) e^{i\boldsymbol{\kappa}\cdot\boldsymbol{r}} \boldsymbol{p} \psi_{v(\boldsymbol{q}-\gamma\boldsymbol{K})\sigma}(\boldsymbol{r}). \tag{4.34}$$

We use $\boldsymbol{A}_0(\boldsymbol{\kappa}, \xi) = A_0(\boldsymbol{\kappa}, \xi)\hat{\boldsymbol{e}}_{\xi\boldsymbol{\kappa}}$ as well as the relations $\psi_{n\boldsymbol{k}\sigma}(\boldsymbol{r} + \boldsymbol{R}) = e^{i\boldsymbol{k}\cdot\boldsymbol{R}} \psi_{n\boldsymbol{k}\sigma}(\boldsymbol{r})$ and $\sum_{\boldsymbol{R}} e^{i\boldsymbol{k}\cdot\boldsymbol{R}} = N \sum_{\boldsymbol{G}} \delta_{\boldsymbol{k},\boldsymbol{G}}$ and rewrite Eq. (4.34) with integrals over Wigner-Seitz cells (WSC):

$$\begin{aligned} M = & -\frac{e}{m_0} \boldsymbol{A}_0(\boldsymbol{\kappa}, \xi) \sum_{\boldsymbol{q}} f^{*}_{vc\,\nu}(\boldsymbol{q}) \\ & \times \sum_{\boldsymbol{R}} \int_{\mathrm{WSC}} \mathrm{d}\boldsymbol{r}\, \psi^{*}_{c(\boldsymbol{q}+\alpha\boldsymbol{K})\tau}(\boldsymbol{r} + \boldsymbol{R}) e^{i\boldsymbol{\kappa}\cdot(\boldsymbol{r}+\boldsymbol{R})} \boldsymbol{p} \psi_{v(\boldsymbol{q}-\gamma\boldsymbol{K})\sigma}(\boldsymbol{r} + \boldsymbol{R}) \\ = & -\frac{e}{m_0} A_0(\boldsymbol{\kappa}, \xi) N \delta_{\tau\sigma} \sum_{\boldsymbol{G}} \delta_{\boldsymbol{\kappa}-\boldsymbol{K},\boldsymbol{G}} \sum_{\boldsymbol{q}} f^{*}_{vc\,\nu}(\boldsymbol{q}) \\ & \times \int_{\mathrm{WSC}} \mathrm{d}\boldsymbol{r}\, e^{-i(\boldsymbol{q}+\alpha\boldsymbol{K})\cdot\boldsymbol{r}} u^{*}_{c(\boldsymbol{q}+\alpha\boldsymbol{K})}(\boldsymbol{r}) e^{i\boldsymbol{\kappa}\cdot\boldsymbol{r}} \hat{\boldsymbol{e}}_{\xi\boldsymbol{\kappa}} \frac{\hbar}{i} \nabla \left[e^{i(\boldsymbol{q}-\gamma\boldsymbol{K})\cdot\boldsymbol{r}} u_{v(\boldsymbol{q}-\gamma\boldsymbol{K})}(\boldsymbol{r}) \right]. \end{aligned} \tag{4.35}$$

The functions $u_{n\boldsymbol{k}}(\boldsymbol{r})$ denote the lattice-periodic part of the Bloch functions $\psi_{n\boldsymbol{k}}(\boldsymbol{k}) = e^{i\boldsymbol{k}\cdot\boldsymbol{r}}u_{n\boldsymbol{k}}(\boldsymbol{r})$. In general, one can neglect Umklapp processes, i.e., one can set $\boldsymbol{G} = \boldsymbol{0}$, since κ and K are much smaller than the extension of the first Brillouin zone. This yields

$$\begin{aligned} M \;=\; & -\frac{e}{m_0}A_0(\boldsymbol{\kappa},\xi)N\delta_{\tau\sigma}\delta_{\boldsymbol{\kappa},\boldsymbol{K}}\sum_{\boldsymbol{q}} f^*_{vc\nu}(\boldsymbol{q})\int_{\text{WSC}} \mathrm{d}\boldsymbol{r}\; u^*_{c(\boldsymbol{q}+\alpha\boldsymbol{K})}(\boldsymbol{r})\hat{\boldsymbol{e}}_{\xi\boldsymbol{\kappa}} \\ & \times\left[\hbar(\boldsymbol{q}-\gamma\boldsymbol{K})u_{v(\boldsymbol{q}-\gamma\boldsymbol{K})}(\boldsymbol{r}) + \frac{\hbar}{i}\nabla u_{v(\boldsymbol{q}-\gamma\boldsymbol{K})}(\boldsymbol{r})\right]. \end{aligned} \tag{4.36}$$

To obtain expressions for the dipole and quadrupole oscillator strength, we use $\boldsymbol{k}\cdot\boldsymbol{p}$ perturbation theory and keep all terms up to first order in $\boldsymbol{q}$ and $\boldsymbol{K}$. It is [85, 162]

$$u_{m\boldsymbol{k}}(\boldsymbol{r}) \approx u_{m\boldsymbol{0}}(\boldsymbol{r}) + \frac{\hbar}{m_0}\sum_{n\neq m}\frac{\boldsymbol{k}\cdot\boldsymbol{p}_{nm}}{(E_m - E_n)}u_{n\boldsymbol{0}}(\boldsymbol{r}) + \ldots \tag{4.37}$$

with

$$\boldsymbol{p}_{mn} = \langle u_{m\boldsymbol{0}}\,|\boldsymbol{p}|\,u_{n\boldsymbol{0}}\rangle \tag{4.38}$$

and the energy $E_n = E_n(\boldsymbol{k}=\boldsymbol{0})$ of the band n at the Γ point. Due to the orthogonality relation of the Bloch functions

$$\int \mathrm{d}\boldsymbol{r}\;\psi^*_{n\boldsymbol{k}\sigma}(\boldsymbol{r})\psi_{n'\boldsymbol{k}'\sigma'}(\boldsymbol{r}) = \delta_{n,n'}\delta_{\boldsymbol{k},\boldsymbol{k}'}\delta_{\sigma,\sigma'} \tag{4.39}$$

the first summand in the integral of Eq. (4.36) vanishes up to first order in $\boldsymbol{q}$ and $\boldsymbol{K}$. We obtain

$$\begin{aligned} M = -\frac{e\hbar}{m_0^2}A_0(\boldsymbol{\kappa},\xi)\delta_{\tau\sigma}\delta_{\boldsymbol{\kappa},\boldsymbol{K}}\sum_{\boldsymbol{q}} f^*_{vc\nu}(\boldsymbol{q})\,[\langle u_{c\boldsymbol{0}}|\,\hat{\boldsymbol{e}}_{\xi\boldsymbol{\kappa}}\cdot\boldsymbol{p}\,|u_{v\boldsymbol{0}}\rangle & \\ + \langle u_{c\boldsymbol{0}}|\,(\hat{\boldsymbol{e}}_{\xi\boldsymbol{\kappa}}\cdot\boldsymbol{p})M_v(\boldsymbol{p}\cdot(\boldsymbol{q}-\gamma\boldsymbol{K}))\,|u_{v\boldsymbol{0}}\rangle & \\ + \langle u_{c\boldsymbol{0}}|\,((\boldsymbol{q}+\alpha\boldsymbol{K})\cdot\boldsymbol{p})M_c(\boldsymbol{p}\cdot\hat{\boldsymbol{e}}_{\xi\boldsymbol{\kappa}})\,|u_{v\boldsymbol{0}}\rangle]\,, & \end{aligned} \tag{4.40}$$

where we used

$$N\,\langle u_{c\boldsymbol{q}}\,|\hat{\boldsymbol{e}}_{\xi\boldsymbol{\kappa}}\cdot\boldsymbol{p}|\,u_{v\boldsymbol{q}}\rangle_{\text{WSC}} = \langle u_{c\boldsymbol{q}}\,|\hat{\boldsymbol{e}}_{\xi\boldsymbol{\kappa}}\cdot\boldsymbol{p}|\,u_{v\boldsymbol{q}}\rangle \tag{4.41}$$

and defined

$$M_m = \sum_{n\neq m}\frac{|u_{n\boldsymbol{0}}\rangle\,\langle u_{n\boldsymbol{0}}|}{(E_m - E_n)}. \tag{4.42}$$

The sum over $\boldsymbol{q}$ can be evaluated using

$$\frac{1}{\sqrt{N}}\sum_{\boldsymbol{q}} q_i^{\chi} f_{vc\nu}(\boldsymbol{q}) = (-i)^{\chi}\frac{\partial^{\chi}}{\partial\beta_i^{\chi}}F_{vc\nu}(\boldsymbol{\beta})\bigg|_{\boldsymbol{\beta}=\boldsymbol{0}} \tag{4.43}$$

and we arrive at

$$\begin{aligned} M \;=\; & -\frac{e\hbar}{m_0^2}A_0(\boldsymbol{\kappa},\xi)\sqrt{N}\delta_{\tau\sigma}\delta_{\boldsymbol{\kappa},\boldsymbol{K}}\lim_{\boldsymbol{r}\to\boldsymbol{0}}\Big[\hat{\boldsymbol{e}}_{\xi\boldsymbol{\kappa}}\cdot\boldsymbol{p}_{cv}\,F^*_{vc\nu}(\boldsymbol{r}) \\ & +(\tilde{\boldsymbol{M}}_v + \tilde{\boldsymbol{M}}_c)\cdot\,[i\nabla F^*_{vc\nu}(\boldsymbol{r})] + (-\gamma\tilde{\boldsymbol{M}}_v + \alpha\tilde{\boldsymbol{M}}_c)\cdot\,[F^*_{vc\nu}(\boldsymbol{r})\boldsymbol{K}]\Big]\,, \end{aligned} \tag{4.44}$$

where we replaced $\boldsymbol{\beta}$ with $\boldsymbol{r}$ and defined the vectors

$$\tilde{\boldsymbol{M}}_v = \langle u_{c\boldsymbol{0}}|\,(\hat{\boldsymbol{e}}_{\xi\boldsymbol{\kappa}}\cdot\boldsymbol{p})M_v\boldsymbol{p}\,|u_{v\boldsymbol{0}}\rangle\,, \tag{4.45a}$$

$$\tilde{\boldsymbol{M}}_c = \langle u_{c\boldsymbol{0}}|\,\boldsymbol{p}M_c(\hat{\boldsymbol{e}}_{\xi\boldsymbol{\kappa}}\cdot\boldsymbol{p})\,|u_{v\boldsymbol{0}}\rangle\,. \tag{4.45b}$$

In $\mathrm{Cu_2O}$ the first term in Eq. (4.44) or $\boldsymbol{p}_{cv}$ vanishes since valence and conduction band have the same parity. Note that for $\boldsymbol{K}=\boldsymbol{0}$ we would obtain the expression for dipole-allowed but parity-forbidden transitions in semiconductors. The sum $\tilde{\boldsymbol{M}}_v+\tilde{\boldsymbol{M}}_c$ equals the vector $\boldsymbol{M}_{cv}$ of Ref. [285] except for a factor $1/m_0$:

$$\boldsymbol{M}_{cv}=\frac{1}{m_0}\left[\sum_{n\neq c}\frac{\boldsymbol{p}_{cn}}{E_c-E_n}\left(\hat{\boldsymbol{e}}_{\xi\boldsymbol{K}}\cdot\boldsymbol{p}_{nv}\right)-\sum_{n\neq v}\frac{\boldsymbol{p}_{nv}}{E_n-E_v}\left(\hat{\boldsymbol{e}}_{\xi\boldsymbol{K}}\cdot\boldsymbol{p}_{cn}\right)\right]. \tag{4.46}$$

The term $\delta_{\tau\sigma}$ has to be replaced by $\sqrt{2}\delta_{S,0}$ when using the eigenstates of the total spin $S=S_{\mathrm{e}}+S_{\mathrm{h}}=\tau-\sigma$ [127].

The main problem is now to derive transition rules and to find an expression for the oscillator strength, which is given in the same formalism as the ansatz (4.23) of the exciton wave function in Sec. 4.3. This will be done now.

The operators M_c and M_v are projection operators. For reasons of symmetry these operators have to transform according to the irreducible representation Γ_1^+ of O_{h}. On the other hand, the operator $\boldsymbol{p}$ transforms according to Γ_4^-. The symmetry of the operator between the Bloch functions in Eq. (4.45) is therefore

$$\Gamma_4^-\otimes\Gamma_1^+\otimes\Gamma_4^-=\Gamma_1^+\oplus\Gamma_3^+\oplus\Gamma_4^+\oplus\Gamma_5^+. \tag{4.47}$$

The symmetry of the Bloch functions (without spin) is

$$\Gamma_5^+\otimes\Gamma_1^+=\Gamma_5^+. \tag{4.48}$$

Consequently, the expression (4.45) does not vanish only if the operator has the symmetry Γ_5^+ [169]. We can then consider the coupling coefficients for the case $\Gamma_4^-\otimes\Gamma_4^-\rightarrow\Gamma_5^+$. With the basis functions $|X\rangle$, $|Y\rangle$, $|Z\rangle$ of Γ_4^- and the basis functions $|\tilde{X}\rangle=|YZ\rangle$, $|\tilde{Y}\rangle=|ZX\rangle$, and $|\tilde{Z}\rangle=|XY\rangle$ of Γ_5^+, we see that, e.g., the Γ_5^+ like part of the products $|X\rangle_1|Y\rangle_2$ and $|Y\rangle_1|X\rangle_2$ transforms as $|\tilde{Z}\rangle/\sqrt{2}$ [90]. So we write

$$\langle\tilde{Z}|(|X\rangle_1|Y\rangle_2)=\frac{1}{\sqrt{2}},\quad\langle\tilde{Z}|(|Y\rangle_1|X\rangle_2)=\frac{1}{\sqrt{2}}, \tag{4.49}$$

and the expressions obtained via cyclic permutation.

In Sec. 4.2 we have introduced the quasi-spin $I=1$. If we compare the states $|I,M_I\rangle$ with the three functions $|u_{v\boldsymbol{0}}^{xy}\rangle$, $|u_{v\boldsymbol{0}}^{yz}\rangle$, and $|u_{v\boldsymbol{0}}^{zx}\rangle$ transforming according to Γ_5^+, it is [83]

$$|1,+1\rangle_I=-\left(|u_{v\boldsymbol{0}}^{yz}\rangle+i\,|u_{v\boldsymbol{0}}^{zx}\rangle\right)/\sqrt{2}, \tag{4.50a}$$

$$|1,0\rangle_I=|u_{v\boldsymbol{0}}^{xy}\rangle, \tag{4.50b}$$

$$|1,-1\rangle_I=\left(|u_{v\boldsymbol{0}}^{yz}\rangle-i\,|u_{v\boldsymbol{0}}^{zx}\rangle\right)/\sqrt{2}. \tag{4.50c}$$

In the envelope function of the exciton the angular dependence is given by the spherical harmonics Y_{LM}. We know that in Eq. (4.44) the gradient of the envelope function at $\boldsymbol{r}=\boldsymbol{0}$ is non-zero only if $L=1$ holds. Furthermore, the envelope function itself vanishes at $\boldsymbol{r}=\boldsymbol{0}$ if $L\neq 0$ holds.

We can now give a simple expression for the oscillator strength by combining all remarks given above. Let us assume that the light is polarized in x-direction, i.e., $\hat{\boldsymbol{e}}_{\xi\boldsymbol{K}}=\hat{\boldsymbol{e}}_x$. Let us furthermore write the function $|\Psi_{\nu\boldsymbol{K}}\rangle$ of the exciton in the form of Eq. (4.23), where the spins, the envelope with the angular momentum L and the function of the hole with the quasi-spin I enter. The dipole-term in Eq. (4.44) is then proportional to

$$\begin{aligned}
& \lim_{\boldsymbol{r}\to\boldsymbol{0}} \langle S=0,\, M_S=0|\left(\langle u^{xy}_{v\boldsymbol{0}}|\,\frac{\partial}{\partial y}+\langle u^{zx}_{v\boldsymbol{0}}|\,\frac{\partial}{\partial z}\right)|\Psi_{\nu\boldsymbol{K}}\rangle \\
= \; & \lim_{r\to 0}\frac{\partial}{\partial r}\,\langle S=0,\, M_S=0| \\
& \times\left(\langle I=1,\, M_I=0|\,(-i)\sqrt{\frac{3}{8\pi}}\,(\langle L=1,\, M_L=1|+\langle L=1,\, M_L=-1|)\right. \\
& \qquad \left. -\frac{i}{\sqrt{2}}(\langle I=1,\, M_I=-1|+\langle I=1,\, M_I=1|)\,\sqrt{\frac{3}{4\pi}}\,\langle L=1,\, M_L=0|\right)|\Psi_{\nu\boldsymbol{K}}\rangle \\
= \; & -i\sqrt{\frac{3}{4\pi}}\lim_{r\to 0}\frac{\partial}{\partial r}({}_D\langle 2,\, 1|+{}_D\,\langle 2,\, -1|)\,|\Psi_{\nu\boldsymbol{K}}\rangle
\end{aligned} \tag{4.51}$$

Here the state $|F_t,\, M_{F_t}\rangle_D$ for the dipole transition (D) is a short notation for

$$|(S_\mathrm{e},\, S_\mathrm{h})\, S,\, I;\, I+S,\, L;\, F_t,\, M_{F_t}\rangle = |(1/2,\, 1/2)\, 0,\, 1;\, 1,\, 1;\, F_t,\, M_{F_t}\rangle\,, \tag{4.52}$$

in which the coupling scheme of the spins and angular momenta is different from the one of Eq. (4.22) due to the requirement that S must be a good quantum number:

$$S_\mathrm{e}+S_\mathrm{h}=S \quad\to\quad (I+S)+L=F_t. \tag{4.53}$$

As the quantization axis we choose the z-axis, which is parallel to one of the principal axes of the crystal lattice. In accordance, the quadrupole term can be written as

$$\begin{aligned}
& \lim_{\boldsymbol{r}\to\boldsymbol{0}} \langle S=0,\, M_S=0|\,(\langle u^{xy}_{v\boldsymbol{0}}|\,K_y+\langle u^{zx}_{v\boldsymbol{0}}|\,K_z)\,|\Psi_{\nu\boldsymbol{K}}\rangle \\
= \; & \lim_{r\to 0}\langle S=0,\, M_S=0|\,\frac{1}{\sqrt{4\pi}}\,\langle L=0,\, M_L=0|\left(\langle I=1,\, M_I=0|\,K_y\right. \\
& \qquad\qquad \left. -\frac{i}{\sqrt{2}}(\langle I=1,\, M_I=-1|+\langle I=1,\, M_I=1|)K_z\right)|\Psi_{\nu\boldsymbol{K}}\rangle \\
= \; & \lim_{r\to 0}\frac{1}{\sqrt{4\pi}}\left({}_Q\,\langle 1,\, 0|\,K_y-\frac{i}{\sqrt{2}}({}_Q\langle 1,\, -1|+{}_Q\,\langle 1,\, 1|)K_z\right)|\Psi_{\nu\boldsymbol{K}}\rangle
\end{aligned} \tag{4.54}$$

with the state $|F_t,\, M_{F_t}\rangle_Q$ for the quadrupole transition (Q) being a short notation for

$$|(S_\mathrm{e},\, S_\mathrm{h})\, S,\, I;\, I+S,\, L;\, F_t,\, M_{F_t}\rangle = |(1/2,\, 1/2)\, 0,\, 1;\, 1,\, 0;\, F_t,\, M_{F_t}\rangle\,. \tag{4.55}$$

Note that this state is similar to the one of Eq. (4.52) but only L is set to zero.

The same calculations can be performed if the light is polarized in y or z direction. We finally arrive at the following expression for the relative oscillator strength:

$$f^{\mathrm{rel}}_{\xi\nu\boldsymbol{K}} = \left|\lim_{r\to 0}\left[-i(\tilde{M}_v^*+\tilde{M}_c^*)\frac{\partial}{\partial r}\langle T^D_{\xi\boldsymbol{K}}|\Psi_{\nu\boldsymbol{K}}\rangle+(-\gamma\tilde{M}_v^*+\alpha\tilde{M}_c^*)\frac{K}{\sqrt{6}}\langle T^Q_{\xi\boldsymbol{K}}|\Psi_{\nu\boldsymbol{K}}\rangle\right]\right|^2. \tag{4.56}$$

For the dipole term in Eq. (4.56) the two transverse states $|T^D_{\xi\boldsymbol{K}}\rangle$ are given by

$$|T^D_{\xi\boldsymbol{K}}\rangle=\sum_{i=1}^{3}\hat{e}_{\xi\boldsymbol{K}i}|\pi^D_i\rangle, \qquad \xi=1,\, 2 \tag{4.57}$$

with the three components of the polarization vector $\hat{\boldsymbol{e}}_{\xi\boldsymbol{K}}$ and three states which transform according to Γ_4^-:

$$|\pi_x^D\rangle = \frac{i}{\sqrt{2}}\left[|2,\,-1\rangle_D + |2,\,1\rangle_D\right], \tag{4.58a}$$

$$|\pi_y^D\rangle = \frac{1}{\sqrt{2}}\left[|2,\,-1\rangle_D - |2,\,1\rangle_D\right], \tag{4.58b}$$

$$|\pi_z^D\rangle = \frac{i}{\sqrt{2}}\left[|2,\,-2\rangle_D - |2,\,2\rangle_D\right]. \tag{4.58c}$$

Note that there is a third linear combination of the states in Eq. (4.58), which is connected with a longitudinal polarization:

$$|L_{\boldsymbol{K}}^D\rangle = \sum_{i=1}^{3} \hat{K}_i |\pi_i^D\rangle. \tag{4.59}$$

Here we set $\hat{\boldsymbol{K}} = \boldsymbol{K}/K$. This state will be important for the nonanalytic exchange interaction in Sec. 9.3.3.

The state $|T_{\xi\boldsymbol{K}}^Q\rangle$ in the quadrupole term of Eq. (4.56) reads

$$|T_{\xi\boldsymbol{K}}^Q\rangle = \sum_{i=1}^{3} \hat{e}_{\xi\boldsymbol{K}i} |\pi_i^Q\rangle, \qquad \xi = 1,\,2 \tag{4.60}$$

with the three states which transform according to Γ_5^+:

$$\left|\pi_x^Q\right\rangle = \hat{K}_y\,|1,\,0\rangle_Q + \hat{K}_z \frac{i}{\sqrt{2}}\left[|1,\,-1\rangle_Q + |1,\,1\rangle_Q\right], \tag{4.61a}$$

$$\left|\pi_y^Q\right\rangle = \hat{K}_x\,|1,\,0\rangle_Q + \hat{K}_z \frac{1}{\sqrt{2}}\left[|1,\,-1\rangle_Q - |1,\,1\rangle_Q\right], \tag{4.61b}$$

$$\left|\pi_z^Q\right\rangle = \hat{K}_y \frac{1}{\sqrt{2}}\left[|1,\,-1\rangle_Q - |1,\,1\rangle_Q\right] + \hat{K}_x \frac{i}{\sqrt{2}}\left[|1,\,-1\rangle_Q + |1,\,1\rangle_Q\right]. \tag{4.61c}$$

The quadrupole interaction appears due to a finite wave vector. The exciton states, which have the symmetry Γ_5^+ at $K = 0$, couple with the finite wave vector leading to a finite polarization proportional to K.

Using the wave function of Eq. (4.23) in spatial representation, we find

$$\begin{aligned}
\lim_{r\to 0} \frac{\partial}{\partial r}\,{}_D\left\langle 2,\,M'_{F_t}\middle|\Psi_{\nu\boldsymbol{K}}\right\rangle = \sum_{NJFF_t}\sum_{M_{S_\mathrm{e}}M_I} & c_{N1JFF_tM'_{F_t}}\,\frac{1}{3}\sqrt{\frac{10}{\alpha^5}}(-1)^{F-J-3M_{S_\mathrm{e}}-M_I+3M'_{F_t}+\frac{3}{2}} \\
& \times\,\left[(N+1)(N+3)(2J+1)(2F+1)(2F_t+1)\right]^{\frac{1}{2}} \\
& \times \begin{pmatrix} F & \frac{1}{2} & F_t \\ M'_{F_t}-M_{S_\mathrm{e}} & M_{S_\mathrm{e}} & -M'_{F_t} \end{pmatrix} \\
& \times \begin{pmatrix} 1 & J & F \\ M'_{F_t}-M_I & M_I-M_{S_\mathrm{e}} & M_{S_\mathrm{e}}-M'_{F_t} \end{pmatrix}
\end{aligned}$$

$$\times \begin{pmatrix} 1 & \frac{1}{2} & J \\ M_I & -M_{S_\mathrm{e}} & M_{S_\mathrm{e}} - M_I \end{pmatrix} \begin{pmatrix} 1 & 1 & 2 \\ M_I & M'_{F_t} - M_I & -M'_{F_t} \end{pmatrix} \tag{4.62}$$

and

$$\lim_{r\to 0} {}_Q\left\langle 1,\, M'_{F_t} \middle| \Psi_{\nu \boldsymbol{K}} \right\rangle = \sum_{NFF_t} \sum_{M_{S_\mathrm{e}}} c_{N0FFF_tM'_{F_t}} \sqrt{\frac{2}{\alpha^3}} (-1)^{F-2M_{S_\mathrm{e}}+\frac{1}{2}} \left[(2F+1)(2F_t+1)\right]^{\frac{1}{2}}$$

$$\times \begin{pmatrix} F & \frac{1}{2} & F_t \\ M'_{F_t} - M_{S_\mathrm{e}} & M_{S_\mathrm{e}} & -M'_{F_t} \end{pmatrix} \begin{pmatrix} 1 & \frac{1}{2} & F \\ M'_{F_t} & -M_{S_\mathrm{e}} & M_{S_\mathrm{e}} - M'_{F_t} \end{pmatrix}. \tag{4.63}$$

We can finally make an assumption as regards the size of the parameters $\tilde{M}_v$ and $\tilde{M}_c$. Since in Cu_2O the uppermost valence bands as well as the lowermost conduction band have positive parity, we see from Eq. (4.45) that only bands with negative parity will contribute to the sums in Eq. (4.42). In Cu_2O there are only two bands of negative parity, which lie 449 meV above the lowest conduction band and 5.6 eV below the highest conduction band [162]. Hence, as regards the denominators of the form $(E_m - E_n)$ in M_c and M_v, the small energy difference between the Γ_7^+ and the Γ_8^+ valence band due to the spin-orbit coupling plays a minimal role. Furthermore, the denominator $(E_c - E_n)$ in M_c is much smaller than the denominator $(E_v - E_n)$ in M_v and it is $M_c \gg M_v$. We therefore neglect M_v in the following. As a consequence, to obtain absolute oscillator strengths, only one parameter η in the final expression

$$f_{\xi\nu\boldsymbol{K}} = \eta \left| \lim_{r\to 0} \left[-i\frac{\partial}{\partial r} \langle T^D_{\xi\boldsymbol{K}} | \Psi_{\nu\boldsymbol{K}} \rangle + \frac{\alpha K}{\sqrt{6}} \langle T^Q_{\xi\boldsymbol{K}} | \Psi_{\nu\boldsymbol{K}} \rangle \right] \right|^2 \tag{4.64}$$

has to be determined via a comparison with experimental values. Note that when evaluating the oscillator strength a mixing term between the dipole and the quadrupole term appears. This is due to the fact that parity is no longer a good quantum number for finite values of K.

To sum up, when calculating oscillator strengths of excitons in Cu_2O three important points need to be considered:

(i) Dipole transitions in Cu_2O are parity forbidden. Hence, the transition matrix element is proportional to the gradient of the envelope function at $r = |\boldsymbol{r}| = 0$ and the exciton state must have a component with angular momentum $L = 1$. For quadrupole transitions the transition matrix element is proportional to the envelope function at $r = 0$, for which reason it must have a component with angular momentum $L = 0$.

(ii) As the dipole and quadrupole operator do not change the total spin $S = S_\mathrm{e} + S_\mathrm{h}$ of the electron and the hole, the exciton state must have a component with $S = 0$.

(iii) The total symmetry of the exciton state must be identical to the symmetry Γ_4^- of the dipole operator or Γ_5^+ of the quadrupole operator [7]. More generally, we can make the following statement[4] if a transition of a specific order (dipole, quadrupole, ...) is possible due to the symmetries of the bands of the crystal: Assume that an operator transforms according to the irreducible parts D^i of the full rotation group. Then transitions may take place to those exciton states whose symmetries Γ_exc at the Γ-point are compatible with the lists of irreducible representations obtained from the compatibility relations of the D^i with the irreducible representations of the point group of the

---

[4] This definition is a generalization of statements in Refs. [7] and [12].

crystal[5]. When classifying the eigenstates of the Hamiltonian, the irreducible representations of the cubic group play the same role in as the angular momentum quantum number L in the case of full rotational symmetry [85].

In semiconductor optics one often speaks of ortho- and para-excitons. These terms are connected with the possibility to excite exciton states from the ground state of the solid. In the ground state of the semiconductor the total spin of all electrons is zero. During the optical excitation of one electron into the conduction band the spin of this electron normally stays unchanged since the electric field of light does not act on spin. Therefore, the total spin of the exciton is zero and one speaks of a singlet exciton. On the other hand, there is the possibility of an interaction between the magnetic field of light and the spin, which results in a spin flip. The total spin of the created triplet exciton is consequently one.

Sometimes different names for the excitons of spin $S = 0$ and $S = 1$ are used:

- $S = 0$: singlet, ortho- or bright exciton,
- $S = 1$: triplet, para- or dark exciton.

The latter names refer to the fact that triplet excitons are spin-flip forbidden and thus have a small oscillator strength [12]. Since angular momentum and spin are often no good quantum numbers in a solid or crystal structure, it is not generally the case that the ortho-exciton is non-degenerate and that the para-exciton is threefold degenerate. It can even be the other way round as it is often found for zincblende-type crystals [12] (cf. also Sec. 5.2).

4.4.1 Two-photon absorption

Here we will shortly discuss the oscillator strength in two-photon absorption experiments. While in one photon absorption excitons of symmetry Γ_4^- are dipole-allowed [38], the selection rules for two-photon absorption [287–289] are different and excitons of symmetry Γ_5^+ can be optically excited.

When considering one-photon absorption one generally treats the operator $\boldsymbol{A}\cdot\boldsymbol{p}$ with the vector potential $\boldsymbol{A}$ of the radiation field in first order perturbation theory. The dipole operator then transforms according to the irreducible representation D^1 of the full rotation group. In two-photon absorption one needs the operator $\boldsymbol{A}\cdot\boldsymbol{p}$ twice and thus the product $D^1 \otimes D^1 = D^0 \oplus D^1 \oplus D^2$ is of importance [90]. In Cu_2O the reduction of these irreducible representations by the cubic group O_h has to be considered and one obtains

$$\Gamma_4^- \otimes \Gamma_4^- = \Gamma_1^+ \oplus \Gamma_4^+ \oplus (\Gamma_3^+ \oplus \Gamma_5^+). \tag{4.65}$$

In two-photon absorption the spin $S = S_\mathrm{e} + S_\mathrm{h} = 0$ remains unchanged and the exciton state must have an $L = 0$ component. Hence, the correct expression for the relative oscillator strength is given by

$$f_{\xi\nu\boldsymbol{K}}^{\mathrm{rel}} = \left|\lim_{r\to 0}\langle T_{\xi\boldsymbol{K}}^{TP}|\Psi_{\nu\boldsymbol{K}}\rangle\right|^2. \tag{4.66}$$

The state $|T_{\xi\boldsymbol{K}}^{TP}\rangle$ transforms according to Γ_5^+. Here we have to consider the polarizations of both photons. By choosing, e.g., one photon to be polarized in x direction and one photon to be polarized in y direction, only one component of the Γ_5^+ exciton states, the xy component, can be

---

[5] For magnetic dipole transitions the corresponding irreducible representation is Γ_4^+ [286].

excited optically. The following three states, which transform according to Γ_5^+, enter $|T_{\xi\boldsymbol{K}}^{TP}\rangle$:

$$\left|\pi_{xy}^{TP}\right\rangle = |1,\,0\rangle_{TP}\,, \tag{4.67a}$$

$$\left|\pi_{yz}^{TP}\right\rangle = \frac{i}{\sqrt{2}}\left[|1,\,-1\rangle_{TP} - |1,\,1\rangle_{TP}\right], \tag{4.67b}$$

$$\left|\pi_{zx}^{TP}\right\rangle = \frac{1}{\sqrt{2}}\left[|1,\,-1\rangle_{TP} + |1,\,1\rangle_{TP}\right], \tag{4.67c}$$

with $|F_t,\,M_{F_t}\rangle_{TP} = |F_t,\,M_{F_t}\rangle_Q$ [cf. Eq. (4.55)]. For all evaluations of the two-photon oscillator strength we will assume the case described with one photon being polarized in x direction and one photon being polarized in y direction. Hence, we set $|T_{\xi\boldsymbol{K}}^{TP}\rangle = \left|\pi_{xy}^{TP}\right\rangle$.

4.4.2 Hydrogen-like model

Here we will shortly discuss the special case of dipole transitions in the hydrogen like model. The oscillator strength is according to Eqs. (4.44)-(4.46) proportional to

$$f_{\xi\nu\boldsymbol{0}} \sim \left|F_{vc\,\nu}^{*}(\boldsymbol{0})\hat{\boldsymbol{e}}_{\xi\boldsymbol{\kappa}}\cdot\boldsymbol{p}_{cv} + i\hbar(\nabla F_{vc\,\nu}^{*}(\boldsymbol{r})|_{\boldsymbol{r}=\boldsymbol{0}})\cdot\boldsymbol{M}_{cv}\right|^2. \tag{4.68}$$

In general, the first summand with $F_{vc\,\nu}^{*}(\boldsymbol{0})$ dominates the sum and we may neglect the other term at first. Inserting the solution (2.220) for $U_{\nu\boldsymbol{K}}$, we find a nonvanishing oscillator strength only for $L=0$, i.e., for S-excitons:

$$f_{\xi\nu\boldsymbol{0}}(\mathrm{allowed}) \sim |F_{vc\,\nu}(\boldsymbol{0})|^2\,|\hat{\boldsymbol{e}}_{\xi\boldsymbol{\kappa}}\cdot\boldsymbol{p}_{cv}|^2 = |\hat{\boldsymbol{e}}_{\xi\boldsymbol{\kappa}}\cdot\boldsymbol{p}_{cv}|^2\,\frac{V_{\mathrm{uc}}}{\pi a_{\mathrm{exc}}^3}\frac{1}{n^3}\,\delta_{L,0}. \tag{4.69}$$

If $\boldsymbol{p}_{cv}$ vanishes, e.g., due to the same parity of the Bloch function of conduction band and valence band, we have to consider the second term in Eq. (4.68). This yields the oscillator strength of P excitons:

$$f_{\xi\nu\boldsymbol{0}}(\mathrm{forbidden}) \sim |(\nabla F_{vc\,\nu}^{*}(\boldsymbol{r})|_{\boldsymbol{r}=\boldsymbol{0}})\cdot\boldsymbol{M}_{cv}|^2 = \hbar^2\,|\boldsymbol{M}_{cv}|^2\,\frac{V_{\mathrm{uc}}}{3\pi a_{\mathrm{exc}}^5}\frac{n^2-1}{n^5}\,\delta_{L,1}. \tag{4.70}$$

Note that both transitions are dipole-allowed; we use the terms “allowed” and “forbidden” as in Ref. [7], i.e., they refer to the symmetry of the bands. In the literature they are sometimes called both allowed [290, 291]. An observation of dipole-forbidden states is weakly possible in one-photon transitions if they are quadrupole or magnetic dipole-allowed and not masked by another dipole-allowed transition in the same spectral range. On the other hand, they can be observed in phonon-assisted transitions or in two-photon transitions, for which the selection rules differ.

If the energy of the photon which excites the exciton exceeds the band-gap energy, the hydrogen-like continuum states[6]

$$\begin{aligned} F_{vc\,kLM}(\boldsymbol{r}) \;=\; & \frac{(2ikr)^L}{(2L+1)!}e^{\frac{\pi\alpha}{2}}\sqrt{\frac{2\pi k^2}{R\alpha\sinh(\pi\alpha)}}\prod_{j=0}^{L}\sqrt{j^2+\alpha^2} \\ & \times e^{-ikr}{}_1F_1(1+L+i\alpha;\,2L+2;\,2ikr)Y_{LM}(\vartheta,\,\varphi) \end{aligned} \tag{4.71}$$

---

[6] See Appendix A.3. These continuum states actually describe free electron and hole states of the one electron or band model [7]. We take the continuum states from Ref. [139] (without being certain if Eq. (2.221) is fulfilled). Note that continuum states sometimes differ in literature due to their normalization factors [62, 247, 292, 293].

with

$$\alpha=\sqrt{\frac{R_{\mathrm{exc}}}{E_k}}\quad\text{and}\quad E_k=\frac{\hbar^2k^2}{2\mu}\tag{4.72}$$

have to be used instead of $F_{vc\nu}$. We obtain

$$f_{\xi\alpha\boldsymbol{0}}(\text{allowed})\ \sim\ |\hat{\boldsymbol{e}}_{\xi\boldsymbol{\kappa}}\cdot\boldsymbol{p}_{cv}|^2\,\frac{\alpha e^{\pi\alpha}}{2\sinh(\pi\alpha)}\frac{V_{\mathrm{uc}}k^2}{R}\,\delta_{L,0},\tag{4.73a}$$

$$f_{\xi\alpha\boldsymbol{0}}(\text{forbidden})\ \sim\ \hbar^2\,|\boldsymbol{M}_{cv}|^2\,\frac{\alpha(1+\alpha^2)e^{\pi\alpha}}{6\sinh(\pi\alpha)}\frac{V_{\mathrm{uc}}k^4}{R}\,\delta_{L,1}.\tag{4.73b}$$

The formula (4.73a) can be decomposed into the absorption of free pairs and the so-called Sommerfeld factor [10, 62, 139]. Hence, one can see that the Coulomb interaction significantly affects the motion of the particles above the ionization continuum (cf. Fig. 3.2).

The formulas (4.73a) and (4.73b) hold only if the energy of the exciton is in the vicinity of the band gap energy. Otherwise the effective mass approach is not applicable and the quasi-particles do not show similarities with free electrons. Finally, we would like to note that transitions of excitons in semiconductors with indirect band gap can be found in Refs. [7, 10, 62] and that the excitation of two excitons by one photon is treated in Ref. [7].

Intraexcitonic transitions Since the exciton is comparable to a hydrogen atom, it is also possible to observe intraexcitonic transitions, i.e., transitions between sublevels of the exciton, corresponding to the Lyman series of the hydrogen atom. There are only two important facts to be considered in this comparison with regard to spectroscopy:

- The hydrogen atom already exists before light is sent on it. The electron is then excited by light from the ground state $1s$ to the np states with $n\geq 2$. In semiconductors the excitons have to be created at first by light.
- In the case of excitons there is no Doppler broadening, because they can be created on a distinct point of their dispersion relation [12].

For excitons the same selection rules hold as for the hydrogen atom:

$$\Delta L=\pm 1,\ \Delta M=0,\pm 1,\ \Delta s=0.\tag{4.74}$$

Therefore transitions between ortho- and para-exciton states are dipole forbidden. However, in the case of excitons the magnetic quantum number has to be replaced by the symmetry of the exciton [36, 87].

The observation of the excitonic Lyman series is possible using differential transmission or pump-and-probe spectroscopy. Early examples on Si and Ge including transitions from the $1S$ state to different $2P$ states can be found in Refs. [294–296]. Corresponding transitions in Cu$_2$O are treated in Refs. [87, 297–301]. There are several points limiting the possibility of observing such transitions:

- Due to the small transition energy often THz spectroscopy has to be used.
- The transitions should not be masked by other transitions like, e.g., phononic transitions.
- The excitonic lifetime should be long enough to obtain a high excitonic density under pumping. Therefore, indirect semiconductors and semiconductors with dipole forbidden transitions are often used in experiments.

4.5 Results and discussion

4.5.1 $F = 5/2$ and $7/2$ excitonic lines of cuprous oxide

In this section we apply the method presented in Secs. 4.2 and 4.3 and repeat the analysis of Ref. [36]. Deviations from the results in Ref. [36] are observed and discussed. Using the parameters $\Delta = 0.1338\,\mathrm{eV}$, $\gamma_1' = 2.78$, $\mu' = 0.47$ from Ref. [72], the parameter δ' has been determined in Ref. [36] by comparing theoretical results with experimental absorption spectra.

In the spherical approximation F and M_F are good quantum numbers. Including the cubic part of the Hamiltonian H_d, the reduction of the irreducible representations D^F of the rotation group by the cubic group O_h has to be considered [169]. With the additional factor Γ_2^+ as described in Sec. 4.4, we obtain for the symmetry of the envelope function and the hole

$$\tilde{D}^{\frac{1}{2}} = D^{\frac{1}{2}} \otimes \Gamma_2^+ = \Gamma_6^- \otimes \Gamma_2^+ = \Gamma_7^- , \tag{4.75a}$$
$$\tilde{D}^{\frac{3}{2}} = D^{\frac{3}{2}} \otimes \Gamma_2^+ = \Gamma_8^- \otimes \Gamma_2^+ = \Gamma_8^- , \tag{4.75b}$$
$$\tilde{D}^{\frac{5}{2}} = D^{\frac{5}{2}} \otimes \Gamma_2^+ = (\Gamma_7^- \oplus \Gamma_8^-) \otimes \Gamma_2^+ = \Gamma_6^- \oplus \Gamma_8^- , \tag{4.75c}$$
$$\tilde{D}^{\frac{7}{2}} = D^{\frac{7}{2}} \otimes \Gamma_2^+ = (\Gamma_6^- \oplus \Gamma_7^- \oplus \Gamma_8^-) \otimes \Gamma_2^+ = \Gamma_7^- \oplus \Gamma_6^- \oplus \Gamma_8^- . \tag{4.75d}$$

The Hamiltonian couples only states with even or odd values of L. Since in the simple-band model only states with $L = 1$ are dipole-allowed, we only include states with odd values of L in our basis. This is the reason for the negative parities in Eq. (4.75). Furthermore, we can neglect the central-cell corrections and the exchange interaction in the following since they only affect states with $L = 0$.

As can be seen from Eqs. (4.75c) and (4.75d) the states with $F = 5/2$ and $F = 7/2$ split into five states with the symmetries Γ_6^-, Γ_7^-, and Γ_8^-. The degeneracies of these states are two for Γ_6^- and Γ_7^- and four for Γ_8^-. Including the symmetry Γ_6^+ of the electron spin, we obtain the symmetry of the exciton and can determine which of these states are dipole-allowed, viz.,

$$\Gamma_6^- \otimes \Gamma_6^+ = \Gamma_1^- \oplus \Gamma_4^- , \tag{4.76a}$$
$$\Gamma_7^- \otimes \Gamma_6^+ = \Gamma_2^- \oplus \Gamma_5^- , \tag{4.76b}$$
$$\Gamma_8^- \otimes \Gamma_6^+ = \Gamma_3^- \oplus \Gamma_4^- \oplus \Gamma_5^- . \tag{4.76c}$$

Since only the threefold degenerate states of symmetry Γ_4^- are dipole-allowed, four lines are visible in experiments at the most. However, in Ref. [36] only three lines could be observed.

We solve the generalized eigenvalue problem (4.24) in the complete basis of Eq. (4.22) with the additional quantum number F_t, determine the states of symmetry Γ_4^-, and calculate the oscillator strengths. Even though the states with $F = 5/2$ and $F = 7/2$ lie energetically very close together in the spherical approximation, it is inappropriate to consider only basis functions with these two values of F in our ansatz. Including all states with $F \leq 15/2$, we obtain a clearly different result in comparison to the one of Ref. [36]. In Fig. 4.1(a) we depict the results of Ref. [36] for the principal quantum number $n = 4$ by green diamonds and our results by circles. For the $9j$-symbol in Eq. (F.8) we use the relations given in Refs. [248, 302], so that our result differs by an exchange of the first two rows in the $9j$-symbol of Eq. (14) of Ref. [36] or of Eq. (A2) of Ref. [78]. We are convinced that the formulas given in Refs. [248, 302] are correct as the quantum numbers in the rows of the $9j$-symbol appear in the same order as they appear in our basis states. An odd

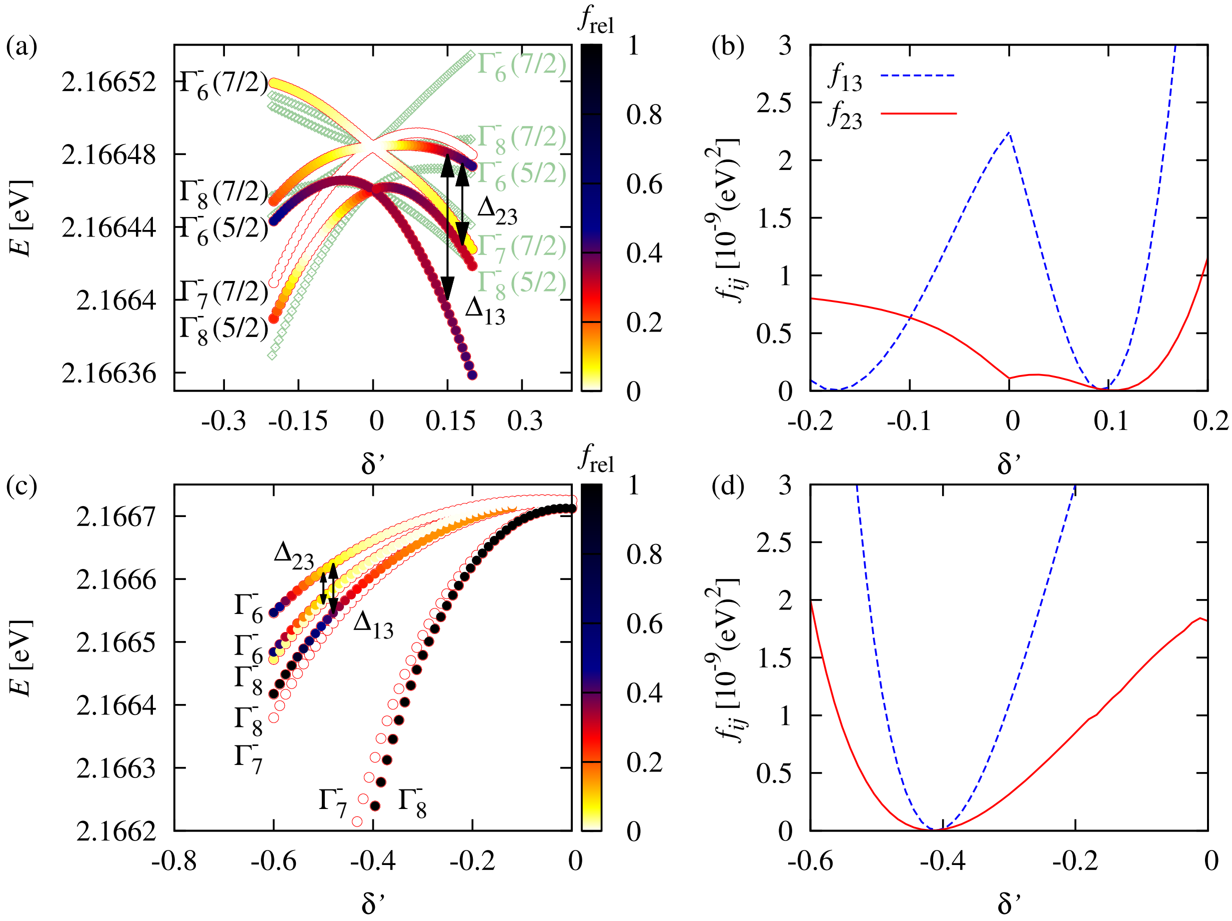

Figure 4.1.: (a) Comparison of the results of Ref. [36] (green diamonds) and the results obtained by the method described in Secs. 4.2 and 4.3 (circles). The splitting of the $F = 5/2$ and $F = 7/2$ states due to the cubic part of the Hamiltonians is depicted for the principal quantum number $n = 4$. Our symmetry assignment (left) differs from the one of Ref. [36] (right). The color bar shows the relative oscillator strengths in arbitrary units. The state assigned with $\Gamma_6^-(7/2)$ has only small oscillator strength. The parameters Δ_{13} and Δ_{23} denote the line spacings between the remaining dipole-allowed states. (b) The functions $f_{13}(\delta')$ and $f_{23}(\delta')$ as defined in Eq. (4.78). The value $\delta' \approx 0.1$, for which both function values are minimal, is the value of this material parameter in Cu_2O if $\mu' = 0.47$ and $\eta_i = 0$ holds. The kinks at $\delta' = 0$ are due to the definition of the quantities Δ_{13} and Δ_{23}. (c), (d) Same calculation but for the material parameters Δ, γ_1', μ', and η_i obtained from band structure calculations [37, 279] (cf. Table 2.2). The assignment of F quantum numbers is omitted. The optimum value for δ' is here $\delta' = -0.408$. For further information see text.

permutation of rows can lead to a change in the sign of the $9j$-symbol depending on the quantum numbers included [248] (cf. also Appendix F.1). Therefore, our assignment of the lines with the symmetries Γ_6^-, Γ_7^-, Γ_8^- in Fig. 4.1(a) differs from the one of Ref. [36].

For the states of Γ_4^--symmetry we calculate relative dipole oscillator strengths via

$$f_{\mathrm{rel}} \sim \left| \lim_{r\to 0} \frac{\partial}{\partial r} \left\langle \pi_z^D \middle| \Psi(\boldsymbol{r}) \right\rangle \right|^2 \tag{4.77}$$

with the wave function of Eq. (4.23) in spatial representation and the state $\left|\pi_z^D\right\rangle$ of Eq. (4.58) (cf. Sec. 4.4). Its specific form shows that we assume the incident light to be linearly polarized in z direction [169]. The oscillator strengths of the states calculated are also depicted in Fig. 4.1(a).

In Ref. [36] it has been discussed that also components of the order $\boldsymbol{p}^4$ should be included in the Hamiltonian to obtain more reliable values for the oscillator strengths. However, the effect of these terms is considered to be very weak for the states investigated here and is may only be important for the $1S$ exciton state [162]. Indeed, the effect of $\boldsymbol{p}^4$-terms significantly decreases with increasing principal quantum number n but a corresponding decrease of the oscillator strength between the $n = 4$ states and the $n = 5$ states cannot be observed experimentally [36]. This shows that an effect of $\boldsymbol{p}^4$-terms is not present at all. We therefore neglect these higher order terms in $\boldsymbol{p}$.

In Fig. 4.1(a) the state assigned with $\Gamma_6^-(7/2)$ has only small oscillator strength, which validates the fact that only three lines can be observed experimentally in absorption spectra. Furthermore, the two lines assigned with $\Gamma_6^-(7/2)$ and $\Gamma_8^-(5/2)$ could hardly be resolved in experiments for $\delta' \geq 0.1$.

To determine the correct value of δ', we consider the energetic spacing between the lines. We use the same nomenclature as in Ref. [36]; i.e., the spacing between the state with the highest energy and the state with the lowest energy is called Δ_{13} while the spacing between the state with the highest energy and the state with the second highest energy is called Δ_{23} [see Fig. 4.1(a)]. Note that, e.g., the state with the lowest energy is $\Gamma_8^-(5/2)$ for $\delta' < 0$ and $\Gamma_6^-(5/2)$ for $\delta' > 0$ so that there are different lines entering Δ_{13} and Δ_{23} depending on δ'. Since the spacings depend on the value of δ' and the principal quantum number n, we use the notation $\Delta_{ij}(\delta', n)$. Minimizing the functions

$$f_{ij}(\delta') = \sum_{n=4}^{8} \left(\Delta_{ij}(\delta', n) - \Delta_{ij}^{\mathrm{exp}}(n) \right)^2, \tag{4.78}$$

where $\Delta_{ij}^{\mathrm{exp}}(n)$ denote the spacings in the experimental absorption spectrum, we obtain almost the same value of δ' irrespective of the indices ij as can be seen from Fig. 4.1(b). The final value is

$$\delta' = 0.1, \tag{4.79}$$

which is clearly different from the value $\delta' = -0.1$ of Ref. [36].

Even though the values $\mu' = 0.47$ and $\delta' = 0.1$ reproduce the experimental results of excitonic absorption spectra very well, we cannot disregard that these values originate from the valence band structure of $\mathrm{Cu_2O}$. In Ref. [36] it has already been noted that a negative value of δ' is expected due to a comparison with band structure calculations [279]. However, our calculations do not provide a negative value even if we include the state assigned with $\Gamma_6^-(7/2)$ in our calculations.

A fit to band structure calculations yields [37] $\mu' = 0.0586$ and $\delta' = -0.404$ as already mentioned in Sec. 4.2. These values are clearly different from the results of the above calculation. Therefore, we assume that there is more than one combination of the parameters μ' and δ' yielding the correct spacings between the observed exciton states.

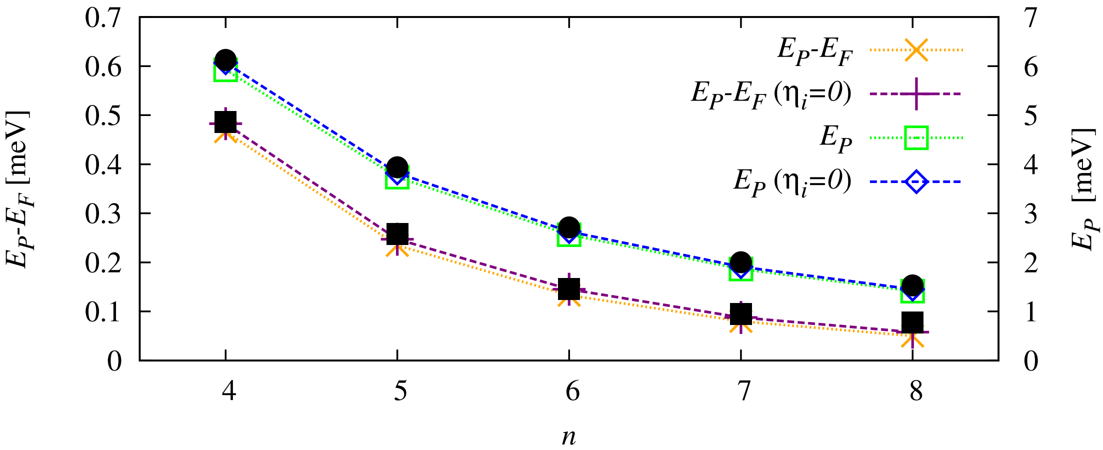

Figure 4.2.: Binding energies E_P of the dipole-allowed P excitons and the energy difference between these excitons and the average energy of the dipole-allowed F excitons. Black dots and circles denote experimental data. Theoretical results are depicted by linespoints. The best agreement between theory and experiment is obtained for $\delta' \approx -0.42$. Without the η_i-dependent terms of Eq. (4.6) an even better agreement can be obtained for $\delta' = -0.408$.

To prove our assumption, we perform the same analysis again, using the parameters $\Delta = 0.131\,\mathrm{eV}$, $\gamma_1' = 2.77$, and $\mu' = 0.0586$ as given values. We now also include the terms with the coefficients η_i of the Hamiltonian (4.6) of the hole. We restrict the analysis to negative values of δ'. The results are depicted in Fig. 4.1(c) and 4.1(d). Note that the value of $\mu' = 0.0586$ is so small that the states with different quantum number F are hardly separated for $\delta' = 0$. Since these states mix for finite δ' it is therefore inappropriate to give the symmetries of the states in the form $\Gamma_i^-(F)$ and we omit the assignment with F. Furthermore, the spacing between the lower lying Γ_6^- state and the higher lying Γ_8^- state, which has a very small oscillator strength, is so small that it can hardly be resolved in experiments. This proves again that there are only three lines observable in experiments. Our calculations yield

$$\delta' = -0.408, \tag{4.80}$$

which is in excellent agreement with the expected value of $\delta' = -0.404$.

In Fig. 4.2 we depict the binding energies E_P of the dipole-allowed P excitons as well as the energy difference between these excitons and the average energy of the dipole-allowed F excitons. We use the nomenclature of Ref. [36] so that the P excitons are the energetically lower lying states of symmetry Γ_7^- and Γ_8^- in Fig. 4.1(c) whereas the F excitons are the remaining states in this Figure. We obtain a good agreement between theory and experiment for a slightly different value of $\delta' \approx -0.42$.

Small uncertainties in the material parameters still remain but can be explained in terms of some approximations made, e.g., the parameters A_i and B_i taken from Ref. [37] are fit parameters to band structure calculations and are hence afflicted with errors. Another influence on the exciton spectrum are phonons (cf. Chapter 3), which our theory does not account for and which also make an experimental determination of the correct position of exciton resonances difficult [30]. Finally, we think that out of the several combinations of μ' and δ', which reproduce the exciton spectrum, the parameters obtained from band structure calculations are the correct ones to describe this spectrum.

4.5.2 $\boldsymbol{K}$-dependent splitting

In this section we discuss the K-dependent line splitting observed in Refs. [82–84] in terms of the complex valence band structure of Cu_2O. The Hamiltonian (4.7) depends only on the relative coordinate $\boldsymbol{r} = \boldsymbol{r}_\mathrm{e} - \boldsymbol{r}_\mathrm{h}$ of electron and hole. For this reason the momentum of the center of mass $\hbar\boldsymbol{K}$ is a constant of motion [267]. About ten years ago the K-dependent line splitting of the $1S$ exciton state was observed and explained in terms of a K-dependent short-range exchange interaction of the form [82–84]

$$\begin{aligned} J(\boldsymbol{K}) &= \Delta_1 \begin{pmatrix} K^2 & 0 & 0 \\ 0 & K^2 & 0 \\ 0 & 0 & K^2 \end{pmatrix} + \Delta_3 \begin{pmatrix} 3K_1^2 - K^2 & 0 & 0 \\ 0 & 3K_2^2 - K^2 & 0 \\ 0 & 0 & 3K_3^2 - K^2 \end{pmatrix} \\ &+ \Delta_5 \begin{pmatrix} 0 & K_1K_2 & K_1K_3 \\ K_1K_2 & 0 & K_2K_3 \\ K_1K_3 & K_2K_3 & 0 \end{pmatrix}, \end{aligned} \tag{4.81}$$

Fitting this ansatz to experimental spectra of the $1S$ exciton yielded

$$\Delta_1 = -8.6\ \mu\mathrm{eV}, \quad \Delta_3 = -1.3\ \mu\mathrm{eV}, \quad \Delta_5 = 2\ \mu\mathrm{eV}. \tag{4.82}$$

However, it has been reported that a K-dependent short-range exchange interaction is far too small to cause the large line splitting observed [162].

As has already been stated in Sec. 4.1, when considering the ortho-exciton states each of these states can have a larger contribution of one of the orbital Bloch functions xy, yz, or zx without a violation of symmetry, respectively. However, if one orbital Bloch component predominates, the anisotropic dispersion of the Bloch function will lead to an anisotropic dispersion of the excitons. Thus, the K-dependent line splitting of the ortho-exciton observed in Refs. [82–84] should be a direct consequence of the disparity in the orbital Bloch components of this exciton. Therefore, we think that the I-dependent terms in Eq. (4.7) are the reason for this splitting and we will show that these terms are of the same form as the ones in Eq. (4.81). Since $\eta_i \ll \gamma_i$ holds in Eq. (4.6), we set $\eta_i = 0$ in the following.

Inserting the well-known coordinates and momenta of relative and center of mass motion of Eq. (2.198) with $\boldsymbol{P} = \hbar\boldsymbol{K}$ in Eq. (4.7) leads to a coupling term between these motions in the kinetic energy [266, 267]:

$$H = T_\mathrm{r}(\boldsymbol{p}) + T_\mathrm{c}(\boldsymbol{p},\, \boldsymbol{K}) + T_\mathrm{t}(\boldsymbol{K}) + V(\boldsymbol{r}). \tag{4.83}$$

In Ref. [267] a different transformation of coordinates was proposed, by which the coupling term T_c vanishes. This transformation reads

$$(\boldsymbol{p}_\mathrm{h})_i = \sum_j \boldsymbol{A}_{ij} K_j - p_i, \tag{4.84a}$$

$$(\boldsymbol{p}_\mathrm{e})_i = \sum_j (\hbar\delta_{ij}\boldsymbol{1} - \boldsymbol{A}_{ij}) K_j + p_i, \tag{4.84b}$$

where the terms $\boldsymbol{A}_{ij}$ are assumed to be spin matrices. However, in the calculations of Ref. [267] the spin-orbit coupling was assumed to be infinitely large so that only states with $J = 3/2$ were considered. We will now calculate the appropriate matrices $\boldsymbol{A}_{ij}$ for the Hamiltonian (4.7) and compare the resulting expression for $T_{\mathrm{t}}(\boldsymbol{K})$ with the ansatz for the exchange interaction in Refs. [82–84].

We define the matrices

$$\boldsymbol{I}_{ij} = 3\left\{\boldsymbol{I}_i,\, \boldsymbol{I}_j\right\} - 2\hbar^2\delta_{ij}\boldsymbol{1} \tag{4.85}$$

according to [79] and note that these operators form a closed subset with respect to the symmetric product $\{a, b\} = \frac{1}{2}(ab + ba)$ (see Appendix C.1). Therefore, we make the ansatz

$$\begin{aligned} \boldsymbol{A}_{jj} &= \hbar^2 C_1 \boldsymbol{1} + \frac{1}{3}C_2\boldsymbol{I}_{jj} + \frac{1}{3}C_3\boldsymbol{I}_{kl}, & \text{(4.86a)} \\ \boldsymbol{A}_{jk} &= \hbar^2 C_4 \boldsymbol{1} + \frac{1}{3}C_5\boldsymbol{I}_{jk} + \frac{1}{3}C_6\boldsymbol{I}_{ll}, & \text{(4.86b)} \end{aligned}$$

with $j \neq l \neq k \neq j$, which respects the cubic symmetry of the solid. Inserting Eqs. (4.84a) and (4.84b) into the kinetic part of Eq. (4.7) and setting the coupling term $T_{\mathrm{c}} = 0$, we can determine the coefficients C_i. The K-dependent part of the kinetic energy is then exactly of the same form as the exchange interaction terms in Refs. [82–84]:

$$T_{\mathrm{t}}(\boldsymbol{K}) = \Omega_1 K^2\boldsymbol{1} - \frac{\Omega_3}{\hbar^2}(K_1^2\boldsymbol{I}_{11} + \text{c.p.}) - \frac{2\Omega_5}{3\hbar^2}(K_1K_2\boldsymbol{I}_{12} + \text{c.p.}) \tag{4.87}$$

or

$$\begin{aligned} T_{\mathrm{t}}(\boldsymbol{K}) &= \Omega_1 \begin{pmatrix} K^2 & 0 & 0 \\ 0 & K^2 & 0 \\ 0 & 0 & K^2 \end{pmatrix} + \Omega_3 \begin{pmatrix} 3K_1^2 - K^2 & 0 & 0 \\ 0 & 3K_2^2 - K^2 & 0 \\ 0 & 0 & 3K_3^2 - K^2 \end{pmatrix} \\ &+ \Omega_5 \begin{pmatrix} 0 & K_1K_2 & K_1K_3 \\ K_1K_2 & 0 & K_2K_3 \\ K_1K_3 & K_2K_3 & 0 \end{pmatrix}, \end{aligned} \tag{4.88}$$

where K is now given in units of $K_0 \approx 2.62\,\mathrm{m}^{-1}$, i.e., the value at the exciton-photon resonance [84]. The dependency of the coefficients C_i and Ω_i on the Luttinger parameters is given in Appendix C.1.

Since our coefficients Ω_i cannot be directly compared with the according coefficients Δ_i in Refs. [82–84], we use a different symbol to illustrate this fact. The impossibility of a direct comparison arises due to three important facts:

First, the operator $T_{\mathrm{t}}(\boldsymbol{K})$ describes the kinetic energy related to the motion of the center of mass, whereas Eq. (4.81) only describes the "exchange interaction", i.e., the interaction without the spherically symmetric part of the kinetic energy. Therefore, it is $\Omega_1 \hat{=} \hbar^2K^2/(2M) + \Delta_1$, $\Omega_3 \hat{=} \Delta_3$, and $\Omega_5 \hat{=} \Delta_5$ with the exciton mass of the simple-band model $M = m_{\mathrm{e}} + m_{\mathrm{h}} \approx 1.64\,m_0$.

Furthermore, the central-cell corrections apply for the $1S$ exciton. However, the calculations on these corrections performed by Kavoulakis *et al.* [162] were done within the simple band model and the unknown coefficients were obtained by comparing results to experimental data. Effects due to the complex valence band structure may therefore be already included in those central-cell corrections so that we cannot separate the true central-cell effects from the effects due to $T_{\mathrm{t}}(\boldsymbol{K})$.

Finally, since the coefficients Δ_i were obtained from experimental data, we have to consider that the K-dependent splitting is also influenced by the binding energy of the exciton. Therefore, $T_{\mathrm{t}}(\boldsymbol{K})$

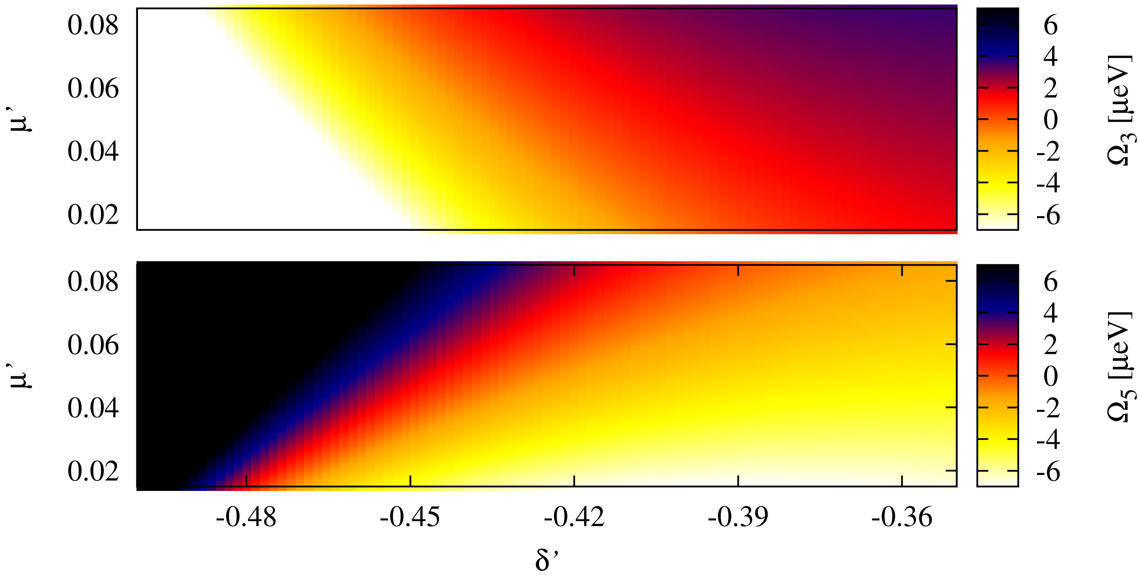

Figure 4.3.: The values of the coefficients (a) Ω_3 and (b) Ω_5 of Eq. (4.88) as functions of μ' and δ'. For further information see text.

has to either be included in the matrix diagonalization or at least be treated within perturbation theory as was done in Ref. [267].

However, Fig. 4.3 shows that there are significant changes in the values of the coefficients Ω_3 and Ω_5 if the parameters μ' and δ' are only slightly varied from $\mu' = 0.0586$ and $\delta' = -0.404$. Consequently, a more comprehensive analysis of $T_{\mathrm{t}}(\boldsymbol{K})$ would not give more reliable results due to the small uncertainties in μ' and δ', which have been discussed at the end of Sec. 4.5.1.

Therefore, we present only a very simple analysis of $T_{\mathrm{t}}(\boldsymbol{K})$: Using $\gamma_1' = 2.77$ as a given value, we solve the equations

$$-1.3\ \mu\mathrm{eV} = \Omega_3(\mu', \delta'), \tag{4.89a}$$

$$2.0\ \mu\mathrm{eV} = \Omega_5(\mu', \delta'), \tag{4.89b}$$

for μ' and δ' and obtain $\mu' \approx 0.0583$ and $\delta' \approx -0.442$. Inserting these results in $\Omega_1(\mu', \delta')$ yields $\Omega_1 \approx 2.15\ \mu\mathrm{eV}$ or $\Omega_1 - \hbar^2 K^2/(2M) \approx -13.73\ \mu\mathrm{eV}$. Of course, the deviation from the experimental value $\Delta_1 = -8.6\ \mu\mathrm{eV}$ could now be explained in terms of the simplicity of this analysis.

However, we have proven that there is clear evidence that the valence band structure or the term $T_{\mathrm{t}}(\boldsymbol{K})$ describing the kinetic energy of the motion of the center of mass of the exciton is the cause for the K-dependent behavior of the $1S$ exciton observed in Refs. [82–84], whereas a K-dependent short-range interaction can most likely be excluded [162]. A detailed analysis of the exchange interaction will be given in the next Chapter 5.

5

$\boldsymbol{K}$-dependent exchange interaction of the 1S ortho-exciton in Cu_2O

When investigating exciton spectra of Cu_2O using high resolution spectroscopy and crystals of high quality, two of the most striking experimental findings are the observation of F excitons and a splitting of the 1S exciton depending on its total momentum $\hbar K$. Both effects cannot be understood within a simple effective mass model. Therefore, the K-dependent splitting of the 1S exciton was attributed by Dasbach *et al.* [82–84] to a K-dependent exchange interaction. This is beyond the scope of the common treatment of the exchange interaction for Cu_2O, where only a K-independent analytic exchange and a vanishing nonanalytic exchange interaction are considered.

Since we have shown in Sec. 4.5.2 that the observed splitting could also be explained by taking full account of the anisotropic dispersion of the Γ_5^+ orbital Bloch states, we believe that the influence of a K dependent exchange interaction on the 1S ortho-exciton in Cu_2O deserves a closer investigation as it is *a priori* unknown whether dispersion *and* exchange interaction are of the same size.

Although a preliminary investigation as regards the presence of a K-dependent exchange interaction was undertaken by Kavoulakis *et al.* [162], their treatment was limited to the nonanalytic part of the exchange interaction only and lacking a consideration of the complete valence band structure of Cu_2O. Going beyond the common treatment of the exchange interaction, where usually only the leading terms of the analytic and the nonanalytic exchange interaction are considered, we derive in Sec. 5.1 general expressions for both the analytic and nonanalytic part of the exchange interaction for all direct excitons up to basically arbitrary order in K using $\boldsymbol{k}\cdot\boldsymbol{p}$ perturbation theory. This allows us not only to show the unknown fact that the appearance of a K-dependent exchange interaction is inseparably connected to a K-independent exchange interaction of P and D excitons but also to estimate the magnitude of the K-dependent terms from microscopic calculations for both parts of the interaction. This is furthermore in contrast to the simple group theoretical treatment of the exchange interaction of Refs. [82–84], which leads to K-dependent terms of the correct form but does not yield the their prefactors. Since every K-dependent energy as regards states of the symmetry Γ_5^+ must lead to matrices of the form presented in Ref. [83], the unambiguous assignment of the experimentally observed K dependent splitting to the exchange interaction is not possible by these means. In Sec. 5.2 we point out the specific properties of excitons in Cu_2O and explain that in contrast to other direct semiconductors the size of the spin orbit interaction has a significant influence on the exciton dispersion in Cu_2O. Considering the special properties of the 1S exciton, we also explain why the effect of the valence band structure is strong especially for this exciton. The analytic and the nonanalytic exchange interaction of the 1S exciton of cuprous oxide are investigated in Sec. 5.3.1 and Sec. 5.3.2, respectively. We show that the magnitude of the exchange interaction is far too small to explain the observed K-dependent splitting [82–84].

Moreover, as regards the nonanalytic exchange interaction, we go beyond the treatment of Kavoulakis *et al.* [162] and pay special attention to its angular dependency in Sec. 5.3.2. This allows us to prove the occurrence of a coupling between longitudinal and transverse excitons in Cu$_2$O due to the K-dependent terms of this part of the exchange interaction. Hence, we show that all three ortho-exciton states couple to light if the wave vector is not oriented in a direction of high symmetry. Essential parts of this Chapter have been published in Ref. [43].

5.1 Exchange interaction

In this section we derive the K-dependent terms of the analytic and the nonanalytic exchange interaction based on the main expressions of the exchange interaction given in Refs. [7, 12, 162, 303, 304]. Even though the exchange interaction has not only been investigated for bulk semiconductors [303, 305], but also for quantum dots [306] and quantum wells [307], its microscopic description includes the Bloch functions and therefore the band structure of the semiconductor, for which reason its calculation is difficult [163, 304].

Within the scope of the simple band model the wave function $\Psi^{\sigma\tau}_{vc,\,\nu\boldsymbol{K}}$ of an exciton is given by Eq. (4.29):

$$\Psi^{\sigma\tau}_{vc,\,\nu\boldsymbol{K}} = \sum_{\boldsymbol{q}} f_{vc\,\nu}(\boldsymbol{q})\Phi^{\sigma\tau}_{vc}(\boldsymbol{q}-\gamma\boldsymbol{K},\,\boldsymbol{q}+\alpha\boldsymbol{K}) \tag{5.1}$$

with the envelope function $f_{vc\nu}(\boldsymbol{q})$ of Eq. (4.30), the constant factors $\alpha = m_{\mathrm{e}}/(m_{\mathrm{e}}+m_{\mathrm{h}})$ and $\gamma = 1-\alpha$, and the function $\Phi^{\sigma\tau}_{vc}$ of Eq. (2.145). In the Wannier equation the exchange energy is missing since it is often treated as a correction to the hydrogen-like solution [7]. In general, the exchange energy between two exciton states $\Psi^{\sigma\tau}_{vc\,\nu\boldsymbol{K}}$ and $\Psi^{\sigma'\tau'}_{v'c'\,\nu'\boldsymbol{K}'}$ reads [7, 303]

$$\begin{aligned}E_{\mathrm{exch}}(vc\,\nu\boldsymbol{K},\,v'c'\,\nu'\boldsymbol{K}') = {}& \delta_{\sigma\tau}\delta_{\sigma'\tau'}\delta_{\boldsymbol{K},\boldsymbol{K}'}\sum_{\boldsymbol{q}\boldsymbol{q}'} f^{*}_{vc\,\nu}(\boldsymbol{q})f_{v'c'\,\nu'}(\boldsymbol{q}')\int \mathrm{d}\boldsymbol{r}_1\int \mathrm{d}\boldsymbol{r}_2\\ &\times \psi^{*}_{c\boldsymbol{q}}(\boldsymbol{r}_1)\psi_{v\boldsymbol{q}-\boldsymbol{K}}(\boldsymbol{r}_1)\frac{e^2}{4\pi\varepsilon_0\varepsilon\,|\boldsymbol{r}_1-\boldsymbol{r}_2|}\psi_{c'\boldsymbol{q}'}(\boldsymbol{r}_2)\psi^{*}_{v'\boldsymbol{q}'-\boldsymbol{K}'}(\boldsymbol{r}_2).\end{aligned} \tag{5.2}$$

The exchange energy includes the term $\delta_{\sigma\tau}\delta_{\sigma'\tau'}$. Introducing the total spin $S = S_{\mathrm{e}} + S_{\mathrm{h}} = \tau - \sigma$ of electron and hole, this term can be written with singlet and triplet states as $2\delta_{S,0}$ [127].

5.1.1 Wannier representation

We treat at first the exchange interaction in Wannier representation. The corresponding expression of Eq. (5.2) in position space can be obtained after some lengthy calculations using the Wannier functions

$$a_{n\boldsymbol{R}}(\boldsymbol{r}) = \frac{1}{\sqrt{N}}\sum_{\boldsymbol{k}} e^{-i\boldsymbol{k}\cdot\boldsymbol{R}}\psi_{n\boldsymbol{k}}(\boldsymbol{r}) \tag{5.3}$$

and the relation $a_{n\boldsymbol{R}_1}(\boldsymbol{r}+\boldsymbol{R}_2) = a_{n\boldsymbol{R}_1-\boldsymbol{R}_2}(\boldsymbol{r})$ [303]:

$$E_{\mathrm{exch}} = 2\delta_{S,0}\delta_{\boldsymbol{K},\boldsymbol{K}'}\sum_{\boldsymbol{R}} e^{i\boldsymbol{K}\cdot\boldsymbol{R}}\int \mathrm{d}\boldsymbol{r}_1\int \mathrm{d}\boldsymbol{r}_2\,\frac{\rho^{*}_{vc\,\nu\boldsymbol{K}}(\boldsymbol{r}_1)\rho_{v'c'\,\nu'\boldsymbol{K}}(\boldsymbol{r}_2)}{4\pi\varepsilon_0\varepsilon\,|\boldsymbol{r}_1-\boldsymbol{r}_2-\boldsymbol{R}|}. \tag{5.4}$$

Here the localized charge density or transition density [7, 303]

$$\rho_{vc\nu\boldsymbol{K}}(\boldsymbol{r}) = e\sum_{\boldsymbol{\beta}} U_{vc\nu\boldsymbol{K}}(\boldsymbol{\beta}) a_{c\boldsymbol{\beta}}(\boldsymbol{r}) a^{*}_{v\boldsymbol{0}}(\boldsymbol{r}) \tag{5.5}$$

with the function $U_{vc\nu\boldsymbol{K}}$ of Eq. (2.220) enters the formula for the exchange interaction.

The exchange interaction is generally divided into the short-range part, which is the summand with $\boldsymbol{R} = \boldsymbol{0}$ in Eq. (5.4), and the dipole-dipole or long-range contribution, which are the remaining terms of Eq. (5.4). The long-range part is often evaluated [7, 308] using a Taylor expansion of $1/\left|\boldsymbol{r}_1 - \boldsymbol{r}_2 - \boldsymbol{R}\right|$:

$$\frac{1}{\left|\boldsymbol{r}_1 - \boldsymbol{r}_2 - \boldsymbol{R}\right|} \approx \frac{1}{R} - (\boldsymbol{r}_2 - \boldsymbol{r}_1)\cdot\frac{\boldsymbol{R}}{R^3} - (\boldsymbol{r}_2 - \boldsymbol{r}_1)^2\frac{1}{2R^3} + \left[(\boldsymbol{r}_2 - \boldsymbol{r}_1)\cdot\boldsymbol{R}\right]^2\frac{3}{2R^5} + \mathcal{O}(R^{-4}). \tag{5.6}$$

Since the charge

$$Q_{vc\nu\boldsymbol{K}} = \int \mathrm{d}\boldsymbol{r}\,\rho_{vc\nu\boldsymbol{K}}(\boldsymbol{r}) = 0, \tag{5.7}$$

vanishes, the long-range part reads

$$E^{\mathrm{LR}}_{\mathrm{exch}} = 2\delta_{S,0}\delta_{\boldsymbol{K},\boldsymbol{K}'}\sum_{\boldsymbol{R}\neq\boldsymbol{0}} e^{i\boldsymbol{K}\cdot\boldsymbol{R}}\frac{1}{4\pi\varepsilon_0\varepsilon}\frac{1}{R^5}\left[\boldsymbol{\mu}^{*}_{vc\nu\boldsymbol{K}}\cdot\boldsymbol{\mu}_{v'c'\nu'\boldsymbol{K}}R^2 - 3(\boldsymbol{\mu}^{*}_{vc\nu\boldsymbol{K}}\cdot\boldsymbol{R})(\boldsymbol{\mu}_{v'c'\nu'\boldsymbol{K}}\cdot\boldsymbol{R})\right]. \tag{5.8}$$

Therefore, the long-range part will occur if the transition density has a dipole moment

$$\boldsymbol{\mu}_{vc\nu\boldsymbol{K}} = \int \mathrm{d}\boldsymbol{r}\;\boldsymbol{r}\rho_{vc\nu\boldsymbol{K}}(\boldsymbol{r}). \tag{5.9}$$

If we set $\boldsymbol{K} = \boldsymbol{0}$ in Eq. (5.8), the term will vanish since it then describes the interaction between one dipole located at $\boldsymbol{R} = \boldsymbol{0}$ and other dipoles, which are in a perfect symmetric (cubic) arrangement [7]. For $\boldsymbol{K} \neq \boldsymbol{0}$, the long-range part reads [7, 303]

$$E^{\mathrm{LR}}_{\mathrm{exch}} = 2\delta_{S,0}\delta_{\boldsymbol{K},\boldsymbol{K}'}\frac{1}{3\varepsilon_0\varepsilon V_{\mathrm{uc}}}\left[\frac{3}{K^2}(\boldsymbol{\mu}^{*}_{vc\nu\boldsymbol{K}}\cdot\boldsymbol{K})(\boldsymbol{\mu}_{v'c'\nu'\boldsymbol{K}}\cdot\boldsymbol{K}) - \boldsymbol{\mu}^{*}_{vc\nu\boldsymbol{K}}\cdot\boldsymbol{\mu}_{v'c'\nu'\boldsymbol{K}}\right] + \mathcal{O}(K^2a^2). \tag{5.10}$$

for exciton in a cubic crystal. This expression depends only on the angle θ between $\boldsymbol{\mu}^{*}_{vc\nu\boldsymbol{K}}$ or $\boldsymbol{\mu}_{v'c'\nu'\boldsymbol{K}}$ and $\boldsymbol{K}$. The expression for the short-range term reads

$$E^{\mathrm{SR}}_{\mathrm{exch}} = 2\delta_{S,0}\delta_{\boldsymbol{K},\boldsymbol{K}'}\int \mathrm{d}\boldsymbol{r}_1\int \mathrm{d}\boldsymbol{r}_2\,\frac{\rho^{*}_{vc\nu\boldsymbol{K}}(\boldsymbol{r}_1)\rho_{v'c'\nu'\boldsymbol{K}}(\boldsymbol{r}_2)}{4\pi\varepsilon_0\varepsilon\left|\boldsymbol{r}_1 - \boldsymbol{r}_2\right|}. \tag{5.11}$$

We can finally make use of the fact that a Wannier functions $a_{m\boldsymbol{R}}$ is localized about $\boldsymbol{R}$ to obtain

$$\rho_{vc\nu\boldsymbol{K}}(\boldsymbol{r}) \approx eU_{vc\nu\boldsymbol{K}}(\boldsymbol{0})a_{c\boldsymbol{0}}(\boldsymbol{r})a^{*}_{v\boldsymbol{0}}(\boldsymbol{r}), \tag{5.12}$$

$$\boldsymbol{\mu}_{vc\nu\boldsymbol{K}} \approx eU_{vc\nu\boldsymbol{K}}(\boldsymbol{0})\int \mathrm{d}\boldsymbol{r}\;\boldsymbol{r}a_{c\boldsymbol{0}}(\boldsymbol{r})a^{*}_{v\boldsymbol{0}}(\boldsymbol{r}), \tag{5.13}$$

with

$$U_{vc\nu\boldsymbol{K}}(\boldsymbol{0}) = \sqrt{\frac{V_{\mathrm{uc}}}{\pi a^3_{\mathrm{exc}}n^3}}\delta_{L,0}\delta_{M,0} \tag{5.14}$$

and the volume V_{uc} of one unit cell of the solid. Since the hydrogen-like wave functions vanish at $\boldsymbol{\beta} = \boldsymbol{0}$ for $L \neq 0$, the exchange interaction is especially important for S excitons. Furthermore, the relative symmetries of the functions $a^{*}_{v\boldsymbol{0}}(\boldsymbol{r})$ and $a_{c\boldsymbol{0}}(\boldsymbol{r})$ have to be appropriate to obtain a dipole moment. If the exciton is dipole-forbidden, one can still obtain a small dipole moment due to contributions from nearest neighbors, which leads to the exchange interaction for P excitons. In this case the summands with the smallest values of $\boldsymbol{\beta} \neq \boldsymbol{0}$ are important in Eq. (5.5).

5.1.2 Fourier representation

We may now treat the exchange interaction in Fourier representation [162, 304, 309]. Inserting the Fourier transform [85, 304]

$$\frac{1}{r} = \frac{4\pi}{NV_{\mathrm{uc}}} \sum_{\boldsymbol{G}} \sum_{\boldsymbol{k}\in\mathrm{BZ}} \frac{1}{(\boldsymbol{k}+\boldsymbol{G})^2} e^{i(\boldsymbol{k}+\boldsymbol{G})\cdot\boldsymbol{r}} \tag{5.15}$$

with reciprocal lattice vectors $\boldsymbol{G}$ in Eq. (5.2), we can write the exchange energy as

$$E_{\mathrm{exch}} = 2\delta_{S,0}\delta_{\boldsymbol{K},\boldsymbol{K}'} \sum_{\boldsymbol{G}} \frac{m^{*}_{vc\,\nu}(\boldsymbol{K},\,\boldsymbol{G}) m_{v'c'\,\nu'}(\boldsymbol{K},\,\boldsymbol{G})}{\varepsilon_0 \varepsilon V_{\mathrm{uc}} (\boldsymbol{K}+\boldsymbol{G})^2} \tag{5.16}$$

with

$$m_{vc\,\nu}(\boldsymbol{K},\,\boldsymbol{G}) = \frac{e}{\sqrt{N}} \sum_{\boldsymbol{q}} f_{vc\,\nu}(\boldsymbol{q}) \left\langle u_{v\boldsymbol{q}-\gamma\boldsymbol{K}} \left| e^{-i\boldsymbol{G}\cdot\boldsymbol{r}} \right| u_{c\boldsymbol{q}+\alpha\boldsymbol{K}} \right\rangle . \tag{5.17}$$

The functions $u_{n\boldsymbol{k}}(\boldsymbol{r})$ denote the lattice-periodic part of the Bloch functions $\psi_{n\boldsymbol{k}}(\boldsymbol{k}) = e^{i\boldsymbol{k}\cdot\boldsymbol{r}} u_{n\boldsymbol{k}}(\boldsymbol{r})$ [85]. In the representation of Eq. (5.16) the exchange energy can be divided into the nonanalytic part $E^{\mathrm{NA}}_{\mathrm{exch}}$, which is the summand with $\boldsymbol{G}=\boldsymbol{0}$, and the analytic part $E^{\mathrm{A}}_{\mathrm{exch}}$, which is the sum of the remaining terms. Note that if the exchange energy is formulated in the Wannier representation instead of the representation with Bloch functions, it is generally separated into the long-range and the short-range part. However, according to Refs. [303, 304, 310] there is no identity between the nonanalytic exchange and the long-range part or between the analytic exchange and the short-range part but only a close correspondence.

In the limit $Ka \ll 1$ one obtains the simple expression [7, 303]

$$E^{\mathrm{NA}}_{\mathrm{exch}} = 2\delta_{S,0}\delta_{\boldsymbol{K},\boldsymbol{K}'} \frac{1}{\varepsilon_0 \varepsilon V_{\mathrm{uc}} K^2} (\boldsymbol{\mu}^{*}_{vc\,\nu\boldsymbol{K}} \cdot \boldsymbol{K})(\boldsymbol{\mu}_{v'c'\,\nu'\boldsymbol{K}} \cdot \boldsymbol{K}) + \mathcal{O}(K^2 a^2) \tag{5.18}$$

for the nonanalytic exchange energy of excitons in a cubic crystal. The expression (5.18) depends only on the two angles between $\boldsymbol{K}$ and the dipole moments $\boldsymbol{\mu}^{*}_{vc\,\nu\boldsymbol{K}}$ or $\boldsymbol{\mu}_{v'c'\,\nu'\boldsymbol{K}}$ [cf. Eq. (5.9)]. If $\boldsymbol{\mu}$ is parallel or perpendicular to $\boldsymbol{K}$, one speaks of longitudinal or transverse excitons, respectively [7]. The nonanalytic exchange energy therefore causes a longitudinal-transverse splitting (LT-splitting) of spin singlet states near $K=0$. It is obvious that the nonanalytic exchange energy is nonzero only for longitudinal excitons and that it is therefore connected to a macroscopic polarization. Thus, the effect can be compared to the LT-splitting of phonons. Since the splitting between transverse and longitudinal excitons depends on $\left|\mu_{vc\,\nu\boldsymbol{K}}\right|^2$ for $vc\,\nu = v'c'\,\nu'$, it is proportional to the oscillator strength $f_{\xi\nu\boldsymbol{0}}$ for exciting one exciton from the ground state of the solid by light. This oscillator strength reads for $Ka \ll 1$ [7]

$$f_{\xi\nu 0} = \frac{4\delta_{S,0}}{\hbar^2 e^2 m_0} E_{\nu\boldsymbol{K}} \left|\hat{\boldsymbol{e}}_{\xi\boldsymbol{K}} \cdot \boldsymbol{\mu}_{vc\,\nu\boldsymbol{K}}\right|^2 \tag{5.19}$$

with the energy $E_{\nu\boldsymbol{K}}$ of the exciton state given in Eq. (2.205), the free electron mass m_0 and the polarization vector $\hat{\boldsymbol{e}}_{\xi\boldsymbol{K}}$ perpendicular to $\boldsymbol{K}$. Thus, the splitting caused by $E^{\mathrm{NA}}_{\mathrm{exch}}$ is identical to the LT-splitting when treating polaritons [311] and it is of appreciable size only if the exciton is dipole allowed.

It is now important to note that light is always transversely polarized and that only transverse excitons are produced in optical absorption [312] [cf. Eq. (5.19)]. Longitudinal excitons cannot be seen in optical absorption spectra. Thus, the LT-splitting in the case of polaritons increases the transverse excitons by an energy Δ_{LT}. On the other hand, the LT-splitting connected to the nonanalytic exchange interaction increases the energy of the longitudinal excitons by the same amount Δ_{LT}. Finally, both states are again degenerate at $K = 0$, which is required for reasons of symmetry.

We can see from Eq. (5.18) that longitudinal and transverse exciton states are not coupled for $Ka \ll 1$. As has been stated in Ref. [7], this uncoupling is "accidental" since it is expected that these states are decoupled only if they transform according to different irreducible representations of the group of $\boldsymbol{K}$ [313, 314]. However, the higher order terms $\mathcal{O}(K^2a^2)$ in Eq. (5.18) may lead to a coupling of longitudinal and transverse exciton states unless they transform according to different irreducible representations. This will be shown for $\mathrm{Cu_2O}$ in Sec. 5.3.2. If a coupling occurs, the longitudinal states will become observable in experiments due to the admixture of transverse states [312].

We can now take a closer look at $m_{vc\nu}(\boldsymbol{K},\,\boldsymbol{G})$ using $\boldsymbol{k}\cdot\boldsymbol{p}$ perturbation theory. It is [85, 162]

$$u_{m\boldsymbol{k}}(\boldsymbol{r}) \approx u_{m\boldsymbol{0}}(\boldsymbol{r}) + \frac{\hbar}{m_0}\sum_{n\neq m}\frac{\boldsymbol{k}\cdot\boldsymbol{p}_{nm}}{(E_m-E_n)}u_{n\boldsymbol{0}}(\boldsymbol{r}) + \frac{\hbar^2}{m_0^2}\left[\sum_{n\neq m,l\neq m}\frac{[\boldsymbol{k}\cdot\boldsymbol{p}_{nl}]\,[\boldsymbol{k}\cdot\boldsymbol{p}_{lm}]}{(E_m-E_n)(E_m-E_l)}u_{n\boldsymbol{0}}(\boldsymbol{r}) - \sum_{n\neq m,l\neq m}\frac{[\boldsymbol{k}\cdot\boldsymbol{p}_{mm}]\,[\boldsymbol{k}\cdot\boldsymbol{p}_{nm}]\,\delta_{nl}}{(E_m-E_n)(E_m-E_l)}u_{n\boldsymbol{0}}(\boldsymbol{r})\right] \tag{5.20}$$

with $\boldsymbol{p}_{mn} = \langle u_{m\boldsymbol{0}}\,|\boldsymbol{p}|\,u_{n\boldsymbol{0}}\rangle$ and the energy $E_n = E_n(\boldsymbol{k} = \boldsymbol{0})$ of the band n at the Γ point. We assume that the point group of the solid contains inversion as a group element. Then the term $\boldsymbol{p}_{mm}$ vanishes for reasons of parity. Using the expression (5.20), we obtain up to second order in $\boldsymbol{K}$ and $\boldsymbol{q}$:

$$\begin{aligned} m_{vc\nu}(\boldsymbol{K},\,\boldsymbol{G}) \approx \frac{e}{\sqrt{N}}\sum_{\boldsymbol{q}} f_{vc\nu}(\boldsymbol{q})\Bigg[& I_{vc}(\boldsymbol{G}) + \frac{\hbar}{m_0}\sum_{n\neq v}\frac{(\boldsymbol{q}-\gamma\boldsymbol{K})\cdot\boldsymbol{p}_{vn}}{(E_v-E_n)}I_{nc}(\boldsymbol{G}) \\ & + \frac{\hbar}{m_0}\sum_{n\neq c}\frac{(\boldsymbol{q}+\alpha\boldsymbol{K})\cdot\boldsymbol{p}_{nc}}{(E_c-E_n)}I_{vn}(\boldsymbol{G}) \\ & + \frac{\hbar^2}{m_0^2}\sum_{n\neq v,m\neq c}\frac{[(\boldsymbol{q}-\gamma\boldsymbol{K})\cdot\boldsymbol{p}_{vn}]\,[(\boldsymbol{q}+\alpha\boldsymbol{K})\cdot\boldsymbol{p}_{mc}]}{(E_v-E_n)(E_c-E_m)}I_{nm}(\boldsymbol{G}) \\ & + \frac{\hbar^2}{m_0^2}\sum_{n\neq c,m\neq c}\frac{[(\boldsymbol{q}+\alpha\boldsymbol{K})\cdot\boldsymbol{p}_{nm}]\,[(\boldsymbol{q}+\alpha\boldsymbol{K})\cdot\boldsymbol{p}_{mc}]}{(E_c-E_n)(E_c-E_m)}I_{vn}(\boldsymbol{G}) \\ & + \frac{\hbar^2}{m_0^2}\sum_{n\neq v,m\neq v}\frac{[(\boldsymbol{q}-\gamma\boldsymbol{K})\cdot\boldsymbol{p}_{mn}]\,[(\boldsymbol{q}-\gamma\boldsymbol{K})\cdot\boldsymbol{p}_{vm}]}{(E_v-E_n)(E_v-E_m)}I_{nc}(\boldsymbol{G})\Bigg]. \end{aligned} \tag{5.21}$$

Here we have defined $I_{mn}(\boldsymbol{G}) = \left\langle u_{m\boldsymbol{0}} \left| e^{-i\boldsymbol{G}\cdot\boldsymbol{r}} \right| u_{n\boldsymbol{0}} \right\rangle$. The sum over $\boldsymbol{q}$ can be evaluated using

$$\frac{1}{\sqrt{N}} \sum_{\boldsymbol{q}} q_i^{\chi} q_j^{\varphi} f_{vc\nu}(\boldsymbol{q}) = (-i)^{\chi+\varphi} \frac{\partial^{\chi}}{\partial \beta_i^{\chi}} \frac{\partial^{\varphi}}{\partial \beta_j^{\varphi}} F_{vc\nu}(\boldsymbol{\beta}) \bigg|_{\boldsymbol{\beta}=\boldsymbol{0}} \tag{5.22}$$

with $\chi,\ \varphi = 0, 1, 2$.

It is evident that the derivatives of the function $F_{vc\nu}$ at the origin must enter the exchange interaction since we could also treat the interaction in the Wannier representation [303] and obtain higher order terms using a Taylor expansion at $\boldsymbol{\beta} = \boldsymbol{0}$.

Due to the special properties of the wave functions $F_{vc\nu}$, the expression (5.22) is nonzero only if $\varphi + \chi = L$ holds. Therefore, we see that the leading term in Eq. (5.21) describes the K-independent exchange interaction of S excitons. The terms of higher order show that the appearance of a K-dependent exchange interaction of S excitons is inseparably connected to a K *in*dependent exchange interaction of P and D excitons. As the function $m_{vc\nu}(\boldsymbol{K},\ \boldsymbol{G})$ enters quadratically the exchange energy (5.16), the relative size of the K-dependent exchange energy of S excitons and the K *in*dependent exchange energy of P excitons can estimated comparing

$$\left|F_{vc\nu}(\boldsymbol{0})\right|^2 K_0^2 = \frac{V_{\mathrm{uc}}}{\pi a_{\mathrm{exc}}^3} \frac{1}{n^3} K_0^2\ \delta_{L,\,0} \tag{5.23}$$

with

$$\left| \frac{\partial}{\partial \boldsymbol{\beta}} F_{vc\nu}(\boldsymbol{\beta}) \bigg|_{\boldsymbol{\beta}=\boldsymbol{0}} \right|^2 = \frac{V_{\mathrm{uc}}}{3\pi a_{\mathrm{exc}}^5} \frac{n^2-1}{n^5}\ \delta_{L,\,1}. \tag{5.24}$$

Here we have introduced the value K_0 of K at the exciton photon resonance [7, 12]. Note that there are always polaritons and no excitons in bulk semiconductors due to the coupling between excitons and photons. However, if this coupling is weak, it is common to speak of excitons and treat the interaction within perturbation theory [7].

For the nonanalytic exchange interaction, the expression (5.21) simplifies due to $I_{mn}(\boldsymbol{0}) = \delta_{mn}$:

$$\begin{aligned} m_{vc\nu}(\boldsymbol{K},\ \boldsymbol{0}) \approx \frac{e}{\sqrt{N}} \sum_{\boldsymbol{q}} f_{vc\nu}(\boldsymbol{q}) \Bigg\{ &-\frac{\hbar}{m_0} \frac{\boldsymbol{K}\cdot\boldsymbol{p}_{vc}}{E_v - E_c} + \frac{\hbar^2}{m_0^2} \sum_{n\neq v,c} \Bigg[\frac{[(\boldsymbol{q}-\gamma\boldsymbol{K})\cdot\boldsymbol{p}_{vn}]\ [(\boldsymbol{q}+\alpha\boldsymbol{K})\cdot\boldsymbol{p}_{nc}]}{(E_v-E_n)(E_c-E_n)} \\ &+ \frac{[(\boldsymbol{q}+\alpha\boldsymbol{K})\cdot\boldsymbol{p}_{vn}]\ [(\boldsymbol{q}+\alpha\boldsymbol{K})\cdot\boldsymbol{p}_{nc}]}{(E_c-E_v)(E_c-E_n)} + \frac{[(\boldsymbol{q}-\gamma\boldsymbol{K})\cdot\boldsymbol{p}_{nc}]\ [(\boldsymbol{q}-\gamma\boldsymbol{K})\cdot\boldsymbol{p}_{vn}]}{(E_v-E_c)(E_v-E_n)} \Bigg] \Bigg\}. \end{aligned} \tag{5.25}$$

It can easily be seen that $m_{vc\nu}(\boldsymbol{0},\ \boldsymbol{0}) = 0$ holds, for which reason the nonanalytic exchange interaction does not diverge at $K = 0$. The different terms describe the nonanalytic exchange energy of S excitons (K-independent and K-dependent) and of P excitons. In the literature usually only the leading terms of the exchange energy are treated, which are given by

$$E_{\mathrm{exch}}^{\mathrm{A}} = 2\delta_{S,0}\delta_{\boldsymbol{K},\boldsymbol{K}'} \sum_{\boldsymbol{G}\neq\boldsymbol{0}} \frac{e^2}{\varepsilon_0 \varepsilon V_{\mathrm{uc}} \boldsymbol{G}^2} F_{vc\nu}^{*}(\boldsymbol{0}) F_{v'c'\nu'}(\boldsymbol{0}) I_{vc}^{*}(\boldsymbol{G}) I_{v'c'}(\boldsymbol{G}), \tag{5.26a}$$

$$E_{\mathrm{exch}}^{\mathrm{NA}} = 2\delta_{S,0}\delta_{\boldsymbol{K},\boldsymbol{K}'} \frac{e^2}{\varepsilon_0 \varepsilon V_{\mathrm{uc}} \boldsymbol{K}^2} F_{vc\nu}^{*}(\boldsymbol{0}) F_{v'c'\nu'}(\boldsymbol{0}) \left(\frac{\hbar}{m_0}\right)^2 \frac{[\boldsymbol{K}\cdot\boldsymbol{p}_{vc}^{*}]\ [\boldsymbol{K}\cdot\boldsymbol{p}_{v'c'}]}{(E_v-E_c)(E_{v'}-E_{c'})}. \tag{5.26b}$$

Note that $E_{\mathrm{exch}}^{\mathrm{NA}}$ depends on $1/K^2$ and that this term cancels with the K^2 of the numerator. So $E_{\mathrm{exch}}^{\mathrm{NA}}$ depends only on the direction of $\boldsymbol{K}$ but not on its amount $K = |\boldsymbol{K}|$. This explains the term “nonanalytic”.

5.2 Ortho- and para-excitons in cuprous oxide

In this section we discuss and partially reiterate some specific properties of Cu_2O and especially the ortho- and the para-excitons, which are needed to investigate the exchange interaction for this semiconductor. First, we have to consider the band structure of Cu_2O. Neglecting the spin-orbit coupling, the uppermost valence band has the symmetry Γ_5^+ and is threefold degenerate at the center of the Brillouin zone. This degeneracy is accounted for by the quasi-spin $I = 1$ [36, 72, 79, 126], which is a convenient abstraction to denote the three spatial functions $\phi_{v,\,xy}$, $\phi_{v,\,yz}$ and $\phi_{v,\,zx}$ [126, 162]. Especially, the relation between the states $|I,\, M_I\rangle$ and the functions $\phi_{v,\,xy}$, $\phi_{v,\,yz}$ and $\phi_{v,\,zx}$ is given by analogy with Eq. (4.50) [83].

The spin-orbit coupling between the spin S_h of a hole in the valence band and the quasi-spin I splits the sixfold degenerate band (now including the hole spin) into a higher lying twofold-degenerate band (Γ_7^+) and a lower lying fourfold-degenerate band (Γ_8^+) (see Fig. 2.14), which are characterized by the effective hole spins $J = I + S_\mathrm{h} = 1/2$ and $J = 3/2$, respectively. Due to the nonspherical symmetry of the solid and interband interactions, the valence bands are not parabolic but deformed. This leads to a coupling between the yellow and the green exciton series as described comprehensively in Chapters 4 and 6.

The coupling between the valence bands or the anisotropic dispersion of the orbital Γ_5^+ Bloch functions is considered in complete Hamiltonian of excitons (cf. Secs. 4.2 and 4.3)

$$H = E_\mathrm{g} - \frac{e^2}{4\pi\varepsilon_0\varepsilon_{\mathrm{s}1}}\frac{1}{\beta} + H_s + H_d + H_\mathrm{so} + H_\mathrm{exch} + V_\mathrm{CCC}. \tag{5.27}$$

via the H_d-term of Eq. (4.17). The term H_s of Eq. (4.15) describes the average kinetic energy without the nonparabolicity and the coupling between the bands. The anisotropic dispersion of the orbital Γ_5^+ Bloch functions is in direct competition with the spin orbit coupling H_so of Eq. (4.2), which is diagonalized by introducing the effective hole spin J. For an infinite spin orbit coupling $\Delta \to \infty$ the Γ_7^+ valence band would be parabolic at the Γ point. However, as $\Delta = 0.131\,\mathrm{eV}$ [37] is comparatively small in Cu_2O, the nonparabolicity of Γ_7^+ and Γ_8^+ valence band already occurs in the vicinity of the Γ point with a simultaneous mixing of both bands.

The H_d term was first introduced by Baldereschi *et al.* (see, e.g., Refs. [77–81] and further references therein) to describe the situation for an uppermost Γ_8^+ valence band in semiconductors like germanium mathematically correct. The decisive breakthrough of their description is the use of modified Bloch functions, i.e., Bloch functions with a lattice periodic part u, which does not depend on the wave vector k. These functions form a complete basis and are thus just as suitable to describe excited states of the solid. The modification of Baldereschi *et al.* is always required if the lattice periodic part of the common Bloch function varies strongly with k. Only due to the constant lattice periodic part the Coulomb interaction between electron and hole will be proportional to $1/r$ if the Wannier equation is transformed from momentum space to position space via a Fourier transformation. The exciton envelope function in the formalism of Balderschi *et al.* then contains only constant Γ_7^+ and Γ_8^+ components, i.e., the spin states with $J = 1/2$ and $J = 3/2$ given below.

A simple restriction to the Γ_7^+ band neglecting the Γ_8^+ band and considering the nonparabolicity via k^4 terms does not treat the problem correctly. Consequently, the exchange interaction has to be treated within the same formalism, for which reason we use $\boldsymbol{k}\cdot\boldsymbol{p}$ perturbation theory at the Γ point. This is in contrast to the treatment by Kavoulakis *et al.* [162] and to the best of our knowledge this has not been done before.

Since the radius of the $1S$ exciton is very small, it is an intermediate exciton between a Frenkel exciton and a Wannier exciton [7]. Therefore, the $1S$ exciton cannot be described within the effective mass approach due to its large extension in momentum space. However, we neglect the central cell corrections in the following. The usage of the kinetic energy in the form of Eqs. (4.15) and (4.17) and the neglect of higher order terms in p is then justified if we use an average curvature of the bands instead of the curvature at the center of the Brillouin zone. Hence, the Bohr radius of the $1S$ exciton is smaller than the one of excitons with $n \geq 2$. Furthermore, we have to replace the dielectric constant $\varepsilon_{\mathrm{s1}} = 7.5$ by its high-frequency value $\varepsilon_{\mathrm{b2}} = 6.46$ [162].

Let us consider at first the Hamiltonian (5.27) without the H_d term and the exchange interaction. In this case we can treat spins and Wannier or Bloch functions separately from the envelope function. The yellow and green exciton series are described by the two states with $J = 1/2$ of symmetry Γ_7^+

$$\left|\frac{1}{2},+\frac{1}{2}\right\rangle_J = \sqrt{\frac{2}{3}}\,|{+1}\rangle_I\,|{\downarrow}\rangle_{\mathrm{h}} - \frac{1}{\sqrt{3}}\,|0\rangle_I\,|{\uparrow}\rangle_{\mathrm{h}}\,, \tag{5.28a}$$

$$\left|\frac{1}{2},-\frac{1}{2}\right\rangle_J = \frac{1}{\sqrt{3}}\,|0\rangle_I\,|{\downarrow}\rangle_{\mathrm{h}} - \sqrt{\frac{2}{3}}\,|{-1}\rangle_I\,|{\uparrow}\rangle_{\mathrm{h}}\,. \tag{5.28b}$$

and the four states with $J = 3/2$ of symmetry Γ_8^+

$$\left|\frac{3}{2},+\frac{3}{2}\right\rangle_J = |{+1}\rangle_I\,|{\uparrow}\rangle_{\mathrm{h}}\,, \tag{5.29a}$$

$$\left|\frac{3}{2},+\frac{1}{2}\right\rangle_J = \frac{1}{\sqrt{3}}\,|1\rangle_I\,|{\downarrow}\rangle_{\mathrm{h}} + \sqrt{\frac{2}{3}}\,|0\rangle_I\,|{\uparrow}\rangle_{\mathrm{h}}\,. \tag{5.29b}$$

$$\left|\frac{3}{2},-\frac{1}{2}\right\rangle_J = \sqrt{\frac{2}{3}}\,|0\rangle_I\,|{\downarrow}\rangle_{\mathrm{h}} + \frac{1}{\sqrt{3}}\,|{-1}\rangle_I\,|{\uparrow}\rangle_{\mathrm{h}}\,, \tag{5.29c}$$

$$\left|\frac{3}{2},-\frac{3}{2}\right\rangle_J = |{-1}\rangle_I\,|{\downarrow}\rangle_{\mathrm{h}}\,. \tag{5.29d}$$

If we now add the electron spin and the Wannier function $\phi_{c,\,s}$ of the conduction band, which transform together according to $\Gamma_6^+ \otimes \Gamma_1^+ = \Gamma_6^+$, we obtain states with the total momentum $G = J + S_{\mathrm{e}} = 0$ and $G = 1$. Subsequently, these states have to be multiplied by the hydrogen-like envelope function $F_\nu(\boldsymbol{\beta}) = F_{nLM}(\boldsymbol{\beta})$ [cf. Sec. 2.5.2].

In the Cartesian basis the ground states of the yellow exciton are (cf. Ref. [83])

$$|P\rangle = F_{1,0,0}(\boldsymbol{\beta})\,|0,\,0\rangle_G\,, \tag{5.30a}$$
$$|O_{xy}\rangle = F_{1,0,0}(\boldsymbol{\beta})\,|1,\,0\rangle_G\,, \tag{5.30b}$$
$$|O_{yz}\rangle = F_{1,0,0}(\boldsymbol{\beta})\,[|1,\,-1\rangle_G - |1,\,+1\rangle_G]\,/\sqrt{2}, \tag{5.30c}$$
$$|O_{zx}\rangle = iF_{1,0,0}\,[\boldsymbol{\beta})(|1,\,-1\rangle_G + |1,\,+1\rangle_G]\,/\sqrt{2}. \tag{5.30d}$$

The state $|P\rangle$ of symmetry Γ_2^+ is the para-exciton state and the states $|O_{ij}\rangle$ of symmetry Γ_5^+ are the ortho-exciton states. It is possible to express these states using the eigenstates of the spin $S = S_{\mathrm{e}} + S_{\mathrm{h}}$ [83]:

$$|P\rangle = \frac{1}{\sqrt{6}} F_{1,0,0}(\boldsymbol{\beta})\phi_{c,\,s} \Big[\sqrt{2}\phi_{v,\,xy}\,|1,\,0\rangle_S + (-\phi_{v,\,yz} + i\phi_{v,\,zx})\,|1,\,+1\rangle_S + (\phi_{v,\,yz} + i\phi_{v,\,zx})\,|1,\,-1\rangle_S\Big]\,, \tag{5.31a}$$

$$|O_{xy}\rangle = \frac{-1}{\sqrt{6}} F_{1,0,0}(\boldsymbol{\beta})\phi_{c,\,s} \Big[-\sqrt{2}\phi_{v,\,xy}\,|0,\,0\rangle_S + (\phi_{v,\,yz} - i\phi_{v,\,zx})\,|1,\,+1\rangle_S + (\phi_{v,\,yz} + i\phi_{v,\,zx})\,|1,\,-1\rangle_S\Big]\,, \tag{5.31b}$$

$$|O_{yz}\rangle = \frac{1}{\sqrt{6}} F_{1,0,0}(\boldsymbol{\beta})\phi_{c,\,s} \Big[\phi_{v,\,xy}\,|1,\,+1\rangle_S + \phi_{v,\,xy}\,|1,\,-1\rangle_S + i\sqrt{2}\phi_{v,\,yz}\,|0,\,0\rangle_S + \sqrt{2}\phi_{v,\,zx}\,|1,\,0\rangle_S\Big]\,, \tag{5.31c}$$

$$|O_{zx}\rangle = \frac{-i}{\sqrt{6}} F_{1,0,0}(\boldsymbol{\beta})\phi_{c,\,s} \Big[\phi_{v,\,xy}\,|1,\,+1\rangle_S - \phi_{v,\,xy}\,|1,\,-1\rangle_S + \sqrt{2}\phi_{v,\,yz}\,|1,\,0\rangle_S + i\sqrt{2}\phi_{v,\,zx}\,|0,\,0\rangle_S\Big]\,. \tag{5.31d}$$

One can see that the para-exciton state does not contain a singlet component, i.e., a component with $S = 0$. Therefore, this state is spin-flip forbidden in optical excitations, which explains the term “para” or “dark” exciton [30]. However, we may note at this point that the ortho- and para-exciton states are not eigenstates of the operators S^2 and S_z. Therefore, it may be misleading to speak of singlet and triplet states [30, 82].

The exciton states are generally mixed by the H_d term (4.17) due to the coupling between L and I. Since parity is a good quantum number in $\mathrm{Cu_2O}$, the H_d term mixes only exciton states with even values of L or with odd values of L [72]. Therefore, D excitons are admixed to S excitons and vice versa. The coupling due to the H_d term leads to an energy gain in the system, which was discussed in Sec. 4.1.

As the radius of the yellow $1S$ exciton is small in position space, it is extended in momentum space, for which reason we expect its coupling to the green series to be strong. Due to the admixture, the yellow ortho-exciton becomes more and more a pure singlet state as the total spin $S = S_{\mathrm{e}} + S_{\mathrm{h}}$ is a good quantum number in the limit of $\Delta = 0$.

In this limiting case with $\Delta = 0$, the introduction of the effective hole spin J would not be necessary. The exciton wave function could be written as the product of a space function, which also depends on I, and a spin function. Without the H_d term the ground states of the exciton would then read

$$|P_{1,j}\rangle = F_{1,0,0}(\boldsymbol{\beta})\phi_{c,\,s}\phi_{v,\,j}\,|1,\,1\rangle_S\,, \tag{5.32a}$$

$$|P_{0,j}\rangle = F_{1,0,0}(\boldsymbol{\beta})\phi_{c,\,s}\phi_{v,\,j}\,|1,\,0\rangle_S\,, \tag{5.32b}$$

$$|P_{-1,j}\rangle = F_{1,0,0}(\boldsymbol{\beta})\phi_{c,\,s}\phi_{v,\,j}\,|1,\,-1\rangle_S\,, \tag{5.32c}$$

$$|O_{j}\rangle = F_{1,0,0}(\boldsymbol{\beta})\phi_{c,\,s}\phi_{v,\,j}\,|0,\,0\rangle_S\,, \tag{5.32d}$$

with $j = xy,\, yz,\, zx$. In this case there are also three ortho-exciton states. The para- and ortho-exciton states are true triplet states ($S = 1$) and singlet states ($S = 0$), respectively.

The Hamiltonian (5.27) is given for $K = 0$. In the general case with $K \neq 0$ additional terms appear (cf. Sec. 4.5.2):

$$T_{\mathrm{t}}(\boldsymbol{K}) = \Omega_1 K^2 \mathbf{1} - \Omega_3 \left[K_1^2(3\boldsymbol{I}_1^2 - 2\hbar^2\mathbf{1}) + \text{c.p.}\right]/\hbar^2 \\ - \Omega_5 \left[K_1 K_2(\boldsymbol{I}_1\boldsymbol{I}_2 + \boldsymbol{I}_2\boldsymbol{I}_1) + \text{c.p.}\right]/\hbar^2 \tag{5.33}$$

As can be seen, these K^2-dependent terms are 3×3 matrices and can again be divided into an H_s-term, an H_d-term of spherical symmetry and an H_d-term of cubic symmetry, i.e., we can write

$$T_{\mathrm{t}}(\boldsymbol{K}) = (\Omega_1)\, K^2 - \left(\frac{\Omega_5 + 2\Omega_3}{15\hbar^2}\right)\left(K^{(2)} \cdot I^{(2)}\right) \\ + \left(\frac{\Omega_5 - 3\Omega_3}{18\hbar^2}\right)\left(\frac{\sqrt{70}}{5}\left[K^{(2)} \times I^{(2)}\right]_0^{(4)} + \sum_{k=\pm 4}\left[K^{(2)} \times I^{(2)}\right]_k^{(4)}\right). \tag{5.34}$$

To describe the exciton series in Cu$_2$O correctly, the Schrödinger equation with the operators (5.27) and (5.33) has to be solved for fixed values of K. However, as the effect of the K^2-dependent terms on the relative motion is small, the effect of $T_{\mathrm{t}}(\boldsymbol{K})$ can be treated within order perturbation theory.

It has been shown in Sec. 4.5.2 that the coefficients Ω_I in $T_{\mathrm{t}}(\boldsymbol{K})$ are of the correct order of magnitude to describe the K-dependent splitting of the $1S$ exciton state, which was observed experimentally and originally assigned to the exchange interaction in Refs. [82–84]. In the next section 5.3 we will show that the exchange interaction is far too small to explain this splitting.

Before we treat the exchange interaction, let us consider the two limiting cases of $\Delta \to \infty$ and $\Delta = 0$. As a complement to the discussion of the H_d term given in Sec. 4.3, we want to stress the influence of Δ on the exciton dispersion in combination with the H_d term. Furthermore, we want to discuss why the effects of the interband coupling are strong especially for the $1S$ exciton.

In the limiting case of $\Delta \to \infty$ only the yellow series or the band of symmetry Γ_7^+ is important and we can neglect the states with $J = 3/2$. Due to symmetry considerations, the functions $\phi_{v,\,xy}$, $\phi_{v,\,yz}$ and $\phi_{v,\,zx}$ contribute with the same magnitude to the Γ_7^+ band. Hence, the anisotropy of the Γ_5^+-Bloch functions is compensated in the Γ_7^+-band. Calculating the expectation value of $T_{\mathrm{t}}(\boldsymbol{K})$ between the exciton states would provide a 3×3 matrix proportional to $K^2\mathbf{1}$, which describes the parabolic dispersion of the Γ_7^+-band. The off-diagonal terms would vanish.

Only due to the admixture of the green series for finite Δ one orbital Bloch component can predominate in the exciton function. This admixture takes place since the associated symmetry reduction or elliptical deformation of the exciton state leads to an energy gain in the system as has been discussed in Sec. 4.1. For the resulting exciton functions the off-diagonal terms still appear in the expectation value of $T_{\mathrm{t}}(\boldsymbol{K})$. Therefore, we can speak of a kind of Δ dependent squeezing of the two terms with prefactors Ω_3 and Ω_5.

The admixture can also be understood from group theoretical considerations using the exciton function in momentum space with Bloch functions $\psi_{n\boldsymbol{k}}$ [cf. Eq. (5.1)]: Only directly at the Γ point or the center of the Brillouin zone the Bloch functions of the valence bands have the symmetry Γ_7^+ and Γ_8^+ and are twofold or fourfold degenerate, respectively. For finite values of $\boldsymbol{k}$ the reduction of these irreducible representations of O_{h} by the group of $\boldsymbol{k}$ has to be considered. If we assume, e.g., the wave vector to be oriented in [100] direction, this group is $C_{4\mathrm{v}}$ and the irreducible representations are reduced to Γ_7 and $\Gamma_6 \oplus \Gamma_7$. The two states of symmetry Γ_7 are mixed by the H_d term. For other directions of $\boldsymbol{k}$ the reduction of the irreducible representations Γ_7^+ and Γ_8^+ is different. Thus, a K-dependent coupling between the bands occurs. The mixing of the bands becomes more strongly for smaller values of Δ, which leads to stronger deviations of the uppermost valence band from a true parabolic behavior. As the radius of the $1S$ exciton is small in position space, it is extended in momentum space, for which reason we expect the coupling between the green and the yellow series to be strong.

The situation in $\mathrm{Cu_2O}$ clearly differs from that of other semiconductors like GaAs [81] where the Γ_8^+ valence band is energetically far above the Γ_7^+ band. In this case a K-dependent splitting will also appear for $\Delta \to \infty$ since the Γ_8^+ band already shows a disparity in the orbital Bloch components, which leads, e.g., to the splitting between light holes and heavy holes for $k \neq 0$. In $\mathrm{Cu_2O}$ only the admixture between yellow and green exciton series can explain the observed K-dependent splitting of the $1S$ exciton.

5.3 Exchange interaction for cuprous oxide

In this section we want to estimate the maximum size of the exchange interaction for the exciton ground state in $\mathrm{Cu_2O}$ following the explanations given in Refs. [83, 162]. Note that it would be necessary to solve the full exciton Hamiltonian (5.27) including all K-dependent terms to determine the true size of the exchange interaction. As has been stated in Sec. 5.2, parity is a good quantum number and the exciton ground state contains mainly S like but also D like envelope functions. Due to the results of Sec. 5.1 the (K-dependent and K-independent) exchange interaction is strongest if the envelope function is purely S like and if $n = 1$ holds. Furthermore, for the exchange interaction only the singlet component of the states is of importance. From Eqs. (5.31) and (5.32) we see that we can set

$$\rho^{(P)}_{vc\nu\boldsymbol{K}}(\boldsymbol{r}) = 0, \tag{5.35a}$$

$$\rho^{(O)}_{vc\nu\boldsymbol{K}}(\boldsymbol{r}) = c_\rho e \sum_{\boldsymbol{\beta}} U_{vc\nu\boldsymbol{K}}(\boldsymbol{\beta}) \phi_{c,\,s}(\boldsymbol{r}-\boldsymbol{\beta}) \phi^*_{v,\,j}(\boldsymbol{r}), \tag{5.35b}$$

with $j = xy,\ yz,\ zx$. The prefactor c_ρ is of the order 1. Even though the exchange energy is not diagonal with respect to ν, we consider only the dominant contribution $E_{\mathrm{exch}}(vc\,1S\,\boldsymbol{K},\ v'c\,1S\,\boldsymbol{K}')$ with $\nu = \nu' = 1S$ or more precisely $\nu = (n, L, M) = (1, 0, 0)$.

5.3.1 Analytic exchange interaction

The K-dependence of the analytic exchange interaction has been neglected in Ref. [162] and will be treated here. We estimate its magnitude to show that the K-dependent splitting of the $1S$ exciton state treated in Refs. [82–84] cannot be explained in terms of the exchange interaction.

In the case of the analytic exchange interaction we consider only the zero and first order terms in the function $m_{vc\nu}(\boldsymbol{K},\, \boldsymbol{G})$ of Eq. (5.21). As can be seen from Eq. (5.16), the analytic exchange energy depends on $m^*_{vc\,\nu}(\boldsymbol{K},\, \boldsymbol{G}) m_{v'c'\,\nu'}(\boldsymbol{K},\, \boldsymbol{G})$. When calculating the exchange energy the second order terms in $m_{v'c'\,\nu'}(\boldsymbol{K},\, \boldsymbol{G})$ have to be multiplied with the zero order term of $m^*_{vc\,\nu}(\boldsymbol{K},\, \boldsymbol{G})$ and vice versa. Since the zero order term is a diagonal 3×3 matrix, the resulting K^2 dependent terms cannot describe a K-dependent splitting of the exciton ground state. Furthermore, we will estimate the size of these terms in the following and show that they are negligibly small. We can write

$$\begin{aligned} m_{vc\nu}(\boldsymbol{K},\,\boldsymbol{G}) \approx \frac{ec_\rho}{\sqrt{N}} \sum_{\boldsymbol{q}} f_{vc\nu}(\boldsymbol{q}) \Bigg[I_{vc}(\boldsymbol{G}) \\ + \frac{\hbar}{m_0} \left\{ \sum_{n\neq v} \frac{(\boldsymbol{q}-\gamma\boldsymbol{K})\cdot\boldsymbol{p}_{vn}}{(E_v-E_n)} I_{nc}(\boldsymbol{G}) + \sum_{n\neq c} \frac{(\boldsymbol{q}+\alpha\boldsymbol{K})\cdot\boldsymbol{p}_{nc}}{(E_c-E_n)} I_{vn}(\boldsymbol{G}) \right\} \Bigg] \\ = ec_\rho F_{vc\nu}(\boldsymbol{0}) I_{vc}(\boldsymbol{G}) \\ + ec_\rho \frac{\hbar}{m_0} \left[(-i\nabla_{\boldsymbol{\beta}}) F_{vc\nu}(\boldsymbol{\beta})\right]_{\boldsymbol{\beta}=\boldsymbol{0}} \cdot \left\{ \sum_{n\neq v} \frac{\boldsymbol{p}_{vn} I_{nc}(\boldsymbol{G})}{(E_v-E_n)} + \sum_{n\neq c} \frac{\boldsymbol{p}_{nc} I_{vn}(\boldsymbol{G})}{(E_c-E_n)} \right\} \\ + ec_\rho \frac{\hbar}{m_0} F_{vc\nu}(\boldsymbol{0}) \left\{ \sum_{n\neq v} \frac{-\gamma\boldsymbol{K}\cdot\boldsymbol{p}_{vn}}{(E_v-E_n)} I_{nc}(\boldsymbol{G}) + \sum_{n\neq c} \frac{\alpha\boldsymbol{K}\cdot\boldsymbol{p}_{nc}}{(E_c-E_n)} I_{vn}(\boldsymbol{G}) \right\}. \end{aligned} \tag{5.36}$$

If we now set $\nu = \nu' = 1S$, the gradient of $F_{vc\,1S}(\boldsymbol{\beta})$ at $\boldsymbol{\beta} = \boldsymbol{0}$ vanishes. Finally, we have

$$\begin{aligned} E_{\mathrm{exch}}^{\mathrm{A}} = 2\delta_{S,0}\delta_{\boldsymbol{K},\boldsymbol{K}'} \frac{e^2 c_\rho^2}{\varepsilon_0\varepsilon_{\mathrm{b}2}\pi a_{\mathrm{exc}}^3} \sum_{\boldsymbol{G}\neq\boldsymbol{0}} \frac{1}{(\boldsymbol{K}+\boldsymbol{G})^2} \\ \times \left[I_{v'c}(\boldsymbol{G}) + \frac{\hbar}{m_0} \left\{ \sum_{n\neq v'} \frac{-\gamma\boldsymbol{K}\cdot\boldsymbol{p}_{v'n}}{(E_{v'}-E_n)} I_{nc}(\boldsymbol{G}) + \sum_{n\neq c} \frac{\alpha\boldsymbol{K}\cdot\boldsymbol{p}_{nc}}{(E_c-E_n)} I_{v'n}(\boldsymbol{G}) \right\} \right] \\ \times \left[I_{vc}(\boldsymbol{G}) + \frac{\hbar}{m_0} \left\{ \sum_{n\neq v} \frac{-\gamma\boldsymbol{K}\cdot\boldsymbol{p}_{vn}}{(E_v-E_n)} I_{nc}(\boldsymbol{G}) + \sum_{n\neq c} \frac{\alpha\boldsymbol{K}\cdot\boldsymbol{p}_{nc}}{(E_c-E_n)} I_{vn}(\boldsymbol{G}) \right\} \right]^* . \end{aligned} \tag{5.37}$$

The component with $\boldsymbol{K} = \boldsymbol{0}$ describes the experimentally observed splitting[1] between ortho- and para-excitons of 12 meV [309, 315, 316]. Therefore, we set

$$12\,\mathrm{meV} = \frac{2e^2 c_\rho^2}{\varepsilon_0\varepsilon_{\mathrm{b}2}\pi a_{\mathrm{exc}}^3} \sum_{\boldsymbol{G}\neq\boldsymbol{0}} \frac{1}{\boldsymbol{G}^2} \left|I_{vc}(\boldsymbol{G})\right|^2 . \tag{5.38}$$

A restriction to the six summands with the smallest value $\boldsymbol{G}_0$ of $\boldsymbol{G}$ as in Ref. [162] is in general not correct. Due to the symmetry of the Bloch functions, other values of $\boldsymbol{G}$ will contribute even more strongly to the sum in Eq. (5.37). Indeed, it is worth mentioning that the symmetry group of the lattice in Cu$_2$O is only isomorphic to the cubic group O_{h} [12]. Since the Cu atoms in Cu$_2$O

---

[1] In the case of Cu$_2$O this splitting is extremely small [17] resulting from the fact that the singlet exciton is only quadrupole allowed (cf. Sec. 2.6 and Chapter 9).

form an fcc sublattice, it can be seen from the unit cell of $\mathrm{Cu_2O}$ that the lattice is not invariant under reflections but under a glide reflection with a translation of $a/2$ (see also supplementary material of Ref. [30]), where a denotes the lattice constant $a = 4.26 \times 10^{-10}\,\mathrm{m}$ of $\mathrm{Cu_2O}$ [171, 172, 273]. The Bloch functions must be invariant under this operation. If we write $u_{n\boldsymbol{K}}(\boldsymbol{r}) = \sum_{\boldsymbol{G}} C_{n\boldsymbol{K}}(\boldsymbol{G}) e^{i\boldsymbol{G}\cdot\boldsymbol{r}}$ [85], we see that the vector components of $\boldsymbol{G}$ can only take whole-number multiples of $4\pi/a$ instead of $2\pi/a$.

The K-dependence of the analytic exchange interaction arises from the $\boldsymbol{K}\cdot\boldsymbol{p}_{mn}$-terms and the factor $1/(\boldsymbol{K}+\boldsymbol{G})^2$ in Eq. (5.37). At first, we will estimate the effect of the $\boldsymbol{K}\cdot\boldsymbol{p}_{mn}$-terms. Due to reasons of symmetry, the terms linear in K must vanish when evaluating the product in Eq. (5.37). The K^2-dependent terms are of the same order of magnitude as the second order terms in the function $m_{vc\nu}(\boldsymbol{K},\boldsymbol{G})$, which we have neglected. We can now use Eq. (5.38) to give an upper limit for their magnitude and to prove that their neglection is justified. Using the values $|\boldsymbol{p}_{nm}|/\hbar \approx 1.3 \times 10^9\,\mathrm{m}^{-1}$ and $(E_m - E_n) \geq \Delta E = 449\,\mathrm{meV}$ given in Ref. [162], we obtain

$$\left(\frac{\hbar}{m_0}\left|\boldsymbol{p}_{nm}\right| K_0 \frac{1}{\Delta E}\right)^2 \times 12\,\mathrm{meV} \approx 0.4\,\mu\mathrm{eV}. \tag{5.39}$$

We see that this part of the analytic exchange interaction is very small.

However, we have shown in Sec. 5.1 that a K-dependent exchange interaction of S excitons is connected to a K-independent analytic exchange interaction of P excitons. Using the result of Eq. (5.39), we can estimate the size of the analytic exchange energy of the $2P$ excitons via Eqs. (5.23) and (5.24). With the exciton Bohr radius $a_{\mathrm{exc}} = 0.53$ nm of the $1S$ exciton, the corresponding value $a_{\mathrm{exc}} = 1.1$ nm for P excitons [162] and $K_0 = 2.62 \times 10^7\,\mathrm{m}^{-1}$ [83], the maximum size of the analytic exchange energy of the $2P$ excitons is

$$\frac{(0.53)^3}{3(1.1)^5(0.0262)^2}\,\frac{2^2-1}{2^5} \times 0.4\ \mu\mathrm{eV} \approx 1.6\ \mu\mathrm{eV}. \tag{5.40}$$

We see that also this energy is negligibly small. Furthermore, the line widths of the P excitons in $\mathrm{Cu_2O}$ are too large to detect a splitting in the order of a few μeV.

Let us now treat the K-dependence arising from the prefactor $1/(\boldsymbol{K}+\boldsymbol{G})^2$. This factor can written as a Fourier series at $\boldsymbol{K} = \boldsymbol{0}$ for $\boldsymbol{K} \ll \boldsymbol{G}$,

$$\frac{1}{(\boldsymbol{K}+\boldsymbol{G})^2} \approx \frac{1}{G^2} - \frac{2}{G^4}\left[\boldsymbol{K}\cdot\boldsymbol{G}\right] + \frac{1}{G^6}\boldsymbol{G}^T\left[-\boldsymbol{1}K^2 + 4\boldsymbol{K}\cdot\boldsymbol{K}^{\mathrm{T}}\right]\boldsymbol{G}. \tag{5.41}$$

Inserting this expression in Eq. (5.37), the term proportional to K vanishes for reasons of symmetry. The magnitude of the K^2-dependent term can be estimated assuming that K is oriented in [100] direction and using the reciprocal lattice vectors with the smallest modulus $4\pi/a$. This gives an upper limit of

$$12\,\mathrm{meV} \times 3K_0^2\left(\frac{a}{4\pi}\right)^2 \approx 28\,\mathrm{neV} \tag{5.42}$$

for the prefactor of those K^2-dependent terms in Eq. (5.37) which originate from the Fourier expansion of $1/(\boldsymbol{K}+\boldsymbol{G})^2$. We see that not only the result of Eq. (5.39) but also the result of Eq. (5.42) is at least one magnitude smaller than the experimentally observed values for the K-dependent splitting of the $1S$ exciton [83]. As the estimated values are upper limits for the prefactors, the actual magnitude of the analytic exchange interaction is generally much smaller.

However, using group theoretical considerations, it is obvious that in both cases the K^2-dependent terms can be written as a sum of the invariant matrices $\boldsymbol{1}K^2$, $(3K_i^2 - K^2)(\hat{\boldsymbol{e}}_i \cdot \hat{\boldsymbol{e}}_i^{\mathrm{T}})$ and $K_iK_j(\hat{\boldsymbol{e}}_i \cdot \hat{\boldsymbol{e}}_j^{\mathrm{T}})$

with $i, j = 1, 2, 3$ and $i \neq j$, since every K-dependent energy as regards states of the symmetry Γ_5^+ must lead to matrices of this form [83, 90]. This can be seen, e.g., from Eq. (5.33), where the dispersion of the exciton is described by the same matrices. Hence, the K-dependent splitting of the $1S$ exciton states must in any case be described by matrices of this form [83]. However, from the experimental point of view the physical origin of these matrices is *a priori* unknown. In Refs. [82–84] it has been assumed that the exchange interaction is responsible for the K-dependent splitting.

We have now shown that the K-dependent analytic exchange interaction is negligibly small in Cu_2O and that it cannot explain the K-dependent splitting of the $1S$ exciton. Furthermore, due to the specific form of the exchange interaction, it would not be experimentally distinguishable from the dispersion of the exciton described by Eq. (5.33).

Only the K-dependent nonanalytic exchange interaction may contribute to the splitting of the $1S$ ortho-exciton. This will be investigated in the following section 5.3.2.

5.3.2 Nonanalytic exchange interaction

We will now treat the nonanalytic exchange interaction for Cu_2O. As the conduction band and the valence band in Cu_2O have the same (positive) parity and the momentum operator $\boldsymbol{p}$ has negative parity, the matrix element $\boldsymbol{p}_{vc} = \langle u_{v\boldsymbol{0}} \left| \boldsymbol{p} \right| u_{c\boldsymbol{0}} \rangle$ vanishes. Therefore, the main contribution to the nonanalytic exchange interaction comes from the term in square brackets in Eq. (5.25).

We can see again the close connection between the nonanalytic exchange interaction and the oscillator strength: Inserting the $q\,K$ dependent terms of Eq. (5.25) into Eq. (5.16), one obtains the K-independent nonanalytic exchange energy of P excitons. Since these excitons are dipole-allowed, their oscillator strength is also K-independent. The exchange energy exactly equals the LT-splitting when treating P exciton-polaritons. The K^2-dependent terms of Eq. (5.25) will lead to a K^2-dependent exchange energy for the S excitons. These excitons are quadrupole allowed and their oscillator strength is also K^2-dependent. For reasons of symmetry, the energy difference between longitudinal and transverse S excitons at $K = 0$ is exactly zero, as well.

In the following, we will concentrate on the K^2-dependent exchange energy of the $1S$ excitons to estimate its magnitude and investigate its angle dependency. Due to the close connection between exchange energy and oscillator strength, we expect the ratio of the K^2-dependent exchange energy of S excitons and the K-independent exchange energy of P excitons to be of the same size as the ratio of the corresponding oscillator strengths.

We can write

$$m_{vc\,1S}(\boldsymbol{K}, \boldsymbol{0}) \approx \frac{ec_{\rho}\hbar^2}{m_0^2} F_{vc\,1S}(\boldsymbol{0}) \left(\langle u_{v\boldsymbol{0}} | \left(\boldsymbol{K} \cdot \boldsymbol{p} \right) \left[\sum_{n \neq v,c} g_{vc}(E_n) \left| u_{n\boldsymbol{0}} \right\rangle \left\langle u_{n\boldsymbol{0}} \right| \right] \left(\boldsymbol{K} \cdot \boldsymbol{p} \right) | u_{c\boldsymbol{0}} \rangle \right) \tag{5.43}$$

with

$$g_{vc}(E_n) = \frac{\gamma\alpha(E_v - E_c) - \alpha^2(E_v - E_n) + \gamma^2(E_c - E_n)}{(E_v - E_n)(E_c - E_n)(E_v - E_c)}. \tag{5.44}$$

Using group theory, we can determine the non-vanishing terms of the exchange energy. The operator in square brackets in Eq. (5.43) is a projection operator. For reasons of symmetry this operator has to transform according to the irreducible representation Γ_1^+. On the other hand, the operator $\boldsymbol{p}$ transforms according to Γ_4^-. The symmetry of the operator between the Bloch functions is therefore

$$\Gamma_4^- \otimes \Gamma_1^+ \otimes \Gamma_4^- = \Gamma_1^+ \oplus \Gamma_3^+ \oplus \Gamma_4^+ \oplus \Gamma_5^+. \tag{5.45}$$

The symmetry of the Bloch functions is

$$\Gamma_5^+ \otimes \Gamma_1^+ = \Gamma_5^+. \tag{5.46}$$

Consequently, the expression (5.43) does not vanish only if the operator has the symmetry Γ_5^+ [169]. As in Sec. 4.4 and especially Eq. (4.49), we can then consider the coupling coefficients for the case $\Gamma_4^- \otimes \Gamma_4^- \rightarrow \Gamma_5^+$. Writing the exchange energy as a 3×3 matrix with the valence band functions given in the order $\phi_{v,\,yz}$, $\phi_{v,\,zx}$, $\phi_{v,\,xy}$, we finally obtain the expression

$$E_{\mathrm{exch}}^{\mathrm{NA}} = \Delta_Q \frac{K^2}{K_0^2} \begin{pmatrix} \hat{K}_y^2 \hat{K}_z^2 & \hat{K}_z^2 \hat{K}_y \hat{K}_x & \hat{K}_y^2 \hat{K}_x \hat{K}_z \\ \hat{K}_z^2 \hat{K}_y \hat{K}_x & \hat{K}_z^2 \hat{K}_x^2 & \hat{K}_x^2 \hat{K}_y \hat{K}_z \\ \hat{K}_y^2 \hat{K}_x \hat{K}_z & \hat{K}_x^2 \hat{K}_y \hat{K}_z & \hat{K}_x^2 \hat{K}_y^2 \end{pmatrix} \tag{5.47}$$

for the nonanalytic exchange energy with $\hat{\boldsymbol{K}} = \boldsymbol{K}/K$. Contrary to dipole allowed excitons, the nonanalytic exchange energy depends on the fourth power of the angular coordinates of $\boldsymbol{K}$.

We can now explicitly give the coefficient Δ_Q of Refs. [82–84] from microscopic calculations and estimate its size using Eq. (5.23) and the values $|\boldsymbol{p}_{nm}|/\hbar \approx 1.3 \times 10^9\,\mathrm{m}^{-1}$ and $(E_m - E_n) \geq \Delta E = 449\,\mathrm{meV}$ given in Ref. [162]:

$$\Delta_Q = \frac{6 c_\rho^2 e^2 K_0^2}{\varepsilon_0 \varepsilon_{\mathrm{b}2} V_{\mathrm{uc}}} \frac{\hbar^4}{m_0^4} |F_{vc\,1S}(\boldsymbol{0}) \sum_{n \neq v,c} g_{vc}(E_n) p_{nc} p_{vn}|^2 \approx 9\,\mathrm{neV}. \tag{5.48}$$

This value is significantly smaller than the result $\Delta_Q = 5\,\mu\mathrm{eV}$ from Ref. [82]. We see that also the K-dependent nonanalytic exchange interaction is negligibly small in $\mathrm{Cu_2O}$.

As has been stated in Sec. 5.1, it is nevertheless interesting to investigate the possible coupling between longitudinal and transverse exciton states. In general, these states are not uncoupled. However, in the case of the ortho-exciton this restriction holds only if the K vector is parallel to one of the main symmetry axes of the crystal. We will show that a general direction of the K vector an LT coupling appears, for which reason all three exciton states couple to light with a polarization not being orthogonal to the wave vector involved. From the experimental point of view it is obvious that longitudinal and transverse exciton states are not eigenstates of the complete K-dependent Hamiltonian of excitons if K is oriented in an arbitrary direction since there are three observable states and not only two or one [82–84].

We start with $\boldsymbol{K}$ being oriented in [100] direction. In this case the cubic symmetry is reduced to the group $C_{4\mathrm{v}}$, which leaves $\boldsymbol{K}$ invariant. Since $K_y = K_z = 0$ holds, the nonanalytic exchange interaction (5.47) is zero. Therefore, we are allowed to choose appropriate linear combinations of the states $\phi_{v,\,yz}$, $\phi_{v,\,zx}$, $\phi_{v,\,xy}$ such that $\boldsymbol{\mu}_{vc\nu\boldsymbol{K}} \parallel \boldsymbol{K}$ and $\boldsymbol{\mu}_{vc\nu\boldsymbol{K}} \perp \boldsymbol{K}$ holds. To this aim, we insert the charge density

$$\rho_{vc,\,\nu\boldsymbol{K}}(\boldsymbol{r}) = c_\rho e \sum_{\boldsymbol{\beta}} U_{vc\nu\boldsymbol{K}}(\boldsymbol{\beta}) \phi_{c,\,s}(\boldsymbol{r} - \boldsymbol{\beta}) \left[c_{yz} \phi_{v,\,yz}^*(\boldsymbol{r}) + c_{zx} \phi_{v,\,zx}^*(\boldsymbol{r}) + c_{xy} \phi_{v,\,xy}^*(\boldsymbol{r}) \right] \tag{5.49}$$

into

$$\boldsymbol{\mu}_{vc\nu\boldsymbol{K}} = \int \mathrm{d}\boldsymbol{r}\; \boldsymbol{r} \rho_{vc\nu\boldsymbol{K}}(\boldsymbol{r}). \tag{5.50}$$

Using Eq. (5.3) and considering again the coupling coefficients for the case $\Gamma_4^- \otimes \Gamma_4^- \rightarrow \Gamma_5^+$ [cf. Eq. (4.49)], we obtain

$$\boldsymbol{\mu}_{vc\nu\boldsymbol{K}} \sim \begin{pmatrix} K_y c_{xy} + K_z c_{zx} \\ K_z c_{yz} + K_x c_{xy} \\ K_x c_{zx} + K_y c_{yz} \end{pmatrix}. \tag{5.51}$$

Hence, the two transverse states for $\boldsymbol{K} \parallel [100]$ are given by $c_{xy} = 1$, $c_{yz} = c_{zx} = 0$ and $c_{zx} = 1$, $c_{yz} = c_{xy} = 0$. This is not unexpected since the K vector causes a symmetry breaking in x direction, which affects the functions $\phi_{v,\,xy}$ and $\phi_{v,\,zx}$ in a different way than $\phi_{v,\,yz}$.

The fact that longitudinal and transverse exciton states are decoupled for $\boldsymbol{K} \parallel [100]$ can also be understood from group theoretical considerations: The exciton states transform according to Γ_5^+ in O_h while the dipole operator transforms according to the irreducible representation D^1 of the full rotation group or according to Γ_4^- in O_h. As the cubic symmetry reduces to $C_{4\mathrm{v}}$, we have to consider the reduction of the irreducible representations of the cubic group O_h by the group $C_{4\mathrm{v}}$:

$$\Gamma_5^+ \rightarrow \Gamma_4 \oplus \Gamma_5, \tag{5.52a}$$

$$\Gamma_4^- \rightarrow \Gamma_1 \oplus \Gamma_5. \tag{5.52b}$$

Comparing both equations, we immediately see that the two Γ_5 states are transverse states and that the Γ_4 state is a longitudinal state. Since there are now exciton states transforming according to Γ_5 and a dipole operator which transforms according to Γ_5, these exciton states can be excited by light. This describes the fact that the $1S$ exciton becomes quadrupole On the other hand, as the transverse states and the longitudinal state transform according to different irreducible representations, no coupling between these states occurs.

Let us now consider the exchange interaction (5.47) for an arbitrary $\boldsymbol{K}$ with all vector components $K_i \neq 0$. The eigenvalues λ_i and eigenvectors v_i of the 3×3 matrix in Eq. (5.47) read

$$\lambda_1 = 0, \quad v_1 = \frac{1}{\sqrt{a^2 + b^2}} \left(-b,\, a,\, 0\right)^\mathrm{T}, \tag{5.53a}$$

$$\lambda_2 = 0, \quad v_2 = \frac{1}{\sqrt{a^2 + c^2}} \left(-c,\, 0,\, a\right)^\mathrm{T}, \tag{5.53b}$$

$$\lambda_3 = a^2 + b^2 + c^2, \quad v_3 = \frac{1}{\sqrt{a^2 + b^2 + c^2}} \left(a,\, b,\, c\right)^\mathrm{T}, \tag{5.53c}$$

with the abbreviations $a = \hat{K}_y \hat{K}_z$, $b = \hat{K}_z \hat{K}_x$ and $c = \hat{K}_x \hat{K}_y$. Even though there is only one state with an eigenvalue $\lambda \neq 0$, we have to prove that this state is connected with a longitudinal polarization. Inserting v_3 into Eq. (5.51) yields

$$\boldsymbol{\mu}_{vc\,\nu\boldsymbol{K}} \sim \boldsymbol{K} - K \left(\hat{K}_x^3,\, \hat{K}_x^3,\, \hat{K}_x^3\right)^\mathrm{T}. \tag{5.54}$$

Due to the second term, the dipole moment is not parallel to $\boldsymbol{K}$. Therefore, we have shown that longitudinal and transverse exciton states are coupled by the nonanalytic exchange interaction (5.47) if $\boldsymbol{K}$ is not oriented in a direction of high symmetry. Furthermore, we see that two eigenstates of the matrix in Eq. (5.47) are degenerate. If the nonanalytic exchange interaction were the only reason for the K-dependent splitting of the $1S$ exciton, only two states would be observable in experiments for any direction of $\boldsymbol{K}$.

6

Even exciton series in Cu_2O

The investigations of excitonic absorption spectra in cuprous oxide in Chapter 4 have shown that it is indispensable to account for the complex valence band structure in the theory of excitons. In Cu_2O parity is a good quantum number and thus the exciton spectrum falls into two parts: The dipole-active exciton states of negative parity and odd angular momentum, which can be observed in one-photon absorption (Γ_4^- symmetry) and the exciton states of positive parity and even angular momentum, which can be observed in two-photon absorption (Γ_5^+ symmetry). The unexpected observation of D excitons in two-photon absorption has given first evidence that the dispersion properties of the Γ_5^+ orbital valence band is giving rise to a coupling of the yellow and green exciton series [72].

The yellow and green exciton series share the same threefold degenerate Γ_5^+ orbital valence band state. This state splits due to spin-orbit interaction into an upper twofold degenerate Γ_7^+ valence band (yellow series) and a lower fourfold degenerate Γ_8^+ valence band (green series). The band structure of both bands is essentially determined by the anisotropic dispersion properties of the orbital state. The threefold degeneracy of the orbital state is lifted as soon as a non-zero $\boldsymbol{k}$ vector gets involved, with new eigenvectors depending on the orientation of $\boldsymbol{k}$. A consequence of the splitting of the orbital state is a partial quenching of the spin-orbit interaction. This $\boldsymbol{k}$ dependent quenching is not only responsible for a remarkable non-parabolicity of the two top valence bands but leads likewise to a $\boldsymbol{k}$ dependent mixing of the Γ_7^+ and Γ_8^+ Bloch states and can thus cause a mixing of the yellow and green exciton series. A mixing of both series is favored by the large Rydberg energy of approximately 100 meV, a corresponding large exciton extension in k space and the small spin-orbit splitting of only 130 meV.

A Hamiltonian that is able to cope with a coupled system of yellow and green excitons must take explicit care of the dispersion properties of the orbital valence band state and has to include the spin-orbit interaction. Such a kind of Hamiltonian was first introduced by Uihlein *et al.* [72] for explaining the unexpected fine structure splitting observed in the two-photon absorption spectrum of Cu_2O. They used a simplified spherical dispersion model for the Γ_5^+ orbital valence band with an identical splitting into longitudinal and transverse states independent of the orientation of $\boldsymbol{k}$. This simplification had the appealing advantage that the total angular momentum remains a good quantum number so that the exciton problem could be reduced to calculate the eigenvalues of a system of coupled radial wave functions. A problem in their paper is the incorrect notation of the $1S$ green and $2S$ yellow excitons states. Both notations need to be exchanged to be consistent with their calculations. Although the spherical model can explain many details of the experimental findings, one has to be aware of its limitations. A more realistic Hamiltonian being compliant with the real band structure by including terms of cubic symmetry has already proved its validity by explaining the puzzling fine structure of the odd parity states in Cu_2O (see Chapter 4 and Ref. [38]). The intention of this Chapter is to show that the same kind of Hamiltonian can likewise describe the fine structure splitting of the even parity excitons.

However, when comparing the even parity and odd parity exciton systems, it is obvious that the even exciton system is a much more challenging problem. One reason for this is the close resonance of the green $1S$ exciton with the even parity states of the yellow series with principal quantum number $n \geq 2$. This requires a very careful calculation of the binding energy of the green $1S$ exciton. Furthermore, the binding energy of the yellow $1S$ exciton is much larger than expected from a simple hydrogen like series, inter alia, due to a less effective screening of the Coulomb potential at distances comparable to the polaron radius. Moreover, a breakdown of the electronic screening is expected at even much shorter distances, but a proper treatment is exceeding the limits of the continuum approximation. Hence, we introduce a δ-function like central cell correction term that should account for all kinds of short range perturbations affecting the immediate neighborhood of the central cell. The magnitude of this term is treated as a free parameter that can be adjusted to the experimental findings. It is important to note that a change of this parameter leads to a significant shift of the green $1S$ exciton with respect to the higher order states of the yellow series and has therefore a high impact on the energies and the compositions of the resulting coupled exciton states. Taking this in mind it is fundamental that one can likewise achieve a match to the relative oscillator strengths of the involved states.

Dealing with the even parity system of Cu_2O is also confronting us with the problem of a proper treatment of the $1S$ exciton with respect to its very small radius since a small exciton radius means a large extension of the exciton in k space. The challenge is therefore to meet the band structure of the valence band in a much larger vicinity of the Γ point. For coping with this situation, we include in the kinetic energy of the hole all terms in the fourth power of p being compliant with the octahedral symmetry of Cu_2O. The parameters of these terms are carefully adjusted to get a best fit to the band structure in the part of the k space being relevant for the $1S$ exciton. All these modifications are discussed in Sec. 6.1 on the central-cell corrections.

Despite of these corrections, it is important to note that the Hamiltonian is essentially the same as the one being applied to the odd exciton system in Chapter 4. The fundamental modifications presented here are irrelevant for the odd parity system because of their δ function like nature or their specific form affecting only exciton states with a small radius. Hence, we present a consistent theoretical model for the complete exciton spectrum of Cu_2O.

Comparing our results to experimental data in Sec. 6.2, we can prove very good agreement as regards not only the energies but also the oscillator strengths since our method of solving the Schrödinger equation allows us also to calculate relative oscillator strengths for one-photon and two-photon absorption. This agreement between theory and experiment is important not only for the investigation of exciton spectra in electric or combined electric and magnetic fields. A correct theoretical description of excitons is indispensable if Rydberg excitons will be used in the future in quantum information technology or used to attain a deeper understanding of quasi-particle interactions in semiconductors [30, 45]. Furthermore, this agreement is a prerequisite for a future search for exceptional points in the exciton spectrum [35]. Essential parts of this Chapter have been published in Ref. [46].

6.1 Central-cell corrections

Due to its small radius, the $1S$ exciton in Cu_2O is an exciton intermediate between a Frenkel and a Wannier exciton [7]. Hence, appropriate corrections are needed to describe this exciton state correctly. The corrections, which allow for the best possible description of the exciton problem within the continuum approximation of the solid, are called central-cell corrections and have first been treated by Uihlein *et al.* [72, 317] and Kavoulakis *et al.* [162] for Cu_2O. While Uihlein *et al.* [72] accounted for these corrections only in a simplified way by using a semi-empirical contact potential $V = -V_0\delta(\boldsymbol{r})$, the treatment of Kavoulakis *et al.* [162] did non account for the band structure and the effect of the central-cell corrections was discussed only on the $1S$ state and only using perturbation theory. By considering the complete valence band structure of Cu_2O in combination with a non-perturbative treatment of the central-cell corrections, we present a more accurate treatment of the whole yellow (and green) exciton series in Cu_2O. Corrections beyond the frame of the continuum approximation will not be treated here. However, these corrections may describe remaining small deviations between experimental and theoretical results.

The central-cell corrections as discussed in Ref. [162] comprise three effects, which are (i) the appearance of terms of higher-order in the momentum $\boldsymbol{p}$ in the kinetic energies of electron and hole, (ii) the momentum- and frequency-dependence of the dielectric function ε, and (iii) the appearance of an exchange interaction, which depends on the momentum of the center of mass. These effects will be discussed in the following.

6.1.1 Band structure of Cu_2O

Since the radius of the yellow $1S$ exciton is small, the extension of its wave function in momentum space is accordingly large. Hence, we have to consider terms of the fourth power of $\boldsymbol{p}$ in the kinetic energy of the electron and the hole. The inclusion of p^4 terms in Eqs. (4.6) and (4.8) leads to an extended and modified Hamiltonian in the sense of Altarelli, Baldereschi and Lipari [77–81] or Suzuki and Hensel [318].

The extended Hamiltonian must be compatible with the symmetry O_h of the crystal and transform according to the irreducible representation Γ_1^+. All the terms of the fourth power of $\boldsymbol{p}$ span a fifteen-dimensional space with the basis functions p_i^4, $p_i^3 p_j$, $p_i^2 p_j^2$, $p_i p_j p_k^2$, with $i, j, k \in \{1, 2, 3\}$ and $i \neq j \neq k \neq i$. Including the quasi-spin I and using group theory, one can find six linear combinations of p^4 terms, which transform according to Γ_1^+ [90] (see Appendix C.2). Using the results of Appendix C.2, we can write the kinetic energy of the electron and the hole as

$$H_\mathrm{e}(\boldsymbol{p}_\mathrm{e}) = \frac{1}{2\hbar^2 m_\mathrm{e}} \left\{ (\hbar^2 + \lambda_1 a^2 \boldsymbol{p}_\mathrm{e}^2)\boldsymbol{p}_\mathrm{e}^2 + \lambda_2 a^2 \left[p_\mathrm{e1}^2 p_\mathrm{e2}^2 + \mathrm{c.p.} \right] \right\} \tag{6.1}$$

and

$$\begin{aligned} H_\mathrm{h}(\boldsymbol{p}_\mathrm{h}) = \; & H_\mathrm{so} + \frac{1}{2\hbar^4 m_0} \Big\{ (\gamma_1 + 4\gamma_2)\hbar^2(\hbar^2 + \xi_1 a^2 \boldsymbol{p}_\mathrm{h}^2)\boldsymbol{p}_\mathrm{h}^2 + \xi_2 a^2 \hbar^2 \left[p_\mathrm{h1}^2 p_\mathrm{h2}^2 + \mathrm{c.p.} \right] \\ & - 6\gamma_2(\hbar^2 + \xi_3 a^2 \boldsymbol{p}_\mathrm{h}^2) \left[p_\mathrm{h1}^2 \boldsymbol{I}_1^2 + \mathrm{c.p.} \right] - 12\gamma_3(\hbar^2 + \xi_4 a^2 \boldsymbol{p}_\mathrm{h}^2) \left[p_\mathrm{h1} p_\mathrm{h2} \{\boldsymbol{I}_1, \boldsymbol{I}_2\} + \mathrm{c.p.} \right] \\ & + 2(\eta_1 + 2\eta_2)\hbar^2 \left[\boldsymbol{p}_\mathrm{h}^2 \, \boldsymbol{I} \cdot \boldsymbol{S}_\mathrm{h} \right] - 12\eta_2 \hbar^2 \left[p_\mathrm{h1}^2 \boldsymbol{I}_1 \boldsymbol{S}_\mathrm{h1} + \mathrm{c.p.} \right] \end{aligned}$$

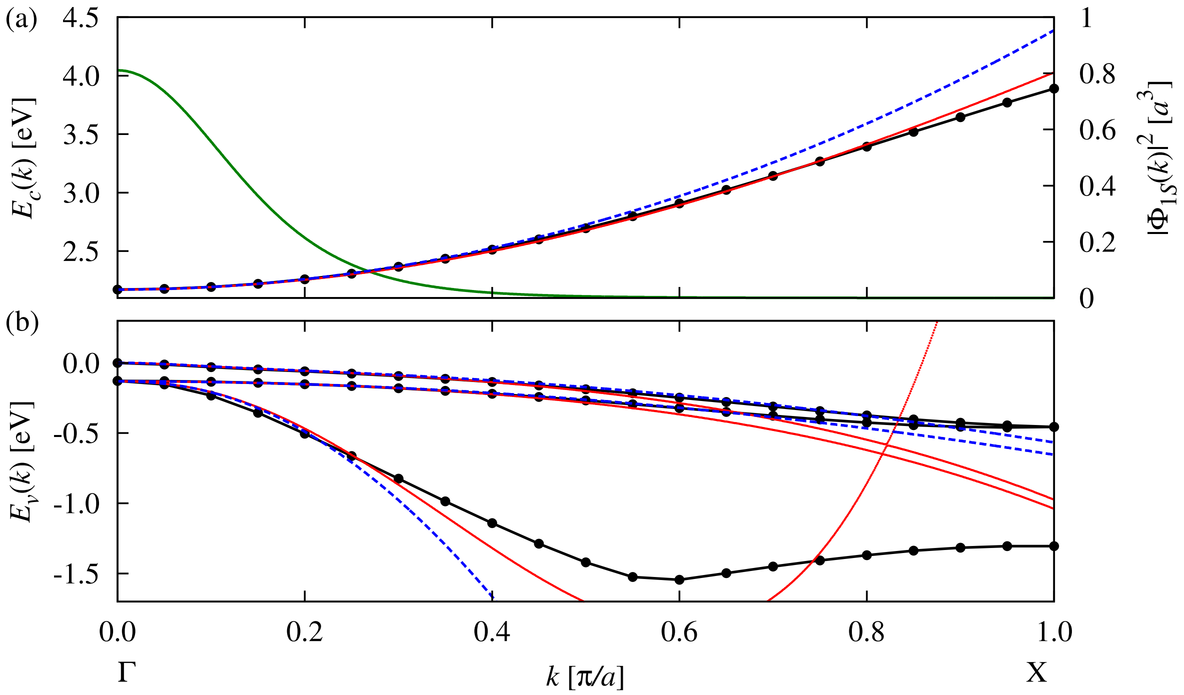

Figure 6.1.: Fits to the band structure obtained via spin density functional theory calculations [279] (black linespoints) for (a) conduction band and (b) valence bands of Cu$_2$O for the [100] direction using the expressions (6.1) and (6.2) (red lines). The green solid line shows the function $|\Phi_{1S}(\boldsymbol{k})|^2$ for $a_{\mathrm{exc}}^{(1S)} = a$ in units of a^3. One can see that the differences between the fit using quartic terms and the fit of Ref. [37] (blue dashed lines) neglecting these terms are small in the range of extension of $|\Phi_{1S}(\boldsymbol{k})|^2$. Note that $|\Phi_{1S}(\boldsymbol{k})|^2$ is not shown in the lower panel for reasons of clarity.

$$- 12\eta_3\hbar^2 \left[p_{\mathrm{h}1}p_{\mathrm{h}2}(\boldsymbol{I}_1\boldsymbol{S}_{\mathrm{h}2} + \boldsymbol{I}_2\boldsymbol{S}_{\mathrm{h}1}) + \mathrm{c.p.}\right] - 6\xi_5 a^2 \left[(p_{\mathrm{h}1}^4 + 6p_{\mathrm{h}2}^2p_{\mathrm{h}3}^2)\boldsymbol{I}_1^2 + \mathrm{c.p.}\right]$$

$$- 12\xi_6 a^2 \left[(p_{\mathrm{h}1}^2 + p_{\mathrm{h}2}^2 - 6p_{\mathrm{h}3}^2)p_{\mathrm{h}1}p_{\mathrm{h}2}\left\{\boldsymbol{I}_1,\, \boldsymbol{I}_2\right\} + \mathrm{c.p.}\right]\Big\} \tag{6.2}$$

with the lattice constant a and the unknown parameters λ_i and ξ_i. Note that the values of parameters η_i are smaller than the Luttinger parameters γ_i (see Table 2.2). Hence, we expect the terms of the form $p^4 I S_{\mathrm{h}}$ to be negligibly small.

After replacing $H_{\mathrm{e}}(\boldsymbol{p}_{\mathrm{e}}) \to H_{\mathrm{e}}(\hbar\boldsymbol{k})$ and $H_{\mathrm{h}}(\boldsymbol{p}_{\mathrm{h}}) \to -H_{\mathrm{h}}(\hbar\boldsymbol{k})$, we can determine the eigenvalues of these Hamiltonians and fit them as in Ref. [37] for $|\boldsymbol{k}| < \pi/a$ to the band structure of Cu$_2$O obtained via spin density functional theory calculations [279].

To obtain a reliable result, we perform a least-squares fit with a weighting function. Even though the exciton ground state will show deviations from a pure hydrogen-like $1S$ state, we expect that the radial probability density can be described qualitatively by that function. Hence, we use the modulus squared of the Fourier transform $\Phi_{1S}(\boldsymbol{k}) = \mathcal{F}(\Psi_{1S})(\boldsymbol{k})$ of the hydrogen-like function

$$\Psi_{1S}(\boldsymbol{r}) = \left[e^{-r/a_{\mathrm{exc}}^{(1S)}}\right] / \left[\pi\left(a_{\mathrm{exc}}^{(1S)}\right)^3\right]^{1/2} \tag{6.3}$$

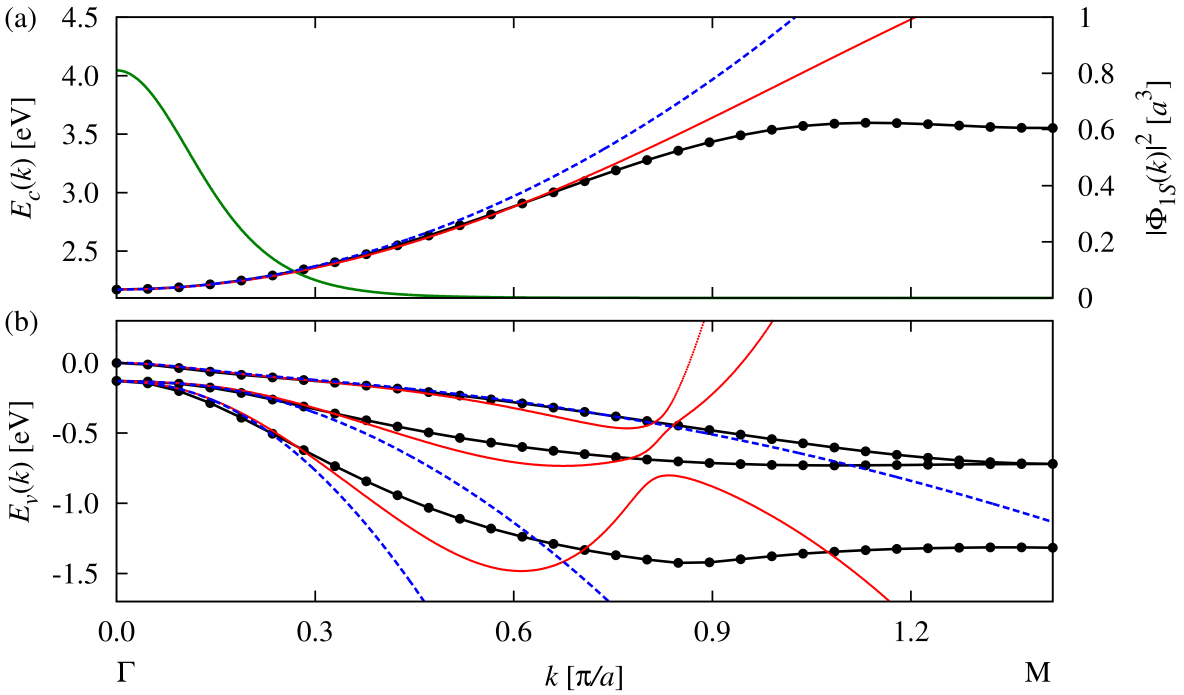

Figure 6.2.: Same as Fig. 6.1 for the [110] direction.

as the weighting function for the fit. It reads [227]

$$|\Phi_{1S}(\boldsymbol{k})|^2 \quad \sim \quad \left| \frac{1}{\sqrt{(2\pi)^3}} \int \mathrm{d}\boldsymbol{r}\ \Psi_{1S}(\boldsymbol{r}) e^{-i\boldsymbol{k}\boldsymbol{r}} \right|^2 = \left[2a_{\mathrm{exc}}^{(1S)}\right]^3 / \left[\sqrt{\pi} + \sqrt{\pi} k^2 \left(a_{\mathrm{exc}}^{(1S)}\right)^2\right]^4 \tag{6.4}$$

with the radius $a_{\mathrm{exc}}^{(1S)}$ of the $1S$ exciton state. Although we do not *a priori* know the true value of $a_{\mathrm{exc}}^{(1S)}$, the experimental value of the binding energy of the $1S$ state [7, 72] as well as the calculations of Ref. [162] indicate that it is on the order of one or two times the lattice constant $a = 0.427\,\mathrm{nm}$ [171, 172, 273]. For the fit to the band structure we assume a small value of $a_{\mathrm{exc}}^{(1S)} = a$ as a lower limit in the sense of a safe estimate since then the extension of the exciton wave function in Fourier space is larger. In doing so, we will now show that even if the radius of the $1S$ exciton were smaller or equal to the lattice constant a, there would not be contributions of the p^4 terms of the band structure.

The results of the fit are depicted as red solid lines in Figs. 6.1, 6.2, and 6.3. For a comparison, we also show the fit neglecting the quartic terms in the momenta (blue dashed lines) [37]. The values of the fit parameters are

$$\begin{aligned} \lambda_1 &= -\,1.109 \times 10^{-2}, & \lambda_2 &= -\,2.052 \times 10^{-2}, \\ \xi_1 &= -\,1.389 \times 10^{-1}, & \xi_4 &= -\,1.518 \times 10^{-1}, \\ \xi_2 &= 2.353 \times 10^{-3}, & \xi_5 &= 9.692 \times 10^{-4}, \\ \xi_3 &= -\,1.523 \times 10^{-1}, & \xi_6 &= -\,8.385 \times 10^{-4}. \end{aligned} \tag{6.5}$$

As can be seen, e.g., from Fig. 6.2, the fit including the quartic terms is only slightly better than the fit with the quadratic terms for small k. A clear difference between the fits can be seen only for

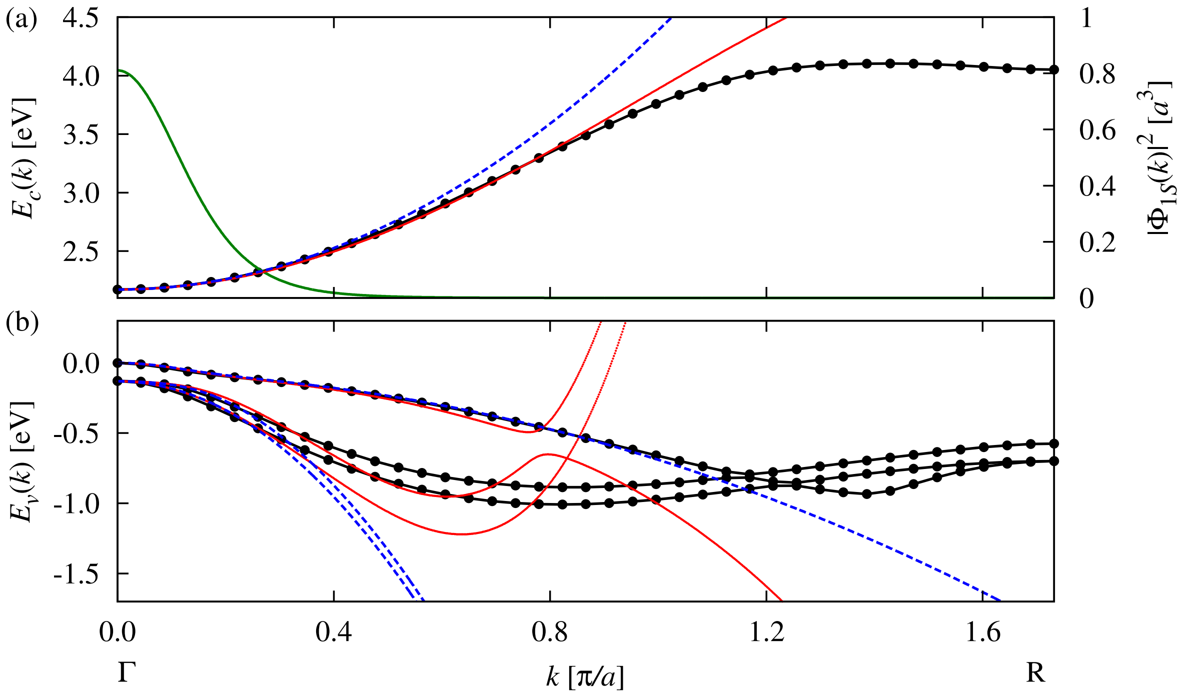

Figure 6.3.: Same as Fig. 6.1 for the [111] direction.

large values of k as regards the valence bands: Since some of the pre-factors of the quartic terms are positive, the energy of the valence bands in the fitted model increases for larger values of k.

Considering the minor differences between the fits for small k and the small extension of the $1S$ exciton function in k space even for $a_{\mathrm{exc}}^{(1S)} = a$ (see, e.g., Fig. 6.1), the quartic terms will hardly affect this exciton state and can be neglected. These arguments still hold if, e.g., $a_{\mathrm{exc}}^{(1S)} = 0.2a$ is assumed.

In the work of Ref. [162] the introduction of p^4 terms seemed necessary to explain the experimentally observed large mass of the $1S$ exciton. However, the experimental observations are already well described by quadratic terms in p when considering the complete valence band structure (cf. Chapter 4). As we already stated in Sec. 5.2, a simple restriction to the Γ_7^+ band neglecting the Γ_8^+ band and considering the nonparabolicity of the Γ_7^+ band via p^4 terms as has been done in Ref. [162] does not treat the problem correctly.

6.1.2 Dielectric constant

In the case of the $1S$ exciton in Cu_2O the relative motion of the electron and the hole is sufficiently fast that phonons cannot follow it and corrections on the dielectric constant need to be considered.

In general, the electron and the hole are coupled to longitudinal optical phonons via the Fröhlich interaction [74, 242] and to longitudinal acoustic phonons via the deformation potential coupling [74, 221] (cf. Sec. 3.1.1). While in the case of optical phonons the ions of the solid are displaced in antiphase and thus create a dipole moment in the unit cell of a polar crystal, the ions are displaced in phase in the case of acoustic phonons and no dipole moment is created. Hence, one expects that the interaction between electron or hole and optical phonons is much larger than the interaction with acoustic phonons in polar crystals[1] [12, 322].

If the frequency of the relative motion of electron and hole is high enough so that the ions of the solid cannot follow it, the Coulomb interaction between electron and hole is screened by the high-frequency or background dielectric constant ε_{b} [7, 97]. This dielectric constant describes the electronic polarization, which can follow the motion of electron and hole very quickly [10].

For lower frequencies of the relative motion the contribution of the phonons to the screening becomes important and the dielectric function ε becomes frequency dependent. In many semiconductors the frequency of the relative motion in exciton states with a principal quantum number of $n \geq 2$ is so small that the low-frequency or static dielectric constant ε_{s} can be used [12], which involves the electronic polarization *and* the displacement of the ions [10]. Note that we use the notation ε_{b}, ε_{s} instead of ε_∞, ε_0 to avoid the risk of confusion with the electric permittivity ε_0 [10, 12].

The transition from $-e^2/4\pi\varepsilon_0\varepsilon_{\mathrm{s}}r$ to $-e^2/4\pi\varepsilon_0\varepsilon_{\mathrm{b}}r$, which takes place when the frequency of the electron or the hole is of the same size as the frequency of the phonon [10], had been investigated in detail by Haken in Refs. [10, 322–326]. He considered at first the interaction between the electron or the hole and the phonons and then constructed the exciton from the resulting particles with polarisation clouds, i.e., the polarons. The change of the Coulomb interaction between both particles was then explained in terms of an exchange of phonons, i.e., of virtual quanta of the polarization field [10].

The final result for the interaction in the transition region between $-e^2/4\pi\varepsilon\varepsilon_{\mathrm{s}}r$ and $-e^2/4\pi\varepsilon\varepsilon_{\mathrm{b}}r$ was the so-called Haken potential [7, 12, 227, 324–326]

$$V(r) \quad = \quad -\frac{e^2}{4\pi\varepsilon_0 r}\left[\frac{1}{\varepsilon_{\mathrm{s}}}+\frac{1}{2\varepsilon^*}\left(e^{-r/\rho_{\mathrm{h}}}+e^{-r/\rho_{\mathrm{e}}}\right)\right]. \tag{6.6}$$

Here ρ_{e} and ρ_{h} denote the polaron radii

$$\rho_{\mathrm{e/h}}=\sqrt{\frac{\hbar}{2m^*_{\mathrm{e/h}}\omega_{\mathrm{LO}}}} \tag{6.7}$$

with the frequency ω_{LO} of the optical phonon and ε^* being given by

$$\frac{1}{\varepsilon^*}=\frac{1}{\varepsilon_{\mathrm{b}}}-\frac{1}{\varepsilon_{\mathrm{s}}}. \tag{6.8}$$

Note that in the result of Haken [322, 327] the polaron masses m_i^* instead of the bare electron and hole masses have to be used in the polaron radii and the kinetic energies (cf. Sec. 3.41). Furthermore, the lattice relaxation due to the interaction of excitons and phonons decreases the band gap energy for electrons and holes. However, since the value of E_{g} for $\mathrm{Cu_2O}$ has been determined in Ref. [30] from the experimental exciton spectrum, the polaron effect is already accounted for in the band gap energy [12].

Note that the above results were derived in the simple band model and by assuming only one optical phonon branch contributing to the Fröhlich interaction. To the best of our knowledge there is no model accounting for more than one optical phonon branch [10, 162, 327], which complicates the correct treatment of $\mathrm{Cu_2O}$, where two LO phonons contribute to the Fröhlich interaction. Even though there are theories for polarons in the degenerate band case [217, 304, 328], we will use only

---

[1] At this point we also want to note the existence of exciton-phonon boundstates [319–321], new quasi-particles, which describe the coupling of different electron-phonon states, if the LO-phonon energy and the excitonic binding energy are of comparable size.

the leading, spherically symmetric terms, in which only the isotropic effective mass of the hole or only the Luttinger parameter γ_1 enters. Of course, there are further terms of cubic symmetry, which also depend on the other Luttinger parameters. However, since already γ_1 is at least by a factor of 2 larger than the other Luttinger parameters, we expect the further terms in the Haken potentials to be smaller than the leading term used here. Since the effect of the Haken potential on the exciton spectrum is not crucial, as will be seen from Fig. 6.5, the neglection of further terms in the polaron potentials will then be *a posteriori* justified.

Furthermore, the Haken potential (6.6) cannot describe the non-Coulombic electron-hole interaction for very small values of r, which is due to the finite size of electron and hole [7]. The conditions of validity of the potential (6.6) have been discussed, e.g., by Haken in Ref. [10].

When treating the Haken potential numerically for different polar crystals, the experimental and theoretical binding energies of the exciton states sometimes do not agree, for which reason corrections, sometimes phenomenologically, to the Haken potential have been introduced [216, 329–331] leading to clearly better results. One of these refined formulas is the potential proposed by Pollmann and Büttner [216, 327]

$$V(r) \;=\; -\frac{e^2}{4\pi\varepsilon_0 r}\left[\frac{1}{\varepsilon_{\mathrm{s}}}+\frac{1}{\varepsilon^*}\left(\frac{m_{\mathrm{h}}}{\Delta m}e^{-r/\rho_{\mathrm{h}}}-\frac{m_{\mathrm{e}}}{\Delta m}e^{-r/\rho_{\mathrm{e}}}\right)\right], \tag{6.9}$$

in which the bare electron and hole masses have to be used and where Δm is given by $\Delta m = m_{\mathrm{h}} - m_{\mathrm{e}}$. Hence, we take the statements given above as a reason to propose the following phenomenological potentials for Cu_2O, which are motivated by the formula of Haken and by the formula of Pollmann and Büttner:

$$V^{\mathrm{H}}(r) = -\frac{e^2}{4\pi\varepsilon_0 r}\left[\frac{1}{\varepsilon_{\mathrm{s1}}}+\frac{1}{2\varepsilon_1^*}\left(e^{-r/\rho_{\mathrm{h1}}}+e^{-r/\rho_{\mathrm{e1}}}\right)+\frac{1}{2\varepsilon_2^*}\left(e^{-r/\rho_{\mathrm{h2}}}+e^{-r/\rho_{\mathrm{e2}}}\right)\right] \tag{6.10a}$$

and

$$\begin{aligned} V^{\mathrm{PB}}(r) \;=\; & -\frac{e^2}{4\pi\varepsilon_0 r}\left[\frac{1}{\varepsilon_{\mathrm{s1}}}+\frac{1}{\varepsilon_1^*}\left(\frac{m_0}{m_0-m_{\mathrm{e}}\gamma_1}e^{-r/\rho_{\mathrm{h1}}}-\frac{m_{\mathrm{e}}\gamma_1}{m_0-m_{\mathrm{e}}\gamma_1}e^{-r/\rho_{\mathrm{e1}}}\right)\right.\\ & \left.+\frac{1}{\varepsilon_2^*}\left(\frac{m_0}{m_0-m_{\mathrm{e}}\gamma_1}e^{-r/\rho_{\mathrm{h2}}}-\frac{m_{\mathrm{e}}\gamma_1}{m_0-m_{\mathrm{e}}\gamma_1}e^{-r/\rho_{\mathrm{e2}}}\right)\right]. \end{aligned} \tag{6.10b}$$

Here we use

$$\frac{1}{\varepsilon_i^*}=\frac{1}{\varepsilon_{\mathrm{b}i}}-\frac{1}{\varepsilon_{\mathrm{s}i}} \tag{6.11}$$

and

$$\rho_{\mathrm{e}i}=\sqrt{\frac{\hbar}{2m_{\mathrm{e}}\omega_{\mathrm{LOi}}}},\qquad \rho_{\mathrm{h}i}=\sqrt{\frac{\hbar\gamma_1}{2m_0\omega_{\mathrm{LOi}}}}, \tag{6.12}$$

where the energies of the phonons and the values of the dielectric constants are given in Table 2.2. As has been done in Ref. [327] for perovskite $CH_3NH_3PbI_3$, we use V_{H} or V_{PB} in the Schrödinger equation without an additional fit parameter and find out which of these potentials describes the exciton spectrum of Cu_2O best. Since for the polaron radii ρ_{e} and ρ_{h} $1.6a \leq \rho \leq 4.4a$ holds, we expect the Haken or the Pollmann-Büttner potential to have a significant influence on the exciton states with $n \leq 2$.

As the Fröhlich coupling constant (3.39) is small in Cu_2O, i.e., it is $\alpha^{\mathrm{F}} \lesssim 0.2$ for the two optical phonons and both the electron and the hole [279], the bare electron and hole masses differ from the polaron masses by at most 3%. Hence, we can calculate with the bare masses when using V_{H}.

Besides the frequency dependence of the dielectric function also its momentum dependence becomes important if the exciton radius is on the order of the lattice constant. This momentum dependence of the dielectric function arises from the electronic polarization [162, 332].

When treating the excitons of $\mathrm{Cu_2O}$ in momentum space, the wave functions of the $n \geq 2$ states are localized about $k = 0$ so that for these states the k-dependence of ε is not important. However, for the $1S$ state $a_{1S} \approx a$ holds and thus this state is screened by ε at higher momenta k [162]. Considering the Coulomb interaction for the $1S$ exciton in k space,

$$V(k,\,\omega) = -\frac{1}{\sqrt{(2\pi)^3}}\,\frac{e^2}{\varepsilon_0\varepsilon(k,\,\omega)k^2}, \tag{6.13}$$

Kavoulakis *et al.* [162] derived a correction term by assuming

$$\frac{1}{\varepsilon(k,\omega)} \approx \frac{1}{\varepsilon_{\mathrm{b}} - d(ka)^2} \approx \frac{1}{\varepsilon_{\mathrm{b}}} + \frac{d(ka)^2}{\varepsilon_{\mathrm{b}}^2} \tag{6.14}$$

valid for $E_{\mathrm{g}}/\hbar \gg \omega \gg \omega_{\mathrm{LO}}$ with a small unknown constant d. Inserting Eq. (6.14) in Eq. (6.13) and Fourier transforming the second expression, one obtains the following correction term to the Coulomb interaction:

$$V_d(\boldsymbol{r}) = -da^2\frac{e^2}{\varepsilon_0\varepsilon_{\mathrm{b}}^2}V_{\mathrm{uc}}\,\delta(\boldsymbol{r}) = -V_0V_{\mathrm{uc}}\delta(\boldsymbol{r}). \tag{6.15}$$

Following the calculation of Ref. [332] on the dielectric function and using the lowest Γ_8^- conduction band and the highest Γ_7^+ valence band, Kavoulakis *et al.* [162] estimated the value of d to $d \approx 0.18$ [162].

Note that in general a Kronecker delta would appear in Eq. (6.15) [7]. However, as we treat the exciton problem in the continuum approximation, this Kronecker delta is replaced by the delta function times the volume $V_{\mathrm{uc}} = a^3$ of one unit cell. Thus, the parameter V_0 has the unit of an energy.

We have already stated above that the Haken potential cannot describe the electron-hole interaction correctly for very small r. Therefore, we now assume that the potential (6.15) is not only due to the momentum dependence of the dielectric function but that it also accounts for deviations from the Haken potential at small r. Hence, we will treat V_0 as an unknown fit parameter in the following.

6.1.3 Exchange interaction

In the Wannier equation or Hamiltonian of excitons the exchange interaction is generally not included but regarded as a correction to the hydrogen-like solution [7]. We have presented a comprehensive discussion of the exchange interaction in $\mathrm{Cu_2O}$ in Chapter 5, where we could show, in accordance with Ref. [162], that corrections to the exchange interaction due to a finite momentum $\hbar\boldsymbol{K}$ of the center of mass of the exciton are negligibly small. Hence, only the K-independent part of the exchange interaction [72, 303, 304]

$$H_{\mathrm{exch}}(\boldsymbol{r}) = J_0\left(\frac{1}{4} - \frac{1}{\hbar^2}\boldsymbol{S}_{\mathrm{e}}\cdot\boldsymbol{S}_{\mathrm{h}}\right)V_{\mathrm{uc}}\delta(\boldsymbol{r}) \tag{6.16}$$

needs to be considered. Note, however, that the K-independent analytic exchange interaction is generally not part of the central-cell corrections, for which reason we will always write it separately in the Hamiltonian of the exciton.

Within the simple hydrogen-like model the exchange interaction would only affect the nS exciton states as these states have a nonvanishing probability density at $r=0$. However, when considering the complete valence band structure, the exciton states with even or with odd values of L are coupled, and thus the exchange interaction will affect the whole even exciton series.

It is well known from experiments that the splitting between the yellow $1S$ ortho- and the yellow $1S$ para-exciton amounts to about 12 meV [309, 315, 316]. Hence, we have to choose the value of J_0 such that this splitting is reflected in the theoretical spectrum.

6.1.4 Summary

Following the explanations given in Secs. 6.1.2 and 6.1.3, the term $H_{\mathrm{exch}}+V_{\mathrm{CCC}}$ in the Hamiltonian of Eq. (4.7) takes one of the following forms [cf. Eqs. (6.10a), (6.10b), (6.15), and (6.16)]:

$$\begin{aligned} H_{\mathrm{exch}}(\boldsymbol{r})+V_{\mathrm{CCC}}^{\mathrm{H}}(\boldsymbol{r}) &= -\frac{e^2}{4\pi\varepsilon_0 r}\left[\frac{1}{2\varepsilon_1^*}\left(e^{-r/\rho_{\mathrm{h}1}}+e^{-r/\rho_{\mathrm{e}1}}\right)+\frac{1}{2\varepsilon_2^*}\left(e^{-r/\rho_{\mathrm{h}2}}+e^{-r/\rho_{\mathrm{e}2}}\right)\right] \\ &\quad +\left[-V_0+J_0\left(\frac{1}{4}-\frac{1}{\hbar^2}\boldsymbol{S}_{\mathrm{e}}\cdot\boldsymbol{S}_{\mathrm{h}}\right)\right]V_{\mathrm{uc}}\delta(\boldsymbol{r}), \end{aligned} \tag{6.17a}$$

$$\begin{aligned} H_{\mathrm{exch}}(\boldsymbol{r})+V_{\mathrm{CCC}}^{\mathrm{PB}}(\boldsymbol{r}) &= -\frac{e^2}{4\pi\varepsilon_0 r}\left[\frac{1}{\varepsilon_1^*}\left(\frac{m_0}{m_0-m_{\mathrm{e}}\gamma_1}e^{-r/\rho_{\mathrm{h}1}}-\frac{m_{\mathrm{e}}\gamma_1}{m_0-m_{\mathrm{e}}\gamma_1}e^{-r/\rho_{\mathrm{e}1}}\right)\right. \\ &\quad \left.+\frac{1}{\varepsilon_2^*}\left(\frac{m_0}{m_0-m_{\mathrm{e}}\gamma_1}e^{-r/\rho_{\mathrm{h}2}}-\frac{m_{\mathrm{e}}\gamma_1}{m_0-m_{\mathrm{e}}\gamma_1}e^{-r/\rho_{\mathrm{e}2}}\right)\right] \\ &\quad +\left[-V_0+J_0\left(\frac{1}{4}-\frac{1}{\hbar^2}\boldsymbol{S}_{\mathrm{e}}\cdot\boldsymbol{S}_{\mathrm{h}}\right)\right]V_{\mathrm{uc}}\delta(\boldsymbol{r}). \end{aligned} \tag{6.17b}$$

Note that while the operators with $\delta(\boldsymbol{r})$ affect only the exciton series with even values of L, the Haken or Pollmann and Büttner potential affect all exciton states [10]. A comparison of our results with the experimental values of Refs. [30, 36, 72, 173, 176] will allow us, in Sec. 6.2, to determine the size of the unknown parameters V_0 and J_0.

We now express the Hamiltonian (4.7) with the corrections in terms of irreducible tensors and write the Schrödinger equation as a generalized eigenvalue problem by analogy with Eq. (4.24) using the complete basis of Sec. 4.3. This eigenvalue problem is then solved using an appropriate LAPACK routine [284]. Note that the presence of the delta functions in Eq. (6.17) makes the whole problem more complicated than in Sec. 4.3 since not only the eigenvalues but also the wave functions at $r=0$ have to converge. However, for a specific value of the scaling parameter α in Eq. (4.21) it is not possible to obtain convergence for all exciton states of interest. Therefore, we solve the Schrödinger equation initially without the $\delta(\boldsymbol{r})$ dependent terms. We then select the converged eigenvectors and with these we set up a second generalized eigenvalue problem now including the $\delta(\boldsymbol{r})$ dependent terms. This problem is again solved using an appropriate LAPACK routine [284] and provides the correct converged eigenvalues of the Hamiltonian.

6.2 Results and discussion

In this section we determine the values of the parameters J_0 and V_0 and discuss the complete exciton spectrum of Cu_2O.

The parameter J_0 describes the strength of the exchange interaction. It is well known that the exchange interaction mainly affects the $1S$ exciton and that the splitting between the ortho- and the para-exciton state amounts to 11.8 meV [72, 176, 309, 315, 316]. By choosing

$$J_0 = 0.792 \pm 0.068\,\mathrm{eV} \tag{6.18}$$

we obtain the correct value of this splitting irrespective of whether using the Haken or the Pollman-Büttner potential [cf. Eq. (6.17)].

Figure 6.4 show the effect of the correction with the coefficient V_0 on the spectrum for the Haken and the Pollman-Büttner potential, respectively. As can be seen from these figures, the exchange splitting of the $1S$ state hardly changes when varying the value V_0. Hence, we can determine V_0 almost independently of J_0. In these figures we also show the relative oscillator strength for two-photon absorption. For the states of Γ_5^+-symmetry we calculate relative oscillator strengths via Eq. (4.66) with $|T^{TP}_{\xi\boldsymbol{K}}\rangle = |\pi^{TP}_{xy}\rangle$.

To find the optimum value of V_0, we compare our results to the energies of the even parity exciton states given in Refs. [37, 41, 72, 173, 176, 333]. However, we can see from Fig. 6.4 that there is no value of V_0 for which all theoretical results take the values of the experimentally determined energies. This is not unexpected since the central-cell corrections are only an attempt to account for the specific properties of the $1S$ exciton within the continuum limit of Wannier excitons and are not an exact description of this exciton state. Hence, we do not expect a perfect agreement between theory and experiment.

Small deviations from the experimental values could also be explained by small uncertainties in the Luttinger parameters γ_i, η_i [37] or the band gap energy [30] as well as by a finite temperature or small strains in the crystal. On the other hand, it is also possible that the experimental values are affected by uncertainties. This can be seen, e.g., when comparing the slightly different experimental results of Refs. [37] and [41, 173].

Note that the almost perfect agreement between theoretical and experimental results in Refs. [72, 317] could only be obtained by taking also γ_1', μ' and Δ as fit parameters to the experiment. However, these parameters are connected to the band structure in $\mathrm{Cu_2O}$ [279] and cannot be chosen arbitrarily as discussed in Sec. 4.5.1.

It can be seen from Fig. 6.4 that the oscillator strength of the exciton state at $E \approx 2.143\,\mathrm{eV}$ changes rapidly with increasing V_0. From the experimental results of Refs. [72, 317] we know that the two exciton states at $E = 2.1378\,\mathrm{eV}$ and $E = 2.1544\,\mathrm{eV}$ are well separated from the other exciton states and that the phonon background is small. Hence, the ratio of the relative two-photon oscillator strengths (cf. Sec. 4.4.1) can be calculated quite accurately to $\sim$ 16.

We now choose the value of V_0 such that the ratio of the calculated two-photon oscillator strengths reaches the same value and obtain

$$V_0 = 0.539 \pm 0.027\,\mathrm{eV} \tag{6.19}$$

when using the Haken potential [cf. Eq. (6.17a)] or

$$V_0 = 0.694 \pm 0.027\,\mathrm{eV} \tag{6.20}$$

when using the Pollmann-Büttner potential [cf. Eq. (6.17b)]. Note that the error bars for V_0 are chosen such that the ratio of the oscillator strengths lies between 14 and 18.

Having determined the most suitable values of V_0 and J_0, we can now turn our attention to the exciton Bohr radius $a_{\mathrm{exc}}^{(1S)}$ of the $1S$ ortho-exciton and to the correct assignment of the $n = 2$ exciton states.

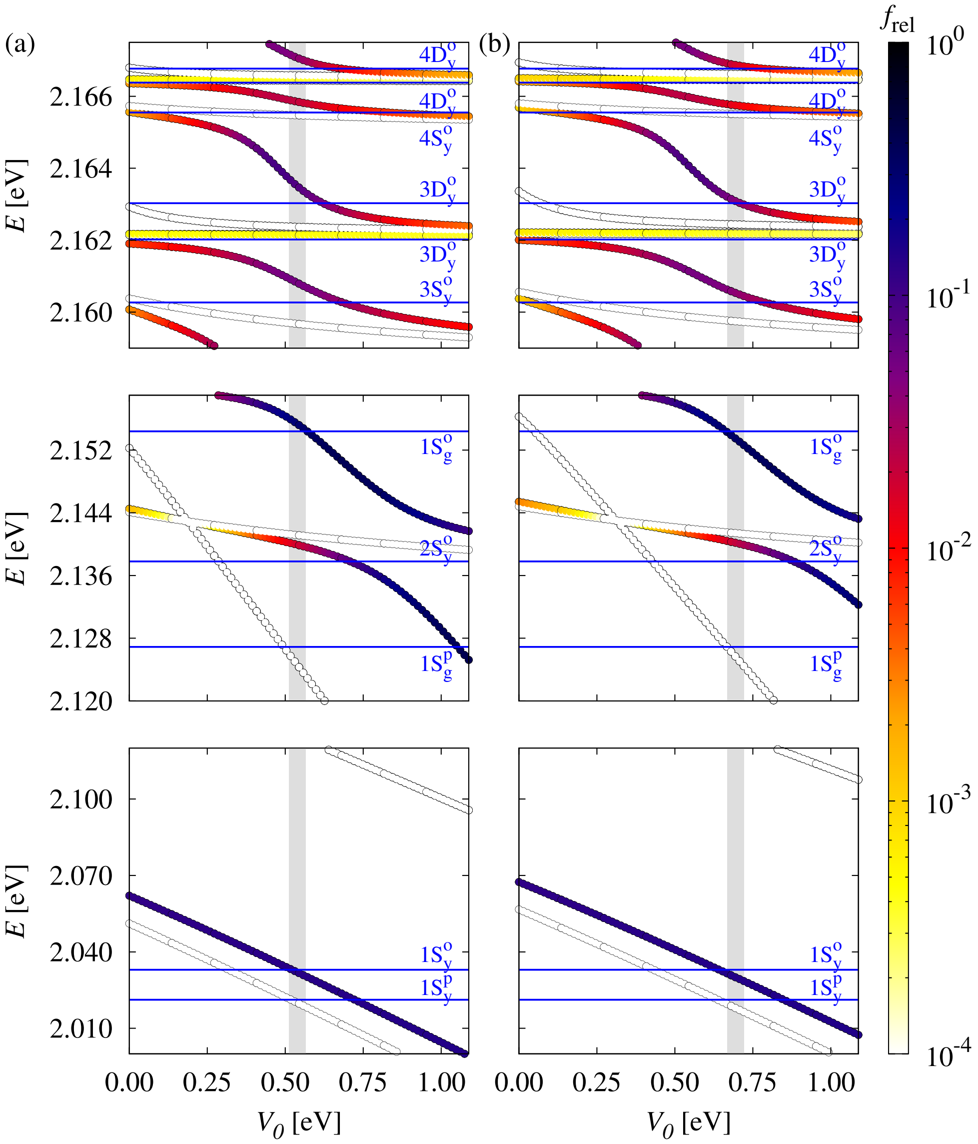

Figure 6.4.: (a) Behavior of the even exciton states as functions of V_0 when using $V_{\mathrm{CCC}}^{\mathrm{H}}$ [see Eq. (6.17a)]. The color bar shows the relative oscillator strengths for two-photon absorption. The blue straight lines denote the position of the dipole-allowed Γ_5^+ S and D exciton states observed in the experiment. We also show the positions of the $1S$ paraexcitons ($1S_{\mathrm{y/g}}^{\mathrm{p}}$). The gray area indicates the optimum range of $V_0 = 0.539 \pm 0.027\,\mathrm{eV}$, where the ratio of the relative oscillator strengths of the yellow $2S$ and the green $1S$ state amounts to $\sim$ 16. The effect of the central-cell corrections on the whole even exciton spectrum is evident. (b) Same calculation but with $V_{\mathrm{CCC}}^{\mathrm{PB}}$ [see Eq. (6.17b)]. One can see only slight differences for the $n = 1$ and $n = 2$ exciton states when comparing the results to panel (a). The gray area indicates the optimum range of $V_0 = 0.694 \pm 0.027\,\mathrm{eV}$. For further information see text.

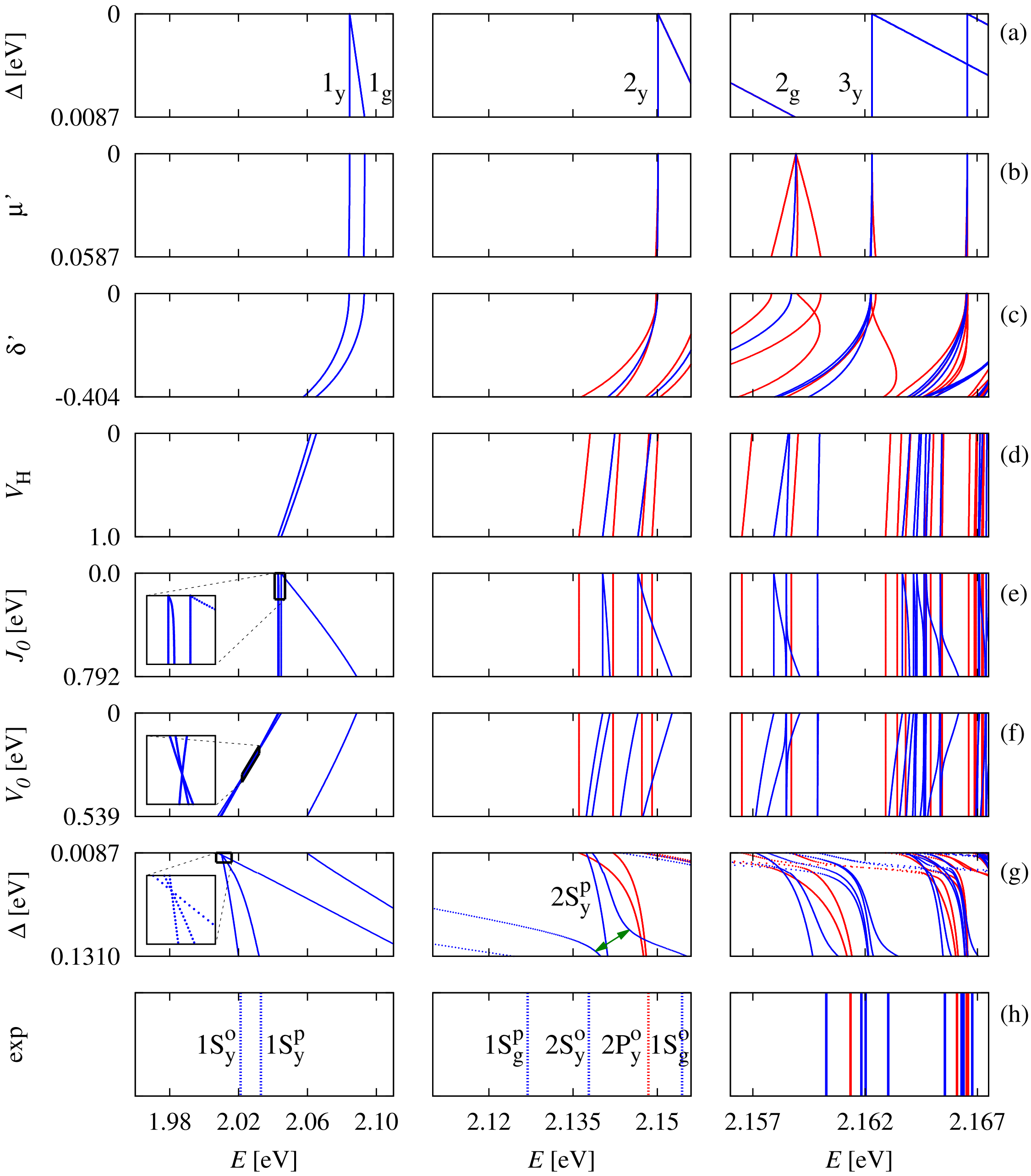

Figure 6.5.: Exciton spectrum of the even (blue) and odd (red) exciton states when increasing all material parameters from zero (top) to their correct values (bottom) and using $V_{\mathrm{CCC}}^{\mathrm{H}}$ [cf. Eq. (6.17b)]. In (g) and (h) the para- and ortho-exciton states are denoted by an upper index p and o. The final results at the bottom of (g), which are also listed in Table 6.2, can then be compared to the position of the exciton states obtained from experiments (h). Note that due to the marked anticrossing [green arrow in the second panel of (g)] the assignment of the green $1S$ state and the yellow $2S$ state changes. For further information see text.

To determine the radius $a_{\mathrm{exc}}^{(1S)}$, we evaluate

$$\langle\Psi|r|\Psi\rangle = \sum_{N'}\sum_{NLJFF_tM_{F_t}}\sum_{j=-2}^{2} c_{N'LJFF_tM_{F_t}} c_{NLJFF_tM_{F_t}} \frac{\alpha(R_2)_{NL}^{j}}{N+L+j+1}\delta_{N',N+j} \tag{6.21}$$

with the wave function Ψ of Eq. (4.23) and compare the result with the formula [174]

$$\langle r\rangle = \frac{1}{2}a_{\mathrm{exc}}\left[3n^2 - L(L+1)\right] \tag{6.22}$$

known from the hydrogen atom, where we set $n = 1$ and $L = 0$. Note that the function $(R_2)_{NL}^{j}$ in Eq. (6.21) is taken from the recursion relations of the Coulomb-Sturmian functions in Appendix E. We obtain

$$a_{\mathrm{exc}}^{(1S)} \approx 0.793\,\mathrm{nm} \approx 1.86\,a \tag{6.23}$$

when using the Haken potential or

$$a_{\mathrm{exc}}^{(1S)} \approx 0.810\,\mathrm{nm} \approx 1.90\,a \tag{6.24}$$

when using the Pollmann-Büttner potential. In both cases the radius of the $1S$ ortho-exciton is large enough that the corrections to the kinetic energy discussed in Sec. 6.1.1 can certainly be neglected.

Let us now proceed to the correct assignment of the $n = 2$ exciton states. Since in the investigation of Uihlein *et al.* [72, 317] the wrong values for the Luttinger parameters were used (cf. Chapter 4), it is not clear whether the state at $E = 2.1544\,\mathrm{eV}$ can still be assigned as the yellow $2S$ ortho-exciton state and the state at $E = 2.1378\,\mathrm{eV}$ as the green $1S$ ortho-exciton state when using the correct Luttinger parameters.

To demonstrate from which hydrogen-like states the experimentally observed exciton states originate, we find it instructive to start from the hydrogen-like spectrum with almost all material parameters set to zero and then increase these material parameters successively to their true values. This is shown in Fig. 6.5.

At first all material parameters except for γ_1' are set to zero, so that a true hydrogen-like spectrum is obtained, where the yellow (y) and green (g) exciton states are degenerate. This spectrum is shown in the panel (a) of Fig. 6.5. When increasing the spin-orbit coupling constant Δ in Fig. 6.5(a), the degeneracy between the green and the yellow exciton series is lifted. The increase of the Luttinger parameters μ' and δ' in the panels (b) and (c) furthermore lifts the degeneracy between the exciton states of different angular momentum L. Since the effect of the parameters η_1', ν and τ on the exciton spectrum is small they are immediately set from zero to their correct values between the panels (c) and (d). The Haken potential does not change degeneracies but slightly lowers the energy of the exciton states in Fig. 6.5(d). The exchange energy described by the constant J_0 lifts the degenercy between ortho- and para-exciton states in Fig. 6.5(e). As the operator $\delta(\boldsymbol{r})$ affects only the states of even parity (blue lines), the energy of the odd exciton states (red lines) remains unchanged in Fig. 6.5(f). Note that we increase Δ in two steps to its true value of $\Delta = 0.131\,\mathrm{eV}$ for reasons of clarity. Hence, at the bottom of Fig. 6.5(g) all material values have been increased to their true values. For a comparison, we show in panel (h) the position of the experimentally observed states. Following the exciton states from panel (a) to (g), it is possible to assign them with the notation $nL_{\mathrm{y/g}}^{\mathrm{p/o}}$, where the upper index denotes a para- or an ortho-exciton state and the lower index a yellow or a green state.

The results presented in Fig. 6.5 suggest to assign the exciton state at $E = 2.1378\,\mathrm{eV}$ to the green $1S$ ortho-exciton state. However, one can observe an anticrossing between the green $1S$ state and the yellow $2S$ state, which is indicated by a green arrow in Fig. 6.5(g). Hence, the assignment has to be changed. As a proof, we can calculate the percentage of the $J = 3/2$ component of these states, i.e., their green part, by evaluating

$$\mathrm{gp} = \langle\Psi|P|\Psi\rangle \tag{6.25}$$

with the projection operator

$$P = \sum_{M_J=-3/2}^{3/2} \left|\frac{3}{2},\, M_J\right\rangle\left\langle\frac{3}{2},\, M_J\right| \tag{6.26}$$

and the exciton wave function $|\Psi\rangle$. For the summands we find

$$\begin{aligned}\left\langle\Psi\middle|\frac{3}{2},\, M_J\right\rangle\left\langle\frac{3}{2},\, M_J\middle|\Psi\right\rangle = {} & \sum_{j=-1}^{1}\sum_{NLFF_tM_{F_t}}\sum_{F'F'_tM'_{F_t}}\sum_{M_{S_\mathrm{e}}M_L}\frac{(R_1)^j_{NL}}{N+L+j+1}\\ & \times c_{(N+j)LJF'F'_tM'_{F_t}}c_{NLJFF_tM_{F_t}}(-1)^{F+F'+M_{F_t}+M'_{F_t}-2J+2M_J-1}\\ & \times \left[(2F+1)(2F_t+1)(2F'+1)(2F'_t+1)\right]^{\frac{1}{2}}\\ & \times \begin{pmatrix} F & \frac{1}{2} & F_t \\ M_L+M_J & M_{S_\mathrm{e}} & -M_{F_t}\end{pmatrix}\begin{pmatrix} L & J & F \\ M_L & M_J & -M_L-M_J\end{pmatrix}\\ & \times \begin{pmatrix} F' & \frac{1}{2} & F'_t \\ M_L+M_J & M_{S_\mathrm{e}} & -M'_{F_t}\end{pmatrix}\begin{pmatrix} L & J & F' \\ M_L & M_J & -M_L-M_J\end{pmatrix}.\end{aligned} \tag{6.27}$$

The function $(R_1)^j_{NL}$ is taken from the recursion relations of the Coulomb-Sturmian functions.

The green part gp of the state at $E \approx 2.1544\,\mathrm{eV}$ is distinctly higher ($\mathrm{gp} \approx 40\%$) than the green part of the exciton state at $E \approx 2.1378\,\mathrm{eV}$ ($\mathrm{gp} \approx 11\%$). However, since also $\mathrm{gp} \approx 40\%$ is significantly smaller than one, we see that the assignment of this exciton state as the ground state of the green series is questionable and shows the significant deviations from the hydrogen-like model. The green $1S$ exciton state is distributed over the yellow states. Note that in Ref. [72] also the state of higher energy had a larger green part than the state of lower energy. However, in Fig. 2 of Ref. [72] the assignment is reversed since the limit of $\mu' \to 0$ was used to designate the states. It seems obvious that a similar anticrossing between the green $1S$ state and the yellow $2S$ state was disregarded. A considerable effect of the interaction between the green and yellow series is the change in the oscillator strength of the states. The oscillator strength of the $2S_y$ state is much smaller than expected when assuming two independent, i.e., green and yellow, series [72, 317] (cf. also Tables 6.2 and 6.3).

For reasons of completeness, we give the size of the green $1S$ and the yellow $2S$ state by evaluating Eq. (6.21). Since these states are strongly mixed and a correct assignment with a principal quantum number n is not possible, we do not use the formula (6.22). We obtain

$$\begin{aligned} \langle r \rangle (2S_y) &\approx 4.32\,\mathrm{nm} \approx 10.1\,a, &\text{(6.28a)}\\ \langle r \rangle (1S_g) &\approx 5.32\,\mathrm{nm} \approx 12.5\,a, &\text{(6.28b)}\end{aligned}$$

when using the Haken potential or

$$\begin{aligned} \langle r \rangle (2S_y) &\approx 4.39\,\mathrm{nm} \approx 10.3\,a, &\text{(6.29a)}\\ \langle r \rangle (1S_g) &\approx 4.09\,\mathrm{nm} \approx 9.58\,a, &\text{(6.29b)}\end{aligned}$$

when using the Pollmann-Büttner potential. We see that in both cases the values of $\langle r \rangle$ for the green $1S$ and the yellow $2S$ state are of the same size. This is expected due to the strong mixing of both states.

The resonance of the green $1S$ state with the yellow exciton series and the mixing of all even exciton states via the cubic band structure leads to an admixture of D and G states to the green $1S$ state. Hence, the three Γ_5^+ states which we assigned with $1S_\mathrm{g}$ are elliptically deformed and invariant only under the subgroup $D_{4\mathrm{h}}$ of O_h (cf. Sec. 4.1 and Ref. [90]). The lower symmetry of the envelope function allows for a smaller mean distance between electron and hole in a specific direction, which leads to a gain of energy due to the Coulomb interaction (cf. Sec. 4.1). As regards the xy-component, the symmetry axis of the according subgroup $D_{4\mathrm{h}}$ is the z-axis of the crystal. Since for this state the expectation values $\left\langle \Psi \middle| x^2 \middle| \Psi \right\rangle$ and $\left\langle \Psi \middle| y^2 \middle| \Psi \right\rangle$ are identical, we can calculate the semi-principal axes of the elliptically deformed state by evaluating

$$\begin{aligned} \left\langle \Psi \middle| x^2 \middle| \Psi \right\rangle &= \left\langle \Psi \middle| (r^2 - z^2)/2 \middle| \Psi \right\rangle \\ &= \sum_{N'L'J'F'F_t'M_{F_t}'} \sum_{NLJFF_tM_{F_t}} c_{N'L'J'F'F_t'M_{F_t}'} c_{NLJFF_tM_{F_t}} \\ &\times \alpha^2 \left\langle \Pi' \middle| \frac{1}{3} r^2 - \frac{1}{3\sqrt{6}} X_0^{(2)} \middle| \Pi \right\rangle \end{aligned} \tag{6.30}$$

and

$$\begin{aligned} \left\langle \Psi \middle| z^2 \middle| \Psi \right\rangle &= \sum_{N'L'J'F'F_t'M_{F_t}'} \sum_{NLJFF_tM_{F_t}} c_{N'L'J'F'F_t'M_{F_t}'} c_{NLJFF_tM_{F_t}} \\ &\times \alpha^2 \left\langle \Pi' \middle| \frac{1}{3}\sqrt{\frac{2}{3}} X_0^{(2)} + \frac{1}{3} r^2 \middle| \Pi \right\rangle \end{aligned} \tag{6.31}$$

with the wave function Ψ of Eq. (4.23) and the matrix elements $\langle \Pi' | X_0^{(2)} | \Pi \rangle$ and $\langle \Pi' | r^2 | \Pi \rangle$ listed in Appendix F.1. We obtain

$$\left\langle x^2 \right\rangle \approx 116.4\,a^2, \qquad \left\langle z^2 \right\rangle \approx 29.9\,a^2, \tag{6.32}$$

when using the Haken potential or

$$\left\langle x^2 \right\rangle \approx 68.6\,a^2, \qquad \left\langle z^2 \right\rangle \approx 25.1\,a^2, \tag{6.33}$$

when using the Pollmann-Büttner potential. The significant differences in $\left\langle x^2 \right\rangle$ and $\left\langle z^2 \right\rangle$ show again the strong resonance of the green $1S$ state with the yellow series as well as the strong admixture

Table 6.1.: Decomposition of the irreducible representations of the rotation group or the angular momentum states by the cubic group O_h. Note that the quasi-spin I already enters the momentum F via J. The irreducible representations denote the symmetry of the envelope function (L), the combined symmetry of envelope and hole (F) or the complete symmetry of the exciton (F_t).

L		$F = L + J\,(J = \frac{1}{2})$		$F_t = F + S_\mathrm{e}$	
0	Γ_1^+	$\frac{1}{2}$	Γ_7^+	0	Γ_2^+
				1	Γ_5^+
1	Γ_4^-	$\frac{1}{2}$	Γ_7^-	0	Γ_2^-
				1	Γ_5^-
		$\frac{3}{2}$	Γ_8^-	1	Γ_4^-
				2	$\Gamma_3^- \oplus \Gamma_5^-$
2	$\Gamma_3^+ \oplus \Gamma_5^+$	$\frac{3}{2}$	Γ_8^+	1	Γ_5^+
				2	$\Gamma_3^+ \oplus \Gamma_4^+$
		$\frac{5}{2}$	$\Gamma_6^+ \oplus \Gamma_8^+$	2	$\Gamma_3^+ \oplus \Gamma_4^+$
				3	$\Gamma_1^+ \oplus \Gamma_4^+ \oplus \Gamma_5^+$
3	$\Gamma_2^- \oplus \Gamma_4^- \oplus \Gamma_5^-$	$\frac{5}{2}$	$\Gamma_6^- \oplus \Gamma_8^-$	2	$\Gamma_3^- \oplus \Gamma_4^-$
				3	$\Gamma_1^- \oplus \Gamma_4^- \oplus \Gamma_5^-$
		$\frac{7}{2}$	$\Gamma_6^- \oplus \Gamma_7^- \oplus \Gamma_8^-$	3	$\Gamma_1^- \oplus \Gamma_4^- \oplus \Gamma_5^-$
				4	$\Gamma_2^- \oplus \Gamma_3^- \oplus \Gamma_4^- \oplus \Gamma_5^-$

L		$F = L + J\,(J = \frac{3}{2})$		$F_t = F + S_\mathrm{e}$	
0	Γ_1^+	$\frac{3}{2}$	Γ_8^+	1	Γ_5^+
				2	$\Gamma_3^+ \oplus \Gamma_4^+$

of states with $L \geq 2$. We finally want to note that, due to the coupling of the yellow and green series, the green $1S$ has to be regarded as an excited state in the complete exciton spectrum and not as the ground state of the green series. In particular, the green $1S$ state is orthogonal to the true ground state of the complete spectrum, i.e., to the yellow $1S$ state.

Let us now discuss the other exciton states. To determine the number of para- and ortho-exciton states as well as their degeneracies for the different values of L, one can use group theoretical considerations. In the spherical approximation, in which the cubic part of the Hamiltonian is neglected ($\delta' = 0$), the momentum $F = J + L$ is a good quantum number for the states of negative parity since the exchange interaction does not act on these states. The states of positive parity can be classified by the total momentum $F_t = F + S_\mathrm{e}$ in the spherical approximation.

If the complete cubic Hamiltonian is treated, the reduction of the irreducible representations D^F or D^{F_t} of the rotation group by the cubic group O_h has to be considered [169]. This is shown in Table 6.1. As has already been stated in Sec. 4.3, a normal spin one transforms according to the irreducible representation Γ_4^+ of the cubic group whereas the quasi-spin I transforms according to $\Gamma_5^+ = \Gamma_4^+ \otimes \Gamma_2^+$. Therefore, one has to include the additional factor Γ_2^+ when determining the symmetry of an exciton state [36, 72]. This symmetry is given by the symmetry of the envelope function, the valence band, and the conduction band:

$$\Gamma_\mathrm{exc} = \Gamma_\mathrm{env} \otimes \Gamma_\mathrm{v} \otimes \Gamma_\mathrm{c}. \tag{6.34}$$

Only states of symmetry Γ_4^- are dipole allowed in one-photon absorption and only states of symmetry Γ_5^+ are dipole allowed in two-photon absorption. Hence, we see from Table 6.1 that there are at the most one P state and four F states or one S and two D states for each principal quantum number n, which can be observed in experiments.

Since the exchange interaction does not act on the exciton states with negative parity, one can use the irreducible representations of the second column of Table 6.1 to classify these exciton states [36]. For the exciton states of positive parity the irreducible representations of the third column are needed. Note that the cubic part of the Hamiltonian mixes the S and D exciton states of symmetry Γ_5^+. Hence, the exchange interaction acts only on the D excitons of symmetry Γ_5^+ via their S component. The degeneracies between the D states of symmetry Γ_3^+ and Γ_4^+ or Γ_1^+ and Γ_4^+ is not lifted, respectively (cf. the third column of Table 6.1).

Since neither J nor F are good quantum numbers due to the cubic symmetry of our Hamiltonian, we do not use the nomenclature $n^{2J+1}L_F$ of Refs. [72, 317]. Although L is likewise no good quantum number, the assignment of the exciton states by using S, P, D, F and G to denote the angular momentum is still common (see, e.g., Refs. [36, 37]). Hence, we feel obliged to classify the states by introducing the notation $nL_\mathrm{y/g}$ for comparison with other works but also stress that this is generally not instructive due to the large deviations from the hydrogen-like model (cf. also Chapter 4). By the index y or g we denote the yellow or the green exciton series, respectively. To be more correct, we will also give the symmetry of the exciton states in terms of the irreducible representations of Table 6.1. These symmetries can be determined by regarding the eigenvectors of the generalized eigenvalue problem mentioned in Sec. 6.1.4 (for a more detailed description see Sec. 4.3).

In the Tables 6.2 and 6.3 we now give a direct comparison between experimental and theoretical exciton energies for all states with $n \leq 5$. One can see that the results with the Haken potential listed in Tab. 6.2 show a better agreement with the experimental values than the results with the Pollmann-Büttner potential listed in Tab. 6.3. Hence, we have chosen the central-cell corrections with the Haken potential for the calculation of Fig. 6.5.

Note that for each n the relative oscillator strength of one nD state is larger than the relative oscillator strengths of the nS state in accordance with the experimental results of Ref. [72]. The Haken potential or the Pollmann-Büttner potential also slightly affects the odd exciton series and especially the $2P$ exciton state. These potentials shift the energy of the Γ_4^- (resp. Γ_8^-) $2P$ exciton state by an amount of 210 μeV (Haken) or 880 μeV (Pollmann-Büttner) towards lower energies.

Table 6.2.: Comparison of calculated energies E_{theor} to experimental values E_{exp} (References given behind experimental values) when using the central-cell corrections with the Haken potential (6.17a). Note that we use $E_{\mathrm{g}} = 2.17202\,\mathrm{eV}$ instead of $E_{\mathrm{g}} = 2.17208\,\mathrm{eV}$ [30] to obtain a better agreement. The assignment of the states in the first column is motivated by Fig. 6.5 but is generally not instructive due to the large deviations from the hydrogen-like model. Hence, we also give the symmetry of the states. In the case of the P and F excitons we do not give the symmetry of the complete exciton state but only the combined symmetry of envelope and hole. As regards the $5G$ excitons we only give the average energy of the states of symmetry Γ_5^+. The value in the fourth column gives the relative oscillator strength in one-photon absorption (nP, nF excitons; see Sec. 4.4) or in two-photon absorption (nS, nD, nG excitons; see Sec. 4.4.1). Note that due to the interaction with the $1S_{\mathrm{g}}$ state the oscillator strength of the $2S_{\mathrm{y}}$ state is much smaller than expected when assuming two independent, i.e., green and yellow, series. The value in the last column indicates the percentage of the $J = 3/2$ component of the state, i.e., the green part. Due to the interaction between the yellow and the green exciton series the green $1S$ state is spread over several yellow exciton states. The green states with $n \geq 2$ are located far above the states listed here.

State		E_{exp} [eV]	E_{theor} [eV]	f_{rel}	gp [%]
$1S_{\mathrm{y}}$	Γ_2^+	2.0212 [176]	2.0200	–	5.49
$1S_{\mathrm{y}}$	Γ_5^+	2.0330 [72]	2.0320	26.60	7.22
$1S_{\mathrm{g}}$	$\Gamma_{3/4}^+$	2.1269 [333]	2.1245	–	71.62
$2S_{\mathrm{y}}$	Γ_5^+	2.1378 [72]	2.1399	3.55	10.88
$2S_{\mathrm{y}}$	Γ_2^+	–	2.1412	–	1.43
$2P_{\mathrm{y}}$	Γ_8^-	2.1484 [30]	2.1475	351.4	1.91
$2P_{\mathrm{y}}$	Γ_7^-	–	2.1480	–	1.30
$1S_{\mathrm{g}}$	Γ_5^+	2.1544 [72]	2.1553	56.01	36.88
$3S_{\mathrm{y}}$	Γ_2^+	–	2.15967	–	0.48
$3S_{\mathrm{y}}$	Γ_5^+	2.16027 [41, 173]	2.16080	10.34	4.49
$3P_{\mathrm{y}}$	Γ_8^-	2.16135 [30]	2.16119	147.3	0.93
$3P_{\mathrm{y}}$	Γ_7^-	–	2.16141	–	0.63
$3D_{\mathrm{y}}$	$\Gamma_{3/4}^+$	2.16183 [41, 173]	2.16213	–	0.31
$3D_{\mathrm{y}}$	Γ_5^+	2.16202 [41, 173]	2.16215	0.09	0.30
$3D_{\mathrm{y}}$	$\Gamma_{1/4}^+$	–	2.16217	–	0.25
$3D_{\mathrm{y}}$	$\Gamma_{3/4}^+$	–	2.16237	–	0.46
$3D_{\mathrm{y}}$	Γ_5^+	2.16303 [41, 173]	2.16348	15.04	8.49
$4S_{\mathrm{y}}$	Γ_2^+	–	2.16547	–	0.21
$4S_{\mathrm{y}}$	Γ_5^+	2.16555 [41, 173]	2.16584	3.79	1.53

$4P_{\mathrm{y}}$	Γ_8^-	2.16609 [30]	2.16604	67.43	0.45
$4P_{\mathrm{y}}$	Γ_7^-	–	2.16614	–	0.32
$4D_{\mathrm{y}}$	$\Gamma_{3/4}^+$	2.16629 [41, 173]	2.16644	–	0.19
$4D_{\mathrm{y}}$	Γ_5^+	2.16638 [41, 173]	2.16645	0.07	0.19
$4D_{\mathrm{y}}$	$\Gamma_{1/4}^+$	–	2.16646	–	0.16
$4F_{\mathrm{y}}$	Γ_7^-	–	2.16653	–	0.12
$4F_{\mathrm{y}}$	Γ_8^-	2.16652 [36]	2.16654	0.066	0.10
$4F_{\mathrm{y}}$	Γ_8^-	2.16654 [36]	2.16656	0.002	0.08
$4F_{\mathrm{y}}$	Γ_6^-	2.16654 [36]	2.16657	0.010	0.08
$4F_{\mathrm{y}}$	Γ_6^-	2.16658 [36]	2.16660	0.011	0.06
$4D_{\mathrm{y}}$	$\Gamma_{3/4}^+$	–	2.16658	–	0.22
$4D_{\mathrm{y}}$	Γ_5^+	2.16677 [41, 173]	2.16704	6.86	3.67
$5S_{\mathrm{y}}$	Γ_2^+	–	2.16798	–	0.10
$5S_{\mathrm{y}}$	Γ_5^+	2.16801 [41, 173]	2.16816	2.02	0.81
$5P_{\mathrm{y}}$	Γ_8^-	2.16829 [30]	2.16825	32.82	0.25
$5P_{\mathrm{y}}$	Γ_7^-	–	2.16830	–	0.18
$5D_{\mathrm{y}}$	$\Gamma_{3/4}^+$	2.16841 [41, 173]	2.16846	–	0.11
$5D_{\mathrm{y}}$	Γ_5^+	2.16846 [41, 173]	2.16846	0.05	0.12
$5D_{\mathrm{y}}$	$\Gamma_{1/4}^+$	–	2.16847	–	0.10
$5F_{\mathrm{y}}$	Γ_7^-	–	2.16850	–	0.09
$5F_{\mathrm{y}}$	Γ_8^-	2.16851 [36]	2.16850	0.069	0.07
$5F_{\mathrm{y}}$	Γ_8^-	2.16852 [36]	2.16852	0.000	0.06
$5F_{\mathrm{y}}$	Γ_6^-	2.16852 [36]	2.16852	0.002	0.06
$5F_{\mathrm{y}}$	Γ_6^-	2.16855 [36]	2.16855	0.001	0.04
$5D_{\mathrm{y}}$	$\Gamma_{3/4}^+$	–	2.16854	–	0.11
$5\bar{G}_{\mathrm{y}}$	Γ_5^+	–	2.16855	0.00	0.03
$5D_{\mathrm{y}}$	Γ_5^+	2.16860 [41, 173]	2.16879	4.30	2.22

Table 6.3.: Same comparison as in Table 6.2 but when using the central-cell corrections with the Pollmann-Büttner potential (6.17b). Especially for the states with $n < 3$ differences in the calculated energies can be observed when using the different corrections (6.17a) or (6.17b).

State		E_{exp} [eV]	E_{theor} [eV]	f_{rel}	gp [%]
$1S_{\text{y}}$	Γ_2^+	2.0212 [176]	2.0180	–	5.49
$1S_{\text{y}}$	Γ_5^+	2.0330 [72]	2.0300	27.90	6.83
$1S_{\text{g}}$	$\Gamma_{3/4}^+$	2.1269 [333]	2.1254	–	65.53
$2S_{\text{y}}$	Γ_5^+	2.1378 [72]	2.1401	4.22	11.16
$2S_{\text{y}}$	Γ_2^+	–	2.1414	–	1.31
$2P_{\text{y}}$	Γ_8^-	2.1484 [30]	2.1482	292.3	1.72
$2P_{\text{y}}$	Γ_7^-	–	2.1486	–	1.20
$1S_{\text{g}}$	Γ_5^+	2.1544 [72]	2.1535	65.25	42.41
$3S_{\text{y}}$	Γ_2^+	–	2.15974	–	0.44
$3S_{\text{y}}$	Γ_5^+	2.16027 [41, 173]	2.16053	7.83	3.29
$3P_{\text{y}}$	Γ_8^-	2.16135 [30]	2.16138	125.9	0.86
$3P_{\text{y}}$	Γ_7^-	–	2.16158	–	0.60
$3D_{\text{y}}$	$\Gamma_{3/4}^+$	2.16183 [41, 173]	2.16217	–	0.28
$3D_{\text{y}}$	Γ_5^+	2.16202 [41, 173]	2.16219	0.07	0.29
$3D_{\text{y}}$	$\Gamma_{1/4}^+$	–	2.16221	–	0.24
$3D_{\text{y}}$	$\Gamma_{3/4}^+$	–	2.16243	–	0.41
$3D_{\text{y}}$	Γ_5^+	2.16303 [41, 173]	2.16308	8.42	4.87
$4S_{\text{y}}$	Γ_2^+	–	2.16550	–	0.19
$4S_{\text{y}}$	Γ_5^+	2.16555 [41, 173]	2.16575	2.45	0.98
$4P_{\text{y}}$	Γ_8^-	2.16609 [30]	2.16612	58.29	0.43
$4P_{\text{y}}$	Γ_7^-	–	2.16621	–	0.31
$4D_{\text{y}}$	$\Gamma_{3/4}^+$	2.16629 [41, 173]	2.16646	–	0.17
$4D_{\text{y}}$	Γ_5^+	2.16638 [41, 173]	2.16647	0.53	0.18
$4D_{\text{y}}$	$\Gamma_{1/4}^+$	–	2.16648	–	0.15
$4F_{\text{y}}$	Γ_7^-	–	2.16653	–	0.12
$4F_{\text{y}}$	Γ_8^-	2.16652 [36]	2.16654	0.078	0.10
$4F_{\text{y}}$	Γ_8^-	2.16654 [36]	2.16657	0.002	0.08
$4F_{\text{y}}$	Γ_6^-	2.16654 [36]	2.16657	0.009	0.08

$4F_{\mathrm{y}}$	Γ_6^-	2.16658 [36]	2.16660	0.010	0.05
$4D_{\mathrm{y}}$	$\Gamma_{3/4}^+$	–	2.16661	–	0.19
$4D_{\mathrm{y}}$	Γ_5^+	2.16677 [41, 173]	2.16686	3.24	1.82
$5S_{\mathrm{y}}$	Γ_2^+	–	2.16800	–	0.09
$5S_{\mathrm{y}}$	Γ_5^+	2.16801 [41, 173]	2.16811	1.17	0.48
$5P_{\mathrm{y}}$	Γ_8^-	2.16829 [30]	2.16829	28.17	0.24
$5P_{\mathrm{y}}$	Γ_7^-	–	2.16834	–	0.17
$5D_{\mathrm{y}}$	$\Gamma_{3/4}^+$	2.16841 [41, 173]	2.16847	–	0.10
$5D_{\mathrm{y}}$	Γ_5^+	2.16846 [41, 173]	2.16847	0.04	0.12
$5D_{\mathrm{y}}$	$\Gamma_{1/4}^+$	–	2.16848	–	0.09
$5F_{\mathrm{y}}$	Γ_7^-	–	2.16850	–	0.09
$5F_{\mathrm{y}}$	Γ_8^-	2.16851 [36]	2.16851	0.078	0.07
$5F_{\mathrm{y}}$	Γ_8^-	2.16852 [36]	2.16852	0.000	0.06
$5F_{\mathrm{y}}$	Γ_6^-	2.16852 [36]	2.16853	0.001	0.06
$5F_{\mathrm{y}}$	Γ_6^-	2.16855 [36]	2.16855	0.001	0.04
$5D_{\mathrm{y}}$	$\Gamma_{3/4}^+$	–	2.16855	0.00	0.03
$5\bar{G}_{\mathrm{y}}$	Γ_5^+	–	2.16856	–	0.07
$5D_{\mathrm{y}}$	Γ_5^+	2.16860 [41, 173]	2.16868	1.68	0.92

7 Magnetoexcitons in cuprous oxide

We have shown in Chapters 4 and 6 that even without external fields the hydrogen-like model of excitons is incapable of describing the fine structure splitting observed experimentally and that it is inevitable to account for the complex valence band structure and the cubic symmetry O_h of $\mathrm{Cu_2O}$ in a quantitative theory.

This is all the more important in the presence of an external magnetic field, which reduces the symmetry of $\mathrm{Cu_2O}$ to a lower symmetry. For this reason one expects an extremely complex splitting of exciton lines in absorption spectra, in which also anticrossings appear. Hence, earlier theoretical treatments of these spectra using a hydrogen-like model were unable to describe the vast number of lines observed in experiments (see Refs. [71, 207, 334, 335] and further references therein).

Due to the specific material parameters in $\mathrm{Cu_2O}$, the exciton radius a_exc is much larger than the Bohr radius a_0 known from atomic physics. This makes excitons attractive for investigations in external fields [35] since the region of "high magnetic fields" can be reached within several Tesla, in contrast to the hydrogen atom, where this region begins above several hundreds of Tesla [35, 71].

The work on magnetoexcitons presented in this Chapter has been done in collaboration with the group of M. Bayer, D. Fröhlich, and M. Aßmann of the TU Dortmund. They used high resolution spectroscopy and natural crystals to obtain complex experimental absorption spectra for the $n \leq 7$ exciton states in Faraday configuration with a significantly better resolution than in previous work on this topic[1] [71, 207, 334, 335]. The experimenal setup is described in Ref. [39].

In this Chapter we present the theory for the exciton absorption spectra of $\mathrm{Cu_2O}$ in an external magnetic field in Secs. 7.1 and 7.2 and discuss the calculation of relative oscillator strengths for different orientations of the external magnetic field in Sec. 7.3. In Sec. 7.4 we investigate the symmetry of the Hamiltonian and compare theoretical with experimental spectra for different orientations of the magnetic field. We especially discuss the dependence of the spectra on the direction of the external magnetic field, which is well described by the anisotropic band structure and which cannot be understood from a simple hydrogen-like model. The comparison of theory and experiment shows an excellent agreement. It furthermore allows for the determination of a yet not precisely determined material parameter of $\mathrm{Cu_2O}$, i.e., the fourth Luttinger parameter κ. Essential parts of this Chapter have been published in Ref. [39] as part of a joined publication together with the experimental group of the TU Dortmund.

---

[1] See especially Refs. [71, 171, 207, 334–336] for previous works on excitons in external fields and Refs. [337, 338] for excitons in the presence of strain. The behavior of the $1S$-exciton under magnetic fields and strain has been studied, e.g., in Refs. [339–341].

7.1 Excitons in external fields

In this section we discuss the correct treatment of the effects on excitonic states when applying external fields to a solid. This will be done following the descriptions in Ref. [7] and using the results of Sec. 2.5.2. A treatment of excitons in external strain fields[2] can be found in [163].

7.1.1 Constant electric field

In a constant electric field the Stark term

$$-e\sum_{l=1}^{N}\boldsymbol{E}\cdot\boldsymbol{r}_l \tag{7.1}$$

has to be added to the Hamiltonian of Eq. (2.103). For reasons of simplicity we assume $\boldsymbol{E}$ to be oriented along the z-axis. The effects of external fields are usually small enough to treat them in perturbation theory. Therefore, we have to calculate matrix elements including the exciton ground state and different excited states. Some of those matrix elements vanish in advance, i.e., those with two wave functions of the same parity and those with states of different translational symmetry (due to the invariance of the Stark term under coordinate translation when neglecting irrelevant additive factors). Especially the the matrix element including two ground state functions Φ_0 (2.126) vanishes. The remaining matrix elements are

$$\int \Psi_{\nu\boldsymbol{K}}^{*}\sum_{l=1}^{N} z_l\Psi_{\nu'\boldsymbol{K}}\,\mathrm{d}\boldsymbol{r}_1\dots\mathrm{d}\boldsymbol{r}_N \tag{7.2a}$$

and

$$\int \Psi_{\nu\boldsymbol{0}}^{*}\sum_{l=1}^{N} z_l\Phi_0\,\mathrm{d}\boldsymbol{r}_1\dots\mathrm{d}\boldsymbol{r}_N. \tag{7.2b}$$

The first matrix element will vanish if the two exciton states $\Psi_{\nu\boldsymbol{K}}$ and $\Psi_{\nu'\boldsymbol{K}}$ do not describe the same electron *or* the same hole. Inserting the exciton wave function (2.220) in (7.2a) and neglecting two-center elements of z, one obtains

$$\sum_{\boldsymbol{\beta}} U_{\nu\boldsymbol{K}}^{*}(\boldsymbol{\beta})z_{mm'}(\boldsymbol{\beta})U_{\nu'\boldsymbol{K}}(\boldsymbol{\beta}) \tag{7.3}$$

with the abbreviation

$$z_{mm'}(\boldsymbol{\beta})=\int \mathrm{d}\boldsymbol{x}\; a_{m\boldsymbol{\beta}}^{*}(\boldsymbol{x})z a_{m'\boldsymbol{\beta}}(\boldsymbol{x}). \tag{7.4}$$

Here the Wannier functions (2.125) enter and m, m' denote the bands from which the exciton states are built. If $\Psi_{\nu\boldsymbol{K}}$ and $\Psi_{\nu'\boldsymbol{K}}$ have the hole in common, electronic states are labeled by m and m'; if $\Psi_{\nu\boldsymbol{K}}$ and $\Psi_{\nu'\boldsymbol{K}}$ have the electron in common, states of the hole are labeled by m and m'.

When considering the so-called *interband mixing* ($m \neq m'$), the matrix elements are usually very small compared to the difference in the energy of the states $\Psi_{\nu\boldsymbol{K}}$ and $\Psi_{\nu'\boldsymbol{K}}$. These elements will

---

[2] At this point we want to state that it is possible to trap excitons in harmonic strain traps [199, 342].

cause small quadratic effects [7]. In case of the *intraband mixing* ($m = m'$) we substitute $\boldsymbol{x}' = \boldsymbol{x} - \boldsymbol{\beta}$ in Eq. (7.4) to obtain

$$z_{mm}(\boldsymbol{\beta}) = \int \mathrm{d}\boldsymbol{x}'\; a^*_{m\boldsymbol{\beta}}(\boldsymbol{x}')(z' + \boldsymbol{\beta} \cdot \hat{\boldsymbol{e}}_z) a_{m\boldsymbol{\beta}}(\boldsymbol{x}') = 0 + \boldsymbol{\beta} \cdot \hat{\boldsymbol{e}}_z \tag{7.5}$$

if the crystal is symmetric under inversion. Furthermore, if the two bands involved are denoted by c and v, the full matrix element reads

$$-eE \sum_{\boldsymbol{\beta}} U^*_{vc\,\nu\boldsymbol{K}}(\boldsymbol{\beta})(\boldsymbol{\beta} \cdot \hat{\boldsymbol{e}}_z) U_{vc\,\nu'\boldsymbol{K}}(\boldsymbol{\beta}) \tag{7.6}$$

or with Eq. (2.220):

$$-e\boldsymbol{E} \cdot \sum_{\boldsymbol{\beta}} F^*_\nu(\boldsymbol{\beta})\boldsymbol{\beta} F_{\nu'}(\boldsymbol{\beta}) \tag{7.7}$$

According to the above derivation it is now justified to add the simple term

$$-e\boldsymbol{E} \cdot \boldsymbol{r} = -e\boldsymbol{E} \cdot \boldsymbol{r}_\mathrm{e} + e\boldsymbol{E} \cdot \boldsymbol{r}_\mathrm{h} \tag{7.8}$$

to the Hamiltonian (2.199) of the effective two-particle model if an external electric field is present.

The application of an external dc electric field leads in perturbation theory, as in atomic physics, to a quadratic or linear Stark effect, i.e., the exciton resonances are splitted and shifted. This can be illustrated by a simple model. Let us assume that there are only two exciton states $|S\rangle$ and $|P\rangle$ with the energies E_S and E_P and opposite parities. Since the operator $-e\boldsymbol{E} \cdot \boldsymbol{r}$ of Eq. (7.8) couples only states with opposite parity, a matrix representation of the complete Hamiltonian $H_\mathrm{ges} = H - e\boldsymbol{E} \cdot \boldsymbol{r}$ reads

$$H_\mathrm{ges} = \begin{pmatrix} E_S & -e\left\langle S \left| \boldsymbol{E} \cdot \boldsymbol{r} \right| P \right\rangle \\ -e\left\langle P \left| \boldsymbol{E} \cdot \boldsymbol{r} \right| S \right\rangle & E_P \end{pmatrix} = \begin{pmatrix} E_S & \gamma_{SP} \\ \gamma_{SP} & E_P \end{pmatrix}. \tag{7.9}$$

After introducing the abbreviations $E_\mathrm{a} = (E_S + E_P)/2$ and $E_\mathrm{d} = (E_S - E_P)/2$, the eigenenergies of H_ges are

$$E_{1,2} = E_\mathrm{a} \pm \sqrt{E_\mathrm{d}^2 + \gamma_{SP}^2}. \tag{7.10}$$

If we now consider the two limiting cases of $E_\mathrm{d} \to 0$ and $E_\mathrm{d} \gg \gamma_{SP}$, we obtain the linear Stark effect ($\sim E$) for almost degenerate states,

$$E_{1,2} = E_\mathrm{a} \pm e\left\langle S \left| \boldsymbol{E} \cdot \boldsymbol{r} \right| P \right\rangle, \tag{7.11}$$

and the quadratic Stark effect ($\sim E^2$) if the perturbation by the electric field is small in comparison to the energetic difference of the two states involved

$$E_{1,2} = E_\mathrm{a} \pm E_\mathrm{d} \left[1 + \frac{e^2 \left| \left\langle S \left| \boldsymbol{E} \cdot \boldsymbol{r} \right| P \right\rangle \right|^2}{2E_\mathrm{d}^2} \right]. \tag{7.12}$$

In general, one has to consider all exciton states when treating the Stark effect. Within the simple hydrogen-like model of excitons one can evaluate the matrix elements $\langle F_{n'L'M'} | eEz | F_{nLM} \rangle$ to show that the Stark effect is strongest between exciton states with $\Delta n = 0$ and $\Delta L = \pm 1$ [343]. However, even within the hydrogen-like model one has to consider the total symmetry of the exciton. In doing so, it can be shown that, e.g., in Faraday configuration with an electric field in [110] direction and with light, which is linearly polarized in $[1\bar{1}0]$ direction, no coupling between S and P excitons occurs [173].

In absorption spectroscopy experiments on excitons in external electric fields one has to consider the attenuation of the field by free charge carriers in the crystal. The laser light excites not only excitons but also free charge carriers at impurity atoms or vacancies, which are then separated by the applied electric field and thus set up an electric field counteracting the external field. This effect can be minimized by reducing the laser power and by applying an alternating electric field [173].

Due to the electric field the bands in the solid are also tilted, for which reason the wave functions of hole and electron can tunnel into the gap. Thus the band-to-band absorption tail is red-shifted and an oscillatory structure appears in the range of the continuum states [12]. To observe the Stark effect the value eEa_{exc} has to be comparable with or larger than the width Δ_{LT} of the absorption bands[3]. However, these strong fields can destroy the exciton by two effects:

- The exciton tunnels through the Coulomb barrier.
- Other carriers are accelerated in the electric field to an amount that they ionize the exciton in a collision (impact ionization).

Hence, it is difficult to observe the Stark effect in experiments for excitons with high principal quantum numbers. Furthermore, high electric fields may cause currents, which can heat the semiconductor and thus lead to dissipative effects.

Within the hydrogen-like model of excitons one can estimate the electric field strength at which the ionization of the exciton occurs by considering the potential difference across the extension of the exciton wave function [173, 344]. Setting

$$\Delta\Phi = deE = 2\langle r\rangle eE = \frac{R_{\mathrm{exc}}}{n^2}, \tag{7.13}$$

with the dipole moment d, we obtain

$$E = \frac{R_{\mathrm{exc}}}{ea_{\mathrm{exc}}\left[3n^2 - L(L+1)\right] n^2}. \tag{7.14}$$

The first experimental observation of the Stark effect has been reported in 1954 by Gross *et al.* [345] using $\mathrm{Cu_2O}$. A discussion of the Stark effect on crystals without inversion symmetry can, e.g., be found in [7, 346, 347]. Recently, an investigation of high-resolution absorption spectra of excitons in electric fields in $\mathrm{Cu_2O}$ has been published [41].

7.1.2 Constant magnetic field

According to the results of the previous section on electric fields, we can describe the effect of a uniform external magnetic field on exciton states simply by performing the minimal substitution in the effective two-particle model. The Hamiltonian (2.197) then reads

$$H_{\mathrm{e-h}} = E_{\mathrm{g}} + \frac{1}{2m_{\mathrm{e}}}(\boldsymbol{p}_{\mathrm{e}} + e\boldsymbol{A}(\boldsymbol{r}_{\mathrm{e}}))^2 + \frac{1}{2m_{\mathrm{h}}}(\boldsymbol{p}_{\mathrm{h}} - e\boldsymbol{A}(\boldsymbol{r}_{\mathrm{h}}))^2 - \frac{e^2}{4\pi\varepsilon_0\varepsilon\left|\boldsymbol{r}_{\mathrm{e}} - \boldsymbol{r}_{\mathrm{h}}\right|} \tag{7.15}$$

with the vector potential

$$\boldsymbol{A}(\boldsymbol{r}) = \frac{1}{2}(\boldsymbol{B}\times\boldsymbol{r}). \tag{7.16}$$

---

[3] For the LT-splitting see, e.g., Sec. 5.1.2.

Additionally, since electron and hole are spin-$\frac{1}{2}$-particles, the term

$$H_B = \mu_\mathrm{B}\left[g_c\boldsymbol{S}_\mathrm{e} + g_v\boldsymbol{S}_\mathrm{h}\right]\cdot\boldsymbol{B}/\hbar \tag{7.17}$$

with the g-values of the conduction band and the valence band[4] has to be added to $H_{\mathrm{e-h}}$.

It is now possible to define a generalized momentum operator [348]

$$\boldsymbol{P} = \sum_{i=1}^{2}(\boldsymbol{p}_i + \frac{q_i}{2}\boldsymbol{B}\times\boldsymbol{r}_i) = \boldsymbol{P}_0 - \frac{e}{2}(\boldsymbol{B}\times\boldsymbol{r}), \tag{7.18}$$

which commutes with $H_{\mathrm{e-h}}$ and which is, hence, a constant of motion. Since

$$q_\mathrm{e} = -e = -q_\mathrm{h} \tag{7.19}$$

holds, the components of $\boldsymbol{P}$ commute, i.e., $[\boldsymbol{P}_i,\, \boldsymbol{P}_j] = 0$. Making the ansatz

$$\psi(\boldsymbol{r},\, \boldsymbol{R}) = e^{i(\boldsymbol{K}+\frac{e}{2\hbar}\boldsymbol{B}\times\boldsymbol{r})\cdot\boldsymbol{R}}F(\boldsymbol{r}), \tag{7.20}$$

an eigenvalue equation for $F(\boldsymbol{r})$ can be obtained:

$$\begin{aligned} H_\mathrm{rel}F(\boldsymbol{r}) \quad = \quad & \left[\frac{\hbar^2\boldsymbol{K}^2}{2M} + \frac{1}{2\mu}\boldsymbol{p}^2 - \frac{e^2}{4\pi\varepsilon_0\varepsilon\,|\boldsymbol{r}|} + \frac{e}{2}\left(\frac{1}{m_\mathrm{e}} - \frac{1}{m_\mathrm{h}}\right)\boldsymbol{B}\cdot(\boldsymbol{r}\times\boldsymbol{p})\right. \\ & \left. + \frac{e^2}{8\mu}(\boldsymbol{B}\times\boldsymbol{r})^2 + \frac{e}{M}(\hbar\boldsymbol{K}\times\boldsymbol{B})\cdot\boldsymbol{r} + H_B\right]F(\boldsymbol{r}) = E\,F(\boldsymbol{r}). \end{aligned} \tag{7.21}$$

Beside the paramagnetic term $\sim \boldsymbol{B}\cdot(\boldsymbol{r}\times\boldsymbol{p})$ and the diamagnetic term $\sim (\boldsymbol{B}\times\boldsymbol{r})^2$ the additional field-dependent term $\sim (\hbar\boldsymbol{K}\times\boldsymbol{B})\cdot\boldsymbol{r}$ appears, which describes the quasi-electric field noticed by the exciton due to the motion of the center of mass [7]. This is the so-called *motional Stark effect.*

When applying an external magnetic field one has to compare the size of the cyclotron energy $\hbar\omega_\mathrm{c} = \hbar eB/\mu$ with that of the excitonic Rydberg energy R_exc. The special cases of $\gamma = \hbar\omega_\mathrm{c}/R_\mathrm{exc} \ll 1$ and $\gamma \gg 1$ characterize the weak and strong field limit, respectively. In the weak field limit one can treat the magnetic field as a perturbation. Within perturbation theory other states are weakly admixed to a distinct state. This can be described from a classical point of view as a deformation of the relative motion of the hole and the electron by Lorentz forces or as a squeezing of the wave function because of the additional (diamagnetic) parabolic potential $V = e^2B^2\,(x^2+y^2)/(8m)$. Due to this admixture an angular momentum results, which is proportional to B. This momentum interacts with the magnetic field leading the so-called diamagnetic shift of the energy levels to higher energies:

$$\Delta E_\mathrm{dia} = aB^2. \tag{7.22}$$

The material parameter a, which depends on a_exc and n, increases with increasing quantum number n.

In the strong field limit one has to consider at first the Landau levels and then the Coulomb interaction as a perturbation [349, 350]. The Landau levels describe the energy states of electrons in an external magnetic field, which result from a quantization of the motion of the electrons perpendicular to $\boldsymbol{B}$:

$$E(n_l,\, \boldsymbol{k}_\parallel) = E_0 + \hbar\omega_\mathrm{c}\left(n_l + \frac{1}{2}\right) + \frac{\hbar^2\boldsymbol{k}_\parallel^2}{2m^*}. \tag{7.23}$$

---

[4] The hole and electron g-factors and can significantly deviate from two, because of influences of the crystal symmetry or of the band structure.

E_0 denotes the band extremum for $B = 0$ and the quantum numbers n_l denote the different Landau levels. In the case of parabolic bands the selection rules for intraband and interband transitions read $\Delta n_l = \pm 1$ and $n_{l,\mathrm{CB}} - n_{l,\mathrm{VB}} = 0$, respectively. A theoretical derivation or description of Landau niveaus is given in Ref. [85].

At last, we want to state that an exhaustive review on external fields can be found in Refs. [17, 351] relating to constant fields and in Refs. [352–354] relating to modulation techniques. Further examples for different semiconductors in external fields comprising electric, magnetic and strain fields, are treated, e.g., in Refs. [7, 12] and further references therein.

7.2 Hamiltonian of magnetoexcitons in Cu_2O

The Hamiltonian of an exciton of odd parity in Cu_2O is given by Eq. (4.7) without exchange interaction and central-cell corrections:

$$H = E_{\mathrm{g}} + H_{\mathrm{e}}(\boldsymbol{p}_{\mathrm{e}}) + H_{\mathrm{h}}(\boldsymbol{p}_{\mathrm{h}}) + V(\boldsymbol{r}_e - \boldsymbol{r}_h). \tag{7.24}$$

We do not consider the exciton states of even parity in this chapter since they are dipole-forbidden in one-photon absorption and since a magnetic field does not lead to a mixing of the even and the odd series.

In the presence of an external magnetic field, the corresponding Hamiltonian is obtained via the minimal substitution as has been shown in Sec. 7.1. After introducing relative and center of mass coordinates [355, 356] and setting the position and momentum of the center of mass to zero, the Hamiltonian of the relative motion reads [7, 281, 355–359]

$$H \;=\; E_{\mathrm{g}} + H_{\mathrm{e}}(\boldsymbol{p} + e\boldsymbol{A}(\boldsymbol{r})) + H_{\mathrm{h}}(-\boldsymbol{p} + e\boldsymbol{A}(\boldsymbol{r})) + V(\boldsymbol{r}) + H_B. \tag{7.25}$$

Since the magnetic field $\boldsymbol{B}$ is constant in our experiments, we use the vector potential $\boldsymbol{A} = (\boldsymbol{B}\times\boldsymbol{r})/2$. The term H_B describes the energy of the spins in the magnetic field for the case of degenerate bands [126, 281, 318, 358]:

$$H_B = \mu_{\mathrm{B}}\left[g_c\boldsymbol{S}_{\mathrm{e}} + (3\kappa + g_s/2)\boldsymbol{I} - g_s\boldsymbol{S}_{\mathrm{h}}\right]\cdot\boldsymbol{B}/\hbar. \tag{7.26}$$

Here μ_B denotes the Bohr magneton, $g_s \approx 2$ the g-factor of the hole spin S_{h}, g_c the g-factor of the conduction band or the electron spin S_{e}. The value of the fourth Luttinger parameter κ is unknown and will be determined in Sec. 7.4. In the case of a finite spin-orbit coupling Δ an additional term would generally appear in H_B, which depends on the fifth Luttinger parameter q [126, 281, 318]. However, this term is connected with spin-orbit interactions of higher order [281] and is not considered here.

For the case that the magnetic field is oriented along one of the directions of high symmetry, i.e., along the [001], [110] or [111] direction, we rotate the coordinate system to make the quantization axis coincide with the direction of the magnetic field and then express the Hamiltonian (7.25) in terms of irreducible tensors [79, 248, 281] (see Appendix D.1). We can then and write the Schrödinger equation corresponding to the Hamiltonian (7.25) as a generalized eigenvalue problem by analogy with Eq. (4.24) using the complete basis of Sec. 4.3. The generalized eigenvalue problem is finally solved using an appropriate LAPACK routine [284].

7.3 Oscillator strengths

With the solutions of the eigenvalue problem mentioned at the end of Sec. 7.2 one can directly calculate the relative oscillator strengths for the transitions from the ground state of the solid to the exciton states.

In the presence of an external magnetic field the operator $\boldsymbol{A}_{\mathrm{rad}} \cdot \boldsymbol{p}$, which describes the interaction between the radiation field or light and the exciton and which enters the dipole matrix element, has to be replaced by $\boldsymbol{A}_{\mathrm{rad}} \cdot [\boldsymbol{p} + e\boldsymbol{A}(\boldsymbol{r})]$ due to the minimal substitution. However, the second term is generally small in comparison to the first one and it vanishes in the Faraday configuration considered here [10, 236, 360].

Nevertheless, we have to consider that the magnetic field reduces the symmetry of the system. Furthermore, since the incident light is oriented parallel to $\boldsymbol{B}$ and since we choose the quantization axis parallel to $\boldsymbol{B}$, we have to find the correct linear combinations of the states of Eq. (4.58), which then describe linearly or circularly polarized light for the three orientations of the magnetic field considered here. This will be done in the following.

7.3.1 Magnetic field in [001] direction

In a magnetic field, which is oriented along the [001] direction, the symmetry O_{h} of the system is reduced to $C_{4\mathrm{h}}$ and we have to consider the reduction of the irreducible representation Γ_4^- of O_{h}, which is connected with the dipole operator (cf. Sec. 4.4), by the group $C_{4\mathrm{h}}$:

$$\Gamma_4^- \rightarrow \Gamma_1^- \oplus \Gamma_3^- \oplus \Gamma_4^- . \tag{7.27}$$

On the one hand, using the method of projection operators [169], we can determine the correct linear combinations of the states in Eq. (4.58) which transform according to the irreducible representations of $C_{4\mathrm{h}}$. On the other hand, it is instructive that the correct linear combinations are given according to the direction of $\boldsymbol{K}$ and the polarization vectors $\hat{\boldsymbol{e}}_{\xi\boldsymbol{K}}$ transverse to $\boldsymbol{K}$:

$$\hat{\boldsymbol{K}} = (0,\, 0,\, 1)^{\mathrm{T}}, \qquad \hat{\boldsymbol{e}}_{1\boldsymbol{K}} = (1,\, 0,\, 0)^{\mathrm{T}}, \qquad \hat{\boldsymbol{e}}_{2\boldsymbol{K}} = (0,\, 1,\, 0)^{\mathrm{T}}. \tag{7.28}$$

The correct linear combinations of the states (4.58) are

$$\Gamma_1^- : |L_{\boldsymbol{K}}^D\rangle = |\pi_z^D\rangle, \tag{7.29a}$$

$$\Gamma_3^- : |T_{+\boldsymbol{K}}^D\rangle = -i\left[|T_{1\boldsymbol{K}}^D\rangle + i|T_{2\boldsymbol{K}}^D\rangle\right]/\sqrt{2} = |2,\, -1\rangle_D\,, \tag{7.29b}$$

$$\Gamma_4^- : |T_{-\boldsymbol{K}}^D\rangle = i\left[|T_{1\boldsymbol{K}}^D\rangle - i|T_{2\boldsymbol{K}}^D\rangle\right]/\sqrt{2} = -\,|2,\, 1\rangle_D\,, \tag{7.29c}$$

with

$$|T_{1\boldsymbol{K}}^D\rangle = |\pi_x^D\rangle \qquad \text{and} \qquad |T_{2\boldsymbol{K}}^D\rangle = |\pi_y^D\rangle, \tag{7.30}$$

Since light is always transverse polarized, only states of symmetry Γ_3^- and Γ_4^- are allowed. Note that Γ_3^- and Γ_4^- are connected with circularly polarized light [90]. The sign ± is defined by the direction of rotation of the polarization with respect to $\boldsymbol{K}$. We calculate the relative oscillator strengths by evaluating

$$f_{\xi\nu\boldsymbol{K}}^{\mathrm{rel}} = \left| \lim_{r\to 0} \frac{\partial}{\partial r} \langle T_{\pm\boldsymbol{K}}^D | \Psi_{\nu\boldsymbol{K}} \rangle \right|^2 . \tag{7.31}$$

7.3.2 Magnetic field in [110] direction

In a magnetic field, which is directed in [110] direction, the symmetry O_{h} of the system is reduced to $C_{2\mathrm{h}}$. In this case the reduction of the irreducible representation Γ_4^- of O_{h} by the group $C_{4\mathrm{h}}$ reads

$$\Gamma_4^- \to \Gamma_1^- \oplus \Gamma_2^- \oplus \Gamma_2^- \tag{7.32}$$

The corresponding vectors are

$$\hat{\boldsymbol{K}} = (1,\, 1,\, 0)^{\mathrm{T}}/\sqrt{2}, \qquad \hat{\boldsymbol{e}}_{1\boldsymbol{K}} = (0,\, 0,\, 1)^{\mathrm{T}}, \qquad \hat{\boldsymbol{e}}_{2\boldsymbol{K}} = (1,\, -1,\, 0)^{\mathrm{T}}/\sqrt{2}, \tag{7.33}$$

so that the correct linear combinations of the states (4.58) read

$$\Gamma_1^- : |L_{\boldsymbol{K}}^D\rangle = \left[|\pi_x^D\rangle + |\pi_y^D\rangle\right]/\sqrt{2}, \tag{7.34a}$$

$$\Gamma_2^- : |T_{1\boldsymbol{K}}^D\rangle = |\pi_z^D\rangle, \tag{7.34b}$$

$$\Gamma_2^- : |T_{2\boldsymbol{K}}^D\rangle = \left[|\pi_x^D\rangle - |\pi_y^D\rangle\right]/\sqrt{2}. \tag{7.34c}$$

We see that Γ_1^- is connected with light which is linearly polarized along [110] and that Γ_2^- is connected with transverse polarized light in [001] and [1$\bar{1}$0] direction. Since the states $|T_{1\boldsymbol{K}}^D\rangle$ and $|T_{2\boldsymbol{K}}^D\rangle$ transform according to the same irreducible representation, we can also use the following linear combinations, which describe circularly polarized light:

$$\Gamma_2^- : \mp\frac{i}{\sqrt{2}}\left[|T_{1\boldsymbol{K}}^D\rangle \pm i|T_{2\boldsymbol{K}}^D\rangle\right]. \tag{7.35}$$

We now choose the quantization axis parallel to $\boldsymbol{B}$, i.e., we rotate the coordinate system by the Euler angles $(\alpha,\, \beta,\, \gamma) = (\pi,\, \pi/2,\, \pi/4)$. This coordinate transformation reads

$$\boldsymbol{r}' = \begin{pmatrix} x' \\ y' \\ z' \end{pmatrix} = \frac{1}{\sqrt{2}}\begin{pmatrix} 0 & 0 & \sqrt{2} \\ 1 & -1 & 0 \\ 1 & 1 & 0 \end{pmatrix}\begin{pmatrix} x \\ y \\ z \end{pmatrix} = \boldsymbol{R}\boldsymbol{r}. \tag{7.36}$$

Note that the direction of the x' and y' axis are predefined by the crystal axes. Rotating the states of Eq. (7.34) as well yields

$$|L_{\boldsymbol{K}}'^D\rangle = \left[|2,\, -1\rangle_D - |2,\, 1\rangle_D\right]/\sqrt{2}, \tag{7.37a}$$

$$|T_{1\boldsymbol{K}}'^D\rangle = \sqrt{3}\,|2,\, 0\rangle_D/2 + \left[|2,\, -2\rangle_D + |2,\, 2\rangle_D\right]/\sqrt{8}, \tag{7.37b}$$

$$|T_{2\boldsymbol{K}}'^D\rangle = i\left[|2,\, 2\rangle_D - |2,\, -2\rangle_D\right]/\sqrt{2}. \tag{7.37c}$$

Finally, we calculate the relative oscillator strengths by evaluating

$$f_{\nu\xi\boldsymbol{K}}^{\mathrm{rel}} = \left|\lim_{r\to 0}\frac{\partial}{\partial r}\langle T_{\xi\boldsymbol{K}}'^D|\Psi_{\nu\boldsymbol{K}}\rangle\right|^2 \tag{7.38}$$

for light which is polarized in [001] or in [1$\bar{1}$0] direction.

The fact that $|T_{1\boldsymbol{K}}'^D\rangle$ and $|T_{2\boldsymbol{K}}'^D\rangle$ transform according to the same irreducible representation Γ_2^- has a significant influence on the exciton spectra: In the two other cases $\boldsymbol{B} \parallel [001]$ and $\boldsymbol{B} \parallel [111]$ a certain exciton state can be excited only by σ^+ *or* by σ^- polarized light. For $\boldsymbol{B} \parallel [110]$ it is possible to excite a certain exciton state by $\pi_{x'}$ *and* by $\pi_{y'}$ polarized light or consequently also by σ^+ *and* by σ^- polarized light. The exciton states are thus elliptically polarized. It is obvious that due the lattice of the solid the two directions [001] and [1$\bar{1}$0] are the principal axes of this ellipsoid. These axes are (group-theoretically) not equivalent. Otherwise [110] would not be a twofold but a fourfold axis. One can see from Eq. (7.37) that the phase shift between $|\pi_{x'}\rangle$ and $|\pi_{y'}\rangle$ is $\pi/2$. Hence, we can calculate the ellipticity of the exciton states by evaluating

$$\phi = \arctan\left(\frac{i\,\langle T'^{D}_{1\boldsymbol{K}}|\Psi(\boldsymbol{r})\rangle}{\langle T'^{D}_{2\boldsymbol{K}}|\Psi(\boldsymbol{r})\rangle}\right), \tag{7.39}$$

which is $\pm\pi/2$ or 0 for linearly polarized light and $\pm\pi/4$ for circularly polarized light.

7.3.3 Magnetic field in [111] direction

In a magnetic field, which is directed in [111] direction, the symmetry O_h of the system is reduced to $C_{3\mathrm{i}}$. In this case we have

$$\Gamma_4^- \to \Gamma_1^- \oplus \Gamma_2^- \oplus \Gamma_3^- \tag{7.40}$$

with the vectors

$$\hat{\boldsymbol{K}} = (1,\,1,\,1)^\mathrm{T}/\sqrt{3}, \qquad \hat{\boldsymbol{e}}_{1\boldsymbol{K}} = = (1,\,1,\,-2)^\mathrm{T}/\sqrt{6}, \qquad \hat{\boldsymbol{e}}_{2\boldsymbol{K}} = = (-1,\,1,\,0)^\mathrm{T}/\sqrt{2}. \tag{7.41}$$

The correct linear combinations of the states in Eqs. (4.58) are therefore

$$\Gamma_1^- : |L^D_{\boldsymbol{K}}\rangle \ = \ |\pi^D_z\rangle, \tag{7.42a}$$

$$\Gamma_2^- : |T^D_{+\boldsymbol{K}}\rangle = \ -i\left[|T^D_{1\boldsymbol{K}}\rangle + i|T^D_{2\boldsymbol{K}}\rangle\right]/\sqrt{2}, \tag{7.42b}$$

$$\Gamma_3^- : |T^D_{-\boldsymbol{K}}\rangle = \ \ i\left[|T^D_{1\boldsymbol{K}}\rangle - i|T^D_{2\boldsymbol{K}}\rangle\right]/\sqrt{2}, \tag{7.42c}$$

with

$$\begin{aligned}|T^D_{1\boldsymbol{K}}\rangle &= \left[\left|\pi^D_x\right\rangle + \left|\pi^D_y\right\rangle - 2\left|\pi^D_z\right\rangle\right]/\sqrt{6},\\ |T^D_{2\boldsymbol{K}}\rangle &= \left[-\left|\pi^D_x\right\rangle + \left|\pi^D_y\right\rangle\right]/\sqrt{2}.\end{aligned} \tag{7.43}$$

We now rotate the coordinate system by the Euler angles $(\alpha,\,\beta,\,\gamma) = (0,\,\arccos(1/\sqrt{3}),\,\pi/4)$. This coordinate transformation reads

$$\boldsymbol{r}'' = \begin{pmatrix} x'' \\ y'' \\ z'' \end{pmatrix} = \frac{1}{\sqrt{6}}\begin{pmatrix} 1 & 1 & -2 \\ -\sqrt{3} & \sqrt{3} & 0 \\ \sqrt{2} & \sqrt{2} & \sqrt{2} \end{pmatrix}\begin{pmatrix} x \\ y \\ z \end{pmatrix} = \boldsymbol{R}\,\boldsymbol{r}. \tag{7.44}$$

Rotating the states of Eq. (7.42) yields

$$|L''^D_{\boldsymbol{K}}\rangle = \ |2,\,0\rangle_D\,, \tag{7.45a}$$

$$|T''^D_{+\boldsymbol{K}}\rangle = \ \ i\left[\sqrt{2}\,|2,\,-2\rangle_D - |2,\,1\rangle_D\right]/\sqrt{3}, \tag{7.45b}$$

$$|T''^D_{-\boldsymbol{K}}\rangle = \ -i\left[\sqrt{2}\,|2,\,2\rangle_D + |2,\,-1\rangle_D\right]/\sqrt{3}. \tag{7.45c}$$

We finally calculate the relative oscillator strengths by evaluating

$$f^\mathrm{rel}_{\xi\nu\boldsymbol{K}} = \left|\lim_{r\to 0}\frac{\partial}{\partial r}\langle T''^D_{\pm\boldsymbol{K}}|\Psi_{\nu\boldsymbol{K}}\rangle\right|^2. \tag{7.46}$$

7.4 Comparison of experimental and theoretical results

In this section we will compare the theoretical results for magnetoexcitons with experimental high resolution abosprtion spectra recorded by the group of M. Bayer, D. Fröhlich and M. Aßmann of the TU Dortmund. The emphasis in this section is on the theoretical results. For the experimenal setup and a further discussion of the experimental results we refer to Ref. [39].

First we determine the maximum number of dipole-allowed exciton states via group theoretical considerations. In this way, we can also show that the external magnetic field lifts all degeneracies of the exciton states. In the spherical approximation, in which the cubic part of the Hamiltonian is neglected, the angular momentum F is a good quantum number. However, if the complete Hamiltonian is treated, the reduction of the irreducible representations D^F of the rotation group by the cubic group O_h has to be considered [169].

The symmetry of an exciton state is given by the symmetry of the envelope function, the valence band, and the conduction band:

$$\Gamma_\mathrm{exc} = \Gamma_\mathrm{env} \otimes \Gamma_\mathrm{v} \otimes \Gamma_\mathrm{c}. \tag{7.47}$$

As the quasi-spin I already enters the angular momentum F, we obtain the combined symmetry of the envelope function and the hole in the reduction of the representations D^F of the full rotation group:

$$\begin{aligned}
\tilde{D}^{\frac{1}{2}} &= D^{\frac{1}{2}} \otimes \Gamma_2^+ &&= \Gamma_6^- \otimes \Gamma_2^+ = \Gamma_7^-, && \text{(7.48a)}\\
\tilde{D}^{\frac{3}{2}} &= D^{\frac{3}{2}} \otimes \Gamma_2^+ &&= \Gamma_8^- \otimes \Gamma_2^+ = \Gamma_8^-, && \text{(7.48b)}\\
\tilde{D}^{\frac{5}{2}} &= D^{\frac{5}{2}} \otimes \Gamma_2^+ &&= (\Gamma_7^- \oplus \Gamma_8^-) \otimes \Gamma_2^+ = \Gamma_6^- \oplus \Gamma_8^-, && \text{(7.48c)}\\
\tilde{D}^{\frac{7}{2}} &= D^{\frac{7}{2}} \otimes \Gamma_2^+ &&= (\Gamma_6^- \oplus \Gamma_7^- \oplus \Gamma_8^-) \otimes \Gamma_2^+ = \Gamma_7^- \oplus \Gamma_6^- \oplus \Gamma_8^-. && \text{(7.48d)}
\end{aligned}$$

It can be seen that there are two exciton states for $n = 2$ or $n = 3$ and seven exciton states for $n = 4$ or $n = 5$. Including the symmetry Γ_6^+ of the electron or the conduction band, the total symmetry of the exciton is

$$\begin{aligned}
\Gamma_\mathrm{exc}^{\frac{1}{2}} &= \tilde{D}^{\frac{1}{2}} \otimes \Gamma_6^+ &&= (\Gamma_2^- \oplus \Gamma_5^-), && \text{(7.49a)}\\
\Gamma_\mathrm{exc}^{\frac{3}{2}} &= \tilde{D}^{\frac{3}{2}} \otimes \Gamma_6^+ &&= (\Gamma_3^- \oplus \Gamma_4^- \oplus \Gamma_5^-), && \text{(7.49b)}\\
\Gamma_\mathrm{exc}^{\frac{5}{2}} &= \tilde{D}^{\frac{5}{2}} \otimes \Gamma_6^+ &&= (\Gamma_1^- \oplus \Gamma_4^-) \oplus (\Gamma_3^- \oplus \Gamma_4^- \oplus \Gamma_5^-), && \text{(7.49c)}\\
\Gamma_\mathrm{exc}^{\frac{7}{2}} &= \tilde{D}^{\frac{7}{2}} \otimes \Gamma_6^+ &&= (\Gamma_1^- \oplus \Gamma_4^-) \oplus (\Gamma_2^- \oplus \Gamma_5^-) \oplus (\Gamma_3^- \oplus \Gamma_4^- \oplus \Gamma_5^-), && \text{(7.49d)}
\end{aligned}$$

respectively. Since the symmetries in parentheses belong to degenerate states, there are fourfold and eightfold degenerate states.

In the presence of a magnetic field being oriented along one of the crystal axis, we have to consider the reduction of the irreducible representations of the cubic group O_h by the group $C_{4\mathrm{h}}$ [90]:

$$\begin{aligned}
&\Gamma_1^- \to \Gamma_1^-, \qquad \Gamma_2^- \to \Gamma_2^-, \qquad && \Gamma_3^- \to \Gamma_1^- \oplus \Gamma_2^-,\\
&\Gamma_4^- \to \Gamma_1^- \oplus \Gamma_3^- \oplus \Gamma_4^-, && \Gamma_5^- \to \Gamma_2^- \oplus \Gamma_3^- \oplus \Gamma_4^-.
\end{aligned} \tag{7.50}$$

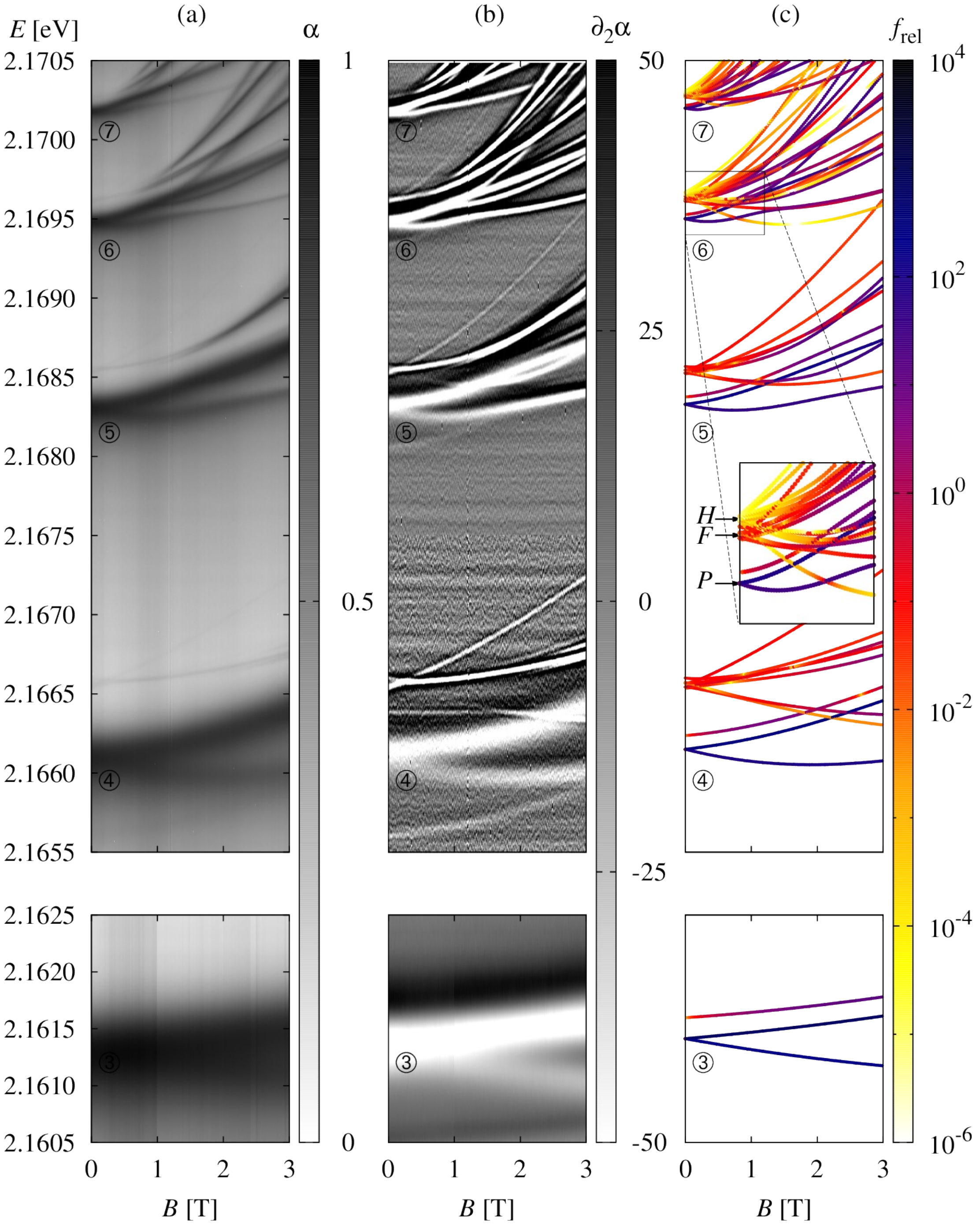

Figure 7.1.: Spectra of the $n = 3 \ldots 7$ excitons in an external magnetic field $\boldsymbol{B} \parallel [001]$ for σ^- polarized light. (a) Experimental absorption spectrum. (b) Second derivative of the experimental absorption spectrum. The absorption constant α and the value of $\partial_2\alpha$ are given in arbitrary units. (c) Theoretical line spectrum for $\kappa = -0.5$. The colorbar shows the calculated relative oscillator strength in arbitrary units. For further information see text.

Inserting these relations in Eq. (7.49), we see that degeneracies are further lifted. Since all irreducible representations of $C_{4\mathrm{h}}$ are one-dimensional, we expect that all degeneracies are lifted so that there are 12 exciton states for $n = 2$ or $n = 3$ and 40 exciton states for $n = 4$ or $n = 5$. Since only the states with the symmetry Γ_3^- and Γ_4^- are dipole-allowed, we immediately see that out of these only 6 states are dipole-allowed for $n = 2$ or $n = 3$ and 20 for $n = 4$ or $n = 5$. In the same manner we can also treat the special cases of a magnetic field being oriented along the [110] and the [111] direction, i.e., we have to consider the reduction of the irreducible representations of the cubic group O_h by the groups $C_{2\mathrm{h}}$ and $C_{3\mathrm{i}}$ [90]. Since all irreducible representations of these groups are one-dimensional we also expect that all degeneracies are lifted and that there are 12 exciton states for $n = 2$ or $n = 3$ and 40 exciton states for $n = 4$ or $n = 5$. However, if we consider only the number of dipole-allowed states we find that there are 6 ($n = 2$, 3) and 20 ($n = 4$, 5) dipole-allowed states for $\boldsymbol{B} \parallel [110]$ but 8 ($n = 2$, 3) and 26 ($n = 4$, 5) dipole-allowed states for $\boldsymbol{B} \parallel [111]$.

For a first overview we show the experimental spectra for $\boldsymbol{B} \parallel [001]$ along with theoretical results for $n = 3 \ldots 7$ in Fig. 7.1. In the special case of $\gamma_2 = \gamma_3 = \eta_i = 0$ the angular momentum L would be a good quantum number and due to the selection rules discussed in Sec. 7.3 only P excitons would be observable in this case. However, even without a magnetic field the complete Hamiltonian couples different exciton states with odd values of L so that also exciton states with higher angular momentum gain a small oscillator strength. This can be seen clearly from the theoretically calculated spectrum in the panel (c) of Fig. 7.1.

Since $L \leq n - 1$ holds, the number of exciton lines for $n \geq 6$ is very high and a quantitative analysis is hardly possible. Hence, we concentrate on the $n = 3$ and $n = 5$ exciton states in the following. The theoretical exciton spectra of these excitons in a magnetic field of $B \leq 3\,\mathrm{T}$ with $\boldsymbol{B} \parallel [001]$ are depicted in Fig. 7.2 along with the exciton states read from experimental data. From Figs. 7.2(b) and 7.2(d) one can clearly distinguish between the contribution of the P excitons and the F excitons at $B = 0\,\mathrm{T}$ (cf. also Sec. 4.5.1). It can be seen that the relative oscillator strength of F excitons significantly increases due to state mixing with growing field strength.

By comparing the experimentally observed line splitting to our results, we can estimate the value of the fourth Luttinger parameter to

$$\kappa = -0.50 \pm 0.10 \tag{7.51}$$

provided that the values listed in Table 2.2 are correct (cf. also the discussion in Sec. 3.3.2). Using this value in our numerical calculations, we obtain an excellent agreement between theory and experiment for both $n = 3$ and $n = 5$ excitons in Fig. 7.2. The value of κ is further confirmed by the fact that only one exciton state can be observed at $B = 3$ T and $E \approx 2.1687$ eV in the experiment for σ^+ polarized light [see Figs. 7.2(a) and 7.2(b)]. Only if $-0.52 < \kappa < -0.46$ holds, theory predicts two nearly degenerate states. For other values of κ, i.e., for $\kappa > -0.4$ or $\kappa < -0.6$, this degeneracy is lifted and two states should be observable in the experiment.

We can now use the value of $\kappa = -0.50$ to calculate the exciton spectra for $\boldsymbol{B} \parallel [110]$ and $\boldsymbol{B} \parallel [111]$. The results are shown in Fig. 7.3. We observe not only an excellent agreement with the experimental results but also see a clear difference between the spectra for the different orientations of the magnetic field. This difference is caused only by the cubic part of the exciton Hamiltonian. We also note that the number of exciton states, which can be observed with σ^+ and σ^- polarized light, differs. In particular, for $\boldsymbol{B} \parallel [110]$ σ^+ and σ^- polarized light belong to the same irreducible representation of $C_{2\mathrm{h}}$. Hence, it is possible to excite a certain exciton state by σ^+ *and* by σ^- polarized light, for which reason all 20 dipole-allowed exciton states can be observed in Fig. 7.3(a) and 7.3(b). As has already been explained in Sec. 7.3.2, the exciton states are connected with

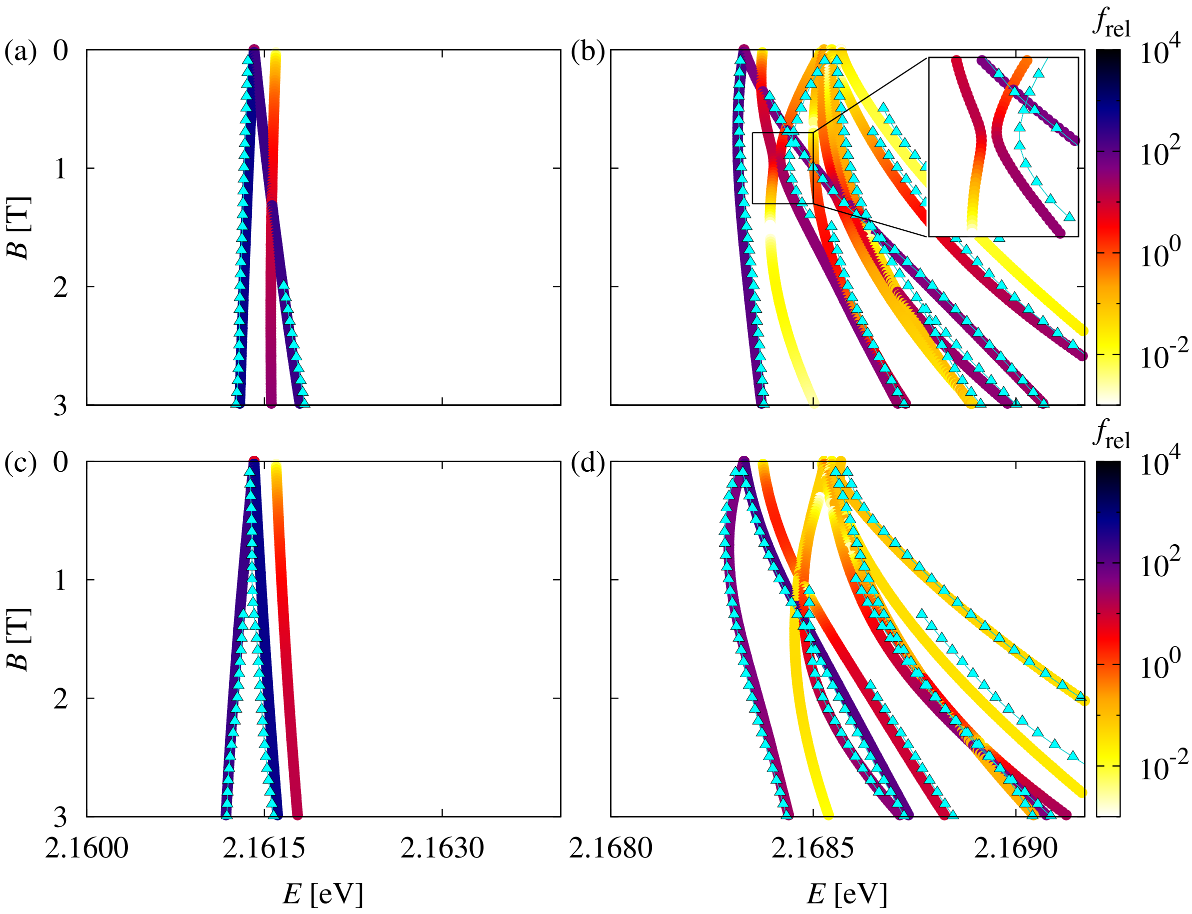

Figure 7.2.: Theoretical line spectrum of the (left) $n = 3$ and (right) $n = 5$ exciton states in an external magnetic field $\boldsymbol{B} \parallel [001]$ for (above) σ^+ and (below) σ^- polarized light. The colorbar shows the calculated relative oscillator strength in arbitrary units. The inset enlarges the most prominent anticrossing in the spectrum. This anticrossing involves the two exciton states, which originate from the Γ_7^- state of Eq. (7.48a) and the Γ_7^- state of Eq. (7.48d) at $B = 0\,\mathrm{T}$. By comparing the theoretical results with the position of those exciton states, which could unambiguously be read out from the experimental spectrum (blue triangles) using the method of the second derivative [37], we can determine the fourth Luttinger parameter κ. An excellent agreement between theory and experiment is obtained for $\kappa = -0.50 \pm 0.10$. As the second derivative does not yield the exact position of the resonances, we have shifted the experimental spectrum by an amount of (a),(c) 100 µeV and (b),(d) 55 µeV.

elliptically polarized light in this configuration. Hence, we also calculated the ellipticity of the states and show the angle ϕ defined in Eq. (7.39) in Fig. 7.4. It can be seen that this angle is clearly different from 0, $\pi/2$ (linearly polarized light) or $\pi/4$ (circularly polarized light).

To compare the theoretically calculated relative oscillator strengths with the experimental values, we analyze the experimental spectra using the method of harmonic inversion, which is presented in detail in Refs. [361, 362]. Within the harmonic inversion the spectra are Fourier transformed

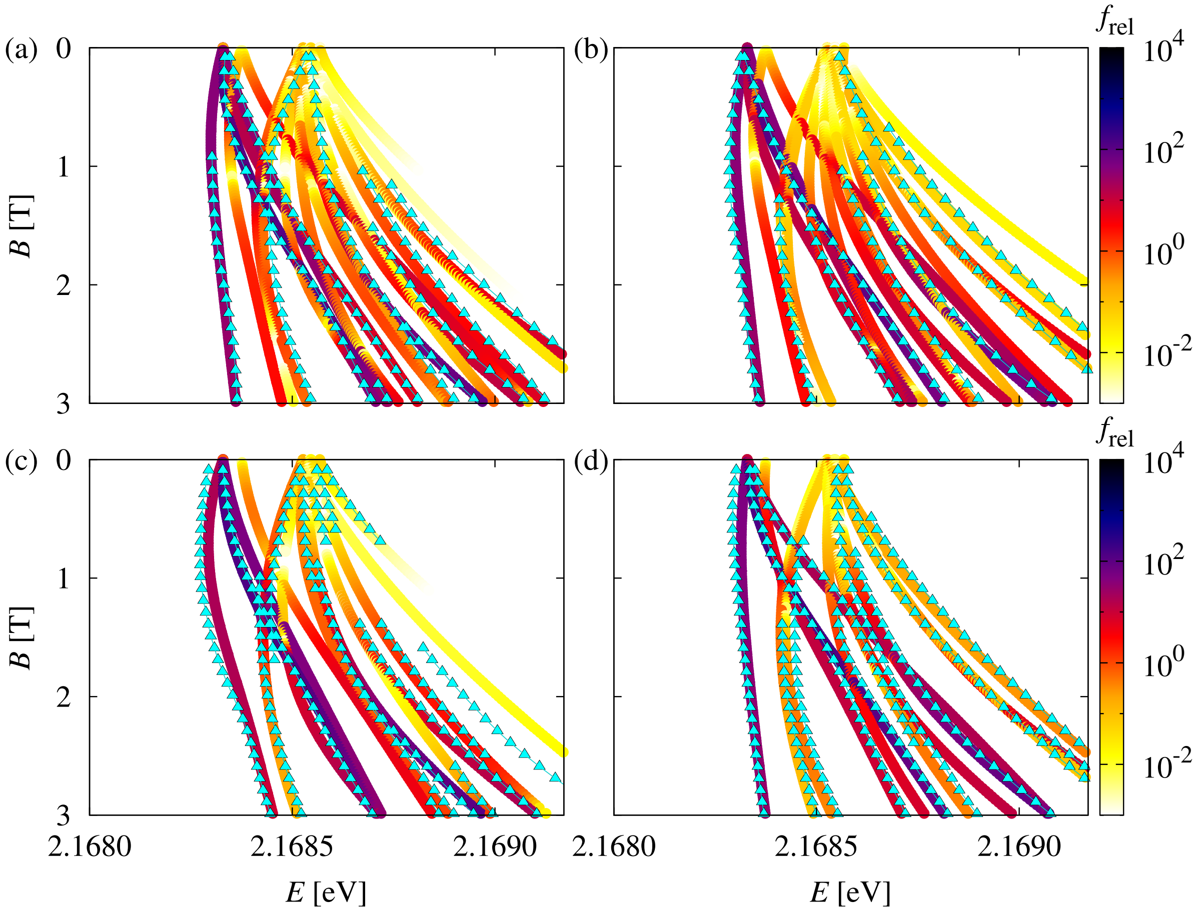

Figure 7.3.: Theoretical line spectrum of the $n = 5$ exciton states in an external magnetic field (above) $\boldsymbol{B} \parallel [110]$ and (below) $\boldsymbol{B} \parallel [111]$ for (left) σ^+ and (right) σ^- polarized light. The colorbar shows the calculated relative oscillator strength in arbitrary units. The exciton states, which could unambiguously be read out from the experiment are again marked by blue triangles. Since σ^+ and σ^- polarized light belong to the same irreducible representation of $C_{2\mathrm{h}}$, it is possible to excite a certain exciton state by σ^+ *and* by σ^- polarized light. Hence, all 20 dipole-allowed exciton states can be observed in panel (a) and in panel (b). Note that we have shifted the experimental spectrum by an amount of 26 µeV.

to find the positions $\mathrm{Re}(E_k)$, widths $\mathrm{Im}(E_k)$ and complex amplitudes d_k of underlying resonances. The spectrum can then be expressed by a sum of Lorentzians

$$G(E) = \mathrm{Im}\left(\sum_k \frac{d_k}{E - E_k}\right). \tag{7.52}$$

The results are presented in Fig. 7.5. For σ^+ and σ^- polarized light one can identify six resonances with exciton states in the theoretical spectrum. For almost all of these resonances we obtain a very good agreement between the modulus $|d|$ of their amplitudes and the theoretically calculated relative oscillator strengths.

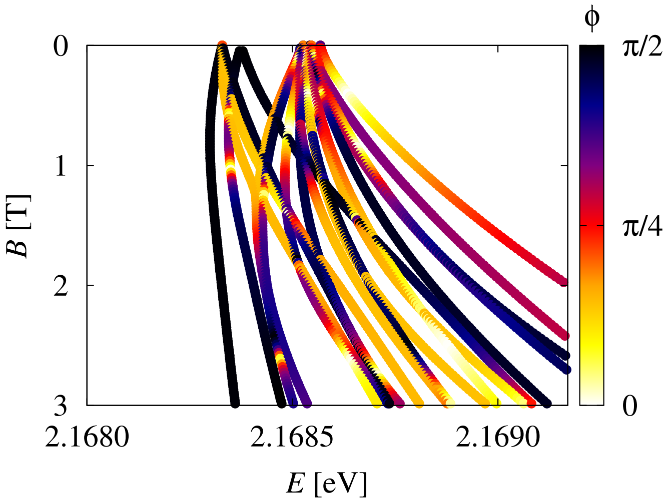

Figure 7.4.: If the external magnetic field is oriented along the [110] direction, the exciton states are connected with elliptically polarized light. The figure shows the angle ϕ defined in Eq. (7.39), which is a measure for the ellipticity of the dipole-allowed exciton states. $\phi = 0$ and $\phi = \pi/2$ describe linear polarization while $\phi = \pi/4$ describes circular polarization.

The harmonic inversion supplies the true position of the resonances, which is generally not identical to the position of the transmission minima due to the asymmetry of the exciton absorption peaks (cf. Chapter 3 and Ref. [30]). Hence, we can compare the results for $\mathrm{Re}(E_k)$ directly to the positions of the exciton states in the theoretical spectrum. This allows us not only to confirm the value of $\kappa = -0.50 \pm 0.10$ but also to determine the first Luttinger parameter more accurately. The best agreements are obtained for $\gamma_1 = 1.73 \pm 0.02$.

In the previous evaluation, we have determined the value of the fourth Luttinger parameter by comparing theoretical and experimental spectra. However, in the theory of Ref. [126] for degenerate valence bands the value of this parameter is inseparably connected with the values of the other three Luttinger parameters γ_i [363]. Hence, we will now shortly prove the consistency of the previously determined value of $\kappa = -0.50 \pm 0.10$ with the results according to Ref. [126]. In Ref. [126] the quantity

$$D^{ij}_{vv'} = \frac{\hbar^2}{2m_0}\delta_{vv'}\delta_{ij} + \frac{1}{m_0^2}\sum_n \frac{\langle u_v\,|p_i|\,u_n\rangle\,\langle u_n\,|p_j|\,u_{v'}\rangle}{E_0 - E_n} \tag{7.53}$$

describes the nonparabolicity of a threefold degenerate valence band with the energy E_0 at the Γ point when neglecting the spin-orbit splitting. The sum is over bands n except for the three valence bands, which are denoted by the indices v and v'. Comparing the Eqs. (21) and (22) of Ref. [126] to the Hamiltonian (7.25), we obtain the following relation between the four Luttinger parameters

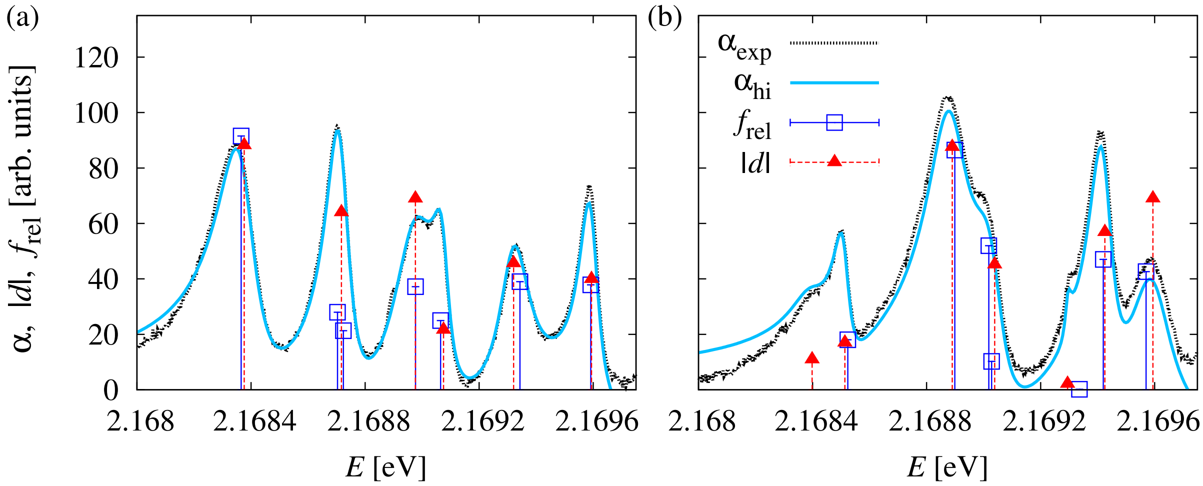

Figure 7.5.: The experimental spectrum (black dotted line) for $\boldsymbol{B} \parallel [001]$ is analyzed using the method of harmonic inversion [361, 362]. The panels show the spectra for (a) σ^+ polarized light at $B = 3\,\mathrm{T}$ and (b) σ^- polarized light at $B = 4\,\mathrm{T}$. Since several exciton states are almost degenerate for σ^- polarized light at $B = 3\,\mathrm{T}$ [cf. Fig. 7.2(d)], we analyze the spectrum at $B = 4\,\mathrm{T}$. The positions and the amplitudes of the resonances obtained are marked by red triangles. The blue solid line shows the function $G(E)$ of Eq. (7.52) for these resonances. Note that in panel (a) the rightmost resonance originates from an $n = 6$ exciton state. Comparing the positions of the resonances to the theoretical spectrum (dark blue squares) yields the optimum values $\gamma_1 = 1.73 \pm 0.02$ and $\kappa = -0.50 \pm 0.10$ for the first and the fourth Luttinger parameter. Furthermore, we obtain a good agreement between the relative oscillator strengths f_{rel} and the modulus $|d|$ of the amplitudes of the resonances.

and the quantity $D^{ij}_{vv'}$:

$$
\begin{aligned}
-\hbar^2(\gamma_1 + 4\gamma_2)/2m_0 &= \quad D^{xx}_{XX}, && (7.54a)\\
-\hbar^2(-6\gamma_2)/2m_0 &= -(D^{xx}_{XX} - D^{yy}_{XX}), && (7.54b)\\
-\hbar^2(-12\gamma_3)/2m_0 &= -2(D^{xy}_{XY} + D^{yx}_{XY}), && (7.54c)\\
e\hbar(3\kappa + 1)/2m_0 &= \quad e(D^{xy}_{XY} - D^{yx}_{XY})/2\hbar. && (7.54d)
\end{aligned}
$$

in accordance with Eq. (44) of Ref. [126].

The matrix elements $\langle u_n | p_i | u_m \rangle$ with the lattice periodic part u_n of the Bloch functions at the Γ point do not vanish only if u_n and u_m have different parity. As the three uppermost valence bands considered here have positive parity, only bands with negative parity give a nonvanishing contribution to $D^{ij}_{vv'}$. There are only two bands Γ_8^- of negative parity in Cu$_2$O, which are located 2.62 eV above and 5.6 eV below the Γ_7^+ valence band [162]. The energy differences $E_0 - E_i$ are thus so large that the spin-orbit coupling between the Γ_7^+ and the Γ_8^+ valence band can be neglected. Hence, this allows us *a posteriori* to assume a threefold degenerate Γ_5^+ valence band and to neglect the spins of the electron and the hole.

Without spins the symmetry of the bands of negative parity is Γ_3^- according to Ref. [51] or according to the relation $\Gamma_3^- \otimes \Gamma_6^+ = \Gamma_8^-$ with the symmetry Γ_6^+ of a spin $S = 1/2$ [90]. The operator $\boldsymbol{p}$ transforms according to Γ_4^-. Therefore, we must consider the coupling coefficients for the case $\Gamma_3^- \otimes \Gamma_4^- \to \Gamma_5^+$:

$$\begin{aligned}
(\langle 3,1| \langle 4,1|) |5,1\rangle &= -\sqrt{3}/2, \\
(\langle 3,1| \langle 4,2|) |5,2\rangle &= \sqrt{3}/2, \\
(\langle 3,2| \langle 4,1|) |5,1\rangle &= -1/2, \\
(\langle 3,2| \langle 4,2|) |5,2\rangle &= -1/2, \\
(\langle 3,2| \langle 4,3|) |5,3\rangle &= 1.
\end{aligned} \tag{7.55}$$

All the other coupling coefficients are zero. Using the energies

$$\begin{aligned}
\Gamma_5^+(v, v' = 1,2,3): &\quad E_0 = 0\,\mathrm{eV}, \\
\Gamma_3^-(n = 1,2): &\quad E_{1,2} = 2.6\,\mathrm{eV}, \\
\Gamma_3^-(n = 3,4): &\quad E_{3,4} = -5.6\,\mathrm{eV},
\end{aligned} \tag{7.56}$$

we obtain

$$\begin{aligned}
D_{12}^{yx} = \frac{1}{m_0^2} \Bigg[&\frac{\langle 5,1 |p_y| 3,1\rangle \langle 3,1 |p_x| 5,2\rangle}{E_0 - E_1} + \frac{\langle 5,1 |p_y| 3,2\rangle \langle 3,2 |p_x| 5,2\rangle}{E_0 - E_2} \\
&+ \frac{\langle 5,1 |p_y| 3,1\rangle \langle 3,1 |p_x| 5,2\rangle}{E_0 - E_3} + \frac{\langle 5,1 |p_y| 3,2\rangle \langle 3,2 |p_x| 5,2\rangle}{E_0 - E_4} \Bigg] = 0,
\end{aligned} \tag{7.57}$$

which finally yields

$$\kappa = -\frac{1}{3}\left(\frac{m_0}{\hbar^2} D_{XY}^{xy} + 1\right) = \left(\gamma_3 - \frac{1}{3}\right) \approx -0.7 \tag{7.58}$$

with $\gamma_3 \approx -0.37$. This value of κ slightly differs from the previously obtained value of $\kappa = -0.50 \pm 0.10$. However, we obtain a very good agreement as regards the sign and the magnitude of this parameter. The small difference may be explained by the neglect of the spins of the quasi-particles.

8

Investigations on the level statistics of magnetoexcitons

For more than 100 years one distinguishes in classical mechanics between two fundamentally different types of motion: regular and chaotic motion. Their appearance strongly depends on the presence of underlying symmetries, which are connected with constants of motion and reduce the degrees of freedom in a given system. If symmetries are broken, the classical dynamics often becomes nonintegrable and chaotic. However, since the description of chaos by trajectories and Lyapunov exponents is not possible in quantum mechanics, it has been unknown for a long time how classical chaos manifests itself in quantum mechanical spectra [364, 365].

Ever since the Bohigas-Giannoni-Schmit conjecture [366], which states that these quantum systems can be described by random matrix theory [367, 368], it has been shown that irregular classical behavior manifests itself in statistical quantities of the corresponding quantum system [369]. In random matrix theory the Hamiltonian of a system is replaced by a random matrix with appropriate symmetries to study the statistical properties of its eigenvalue spectrum [370]; so only universal quantities of a system are considered and detailed dynamical properties are irrelevant. Even though Hamiltonians of dynamical systems are not random in most cases, it is already understood that spectral fluctuations for nonrandom and random Hamiltonians are equivalent [364, 371, 372].

All systems with a Hamiltonian leading to global chaos in the classical dynamics can be assigned to one of three universality classes: the orthogonal, the unitary or the symplectic universality class [364]. To which of these universality classes a given system belongs is determined by the remaining symmetries in the system. Most of the physical systems still have time-reversal or at least one remaining antiunitary symmetry and thus show the statistics of a Gaussion orthogonal ensemble (GOE). Some examples of these systems are spectra of nuclei [373–376], microwave billiards [377–379], molecular spectra [380], impurities [381], and quantum wells [382]. As regards the other universality classes, there are only few examples since systems *without any antiunitary symmetry* [Gaussian unitary ensemble (GUE)] or systems with *time-reversal invariance possessing Kramer's degeneracy but no geometric symmetry at all* [Gaussian symplectic ensemble (GSE)] have to be found [364].

Atoms in constant external fields are among the most important physical systems belonging to the orthogonal universality class [383–385]. Even though an applied magnetic field breaks time-reversal invariance, at least one antiunitary symmetry, e.g., time reversal and a certain parity, remains and GOE statistics is observed [364, 385, 386]. Atoms in external fields are ideal systems to investigate the emergence of quantum chaos both in high-precision experimental measurements and precise quantal calculations, possible because of the availability of the analytically known Hamiltonian (see Refs. [369, 386] and further references therein). Hence, they are a perfectly suitable physical system to study the transition from the Poissonian level statistics, which describes the classically integrable case in the absence of the fields [364, 387], to GOE statistics [385], where the breaking of symmetries due to the external fields leads to a correlation of levels and hence to a strong suppression of crossings [364].

Until now GUE statistics was observable in rather exotic systems such as microwave cavities with ferrite strips [388], atoms in a static electric field and a resonant microwave field of elliptical polarization [389], a kicked rotor or a kicked top [371, 390, 391], the metal-insulator transition in the Anderson model of disordered systems [392], which can be compared to the Brownian-motion model [393], or for billiards in microwave resonators [394], and in graphene quantum dots [395]. Since random matrix theory has already been extended to describe also transitions between the different statistics with analytical functions [370], it is highly desirable to study these transitions theoretically and experimentally. However, due to the small number of physical systems showing GUE statistics, there are only few examples, where transitions from Poissonian to GUE statistics or from GOE to GUE statistics in dependence of a parameter of the system could be studied [371, 390–392, 396]. Often only mathematical models with specifically designed Hamiltonians are introduced to investigate these transitions [370].

Since excitons in semiconductors are often treated as the hydrogen analog of the solid state but also show substantial deviations from this behavior due to the surrounding solid, the question about their level spacing statistics in external fields arises. First experimental investigations of the level spacing statistics in an external magnetic field by M. Aßmann *et al.* [31, 32] give indications on a breaking of antiunitary symmetries, which is, however, attributed to the interaction of excitons and phonons.

In Chapter 4, we have shown that it is indispensable to account for the complete valence band structure of $\mathrm{Cu_2O}$ in a quantitative theory of excitons to explain the striking experimental findings of a fine structure splitting and the observability of F excitons [36]. We have also proven in Chapter 7 that the effect of the valence band structure on the exciton spectra is even more prominent when treating excitons in external fields.

Here we will now show that the simultaneous presence of a cubic band structure and external fields breaks all antiunitary symmetries in the exciton system without the need of phonons. This effect is present in all direct band gap semiconductors with a cubic valence band structure and not restricted to $\mathrm{Cu_2O}$. We prove not only analytically that the antiunitary symmetry known from the hydrogen atom in external fields is broken in the case of excitons, but also numerically, by solving the Schrödinger equation in a complete basis, that the nearest-neighbor spacing (NNS) distribution of exciton states can reveal GUE statistics. Thus, we give the first theoretical evidence for a spatially homogeneous system which breaks all antiunitary symmetries and demonstrate a fundamental difference between atoms in vacuum and excitons.

Having proven the appearance of GUE statistics, we investigate the symmetry breaking for excitons in dependence on system parameters such as the strength and the angle of the magnetic field or the scaled energy [369, 397]. Since the eigenvalue spectrum of the magnetoexciton Hamiltonian shows Poissonian, GOE *or* GUE statistics depending on these parameters, it is an ideal system to investigate the transitions from GOE to GUE statistics or from Poissonian to GUE statistics. To the best of our knowledge, there are only two more systems where both transitions have been studied, i.e., the kicked top [391] and the Anderson model [392]. However, the kicked top is a time-dependent system, which has to be treated within Floquet theory [371, 391], and the Anderson model is rather a model system for a d-dimensional disordered lattice, where parameters such as the disorder and the hopping rate need to be adjusted [392]. Magnetoexcitons are a more realistic physical system allowing for a systematic investigation of transitions between different statistics. In particular, the parameters describing these transitions can be easily adjusted in experiments. Comparing our results with analytical functions from random matrix theory describing the transitions between the statistics [370, 371], we confirm the so-called Wigner surmise [398], which states that the NNS of large random matrices can be approximated by the NNS of 2×2 matrices of the same universality class [370].

In Sec. 8.1 we present a simplified model of excitons in cubic semiconductors in an external magnetic field and introduce an appropriate complete basis to solve the corresponding Schrödinger equation. The methods of solving the Schrödinger equation for fixed values of the external field strenghts or for a constant scaled energy are discussed in Secs. 8.1.1 and 8.1.2, respectively.

Having shown analytically that the presence of the cubic band structure and external fields breaks all antiunitary symmetries and that quasi-particle interactions will not restore these symmetries in Sec. 8.2.1, we investigate the eigenvalue spectrum and the level spacing statistics numerically. At first, we demonstrate the appearance of GOE or GUE statistics for specific directions of an external magnetic field in Sec. 8.2.2. The transitions between different level spacing statistics are then investigated in Secs. 8.3.2 and 8.3.3 after the presentation of the formulas for these transitions in Sec. 8.3.

The model of Sec. 8.1 which includes the complete cubic valence band structure of the solid, can explain the appearance of GUE statistics if the magnetic field is not oriented in one of the symmetry planes of the cubic lattice. However, M. Aßmann *et al.* [31, 32] have observed experimentally that GUE statistics occurs for all orientations of the field. This raises again the question about the influence of the exciton-phonon interaction on the level spacing statistics of the exciton spectra.

In Sec. 8.4 we discuss that the exciton-phonon interaction leads to a finite momentum of the exciton center of mass and thus to the appearance of a magneto Stark effect in an external magnetic field. The motional Stark field connected to this effect then causes in combination with the cubic lattice the breaking of all antiunitary symmetries even if the external field *is* oriented in one of the symmetry planes of the lattice. Hence, we explain the appearance of GUE statistics for all orientations of the external field. Essential parts of this Chapter have been published in Refs. [40, 47, 48].

8.1 Simplified model of excitons in cubic semiconductors

A simplified model of excitons without electron and hole spin will be necessary to determine the level statistics of the system. Only then it is possible to numerically calculate exciton states, which have appropriately high principal quantum numbers, with the given computational memory. In this section we briefly discuss this simplified model of excitons in direct semiconductors with a cubic valence band structure in external fields and present an appropriate basis to solve the corresponding Schrödinger equation.

When applying external fields, the corresponding Hamiltonian is obtained via the minimal substitution. We additionally introduce relative and center of mass coordinates as given in Refs. [348, 355, 356] for external fields. Hence, we replace the coordinates and momenta of electron and hole

with

$$\begin{aligned}
\boldsymbol{r}_{\mathrm{e}} &= \boldsymbol{R} + (m_{\mathrm{h}}/M)\boldsymbol{r}, && (8.1\mathrm{a})\\
\boldsymbol{r}_{\mathrm{h}} &= \boldsymbol{R} - (m_{\mathrm{e}}/M)\boldsymbol{r}, && (8.1\mathrm{b})\\
\boldsymbol{p}_{\mathrm{e}} &= (m_{\mathrm{e}}/M)\boldsymbol{P} + \boldsymbol{p} + e\boldsymbol{A}(\boldsymbol{r}), && (8.1\mathrm{c})\\
\boldsymbol{p}_{\mathrm{h}} &= (m_{\mathrm{h}}/M)\boldsymbol{P} - \boldsymbol{p} + e\boldsymbol{A}(\boldsymbol{r}), && (8.1\mathrm{d})
\end{aligned}$$

where $M = m_{\mathrm{e}} + m_{\mathrm{h}} = m_{\mathrm{e}} + m_0/\gamma_1$ denotes the yellow exciton mass and $\boldsymbol{P}$ is the generalized momentum operator discussed in Sec. 7.1.2. This is an extension of the coordiante transformation in Eq. (2.198) for finite magnetic fields. The Hamiltonian of the exciton reads (cf. Sec. 7.2 and Refs. [7, 281, 355–359])

$$H_{\mathrm{exc}} = V(\boldsymbol{r}) + e\Phi(\boldsymbol{r}) + H_{\mathrm{e}}((m_{\mathrm{e}}/M)\boldsymbol{P} + \boldsymbol{p} + e\boldsymbol{A}(\boldsymbol{r})) + H_{\mathrm{h}}((m_{\mathrm{h}}/M)\boldsymbol{P} - \boldsymbol{p} + e\boldsymbol{A}(\boldsymbol{r})). \qquad (8.2)$$

Here the band gap energy E_{g} is set to zero. The kinetic energy $H_{\mathrm{e}}(\boldsymbol{p}_{\mathrm{e}})$ of the electron and the Coulomb interaction $V(\boldsymbol{r})$ are given by Eqs. (4.8) and (4.9), respectively. We use the vector potential $\boldsymbol{A} = (\boldsymbol{B} \times \boldsymbol{r})/2$ of a constant magnetic field $\boldsymbol{B}$ and the electrostatic potential $\Phi(\boldsymbol{r}) = -\boldsymbol{F} \cdot \boldsymbol{r}$ of a constant electric field $\boldsymbol{F}$. For the kinetic energy of the hole we use the following simplified expression:

$$H_{\mathrm{h}}(\boldsymbol{p}_{\mathrm{h}}) = \frac{1}{2\hbar^2 m_0}\left\{\hbar^2(\gamma_1 + 4\gamma_2)\boldsymbol{p}_{\mathrm{h}}^2 - 6\gamma_2(p_{\mathrm{h}1}^2 \boldsymbol{I}_1^2 + \mathrm{c.p.}) - 12\gamma_3(\{p_{\mathrm{h}1}, p_{\mathrm{h}2}\}\{\boldsymbol{I}_1, \boldsymbol{I}_2\} + \mathrm{c.p.})\right\} \qquad (8.3)$$

with $\boldsymbol{p} = (p_1,\, p_2,\, p_3)$, $\{a, b\} = \frac{1}{2}(ab+ba)$ and c.p. denoting cyclic permutation. The parameters η_i of Eq. (4.6) are set to zero due to their smallness so that only the three Luttinger parameters γ_i describe the behavior and the anisotropic effective mass of the hole. The spin-orbit coupling H_{so} (4.2), which generally enters the kinetic energy of the hole, is neglected, as well, since it is spherically symmetric and therefore does not affect the symmetry properties of the exciton Hamiltonian. The term H_B of Eq. (7.26), which describes the energy of the spins in the magnetic field [126, 281, 318, 358], is likewise neglected as it is invariant under the symmetry operations considered below. This formally corresponds to setting $\kappa = -1/3$ in Eq. (7.26) and neglecting the spins of the electron and the hole.

Since the Hamiltonian depends only on the relative coordinate $\boldsymbol{r}$, the generalized momentum of the center of mass is a good quantum number, i.e., $[\boldsymbol{P},\, H_{\mathrm{exc}}] = \boldsymbol{0}$, and one can generally set $\boldsymbol{P} = \hbar\boldsymbol{K}$ [81, 267, 348]. When neglecting the exciton-phonon interaction, one can especially assume $\boldsymbol{K} \approx \boldsymbol{0}$, as the wave vector of photons, by which the excitons are created, are very close to the origin of the Brillouin zone [7]. Hence, we have

$$H_{\mathrm{exc}} = V(\boldsymbol{r}) + e\Phi(\boldsymbol{r}) + H_{\mathrm{e}}(\boldsymbol{p} + e\boldsymbol{A}(\boldsymbol{r})) + H_{\mathrm{h}}(-\boldsymbol{p} + e\boldsymbol{A}(\boldsymbol{r})). \qquad (8.4)$$

As we will show in Sec. 8.2.1, the symmetry breaking in the system depends on the orientation of the fields with respect to the crystal lattice. We will denote the orientation of $\boldsymbol{B}$ and $\boldsymbol{F}$ in spherical coordinates via

$$\boldsymbol{B}(\varphi,\, \vartheta) = B\begin{pmatrix} \cos\varphi\sin\vartheta, \\ \sin\varphi\sin\vartheta \\ \cos\vartheta \end{pmatrix} \qquad (8.5)$$

and similar for $\boldsymbol{F}$ in what follows.

Before we solve the Schrödinger equation corresponding to the Hamiltonian (8.4), we rotate the coordinate system to make the quantization axis coincide with the direction of the magnetic field and then express Eq. (8.4) in terms of irreducible tensors [79, 248, 281]. We can then calculate a matrix representation of the Schrödinger equation using a complete basis.

Since we neglect the spin-orbit coupling, the term H_B and set $\eta_i = 0$, the Hamiltonian does not depend on the spins S_h and S_h of the electron and the hole. Therefore, we disregard these spins in our basis. As regards the angular momentum part of the basis, we still have to consider that the Hamiltonian (8.4) couples the angular momentum L of the exciton and the quasi-spin I. Hence, we introduce the total momentum $G = L + I$ with the z component M_G. For the radial part of the exciton wave function we again use the Coulomb-Sturmian functions of Sec. 4.3. Finally, we make the ansatz

$$|\Psi\rangle = \sum_{NLGM_G} c_{NLGM_G} \left|N,\, L,\, I,\, G,\, M_G\right\rangle, \tag{8.6}$$

for the exciton wave function with complex coefficients c.

The Schrödinger equation can now be solved for fixed values of the external field strengths or for a fixed value of the scaled energy known from atoms in external fields [397]. Both methods will be presented in the following.

8.1.1 Constant field strength spectra

Inserting the ansatz (8.6) in the Schrödinger equation $H\Psi = E\Psi$ and multiplying from the left with another basis state $\langle \Pi' |$, we obtain a matrix representation of the Schrödinger equation of the form

$$\boldsymbol{D}\boldsymbol{c} = E\boldsymbol{M}\boldsymbol{c}, \tag{8.7}$$

where the external field strengths are assumed to be constant. The vector $\boldsymbol{c}$ contains the coefficients of the expansion (8.6). All matrix elements which enter the hermitian matrices $\boldsymbol{D}$ and $\boldsymbol{M}$ can be calculated similarly to the matrix elements in Appendix F. The generalized eigenvalue problem (8.7) is finally solved using an appropriate Lapack routine [284].

As was already stated in Sec. 4.3, the basis cannot be infinitely large in numerical calculations. Hence, the values of the quantum numbers are chosen in the following way: For each value of $n = N + L + 1 \leq n_\mathrm{max}$ we use

$$\begin{aligned} L &= 0,\, \ldots,\, n-1, \\ G &= \left|L-1\right|,\, \ldots,\, \min(L+1,\, G_\mathrm{max}), \\ M_G &= -G,\, \ldots,\, G. \end{aligned} \tag{8.8}$$

The values G_max and n_max are chosen appropriately large so that as many eigenvalues as possible converge. In our numerical calculations, the maximum number of basis states used is limited by the condition $n_\mathrm{max} \leq 30$ due to the required computer memory.

Note that without an external electric field, parity is a good quantum number and the operators in the Schrödinger equation couple only basis states with even *or* with odd values of L. In this case we consider only basis states with odd values of L as these exciton states can be observed in parity-forbidden semiconductors (cf. Sec. 4.4 and Refs. [36, 44]).

8.1.2 Constant scaled energy spectra

Besides solving the Schrödinger equation or the generalized eigenvalue problem (8.7) for fixed values of the external field strength, it is also possible to use the concept of scaled energy [397]. In classical mechanics the Hamiltonian of a hydrogen atom in external fields possesses a scaling property which allows for reducing the three parameters energy E, magnetic field B and electric field F to two parameters [399, 400]. The corresponding transformation reads

$$\hat{\boldsymbol{r}} = \gamma^{2/3}\boldsymbol{r}, \qquad \hat{\boldsymbol{p}} = \gamma^{-1/3}\boldsymbol{p}, \qquad \hat{\boldsymbol{F}} = \gamma^{-4/3}\boldsymbol{F}, \qquad \hat{E} = \gamma^{-2/3}E, \tag{8.9}$$

with $\gamma = B/B_0$ and $B_0 = 2.3505 \times 10^5\ \mathrm{T}$ [369]. This scaling is not applicable in quantum mechanics since $[\hat{r}_i,\, \hat{p}_j] = i\hbar\gamma^{1/3}\delta_{ij} \neq i\hbar\delta_{ij}$ holds. However, it is possible to define a scaled quantum Hamiltonian by substituting $\hat{\boldsymbol{r}} = \gamma^{2/3}\boldsymbol{r}$ in the Schrödinger equation and introducing the scaled energy $\hat{R} = \gamma^{-2/3}E$.

We will now apply this scaling to the exciton system. Let us write the Hamiltonian of excitons (8.4) in the form

$$H \quad = \quad -\frac{e^2}{4\pi\varepsilon_0\varepsilon}\frac{1}{r} - e\boldsymbol{F}\cdot\boldsymbol{r} + H_0 + (eB)H_1 + (eB)^2H_2 \tag{8.10}$$

with the H_i given in Appendix D.1 but using the simplifications of Sec. 8.1. Due to the effective masses of electron and hole and due to the scaling of the Coulomb energy by the dielectric constant, we introduce exciton Hartree units so that the hydrogen-like part of the Hamiltonian is exactly of the same form as that of the hydrogen Hamiltonian in normal Hartree units [35] (see Appendix B). Variables in exciton Hartree units will be indicated by a tilde sign.

Performing the substitution $\hat{\boldsymbol{r}} = \gamma^{2/3}\tilde{\boldsymbol{r}}/\alpha$ with a convergence parameter α (cf. Sec. 4.3) in the corresponding Schrödinger equation, where we now have to use $\gamma = B/B_0$ with $B_0 = 2.3505 \times 10^5\ \mathrm{T}/(\gamma_1'^2\varepsilon^2)$, and multiplying the resulting equation with $\alpha^2\gamma^{2/3}$, we obtain

$$-\frac{\alpha}{\hat{r}} - \gamma^{4/3}\alpha^3\tilde{\boldsymbol{F}}\cdot\hat{\boldsymbol{r}} + \gamma^{2/3}\tilde{H}_0 + \gamma^{1/3}\alpha^2\tilde{H}_1 + \alpha^4\tilde{H}_2 = \gamma^{-2/3}\alpha^2\tilde{E}. \tag{8.11}$$

As for the hydrogen atom, we define the scaled energy $\hat{E} = \gamma^{-2/3}\tilde{E}$ and scaled electric field strength $\hat{\boldsymbol{F}} = \gamma^{4/3}\tilde{\boldsymbol{F}}$. When using the complete basis of Eq. (8.6), Eq. (8.11) represents a quadratic eigenvalue problem of the form

$$\boldsymbol{A}\boldsymbol{c} + \tau\boldsymbol{B}\boldsymbol{c} = \tau^2\boldsymbol{C}\boldsymbol{c} \tag{8.12}$$

with hermitian matrices $\boldsymbol{A}$, $\boldsymbol{B}$, and $\boldsymbol{C}$ and an eigenvalue $\tau = \gamma^{1/3}$. The eigenvalue problem can be transformed into a standard generalized eigenvalue problem by defining a vector $\boldsymbol{d} = \tau\boldsymbol{c}$:

$$\begin{pmatrix} \boldsymbol{A} & \boldsymbol{B} \\ \boldsymbol{0} & \boldsymbol{1} \end{pmatrix} \begin{pmatrix} \boldsymbol{c} \\ \boldsymbol{d} \end{pmatrix} = \tau \begin{pmatrix} \boldsymbol{0} & \boldsymbol{C} \\ \boldsymbol{1} & \boldsymbol{0} \end{pmatrix} \begin{pmatrix} \boldsymbol{c} \\ \boldsymbol{d} \end{pmatrix}. \tag{8.13}$$

This eigenvalue problem is solved for constant scaled energies $\hat{E}$ using an appropriate LAPACK routine [284] to obtain constant scaled energy spectra, whose level statistics will be analyzed in Sec. 8.3.

We finally note that due to the substitution $\hat{\boldsymbol{r}} = \gamma^{2/3}\tilde{\boldsymbol{r}}/\alpha$ and due to the use of exciton Hartree units, a different value of the free convergence parameter α than in Sec. 4.3 has to be used to obtain convergence for the exciton states with principal quantum number n. This value is given by $\alpha \approx n\gamma^{2/3}$.

8.2 Magnetoexcitons break antiunitary symmetries

We will now prove analytically in Sec. 8.2.1 that the Hamiltonian (8.4) breaks all antiunitary symmetries if the external fields are not oriented in one symmetry plane of the lattice. This result will then be confirmed numerically in Sec. 8.2.2 by solving the corresponding Schrödinger equation as described in Sec. 8.1.1.

8.2.1 Discussion of antiunitary symmetries

The matrices $\boldsymbol{I}_i$ of the quasi-spin $I = 1$ given by Eq. (4.3) are not the standard spin matrices $\boldsymbol{S}_i$ of spin one [401]. However, these matrices obey the commutation rules [126]

$$[\boldsymbol{I}_i,\, \boldsymbol{I}_j] = i\hbar \sum_{k=1}^{3} \varepsilon_{ijk} \boldsymbol{I}_k, \tag{8.14}$$

for which reason a unitary transformation can be found so that $\boldsymbol{U}^\dagger \boldsymbol{I}_i \boldsymbol{U} = \boldsymbol{S}_i$ holds. The corresponding transformation matrix reads

$$\boldsymbol{U} = \frac{1}{\sqrt{2}} \begin{pmatrix} -1 & 0 & 1 \\ -i & 0 & -i \\ 0 & \sqrt{2} & 0 \end{pmatrix}. \tag{8.15}$$

Since in Ref. [401] the behavior of the standard spin matrices under symmetry operations such as time reversal and reflections are given, we will use the matrices $\boldsymbol{S}_i$ instead of the $\boldsymbol{I}_i$ in the following.

In the special case of vanishing Luttinger parameters $\gamma_2 = \gamma_3 = 0$, the exciton Hamiltonian (8.4) is of the same form as the Hamiltonian of a hydrogen atom in external fields. It is well known that for this Hamiltonian there is still one antiunitary symmetry left, viz., the combined symmetry of time inversion K followed by a reflection $S_{\hat{\boldsymbol{n}}}$ at the specific plane spanned by both fields [364]. This plane is given by the normal vector

$$\hat{\boldsymbol{n}} = (\boldsymbol{B} \times \boldsymbol{F}) / \left|\boldsymbol{B} \times \boldsymbol{F}\right| \tag{8.16}$$

or $\hat{\boldsymbol{n}} \perp \hat{\boldsymbol{B}} = \boldsymbol{B}/B$ if $\boldsymbol{F} = \boldsymbol{0}$ holds. Therefore, the hydrogen-like system shows GOE statistics in the chaotic regime.

As the hydrogen atom is spherically symmetric in the field-free case, it makes no difference whether the magnetic field is oriented in z direction or not. However, in a semiconductor with $\delta' \neq 0$ the Hamiltonian has cubic symmetry and the orientation of the external fields with respect to the crystal axis of the lattice becomes important. Any rotation of the coordinate system with the aim of making the z axis coincide with the direction of the magnetic field will also rotate the cubic crystal lattice. The only remaining antiunitary symmetry mentioned above is now broken for the exciton Hamiltonian if the plane spanned by both fields is *not* identical to one of the symmetry planes of the cubic lattice. Even without an external electric field the symmetry is broken if the magnetic field is not oriented in one of these symmetry planes. Only if the plane spanned by both fields is identical to one of the symmetry planes of the cubic lattice, the antiunitary symmetry $KS_{\hat{\boldsymbol{n}}}$ with $\hat{\boldsymbol{n}}$ given by Eq. (8.16) is present since only then the reflection $S_{\hat{\boldsymbol{n}}}$ transforms the lattice into itself.

This criterion can also be expressed in a different way: The antiunitary symmetry known from the hydrogen atom is broken if none of the normal vectors $\hat{\boldsymbol{n}}_i$ of the 9 symmetry planes of the cubic lattice given by

$$\begin{aligned} \hat{\boldsymbol{n}}_1 =&(1,\,0,\,0)^{\mathrm{T}}, & \hat{\boldsymbol{n}}_2 =&(0,\,1,\,0)^{\mathrm{T}}, & \hat{\boldsymbol{n}}_3 =&(0,\,0,\,1)^{\mathrm{T}}, \\ \hat{\boldsymbol{n}}_4 =&(1,\,1,\,0)^{\mathrm{T}}/\sqrt{2}, & \hat{\boldsymbol{n}}_5 =&(0,\,1,\,1)^{\mathrm{T}}/\sqrt{2}, & \hat{\boldsymbol{n}}_6 =&(1,\,0,\,1)^{\mathrm{T}}/\sqrt{2}, \\ \hat{\boldsymbol{n}}_7 =&(1,\,-1,\,0)^{\mathrm{T}}/\sqrt{2}, & \hat{\boldsymbol{n}}_8 =&(0,\,1,\,-1)^{\mathrm{T}}/\sqrt{2}, & \hat{\boldsymbol{n}}_9 =&(-1,\,0,\,1)^{\mathrm{T}}/\sqrt{2}, \end{aligned} \tag{8.17}$$

is parallel to the vector $\hat{\boldsymbol{n}}$ discussed above.

Since the breaking of all antiunitary symmetries depends on the relative orientation of the external fields to all normal vectors $\hat{\boldsymbol{n}}_i$, we can introduce a parameter which is a qualitative measure for the deviation from the cases with antiunitary symmetry:

$$\sigma = \left[\sum_{i=1}^{9} \frac{|\boldsymbol{B}\times\boldsymbol{F}|^2}{|\hat{\boldsymbol{n}}_i\times(\boldsymbol{B}\times\boldsymbol{F})|^2}\right]^{-\frac{1}{2}}. \tag{8.18}$$

For the special case of $\boldsymbol{F}=\boldsymbol{0}$ we define

$$\sigma = \left[\sum_{i=1}^{9} (\hat{\boldsymbol{n}}_i\cdot\hat{\boldsymbol{B}})^{-2}\right]^{-\frac{1}{2}}. \tag{8.19}$$

We have $\sigma = 0$ for the cases with antiunitary symmetry. That symmetry is more and more broken with increasing values of σ.

Under time inversion K and reflections $S_{\hat{\boldsymbol{n}}}$ at a plane perpendicular to a normal vector $\hat{\boldsymbol{n}}$ the vectors of position $\boldsymbol{r}$, momentum $\boldsymbol{p}$ and spin $\boldsymbol{S}$ transform according to [401]

$$K\boldsymbol{r}K^{\dagger} \;=\; \boldsymbol{r}, \qquad K\boldsymbol{p}K^{\dagger} = -\boldsymbol{p}, \qquad K\boldsymbol{S}K^{\dagger} = -\boldsymbol{S}, \tag{8.20}$$

and

$$\begin{aligned} S_{\hat{\boldsymbol{n}}}\boldsymbol{r}S_{\hat{\boldsymbol{n}}}^{\dagger} &= \boldsymbol{r} - 2\hat{\boldsymbol{n}}(\hat{\boldsymbol{n}}\cdot\boldsymbol{r}), \\ S_{\hat{\boldsymbol{n}}}\boldsymbol{p}S_{\hat{\boldsymbol{n}}}^{\dagger} &= \boldsymbol{p} - 2\hat{\boldsymbol{n}}(\hat{\boldsymbol{n}}\cdot\boldsymbol{p}), \\ S_{\hat{\boldsymbol{n}}}\boldsymbol{S}S_{\hat{\boldsymbol{n}}}^{\dagger} &= -\boldsymbol{S} + 2\hat{\boldsymbol{n}}(\hat{\boldsymbol{n}}\cdot\boldsymbol{S}). \end{aligned} \tag{8.21}$$

For all orientations of the external fields the hydrogen-like part of the Hamiltonian (8.4) is invariant under $KS_{\hat{\boldsymbol{n}}}$ with $\hat{\boldsymbol{n}}$ given by Eq. (8.16). However, other parts of the Hamiltonian such as $H_c = (p_1^2\boldsymbol{S}_1^2 + \mathrm{c.p.})$ [see Eq. (8.3)] are not invariant if $\sigma \neq 0$ holds. For example, for the case with $\boldsymbol{B}(0,\,0)$ and $\boldsymbol{F}(\pi/6,\,\pi/2)$, we obtain

$$\begin{aligned} S_{\hat{\boldsymbol{n}}}KH_cK^{\dagger}S_{\hat{\boldsymbol{n}}}^{\dagger} - H_c \;=\; & \frac{1}{8}\Big[2\sqrt{3}(\boldsymbol{S}_2^2 - \boldsymbol{S}_1^2)p_1p_2 + 3(\boldsymbol{S}_1^2p_2^2 + \boldsymbol{S}_2^2p_1^2) \\ & -3(\boldsymbol{S}_1^2p_1^2 + \boldsymbol{S}_2^2p_2^2) + \{\boldsymbol{S}_1,\boldsymbol{S}_2\}\left(2\sqrt{3}(p_2^2 - p_1^2) + 12p_1p_2\right)\Big] \neq 0 \end{aligned} \tag{8.22}$$

with $\hat{\boldsymbol{n}} = (-1/2,\,\sqrt{3}/2,\,0)^{\mathrm{T}}$. Note that even though H_c does not depend on the external fields, the normal vector $\hat{\boldsymbol{n}}$ is determined by these fields via Eq. (8.16). Otherwise, the hydrogen-like part of the Hamiltonian would not be invariant under $KS_{\hat{\boldsymbol{n}}}$.

Since the expression in Eq. (8.22) is not equal to zero, we have shown for $\boldsymbol{B}(0,\,0)$ and $\boldsymbol{F}(\pi/6,\,\pi/2)$ that the generalized time-reversal symmetry of the hydrogen atom is broken for excitons due to the cubic symmetry of the semiconductor. The same calculation can also be performed for other orientations of the external fields. As we have stated above, the antiunitary symmetry remains unbroken only for specific orientations of the fields.

The main advantage of theory over the experiments is that the effects of the band structure and of the exciton-phonon interaction can be treated separately. We performed calculations to demonstrate that, in general, GUE statistics appears for a much simpler system, i.e., only the presence of the cubic lattice and the external fields already breaks all antiunitary symmetries without the need for interactions with other quasi-particles like phonons.

However, one may ask whether these interactions are able to restore the broken symmetries. It is well known that when adding an additional interaction to a Hamiltonian, this interaction will often further reduce the symmetry of the problem and not increase it. Indeed, it is not possible that the effects of the band structure and quasi-particle interactions on the symmetry or the level spacing statistics will cancel each other out, in particular for all values of the external field strengths. The quasi-particle interaction would have to have the same form as the operators in our Hamiltonian to make the commutator of the Hamiltonian and the symmetry operator $KS_{\hat{\boldsymbol{n}}}$ vanish. However, if we, e.g., consider the interaction between excitons and phonons, the interaction operators [cf. Sec. 3.1.3 and Eq. (8.32)] look quite different than the operators in the exciton Hamiltonian (8.2). Hence, phonons or other interactions in the solid do not restore the broken antiunitary symmetries if the external fields are not oriented in one symmetry plane of the solid.

8.2.2 Appearance of GOE and GUE statistics

We will now demonstrate the breaking of all antiunitary symmetries by analyzing the nearest-neighbor spacings (NNS) of the energy eigenvalues corresponding to the Hamiltonian (8.4) [385] for a model system with the arbitrarily chosen set of parameters $E_{\mathrm{g}} = 0$, $\varepsilon = 7.5$, $m_{\mathrm{e}} = m_0$, $\gamma_1' = 2$, $\mu' = 0$, and $\delta' = -0.15$. If we set $\boldsymbol{F} = \boldsymbol{0}$, we expect to obtain GUE statistics in the limit of high energies as long as the magnetic field is not oriented in one of the symmetry planes of the lattice.

Before analyzing the NNS, we have to unfold the spectra to obtain a constant mean spacing [364, 366, 374, 385]. The unfolding procedure separates the average behavior of the non-universal spectral density from universal spectral fluctuations and yields a spectrum in which the mean level spacing is equal to unity [370].

To unfold the spectra, we plot for both cases of constant field strengths and constant scaled energy the number

$$N(E) = \sum_n \Theta(E - E_n) \tag{8.23}$$

of energy levels up to the value E_{max}, up to which all eigenvalues converged. Here $\Theta(x)$ denotes the Heaviside function. We leave out a certain number of low-lying sparse levels to remove individual but nontypical fluctuations [385]. In the case of constant scaled energy it is known that the mean number of levels is proportional to $E^{-2/3}$ in the dense part of the spectrum [385]. Hence, we fit $N(E)$ with $\bar{N}(E) = aE^{-2/3} + b$. In the case of constant field strength no such proportionality is known and we fit $N(E)$ with a cubic polynomial function $\bar{N}(E)$. The level spacings of the unfolded spectrum are then given by $s_n = \bar{N}(E_{n+1}) - \bar{N}(E_n)$ [402].

Since the magnetic field breaks all symmetries in the system and limits the convergence of the solutions of the generalized eigenvalue problem with high energies, the number of level spacings

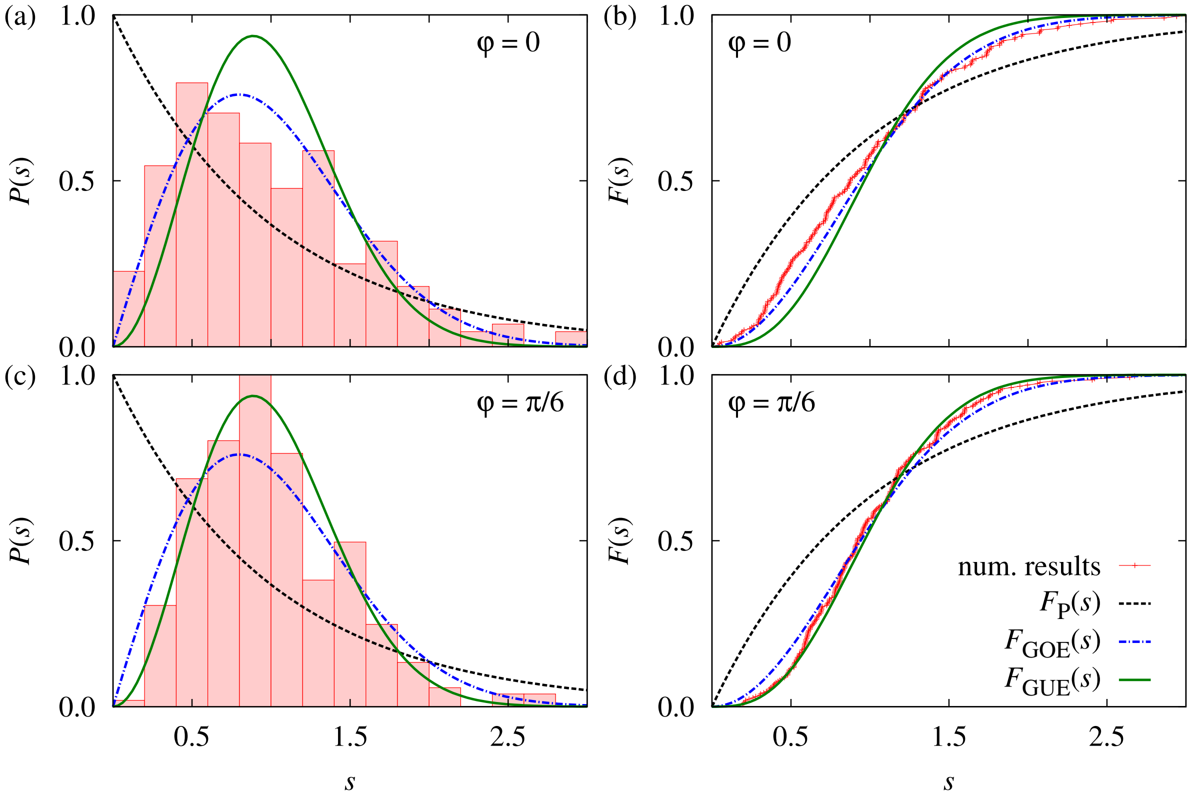

Figure 8.1.: Level spacing probability distribution functions $P(s)$ (left) and cumulative distribution functions $F(s)$ (right) for $\delta' = -0.15$, $B = 3\,\mathrm{T}$, $\vartheta = \pi/6$, and two different values of φ. Besides the numerical data (red boxes or red dots), we also show the corresponding functions of a Poissonian ensemble (black dashed line), GOE (blue dash-dotted line), and GUE (green solid line). Only if the magnetic field is oriented in one of the symmetry planes of the lattice, one antiunitary symmetry is present and GOE statistics can be observed (a,b). In all other cases, all antiunitary symmetries are broken and GUE statistics appears (c,d).

analyzed here is comparatively small and comprises about 250 to 500 exciton states. In this case, the cumulative distribution function [403]

$$F(s) = \int_0^s P(x)\,\mathrm{d}x \tag{8.24}$$

is often more meaningful than histograms of the level spacing probability distribution function $P(s)$.

We will compare our results with the cumulative distribution function corresponding to the level spacing probability distribution functions [31, 366], i.e, the Poissonian distribution

$$P_{\mathrm{P}}(s) = e^{-s} \tag{8.25}$$

for non-interacting energy levels, the Wigner distribution

$$P_{\mathrm{GOE}}(s) = \frac{\pi}{2}\,s e^{-\pi s^2/4}, \tag{8.26}$$

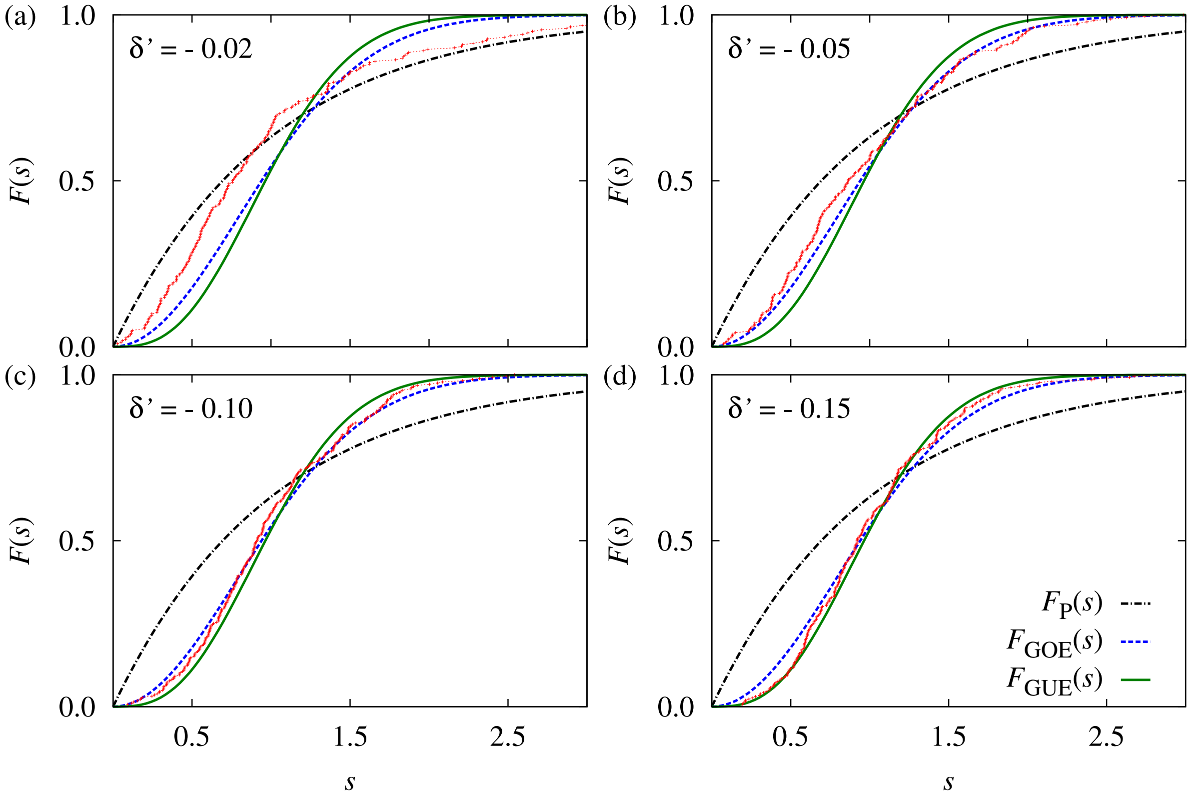

Figure 8.2.: Cumulative distribution function $F(s)$ for increasing values of δ' with $\boldsymbol{B}(\varphi,\,\vartheta) = \boldsymbol{B}(\pi/6,\,\pi/6)$ and $B = 3\,\mathrm{T}$. Besides the numerical data (red dots), we also show the corresponding functions of a Poissonian ensemble (black dash-dotted line), GOE (black dashed line), and GUE (green solid line). For increasing values of δ' the statistics rapidly changes to the one of a Gaussian unitary ensemble (d). Note that we do not show the hydrogen-like case $\delta' = 0$ since we simply obtain transitional form between Poissonian and GOE statistics and since this system is sufficiently well known from literature (see, e.g., Refs. [364, 385, 386] and further references therein).

and the distribution

$$P_{\mathrm{GUE}}(s) = \frac{32}{\pi^2}\,s^2 e^{-4s^2/\pi} \tag{8.27}$$

for systems without any antiunitary symmetry. It can be seen that the most striking difference between the three distributions is the behavior for small values of s. While for the Poissonian distribution the probability of level crossings is nonzero and thus $P_{\mathrm{P}}(0) \neq 0$ holds, in chaotic spectra the symmetry reduction leads to a correlation of levels and hence to a strong suppression of crossings. The most characteristic feature of GOE or GUE statistics is the linear or quadratic level repulsion for small s, respectively.

In Fig. 8.1 we show the results for level spacing probability distribution function and the cumulative distribution function for $\boldsymbol{B}(0,\,\pi/6)$ and $\boldsymbol{B}(\pi/6,\,\pi/6)$ obtained with a constant magnetic field strength of $B = 3\,\mathrm{T}$ and exciton states within a certain energy range. While for $\boldsymbol{B}(0,\,\pi/6)$ the magnetic field is oriented in one of the symmetry planes of the lattice and thus only GOE statistics can be observed, we see clear evidence for GUE statistics as regards the case with $\boldsymbol{B}(\pi/6,\,\pi/6)$.

Note that we have chosen the values $\delta' = -0.15$ and $B = 3\,\mathrm{T}$ to be fixed. It is well known from atomic physics that chaotic effects become more apparent in higher magnetic fields or by using states of higher energies for the analysis. Hence, by increasing B or investigating the statistics of exciton states with higher energies, GUE statistics could probably be observed also for smaller values of $|\delta'|$.

In Fig. 8.2 we show for a fixed value of $B = 3\,\mathrm{T}$ with the orientation $\boldsymbol{B}(\pi/6,\, \pi/6)$ the appearance of GUE statistics when increasing the parameter δ'. Hence, the transition between GOE and GUE statistics can, e.g., be observed by varying the angle φ or the parameter δ' when keeping the strength of the magnetic field fixed. At this point we have to note that an evaluation of numerical spectra for $\delta' > 0$ shows the same appearance of GUE statistics. This is expected since the analytically shown breaking of all antiunitary symmetries in Sec. 8.2.1 is independent of the sign of the material parameters.

M. Aßmann *et al.* [31, 32] have shown experimentally that excitons in $\mathrm{Cu_2O}$ in an external magnetic field obey GUE statistics. However, since their experimental spectra were analyzed exactly for $\boldsymbol{B}(0,\, \pi/6)$, there must be another explanation for this observation than the cubic band structure. M. Aßmann *et al.* [31, 32] have assigned the observation of GUE statistics to the interaction of excitons and phonons. We will discuss the influence of the exciton-phonon interaction on the level statistics in Sec. 8.4.

8.3

GOE-GUE-Poisson transitions in the nearest neighbor spacing distribution of magnetoexcitons

The model system of excitons in external fields shows Poissonian, GOE or GUE statistics in dependence on the energy, the magnetic field strength and the angles ϑ and φ, i.e., in dependence of experimentally adjustable parameters. Thus, our system is perfectly suited to investigate transitions between the different statistics or different symmetry classes when changing one or more of these parameters. In this section we will now investigate these transitions and compare our results to formulas of the random matrix theory.

8.3.1 Transitions between spacing distributions

In Ref. [370] analytical expressions for the spacing distribution functions in the transition region between the different statistics have been derived using random matrix theory for 2×2 matrices. However, at this point we have to note that the transition between different symmetry classes is not universal and that the level spacing distributions are universal only in the Poisson, GOE or GUE limit [404]. Besides the transition formulas derived within random matrix theory, which will be presented in the following, also other interpolating distributions, e.g., for the transition P → GOE have been proposed in the literature [405–409]. When using one of these distributions for the intermediate regime the results of Secs. 8.3.3 and 8.3.2 may be modified. However, since all the transition formulae presented here were derived in the same manner within random matrix theory in Ref. [370], we use these formula for a consistent description of all transitions considered here.

The transition from Poissonian to GOE statistics is described in random matrix theory by

$$P_{\mathrm{P}\to\mathrm{GOE}}(s;\,\lambda) \quad = \quad Cse^{-D^2s^2}\int_0^\infty \mathrm{d}x\, e^{-x^2/4\lambda^2-x}I_0(z) \tag{8.28a}$$

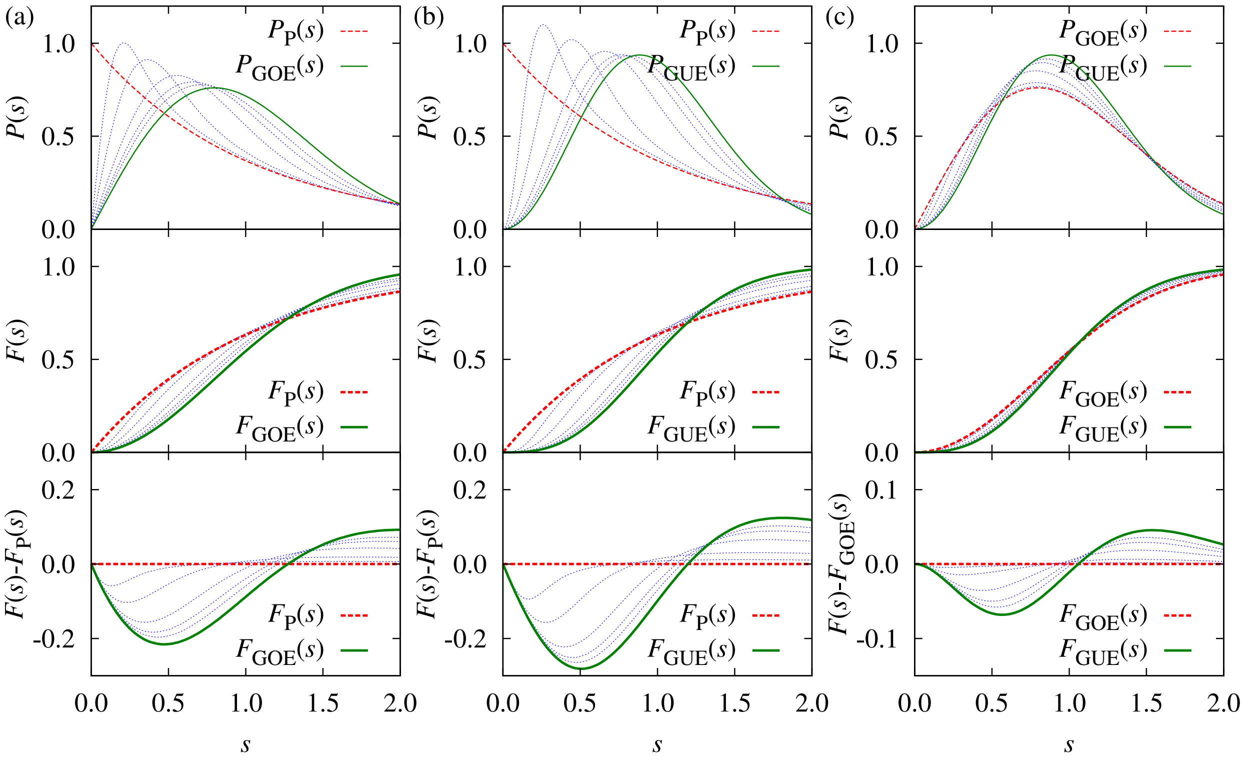

Figure 8.3.: Level spacing probability distribution functions $P(s)$ (first row) and cumulative distribution functions $F(s)$ (second row) for the transitions (a) P → GOE, (b) P → GUE, and (c) GOE → GUE. The blue dotted lines show the transition functions of Eqs. (8.28), (8.29), and (8.30) for $\lambda = 0.1, 0.2, 0.4, 0.6, 0.8$. To visualize the differences between the cumulative distribution functions more clearly, especially for the GOE → GUE transition, we also show in the third row the difference between the distributions for a fixed value of λ and the initial distribution, respectively.

with $z = xDs/\lambda$ and

$$D(\lambda) = \frac{\sqrt{\pi}}{2\lambda} U\left(-\frac{1}{2},\, 0,\, \lambda^2\right), \tag{8.28b}$$

$$C(\lambda) = 2D(\lambda)^2, \tag{8.28c}$$

a parameter λ, the Tricomi confluent hypergeometric function $U(a,\, b,\, z)$ [410] and the modified Bessel function $I_0(z)$ [410]. For the special cases of $\lambda \to 0$ or $\lambda \to \infty$ Poissonian or GOE statistics is obtained, respectively. However, already for $\lambda \gtrsim 0.7$ the transition to GOE statistics is almost completed [370].

The transition from Poissonian to GUE statistics is described by

$$P_{\mathrm{P}\to\mathrm{GUE}}(s;\, \lambda) = Cs^2 e^{-D^2 s^2} \int_0^\infty \mathrm{d}x\, e^{-x^2/4\lambda^2 - x} \frac{\sinh(z)}{z} \tag{8.29a}$$

with $z = xDs/\lambda$ and

$$D(\lambda) = \frac{1}{\sqrt{\pi}} + \frac{1}{2\lambda} e^{\lambda^2} \mathrm{erfc}(\lambda) - \frac{\lambda}{2} \mathrm{Ei}(\lambda^2) + \frac{2\lambda^2}{\sqrt{\pi}} \, {}_2F_2\left(\frac{1}{2}, 1; \frac{3}{2}, \frac{3}{2}; \lambda^2\right), \tag{8.29b}$$

$$C(\lambda) = \frac{4D(\lambda)^3}{\sqrt{\pi}}, \tag{8.29c}$$

the complementary error function erfc [410], the exponential integral Ei [410] and a generalized hypergeometric function ${}_2F_2$ [411].

Finally, the transition from GOE to GUE statistics is given by

$$P_{\mathrm{GOE}\to\mathrm{GUE}}(s;\, \lambda) = Cse^{-D^2s^2} \mathrm{erf}\left(\frac{Ds}{\lambda}\right) \tag{8.30a}$$

with

$$D(\lambda) = \frac{\sqrt{1+\lambda^2}}{\sqrt{\pi}} \left(\frac{\lambda}{1+\lambda^2} + \mathrm{arccot}(\lambda)\right), \tag{8.30b}$$

$$C(\lambda) = 2\sqrt{1+\lambda^2}\, D(\lambda)^2. \tag{8.30c}$$

As in Ref. [370], we calculate the distribution functions for $\lambda = 0.01 \times 1000^{(k-1)/999}$ with $k = 1, \ldots, 1000$ and then numerically integrate the results to obtain the corresponding cumulative distribution functions $F(s;\, \lambda)$. All these functions are shown for different values of λ in Fig. 8.3.

As the transition from Poissonian to GOE statistics has been investigated in detail for the hydrogen atom in external fields [385], we will treat only the two other transitions in the following.

8.3.2 Transition GOE → GUE

Let us start with the transition from GOE to GUE statistics. For this case we solve the generalized eigenvalue problem (8.7) for different orientations of the magnetic field $\boldsymbol{B}(\varphi,\, \vartheta)$ by setting $\vartheta = \pi/6$ and gradually increasing the angle φ from 0 to $\pi/4$. To increase the statistical significance, we analyze and merge the level spacings for $B = 2.8\,\mathrm{T}$, $B = 3.0\,\mathrm{T}$, and $B = 3.2\,\mathrm{T}$ for a given value of φ [385]. The results are finally fitted by the function $F_{\mathrm{GOE}\to\mathrm{GUE}}(s;\, \lambda)$ and shown in Fig. 8.4.

For the special case of $\varphi = 0$ we obtain GOE statistics as expected since the magnetic field is oriented in the symmetry plane of the solid with $\hat{\boldsymbol{n}}_2 = (0,\, 1,\, 0)^{\mathrm{T}}$ [cf. Eq. (8.17)]. When increasing the angle φ, the parameter λ changes rapidly from 0 to 0.5 and hence the transition from GOE to GUE statistics is almost completed for $\varphi \gtrsim 3\pi/48$ (see Fig. 8.5).

The decrease of the parameter λ for $\varphi \gtrsim \pi/8$ in Fig. 8.5 can be explained by considering the orientation of $\boldsymbol{B}$ with respect to all symmetry planes of the lattice. Hence, we calculate the value of the parameter σ of Eq. (8.19) for $\vartheta = \pi/6$ and increasing values of φ. It is obvious that the value of σ increases for $0 \leq \varphi \leq \pi/8$ and decreases for $\pi/8 \leq \varphi \leq \pi/4$ since the magnetic field moves away from the plane with $\hat{\boldsymbol{n}}_2$ and then approaches the plane with $\hat{\boldsymbol{n}}_7$. Therefore, the fact that $\boldsymbol{B}$ approaches the plane with $\hat{\boldsymbol{n}}_7$ for $\varphi \geq \pi/8$ explains the decrease of λ in Fig. 8.4.

8.3.3 Transition Poisson → GUE

Let us now treat the transition from Poissonian to GUE statistics. It is known from the hydrogen atom in external fields that for fixed values of the magnetic field strength B the low-energy part of

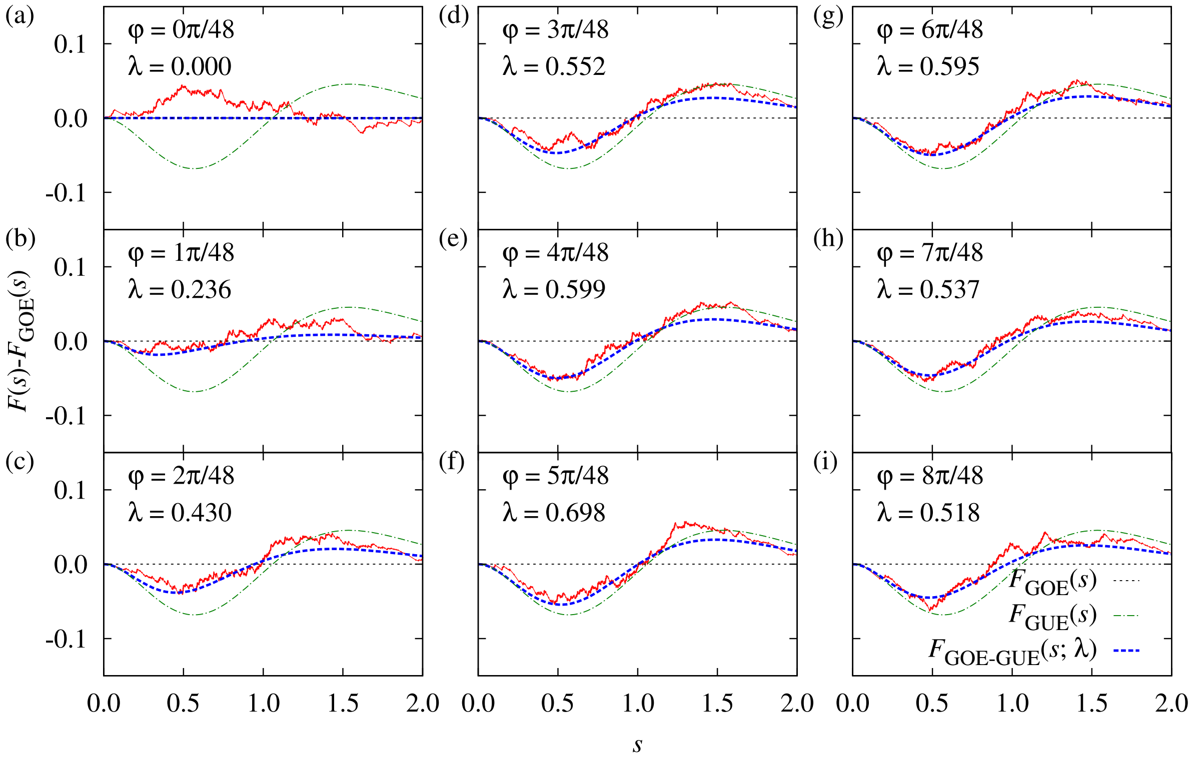

Figure 8.4.: Transition from GOE to GUE statistics for fixed values of the magnetic field strength B and increasing values of the angle φ in $\boldsymbol{B}(\varphi, \vartheta = \pi/6)$. The results are presented in the same way as in the bottom most panel of Fig. 8.3 to show the differences between $F_{\mathrm{GOE}}(s)$ and $F_{\mathrm{GUE}}(s)$ more clearly. The data points (red) were fitted with the analytical function $F_{\mathrm{GOE}\to\mathrm{GUE}}(s;\,\lambda)$. The optimum values of the fit parameter λ are given in each panel, but are also shown in Fig. 8.5. One can observe a good agreement between the numerical data and the analytical function describing the transition between the two statistics in dependence on λ. Only for $\varphi = 0$ the data shows a slight admixture of Poissonian statistics to the expected GOE statistics. For further information see text.

the eigenvalue spectrum will show Poissonian statistics while the high-energy part already shows GOE statistics. For a better level statistics it is appropriate to analyze the spectra with a constant scaled energy $\hat{E}$.

For fixed small values of the scaled energy the corresponding classical dynamics becomes regular and energy eigenvalues of the quantum mechanical system will show purely Poissonian statistics. On the other hand, as we have shown above, GUE statistics is observed best at large energies and for angles φ and ϑ, for which the magnetic field is oriented exactly between two symmetry planes of the lattice. Hence, keeping the values $\varphi = \pi/8$, $\vartheta = \pi/6$, and $\delta' = -0.15$ fixed and increasing the scaled energy, we expect to observe a transition from Poissonian to GUE statistics.

Having unfolded the spectra according to Ref. [385], we fit the numerical results by the function $F_{\mathrm{P}\to\mathrm{GUE}}(s;\,\lambda)$ given in Eq. (8.29). It can be seen from Fig. 8.6 that we obtain a good agreement between the results for our system and the analytical function for all scaled energies $\hat{E} > -0.9$. The

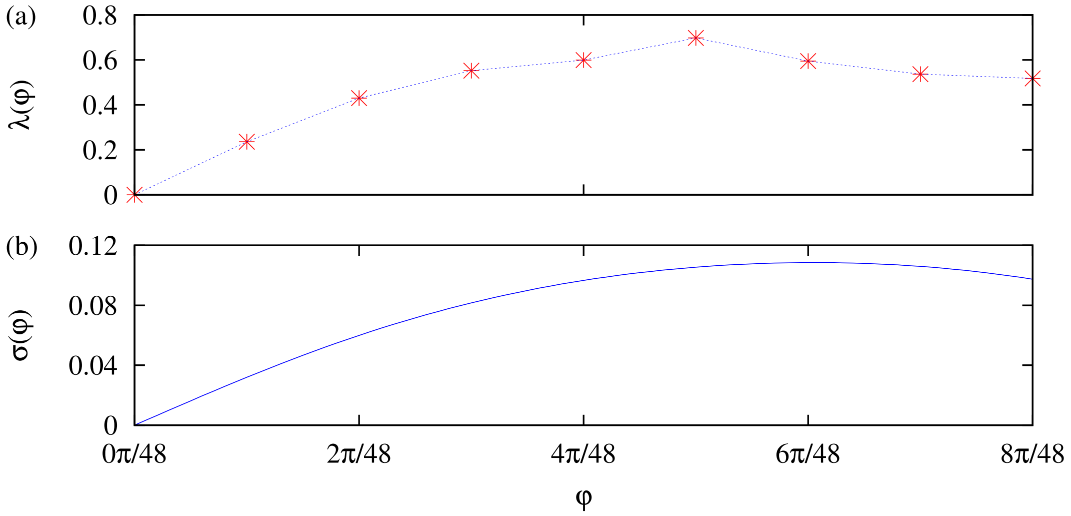

Figure 8.5.: (a) Optimum values of the fit parameter λ in dependence on the angle φ for the situation presented in Fig. 8.4. The blue dashed line only serves as a guide to the eye. (b) The function $\sigma(\varphi)$ of Eq. (8.19) for $\vartheta = \pi/6$. We obtain a qualitatively good agreement between both curves, i.e., as expected, both values $\lambda(\varphi)$ and $\sigma(\varphi)$ increase from zero to a certain value and then decrease for $\varphi \gtrsim \pi/8$.

transition from Poissonian to GUE statistics takes place already at very small values of the scaled energy $-1.2 \lesssim \hat{E} \lesssim -0.6$ (see Fig. 8.7). This differs from the hydrogen atom in external fields where the statistics is still Poisson-like for $\hat{E} \lesssim -0.6$ [385] and can be explained by the presence of the cubic band structure here. Therefore, the presence of the cubic band structure increases the chaos in comparison with the hydrogen atom.

For very small values of the scaled energy $\hat{E} \lesssim -0.8$ a reasonable analysis of the spectra is hardly possible. For these values of $\hat{E}$ we cannot obtain enough converged eigenvalues in the dense part of the spectrum due to the required computer memory. On the other hand, the number of low-lying sparse levels increases. Hence, fitting the number $N(E)$ of energy levels with the function $\bar{N}(E) = aE^{-2/3} + b$ for the unfolding procedure (cf. Sec. 8.2.2) does not lead to good results since the mean number of energy levels is proportional to $E^{-2/3}$ only in the dense part of the spectrum. This effect can already be observed for $\hat{E} = -1.009$ in Fig. 8.6. Note that a change in the unfolding procedure or the fit function would not lead to better results as the problem is connected with the appearance of the low-lying sparse levels. These levels lead to individual but nontypical fluctuations [385].

It is generally assumed that the NNS of large random matrices can be approximated by the NNS of 2×2 matrices of the same universality class [370]. Since we obtained a good agreement when fitting the functions $F_{\mathrm{GOE}\to\mathrm{GUE}}(s;\,\lambda)$ and $F_{\mathrm{P}\to\mathrm{GUE}}(s;\,\lambda)$, which were derived for 2×2 matrices, to our numerical results, we could prove the Wigner surmise [398] for our system.

We finally want to note that all transitions considered here are modelled by Hamiltonians of the form $H = H_\beta + \lambda H_{\beta'}$ [370], where $H_{\beta'}$ has a lower symmetry than H_β. The level statistics is strongly affected by the perturbation $H_{\beta'}$ if the level spacings of H_β, which are smaller than the matrix elements of this Hamiltonian, and the matrix elements of $\lambda H_{\beta'}$ are of comparable size. In the case of $\hbar \to 0$, the transition will take place at even smaller values of λ. Especially, the connection

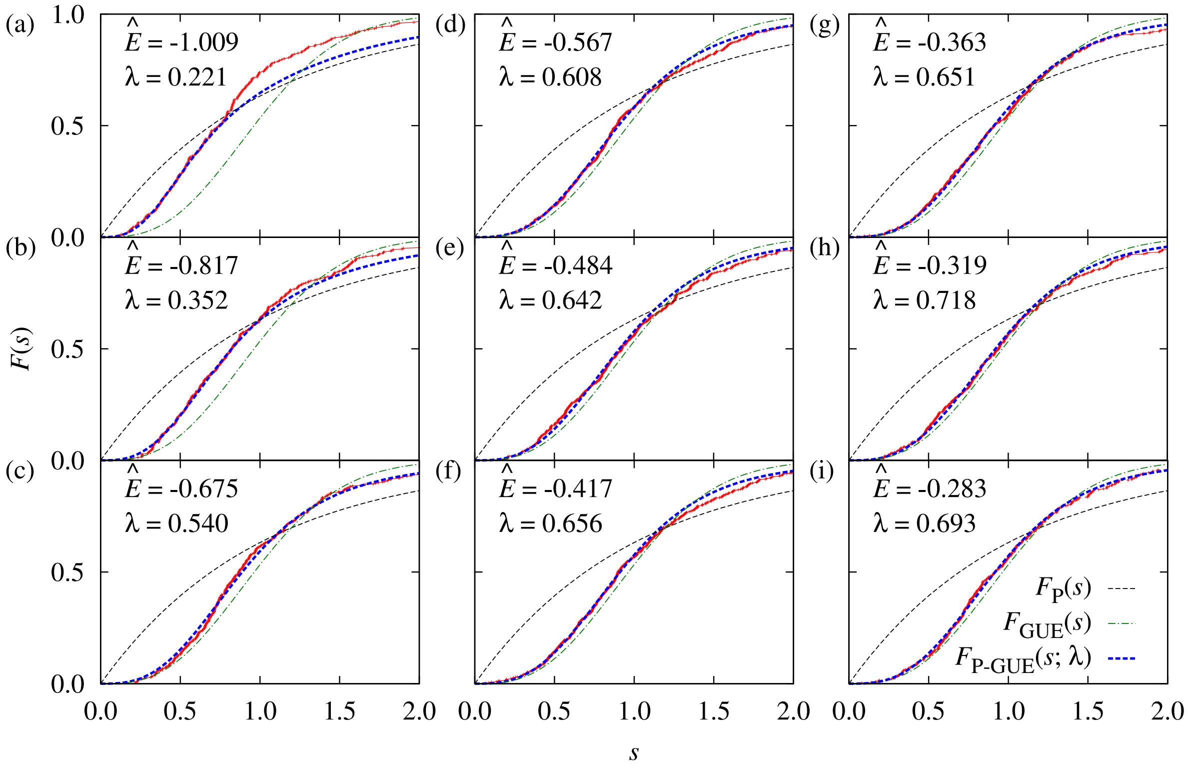

Figure 8.6.: Transition from Poissonian to GUE statistics for fixed values of the angles $\varphi = \pi/8$, $\vartheta = \pi/6$ and increasing values of the scaled energy $\hat{E}$. Except for $\hat{E} = -1.009$ a good agreement between the numerical data and the analytical function $F_{\mathrm{P}\to\mathrm{GUE}}(s;\,\lambda)$ is obtained. For further information see text.

between λ and the parameter σ [cf. Eqs. (8.18) and (8.19)] must depend on $\hbar$. However, we note that the parameter σ has only been introduced phenomenologically to describe the dependency of the transition on the angle between the vector $\hat{\boldsymbol{n}}$ (8.16) or $\hat{\boldsymbol{B}} = \boldsymbol{B}/B$ and the normal vectors $\hat{\boldsymbol{n}}_i$ (8.17) of the symmetry planes of the lattice.

To investigate the dependence of all results on $\hbar$, further and more extensive calculations are necessary, which is beyond the scope of this work. Nevertheless, our model system offers the possibility for an according analysis and we may discuss the effects in a future work.

Changing the two parameters δ' and the scaled energy $\hat{E}$ in numerical calculations allows for investigating arbitrary transitions of the level statistics in the triangle between Poissonian (arbitrary δ', small $\hat{E}$), GOE ($\delta' = 0$, large $\hat{E}$), and GUE statistics ($\delta' \neq 0$, large $\hat{E}$). This has been done in a recent work [50, 412]. As for arbitrary transitions within this triangle no analytical formulas have been derived within random matrix theory so far, also corresponding functions $P(s;\,\lambda_1,\,\lambda_2)$ have been proposed in this work.

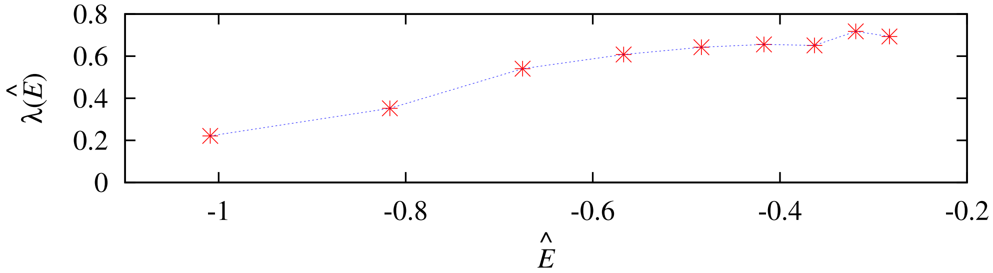

Figure 8.7.: Optimum values of the fit parameter λ in dependence on the scaled energy $\hat{E}$ for the situation presented in Fig. 8.6. The blue dashed line only serves as a guide to the eye. The value of λ increases from a small value at low scaled energies to about $\lambda \approx 0.7$, where the function $F_{\mathrm{P}\to\mathrm{GUE}}(s;\,\lambda)$ almost describes GUE statistics.

8.4 Exciton-phonon interaction breaking all antiunitary symmetries in external magnetic fields

In this section we discuss the case that the plane spanned by the external fields coincides with a symmetry plane of the lattice. Without the exciton-phonon interaction one would expect to observe only GOE statistics according to the explanations given in Sec. 8.2.1. However, recent experiments indicate that the spectrum of magnetoexcitons reveals GUE statistics for *all* orientations of the magnetic field applied [31, 32]. Hence, we will now concentrate on the effects of the exciton-phonon interaction in more detail and show that they lead, in combination with the cubic valence band structure, to a breaking of all antiunitary symmetries for an arbitrary orientation of the external fields.

The Hamiltonian describing the exciton-phonon interaction [85] does not only depend on the relative coordinate $\boldsymbol{r}$ but also on the coordinate of the center of mass $\boldsymbol{R}$. Hence, when considering the Hamiltonian of excitons *and* phonons the momentum of the center of mass $\boldsymbol{P}$ is not a good quantum number, i.e., the Hamiltonian and the operator $\boldsymbol{P}$ no longer commute. Consequently, we are not allowed to set the momentum of the center of mass to zero, as has been done in the calculation of Sec. 8.2.1, but have to treat the complete problem

$$H = H_{\mathrm{exc}} + H_{\mathrm{exc-ph}} + H_{\mathrm{ph}} \tag{8.31}$$

with the exciton Hamiltonian given in Eq. (8.2), the phonon Hamiltonian given in Eq. (2.75), and the exciton-phonon interaction terms (see Secs. 3.1.1 and 3.1.3 and Refs. [7, 73, 85])

$$H_{\mathrm{exc-ph}}^{(\mathrm{LA})} = \sqrt{\frac{\hbar}{2c_{\mathrm{LA}}\rho V}} \sum_{\boldsymbol{q}} \sqrt{q} \left[e^{i\boldsymbol{q}\cdot\boldsymbol{R}} \left(D_{\mathrm{e}} e^{i\frac{\mu}{m_{\mathrm{e}}}\boldsymbol{q}\cdot\boldsymbol{r}} + D_{\mathrm{h}} e^{-i\frac{\mu}{m_{\mathrm{h}}}\boldsymbol{q}\cdot\boldsymbol{r}} \right) a_{\mathrm{LA}}(\boldsymbol{q}) + \mathrm{h.c.} \right], \tag{8.32a}$$

$$H_{\mathrm{exc-ph}}^{(\mathrm{LO})} = \sqrt{\frac{e^2\hbar\omega_{\mathrm{LO}}}{2\varepsilon_0 V}\left(\frac{1}{\varepsilon_{\mathrm{b}}} - \frac{1}{\varepsilon_{\mathrm{s}}}\right)} \sum_{\boldsymbol{q}} \frac{1}{q} \left[e^{i\boldsymbol{q}\cdot\boldsymbol{R}} \left(e^{i\frac{\mu}{m_{\mathrm{e}}}\boldsymbol{q}\cdot\boldsymbol{r}} + e^{-i\frac{\mu}{m_{\mathrm{h}}}\boldsymbol{q}\cdot\boldsymbol{r}} \right) a_{\mathrm{LO}}(\boldsymbol{q}) + \mathrm{h.c.} \right]. \tag{8.32b}$$

Note that the Hamiltonians (8.32) are only the leading terms of the exciton-phonon interaction. Hence, also further terms in Eq. (8.32) could be considered, which may have cubic symmetry. However, here we show that already the operators (8.32) in combination with the complete valence band structure are sufficient to break all antiunitary symmetries in the presence of an external magnetic field.

The consideration of the valence band structure, a finite momentum of the center of mass, the external fields, and the phonons is very complicated. Hence, we concentrate only on the main effects to show that the exciton-phonon interaction will lead to a breaking of all antiunitary symmetries even if the plane spanned by the external fields is identical to a symmetry plane of the lattice.

When considering a finite momentum $\boldsymbol{P} = \hbar\boldsymbol{K}$ of the exciton center of mass in an external magnetic field, the motional Stark effect occurs (cf. Sec. 7.1.2 and Ref. [348]). Since the insertion of a finite momentum of the center of mass in the complete Hamiltonian (8.2) is quite laborious, we treat only the leading term of the motional Stark effect, which has the form [348]

$$H_{\mathrm{ms}} = \frac{\hbar e}{M}(\boldsymbol{K} \times \boldsymbol{B}) \cdot \boldsymbol{r} \tag{8.33}$$

with the isotropic exciton mass $M = m_{\mathrm{e}} + m_{\mathrm{h}} = m_{\mathrm{e}} + m_0/\gamma_1$. Note that this term has the same form as the electric field term in the Hamiltonian (8.2). Hence, the effect of the motional Stark effect is the same as that of an external electric field and we can introduce a total electric field

$$\boldsymbol{F}_{\mathrm{tot}} = \boldsymbol{F} + \boldsymbol{F}_{\mathrm{ms}} = \boldsymbol{F} - \frac{\hbar}{M}(\boldsymbol{K} \times \boldsymbol{B}). \tag{8.34}$$

One could now, in principle, do the same calculation as in Eq. (8.22) to show that the antiunitary symmetry known from the hydrogen atom is broken if the plane spanned by $\boldsymbol{B}$ and $\boldsymbol{F}_{\mathrm{tot}}$ is not identical to one symmetry plane of the solid. However, we have to consider the specific properties, i.e., the size and the orientation, of the motional Stark field $\boldsymbol{F}_{\mathrm{ms}}$ related to the size and the orientation of $\boldsymbol{K}$.

The size of the momentum $\hbar\boldsymbol{K}$ is determined by the interaction between excitons and phonons. Instead of considering the huge number of phonon degrees of freedom, we assume a thermal distribution at a finite temperature T. The direction of $\boldsymbol{K}$ is then evenly distributed over the solid angle and its average size is determined by

$$\frac{3}{2}k_{\mathrm{B}}T = \frac{\hbar^2 K^2}{2M} \tag{8.35}$$

with the Boltzmann constant k_{B}. We assume for all of our calculations a temperature of $T = 0.8\,\mathrm{K}$, which is even slightly smaller than the temperature in experiments [30]. Note that the value of K determined by Eq. (8.35) is of the same order of magnitude as the value estimated via experimental group velocity measurements of the $1S$ ortho-exciton [179, 180]. The relation (8.35) leads to a field strength of

$$F_{\mathrm{ms}} = \sqrt{\frac{3k_{\mathrm{B}}T}{M}}\,B. \tag{8.36}$$

We will now show that the motional Stark field $\boldsymbol{F}_{\mathrm{ms}}$ leads to GUE statistics if the external magnetic field $\boldsymbol{B}$ is oriented in one of the symmetry planes of the lattice. In the general case, the magnetic field then fulfils $\boldsymbol{B} \perp \hat{\boldsymbol{n}}_i$ with one of the nine normal vectors $\hat{\boldsymbol{n}}_i$ given in Eq. (8.17). In

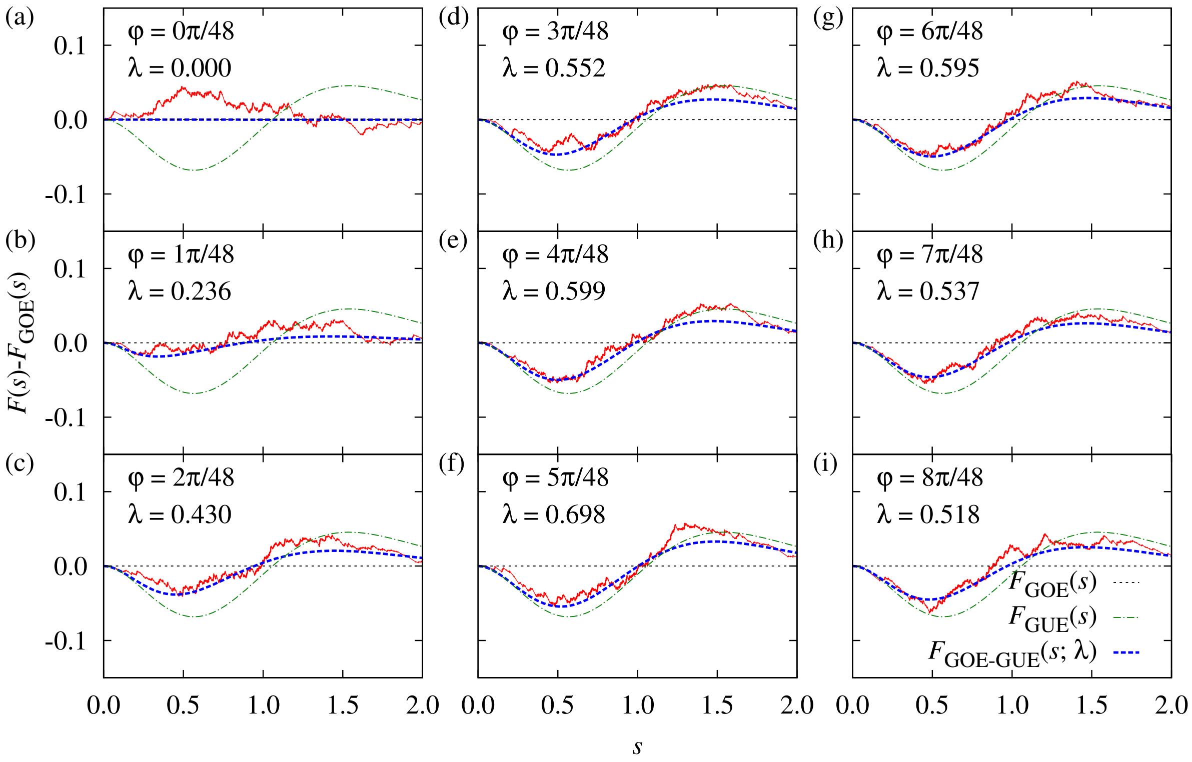

Figure 8.8.: Transition from GOE to GUE statistics when deflecting the field $\boldsymbol{F}_{\mathrm{ms}}$ in Eq. (8.38) from the symmetry plane $y = 0$ by an angle φ_{ms}. For the magnetic field we have set $\boldsymbol{B}(\varphi = 0,\, \vartheta = \pi/6)$ with $B = 3\,\mathrm{T}$. To obtain enough eigenvalues for a statistical evaluation, we used the simplified model of Sec. 8.1, in which the spins of the electron and hole are neglected. To visualize the differences between the cumulative distribution functions more clearly, we subtract $F_{\mathrm{GOE}}(s)$ from them. The data points (red) were fitted with the analytical function $F_{\mathrm{GOE}\to\mathrm{GUE}}(s;\, \lambda)$. The optimum values of the fit parameter λ are given in each panel and are also shown in Fig. 8.9. One can observe a good agreement between the numerical data and the analytical function describing the transition between the two statistics in dependence on λ. For further information see text.

our numerical example we choose the magnetic field

$$\boldsymbol{B} = \boldsymbol{B}(\varphi = 0,\, \vartheta = \pi/6) = \frac{B}{2}\begin{pmatrix} 1 \\ 0 \\ \sqrt{3} \end{pmatrix} \perp \hat{\boldsymbol{n}}_2 \tag{8.37}$$

with a constant field strength of $B = 3\,\mathrm{T}$. The external electric field is set to $\boldsymbol{F} = \boldsymbol{0}$. The motional Stark field is oriented perpendicular to $\boldsymbol{B}$. Hence, we assume it for φ_{ms} to be oriented perpendicular to the magnetic field and to be initially lying in the same symmetry plane $y = 0$ of the lattice. Then $\boldsymbol{F}_{\mathrm{ms}}$ is deflected from this plane, i.e., the field is rotated by an angle φ_{ms} about the axis given

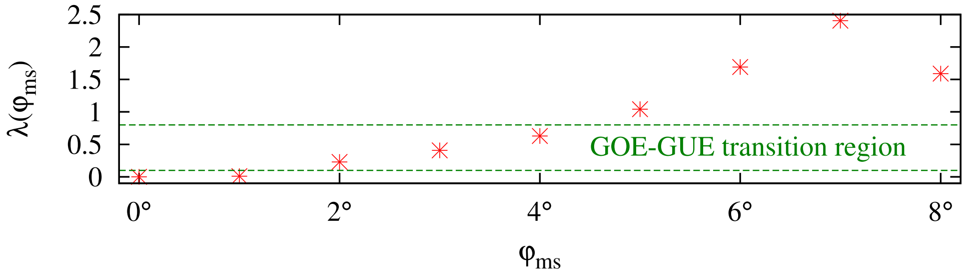

Figure 8.9.: Optimum values of the fit parameter λ in dependence on the angle φ_{ms} for the situation presented in Fig. 8.8. One can see that the value of λ increases very rapidly with increasing φ_{ms}. Already for $\varphi_{\mathrm{ms}} = 5°$ the transition to GUE statistics is completed. As regards the value of λ for $\varphi_{\mathrm{ms}} = 8°$, we have to note that the function $F_{\mathrm{GOE}\to\mathrm{GUE}}(s;\,\lambda)$ only slightly varies for $\lambda \geq 0.8$ and hence small fluctuations in the numerical results will lead to a strong change in λ. For the transition between GOE and GUE statistics only the range of $0.1 \leq \lambda \leq 0.8$ is of importance (green dahed lines) (cf. Sec. 8.3.1). For $\varphi_{\mathrm{ms}} > 8°$ it is always $\lambda > 0.8$ until $\varphi_{\mathrm{ms}} \approx 176°$ [cf. Eq. (8.39)].

by the magnetic field of Eq. (8.37):

$$\boldsymbol{F}_{\mathrm{ms}}(\varphi_{\mathrm{ms}}) = \frac{F_{\mathrm{ms}}}{2}\begin{pmatrix} \sqrt{3}\cos\varphi_{\mathrm{ms}} \\ 2\sin\varphi_{\mathrm{ms}} \\ -\cos\varphi_{\mathrm{ms}} \end{pmatrix}. \tag{8.38}$$

Here F_{ms} is given by Eq. (8.36) with $B = 3\,\mathrm{T}$ and $T = 0.8\,\mathrm{K}$. According to the explanations given in Sec. 8.2.1, we expect to obtain GOE statistics with our numerical results only for the cases $\varphi_{\mathrm{ms}} = 0$ and $\varphi_{\mathrm{ms}} = \pi$, since

$$\hat{\boldsymbol{n}} = (\boldsymbol{B}\times\boldsymbol{F})/\left|\boldsymbol{B}\times\boldsymbol{F}\right| = \frac{1}{2}\begin{pmatrix} -\sqrt{3}\sin\varphi_{\mathrm{ms}} \\ 2\cos\varphi_{\mathrm{ms}} \\ \sin\varphi_{\mathrm{ms}} \end{pmatrix} \tag{8.39}$$

is parallel to $\hat{\boldsymbol{n}}_2$ only for these two values of φ_{ms}. The decisive question is how fast the transition from GOE to GUE statistics takes place if the field $\boldsymbol{F}_{\mathrm{ms}}$ is deflected from the symmetry plane $y = 0$. This is shown in Fig. 8.8.

As we have already stated in Sec. 8.1.1, the number of eigenvalues which can be used for a statistical analysis is limited due to the required computer memory or the limited size of our basis. Therefore, to enhance the number of converged states, we used for the calculation of Fig. 8.8 the simplified model of Sec. 8.1 with $\Delta = H_B = 0$, $m_{\mathrm{e}} = m_0$, $\gamma_1 = 2$ and $\delta' = -0.15$. However, we expect a qualitatively similar behavior for $\mathrm{Cu_2O}$, i.e., when considering $\Delta \neq 0$, as we will discuss and show below.

For a quantitative analysis the results are fitted with the function $F_{\mathrm{GOE}\to\mathrm{GUE}}(s;\,\lambda)$ of Eq. (8.30) describing the transition between both statistics. We show the resulting values of the fit parameter λ in Fig. 8.9. It can be seen that the parameter λ increases very rapidly with increasing values of φ_{ms}. Already for $\varphi_{\mathrm{ms}} = 5°$ the statistics is almost purely GUE statistics. Hence, the motional Stark field has a strong influence on the level spacing statistics. This implies that for a majority of the orientations of $\boldsymbol{F}_{\mathrm{ms}}$ GUE statistics will be observable. Our main argument for the observed

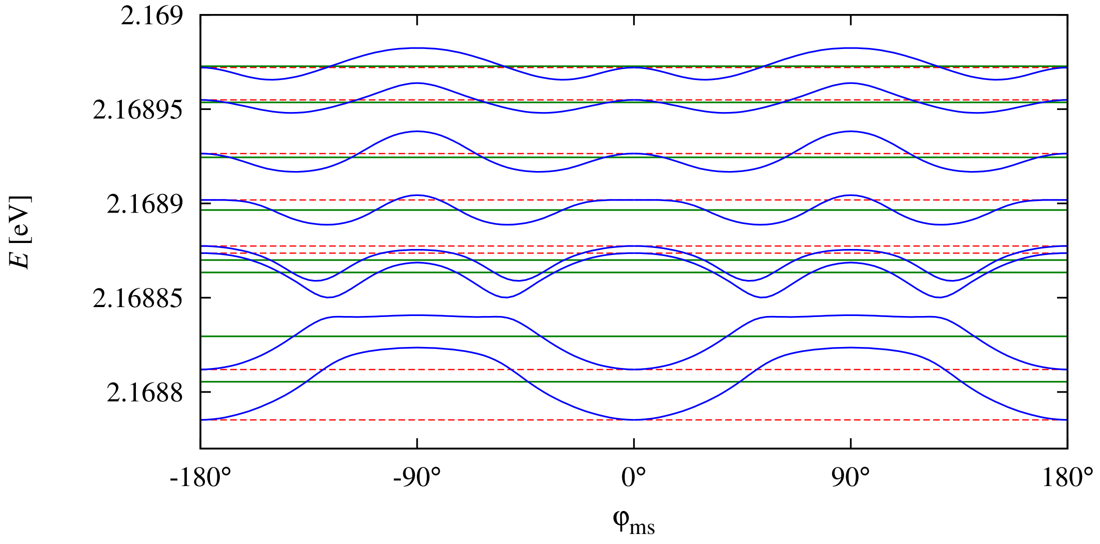

Figure 8.10.: Dependence of the energy of specific exciton states on the angle φ_{ms} of the field $\boldsymbol{F}_{\mathrm{ms}}$. For the magnetic field we have set $\boldsymbol{B}(\varphi = 0,\, \vartheta = \pi/6)$ with $B = 3\,\mathrm{T}$. It can be seen that for φ_{ms} and $\pi + \varphi_{\mathrm{ms}}$ the exciton energies (blue solid lines) are shifted in the same direction with respect to the energy at $\varphi_{\mathrm{ms}} = 0$ (red dashed lines). The average energy (green solid lines) often clearly differs from the energy at $\varphi_{\mathrm{ms}} = 0$.

level statistics is now that since the momentum $\boldsymbol{K}$ and hence also the field $\boldsymbol{F}_{\mathrm{ms}}$ is evenly distributed over the angle φ_{ms}, the exciton spectrum will show GUE statistics on average.

One might argue whether the effects of $\boldsymbol{F}_{\mathrm{ms}}$ cancel each other out if the field is evenly distributed over the solid angle. This can be ruled out when considering the effect of the field on the exciton states for all values of the angle φ_{ms} as shown for a selection of exciton states in Fig. 8.10. It can be seen that the fields $\boldsymbol{F}_{\mathrm{ms}}(\varphi_{\mathrm{ms}})$ and $\boldsymbol{F}_{\mathrm{ms}}(\pi + \varphi_{\mathrm{ms}}) = -\boldsymbol{F}_{\mathrm{ms}}(\varphi_{\mathrm{ms}})$ shift the exciton states in the same direction and not in opposite direction as regards their energies. Hence, on average the exciton states are shifted towards higher or lower energies and do not remain at their position. This argument holds both when using the model with the parameters of Sec. 8.2.2 *and* when using all material parameters of $\mathrm{Cu_2O}$ (see Table 2.2). In Fig. 8.10 the results for $\mathrm{Cu_2O}$ are shown.

Even though we cannot obtain enough converged exciton energies for a statistical analysis when using the parameters of $\mathrm{Cu_2O}$, we can use the small number of converged states to show that the magneto Stark field has the small effect of increasing level spacings, which is a characteristic feature of GUE compared to GOE statistics [cf. Eqs. (8.26) and (8.27)].

To this aim, we consider at first the spectrum of $\mathrm{Cu_2O}$ in a magnetic field $\boldsymbol{B}(\varphi = 0,\, \vartheta = \pi/6)$ to find an avoided crossing (see panel (a) of Fig. 8.11). We then choose the magnetic field strength of $B = 1.98\,\mathrm{T}$, where an avoided crossing appears, to be fixed, and calculate the spectrum in dependence on the angle φ_{ms}. The strength of the motional Stark field is given by Eq. (8.36) with $B = 1.98\,\mathrm{T}$ and $T = 0.8\,\mathrm{K}$. We now calculate the energies of the states for the following three cases, where the magnetic field strength is always given by $B = 1.98\,\mathrm{T}$: (i) $F_{\mathrm{ms}} = 0$, (ii) $F_{\mathrm{ms}} = \sqrt{2k_{\mathrm{B}}T/M}\,B$ and $\varphi_{\mathrm{ms}} = 0$, (iii) $F_{\mathrm{ms}} = \sqrt{2k_{\mathrm{B}}T/M}\,B$ and taking the average of the exciton energies over φ_{ms}. These energies are shown in panel (b) of Fig. 8.11. We assume

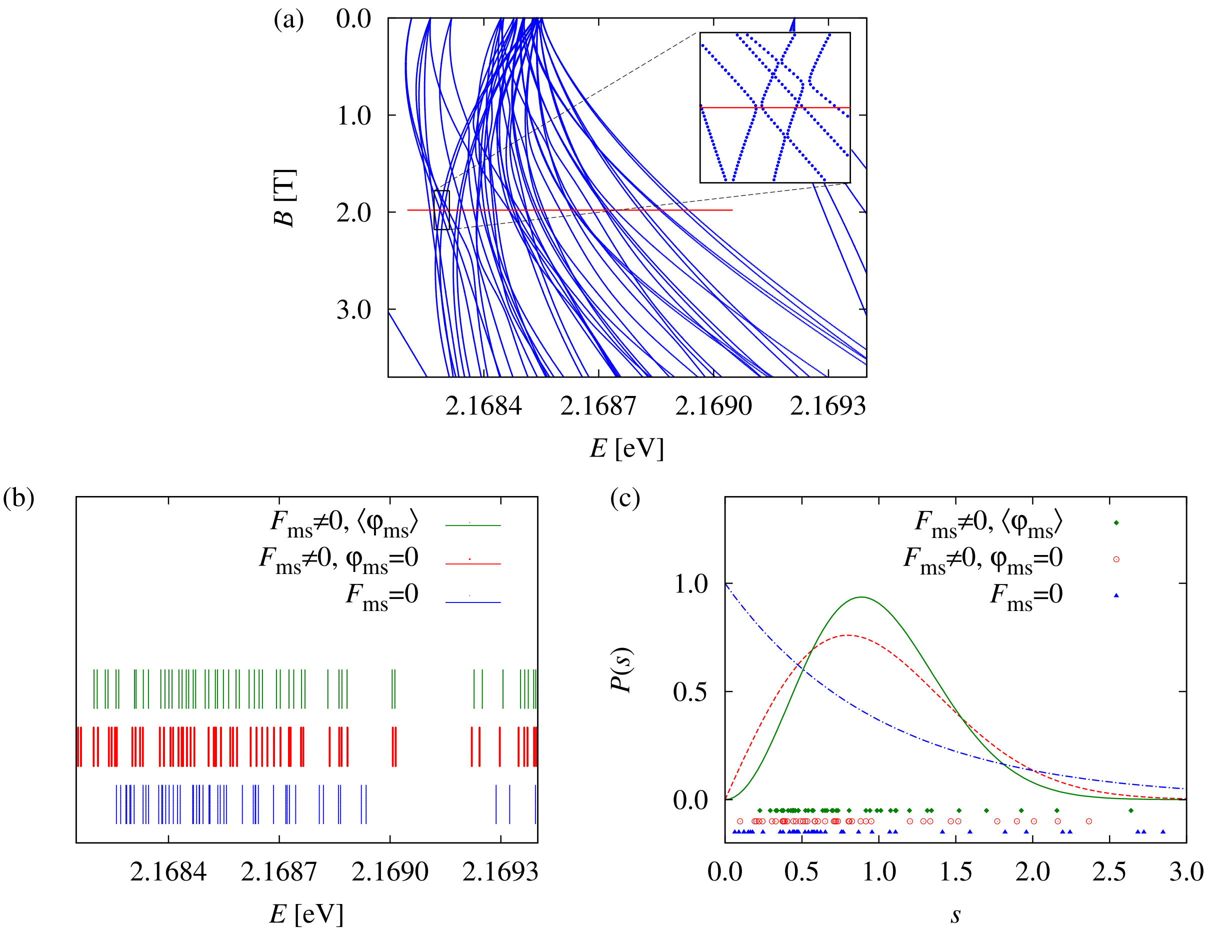

Figure 8.11.: (a) Splitting of the $n = 5$ exciton states of Cu$_2$O in an external magnetic field $\boldsymbol{B} = \boldsymbol{B}(\varphi = 0, \vartheta = \pi/6)$ with $F_{\mathrm{ms}} = 0$. At $B \approx 1.98\,\mathrm{T}$ an avoided crossing can be observed (see inset and red line). (b) Energy of the $n = 5$ states for $B = 1.98\,\mathrm{T}$ and (i) $F_{\mathrm{ms}} = 0$ (blue lines), (ii) $F_{\mathrm{ms}} = 9.57 \times 10^3\,\mathrm{V/m}$ given by Eq. (8.38) with $\varphi_{\mathrm{ms}} = 0$ (red lines), and (iii) F_{ms} given by Eq. (8.38) but taking the position of the states when averaging over $\varphi_{\mathrm{ms}} = 0$ (green lines). (c) Normalized spacings for the three cases considered. It can be seen that the motional Stark effect further suppresses small spacings. For a comparison, we also show the distribution functions for Poissonian statistics (blue dash-dotted line), GOE statistics (red dashed line), and GUE statistics (green solid line).

a constant density of states due to the small energy range considered here. Then the normalized spacings between two neighboring exciton states are determined as $s_i = (E_i - E_{i+1})/\bar{E}$ with $\bar{E}$ denoting the mean value of all spacings considered. One can see from panel (c) of Fig. 8.11 that the level spacings change for the three cases considered. Especially for small values of s the spacing increases, which illustrates the repulsion of levels and the transition to GUE statistics.

Overall, it can be stated that the exciton-phonon interaction leads to a finite momentum of the center of mass of the exciton, which is evenly distributed over the solid angle. The size of this momentum is on average determined by the Boltzmann distribution. In an external magnetic field this finite momentum causes the motional Stark effect. The electric field corresponding to this effect breaks in combination with the cubic lattice all antiunitary symmetries in the system even if the plane spanned by the external fields coincides with one of the symmetry planes of the lattice.

9 Exciton-polaritons in cuprous oxide

Even though the spectrum of Rydberg excitons in Cu_2O can be described quite well in a first approximation by the hydrogen-like model of Wannier, one must keep in mind that excitons are complex many-body states of the solid and, hence, that there are significant limitations to the hydrogen-like model and to the atom-like description of these quasi-particles [61].

Some essential corrections to the hydrogen-like model like the inclusion of the complete cubic valence band structure [77–81, 318], the central-cell corrections [7, 10, 12, 162, 227, 324–326], and the exchange interaction [7, 12, 162, 303, 304] as well as interactions with phonons [74, 221, 242] have already been discussed for excitons Cu_2O in the previous chapters.

There is another fundamental difference between atoms and excitons as regards their interaction with light. By analogy with the interaction of atoms with light one may suppose that absorption of light in a crystal can be described as the excitation of an exciton with the simultaneous disappearance of a photon [7]. Indeed, in the weak-coupling limit, the incident light acts only as a perturbation on the different energy states or excitations of the solid like, e.g., optical phonons, plasmons, excitons or higher band-to-band transitions [12]. In a more general way one can speak of a coupling of light to a dipole-active oscillator. Since the excited states in the solid are connected to a polarization and an oscillating polarization emits again an electromagnetic wave acting back onto the incident wave, there is an interplay between light and matter. If the frequency of light is within the range of the resonance frequency of one oscillator, the coupling is strong and anomalous dipersion can be observed [7]. Due to this coupling excitons and photons cannot be treated as independent entities or good eigenstates, but new quasi-particles must be introduced, which are called polaritons[1] and which represent the quanta of the mixed state of polarization and electromagnetic wave [17, 141, 413–419].

Here we present the theory of exciton-polaritons and its application to Cu_2O. Having extended the Hamiltonian of Chapter 6, which accounts for the complete valence band structure, the exchange interaction, and the central-cell corrections, for a finite momentum $\hbar\boldsymbol{K}$ of the center of mass in Sec 9.1, we present in Sec. 9.2 formulas to calculate dipole and quadrupole oscillator oscillator strengths for the three cases where $\boldsymbol{K}$ coincides with one of the high-symmetry axes of the crystal lattice.

---

[1] The name polariton is a composition of polarization and photon. Related to the corresponding excitation in the solid one also speaks of, e.g., phonon polaritons or exciton polaritons. The quasi-particle resulting from an interaction between excitons, photons *and* phonons is called phonoriton. It has been observed experimentally in Cu_2O [204].

With the solutions of the K-dependent Hamiltonian of excitons, one can then calculate the polariton dispersion. In Sec. 9.3.1 the multi-polariton concept of exciton-polartions is introduced, which is then simplified using the rotating wave approximation discussed in Sec. 9.3.2. Within this approximation it is also possible to include the nonanalytic exchange interaction as shown in Sec. 9.3.3. Since the splitting due to the nonanalytic exchange interaction at $K = 0$ is identical to the longitudinal-transverse splitting (LT-splitting) when treating polaritons, this interaction needs to be considered for a correct treatment of the complete problem. We shortly discuss criteria for spatial or temporal coherence in Sec. 9.3.4, by which statements about the observability of polariton effects for $\mathrm{Cu_2O}$ can be made.

As regards exciton-polaritons in cuprous oxide the $1S$ ortho-exciton is of particular interest as for this state characteristic polariton effects like propagation beats and the conservation of coherence over macroscopic distances have already been demonstrated experimentally [178]. Furthermore, the threefold degeneracy of this state is lifted for finite momentum of the center of mass $\hbar K$, and its oscillator strengths [179] as well as its dispersion are anisotropic (cf. Secs. 4.1 and 4.5.2) [82–84]. All of these effects and the number of experimental results for, e.g., the oscillator strength, the $\boldsymbol{K}$-dependent spectra, and the group velocity [179], with which theoretical results can be compared, make the $1S$ ortho-exciton an ideal candidate for theoretical investigations. Only very recently experiments on the second harmonics generation in $\mathrm{Cu_2O}$ have furthermore validated the polariton character of the $1S$ state and also of the higher nS and nD states [420].

As the $1S$ exciton state lies energetically clearly below the other states, it can be treated separately from these states. In Sec. 9.4, we present a 5×5 matrix model, which allows us to calculate the dispersion of the $1S$ ortho-exciton polariton and to investigate its properties theoretically for any direction of $\boldsymbol{K}$.

In the Secs. 9.5 to 9.7 we present the application of the theory of exciton polaritons to $\mathrm{Cu_2O}$. Starting with the simple hydrogen-like model of excitons, we discuss the effects of the exciton-photon interaction on the giant Rydberg exciton states with a high principal quantum number in Sec. 9.5. As the exciton states of large principal quantum number have a large radius and, thus, a very small extension in momentum space, the effect of the valence band structure can be disregarded here. We show that a strong mixing of exciton states with different principal quantum number n in the resonance region occurs, which can be described correctly only within a multi-polariton framework.

Since especially for the exciton states with a small quantum number $n \leq 4$ the effects of complete valence band structure, the exchange interaction, and the central-cell corrections are large, we use the Hamiltonian of excitons of Sec. 9.1 for these states in Sec. 9.6. This finally yields very complex polariton dispersions. Since due to the cubic lattice the orientation of $\boldsymbol{K}$ with respect to the crystal axes becomes important, we discuss the polariton spectra for the three orientations of $\boldsymbol{K}$ along the axes [001], [110], and [111] of high symmetry.

Using criteria for spatial or temporal coherence, we also discuss the observability of polariton effects for $\mathrm{Cu_2O}$ and show that they can be neglected for exciton states with $n \geq 2$ as regards transmission experiments. This is an important result for future work on $\mathrm{Cu_2O}$ since it allows one to treat excitons as good eigenstates of the solid in theory when comparing theoretical results to transmission spectra.

The only exciton state for which a pronounced polariton effect has been observed in several experiments, the $1S$ ortho-exciton state, will be treated separately in Sec. 9.7. At first, we discuss the effects of a finite momentum $\hbar\boldsymbol{K}$ of the center of mass on the spectrum. The $\boldsymbol{K}$-dependent splitting, which has been discussed in Refs. [82–84] and Sec. 4.5.2, is now treated using the $\boldsymbol{K}$-dependent Hamiltonian in explicit form and including the central-cell corrections. The calculated splittings are in the same order of magnitude as the splittings observed experimentally [82–84].

Furthermore, we are able to compare experimental results for the group velocity [179, 180], the oscillator strengths [178], and spectra for different orientations of $\boldsymbol{K}$ [83] with our numerical results. This can be done using the 5 × 5 matrix model mentioned above. We especially discuss the two cases of the polariton spectra in the planes perpendicular to $[1\bar{1}0]$ and [111]. In the first case the vector $\boldsymbol{K}$ is oriented in a symmetry plane of the lattice so that the polariton states can be classified according to two different irreducible representations. As regards the second case, we are able to compare our results with experimental transmission spectra. Essential parts of this Chapter have been published in Ref. [49].

9.1 $\boldsymbol{K}$-dependent Hamiltonian in Cu_2O

In this section we present the theory of excitons with a finite momentum of the center of mass in Cu_2O, where the cubic valence band structure, the exchange interaction and the central-cell corrections are considered.

The Hamiltonian of the exciton is given by (cf. Chapters 4 and 6)

$$H = E_{\mathrm{g}} + V(\boldsymbol{r}_e - \boldsymbol{r}_h) + H_{\mathrm{e}}(\boldsymbol{p}_{\mathrm{e}}) + H_{\mathrm{h}}(\boldsymbol{p}_{\mathrm{h}}) + H_{\mathrm{exch}} + V_{\mathrm{CCC}} \tag{9.1}$$

with the energy E_{g} of the band gap, the screened Coulomb interaction V (4.9), the kinetic energies of the electron (4.8) and the hole (4.6), the exchange interaction and the central-cell corrections (6.17a). We now introduce relative and center-of-mass coordinates

$$\boldsymbol{r} = \boldsymbol{r}_{\mathrm{e}} - \boldsymbol{r}_{\mathrm{h}}, \tag{9.2a}$$

$$\boldsymbol{R} = \boldsymbol{\alpha}\boldsymbol{r}_{\mathrm{e}} + \boldsymbol{\gamma}\boldsymbol{r}_{\mathrm{h}}. \tag{9.2b}$$

The factors $\boldsymbol{\alpha}$ and $\boldsymbol{\gamma}$ are in general 3×3 or 6×6 matrices with $|\det(\boldsymbol{\alpha}+\boldsymbol{\gamma})| = 1$ [81]. As the Hamiltonian (9.1) depends only on the relative coordinate $\boldsymbol{r} = \boldsymbol{r}_{\mathrm{e}} - \boldsymbol{r}_{\mathrm{h}}$ of electron and hole, the momentum of the center of mass

$$\boldsymbol{P} = \boldsymbol{p}_{\mathrm{e}} + \boldsymbol{p}_{\mathrm{h}} = -i\hbar(\boldsymbol{\alpha}+\boldsymbol{\gamma})\nabla_{\boldsymbol{R}} \tag{9.3}$$

with

$$\nabla_{\boldsymbol{r}_{\mathrm{e}}} = \boldsymbol{\alpha}\nabla_{\boldsymbol{R}} + \nabla_{\boldsymbol{r}}, \tag{9.4a}$$

$$\nabla_{\boldsymbol{r}_{\mathrm{h}}} = \boldsymbol{\gamma}\nabla_{\boldsymbol{R}} - \nabla_{\boldsymbol{r}}, \tag{9.4b}$$

is a constant of motion, i.e., we can set $\boldsymbol{P} = \hbar\boldsymbol{K}$ [81, 267]. According to Ref. [81], the matrices $\boldsymbol{\alpha}$ and $\boldsymbol{\gamma}$ can be chosen arbitrarily, as long as $|\det(\boldsymbol{\alpha}+\boldsymbol{\gamma})| = 1$ holds, but should be adapted to the problem. Note that if we insert Eqs. (9.2) and (9.4) in the Hamiltonian (9.1) in general a coupling term between the relative motion and the motion of center of mass appears. Only for a specific choice of $\boldsymbol{\alpha}$ and $\boldsymbol{\gamma}$ this coupling term vanishes. However, the correct values of $\boldsymbol{\alpha}$ and $\boldsymbol{\gamma}$ are difficult to find (cf. Ref. [267] and Sec. 4.5.2). In particular, the generalized relative and center of mass coordinate transformation of Sec. 4.5.2 holds only if the parameters η_i in the kinetic energy of the hole are set to zero [cf. Eq. (4.6)]. When assuming isotropic coefficients $\boldsymbol{\alpha} = \alpha\boldsymbol{1}$ and $\boldsymbol{\gamma} = (1-\alpha)\boldsymbol{1}$ it is not possible to find a constant value of α for which the relative motion and the motion of the center of mass are decoupled. This is connected to the fact that the exciton mass in Cu_2O is not isotropic. Hence, a more complicated generalized transformation with 3 × 3 or 6 × 6 matrices would be needed.

Here we will use the coordinates and momenta of relative and center of mass motion with $\boldsymbol{\alpha} = m_{\mathrm{e}}/(m_{\mathrm{e}} + m_{\mathrm{h}})\mathbf{1}$ and $\boldsymbol{\gamma} = m_{\mathrm{h}}/(m_{\mathrm{e}} + m_{\mathrm{h}})\mathbf{1}$ known from the hydrogen atom, which are given in Eq. (2.198). We can then write the Hamiltonian in the form

$$H = H_0 + (\hbar K)H_1 + (\hbar K)^2 H_2. \tag{9.5}$$

The first part H_0 is exactly the Hamiltonian of relative motion presented and discussed in Chapter 6, while the last part H_2 describes the motion of the center of mass in the degenerate band case. The term H_1 depends on the relative momentum $\boldsymbol{p}$ and thus couples the relative motion and the motion of the center of mass.

For the case that the wave vector $\boldsymbol{K}$ is oriented along one of the directions of high symmetry, i.e., along [001], [110] or [111], one can rotate the coordinate system to make the quantization axis coincide with the direction of $\boldsymbol{K}$ and then express the Hamiltonian (9.5) in terms of irreducible tensors [79, 248, 281]. Explicit expressions for H_0, H_1, and H_2 for these special orientations of the wave vector $\boldsymbol{K}$ are given in Appendix D.2.

We can then calculate a matrix representation of the Schrödinger equation corresponding to the Hamiltonian (9.5) using the complete basis of Sec 4.3. Here the ansatz for the exciton wave function reads

$$|\Psi_{\nu\boldsymbol{K}}\rangle = \sum_{NLJFF_tM_{F_t}} c^{\nu\boldsymbol{K}}_{NLJFF_tM_{F_t}} |\Pi\rangle\,, \tag{9.6a}$$

$$|\Pi\rangle = |N,\, L;\, (I,\, S_{\mathrm{h}})\, J;\, F,\, S_{\mathrm{e}};\, F_t,\, M_{F_t}\rangle \tag{9.6b}$$

with complex coefficients c. Note that the coefficients here will depend on the wave vector $\boldsymbol{K}$, which enters the Hamiltonian (9.5). The index ν is a number to distinguish the different exciton states.

9.2 Oscillator strengths

Having solved the generalized eigenvalue problem after expressing the Schrödinger equation corresponding to the Hamiltonian (9.5) in the complete basis (9.6b), one can directly calculate the relative dipole and quadrupole oscillator strengths for the transitions from the ground state of the solid to the exciton states as discussed in Sec. 4.4.

Here we choose $\boldsymbol{K}$ to be oriented in [001], [110], or [111] direction and, as in Chapter 7, we also rotate the coordinate system to make the z axis of the new coordinate system coincide with the direction of $\boldsymbol{K}$. The formulas for the oscillator strengths for the three orientations of $\boldsymbol{K}$ will be given in the following.

9.2.1 Wave vector in [001] direction

For $\boldsymbol{K} \parallel [001]$, the symmetry O_{h} of the system is reduced to $C_{4\mathrm{v}}$ and we have to consider the reduction of the irreducible representations of O_{h} by the group $C_{4\mathrm{v}}$ (see Table 9.1). Especially for Γ_4^- it is

$$\Gamma_4^- \to \Gamma_1 \oplus \Gamma_5. \tag{9.7}$$

Table 9.1.: Reduction of the irreducible representations of the cubic group O_{h} by the groups $C_{4\mathrm{v}}\,(\boldsymbol{K} \parallel [001])$, $C_{2\mathrm{v}}\,(\boldsymbol{K} \parallel [110])$, and $C_{3\mathrm{v}}\,(\boldsymbol{K} \parallel [111])$ [90]. Note that only the irreducible representation Γ_5 of $C_{4\mathrm{v}}$ and the irreducible representation Γ_3 of $C_{3\mathrm{v}}$ are two-dimensional. Hence, almost all degeneracies in the exciton spectrum are lifted for $K \neq 0$.

O_{h}	$C_{4\mathrm{v}}$	$C_{2\mathrm{v}}$	$C_{3\mathrm{v}}$
Γ_1^+	Γ_1	Γ_1	Γ_1
Γ_2^+	Γ_3	Γ_2	Γ_2
Γ_3^+	$\Gamma_1 \oplus \Gamma_3$	$\Gamma_1 \oplus \Gamma_2$	Γ_3
Γ_4^+	$\Gamma_2 \oplus \Gamma_5$	$\Gamma_2 \oplus \Gamma_3 \oplus \Gamma_4$	$\Gamma_2 \oplus \Gamma_3$
Γ_5^+	$\Gamma_4 \oplus \Gamma_5$	$\Gamma_1 \oplus \Gamma_3 \oplus \Gamma_4$	$\Gamma_1 \oplus \Gamma_3$
Γ_1^-	Γ_2	Γ_3	Γ_2
Γ_2^-	Γ_4	Γ_4	Γ_1
Γ_3^-	$\Gamma_2 \oplus \Gamma_4$	$\Gamma_3 \oplus \Gamma_4$	Γ_3
Γ_4^-	$\Gamma_1 \oplus \Gamma_5$	$\Gamma_1 \oplus \Gamma_2 \oplus \Gamma_4$	$\Gamma_1 \oplus \Gamma_3$
Γ_5^-	$\Gamma_3 \oplus \Gamma_5$	$\Gamma_1 \oplus \Gamma_2 \oplus \Gamma_3$	$\Gamma_2 \oplus \Gamma_3$

On the one hand, using the method of projection operators [169], we can determine the correct linear combinations of the states in Eqs. (4.58) and (4.61) which transform according to the irreducible representations of $C_{4\mathrm{v}}$. On the other hand, the correct linear combinations are given according to the direction of $\boldsymbol{K}$ and the polarization vectors $\hat{\boldsymbol{e}}_{\xi\boldsymbol{K}}$ transverse to $\boldsymbol{K}$:

$$\hat{\boldsymbol{K}} = (0,\,0,\,1)^{\mathrm{T}}, \qquad \hat{\boldsymbol{e}}_{1\boldsymbol{K}} = (1,\,0,\,0)^{\mathrm{T}}, \qquad \hat{\boldsymbol{e}}_{2\boldsymbol{K}} = (0,\,1,\,0)^{\mathrm{T}}. \tag{9.8}$$

Since light is always transversely polarized, only states of symmetry Γ_5 are allowed. The correct linear combinations of the states (4.58) are

$$\Gamma_1 : |L^D_{\boldsymbol{K}}\rangle = |\pi^D_z\rangle, \tag{9.9a}$$

$$\Gamma_5 : |T^D_{1\boldsymbol{K}}\rangle = |\pi^D_x\rangle \quad \text{and} \tag{9.9b}$$

$$|T^D_{2\boldsymbol{K}}\rangle = |\pi^D_y\rangle, \tag{9.9c}$$

and likewise for the states of Eq. (4.61). If we assume the incident light to be circularly polarized, the oscillator strength is given by

$$f_{\xi\nu\boldsymbol{K}} = \eta \left| \lim_{r\to 0} \left[-i\frac{\partial}{\partial r}\langle T^D_{\pm\boldsymbol{K}}|\Psi_{\nu\boldsymbol{K}}\rangle + \frac{\alpha K}{\sqrt{6}}\langle T^Q_{\pm\boldsymbol{K}}|\Psi_{\nu\boldsymbol{K}}\rangle \right] \right|^2 \tag{9.10}$$

with

$$|T^D_{+\boldsymbol{K}}\rangle = -i\left[|T^D_{1\boldsymbol{K}}\rangle + i|T^D_{2\boldsymbol{K}}\rangle\right]/\sqrt{2} = |2,\,-1\rangle_D\,, \tag{9.11a}$$

$$|T^D_{-\boldsymbol{K}}\rangle = i\left[|T^D_{1\boldsymbol{K}}\rangle - i|T^D_{2\boldsymbol{K}}\rangle\right]/\sqrt{2} = -|2,\,1\rangle_D \tag{9.11b}$$

and

$$|T^Q_{+\boldsymbol{K}}\rangle = -i\left[|T^Q_{1\boldsymbol{K}}\rangle + i|T^Q_{2\boldsymbol{K}}\rangle\right]/\sqrt{2} = |1,\,-1\rangle_Q\,, \tag{9.12a}$$

$$|T^Q_{-\boldsymbol{K}}\rangle = i\left[|T^Q_{1\boldsymbol{K}}\rangle - i|T^Q_{2\boldsymbol{K}}\rangle\right]/\sqrt{2} = -|1,\,1\rangle_Q\,. \tag{9.12b}$$

Note that the sign ± is defined by the direction of rotation of the polarization with respect to $\boldsymbol{K}$.

9.2.2 Wave vector in [110] direction

For $\boldsymbol{K} \parallel [110]$ the symmetry is reduced to $C_{2\mathrm{v}}$ and it is

$$\Gamma_4^- \to \Gamma_1 \oplus \Gamma_2 \oplus \Gamma_4. \tag{9.13}$$

The corresponding vectors are

$$\hat{\boldsymbol{K}} = (1,\, 1,\, 0)^{\mathrm{T}}/\sqrt{2}, \qquad \hat{\boldsymbol{e}}_{1\boldsymbol{K}} = (1,\, -1,\, 0)^{\mathrm{T}}/\sqrt{2}, \qquad \hat{\boldsymbol{e}}_{2\boldsymbol{K}} = (0,\, 0,\, 1)^{\mathrm{T}}, \tag{9.14}$$

so that the correct linear combinations of the states (4.58) read

$$\Gamma_1 : |L_{\boldsymbol{K}}^{D}\rangle = \left[\left|\pi_x^D\right\rangle + \left|\pi_y^D\right\rangle\right]/\sqrt{2}, \tag{9.15a}$$

$$\Gamma_2 : |T_{1\boldsymbol{K}}^{D}\rangle = \left[\left|\pi_x^D\right\rangle - \left|\pi_y^D\right\rangle\right]/\sqrt{2}, \tag{9.15b}$$

$$\Gamma_4 : |T_{2\boldsymbol{K}}^{D}\rangle = \left|\pi_z^D\right\rangle. \tag{9.15c}$$

We now choose the quantization axis parallel to $\boldsymbol{K}$, i.e., we rotate the coordinate system by the Euler angles $(\alpha,\, \beta,\, \gamma) = (\pi,\, \pi/2,\, \pi/4)$. Rotating the states $|L_{\boldsymbol{K}}^{i}\rangle$ and $|T_{\xi\boldsymbol{K}}^{i}\rangle$ as well yields

$$|L_{\boldsymbol{K}}^{\prime D}\rangle = |\pi_{z'}^D\rangle = \left[|2,\, -1\rangle_D - |2,\, 1\rangle_D\right]\sqrt{2}, \tag{9.16a}$$

$$|T_{1\boldsymbol{K}}^{\prime D}\rangle = |\pi_{y'}^D\rangle = i\left[|2,\, 2\rangle_D - |2,\, -2\rangle_D\right]/\sqrt{2}, \tag{9.16b}$$

$$|T_{2\boldsymbol{K}}^{\prime D}\rangle = |\pi_{x'}^D\rangle = \sqrt{3}\,|2,\, 0\rangle_D/2 + \left[|2,\, -2\rangle_D + |2,\, 2\rangle_D\right]/\sqrt{8}, \tag{9.16c}$$

and

$$|L_{\boldsymbol{K}}^{\prime Q}\rangle = |\pi_{z'}^Q\rangle = \Big[|1,\, -1\rangle_Q - |1,\, 1\rangle_Q\Big]/\sqrt{2}, \tag{9.17a}$$

$$|T_{1\boldsymbol{K}}^{\prime Q}\rangle = |\pi_{y'}^Q\rangle = 0, \tag{9.17b}$$

$$|T_{2\boldsymbol{K}}^{\prime Q}\rangle = |\pi_{x'}^Q\rangle = |1,\, 0\rangle_Q. \tag{9.17c}$$

The labels x', y' and z' are meant to indicate that the states are given in the rotated coordinate system. Finally, we calculate the oscillator strengths by evaluating

$$f_{\nu\xi\boldsymbol{K}} = \eta\left|\lim_{r\to 0}\left[-i\frac{\partial}{\partial r}\langle T_{\xi\boldsymbol{K}}^{\prime D}|\Psi_{\nu\boldsymbol{K}}\rangle + \frac{\alpha K}{\sqrt{6}}\langle T_{\xi\boldsymbol{K}}^{\prime Q}|\Psi_{\nu\boldsymbol{K}}\rangle\right]\right|^2 \tag{9.18}$$

for light which is polarized in [001] or in [1$\bar{1}$0] direction.

9.2.3 Wave vector in [111] direction

For $\boldsymbol{K} \parallel [111]$ the symmetry is reduced to $C_{3\mathrm{v}}$ and we have

$$\Gamma_4^- \to \Gamma_1 \oplus \Gamma_3 \tag{9.19}$$

with the vectors

$$\hat{\boldsymbol{K}} = (1,\, 1,\, 1)^{\mathrm{T}}/\sqrt{3}, \qquad \hat{\boldsymbol{e}}_{1\boldsymbol{K}} = (1,\, 1,\, -2)^{\mathrm{T}}/\sqrt{6}, \qquad \hat{\boldsymbol{e}}_{2\boldsymbol{K}} = (-1,\, 1,\, 0)^{\mathrm{T}}/\sqrt{2}. \tag{9.20}$$

The correct linear combinations of the states in Eqs. (4.58) are therefore

$$\Gamma_1 : |L^D_{\boldsymbol{K}}\rangle = \left[|\pi^D_x\rangle + |\pi^D_y\rangle + |\pi^D_z\rangle\right]/\sqrt{3}, \tag{9.21a}$$

$$\Gamma_3 : |T^D_{1\boldsymbol{K}}\rangle = \left[|\pi^D_x\rangle + |\pi^D_y\rangle - 2\,|\pi^D_z\rangle\right]/\sqrt{6} \quad \text{and} \tag{9.21b}$$

$$|T^D_{2\boldsymbol{K}}\rangle = \left[-|\pi^D_x\rangle + |\pi^D_y\rangle\right]/\sqrt{2} \tag{9.21c}$$

Here the Euler angles $(\alpha,\, \beta,\, \gamma) = (0,\, \arccos(1/\sqrt{3}),\, \pi/4)$ are chosen to rotate the coordinate system. Rotating the states of Eq. (9.21) and assuming circularly polarized light yields

$$|L''^D_{\boldsymbol{K}}\rangle = |2,\, 0\rangle_D\,, \tag{9.22a}$$

$$|T''^D_{+\boldsymbol{K}}\rangle = i\left[\sqrt{2}\,|2,\, -2\rangle_D - |2,\, 1\rangle_D\right]/\sqrt{3}, \tag{9.22b}$$

$$|T''^D_{-\boldsymbol{K}}\rangle = -i\left[\sqrt{2}\,|2,\, 2\rangle_D + |2,\, -1\rangle_D\right]/\sqrt{3}, \tag{9.22c}$$

and

$$|L''^Q_{\boldsymbol{K}}\rangle = 2\,|1,\, 0\rangle_Q\,/\sqrt{3}, \tag{9.23a}$$

$$|T''^Q_{+\boldsymbol{K}}\rangle = -i\,|1,\, 1\rangle_Q\,/\sqrt{3}, \tag{9.23b}$$

$$|T''^Q_{-\boldsymbol{K}}\rangle = -i\,|1,\, -1\rangle_Q\,/\sqrt{3}. \tag{9.23c}$$

We finally calculate the oscillator strengths by evaluating

$$f_{\xi\nu\boldsymbol{K}} = \eta\left|\lim_{r\to 0}\left[-i\frac{\partial}{\partial r}\langle T''^D_{\pm\boldsymbol{K}}|\Psi_{\nu\boldsymbol{K}}\rangle + \frac{\alpha K}{\sqrt{6}}\langle T''^Q_{\pm\boldsymbol{K}}|\Psi_{\nu\boldsymbol{K}}\rangle\right]\right|^2. \tag{9.24}$$

9.3 Polaritons - Quantum-mechanical treatment

We will now introduce the Hamiltonian of the exciton-photon interaction in second quantization and show how the dispersion relation of a polariton can be obtained from quantum-mechanical calculations in Sec. 9.3.1. The problem is then simplified by introducing the rotating-wave approximation in Sec. 9.3.2. To obtain the correct treatment of the K-dependent problem, we consider the nonanalytic exchange interaction in Sec. 9.3.3. In Sec. 9.3.4 we shortly present the criteria for the observability of polariton effects.

9.3.1 Polariton transformation

The quantum mechanical theory of polaritons was first developed by Hopfield, Fano, and Agranovich [141, 413, 414]. According to Refs. [140, 141, 282], the second-quantized Hamiltonian for the interaction of excitons and photons,

$$\begin{aligned} H \;=\; \sum_{\xi\boldsymbol{K}}\Bigg[&\hbar\omega_{\xi\boldsymbol{K}}\left(a^\dagger_{\xi\boldsymbol{K}}a_{\xi\boldsymbol{K}} + \frac{1}{2}\right) + \sum_\nu E_{\nu\boldsymbol{K}}\left(B^\dagger_{\nu\boldsymbol{K}}B_{\nu\boldsymbol{K}} + \frac{1}{2}\right) \\ &+ \sum_\nu\left(a^\dagger_{\xi\boldsymbol{K}} + a_{\xi-\boldsymbol{K}}\right)\left\{iC_{\xi\,\nu\boldsymbol{K}}\left(B_{\nu\boldsymbol{K}} - B^\dagger_{\nu-\boldsymbol{K}}\right) + D_{\xi\,\nu\boldsymbol{K}}\left(a_{\xi\boldsymbol{K}} + a^\dagger_{\xi-\boldsymbol{K}}\right)\right\}\Bigg], \end{aligned} \tag{9.25}$$

can be derived either from a microscopic model of excitons with the Hamiltonian describing the interaction between radiation and matter or from the equation of motion for the exciton polarization. In the Hamiltonian (9.25) the operator $B^{\dagger}_{\nu\boldsymbol{K}}$ ($B_{\nu\boldsymbol{K}}$) creates (annihilates) an exciton with energy $E_{\nu\boldsymbol{K}}$. Likewise, the operator $a^{\dagger}_{\xi\boldsymbol{K}}$ ($a_{\xi\boldsymbol{K}}$) creates (annihilates) a photon with polarization ξ and energy $\hbar\omega_{\xi\boldsymbol{K}} = \hbar cK/\sqrt{\varepsilon_{\mathrm{b}2}}$. The coupling coefficients in the exciton-photon and the photon-photon interaction terms of Eq. (9.25) are given by

$$C_{\xi\,\nu\boldsymbol{K}} = \left[\frac{\kappa_{\mathrm{SI}}\pi\beta_{\xi\nu\boldsymbol{K}}E^3_{\nu\boldsymbol{K}}}{\varepsilon_{\mathrm{b}2}\hbar\omega_{\xi\boldsymbol{K}}}\right]^{\frac{1}{2}} \tag{9.26}$$

with $\kappa_{\mathrm{SI}} = 1/4\pi\varepsilon_0$ and

$$D_{\xi\,\nu\boldsymbol{K}} = C^2_{\xi\,\nu\boldsymbol{K}}/E_{\nu\boldsymbol{K}}. \tag{9.27}$$

The polarizability $\beta_{\xi\nu\boldsymbol{K}}$ is proportional to the oscillator strength of the exciton state. With our definition of the oscillator strength $f_{\xi\nu\boldsymbol{K}}$ (cf. Sec. 4.4 and Refs. [178–180]) this proportionality is given by [282, 421, 422]

$$\beta_{\xi\nu\boldsymbol{K}} = \varepsilon_0\varepsilon_{\mathrm{b}2}f_{\xi\nu\boldsymbol{K}}. \tag{9.28}$$

The Hamiltonian (9.25) can be diagonalized by the Hopfield transformation [141, 413], which is similar to the Bogolyubov's uv transformation [423, 424]: New creation and annihilation operators $p^{\dagger}_{\mu\xi\boldsymbol{K}}$ and $p_{\mu\xi\boldsymbol{K}}$ are introduced via

$$a_{\xi\boldsymbol{K}} = \sum_{\mu}\left[u_{\mu\xi\boldsymbol{K}}p_{\mu\xi\boldsymbol{K}} + v^*_{\mu\xi-\boldsymbol{K}}p^{\dagger}_{\mu\xi-\boldsymbol{K}}\right], \tag{9.29a}$$

$$B_{\nu\boldsymbol{K}} = \sum_{\mu}\left[u_{\mu\xi\nu\boldsymbol{K}}p_{\mu\xi\boldsymbol{K}} + v^*_{\mu\xi\nu-\boldsymbol{K}}p^{\dagger}_{\mu\xi-\boldsymbol{K}}\right], \tag{9.29b}$$

to obtain the polariton Hamiltonian

$$H = \sum_{\mu\xi\boldsymbol{K}} E_{\mu\xi\boldsymbol{K}}p^{\dagger}_{\mu\xi\boldsymbol{K}}p_{\mu\xi\boldsymbol{K}} + \text{const.} \tag{9.30}$$

with μ and $E_{\mu\xi\boldsymbol{K}}$ denoting the polariton branches and the polariton energies, respectively. The new operators must obey Bose commutation relations and the Hamiltonian shall be diagonal, i.e.,

$$[p_{\mu\xi\boldsymbol{K}}, H] = E_{\mu\xi\boldsymbol{K}}p_{\mu\xi\boldsymbol{K}} \tag{9.31}$$

must hold. This provides an conditional equation for the polariton energies [140, 414, 425]:

$$\frac{\hbar^2c^2K^2}{E^2_{\mu\xi\boldsymbol{K}}} = \varepsilon_{\mathrm{b}2} + \sum_{\nu}\frac{4\pi\kappa_{\mathrm{SI}}\beta_{\xi\nu\boldsymbol{K}}}{1-(E_{\mu\xi\boldsymbol{K}}/E_{\nu\boldsymbol{K}})^2}. \tag{9.32}$$

Using the phase convention of Hopfield [141], one obtains the following solution for the coefficients of the polariton transformation [140]:

$$u_{\mu\xi\boldsymbol{K}} = \frac{\hbar\omega_{\xi\boldsymbol{K}} + E_{\mu\xi\boldsymbol{K}}}{2\sqrt{\hbar\omega_{\xi\boldsymbol{K}} E_{\mu\xi\boldsymbol{K}} g_{\mu\xi\boldsymbol{K}}}}, \tag{9.33a}$$

$$u_{\mu\xi\nu\boldsymbol{K}} = i\,\frac{E_{\nu\boldsymbol{K}} + E_{\mu\xi\boldsymbol{K}}}{1-(E_{\mu\xi\boldsymbol{K}}/E_{\nu\boldsymbol{K}})^2}\sqrt{\frac{\pi\kappa_{\mathrm{SI}}\beta_{\xi\nu\boldsymbol{K}}}{\varepsilon_{\mathrm{b}2}E_{\mu\xi\boldsymbol{K}}E_{\nu\boldsymbol{K}}g_{\mu\xi\boldsymbol{K}}}}, \tag{9.33b}$$

$$v_{\mu\xi-\boldsymbol{K}} = \frac{\hbar\omega_{\xi\boldsymbol{K}} - E_{\mu\xi\boldsymbol{K}}}{\hbar\omega_{\xi\boldsymbol{K}} + E_{\mu\xi\boldsymbol{K}}}u_{\mu\xi\boldsymbol{K}}, \tag{9.33c}$$

$$v_{\mu\xi\nu-\boldsymbol{K}} = -\frac{E_{\nu\boldsymbol{K}} - E_{\mu\xi\boldsymbol{K}}}{E_{\nu\boldsymbol{K}} + E_{\mu\xi\boldsymbol{K}}}u_{\mu\xi\nu\boldsymbol{K}}, \tag{9.33d}$$

with

$$g_{\mu\xi\boldsymbol{K}} = 1 + \sum_{\nu}\frac{4\pi\kappa_{\mathrm{SI}}\beta_{\xi\nu\boldsymbol{K}}}{\varepsilon_{\mathrm{b}2}\left[1-(E_{\mu\xi\boldsymbol{K}}/E_{\nu\boldsymbol{K}})^2\right]^2}. \tag{9.33e}$$

The polariton operators can also be expressed in terms of exciton and photon operators:

$$p_{\mu\xi\boldsymbol{K}} = w^{(1)}_{\mu\xi\boldsymbol{K}}a_{\xi\boldsymbol{K}} + w^{(2)*}_{\mu\xi-\boldsymbol{K}}a^{\dagger}_{\xi-\boldsymbol{K}} + \sum_{\nu}\left[z^{(1)}_{\mu\xi\nu\boldsymbol{K}}B_{\nu\boldsymbol{K}} + z^{(2)*}_{\mu\xi\nu-\boldsymbol{K}}B^{\dagger}_{\nu-\boldsymbol{K}}\right]. \tag{9.34}$$

Since all creation and annihilation operators of the three (quasi-)particles obey Bose commutation relations, we can determine the coefficients w and z by evaluating

$$\left[p_{\mu\xi\boldsymbol{K}},\, a^{\dagger}_{\xi\boldsymbol{K}}\right] = +w^{(1)}_{\mu\xi\boldsymbol{K}} = u^{*}_{\mu\xi\boldsymbol{K}}, \tag{9.35a}$$

$$\left[p_{\mu\xi\boldsymbol{K}},\, a_{\xi-\boldsymbol{K}}\right] = -w^{(2)*}_{\mu\xi\boldsymbol{K}} = v^{*}_{\mu\xi\boldsymbol{K}}, \tag{9.35b}$$

$$\left[p_{\mu\xi\boldsymbol{K}},\, B^{\dagger}_{\nu-\boldsymbol{K}}\right] = +z^{(1)}_{\mu\xi\nu\boldsymbol{K}} = u^{*}_{\mu\xi\nu\boldsymbol{K}}, \tag{9.35c}$$

$$\left[p_{\mu\xi\boldsymbol{K}},\, B_{\nu\boldsymbol{K}}\right] = -z^{(2)*}_{\mu\xi\nu\boldsymbol{K}} = v^{*}_{\mu\xi\nu\boldsymbol{K}}. \tag{9.35d}$$

The coefficients $w^{(i)}_{\mu\xi\boldsymbol{K}}$ or the sum

$$W_{\mu\xi\boldsymbol{K}} = \sum_{i=1}^{2}|w^{(i)}_{\mu\xi\boldsymbol{K}}|^2 \tag{9.36}$$

then allows one to determine whether the polariton is more photon-like ($W_{\mu\xi\boldsymbol{K}} \to 1$) or more exciton-like ($W_{\mu\xi\boldsymbol{K}} \to 0$).

9.3.2 Rotating-wave approximation

In the literature polaritons are often treated within the so-called rotating-wave approximation [282]. In this case the term with the coefficient D and the anti-resonant terms of the form aB and $a^{\dagger}B^{\dagger}$ are neglected in the Hamiltonian (9.25). The resulting Hamiltonian

$$H = \sum_{\xi\boldsymbol{K}}\left[\hbar\omega_{\xi\boldsymbol{K}}a^{\dagger}_{\xi\boldsymbol{K}}a_{\xi\boldsymbol{K}} + \sum_{\nu}E_{\nu\boldsymbol{K}}B^{\dagger}_{\nu\boldsymbol{K}}B_{\nu\boldsymbol{K}} + \sum_{\nu}C_{\xi\,\nu\boldsymbol{K}}\left(a^{\dagger}_{\xi\boldsymbol{K}}B_{\nu\boldsymbol{K}} + a_{\xi\boldsymbol{K}}B^{\dagger}_{\nu\boldsymbol{K}}\right)\right] \tag{9.37}$$

is then called the Jaynes-Cummings Hamiltonian [426], where the vacuum energy has also been neglected [282] and where the operators $a_{\xi\boldsymbol{K}}$ have been replaced with $ia_{\xi\boldsymbol{K}}$. Note that this replacement does not change the physics of the problem since it only adds global phases to the occupation-number states. The occupation-number operator and the commutation relations remain unchanged.

The coefficient $C_{\xi\,\nu\boldsymbol{K}}$ can be written as [282, 422]

$$C_{\xi\,\nu\boldsymbol{K}}=\left[\frac{\kappa_{\mathrm{SI}}\pi\beta_{\xi\nu\boldsymbol{K}}E_{\nu\boldsymbol{K}}^{3}}{\varepsilon_{\mathrm{b}2}\hbar\omega_{\xi\boldsymbol{K}}}\right]^{\frac{1}{2}}\approx\frac{1}{2}\left(\frac{K_0}{K}\right)^{\frac{1}{2}}\hbar\Omega_{\mathrm{R}} \tag{9.38}$$

with the wave vector at the exciton-photon resonance $K_0=E_{\nu\boldsymbol{K}_0}\sqrt{\varepsilon_{\mathrm{b}2}}/\hbar c$ and the Rabi frequency

$$\Omega_{\mathrm{R}}=E_{\nu\boldsymbol{K}_0}\sqrt{\frac{4\pi\kappa_{\mathrm{SI}}\beta_{\xi\nu\boldsymbol{K}}}{\varepsilon_{\mathrm{b}2}\hbar^{2}}}. \tag{9.39}$$

The rotating wave approximation is generally valid if $\hbar\Omega_{\mathrm{R}}\ll E_{\nu\boldsymbol{K}_0}$ holds. This is, e.g., the case for anorganic semiconductors and especially for $\mathrm{Cu_2O}$ [422].

Close to the resonance ($K\approx K_0$) one can assume $C_{\xi\,\nu\boldsymbol{K}}\approx\hbar\Omega_{\mathrm{R}}/2$. Note that for $K\to 0$ the coupling constant (9.38) diverges, which is *a manifestation of the infrared catastrophe in quantum electrodynamics* [282]. Hence, the simplifications made above are valid only in the vicinity of the exciton-photon resonance. Otherwise, the full Hamiltonian (9.25) has to be diagonalized.

In the rotating-wave approximation the polariton transformation is more simple as there is no interaction between states with different values of $\boldsymbol{K}$. Using the ansatz

$$p_{\mu\xi\boldsymbol{K}}=w_{\mu\xi\boldsymbol{K}}a_{\xi\boldsymbol{K}}+\sum_{i}z_{\mu\xi\nu_i\boldsymbol{K}}B_{\nu_i\boldsymbol{K}}, \tag{9.40}$$

the Bose commutation relations of the creation and annihilation operators, and the condition (9.31) for the polariton operator, one ends up with the eigenvalue problem

$$\boldsymbol{P}_{\xi\{\nu\}\boldsymbol{K}}\boldsymbol{z}_{\mu\xi\{\nu\}\boldsymbol{K}}=E_{\mu\xi\boldsymbol{K}}\boldsymbol{z}_{\mu\xi\{\nu\}\boldsymbol{K}} \tag{9.41}$$

with

$$\boldsymbol{P}_{\xi\{\nu\}\boldsymbol{K}}=\begin{pmatrix}\hbar\omega_{\xi\boldsymbol{K}} & \frac{1}{2}\hbar\Omega_{\mathrm{R},\,\nu_1} & \frac{1}{2}\hbar\Omega_{\mathrm{R},\,\nu_2} & \cdots & \frac{1}{2}\hbar\Omega_{\mathrm{R},\,\nu_n} & \cdots\\ \frac{1}{2}\hbar\Omega_{\mathrm{R},\,\nu_1} & E_{\nu_1\boldsymbol{K}} & 0 & \cdots & 0 & \cdots\\ \frac{1}{2}\hbar\Omega_{\mathrm{R},\,\nu_2} & 0 & E_{\nu_2\boldsymbol{K}} & & \vdots & \\ \vdots & \vdots & & \ddots & 0 & \cdots\\ \frac{1}{2}\hbar\Omega_{\mathrm{R},\,\nu_n} & 0 & \cdots & 0 & E_{\nu_n\boldsymbol{K}} & \\ \vdots & \vdots & & \vdots & & \ddots\end{pmatrix},\quad \boldsymbol{z}_{\mu\xi\{\nu\}\boldsymbol{K}}=\begin{pmatrix}w_{\mu\xi\boldsymbol{K}}\\ z_{\mu\xi\nu_1\boldsymbol{K}}\\ z_{\mu\xi\nu_2\boldsymbol{K}}\\ \vdots\\ z_{\mu\xi\nu_n\boldsymbol{K}}\\ \vdots\end{pmatrix}. \tag{9.42}$$

Knowing the energies $E_{\nu\boldsymbol{K}}$ and the Rabi frequencies $\Omega_{\mathrm{R},\,\nu}$ of the exciton states, one can directly obtain the corresponding polariton energies by determining the eigenvalues of Eq. (9.41). Note that the characteristic polynomial for the eigenvalue problem (9.41) is of a similar form than Eq. (9.32) [427–429],

$$\hbar\omega_{\xi\boldsymbol{K}}=E_{\mu\xi\boldsymbol{K}}+\sum_{j=2}^{n}\frac{\left(\frac{1}{2}\hbar\Omega_{\mathrm{R},\,j}\right)^{2}}{E_{j\boldsymbol{K}}-E_{\mu\xi\boldsymbol{K}}}, \tag{9.43}$$

but due to the approximations made in the rotating wave approximation, the equations are not identical. Finally, as the polariton is a mixed state of a photon and excitons, one can again determine the photon-like part

$$W_{\mu\xi\boldsymbol{K}} = |w_{\mu\xi\boldsymbol{K}}|^2 \tag{9.44}$$

of the polariton or the contribution

$$Z_{\mu\xi\nu\boldsymbol{K}} = |z_{\mu\xi\nu\boldsymbol{K}}|^2 \tag{9.45}$$

of the exciton with the energy $E_{\nu\boldsymbol{K}}$ to the polariton.

9.3.3 Nonanalytic exchange interaction

From the formula (4.64) for the oscillator strength one can see that the exciton-photon coupling affects only the transverse exciton states. However, there is another interaction affecting the longitudinal exciton states: the nonanalytic (NA) exchange interaction. It is well known that the splitting caused by $H^{\mathrm{NA}}_{\mathrm{exch}}$ is identical to the longitudinal-transverse splitting (LT-splitting) when treating polaritons [311]. Hence, it is indispensable to include the nonanalytic exchange interaction in the theory to obtain a correct treatment of the complete problem.

In this section we will derive an expression for the nonanalytic exchange interaction, which can be used in numerical evaluations. We start with the expression (5.16) for the nonanalytic exchange energy between two exciton states $\Psi^{\sigma\tau}_{vc,\,\nu\boldsymbol{K}}$ and $\Psi^{\sigma'\tau'}_{vc,\,\nu'\boldsymbol{K}'}$. This yields the Hamiltonian

$$H^{\mathrm{NA}}_{\mathrm{exch}} = \sum_{\nu\nu'\boldsymbol{K}} \frac{m^*_{\nu\boldsymbol{K}} m_{\nu'\boldsymbol{K}}}{\varepsilon_0 \varepsilon_{\mathrm{b}2} V_{\mathrm{uc}} K^2} B^\dagger_{\nu\boldsymbol{K}} B_{\nu'\boldsymbol{K}} \tag{9.46}$$

in second quantization with the volume V_{uc} of one unit cell and

$$\begin{aligned} m_{\nu\boldsymbol{K}} = \delta_{\sigma\tau} \frac{e}{\sqrt{N}} \sum_{\boldsymbol{q}} f_{vc\,\nu}(\boldsymbol{q}) \Bigg\{ &-\frac{\hbar}{m_0} \frac{\boldsymbol{K}\cdot\boldsymbol{p}_{vc}}{E_v - E_c} + \frac{\hbar^2}{m_0^2} \sum_{n\neq v,c} \Bigg[\frac{[(\boldsymbol{q}-\gamma\boldsymbol{K})\cdot\boldsymbol{p}_{vn}]\,[(\boldsymbol{q}+\alpha\boldsymbol{K})\cdot\boldsymbol{p}_{nc}]}{(E_v - E_n)(E_c - E_n)} \\ &+ \frac{[(\boldsymbol{q}+\alpha\boldsymbol{K})\cdot\boldsymbol{p}_{vn}]\,[(\boldsymbol{q}+\alpha\boldsymbol{K})\cdot\boldsymbol{p}_{nc}]}{(E_c - E_v)(E_c - E_n)} + \frac{[(\boldsymbol{q}-\gamma\boldsymbol{K})\cdot\boldsymbol{p}_{nc}]\,[(\boldsymbol{q}-\gamma\boldsymbol{K})\cdot\boldsymbol{p}_{vn}]}{(E_v - E_c)(E_v - E_n)} \Bigg] \Bigg\} . \end{aligned} \tag{9.47}$$

Here $m_{\nu\boldsymbol{K}}$ is a short notation for the function $m_{vc\,\nu}(\boldsymbol{K},\,\boldsymbol{0})$ of Eq. (5.25). For the definitions of $\Psi^{\sigma\tau}_{vc,\,\nu\boldsymbol{K}}$, $f_{vc\,\nu}(\boldsymbol{q})$, and $\boldsymbol{p}_{mn}$ see Sec. 4.4. The exchange energy includes the term $\delta_{\sigma\tau}\delta_{\sigma'\tau'}$. Introducing the total spin $S = S_{\mathrm{e}} + S_{\mathrm{h}} = \tau - \sigma$ of electron and hole, this term can be written for singlet and triplet states as $2\delta_{S,0}$ [127]. Using Eq. (4.43) and rearranging the different terms in Eq. (9.47) yields

$$m_{\nu\boldsymbol{K}} = \delta_{\sigma\tau} \frac{e\hbar^2}{m_0^2} \frac{K}{(E_c - E_v)} \lim_{\boldsymbol{r}\to\boldsymbol{0}} \Big[(\tilde{\boldsymbol{N}}_v + \tilde{\boldsymbol{N}}_c) \cdot [-i\nabla_{\boldsymbol{r}} F_{vc\,\nu}(\boldsymbol{r})] + (-\gamma\tilde{\boldsymbol{N}}_v + \alpha\tilde{\boldsymbol{N}}_c) \cdot [F_{vc\,\nu}(\boldsymbol{r})\boldsymbol{K}] \Big] \tag{9.48}$$

with the matrices

$$\tilde{\boldsymbol{N}}_v = \langle u_{v\boldsymbol{0}}|\, \boldsymbol{p} M_v(\hat{\boldsymbol{K}}\cdot\boldsymbol{p})\, |u_{c\boldsymbol{0}}\rangle \,, \tag{9.49a}$$

$$\tilde{\boldsymbol{N}}_c = \langle u_{v\boldsymbol{0}}|\, (\hat{\boldsymbol{K}}\cdot\boldsymbol{p}) M_c \boldsymbol{p}\, |u_{c\boldsymbol{0}}\rangle \,. \tag{9.49b}$$

and $\hat{\boldsymbol{K}} = \boldsymbol{K}/K$.

Due to the similarity between Eq. (4.44) and Eq. (9.48), we can perform the same calculation as in Sec. 4.4 to obtain

$$m_{\nu\boldsymbol{K}} \sim K \lim_{r\to 0}\left[-i(\tilde{M}_v+\tilde{M}_c)\frac{\partial}{\partial r}\langle L^D_{\boldsymbol{K}}|\Psi_{\nu\boldsymbol{K}}\rangle + (-\gamma\tilde{M}_v+\alpha\tilde{M}_c)\frac{K}{\sqrt{6}}\langle L^Q_{\boldsymbol{K}}|\Psi_{\nu\boldsymbol{K}}\rangle\right]. \tag{9.50}$$

with the longitudinal states

$$|L^D_{\boldsymbol{K}}\rangle = \sum_{i=1}^{3}\hat{K}_i\,|\pi^D_i\rangle, \qquad |L^Q_{\boldsymbol{K}}\rangle = \sum_{i=1}^{3}\hat{K}_i\,|\pi^Q_i\rangle, \tag{9.51}$$

where $|\pi^D_i\rangle$ and $|\pi^Q_i\rangle$ were defined in Eqs. (4.58) and (4.61). As in Sec. 4.4 we will assume $M_c \gg M_v$ so that we can finally state that $m_{\nu\boldsymbol{K}}$ is proportional to

$$K \lim_{r\to 0}\left[-i\frac{\partial}{\partial r}\langle L^D_{\boldsymbol{K}}|\Psi_{\nu\boldsymbol{K}}\rangle + \frac{\alpha K}{\sqrt{6}}\langle L^Q_{\boldsymbol{K}}|\Psi_{\nu\boldsymbol{K}}\rangle\right]. \tag{9.52}$$

We can see from Eq. (9.46) that there is no interaction between states with different values of $\boldsymbol{K}$, which is the same case as for the Hamiltonian (9.37) of the polariton interaction in the rotating-wave approximation. Knowing the exciton energies $E_{\nu\boldsymbol{K}}$ and the corresponding wave functions $|\Psi_{\nu\boldsymbol{K}}\rangle$, we can simultaneously diagonalize the polariton Hamiltonian and the NA-exchange Hamiltonian by solving the eigenvalue problem

$$\left(\boldsymbol{P}_{\xi\{\nu\}\boldsymbol{K}} + \boldsymbol{N}_{\{\nu\}\boldsymbol{K}}\right)\boldsymbol{z}_{\mu\xi\{\nu\}\boldsymbol{K}} = E_{\mu\xi\boldsymbol{K}}\boldsymbol{z}_{\mu\xi\{\nu\}\boldsymbol{K}} \tag{9.53}$$

with the matrix

$$\boldsymbol{N}_{\{\nu\}\boldsymbol{K}} = \frac{\zeta}{\varepsilon_{\mathrm{b}2}K^2}\begin{pmatrix} 0 & 0 & 0 & \cdots & 0 & \cdots \\ 0 & m^*_{\nu_1\boldsymbol{K}}m_{\nu_1\boldsymbol{K}} & m^*_{\nu_1\boldsymbol{K}}m_{\nu_2\boldsymbol{K}} & \cdots & m^*_{\nu_1\boldsymbol{K}}m_{\nu_n\boldsymbol{K}} & \cdots \\ 0 & m^*_{\nu_2\boldsymbol{K}}m_{\nu_1\boldsymbol{K}} & m^*_{\nu_2\boldsymbol{K}}m_{\nu_2\boldsymbol{K}} & & \vdots & \\ \vdots & \vdots & & \ddots & & \cdots \\ 0 & m^*_{\nu_n\boldsymbol{K}}m_{\nu_1\boldsymbol{K}} & \cdots & & m^*_{\nu_n\boldsymbol{K}}m_{\nu_n\boldsymbol{K}} & \\ \vdots & \vdots & & & \vdots & \ddots \end{pmatrix}, \tag{9.54}$$

and the matrix $\boldsymbol{P}_{\xi\{\nu\}\boldsymbol{K}}$ and vector $\boldsymbol{z}_{\mu\xi\{\nu\}\boldsymbol{K}}$ defined in Eq. (9.42). The constant parameter ζ can be determined by the fact that the splitting caused by $H^{\mathrm{NA}}_{\mathrm{exch}}$ is identical to the LT-splitting.

9.3.4 Observability of polariton effects

We now shortly discuss the criteria for the observability of polariton effects, which were derived by Tait in Ref. [430]. We already stated that there a no "true" excitons and "true" photons in a solid but – due to their interaction – always polaritons. If we now imagined a system without damping or energy sink, i.e., if we set $\gamma = 0$ in the Lorentz model, photons of certain momentum and energy would excite a population of excitons, which would then decay after some time and emit photons being indistinguishable from the incident ones. In this case no absorption would be observed. Therefore, the interaction of excitons and phonons or polaritons and phonons plays an important role for absorption spectra since lattice vibrations can serve as an energy sink.

In the above model, the so-called Rabi flopping [431] takes place, i.e., the energy oscillates coherently between the exciton and the photon state with the frequency $\Omega_{\mathrm{R}}/(2\pi)$. This oscillation is often damped due to the interaction with other polaritons, phonons, or the leakage of photons out of the solid [422, 430]. To obtain the criteria for the observability, Tait included a damping term Γ in the model of polaritons:

$$\frac{\hbar^2 c^2 K^2}{E^2_{\mu\xi\boldsymbol{K}}} = \varepsilon_{\mathrm{b}2} + \sum_{\nu} \frac{4\pi\kappa_{\mathrm{SI}}\beta_{\xi\nu\boldsymbol{K}}E^2_{\nu\boldsymbol{K}}}{E^2_{\nu\boldsymbol{K}} - E^2_{\mu\xi\boldsymbol{K}} - i\Gamma E_{\mu\xi\boldsymbol{K}}}. \tag{9.55}$$

This equation can either be solved for a fixed wave vector K or for a fixed frequency $\omega = E_{\mu\xi\boldsymbol{K}}/\hbar$.

The first case corresponds to nonlinear optical experiments like, e.g., two-photon absorption. For this case a criterion of temporal coherence between the photon and the exciton can be derived [282, 430]. As long as

$$\hbar\Gamma < \hbar\sqrt{\kappa_{\mathrm{SI}}\frac{\pi}{\varepsilon_{\mathrm{b}2}}\beta_{\xi\nu\boldsymbol{K}}E^2_{\nu\boldsymbol{K}_0}} = \frac{\hbar}{2}\Omega_{\mathrm{R}} \tag{9.56}$$

holds, where $\hbar\Gamma$ is the broadening of the linewidth due to damping, the polariton splitting is observable. This criterion can be interpreted in terms of Rabi oscillations, i.e., polariton effects are observable if a coherent energy transfer between an exciton and a photon is possible at least once [422]. Spatial coherence is already provided here by keeping K fixed [282].

The second case corresponds to reflectivity or absorption experiments. Here the coupling between the photon and the exciton must remain coherent during the propagation of the polariton through the solid in the presence of damping [282]. The criterion of spatial coherence reads [282, 422, 432]

$$\hbar\Gamma < \sqrt{\frac{16\pi}{Mc^2}\kappa_{\mathrm{SI}}E^3_{\nu\boldsymbol{K}_0}\beta_{\xi\nu\boldsymbol{K}}} = \frac{\hbar}{2}\Omega_{\mathrm{R}}\sqrt{\frac{16\varepsilon_{\mathrm{b}2}}{Mc^2}E_{\nu\boldsymbol{K}_0}}, \tag{9.57}$$

and it is generally more difficult to satisfy than Eq. (9.56) [422, 433] since $\sqrt{16\varepsilon_{\mathrm{b}2}E_{\nu\boldsymbol{K}_0}/Mc^2} \ll 1$ holds for an exciton mass M on the order of m_0 and an exciton energy on the order of a few eV. The criterion (9.57) is equivalent to $l \gg \lambda$ with λ denoting the light wavelength and $l = v_g/\Gamma$ the mean free path of the exciton [282]. Hence, polariton effects can hardly be observed in semiconductors with very shallow excitons like, e.g., GaAs [282], when using linear optical techniques. Therefore, polariton effects are often investigated using nonlinear optical spectroscopic techniques due to the much less stringent criterion (9.56) [434, 435].

If both of the two criteria are not fulfilled, the damping dominates and the interaction between exciton and photon can be treated within perturbation theory (weak coupling regime).

Note that we can now describe the process of absorption in second quantization: At first, an incident photon excites a polariton state (or a superposition of polariton states). Due to its exciton component, the polariton is coupled to nonradiative states, i.e., to phonons or defects of the crystal, and it can therefore decay. Without this decay mechanism, the polariton would emit a photon after some time, which is indistinguishable from the incident one. Since it is now about polaritons which are excited by photons, the results of Secs. 3.1.4 and 4.4 have to be reinterpreted [7, 414]: It is easily seen that $W_{\nu\boldsymbol{K},0} \sim |C_{\xi\nu\boldsymbol{K}}|^2$ holds for the transition rate of Sec. 4.4. On the other hand, the probability that a polariton will decay to other long-lifetime states (see Fig. 9.1) is proportional to its exciton amplitude, which depends on $|C_{\xi\nu\boldsymbol{K}}|^2$. We can therefore treat $|C_{\xi\nu\boldsymbol{K}}|^2$ as a probability measure for a non-radiative decay (see also Sec. 2.5.4). Therefore, due to the above explanation, the results of Secs. 3.1.4 and 4.4 are still valid[2].

---

[2] In the picture of polaritons another problem arises in connection with Bose-Einstein condensation of excitons: Since the lowest energy states are situated near $\boldsymbol{K} = \boldsymbol{0}$, particles on the lower branch would follow the LPB to $\boldsymbol{K} = \boldsymbol{0}$ and would be transferred into mostly-photon-like states. The condensation must therefore take place entirely within the UPB [7].

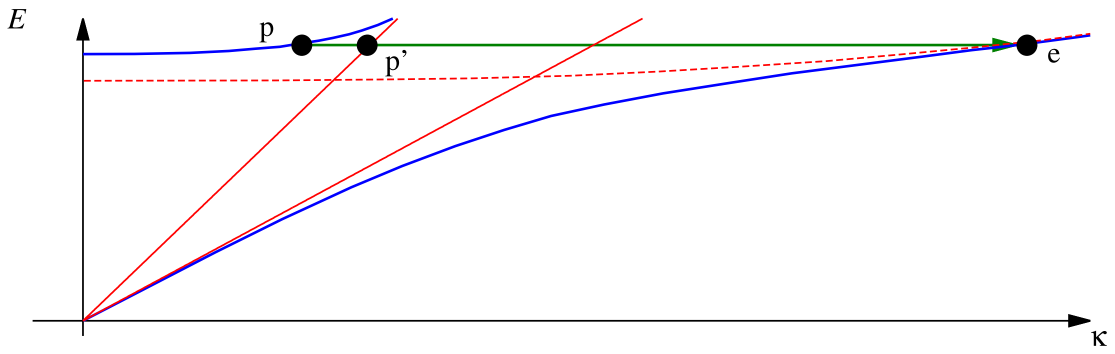

Figure 9.1.: The strongly-mixed polariton state p can be scattered - due to the interaction of the exciton component of the polariton with, e.g., phonons - into a long-lived state e. The photon amplitude of e is very small and a radiative decay of e into a photon p' is unlikely. Adapted from [7].

At last we want to state that the polariton effect can be neglected in specific cases and that a description with excitons and photons is then justified [163, 436]. In some cases the coupling of an electron to the radiation field can be weak. These cases comprise

- spin-flips (triplet excitons),
- longitudinal excitons,
- the inclusion of a third particle (e.g. a phonon) to create the exciton in indirect semiconductors,
- and dipole-forbidden transitions.

In the context of these effects the weak-coupling approach is often (but not always) sufficient for a description [12].

9.4 5×5 matrix model for the $1S$ ortho-exciton polariton

The yellow $1S$ ortho-exciton is well separated from the other exciton states as regards its energy. Hence, it can be treated separately. In this section we set up a model with a 5×5 matrix, which allows calculating the dispersion of the $1S$ ortho-exciton polariton for any direction of $\boldsymbol{K}$ close to the resonance ($K \approx K_0$). This model includes the two photon states with the polarization vectors $\hat{\boldsymbol{e}}_{\xi \boldsymbol{K}}$ and the three ortho-exciton states Ψ_i, which transform according to yz, zx and xy.

First we will treat the oscillator strength and the Rabi frequency. Let us consider the most simple case with $\boldsymbol{K} \parallel [001]$. Due to group theoretical reasons, the three states Ψ_{yz}, Ψ_{zx}, and Ψ_{xy} are good eigenstates of the Hamiltonian. The Ψ_{zx} exciton interacts with the photon in x polarization and the Ψ_{yz} exciton interacts with the photon in y polarization. Let us denote the oscillator strength of these exciton states at the exciton-photon resonance by f_0.

For other orientations of $\boldsymbol{K}$ superpositions of the form $\sum_i a_i\Psi_i$ are eigenstates of the Hamiltonian. From the expression (4.64) or especially from the form of the states $|T^{Q}_{\xi\boldsymbol{K}}\rangle$ (4.60) we can see that the K-dependent oscillator strength of these exciton states is given by

$$f_{1S\,\xi\boldsymbol{K}} = f_0 \left| \begin{pmatrix} \hat{e}_{\xi\boldsymbol{K},y}K_z + \hat{e}_{\xi\boldsymbol{K},z}K_y \\ \hat{e}_{\xi\boldsymbol{K},z}K_x + \hat{e}_{\xi\boldsymbol{K},x}K_z \\ \hat{e}_{\xi\boldsymbol{K},x}K_y + \hat{e}_{\xi\boldsymbol{K},y}K_x \end{pmatrix} \cdot \begin{pmatrix} a_{yz} \\ a_{zx} \\ a_{xy} \end{pmatrix} \right|^2 \tag{9.58}$$

with the components $\hat{e}_{\xi\boldsymbol{K},i}$ of the polarization vector $\hat{\boldsymbol{e}}_{\xi\boldsymbol{K}}$.

For the $1S$ ortho-exciton a K-dependent splitting was observed experimentally in Refs. [82–84] and originally discussed in terms of a K-dependent exchange interaction. However, a closer examination of this interaction in Sec. 5.3 revealed that it is far too weak in $\mathrm{Cu_2O}$ to describe the observed splitting. Instead, it could be shown that the effects due to the cubic valence band structure lead to a K-dependent effective mass and a K-dependent splitting of the $1S$ ortho-exciton (cf. Sec. 4.5.2). Hence, the directional dispersion is the true cause of the experimentally observed splitting. However, in Sec. 4.5.2 the splitting was treated within a perturbation approach and it was already emphasized that the complete K-dependent Schrödinger equation including the central-cell corrections would have to be solved to obtain correct results. This can now be done with the help of the theory of Sec. 9.1.

We have already stated in Sec. 5.3.1 that a K-dependent splitting of a state with the symmetry Γ_5^+ must always have the form

$$\begin{aligned} \boldsymbol{H}_{\mathrm{disp}}(\boldsymbol{K}) =& \Delta_1 \begin{pmatrix} K^2 & 0 & 0 \\ 0 & K^2 & 0 \\ 0 & 0 & K^2 \end{pmatrix} + \Delta_3 \begin{pmatrix} 3K_x^2 - K^2 & 0 & 0 \\ 0 & 3K_y^2 - K^2 & 0 \\ 0 & 0 & 3K_z^2 - K^2 \end{pmatrix} \\ &+ \Delta_5 \begin{pmatrix} 0 & K_xK_y & K_xK_z \\ K_xK_y & 0 & K_yK_z \\ K_xK_z & K_yK_z & 0 \end{pmatrix} \end{aligned} \tag{9.59}$$

for group theoretical reasons. We will prove the consistency with this formula in Sec. 9.7.1 by diagonalizing the Hamiltonian (9.59) for $\boldsymbol{K} \parallel [001]$, $\boldsymbol{K} \parallel [110]$, and $\boldsymbol{K} \parallel [111]$ and fitting the resulting eigenvalues to the numerical results of the complete problem (9.5). This will yield the values of the parameters Δ_1, Δ_3 and Δ_5.

For states of symmetry Γ_5^+ it has been shown in Sec. 5.3.2 that the nonanalytic exchange interaction can be written as

$$\boldsymbol{H}^{\mathrm{NA}}_{\mathrm{exch}}(\boldsymbol{K}) = \frac{\Delta_Q}{K^2} \begin{pmatrix} K_y^2K_z^2 & K_z^2K_yK_x & K_y^2K_xK_z \\ K_z^2K_yK_x & K_z^2K_x^2 & K_x^2K_yK_z \\ K_y^2K_xK_z & K_x^2K_yK_z & K_x^2K_y^2 \end{pmatrix}. \tag{9.60}$$

Contrary to dipole-allowed excitons, the nonanalytic exchange energy depends on the fourth power of the angular coordinates of $\boldsymbol{K}$. The prefactor Δ_Q is connected to the oscillator strength and can be determined for the $1S$ state in the following way: For the special case of $\boldsymbol{K}$ being oriented in [111] direction, the Γ_5^+ state splits into one longitudinal Γ_1 and two transverse Γ_5 states. The longitudinal state is an eigenstate of the operator (9.60) with the eigenvalue $\Delta_Q/3$. An excitation of the longitudinal exciton leads to an oscillating longitudinal polarization. Due to the Maxwell equation $\nabla \cdot \boldsymbol{D} = 0$, the dielectric function must be zero. Hence, we have

$$\varepsilon(\omega,\, K_0)\,[\Gamma_1] = \varepsilon_{\mathrm{b2}} + \frac{\frac{4}{3}f_0\varepsilon_{\mathrm{b2}}}{1 - \left(E_0 + \frac{1}{3}\Delta_Q K_0^2\right)^2 / \left(E_0\right)^2} = 0 \tag{9.61}$$

with the energy $E_0 = \hbar c K_0 / \sqrt{\varepsilon_{\mathrm{b}2}}$ of the Γ_1 exciton at $K = K_0$ without the nonanalytic exchange interaction [cf. also Eq. (9.32)]. This relation can be solved for Δ_Q. Using $f_0 \ll 1$ [178–180], we obtain

$$\Delta_Q = 2 f_0 E_0 / K_0^2 = 2 f_0 \hbar^2 c^2 / \varepsilon_{\mathrm{b}2}. \tag{9.62}$$

Combining all the K-dependent effects for the $1S$ ortho-exciton, we arrive at the Hamiltonian for the $1S$ ortho-exciton polariton in the rotating-wave approximation:

$$\boldsymbol{H} = \begin{pmatrix} \boldsymbol{H}_{\mathrm{ph}} & \boldsymbol{H}_{\mathrm{exc-ph}} \\ \boldsymbol{H}_{\mathrm{exc-ph}}^{\mathrm{T}} & \boldsymbol{H}_{\mathrm{exc}} \end{pmatrix} \tag{9.63}$$

with the 2×2 matrix $\boldsymbol{H}_{\mathrm{ph}}$ containing the photon dispersion,

$$\boldsymbol{H}_{\mathrm{ph}} = \frac{\hbar c K}{\sqrt{\varepsilon_{\mathrm{b}2}}} \begin{pmatrix} 1 & 0 \\ 0 & 1 \end{pmatrix} = E_0 \frac{K}{K_0} \begin{pmatrix} 1 & 0 \\ 0 & 1 \end{pmatrix}, \tag{9.64}$$

a 2×3 matrix $\boldsymbol{H}_{\mathrm{exc-ph}}$ with the Rabi energies $\hbar\Omega_{\mathrm{R}} = E_0 \sqrt{f_0}$,

$$\boldsymbol{H}_{\mathrm{exc-ph}}^{\mathrm{T}} = \frac{1}{2} \hbar\Omega_{\mathrm{R}} \frac{1}{K_0} \begin{pmatrix} (\hat{e}_{1\boldsymbol{K},y} K_z + \hat{e}_{1\boldsymbol{K},z} K_y) & (\hat{e}_{2\boldsymbol{K},y} K_z + \hat{e}_{2\boldsymbol{K},z} K_y) \\ (\hat{e}_{1\boldsymbol{K},z} K_x + \hat{e}_{1\boldsymbol{K},x} K_z) & (\hat{e}_{2\boldsymbol{K},z} K_x + \hat{e}_{2\boldsymbol{K},x} K_z) \\ (\hat{e}_{1\boldsymbol{K},x} K_y + \hat{e}_{1\boldsymbol{K},y} K_x) & (\hat{e}_{2\boldsymbol{K},x} K_y + \hat{e}_{2\boldsymbol{K},y} K_x) \end{pmatrix}, \tag{9.65}$$

and

$$\boldsymbol{H}_{\mathrm{exc}} = E_0 \, \mathbf{1} + \boldsymbol{H}_{\mathrm{disp}}(\boldsymbol{K}) + \boldsymbol{H}_{\mathrm{exch}}^{\mathrm{NA}}(\boldsymbol{K}), \tag{9.66}$$

where $\mathbf{1}$ is the 3×3 identity matrix.

Note that the Rabi energy depends on the square root of the oscillator strength [cf. Eq. (9.39)]. Hence, questions about the sign of the terms $(\hat{e}_{1\boldsymbol{K},y} K_z + \hat{e}_{1\boldsymbol{K},z} K_y)$ in Eq. (9.65) may arise. However, for reasons of symmetry the terms must be linear in $\boldsymbol{K}$. As the photon has negative parity, i.e., since it transforms according to Γ_4^- in O_{h}, the terms have to change the sign if the direction of $\boldsymbol{K}$ is reversed.

The eigenstates of the Hamiltonian (9.63) can be calculated using an appropriate LAPACK routine [284]. The values of f_0 and E_0 as well as the parameters Δ_i can be determined from the solutions of the complete Hamiltonian (9.5).

9.5 Results for the hydrogen-like case

In this section we investigate the effects of the exciton-photon interaction on Rydberg excitons. To this aim, we use the multi-polariton concept for the hydrogen-like model of $\mathrm{Cu_2O}$ within the rotating-wave approximation[3]. The hydrogen-like model is sufficient for the exciton states with $n \gtrsim 5$ as these states have a very small extension in momentum space, which implies that the effect of the valence band structure can be disregarded. Only a small correction term $\delta_{L=1}$ will be included in the exciton energies to obtain an even better agreement with the experimental result of Ref. [30] for the P excitons.

We consider only the transverse exciton states, for which reason the nonanalytic exchange interaction is not needed, and only P excitons, which are dipole-active in $\mathrm{Cu_2O}$. Even though S excitons

---

[3] A treatment of exciton-polaritons in an external magnetic field using the hydrogen-like model of $\mathrm{Cu_2O}$ can be found in Ref. [437].

would have a small finite quadrupole oscillator strength for $K \neq 0$, they are disregarded here. A correct quantitative treatment of exciton-polaritons including the complete valence band structure, the central-cell corrections, the quadrupole oscillator strength and the nonanalytic exchange interaction will be presented in the next section 9.6.

In the simple hydrogen-like model of the yellow exciton series in $\mathrm{Cu_2O}$ (with $\mu' = \delta' = J_0 = V_0 = 0$ and $J = 1/2$) the energies of the P exciton states are given by

$$E_{n\boldsymbol{K}} = E_{\mathrm{g}} - \frac{R_{\mathrm{exc}}}{(n-\delta_{L=1})^2} + \frac{\hbar^2 K^2}{2M} \tag{9.67}$$

with the exciton Rydberg energy

$$R_{\mathrm{exc}} = \frac{m_{\mathrm{e}} e^4}{2\gamma_1' \varepsilon_{\mathrm{s1}}^2 (4\pi\varepsilon_0)^2 \hbar^2}, \tag{9.68}$$

the total exciton mass

$$M = m_{\mathrm{e}} + m_{\mathrm{h}} = m_{\mathrm{e}} + m_0/\gamma_1, \tag{9.69}$$

and the correction factor $\delta_{L=1} = 0.23$ of Ref. [30].

Since the transition between the valence band and the conduction band is parity forbidden in $\mathrm{Cu_2O}$, only the nP excitons can be optically excited in the hydrogen-like model. Their oscillator strengths are given by $f \approx 3.75 \times 10^{-4}(n^2-1)/n^5$ (see Secs. 9.6 and 4.4.2). Hence, the corresponding Rabi frequencies read [421]

$$\Omega_{\mathrm{R},\,n} \;=\; \frac{1}{\hbar}\sqrt{f} E_{n\boldsymbol{K}} \approx \frac{1}{\hbar}\sqrt{3.75\times 10^{-4}\frac{n^2-1}{n^5}}\left(E_{\mathrm{g}} - \frac{R_{\mathrm{exc}}}{(n-\delta_{L=1})^2}\right). \tag{9.70}$$

Inserting Eqs. (9.67) and (9.70) in the eigenvalue problem (9.41)

$$\begin{pmatrix} \hbar\omega_{\xi\boldsymbol{K}} & \frac{1}{2}\hbar\Omega_{\mathrm{R},\,2} & \frac{1}{2}\hbar\Omega_{\mathrm{R},\,3} & \cdots & \frac{1}{2}\hbar\Omega_{\mathrm{R},\,n} \\ \frac{1}{2}\hbar\Omega_{\mathrm{R},\,2} & E_{2\boldsymbol{K}} & 0 & \cdots & 0 \\ \frac{1}{2}\hbar\Omega_{\mathrm{R},\,3} & 0 & E_{3\boldsymbol{K}} & & \vdots \\ \vdots & \vdots & & \ddots & 0 \\ \frac{1}{2}\hbar\Omega_{\mathrm{R},\,n} & 0 & \cdots & 0 & E_{n\boldsymbol{K}} \end{pmatrix} \begin{pmatrix} w_{\mu\xi\boldsymbol{K}} \\ z_{\mu\xi\,2\boldsymbol{K}} \\ z_{\mu\xi\,3\boldsymbol{K}} \\ \vdots \\ z_{\mu\xi\,n\boldsymbol{K}} \end{pmatrix} = E_{\mu\xi\boldsymbol{K}} \begin{pmatrix} w_{\mu\xi\boldsymbol{K}} \\ z_{\mu\xi\,2\boldsymbol{K}} \\ z_{\mu\xi\,3\boldsymbol{K}} \\ \vdots \\ z_{\mu\xi\,n\boldsymbol{K}} \end{pmatrix}, \tag{9.71}$$

we can now determine the polariton energies $E_{\mu\xi\boldsymbol{K}}$. Since in Ref. [30] giant Rydberg excitons up to a principal quantum number of $n = 25$ could be observed, we accordingly include all exciton states with $n \leq 25$ in our calculations.

The polariton dispersion is shown in Fig. 9.2. We can see that the resonances of the excitons with the photon occur for $2.95 \times 10^7\,\frac{1}{\mathrm{m}} \lesssim K \lesssim 3.03 \times 10^7\,\frac{1}{\mathrm{m}}$. If the exciton states are clearly separated from each other, as is the case, e.g., for $n = 2$ and $n = 3$, the polariton is photon-like between the two exciton states. However, for the states with small principal quantum number the effects of the valence band structure and the central-cell corrections are important. Hence, they will be investigated in more detail in Sec. 9.6. As regards the higher exciton states with $n \gtrsim 5$, the polariton is not photon-like any more between each two exciton states and a strong mixing of exciton states in the resonance region occurs. This can be seen clearly in Fig. 9.3, where we show the $n = 5$, $n = 6$, and $n = 7$ exciton component of the polaritons. Outside the resonance region the polariton is exciton-like and only one exciton contributes to the polariton. However, in the vicinity of the resonance many excitons of different principal quantum number contribute to the

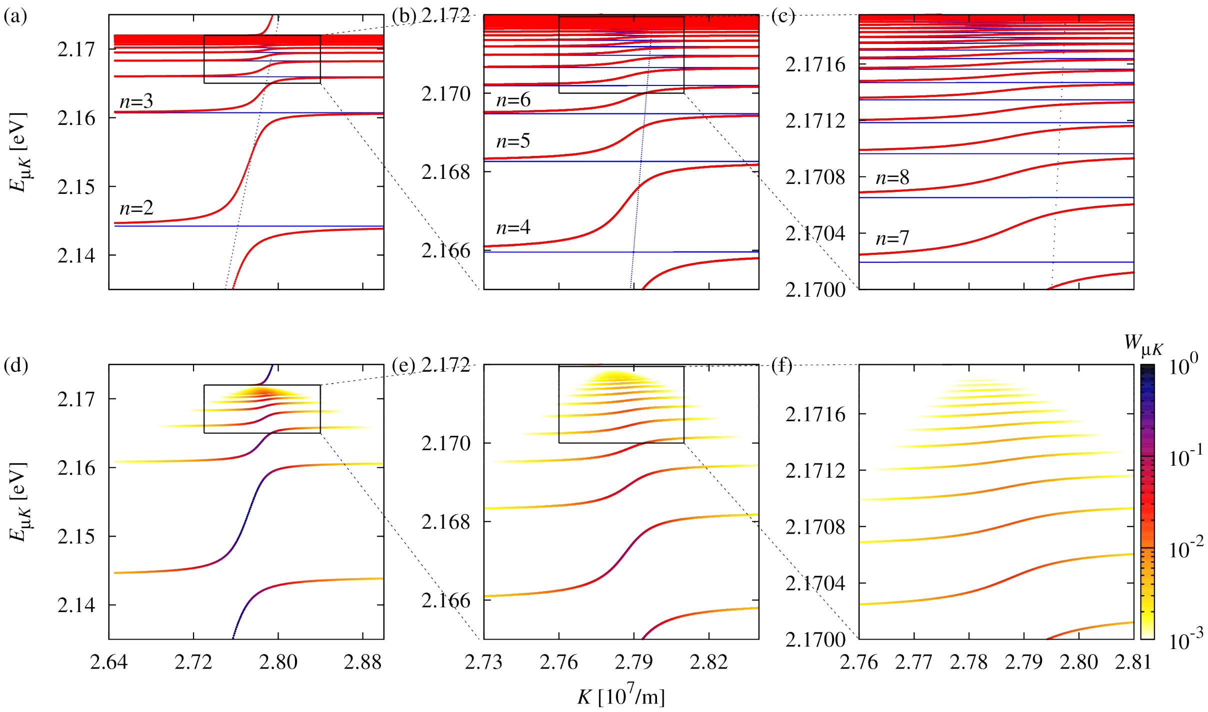

Figure 9.2.: (a)-(c) Polariton dispersion (red) in the rotating-wave approximation when considering all nP excitons with $2 \leq n \leq 25$. The blue lines show the exciton and photon dispersion without interaction. Note that the quadratic dependence of the exciton energies on the wave vector K is too weak to be seen here. Instead, the lines showing the exciton dispersion are almost flat. (d)-(f) The colorbar shows the photon-like part $W_{\mu \boldsymbol{K}}$ of the polariton. If the energy difference between the exciton states is large, e.g., between $n = 2$ and $n = 3$, the polariton is photon-like between the two energies. Otherwise, the polariton is always more exciton-like, which can be seen for $n \gtrsim 6$.

polariton. Therefore, Rydberg polaritons or polaritons corresponding to excitons with $n \gtrsim 5$, must in any case be treated within the multi-polariton framework.

Using the criteria for temporal and spatial coherence presented in Sec. 9.3.4, we can estimate the possible observability of the polariton effects. If we set $n = 2$, the criterion of temporal coherence reads

$$\hbar\Gamma < \frac{\hbar}{2}\Omega_{\mathrm{R}} \approx 6.4\,\mathrm{meV}. \tag{9.72}$$

For the criterion of spatial coherence, we obtain

$$\hbar\Gamma < \frac{\hbar}{2}\Omega_{\mathrm{R}}\sqrt{\frac{16\varepsilon_{\mathrm{b}2}}{Mc^2}E_{\nu\boldsymbol{K}_0}} \approx 0.11\,\mathrm{meV} \tag{9.73}$$

with the isotropic mass $M \approx 1.57m_0$ of the exciton. In Ref. [30] the spectrum of the giant Rydberg excitons has been investigated in an absorption experiment and, thus, experimental values of the

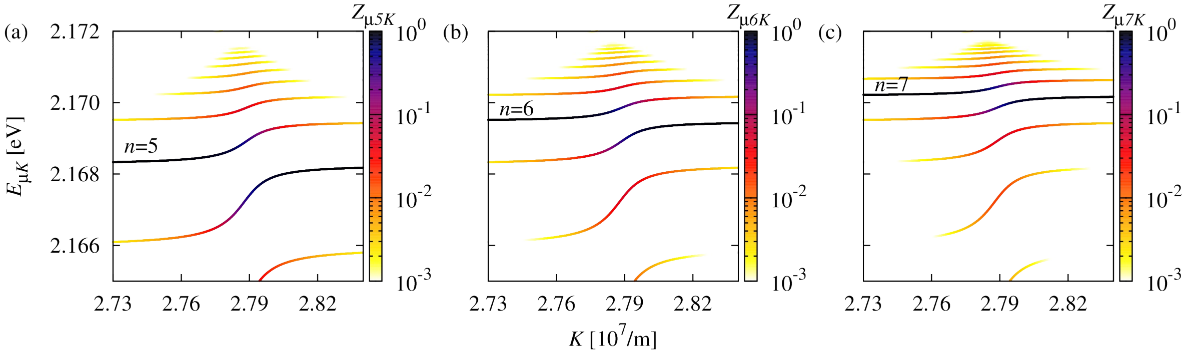

Figure 9.3.: Contribution of the (a) $n = 5$, (b) $n = 6$, (c) $n = 7$ excitons to the polariton dispersion. Except for a very small range in the vicinity of the resonance, the polariton is almost completely exciton-like. Within this region a strong mixing of exciton states with different quantum numbers occurs. Even at the resonance of the photon with the dispersion of the $n = 8$ exciton, still an admixture of the $n = 5$ exciton to the polariton can be observed.

exciton linewidths $\hbar\Gamma$ for the criterion of spatial coherence are known. For $n = 2$ the experimental line width is $\hbar\Gamma = 1.58\,\mathrm{meV}$ [30], which is significantly larger than 0.11 meV. Thus, we expect that the polariton effects for the yellow exciton states with $n \geq 2$ in $\mathrm{Cu_2O}$ may only be observed using nonlinear spectroscopy methods and high quality crystals [434, 435]. As regards the $1S$ ortho-exciton state, the linewidth is small enough to clearly observe polariton effects [178–180].

9.6 Results including VB structure and central-cell corrections

In this section we will treat the exciton-polaritons with $n \leq 4$ in $\mathrm{Cu_2O}$ using the Hamiltonian which accounts for the valence band structure, the exchange interaction, the central-cell corrections, and the finite momentum $\hbar K$ of the center of mass.

The exciton of even and odd parity behave differently in dependence on the momentum $\hbar K$. Those states of the odd series having the symmetry Γ_4^- and a component with $L = 1$, show a finite dipole oscillator strength at $K = 0$. Since the angular momentum L is not a good quantum number in $\mathrm{Cu_2O}$ and since P-like exciton states are admixed to other states of odd parity at $K = 0$ (cf. Chapter 4), all P, F, H, … states of symmetry Γ_4^- have a finite dipole oscillator strength. Hence, for these states already a splitting at $K = 0$ occurs due to the nonanalytic exchange interaction and the exciton-photon coupling. For $K \neq 0$ these states split further depending on the orientation of $\boldsymbol{K}$. For the three orientations [001], [110], and [111] of $\boldsymbol{K}$ considered in the following, we have to consider, e.g., the reduction of the irreducible representations of the cubic group O_h by the groups $C_{4\mathrm{v}}$, $C_{2\mathrm{v}}$, and $C_{3\mathrm{v}}$, respectively, as listed in Table 9.1. However, the K-dependent splitting is of the order of a few μeV and, therefore, cannot be seen when presenting the complete polariton dispersion for $n \leq 4$.

On the other hand, the even exciton states do not have an oscillator strength at $K=0$ so that no splitting occurs. For those even states which have the symmetry Γ_5^+ and an $L=0$-component at $K=0$ the coupling to light via a finite K vector is possible. Since S-like exciton states are admixed to other states of even parity at $K=0$ (cf. Chapter 6), all S, D, G, … states of symmetry Γ_5^+ obtain a finite quadrupole oscillator strength being proportional to K^2. Just as for the odd states a splitting of the order of a few μeV occurs for $K\neq 0$. We will discuss this splitting in connection with the $1S$ ortho-exciton polariton in Sec. 9.7.

At first, we compare our numerical results for the relative oscillator strengths of the $1S$ excitons with the absolute value from the experiment. This will allow us to calculate absolute oscillator strengths for all exciton states. Having determined the correct size of the nonanalytic exchange interaction for the nP excitons and, hence, for all other exciton states, we can then investigate the dispersion of exciton-polaritons for the three orientations of $\boldsymbol{K}$ along the axes of high symmetry.

Since the formula derived in Sec. 4.4 allows us only to calculate relative oscillator strengths $f_{\xi\nu\boldsymbol{K}}^{\mathrm{rel}}$ but not absolute oscillator strengths for the different polarizations ξ and exciton states $\nu\boldsymbol{K}$, we determine the scaling factor η in

$$f_{\xi\nu\boldsymbol{K}}=\eta f_{\xi\nu\boldsymbol{K}}^{\mathrm{rel}} \tag{9.74}$$

by comparing the theoretical result for $f_{\xi\,1S\,\boldsymbol{K}}^{\mathrm{rel}}$ for the $1S$ exciton state at the exciton-photon resonance $K=K_0$ with the experimentally obtained value of [178]

$$f_{\xi\,1S\,\boldsymbol{K}}=3.6\times 10^{-9} \tag{9.75}$$

for $\boldsymbol{K}\parallel[110]$. This yields $\eta=825.9$. Knowing this scaling factor, we can give the absolute oscillator strengths of all exciton states in the following. With this value the oscillator strengths of, e.g., the nP excitons are given by

$$f_{\xi\,nP\,\boldsymbol{K}}=3.75\times 10^{-4}\,\frac{n^2-1}{n^5}. \tag{9.76}$$

Note that there are different definitions of the Rabi energy in the literature [178–180, 282, 421]. While, e.g., in Ref. [282] the oscillator strength is divided by $\varepsilon_{\mathrm{b}2}$ in the Rabi energy, this is not the case in Refs. [178–180, 421]. In our calculations we use the definition without $\varepsilon_{\mathrm{b}2}$ as can be seen from, e.g., from Eq. (9.70). In Ref. [163] not only the oscillator strength of the $1S$ ortho exciton is given but also the oscillator strength of the nP excitons. While it can be seen from the formula of the Rabi energy in Ref. [163] that the definition of $f_{\xi\,1S\,\boldsymbol{K}}$ is without the dielectric constant, the definition of $f_{\xi\,nP\,\boldsymbol{K}}$ remains unclear. The theoretical results, which we present in the following suggest that the value $f_{\xi\,nP\,\boldsymbol{K}}=3\times 10^{-5}\,(n^2-1)/n^5$ given in Ref. [163] is defined differently. Furthermore, just as in atomic physics, it is difficult to determine the ratio of oscillator strengths which differ by orders of magnitude. While the spectrum presented in Ref. [72] may lead to the conclusion that the ratio of the oscillator strengths of the $2P$ and the $1S$ exciton is smaller than the values of Ref. [163] suggest, the spectrum in Ref. [51] seems to confirm these values. However, in the spectrum in Ref. [51] the ratio of the oscillator strengths is so large that it cannot be determined directly from a comparison of the areas beneath the absorption peaks. We chose the absolute value of the oscillator strength or the scaling factor η as described above. We want to note that when varying the size of η the size of the avoided crossing in the polariton dispersion changes proportional to $\sqrt{\eta}$. However, there are no significant deviations in the qualitative bahavior of the polariton dispersion when changing η by one order of magnitude. Hence, even if the absolute values of the oscillator strengths used were defined differently, it would not change the results in a significant way.

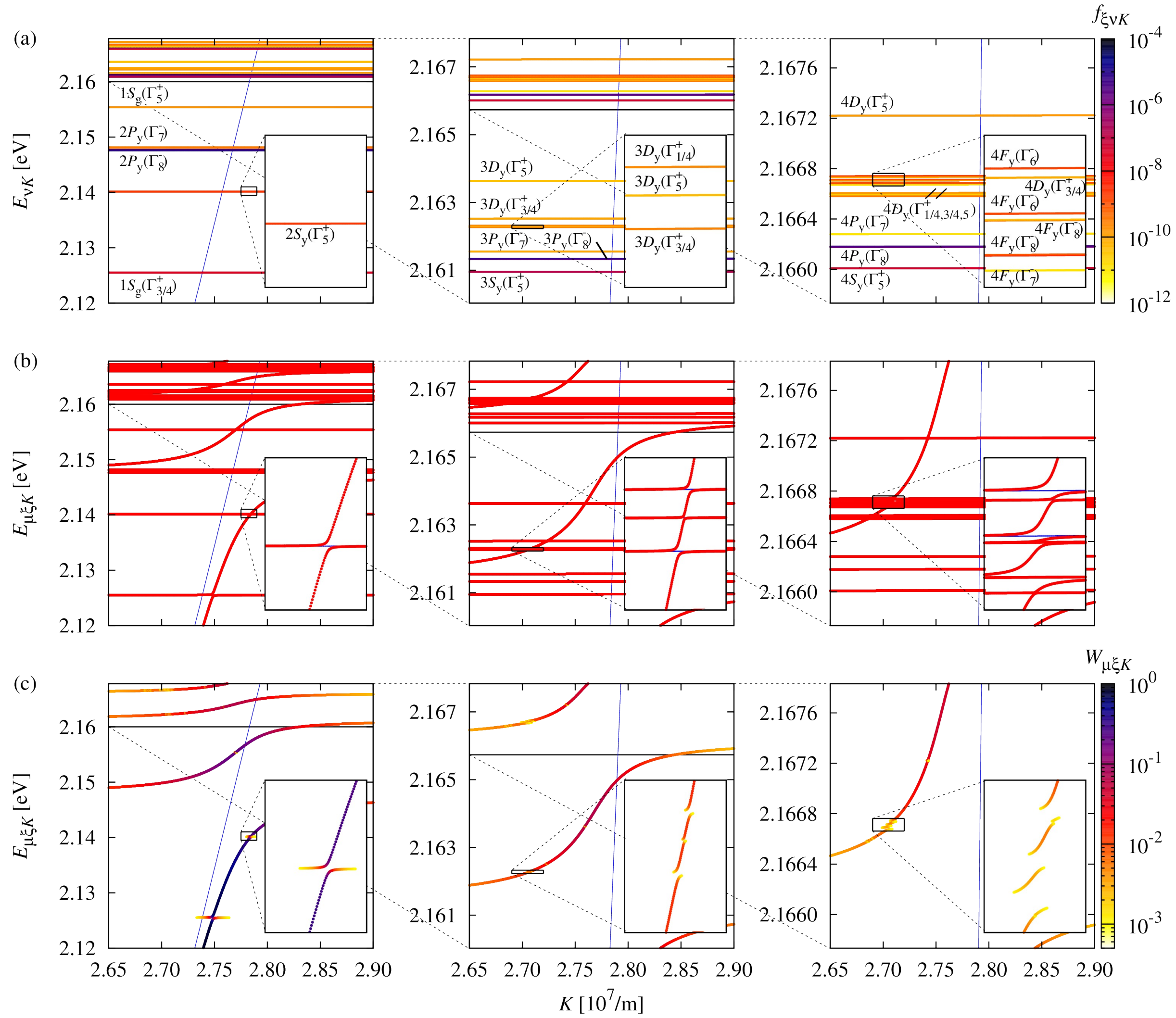

Figure 9.4.: (a) The exciton energies $E_{\nu\boldsymbol{K}}$ in dependence on $K = |\boldsymbol{K}|$ for $\boldsymbol{K} \parallel [001]$. Due to the inclusion of the complete valence band structure and the central cell corrections, the spectrum is much more complicated than in the hydrogen-like case (cf. Fig. 9.2). The colorbar shows the oscillator strengths for $\xi = \sigma_z^{\pm}$ polarized light. For both polarizations the spectrum is identical. We denote from which states at $K = 0$ the exciton states originate (cf. Sec. 6.2). For reasons of space we introduce the abbreviated notation $\Gamma_{i/j}^{\pm}$ to replace $\Gamma_i^{\pm}$, $\Gamma_j^{\pm}$. The blue solid line gives the photon dispersion $\hbar\omega_{\xi\boldsymbol{K}} = \hbar K c/\sqrt{\varepsilon_{\mathrm{b}2}}$. (b) Polariton dispersion obtained by solving the eigenvalue problem (9.53). (c) Photon-like part $W_{\mu\xi\boldsymbol{K}}$ (9.44) of the polariton states. In all cases the mixing of excitons and photons is strongest in the vicinity of an avoided crossing.

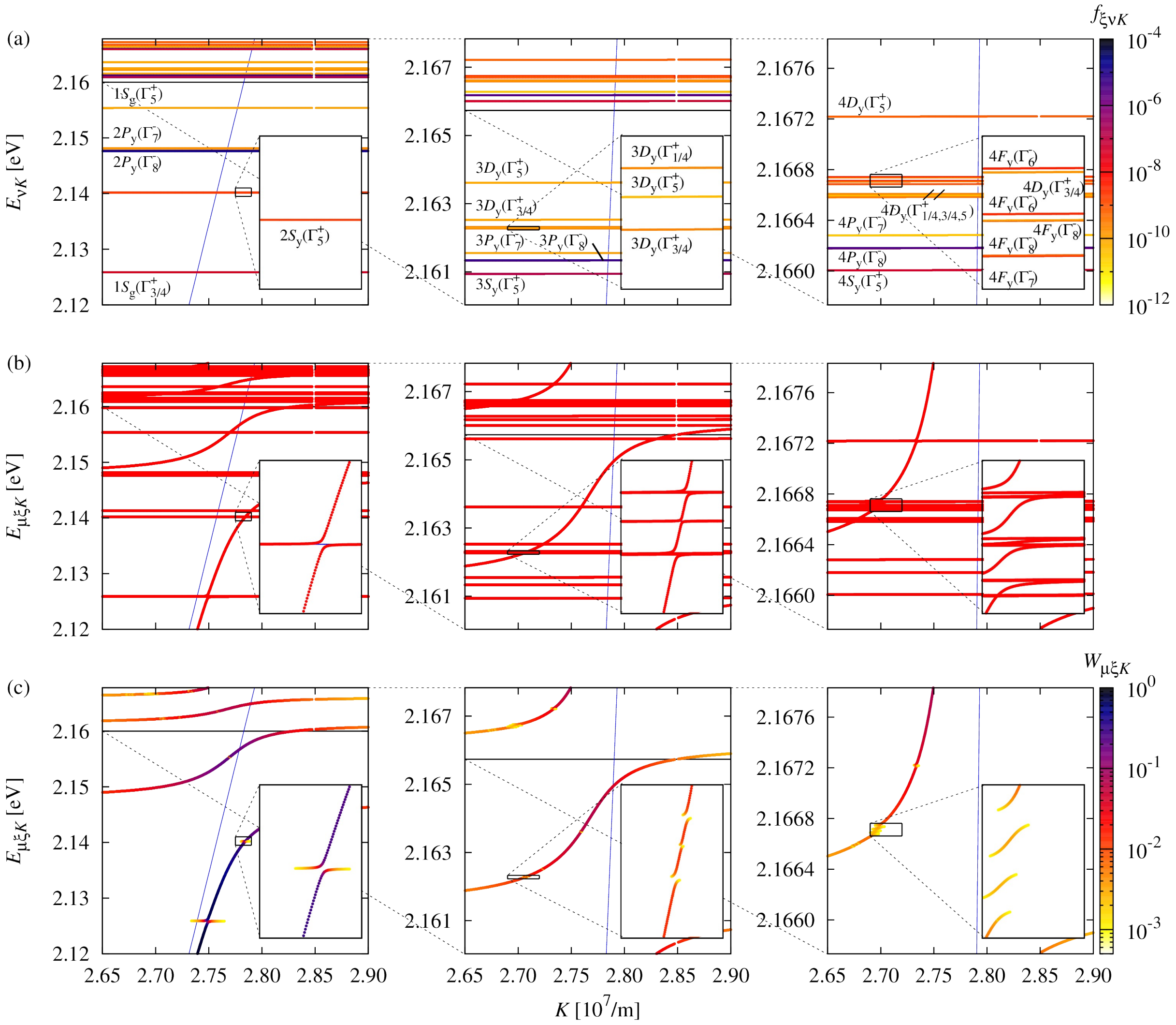

Figure 9.5.: Same spectra as in Fig. 9.4 but for $\boldsymbol{K} \parallel [110]$ and $\xi = \pi_{x'}$ polarized light. For further information see text.

For a complete description of the polariton problem, we also have to include the nonanalytic exchange interaction. The splitting caused by this interaction at $\boldsymbol{K} = \boldsymbol{0}$ must exactly equal the LT-splitting due to the polariton transformation. As the rotating wave approximation does not hold for $\boldsymbol{K} \to \boldsymbol{0}$, we determine at first the polariton energies $E_{\mu\xi\boldsymbol{K}}$ for the transverse exciton states via the conditional equation (9.32)

$$\frac{\hbar^2 c^2 K^2}{\varepsilon_{\mathrm{b}2} E^2_{\mu\xi\boldsymbol{K}}} = 1 + \sum_{\nu} \frac{f_{\xi\nu\boldsymbol{K}}}{1 - (E_{\mu\xi\boldsymbol{K}}/E_{\nu\boldsymbol{K}})^2}. \tag{9.77}$$

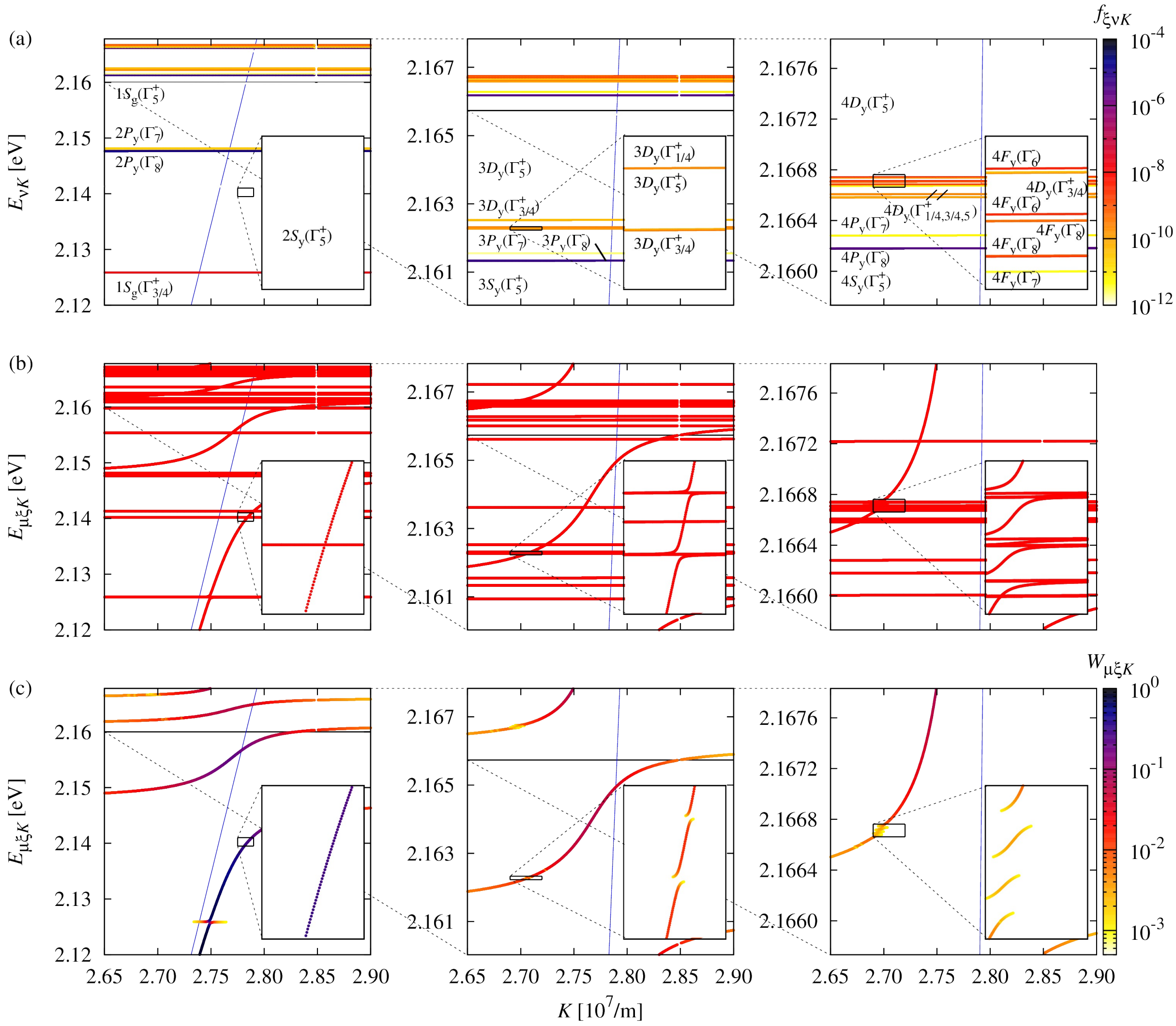

Figure 9.6.: Same spectra as in Fig. 9.4 but for $\boldsymbol{K} \parallel [110]$ and $\xi = \pi_{y'}$ polarized light. Note that the states which have the symmetry Γ_5^+ for $K = 0$ are dipole-forbidden in this case. For further information see text.

This equation can be rewritten so that the polariton energies are the roots of the function

$$F(E_{\mu\xi\boldsymbol{K}}) = 1 - \frac{\hbar^2\omega_{\xi\boldsymbol{K}}^2}{E_{\mu\xi\boldsymbol{K}}^2} + \sum_{\nu} \frac{f_{\nu\xi\boldsymbol{K}} E_{\nu\boldsymbol{K}}^2}{E_{\nu\boldsymbol{K}}^2 - E_{\mu\xi\boldsymbol{K}}^2}, \tag{9.78}$$

where the photon energy $\hbar\omega_{\xi\boldsymbol{K}} = \hbar K c/\sqrt{\varepsilon_{\mathrm{b}2}}$ is used. Note that a root of $F(E_{\mu\xi\boldsymbol{K}})$ is always located between any neighboring pair of the exciton energies $E_{\nu\boldsymbol{K}}$, $E_{\nu+1\,\boldsymbol{K}}$ [427–429].

We calculate the effect of the nonanalytic exchange interaction on the longitudinal states for $\boldsymbol{K} \to \boldsymbol{0}$ by diagonalizing the matrix $\boldsymbol{N}_{\{\nu\}\boldsymbol{K}}$ given in Eq. (9.54). As the size of the nonanalytic exchange is a priori unknown, we have scaled the matrix $\boldsymbol{N}_{\{\nu\}\boldsymbol{K}}$ with a parameter ζ. We vary the

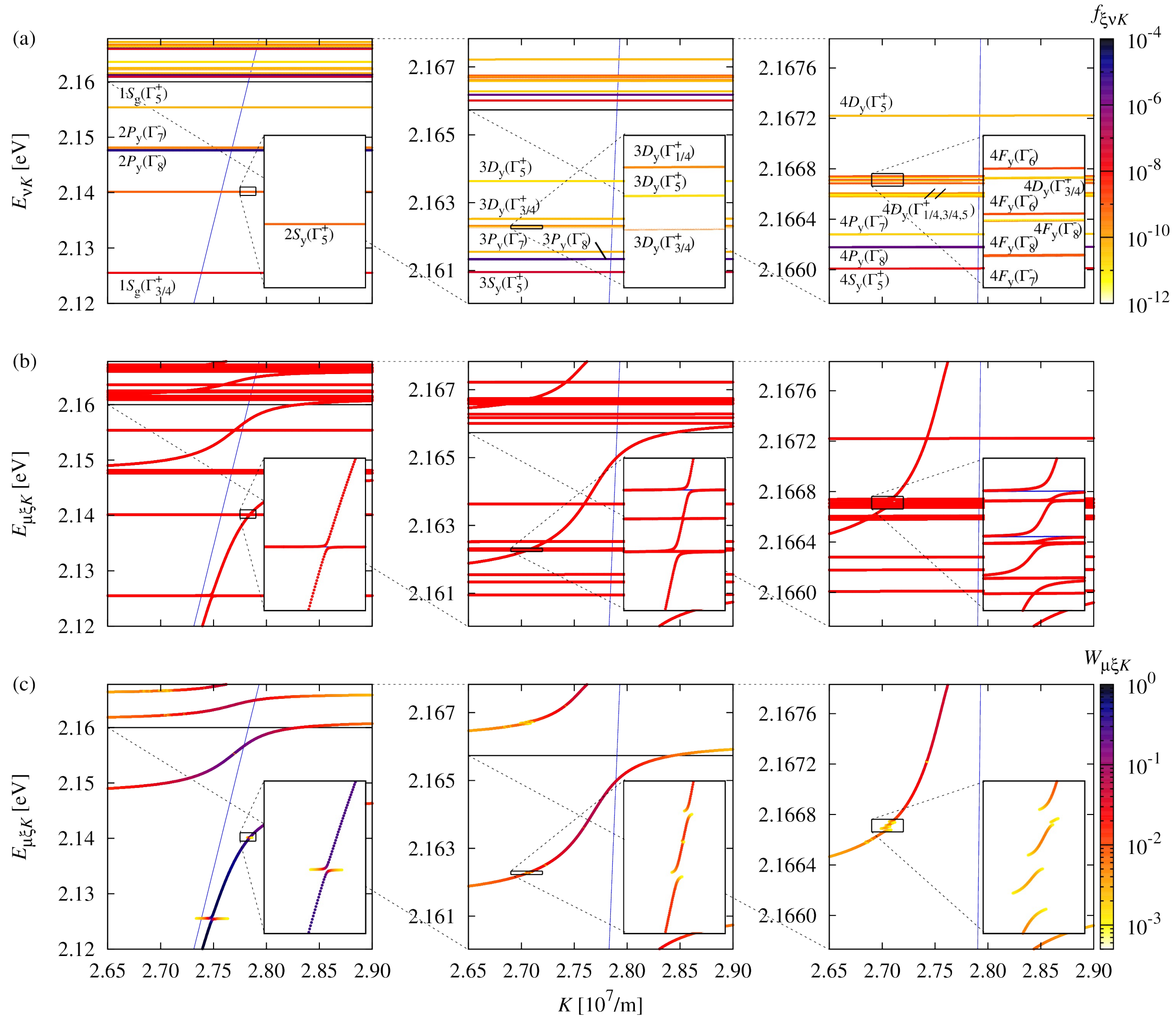

Figure 9.7.: Same spectra as in Fig. 9.4 but for $\boldsymbol{K} \parallel [111]$ and $\xi = \sigma^{\pm}_{z''}$ polarized light. For both polarizations the spectrum is identical. The oscillator strength of the $4F(\Gamma_7^-)$ state is too weak to be seen here. For further information see text.

parameter ζ in such a way that the energies of the longitudinal and transverse nP exciton states are identical. This yields $\zeta = 213.5 \pm 2.0$.

Of prime interest are the polariton dispersions in the vicinity of the exciton phonon resonance. In this range of K the rotating wave approximation is valid and we solve the eigenvalue problem of Eq. (9.53). Note that the errors arising due to the use of the rotating-wave approximation are smaller than the error due to uncertainties in $\varepsilon_{\mathrm{b2}}$.

The results for the three different orientations of $\boldsymbol{K}$ considered here are presented in Figs. 9.4-9.7. In the panels (a) of these figures we show the exciton spectrum in dependence on $K = |\boldsymbol{K}|$. Since the changes in the energy in dependence on K are in the order of tens of μeV, the exciton states appear as straight horizontal lines.

It can be seen that the spectrum is much more complicated than for the hydrogen-like case in Fig. 9.2. Even for vanishing momentum of the center of mass, the complete valence band structure already leads to a complicated fine structure splitting and to a mixing of the exciton states with even or odd parity. This explains the observability of F excitons in absorption spectra due to the admixture of P excitons (cf. Ref. [36] and Chapter 4). Due to the finite momentum of the center of mass S and D excitons also obtain a small quadrupole oscillator strength.

We state in the panels (a) of the Figs. 9.4-9.7 from which states at $K = 0$ the exciton states originate. We use the nomenclature $nL_{\mathrm{y/g}}(\Gamma_i^{\pm})$ of Sec. 6.2 with the abbreviations y and g for yellow and green. In the case of the P and F excitons we do not give the symmetry of the complete exciton state but only the combined symmetry of envelope and hole [36].

In the panels (b) of the Figs. 9.4-9.7 we show the polariton dispersions. Only for the P excitons, which have a comparatively large oscillator strength, significant deviations between the polariton spectrum and the exciton spectrum can be observed. The insets in the panels show that also for the other exciton states avoided crossings appear due to their finite oscillator strength. However, the panels (c) of the Figs. 9.4-9.7, which show the photon-like part of the polariton states, indicate that the mixing between excitons and photons is small for these excitons.

In contrast to the hydrogen-like case, the multi-polariton framework has to be used also for the exciton states with small principal quantum numbers. This can be seen in the middle and right panel in the last row of the figures: Due to the proximity of the nS and nP states as well as that of the nF states, avoided crossings are not well-separated and a single-polariton concept would lead to different results. The large avoided crossings of the P excitons clearly affect the other avoided crossings as they shift them away from the position where the dispersion of light and the dispersion of the other exciton states cross.

Since the K-dependent shift of the exciton energies is on the order of tens of μeV, the exciton energies are almost the same for the three orientations of $\boldsymbol{K}$ considered here. The main difference between the spectra for $\boldsymbol{K} \parallel [001]$, $\boldsymbol{K} \parallel [110]$ or $\boldsymbol{K} \parallel [111]$ is the values of the oscillator strengths due to the different symmetry breaking (cf. Table 9.1). Therefore, also the polariton dispersions are clearly different especially in the vicinity of the avoided crossings.

Note that we do not show the polariton dispersion for exciton states with $n \geq 5$ since the number of states with a finite oscillator strength increases rapidly. However, the oscillator strengths of the G, H, … exciton states are very small so that polariton effects are likewise very small. Hence, we do not expect to observe considerably new effects for the exciton-polaritons with $n \geq 5$.

9.7 Yellow 1S ortho-exciton polariton

We now come to the yellow 1S ortho-exciton polariton. In Sec. 9.7.1 we discuss at first the effect of finite momentum of the center of mass $\hbar K \neq 0$ on the exciton spectrum. We especially pay attention to the small quadrupole oscillator strength [178] and the $\boldsymbol{K}$-dependent splitting of this state [82–84]. We discuss why a direct comparison to experimental values for this splitting is not possible and that polariton effects always need to be considered for this state. Including these effects, we present the polariton dispersion, determine the group velocity [179, 180] as well as the spectra for rotations about the $[1\bar{1}0]$ and the $[111]$ axis and compare them with experimental values [82, 83] in Sec. 9.7.2.

9.7.1 $\boldsymbol{K}$-dependent splitting

As has already been stated in Sec. 9.6, we have to consider the reduction of the irreducible representations of the cubic group O_{h} by the groups $C_{4\mathrm{v}}$, $C_{2\mathrm{v}}$, and $C_{3\mathrm{v}}$ for the three cases of $\boldsymbol{K}$ being oriented along the [001], [110], or the [111] direction, respectively. In particular for an exciton state having the symmetry $\Gamma_5^{\pm}$ at $K=0$ degeneracies are lifted for $K \neq 0$.

We therefore observe a splitting of the $1S_{\mathrm{y}}(\Gamma_5^{+})$ ortho-exciton state depending on K when solving the full K-dependent Hamiltonian (9.5) of excitons in $\mathrm{Cu_2O}$. This splitting is shown in Fig. 9.8. It was observed experimentally in Refs. [82–84] and originally discussed in terms of a K-dependent exchange interaction. However, a closer examination of this interaction revealed that it is far too weak in $\mathrm{Cu_2O}$ to describe the observed splitting (cf. Sec. 5.3). Instead, it could be shown in Sec. 4.5.2 that the effects due to the cubic valence band structure lead to a K-dependent effective mass and a K-dependent splitting of the $1S$ ortho-exciton. Hence, the directional dispersion is the true cause of the experimentally observed splitting. Note, however, that in Sec. 4.5.2 the splitting was treated within a perturbation approach and that it was already emphasized that the complete K-dependent Schrödinger equation including the central-cell corrections would have to be solved to obtain correct results. This has now been done.

As the $1S$ ortho-exciton state exciton state has the symmetry Γ_5^{+} for $K=0$, we expect for $\boldsymbol{K} \parallel [001]$ and $\boldsymbol{K} \parallel [111]$ a splitting into two degenerate and one non-degenerate state. For $\boldsymbol{K} \parallel [110]$ all degeneracies are lifted (cf. Table 9.1). We have already stated in Chapter 5 that a K-dependent splitting of a state with the symmetry Γ_5^{+} must always have the form of Eq. (9.59) for group theoretical reasons. We can prove the consistency with this formula by diagonalizing the Hamiltonian (9.59) for $\boldsymbol{K} \parallel [001]$, $\boldsymbol{K} \parallel [110]$, and $\boldsymbol{K} \parallel [111]$ and fitting the resulting eigenvalues to our numerical results obtained with the full exciton Hamiltonian (9.1) in Fig. 9.8. For the different orientations of $\boldsymbol{K}$ these eigenvalues read

$$\begin{aligned} [001]: \quad & \lambda_{1,2} = (\Delta_1 - \Delta_3)K^2, \\ & \lambda_3 = (\Delta_1 + 2\Delta_3)K^2, \end{aligned} \tag{9.79a}$$

$$\begin{aligned} [110]: \quad & \lambda_1 = (\Delta_1 - \Delta_3)K^2, \\ & \lambda_{2,3} = (\Delta_1 + \Delta_3/2 \pm \Delta_5/2)K^2, \end{aligned} \tag{9.79b}$$

$$\begin{aligned} [111]: \quad & \lambda_{1,2} = (\Delta_1 - \Delta_5/3)K^2, \\ & \lambda_3 = (\Delta_1 + 2\Delta_5/3)K^2. \end{aligned} \tag{9.79c}$$

The values of the fit parameters Δ_1, Δ_3, and Δ_5 are given in Table 9.2. Since we have only three independent parameters Δ_i but seven exciton states to be fitted, the consistency is proven by the fact that we obtain the same values of the parameters Δ_i in all fits.

When performing the fit, it is not necessary to account for the K-dependent nonanalytic exchange interaction. In Sec. 9.4 a formula for the size of the nonanalytic exchange interaction of the $1S$ exciton was derived:

$$\Delta_Q = 2f_0E_0/K_0^2. \tag{9.80}$$

Here $f_0 = 3.6\times10^{-9}$ and E_0 denote the oscillator strength and the energy of the transverse exciton for $\boldsymbol{K} \parallel [001]$ at the exciton-photon resonance K_0, respectively. From the numerical results we obtain

$$K_0 = 2.614\times10^{7}\,\frac{1}{\mathrm{m}}, \qquad E_0 = 2.032\,\mathrm{eV} \tag{9.81}$$

and, therefore,

$$\Delta_Q = 2.135\times10^{-17}\,\mu\mathrm{eV\,m^2}. \tag{9.82}$$

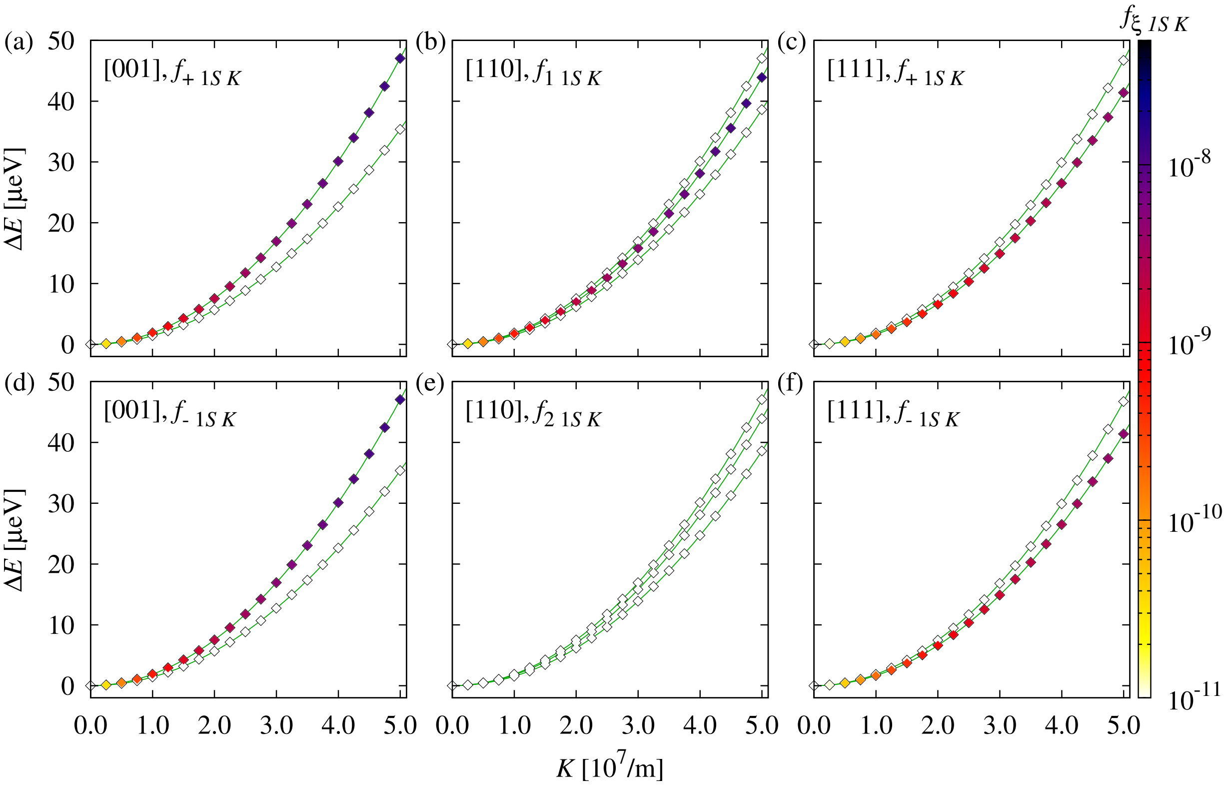

Figure 9.8.: Energy of the $1S_\mathrm{y}(\Gamma_5^+)$ ortho-exciton state in dependence of $K = |\boldsymbol{K}|$. We do not plot the absolute energies but the energy difference $\Delta E = E^\mathrm{o}_{1S,\boldsymbol{K}} - E^\mathrm{o}_{1S,\boldsymbol{0}}$ to show the small increase of the energy for $K \neq 0$. The 1*S* exciton obtains a finite oscillator strength for $K \neq 0$, which increases quadratically with *K*. Furthermore, a *K*-dependent splitting of the three ortho-exciton states can be observed. The green solid lines are the fits of the eigenvalues (9.79) of the Hamiltonian (9.59) to the numerical results. For further information see text.

Table 9.2.: Results for the three coefficients Δ_i when fitting the eigenvalues of Eq. (9.79) to the theoretical spectra of Fig. 9.8 for the different orientations of $\boldsymbol{K}$. For the [001] direction and the [111] direction the values Δ_5 and Δ_3 cannot be determined, respectively. All results are given in $10^{-14}\,\mu\mathrm{eV\,m}^2$. For a comparison, we also list the experimentally determined values of Refs. [82–84]. For further information see text.

	[001]	[110]	[111]	expt
Δ_1	1.727	1.729	1.728	1.074
Δ_3	−0.156	−0.155	-	−0.189
Δ_5	-	0.213	0.213	0.292

Obviously, the nonanalytic exchange interaction is two to three orders of magnitude smaller than the anisotropic dispersion (cf. Table 9.2).

The experimentally observed splitting was described by the ansatz (9.59) as well [82–84]. However, we cannot directly compare our values of the fit parameters to the results of Refs. [82–84]. As we have already stated in Sec. 9.3.4, in transmission and absorption experiments the frequency is well defined while the value of K is uncertain. Instead, several K values contribute to these spectra, which makes it difficult to interpret them. This has even been demonstrated experimentally for the $1S$ ortho-exciton: The observation of quantum beats [178] and measurements of the group velocity [179, 180] indicate a pronounced polariton effect. Hence, the assumption of a fixed value of $K = K_0$ in the evaluation of the results in Refs. [82–84] is not justified. Since in the experiment the value of K is uncertain and only its magnitude can be estimated, it is only possible to compare whether our results and the results of Refs. [82–84] for the parameters Δ_i are of the correct order of magnitude.

When comparing the results, we have to note that the values of the Δ_i are given with respect to K_0 and that the factor Δ_1 of Refs. [82–84] only describes the "exchange interaction", i.e., the interaction without the spherically symmetric part of the kinetic energy. Therefore, we have to compare $\Delta_1/K_0^2 + \hbar^2/2M$, Δ_3/K_0^2, and Δ_5/K_0^2 with our results of the parameters Δ_i. Here $M = m_{\mathrm{e}}+m_{\mathrm{e}} \approx 1.64m_0$ is the value of the isotropic exciton mass used in Refs. [82–84]. Furthermore, in the evaluation of the experiments the value of Δ_1 could not be determined from the observed splitting of states since the curvature of the dispersion parabola is not accessible in transmission experiments. For this reason, Δ_1 had to be determined by using the isotropic mass $M = 3m_0$ of the $1S$ ortho-exciton, which was obtained via resonant Raman scattering [438]. Note that also in the evaluation of Ref. [438] again a hydrogen-like model of excitons was used. All this explains the discrepancy when comparing our results with the value of Δ_1 from Refs. [82–84].

Within our model the average mass of the $1S$ ortho-exciton is

$$M = \frac{\hbar^2}{2K^2}\left(\frac{1}{3}\mathrm{Tr}\left[\boldsymbol{H}_{\mathrm{disp}}(\boldsymbol{K})\right]\right)^{-1} = \frac{\hbar^2}{2\Delta_1} = 2.2\,m_0, \tag{9.83}$$

which is significantly larger than the sum $M = m_{\mathrm{e}} + m_{\mathrm{h}} = m_{\mathrm{e}} + m_0/\gamma_1 \approx 1.56m_0$ of the isotropic quasi-particle masses. However, there is a clear deviation from the experimentally determined value of $M = (3.0 \pm 0.2)m_0$ [153, 258, 438]. The disparity in the masses can be explained by the fact that the electron and the hole are not bare particles but polarize the surrounding lattice and are thus accompanied by clouds of longitudinal optical phonons [12]. Hence, in the experiment always polaron masses are measured which are larger than the bare particle masses [12]. Although we accounted for this effect via the Haken potential in the Hamiltonian (9.1), we already stated in Sec. 6.1.2 that there are some difficulties in applying this theory to $\mathrm{Cu_2O}$ due to the existence of two optical phonons contributing to the Fröhlich interaction and due to the small distance between the electron and the hole in the exciton ground state, for which the Haken potential cannot describe the non-Coulombic electron-hole interaction.

For the other two coefficients Δ_3 and Δ_5 a good agreement is obtained, in particular, as regards the sign of the parameters (see Table 9.2). Note, however, that in Refs. [82–84] Δ_Q has been assumed to be of the same order of magnitude as the parameters Δ_i and that it has been included in the fit of the experimental data. This affects the values for Δ_3 and Δ_5 and is, therefore, another reason for the difference between the experimental and the theoretical values in Table 9.2.

We can underpin the fact that in the experiment a distribution of the exciton momentum $\hbar K$ plays a role. With the parameters Δ_i of Table 9.2 we calculate for the three orientations $\boldsymbol{K} \parallel [001]$, $\boldsymbol{K} \parallel [110]$, and $\boldsymbol{K} \parallel [111]$, those values of K, for which the differences between the eigenvalues of the Hamiltonian (9.59) are identical to the experimentally observed splittings of Refs. [82–84]. The results are listed in Table 9.3. One can see that there is no consistent result for K.

Table 9.3.: Experimentally observed splittings between the components of the $1S$ ortho-exciton [84]. Here $\tilde{\Delta}_{12}$ and $\tilde{\Delta}_{23}$ denote the energy differences $\tilde{\Delta}_{ij} = E_i - E_j$ with E_1 being the $1S$ ortho state of highest energy and E_3 being the $1S$ ortho state of smallest energy. We calculate the eigenvalues of the Hamiltonian (9.59) and choose the value of K in such a way that the differences between the eigenvalues equal the experimental splittings. It can be seen that when using the parameters Δ_i of Table 9.2 no consistent value for K can be obtained. For further information see text.

	$\tilde{\Delta}_{12}\,[\mu\mathrm{eV}]$	$K\,[10^7\,\frac{1}{\mathrm{m}}]$	$\tilde{\Delta}_{23}\,[\mu\mathrm{eV}]$	$K\,[10^7\,\frac{1}{\mathrm{m}}]$
[001]	0.0	–	4.3	3.02
[110]	1.6	3.54	2.1	3.15
[111]	4.3	4.51	0.0	–

Finally, differences between the experimental and theoretical values of the parameters Δ_i could furthermore be explained in terms of small strains in the crystal [83] and uncertainties in the experimental values (cf. the large error bars in the figures of Ref. [82]). In particular, the fact that the experimental spectra are not identical when changing the angle of the laser beam by the same amount in opposite directions in Ref. [82] shows the presence of strains.

We wish to note that also K-dependent splittings in the same order of magnitude are obtained, e.g., for the $2P$ exciton state. However, these splittings cannot be observed experimentally due to the large linewidth of the $2P$ exciton.

9.7.2 Polariton dispersion

As the $1S$ ortho state shows a pronounced polariton effect, we will now come to its polariton dispersion, which can be calculated using the 5×5 matrix model of Sec. 9.4. For the subsequent calculations we will use the parameters

$$f_0 = 3.6 \times 10^{-9}, \quad E_0 = 2.0239\,\mathrm{eV} \tag{9.84}$$

of Ref. [178], which yield

$$K_0 = 2.618 \times 10^7\,\frac{1}{\mathrm{m}}, \quad \Delta_Q = 2.135 \times 10^{-17}\,\mu\mathrm{eV}\,\mathrm{m}^2. \tag{9.85}$$

We also use the average values of the theoretical results for the parameters Δ_i in Table 9.2:

$$\begin{aligned} \Delta_1 &= 1.728 \times 10^{-14}\,\mu\mathrm{eV}\,\mathrm{m}^2, \\ \Delta_3 &= -0.1555 \times 10^{-14}\,\mu\mathrm{eV}\,\mathrm{m}^2, \\ \Delta_5 &= 0.213 \times 10^{-14}\,\mu\mathrm{eV}\,\mathrm{m}^2. \end{aligned} \tag{9.86}$$

In Fig. 9.9 we first present the results for $\boldsymbol{K}$ being oriented along one of the axes of high symmetry. The longitudinal exciton states do not couple to photons and, therefore, their dispersion appears as almost horizontal lines. In particular, it can be seen that for $\boldsymbol{K} \parallel [110]$ and light being polarized along $\hat{\boldsymbol{e}}_{2\boldsymbol{K}}$ no exciton-photon coupling occurs. For the transverse states we show the photon-like part for the two polarizations.

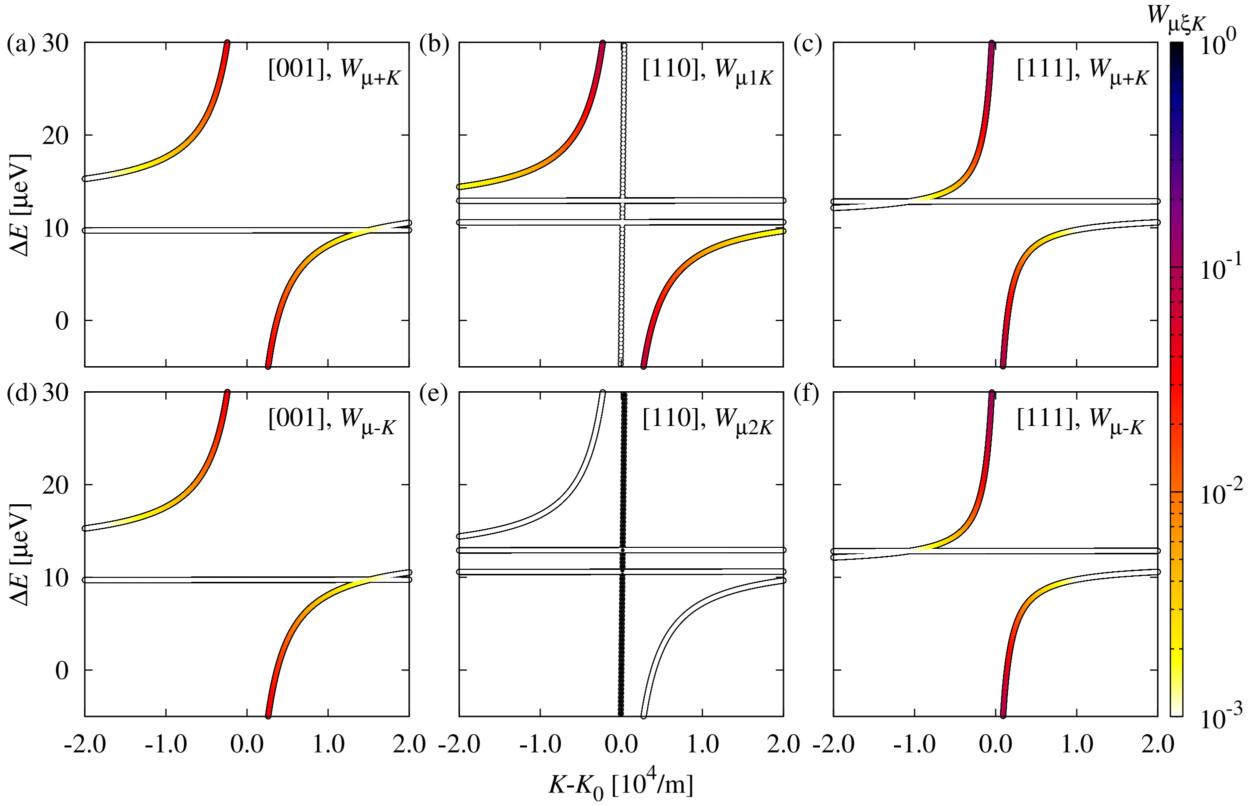

Figure 9.9.: Dispersion of the $1S$ ortho-exciton polariton calculated using the 5×5 matrix model of Sec. 9.4. For the different orientations of $\boldsymbol{K}$ we give the photon-like part $W_{\mu\xi\boldsymbol{K}}$ for the two polarizations ξ. It can be seen that for $\boldsymbol{K} \parallel [110]$ and light being polarized along $\hat{\boldsymbol{e}}_{2\boldsymbol{K}}$ no exciton-photon coupling occurs. We do not plot the absolute energies but the energy difference $\Delta E = E - E_0$.

In Ref. [179] the group velocity of the $1S$ ortho-exciton polariton has been measured as function of the photon energy for $\boldsymbol{K} \parallel [110]$. From the dispersion in Fig 9.9(b) and (e), we can directly calculate the group velocity via

$$v_{\mathrm{g}} = \frac{\mathrm{d}\omega}{\mathrm{d}K} = \frac{1}{\hbar}\frac{\mathrm{d}E}{\mathrm{d}K}. \tag{9.87}$$

The result is shown in Fig. 9.10. It can be seen that the group velocity decreases on the lower polariton branch close to the resonance for increasing values of K. However, for large values of K the polariton dispersion approaches the exciton dispersion, which increases quadratically in K, so that v_{g} is then proportional to K. Hence, there must be a minimum value of the group velocity. In the experiment group velocities as low as $40\,\frac{\mathrm{km}}{\mathrm{s}}$ could be measured [179]. However, it was not possible to measure the complete dispersion. In particular, the region of very low group velocities is not experimentally accessible. From Eq. (9.87) and the theoretical results it is possible to calculate all group velocities. The minimum value of v_{g} obtained in our calculations is

$$v_{\mathrm{g,min}} = 1.5\,\frac{\mathrm{km}}{\mathrm{s}}. \tag{9.88}$$

at $K = 2.758\,\frac{1}{\mathrm{m}}$. When comparing our result for the group velocity, i.e., Fig 9.10(b), with the

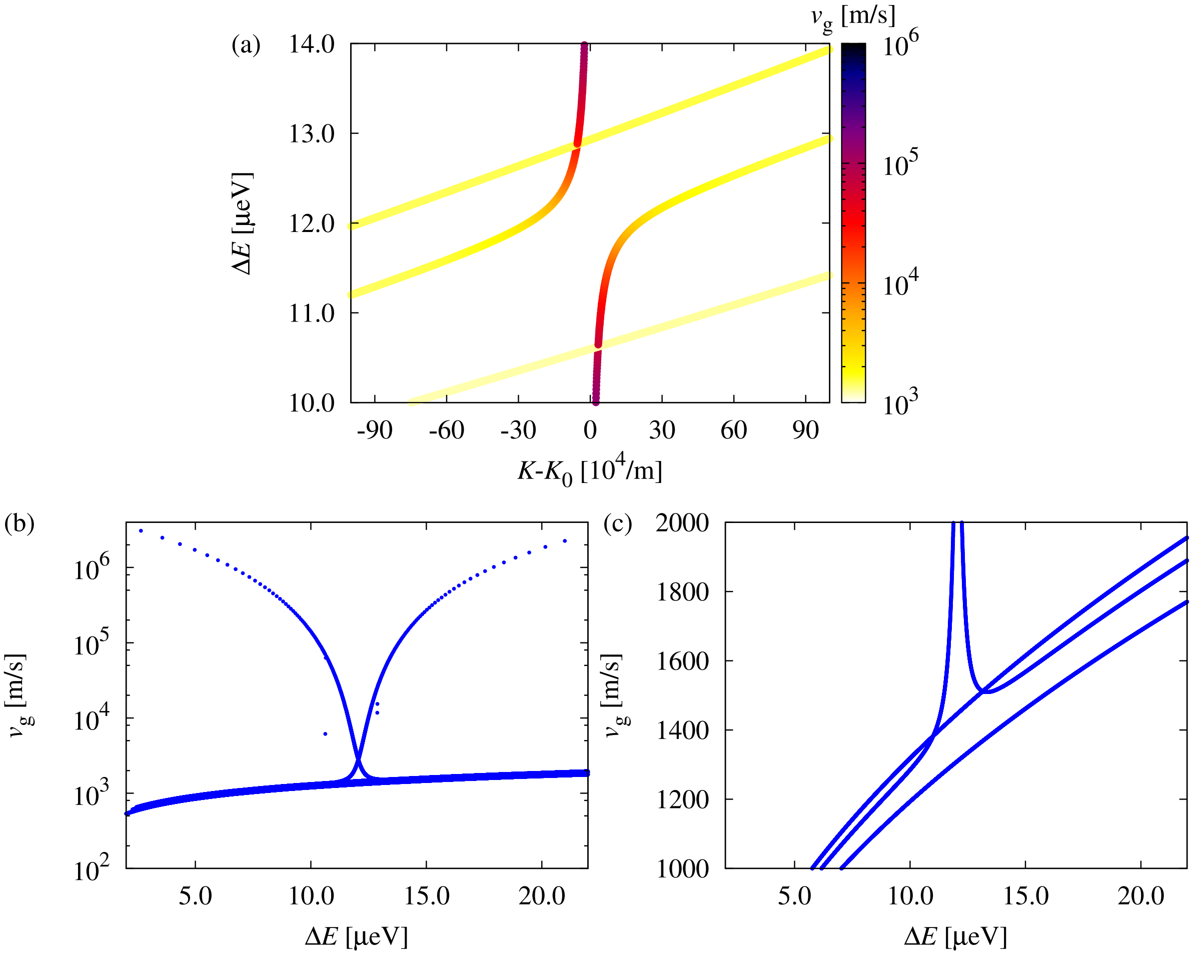

Figure 9.10.: (a) Group velocity v_g (colorscale) of the $1S$ ortho-exciton polariton with $\boldsymbol{K} \parallel [110]$ and $\hat{\boldsymbol{e}}_{1\boldsymbol{K}}$ polarization in dependence on the energy difference $\Delta E = E - E_0$ and the wave vector K. (b)-(c) The group velocity v_g only in dependence on the energy difference $\Delta E = E - E_0$ for a comparison with Fig. 3 of Ref. [179]. The minimum value of v_g depends on f_0 and is given by $v_{\mathrm{g,min}} = 1.5\,\frac{\mathrm{km}}{\mathrm{s}}$.

experimental results of Ref. [179], a very good agreement can be observed.

From the results of the 5×5 matrix model it is also possible to calculate the polarization vector of the photon-like part of the polariton or the orientation of the electric field as $\sum_{i=1}^{2} W_{\mu i \boldsymbol{K}} \hat{\boldsymbol{e}}_{i\boldsymbol{K}}$ and the polarization vector connected with the exciton-like part of the polariton via the symmetric cross product of $\hat{\boldsymbol{e}}_{i\boldsymbol{K}}$ and $\boldsymbol{K}$ [cf. Eq. (9.58)] according to the group theoretical condition $\Gamma_5^+ \otimes \Gamma_4^- \rightarrow \Gamma_4^-$. One obtains for $\Delta_3 = \Delta_5 = 0$ states with purely longitudinal or transverse polarization. However, in the general case, the states are mixed longitudinal-transverse states and the polarization is not parallel to the applied electrical field.

Another interesting point is the polariton energies if the crystal is rotated about the $[1\bar{1}0]$ or the $[111]$ axis (cf. Refs. [82–84]). In the case that the crystal is rotated about the $[1\bar{1}0]$ plane, the K

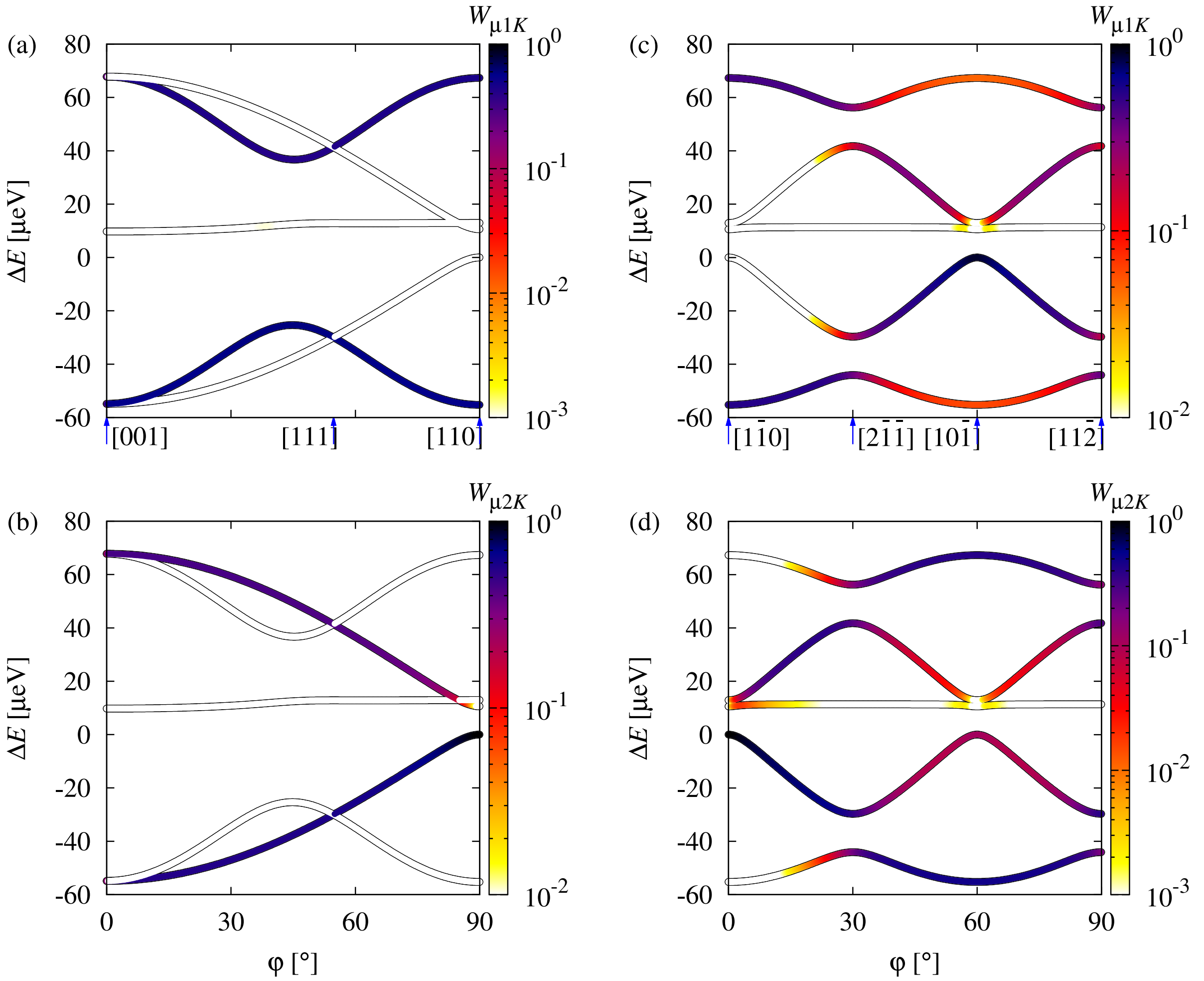

Figure 9.11.: Polariton energies at $K = K_0$ when rotating the vector $\boldsymbol{K}$ in the plane with the normal vector $\hat{\boldsymbol{n}} = (1,\,-1,\,0)/\sqrt{2}$. Again, we only plot the energy difference $\Delta E = E - E_0$. The colorscale denotes the photon-like part of the polariton states. As is discussed in the text, the problem decouples in two problems for the two irreducible representations Γ_1 [panel (a)] and Γ_2 [panel (b)] of the group C_s. (c),(d) Polariton energies at $K = K_0$ when rotating $\boldsymbol{K}$ in the plane with the normal vector $\hat{\boldsymbol{n}} = (1,\,1,\,1)/\sqrt{3}$. Every 60° $\boldsymbol{K}$ is oriented in a direction of high symmetry.

vector passes all three orientations of high symmetry from [001] to [111] and then to [110]:

$$\boldsymbol{K} = \frac{K}{\sqrt{2}} \begin{pmatrix} \sin\varphi \\ \sin\varphi \\ \sqrt{2}\cos\varphi \end{pmatrix}. \tag{9.89}$$

The polarization vectors are given by

$$\hat{\boldsymbol{e}}_{1\boldsymbol{K}} = \frac{1}{\sqrt{2}} \begin{pmatrix} \cos\varphi \\ \cos\varphi \\ -\sqrt{2}\sin\varphi \end{pmatrix}, \qquad \hat{\boldsymbol{e}}_{2\boldsymbol{K}} = \frac{1}{\sqrt{2}} \begin{pmatrix} 1 \\ -1 \\ 0 \end{pmatrix}. \tag{9.90}$$

Independent of the angle φ the symmetry of the problem is always C_{s} [90]. This group contains the identity and a reflection at the plane with the normal vector $\hat{\boldsymbol{n}} = (1,\,-1,\,0)/\sqrt{2}$, which is identical to one of the six σ_{d} reflections of O_{h}. The irreducible representations of C_{s} are either symmetric (Γ_1) or antisymmetric (Γ_2) under reflection. Hence, the complete problem falls into two parts: The linear combinations Ψ_{xy} and $(\Psi_{zx} + \Psi_{yz})/\sqrt{2}$ of the ortho-exciton states transform according to Γ_1 while the linear combination $(\Psi_{zx} - \Psi_{yz})/\sqrt{2}$ transforms according to Γ_2. Furthermore, photons transform in C_{s} also according to Γ_1 ($\hat{\boldsymbol{e}}_{1\boldsymbol{K}}$) and Γ_2 ($\hat{\boldsymbol{e}}_{2\boldsymbol{K}}$). Therefore, the problem decouples group theoretically in a Γ_1 problem with three polariton branches and a Γ_2 problem with only two polariton branches.

We keep the amount of $\boldsymbol{K}$ fixed at $K = K_0$ and increase the angle φ from 0° to 90°. The result is shown in Figs. 9.11(a) and 9.11(b). From the photon-like part of the polaritons we can clearly see the decoupling of the problem. Furthermore, the expected degeneracies of the polariton states occur if $\boldsymbol{K}$ is oriented in [001], [111] or [110] direction.

Let us now discuss the rotation about the [111] axis. The [111] axis is a threefold axis, for which reason after every 60° $\boldsymbol{K}$ is oriented in a direction of the form [110]. Between each two of these cases $\boldsymbol{K}$ is oriented in a direction of the form [112]. We have

$$\boldsymbol{K} = \frac{K}{\sqrt{6}} \begin{pmatrix} \sqrt{3}\cos\varphi + \sin\varphi \\ -\sqrt{3}\cos\varphi + \sin\varphi \\ -2\sin\varphi \end{pmatrix}, \tag{9.91}$$

and the polarization vectors

$$\hat{\boldsymbol{e}}_{1\boldsymbol{K}} = \frac{1}{3} \begin{pmatrix} -1 + \cos\varphi - \sqrt{3}\sin\varphi \\ -1 + \cos\varphi + \sqrt{3}\sin\varphi \\ -1 - 2\cos\varphi \end{pmatrix}, \qquad \hat{\boldsymbol{e}}_{2\boldsymbol{K}} = \frac{1}{3\sqrt{2}} \begin{pmatrix} 2 + \cos\varphi - \sqrt{3}\sin\varphi \\ 2 + \cos\varphi + \sqrt{3}\sin\varphi \\ 2 - 2\cos\varphi \end{pmatrix}. \tag{9.92}$$

The resulting spectrum when varying the angle φ and keeping the amount of $\boldsymbol{K}$ fixed at $K = K_0$ is shown in Figs. 9.11(c) and 9.11(d). In the cases with $\boldsymbol{K}$ being of the form [110] only one exciton state is allowed for the polarization vector of the form [001] and all exciton states are forbidden for the other polarization vector. Note, however, that if we start with the configuration $\boldsymbol{K} \parallel [0\bar{1}0]$, $\hat{\boldsymbol{e}}_{1\boldsymbol{K}} \parallel [00\bar{1}]$, and $\hat{\boldsymbol{e}}_{1\boldsymbol{K}} \parallel [110]$ of Ref. [82] and perform a rotation about the [111] axis, none of the polarization vectors is oriented in the [010] direction at $\varphi = 60°$ while $\boldsymbol{K} \parallel [10\bar{1}]$ holds. Hence, only for $\varphi = 0°$ all exciton states are forbidden for the polarization $\hat{\boldsymbol{e}}_{2\boldsymbol{K}}$ in Fig. 9.11(c) and 9.11(d).

In the cases with $\boldsymbol{K}$ being of the form [112] all exciton states are allowed. Since the difference between $\boldsymbol{K} \parallel [1\bar{1}0]$ and $\boldsymbol{K} \parallel [2\bar{1}\bar{1}]$ are only $\Delta\varphi = 30°$, a rotation about the [111] axis with $\varphi = 4°$ already shows a significant effect on the spectrum as can be seen especially from Fig. 9.11(d).

Exactly for this case with $\varphi = 4°$ and the polarization $\hat{\boldsymbol{e}}_{2\boldsymbol{K}}$ the transmission spectrum of the ortho-exciton polariton has been shown in Ref. [82]. For a comparison, we calculate the polariton dispersion for different values of K and keeping φ fixed to $\varphi = 4°$. The result is shown in Fig. 9.12. It can be seen that for the polarization $\hat{\boldsymbol{e}}_{2\boldsymbol{K}}$ two states have a significant photon amplitude. Hence, these are the two states, which could be observed as very narrow lines in the experimental transmission spectrum [82]. However, while in the experiment the energy difference between the two

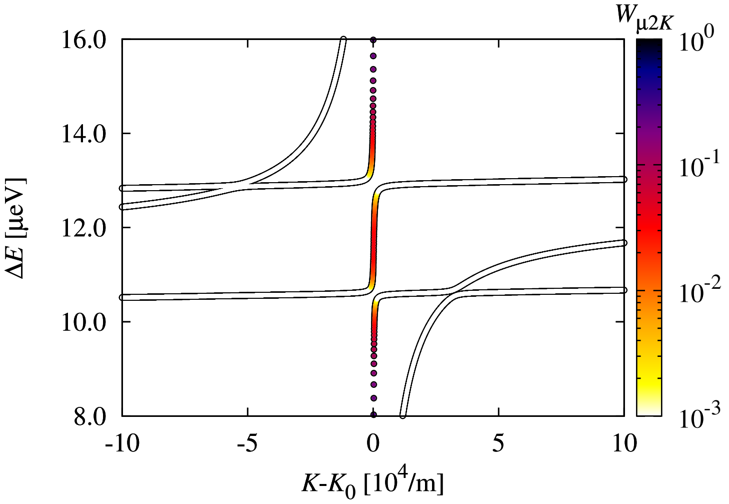

Figure 9.12.: Polariton energies if the vector $\boldsymbol{K}$ is rotated in the plane with the normal vector $\hat{\boldsymbol{n}} = (1,\, 1,\, 1)/\sqrt{3}$ by $\varphi = 4°$ and its amount is varied. Again, we only plot the energy difference $\Delta E = E - E_0$. The colorscale denotes the photon-like part of the polariton states.

states is about $4\,\mu$eV, we obtain only $2.4\,\mu$eV. We can exclude uncertainties in the parameter Δ_1 or the angle φ since a variation of these parameters does not change the size of the splitting. Only a variation of Δ_3 and Δ_5 changes the size of the splitting. However, even if we set these parameters to the experimentally determined values listed in Table 9.2, the splitting increases only to $3.0\,\mu$eV. As we have already stated above, the presence of small strains in the crystal cannot be excluded. These may be the major reason for the observed discrepancy.

Of course, it is also possible that the positions of the transmission maxima in the experiment are not exactly given by the positions of the avoided crossings. In this case, one would have to calculate the transmission spectrum for the polariton dispersion using Pekar's boundary conditions [439]. This is likewise difficult and beyond the scope of this work. Despite all that, we obtain a good qualitative agreement with the experiment.

10

Summary and Outlook

Excitons are of great physical interest since they represent the fundamental optical excitation in semiconductors. Excitons in cuprous oxide (Cu_2O), in particular, have attracted lots of attention in recent years [30, 31, 33–48, 51–55, 278, 440] due to an experiment, where the hydrogen-like absorption spectrum of these quasi-particles could be observed up to a principal quantum number of $n = 25$ [30]. The discovery of these giant Rydberg excitons may pave the way to a deeper understanding of inter-particle interactions in the solid [30] and to applications in quantum information technology [45].

In this context it is indispensable to completely understand the underlying theory of excitons. It was one of the topics of this thesis to investigate the corrections to the simple hydrogen-like model of excitons, which are needed to describe the experimentally observed spectra for Cu_2O. These corrections included the exciton-phonon interaction, the cubic valence band structure, the exchange interaction, the central-cell corrections, and the exciton-photon interaction. The second topic of this thesis were excitonic spectra in external magnetic fields and the breaking of all antiunitary symmetries for magnetoexcitons due to the valence band structure or due to the exciton-phonon interaction.

In Chapter 3 on the exciton-phonon interaction we have calculated the main parameters describing the shape of the excitonic absorption lines for the yellow exciton series of Cu_2O and compared our results to the experimentally observed lines of Ref. [30]. The calculated line width for yellow $2P$-exciton, in particular, lies within the same order of magnitude as the experimental one and differs only by a factor of ~ 3.5, which is a significant improvement on the result of Ref. [74]. Furthermore, we have discussed possible reasons for the large broadening and the large asymmetry of the lines. Of course, some of these special properties of Cu_2O could eventually be included in theory, but only with huge effort.

In Chapter 4 we described the corrections to the hydrogen-like model of excitons due to the cubic valence band structure. We introduced a complete basis to solve the corresponding Schrödinger equation and also derived formulas by which the relative oscillator strength of the exciton states can be determined. An evaluation of the calculated line spacings and oscillator strengths proved that there are several combinations of the parameters μ' and δ' by which the excitonic spectra can be described. However, we assume that the values resulting from band structure calculations are the correct ones. Using the values $\gamma_1' = 2.77$, $\mu' = 0.0586$, and $\delta' = -0.404$, the Luttinger parameters of Cu_2O are $\gamma_1 = 1.76$, $\gamma_2 \approx 0.75$, $\gamma_3 \approx -0.37$. Furthermore, we separated the relative motion and the motion of the center of mass using an appropriate coordinate transformation. The final result allows us to explain the K-dependent line splitting of the $1S$ exciton state in terms of the complex kinetic energy of the motion of the center of mass.

Using $\boldsymbol{k}\cdot\boldsymbol{p}$ perturbation theory, we could derive K-dependent higher order terms of the analytic and nonanalytic exchange interaction of Wannier excitons in Chapter 5. We have discussed the specific properties of Cu_2O and in particular the effects of the valence band structure. Investigating the K-dependent exchange interaction of the $1S$ excitons in this semiconductor, we could show that the K-dependent terms of the analytic and the nonanalytic exchange interaction are negligibly small compared to the effects of the nonisotropic dispersion. A closer examination of the K-dependent nonanalytic exchange interaction exhibited a coupling between longitudinal and transverse exciton states if $\boldsymbol{K}$ is not oriented in a direction of high symmetry.

In Chapter 6 we have treated the exciton spectrum of Cu_2O considering especially the central-cell corrections. A thorough discussion of these corrections revealed that only the frequency and the momentum dependence of the dielectric function $\varepsilon(k,\,\omega)$ have to be accounted for. Due to the estimated size of the $1S$ exciton Bohr radius, corrections to the kinetic energy can be neglected. Hence, only the two parameters V_0 and J_0 are decisive for the relative position of the exciton states. While J_0 describes the splitting of the exciton states into ortho and para components, V_0 changes the relative energy of the states but leaves this splitting between ortho and para component of the same exciton state almost unchanged. Hence, these parameters could be determined almost independently. This means that our results are not very sensitive to the choice of the parameters used. Instead, there is only one combination of both parameters J_0 and V_0 given in Eqs. (6.18)-(6.20), for which our results are in good agreement with the experiment.

We have shown that the central-cell corrections considerably affect the complete even exciton series since the valence band structure couples the $1S$ state to higher exciton states. The frequency dependence of the dielectric function also slightly affects the odd exciton series and lowers, in particular, the energy of the $2P$ exciton state. Furthermore, we have demonstrated that due to the coupling of the yellow and the green exciton series the green $1S$ exciton state is distributed over all yellow states. The results of our theory show a very good agreement with experimental values (see Table. 6.2).

In contrast to earlier works [41], we have presented a closed theory of the complete exciton series in Cu_2O, where we explicitly give the correction potentials (6.17a) or (6.17b). Hence, the introduction of quantum defects or the introduction of different exchange parameters for different exciton states, which take the effect of the central-cell corrections into account only phenomenologically, is redundant [37, 41].

The theory of excitons in semiconductors with a cubic valence band structure has been extended in Chapter 7 to calculate spectra in Faraday configuration in a uniform external magnetic field. Only by taking into account the complex valence band structure of Cu_2O, we could obtain an excellent agreement between theory and experiment as regards not only the relative positions but also the relative oscillator strengths of the exciton states. Furthermore, we have shown significant differences between the spectra for different orientations of the external magnetic field. Comparing the theoretical spectrum for $n=3$ and $n=5$ excitons with experimental results and using the method of harmonic inversion, we were able to determine the fourth Luttinger parameter of cuprous oxide to $\kappa=-0.50\pm0.10$.

The spectrum of excitons in magnetic fields especially shows characteristic level spacing statistics. Investigating the Hamiltonian of excitons in cubic semiconductors we could show in Chapter 8 analytically and numerically that the simultaneous presence of the cubic band structure and external fields can break all antiunitary symmetries in the system. The level spacing statistics of the quantum mechanical spectrum depends on the energy, the field strengths, the field orientations, and on the value of the parameter δ', which determines the strength of the cubic deformation of the band structure. This makes excitons in external fields a prime system to investigate the transitions between different level spacing statistics. Keeping the parameter δ' fixed, we analyzed the transition from GOE to GUE statistics and from Poissonian to GUE statistics. Since we changed only parameters such as the angles of the magnetic field or the scaled energy, which can also be varied in experiments, we think that the transition between the different level statistics could also be investigated experimentally. A comparison with analytical formulas for these transitions derived for 2×2 matrices within random matrix theory showed very good agreements. Hence, we could confirm the Wigner surmise for our model system.

When neglecting the exciton-phonon interaction, this symmetry breaking appears only if the plane spanned by the external fields is not identical to one of the symmetry planes of the cubic lattice of Cu_2O. We have discussed that for these cases the additional presence of the exciton-phonon interaction is not able to restore the broken symmetries.

For the specific orientations of the external fields, where the plane spanned by the fields is identical to one of the symmetry planes of the cubic lattice, the exciton-phonon interaction becomes important. This interaction causes a finite momentum of the exciton center of mass, which leads to the motional Stark effect in an external magnetic field. If the cubic valence band structure is considered, the effective electric field connected with the motional Stark effect finally leads to the breaking of all antiunitary symmetries. Since the exciton-phonon interaction is always present in the solid, we have thus shown that GUE statistics will be observable in all spectra of magnetoexcitons irrespective of the orientation of the external magnetic field, which is in agreement with the experimental observations in Refs. [31, 32]. We are convinced that a closer investigation of excitons in external fields can lead to a better understanding of the connection between quantum and classical chaos.

In Chapter 9 we presented the theory of exciton-polaritons in Cu_2O. In the derivation of the formulas we accounted for all relevant effects, which are needed to describe the spectra theoretically in an appropriate way, i.e., the complete valence band structure, the exchange interaction, and the central-cell corrections. The subsequent polariton transformation can be performed within the so-called rotating-wave approximation. Within this approximation it is straightforward to additionally account for the nonanalytic exchange interaction. As the exciton ground state located energetically far below other exciton states, it can be treated separately. Exploiting the symmetry properties of the $1S$ ortho exciton, we were able to set up a 5×5 matrix model, which allows for the calculation of the corresponding polariton dispersion for any direction of $\boldsymbol{K}$.

The treatment of the polariton effect using the hydrogen-like model already allowed for some first qualitative statements on the dispersion. We could show that for exciton states with a principal quantum number of $n \geq 6$ the polariton is not photon-like any more between each pair of exciton states and that a strong mixing of exciton states in the resonance region occurs. Therefore, only when using the multi-polariton concept, the correct polariton dispersion can be obtained. We also estimated that polariton effects for the yellow exciton states with $n \geq 2$ may only be observed using nonlinear spectroscopy methods and high quality crystals.

The more complex spectrum of excitons when using the full Hamiltonian leads likewise to a more complex polariton dispersion. Since the oscillator strengths of the exciton states differ for the three orientations $\boldsymbol{K}$ considered here, the polariton dispersions differ as well. When including the complete valence band structure, a K-dependent splitting (not only) of the three components of the yellow $1S$ ortho exciton appears. In contrast to Chapter 4, we have solved the complete K-dependent Schrödinger equation numerically including also the correct values for the central-cell corrections of Chapter 6. The splittings calculated are on the same order of magnitude as the splittings observed experimentally [82–84]. However, a direct comparison between theory and experiment is not possible since in transmission experiments the value of K is uncertain.

Using the 5×5 matrix model, we investigated the dispersion of the $1S$ ortho exciton polariton for different orientations of $\boldsymbol{K}$. In a comparison of the results for the group velocity with experimental results we obtained a very good agreement. The calculations allowed us to determine the minimum value of the group velocity to $v_{\mathrm{g,min}} = 1.5\,\frac{\mathrm{km}}{\mathrm{s}}$. We also presented results for the two special cases that the $\boldsymbol{K}$-vector is rotated in planes perpendicular to $[1\bar{1}0]$ and $[111]$. Especially in the second case, another comparison with experimental results was possible for a rotation angle of 4°. The splitting between the two allowed states obtained is smaller than in the experiment. This can, however, be explained in terms of the presence of small strains and uncertainties in the parameters Δ_i.

The research field of giant Rydberg excitons is by far not exploited yet. Building on the investigations on the exciton-photon and the exciton-phonon interaction it is, e.g., possible to calculate transmission spectra from the polariton dispersion obtained via the 5×5 matrix model by assuming Pekar's boundary conditions [439] and applying the Fresnel equations. This would allow for an even better comparison of theoretical results with the experiment and may also lead to an understanding of the shape of the peaks in the spectra.

In connection with the investigations on the impact of the cubic valence band structure, it is interesting to treat the complete problem within classical mechanics using closed orbit theory [441]. An identification of peaks in the Fourier transform of experimental spectra of magnetoexcitons with the classical orbits may allow for a deeper insight in the effects of the valence band structure. The situation might be comparable to the hydrogen atom and molecules in external magnetic fields: When treating the of hydrogen atom in a magnetic field classically, fundamental orbits occur. In the case of molecules, sums of these orbits lead to additional peaks in the spectra due to scattering at the atomic core [442]. It is expected that the valence band structure has a similar effect and that sums of fundamental orbits occur.

In this thesis we have laid the foundation to investigate spectra of excitons in external magnetic fields theoretically. What has not been concerned so far is the simultaneous presence of external magnetic *and* electric fields. Since an electric field leads to a mixing of the even and the odd exciton series, not only the valence band structure but also the exchange interaction and the central-cell corrections need to be considered. This leads to a likewise complex problem. However, using the method of complex rotation, which is known from the hydrogen atom in external fields [35, 443], it is then possible to find not only resonances in the spectra but also exceptional points. The appearance of these points, where not only two eigenvalues but also the corresponding eigenvectors of the Hamiltonian coalesce, has already been proven theoretically for the hydrogen atom in external fields [444]. However, the field strengths at which these points appear are far too high to be reached in experiments. Due to the small Rydberg energy of excitons, the fields where exceptional points appear are expected to be much smaller [35]. Hence, this may allow for the experimental proof of exceptional points.

A Relevant formulas

In this appendix we give some relevant formulas, which are needed in the theory of semiconductors or especially in the theory of excitons.

A.1 Delta functions

In section 2.2.2 we treated phonons in one dimension and found that their wave vectors are discrete due to periodic boundary conditions or the finite size of the crystal. Additionally, these wave vectors have to be inside the first BZ $[-\pi/a,\, \pi/a]$ since plane waves with a too small wavelength cannot be reproduced unambiguously by lattice vibrations (Fig. 2.5). We obtained

$$q = \frac{2\pi m}{L}, \quad m \in \left\{ -\frac{N}{2}, \ldots, \frac{N}{2} - 1 \right\} \tag{A.1}$$

with the length of the solid $L = Na$. In the case of electrons the wave vector can take even larger values since the elctronic wave function is not bound to the atoms, i.e., their wave function depends on the continuous coordinate x. However, due to Bloch's theorem, the energy and the wave function of electrons are periodic in k-space and it is sufficient to restrict oneself to the first BZ [86], as well (see Secs. 2.3.3 and 2.3.4).

In the following we derive some useful relations for the two cases according to the descriptions in [96], which will be used throughout this work and especially in Chapter 2. We start with the electrons, i.e., with a continuous variable x and prove the relation

$$\int_{-L/2}^{L/2} \mathrm{d}x \; e^{i(q-q')x} = L\delta_{q,q'}. \tag{A.2}$$

For $q \neq q'$ it is

$$\int_{-L/2}^{L/2} \mathrm{d}x \; e^{i(q-q')x} = \frac{2\sin\bigl((q-q')\frac{L}{2}\bigr)}{(q-q')}. \tag{A.3}$$

This expression vanishes for $q = 2\pi m/L$ and $q' = 2\pi n/L$ with $m \neq n$. On the other hand, we obtain

$$\int_{-L/2}^{L/2} \mathrm{d}x \; e^{i(q-q')x} = \int_{-L/2}^{L/2} \mathrm{d}x \, 1 = L \tag{A.4}$$

for $q = q'$. Therefore, Eq. (A.2) is correct. In three dimensions this relation reads

$$\int_V \mathrm{d}\boldsymbol{r}\; e^{i(\boldsymbol{q}-\boldsymbol{q}')\cdot\boldsymbol{r}} = V\delta_{\boldsymbol{q},\boldsymbol{q}'}. \tag{A.5}$$

If we now consider the results of Sec. 2.3.3, we may extend Eq. (A.5) for Bloch functions [94]:

$$\begin{aligned}\int_V \mathrm{d}\boldsymbol{r}\; \psi^*_{n\boldsymbol{q}}\psi_{n'\boldsymbol{q}'} &= \int_V \mathrm{d}\boldsymbol{r}\; e^{i(\boldsymbol{q}'-\boldsymbol{q})\cdot\boldsymbol{r}} u^*_{n\boldsymbol{q}}(\boldsymbol{r}) u_{n'\boldsymbol{q}'}(\boldsymbol{r}) \\ &= \sum_{\boldsymbol{G}}\sum_{\boldsymbol{G}'} c^*_{n\boldsymbol{q}-\boldsymbol{G}} c_{n'\boldsymbol{q}'-\boldsymbol{G}'} \int_V \mathrm{d}\boldsymbol{r}\; e^{i(\boldsymbol{q}'-\boldsymbol{q})\cdot\boldsymbol{r}} e^{i(\boldsymbol{G}'-\boldsymbol{G})\cdot\boldsymbol{r}} \\ &= \sum_{\boldsymbol{G}''}\sum_{\boldsymbol{G}} c^*_{n\boldsymbol{q}-\boldsymbol{G}} c_{n'\boldsymbol{q}'-\boldsymbol{G}-\boldsymbol{G}''} \int_V \mathrm{d}\boldsymbol{r}\; e^{i(\boldsymbol{q}'-\boldsymbol{q})\cdot\boldsymbol{r}} e^{i\boldsymbol{G}''\cdot\boldsymbol{r}} \\ &= \sum_{\boldsymbol{G}''} C_{n,n',\boldsymbol{q},\boldsymbol{q}',\boldsymbol{G}''} V\delta_{\boldsymbol{q},\boldsymbol{q}'+\boldsymbol{G}''} \\ &= V\delta_{\boldsymbol{q},\boldsymbol{q}'} C_{n,n',\boldsymbol{q},\boldsymbol{q}',\boldsymbol{0}}. \end{aligned} \tag{A.6}$$

In the last step we assumed $\boldsymbol{q}$ and $\boldsymbol{q}'$ to be within the first BZ. A special case is the integral

$$\int_V \mathrm{d}\boldsymbol{r}\; \psi^*_{n\boldsymbol{q}} e^{i\boldsymbol{k}\cdot\boldsymbol{r}} \psi_{n'\boldsymbol{q}'} = \sum_{\boldsymbol{G}''} C_{n,n',\boldsymbol{q},\boldsymbol{q}',\boldsymbol{G}''} V\delta_{\boldsymbol{q}+\boldsymbol{k},\boldsymbol{q}'+\boldsymbol{G}''} \tag{A.7}$$

with $\boldsymbol{q}+\boldsymbol{k}$ being outside the first BZ. Then we may write $\boldsymbol{q}+\boldsymbol{k} = \tilde{\boldsymbol{q}} + \tilde{\boldsymbol{G}}$ with a reciprocal lattice vector $\tilde{\boldsymbol{G}}$ and a wave vector $\tilde{\boldsymbol{q}}$ being inside the first BZ. Now we obtain

$$\begin{aligned}\int_V \mathrm{d}\boldsymbol{r}\; \psi^*_{n\boldsymbol{q}} e^{i\boldsymbol{k}\cdot\boldsymbol{r}} \psi_{n'\boldsymbol{q}'} &= \sum_{\boldsymbol{G}''} C_{n,n',\boldsymbol{q},\boldsymbol{q}',\boldsymbol{G}''} V\delta_{\tilde{\boldsymbol{q}},\boldsymbol{q}'+\boldsymbol{G}''-\tilde{\boldsymbol{G}}} = V\delta_{\tilde{\boldsymbol{q}},\boldsymbol{q}'} C_{n,n',\boldsymbol{q},\boldsymbol{q}',\tilde{\boldsymbol{G}}} \\ &= V\delta_{\boldsymbol{q}+\boldsymbol{k}-\tilde{\boldsymbol{G}},\boldsymbol{q}'} C_{n,n',\boldsymbol{q},\boldsymbol{q}',\tilde{\boldsymbol{G}}}. \end{aligned} \tag{A.8}$$

If we treat integrals with $n = n'$ and use the effective-mass approximation, i.e.,

$$\psi_{\boldsymbol{k}}(\boldsymbol{r}) = e^{i\boldsymbol{k}\cdot\boldsymbol{r}} u_{\boldsymbol{k}}(\boldsymbol{r}) \approx \frac{1}{\sqrt{V}} e^{i\boldsymbol{k}\cdot\boldsymbol{r}}, \tag{A.9}$$

we may finally write

$$\langle\boldsymbol{q}|e^{i\boldsymbol{k}\cdot\boldsymbol{r}}|\boldsymbol{q}'\rangle = \sum_{\boldsymbol{G}} \delta_{\boldsymbol{q},\boldsymbol{q}'+\boldsymbol{k}+\boldsymbol{G}}, \tag{A.10}$$

but always demand that $\boldsymbol{q}$, $\boldsymbol{q}'$ and $\boldsymbol{k}$ are within the first BZ.

Another important relation is

$$\sum_q e^{iq(x-x')} = L\delta(x-x'), \tag{A.11}$$

which can be proven by integrating both sides of the equation ($u = x - x'$) and using Eq. (A.2):

$$\int_{-L/2}^{L/2} \mathrm{d}u \sum_q e^{iqu} = L\sum_q \delta_{q,0} = L = \int_{-L/2}^{L/2} \mathrm{d}u\; L\delta(u). \tag{A.12}$$

In three dimensions this relation reads

$$\sum_{\boldsymbol{q}} e^{i\boldsymbol{q}\cdot(\boldsymbol{r}-\boldsymbol{r}')} = V\delta(\boldsymbol{r}-\boldsymbol{r}'). \tag{A.13}$$

Now we take a look at the phonon case with discrete position vectors $\boldsymbol{R}_n$. At first, we prove the relation

$$\sum_{n} e^{i(q-q')R_n} = N\sum_{G} \delta_{q,q'+G} \tag{A.14}$$

in one dimension. From

$$(1-e^{iqa})\sum_{n=0}^{N-1} e^{iqR_n} = (1-e^{i2\pi\frac{m}{N}})\sum_{n=0}^{N-1} e^{i(\frac{2\pi}{Na}m)na} = (1-e^{i2\pi m}) \tag{A.15}$$

we see that

$$\sum_{n=0}^{N-1} e^{iqR_n} = 0 \tag{A.16}$$

holds, unless $q=0$. For $q=0$ it is

$$\sum_{n=0}^{N-1} e^{iqR_n} = \sum_{n=0}^{N-1} 1 = N. \tag{A.17}$$

The replacement $q \to q+G$ does not change the results since

$$e^{iGR_n} = e^{i(\frac{2\pi}{a}m)na} = e^{i2\pi mn} = e^0 = 1 \tag{A.18}$$

holds. Therefore, Eq. (A.14) is correct. In three dimensions this relation reads

$$\sum_{\boldsymbol{n}} e^{i(\boldsymbol{q}-\boldsymbol{q}')\cdot\boldsymbol{R_n}} = N\sum_{\boldsymbol{G}} \delta_{\boldsymbol{q},\boldsymbol{q}'+\boldsymbol{G}}. \tag{A.19}$$

The last relation,

$$\sum_{q} e^{iq(R_n-R_m)} = N\delta_{R_n,R_m}, \tag{A.20}$$

can be proven in analogy to Eq. (A.14). Its three-dimensional version reads

$$\sum_{\boldsymbol{q}} e^{i\boldsymbol{q}\cdot(\boldsymbol{R_n}-\boldsymbol{R_m})} = N_xN_yN_z\,\delta_{\boldsymbol{R_n},\boldsymbol{R_m}}. \tag{A.21}$$

We finally note that each state takes a volume of $(2\pi/Na)^3 = (2\pi)^3/V$ in reciprocal space. If we assume the solid to be infinitely large, the wave vectors become quasi-continuous and we can replace the sums in the following way:

$$\sum_{\boldsymbol{k}} \to \frac{V}{(2\pi)^3}\int \mathrm{d}\boldsymbol{k} \tag{A.22}$$

In the long wavelength regime, the integral then extends only over the central part of the BZ with $|\boldsymbol{q}| \ll \pi/a$.

A.2 Second quantization

In this section we shortly introduce the formalism of second quantization, which is used in many chapters throughout this work due to the fact that electrons are fermions and that the many-particle wave function should be antisymmetric when two particles are interchanged. In first quantization the wave function would have to be constructed as a Slater determinant of one-particle wave functions. This determinant fulfills the requirement for asymmetry and vanishes if one of the single particle states is occupied more than once. However, to avoid unwieldy calculations with this determinant the Fock or occupation number representation is used.

Assume that we have a set of ortho-normalized and ordered single-particle wave functions $\psi_{\alpha_i}(x_i)$ with the quantum numbers α_i. These quantum numbers are, e.g., in the case of free electrons the pairs of wave vectors and spins ($\alpha_i = \boldsymbol{k}_i\sigma_i$). The coordinate x_i denotes spin and space variables. Instead of a Slater determinant the many-particle wave function is written in the following form:

$$|\Psi\rangle = |\{n_\alpha\}\rangle = c^\dagger_{\alpha_1} c^\dagger_{\alpha_2} \dots c^\dagger_{\alpha_N} |\{0\}\rangle \,. \tag{A.23}$$

The creation operators $c^\dagger_\alpha$ acting on the vacuum $|\{0\}\rangle$ create states with a finite number of fermions, where the ordering of the operators is of relevance since obey anti-commutation relations:

$$\begin{aligned} \left\{c_\alpha, c^\dagger_{\alpha'}\right\} &= \delta_{\alpha\alpha'}, & \text{(A.24a)} \\ \left\{c_\alpha, c_{\alpha'}\right\} = \left\{c^\dagger_\alpha, c^\dagger_{\alpha'}\right\} &= 0. & \text{(A.24b)} \end{aligned}$$

These relations guarantee the antisymmetry of the state $|\Psi\rangle$ and secure that one single-particle state is at most only once occupied. The operator $c^\dagger_\alpha c_\alpha$ acting on $|\Psi\rangle$ provides the occupation number n_α of the state with quantum number α and the number operator giving the total number of fermions is thus

$$\hat{N} = \sum_\alpha c^\dagger_\alpha c_\alpha. \tag{A.25}$$

Since fermions are indistinguishable, any operator A has to be symmetric in its coordinate representation under a permutation $\pi \in S_n$ of the particle coordinates: $A(x_1, \dots, x_n) = A(x_{\pi(1)}, \dots, x_{\pi(n)})$. Especially for non-interacting particles it is

$$A(x_1, \dots, x_n) = \sum_{l=1}^{n} A_1(x_l). \tag{A.26}$$

If an operator A consists of operators A_ν acting on ν particles in first quantization, it can be expressed in second quantization or Fock representation in terms of annihilation and creation operators in the following manner:

$$A \to \sum_{\alpha_1,\dots,\alpha_\nu} \sum_{\beta_1,\dots,\beta_\nu} \langle\psi_{\alpha_1}\dots\psi_{\alpha_\nu}|\, A_\nu \,|\psi_{\beta_1}\dots\psi_{\beta_\nu}\rangle\, c^\dagger_{\alpha_1}\dots c^\dagger_{\alpha_\nu} c_{\beta_\nu}\dots c_{\beta_1} \tag{A.27}$$

with

$$\begin{aligned} &\langle\psi_{\alpha_1}\dots\psi_{\alpha_\nu}|\, A_\nu \,|\psi_{\beta_1}\dots\psi_{\beta_\nu}\rangle \\ &= \int \mathrm{d}t_1 \dots \int \mathrm{d}t_\nu\, \psi^*_{\alpha_1}(t_1)\dots\psi^*_{\alpha_\nu}(t_\nu) A_\nu(t_1,\dots,t_\nu)\psi_{\beta_1}(t_1)\dots\psi_{\beta_\nu}(t_\nu). \end{aligned} \tag{A.28}$$

In this representation the ν-particle operator at first removes particles in the states β_i and then adds particles in the states α_j.

A.3 Continuum functions of the hydrogen atom

In this section we want to derive the solutions for the ionization continuum of the hydrogen-like exciton problem of Eq. (2.199) following the descriptions in Refs. [139, 247, 292]. With the ansatz

$$F_{kLM}(\boldsymbol{r}) = L_{kL}(r) Y_{LM}(\vartheta, \varphi) \tag{A.29}$$

we obtain the radial Schrödinger equation

$$-\frac{\hbar^2}{2\mu}\frac{1}{r^2}\frac{\partial}{\partial r}\left(r^2\frac{\partial}{\partial r}\right)L_{kL} + \frac{\hbar^2 L(L+1)}{2\mu}\frac{1}{r^2}L_{kL} - \frac{e^2}{4\pi\varepsilon_0\varepsilon}\frac{1}{r}L_{kL} = E_k L_{kL}. \tag{A.30}$$

We can simplify this expression by setting $E_k = \hbar^2 k^2/2\mu$, $\rho = 2ikr$ and $\alpha = \sqrt{R_{\mathrm{exc}}/E_k}$:

$$\frac{1}{\rho^2}\frac{\partial}{\partial \rho}\left(\rho^2\frac{\partial}{\partial \rho}\right)L_{kL} + \left(-\frac{1}{4} - \frac{i\alpha}{\rho} - \frac{L(L+1)}{\rho^2}\right)L_{kL} = 0. \tag{A.31}$$

Similarly to the case with bound solutions, we make the ansatz

$$L_{kL} = \rho^L e^{-\frac{\rho}{2}} T_{kL}(\rho). \tag{A.32}$$

This yields

$$\rho\frac{\partial^2}{\partial \rho^2}T_{kL} + (2L+2-\rho)\frac{\partial}{\partial \rho}T_{kL} + (-i\alpha - L - 1)T_{kL} = 0. \tag{A.33}$$

Since the hypergeomeric function

$${}_1F_1(a;\, b;\, z) = 1 + \frac{a}{b}z + \frac{a(a+1)}{2b(b+1)}z^2 + \ldots = \sum_{m=0}^{\infty}\frac{\Gamma(m+a)}{\Gamma(a)}\frac{\Gamma(b)}{\Gamma(b+m)}\frac{z^m}{m!} \tag{A.34}$$

fulfills the differential equation

$$z\frac{\partial^2}{\partial z^2}{}_1F_1 + (b-z)\frac{\partial}{\partial z}{}_1F_1 - a\,{}_1F_1 = 0, \tag{A.35}$$

the solution of Eq. (A.33), which is regular at $r = 0$, reads $T_{kL} = {}_1F_1(1+L+i\alpha;\, 2L+2;\, \rho)$. We finally obtain

$$L_{kL}(r) = N_{kL}(2ikr)^L e^{-ikr}\,{}_1F_1(1+L+i\alpha;\, 2L+2;\, 2ikr) \tag{A.36}$$

with a normalization constant N_{kL}. To normalize the continuum states, we put the exciton in an imaginary sphere of radius R and demand

$$\int_0^R \mathrm{d}r\, r^2 N_{kL}(2kr)^{2L}\left|{}_1F_1(1+L+i\alpha;\, 2L+2;\, 2ikr)\right|^2 = 1. \tag{A.37}$$

However, the integral does not converge if we let $R \to \infty$. Therefore, we may use

$$ {}_1F_1(a;\, b;\, z) \;=\; \frac{\Gamma(b)e^{i\pi a}z^{-a}}{\Gamma(b-a)}\left[1+\mathcal{O}\left(\frac{1}{|z|}\right)\right]+\frac{\Gamma(b)e^{z}z^{a-b}}{\Gamma(a)}\left[1+\mathcal{O}\left(\frac{1}{|z|}\right)\right] \qquad \text{(A.38)} $$

to obtain [139]

$$ \begin{aligned} F_{kLM}(\boldsymbol{r}) \;&=\; \frac{(2ikr)^L}{(2L+1)!}e^{\frac{\pi\alpha}{2}}\sqrt{\frac{2\pi k^2}{R\alpha\sinh(\pi\alpha)}}\prod_{j=0}^{L}\sqrt{j^2+\alpha^2} \\ &\quad \times e^{-ikr}{}_1F_1(1+L+i\alpha;\, 2L+2;\, 2ikr)Y_{LM}(\vartheta,\, \varphi). \end{aligned} \qquad \text{(A.39)} $$

The product could be replaced by a more simple expression [293]:

$$ \sqrt{\frac{\pi\alpha}{\sinh(\pi\alpha)}}\prod_{j=1}^{L}\sqrt{j^2+\alpha^2} = |\Gamma(L+1\pm i\alpha)|\,. \qquad \text{(A.40)} $$

Finally, we have to note that only specific k-values $k=\pi n/R$ with $n\in\mathbb{Z}$ are allowed, which results from the expression (A.38) if $F_{kLM}(\boldsymbol{r})|_{r=R}=0$ shall hold. This leads to the replacement

$$ \sum_k = \frac{R}{\pi}\sum_k \Delta k \to \frac{R}{\pi}\int \mathrm{d}k, \qquad \text{(A.41)} $$

whenever the sum over all continuum states appears. After the evaluation of the integral, one has to let $R\to\infty$.

A.4 Oscillator strengths using Wannier functions

Here we give some alternative expressions for the oscillator strength of excitons treated in Sec. 4.4 using Wannier functions or the transition density, which are also often found in the literature [7].

The matrix element of Eq. (4.34) can also be written as

$$ M = -\frac{e}{m_0}A_0(\boldsymbol{\kappa},\xi)\sqrt{N}\delta_{S,0}\left[\sum_{\boldsymbol{G}}\delta_{\boldsymbol{\kappa},\boldsymbol{K}+\boldsymbol{G}}\right]\hat{\boldsymbol{e}}_{\xi\boldsymbol{\kappa}}\cdot(e^{i\boldsymbol{\kappa}\cdot\boldsymbol{r}}\boldsymbol{p})_{\nu 0} \qquad \text{(A.42)} $$

with the state $\phi_{c\nu\boldsymbol{0}}(\boldsymbol{r})$ defined in Eq. (2.223) and the term

$$ (e^{i\boldsymbol{\kappa}\cdot\boldsymbol{r}}\boldsymbol{p})_{\nu 0} = \sqrt{2}\int \phi^*_{c\nu\boldsymbol{0}}(\boldsymbol{r})e^{i\boldsymbol{\kappa}\cdot\boldsymbol{r}}\boldsymbol{p}\,a_{v\boldsymbol{0}}(\boldsymbol{r})\,\mathrm{d}\boldsymbol{r}, \qquad \text{(A.43)} $$

which corresponds to the transition of an electron from the initial state $a_{c\boldsymbol{0}}(\boldsymbol{r})$ to the final state $\phi_{c\nu\boldsymbol{0}}(\boldsymbol{r})$. The factor[1] $\sqrt{2}$ results from the usage of a spin singlet wave function Φ_0. Since the absorption coefficient is proportional to $\left|(e^{i\boldsymbol{\kappa}\cdot\boldsymbol{r}}\boldsymbol{p})_{\nu 0}\right|^2$, the factor 2 will then denote the number of electrons which are available for a specific one-electron transition due to spin degeneracy. We can

---

[1] This factor is sometimes omitted in literature. In this case one obtains oscillator strengths and absorption coefficients per electron [7].

neglect Umklapp processes since $\boldsymbol{\kappa}$ and $\boldsymbol{K}$ are much smaller than the extension of the Brillouin zone [236]. Therefore, we set $\boldsymbol{G} = \boldsymbol{0}$ in Eq. (A.42).

To obtain the expression (A.42), we only have to replace the Bloch functions by the Wannier functions of Eq. (2.125):

$$\begin{aligned}
M &= -\frac{e}{m_0}\boldsymbol{A}_0(\boldsymbol{\kappa},\xi)\sum_{\boldsymbol{q}} f^*_{vc\nu}(\boldsymbol{q})\frac{1}{N}\sum_{\boldsymbol{R}\boldsymbol{R}'} e^{-i(\boldsymbol{q}+\alpha\boldsymbol{K})\cdot\boldsymbol{R}'} e^{i(\boldsymbol{q}-\gamma\boldsymbol{K})\cdot\boldsymbol{R}} \int \mathrm{d}\boldsymbol{r}\, a^*_{c\boldsymbol{R}'\tau}(\boldsymbol{r}) e^{i\boldsymbol{\kappa}\cdot\boldsymbol{r}}\boldsymbol{p}\, a_{v\boldsymbol{R}\sigma}(\boldsymbol{r}) \\
&= -\frac{e}{m_0}\boldsymbol{A}_0(\boldsymbol{\kappa},\xi)\sum_{\boldsymbol{R}\boldsymbol{\beta}}\left(\frac{1}{\sqrt{N}}\sum_{\boldsymbol{q}} f^*_{vc\nu}(\boldsymbol{q}) e^{-i\boldsymbol{q}\cdot\boldsymbol{\beta}}\right) e^{-i\alpha\boldsymbol{K}\cdot\boldsymbol{\beta}} \\
&\quad \times\frac{1}{\sqrt{N}} e^{-i\boldsymbol{K}\cdot\boldsymbol{R}} \int \mathrm{d}\boldsymbol{r}\, a^*_{c\boldsymbol{\beta}\tau}(\boldsymbol{r}-\boldsymbol{R}) e^{i\boldsymbol{\kappa}\cdot\boldsymbol{r}}\boldsymbol{p}\, a_{v\boldsymbol{0}\sigma}(\boldsymbol{r}-\boldsymbol{R}) \\
&= -\frac{e}{m_0}\boldsymbol{A}_0(\boldsymbol{\kappa},\xi)\delta_{\tau\sigma}\sum_{\boldsymbol{\beta}} U^*_{vc\nu\boldsymbol{K}}(\boldsymbol{\beta})\left[\frac{1}{\sqrt{N}}\sum_{\boldsymbol{R}} e^{i(\boldsymbol{\kappa}-\boldsymbol{K})\cdot\boldsymbol{R}}\right]\int \mathrm{d}\boldsymbol{r}\, a^*_{c\boldsymbol{\beta}}(\boldsymbol{r}) e^{i\boldsymbol{\kappa}\cdot\boldsymbol{r}}\boldsymbol{p}\, a_{v\boldsymbol{0}}(\boldsymbol{r}). \qquad \text{(A.44)}
\end{aligned}$$

Using $\boldsymbol{A}_0(\boldsymbol{\kappa},\xi) = A_0(\boldsymbol{\kappa},\xi)\hat{\boldsymbol{e}}_{\xi\boldsymbol{\kappa}}$ and the relation $\sum_{\boldsymbol{R}} e^{i(\boldsymbol{\kappa}-\boldsymbol{K})\cdot\boldsymbol{R}} = N\sum_{\boldsymbol{G}}\delta_{\boldsymbol{\kappa},\boldsymbol{K}+\boldsymbol{G}}$, we finally arrive at the expression (A.42). The absorption coefficient can now be written in analogy to[2] Eq. (2.186):

$$\begin{aligned}
\alpha(\omega) &= \frac{2\hbar}{\varepsilon_0 n c\,\omega A_0^2 V}\sum_{\nu\boldsymbol{K}} W_{\nu\boldsymbol{K},0} \\
&= \frac{4\pi e^2}{\varepsilon_0 n c\,\omega m_0^2}\frac{N}{V}\sum_{\nu\boldsymbol{K}}\left|\hat{\boldsymbol{e}}_{\xi\boldsymbol{\kappa}}\cdot(e^{i\boldsymbol{\kappa}\cdot\boldsymbol{r}}\boldsymbol{p})_{\nu 0}\right|^2 \delta_{S,0}\delta_{\boldsymbol{\kappa},\boldsymbol{K}}\,\delta(E^{(0)}_{\nu\boldsymbol{K}} - E^{(1)}_0 - \hbar\omega). \qquad \text{(A.45)}
\end{aligned}$$

We can immediatly see from the delta functions that spin, momentum and energy conservation hold. From Eq. (A.45) the relative oscillator strength is defined in Ref. [7] as the dimensionless quantity [cf. Eq. (2.189)]

$$f_{\nu 0} = 2\left|\hat{\boldsymbol{e}}_{\xi\boldsymbol{\kappa}}(e^{i\boldsymbol{\kappa}\cdot\boldsymbol{r}}\boldsymbol{p})_{\nu 0}\right|^2 / \, m_0(E^{(0)}_{\nu\boldsymbol{K}} - E^{(1)}_0). \qquad \text{(A.46)}$$

A.4.1 Formulation with transition density

The formulas for the oscillator strengths can be expressed using the transition density $\rho_{vc\nu\boldsymbol{K}}(\boldsymbol{r})$ defined in Eq. (5.5) of Sec. 5.1.1. With these expressions one can easily see the close connection between the exchange interaction and the oscillator strength or exciton-photon interaction.

Dipole transition Let us consider the original matrix element (4.28) for the case with $\boldsymbol{\kappa} = \boldsymbol{0}$:

$$M = -\frac{e}{m_0}A_0\delta_{\boldsymbol{K},\boldsymbol{0}}\,\hat{\boldsymbol{e}}_{\xi\boldsymbol{\kappa}}\cdot\langle\Psi^{\sigma\tau}_{vc\nu\boldsymbol{0}}|\sum_l \boldsymbol{p}_l\,|\Phi_0\rangle\,. \qquad \text{(A.47)}$$

Comparing Eq. (A.45) to Eqs. (2.180) and (2.181) it may seem reasonable to make an equivalent replacement:

$$\begin{aligned}
M &= -\frac{ie}{\hbar}A_0\delta_{\boldsymbol{K},\boldsymbol{0}}\,\hat{\boldsymbol{e}}_{\xi\boldsymbol{\kappa}}\cdot\langle\Psi^{\sigma\tau}_{vc\nu\boldsymbol{0}}|\sum_l [H_0,\,\boldsymbol{r}_l]\,|\Phi_0\rangle \qquad \text{(A.48a)} \\
&\approx -\frac{ie}{\hbar}A_0(E^{(0)}_{\nu\boldsymbol{0}} - E^{(1)}_0)\delta_{\boldsymbol{K},\boldsymbol{0}}\,\hat{\boldsymbol{e}}_{\xi\boldsymbol{\kappa}}\cdot\langle\Psi^{\sigma\tau}_{vc\nu\boldsymbol{0}}|\sum_l \boldsymbol{r}_l\,|\Phi_0\rangle\,. \qquad \text{(A.48b)}
\end{aligned}$$

---

[2] In contrast to Ref. [7] we define the absorption coefficient with the sums over ν and $\boldsymbol{K}$ according to Refs. [73, 94].

However, since Φ_0 and $\Psi_{\nu\boldsymbol{K}}$ are not eigenstates[3] of the Hamiltonian (2.103), this replacement is only an approximation. In analogy to Eq. (A.44) we can write

$$M = -\frac{ie}{\hbar} A_0 (E^{(0)}_{\nu\boldsymbol{0}} - E^{(1)}_0) \delta_{\boldsymbol{K},\boldsymbol{0}} \delta_{\tau\sigma}\, \hat{\boldsymbol{e}}_{\xi\boldsymbol{\kappa}} \cdot \sum_{\boldsymbol{\beta}} U^*_{vc\nu\boldsymbol{0}}(\boldsymbol{\beta}) \frac{1}{\sqrt{N}} \sum_{\boldsymbol{R}} \int \mathrm{d}\boldsymbol{r}\; a^*_{c\boldsymbol{\beta}}(\boldsymbol{r})(\boldsymbol{r}+\boldsymbol{R}) a_{v\boldsymbol{0}}(\boldsymbol{r}). \quad \text{(A.49)}$$

The integral $\int \mathrm{d}\boldsymbol{r}\, a^*_{c\boldsymbol{\beta}}(\boldsymbol{r}) a_{v\boldsymbol{0}}(\boldsymbol{r})$ vanishes [308] and we finally have

$$\begin{aligned} M &= -\frac{i}{\hbar} A_0 \sqrt{N} (E^{(0)}_{\nu\boldsymbol{0}} - E^{(1)}_0) \delta_{\boldsymbol{K},\boldsymbol{0}} \delta_{\tau\sigma}\, \hat{\boldsymbol{e}}_{\xi\boldsymbol{\kappa}} \cdot \int \mathrm{d}\boldsymbol{r}\; \boldsymbol{r} \rho^*_{vc\nu\boldsymbol{0}}(\boldsymbol{r}) \\ &= -\frac{i}{\hbar} A_0 \sqrt{N} (E^{(0)}_{\nu\boldsymbol{0}} - E^{(1)}_0) \delta_{\boldsymbol{K},\boldsymbol{0}} \delta_{\tau\sigma}\, (\hat{\boldsymbol{e}}_{\xi\boldsymbol{\kappa}} \cdot \boldsymbol{\mu}^*_{vc\nu\boldsymbol{0}}) \end{aligned} \quad \text{(A.50)}$$

with the localized charge density or transition density $\rho_{vc\nu\boldsymbol{K}}(\boldsymbol{r})$ of Eq. (5.5) [7, 303, 308] and the dipole moment $\boldsymbol{\mu}_{vc\nu\boldsymbol{K}}$ of Eq. (5.9) [308]. Since the Wannier functions $a_{n\boldsymbol{R}}(\boldsymbol{r})$ are localized about $\boldsymbol{R}$, one can use a Taylor expansion of $\rho_{vc\nu\boldsymbol{K}}(\boldsymbol{r})$ in Eq. (A.50) to obtain again the matrix element in the form of Eq. (4.40).

Quadrupole transition The matrix element for the quadrupole transition is obtained when using the first order term $i\boldsymbol{\kappa r}$ of the Taylor expansion of $e^{i\boldsymbol{\kappa r}}$ in Eq. (4.28). The operator in

$$M = -\frac{e}{m_0} \delta_{\boldsymbol{K},\boldsymbol{\kappa}} \langle \Psi^{\sigma\tau}_{vc\nu\boldsymbol{K}} | \sum_l (i\boldsymbol{\kappa}\cdot\boldsymbol{r}_l)(\boldsymbol{A}_0\cdot\boldsymbol{p}_l) | \Phi_0 \rangle \quad \text{(A.51)}$$

can be rewritten in the form

$$\begin{aligned} (i\boldsymbol{\kappa}\cdot\boldsymbol{r})(\boldsymbol{A}_0\cdot\boldsymbol{p}) &= \frac{1}{2}\left[(i\boldsymbol{\kappa}\cdot\boldsymbol{r})(\boldsymbol{A}_0\cdot\boldsymbol{p}) + (i\boldsymbol{q}\cdot\boldsymbol{p})(\boldsymbol{A}_0\cdot\boldsymbol{r})\right] + \frac{1}{2}\left[(i\boldsymbol{\kappa}\cdot\boldsymbol{r})(\boldsymbol{A}_0\cdot\boldsymbol{p}) - (i\boldsymbol{q}\cdot\boldsymbol{p})(\boldsymbol{A}_0\cdot\boldsymbol{r})\right] \\ &= \frac{1}{2}\left[i\boldsymbol{\kappa}(\boldsymbol{r}\otimes\boldsymbol{p} + \boldsymbol{p}\otimes\boldsymbol{r})\boldsymbol{A}_0\right] + \frac{1}{2}\left[(i\boldsymbol{\kappa}\times\boldsymbol{A}_0)\cdot(\boldsymbol{r}\times\boldsymbol{p})\right]. \end{aligned} \quad \text{(A.52)}$$

with the dyadic product $\otimes$. The operator $(\boldsymbol{r}\otimes\boldsymbol{p} + \boldsymbol{p}\otimes\boldsymbol{r})$ is a symmetric tensor and describes the electric quadrupole transition. The operator $(i\boldsymbol{\kappa}\times\boldsymbol{A}_0)\cdot(\boldsymbol{r}\times\boldsymbol{p}) = (\nabla\times\boldsymbol{A})\cdot\boldsymbol{L} = \boldsymbol{B}\cdot\boldsymbol{L}$ describes the magnetic dipole transition. The first operator can be expressed in analogy to Eq. (2.181) as

$$(\boldsymbol{r}\otimes\boldsymbol{p} + \boldsymbol{p}\otimes\boldsymbol{r}) = \frac{im_0}{\hbar}\left[H_0,\, \boldsymbol{r}\otimes\boldsymbol{r}\right]. \quad \text{(A.53)}$$

The matrix element for the electric quadrupole transition then reads

$$M = -\frac{i}{\hbar} A_0 \sqrt{N} (E^{(0)}_{\nu\boldsymbol{K}} - E^{(1)}_0) \delta_{\boldsymbol{K},\boldsymbol{\kappa}} \delta_{\tau\sigma}\, \hat{\boldsymbol{e}}_{\xi\boldsymbol{\kappa}} \cdot \int \mathrm{d}\boldsymbol{r}\; (i\boldsymbol{\kappa}\cdot\boldsymbol{r})\boldsymbol{r} \rho^*_{vc\nu\boldsymbol{K}}(\boldsymbol{r}). \quad \text{(A.54)}$$

If we use the zero order of the Talor expansion of $\rho^*_{vc\nu\boldsymbol{K}}(\boldsymbol{r})$ at $\boldsymbol{\beta} = \boldsymbol{0}$, we obtain the expression for the electric quadrupole transition of S excitons:

$$M = -\frac{ie}{\hbar} A_0 \sqrt{N} (E^{(0)}_{\nu\boldsymbol{K}} - E^{(1)}_0) \delta_{\boldsymbol{K},\boldsymbol{\kappa}} \delta_{\tau\sigma} F^*_{vc,\,\nu}(\boldsymbol{0})\, \hat{\boldsymbol{e}}_{\xi\boldsymbol{\kappa}} \cdot \int \mathrm{d}\boldsymbol{r}\; a^*_{v\boldsymbol{0}}(\boldsymbol{r})(i\boldsymbol{\kappa}\cdot\boldsymbol{r})\boldsymbol{r} a_{c\boldsymbol{0}}(\boldsymbol{r}). \quad \text{(A.55)}$$

---

[3] Compare Secs. 2.3.8 and 2.5.2.

B

Exciton Hartree units

When performing numerical calculations for the hydrogen atom in external fields, often Hartree units are used [35, 445]. These units are obtained by setting the fundamental physical constants e, m_0, $\hbar$ as well as the Bohr radius a_0 to one. As the effective masses of the electron and hole differ from the free electron mass and since the Coulomb interaction is scaled by the dielectric constant ε, we introduce exciton Hartree units. Within these units the hydrogen-like part of the Hamiltonian (8.4) is exactly of the same form as the Hamiltonian of the hydrogen atom in Hartree units [35] and the values of the scaled energies in Sec. 8.1.2 can be compared directly with the values of the scaled energies used in calculations for the hydrogen atom [385]. The exciton Hartree units are obtained by setting $e = \hbar = 1$, $m_0 = \gamma_1'$ and $a_{\mathrm{exc}} = \gamma_1' \varepsilon a_0 = 1$. Since all other physical quantities have to be converted to exciton Hartree units as well, we give the according scaling factors in Table B.1. Variables given in exciton Hartree units are marked by a tilde sign, e.g., $r \to \tilde{r}$.

Table B.1.: Exciton Hartree units converted to SI-units for $\gamma_1' = 2$ and $\varepsilon = 7.5$. For a comparison, we also give the values for normal Hartree units, which are obtained by setting $\gamma_1' = \varepsilon = 1$.

quantity	symbol	exc. Hartree unit	SI ($\gamma_1' = 2$, $\varepsilon = 7.5$)	SI ($\gamma_1' = 1$, $\varepsilon = 1$)
charge	q	e	1.6022×10^{-19} C	1.6022×10^{-19} C
action	S	$\hbar$	1.0546×10^{-34} Js	1.0546×10^{-34} Js
mass	m	m_0/γ_1'	4.5547×10^{-31} kg	9.1094×10^{-31} kg
length	r	$\gamma_1' \varepsilon a_0$	7.9377×10^{-10} m	5.2918×10^{-11} m
momentum	p	$\hbar/\gamma_1' \varepsilon a_0$	1.3286×10^{-25} kgm/s	1.9929×10^{-24} kgm/s
time	t	$\gamma_1' \varepsilon^2 a_0^2 m_0/\hbar$	2.7213×10^{-15} s	2.4189×10^{-17} s
energy	E	$\hbar^2/\gamma_1' \varepsilon^2 a_0^2 m_0$	3.8753×10^{-20} J	4.3597×10^{-18} J
magn. flux dens.	B	$\hbar/\gamma_1'^2 \varepsilon^2 a_0^2 e$	$1.0447 \times 10^{+3}$ T	$2.3505 \times 10^{+5}$ T
el. field strength	F	$\hbar^2/\gamma_1'^2 \varepsilon^3 a_0^3 m_0 e$	$3.0472 \times 10^{+8}$ V/m	$5.1422 \times 10^{+11}$ V/m

C Formulas connected with the VB structure

Here we list several formulas, which are connected with the cubic valence band structure of Cu$_2$O and which are needed in the evaluation of Chapter 4 and Chapter 6.

C.1 The matrices of the quasi-spin $\boldsymbol{I} = 1$

In Sec. 4.5.2 we introduced the matrices

$$\boldsymbol{I}_{ij} = 3\left\{\boldsymbol{I}_i,\, \boldsymbol{I}_j\right\} - 2\hbar^2\delta_{ij}\boldsymbol{1}. \tag{C.1}$$

We will shortly list the main properties of these matrices. The second-rank tensor with the components $\boldsymbol{I}_{ij}$ is symmetric, $\boldsymbol{I}_{ij} = \boldsymbol{I}_{ji}$, and traceless, $\sum_{i=1}^{3}\boldsymbol{I}_{ii} = \boldsymbol{0}$. As already stated in Sec. 4.5.2 the operators $\boldsymbol{I}_{ij}$ form a closed subset with respect to the symmetric product $\{a, b\} = \frac{1}{2}(ab + ba)$:

$$\begin{aligned}
&\left\{\boldsymbol{I}_{jj},\, \boldsymbol{I}_{jj}\right\} = \hbar^2\left(2\hbar^2\boldsymbol{1} - \boldsymbol{I}_{jj}\right), && \left\{\boldsymbol{I}_{jj},\, \boldsymbol{I}_{jk}\right\} = -\frac{\hbar^2}{2}\boldsymbol{I}_{jk},\\
&\left\{\boldsymbol{I}_{jk},\, \boldsymbol{I}_{jk}\right\} = -\frac{3\hbar^2}{4}\left(-2\hbar^2\boldsymbol{1} + \boldsymbol{I}_{jj} + \boldsymbol{I}_{kk}\right), && \left\{\boldsymbol{I}_{jk},\, \boldsymbol{I}_{kl}\right\} = -\frac{3\hbar^2}{4}\boldsymbol{I}_{jl},\\
&\left\{\boldsymbol{I}_{jj},\, \boldsymbol{I}_{kk}\right\} = \hbar^2\left(-\hbar^2\boldsymbol{1} + \boldsymbol{I}_{jj} + \boldsymbol{I}_{kk}\right), && \left\{\boldsymbol{I}_{jj},\, \boldsymbol{I}_{kl}\right\} = \hbar^2\boldsymbol{I}_{kl},
\end{aligned} \tag{C.2}$$

where $j \neq l \neq k \neq j$. The matrices can also be expressed in terms of irreducible tensors [79]:

$$\begin{aligned}
&\boldsymbol{I}_{11} = +\frac{1}{2}\left[I_2^{(2)} + I_{-2}^{(2)} - \sqrt{\frac{2}{3}}I_0^{(2)}\right], && \boldsymbol{I}_{12} = -\frac{i}{2}\left[I_2^{(2)} - I_{-2}^{(2)}\right],\\
&\boldsymbol{I}_{22} = -\frac{1}{2}\left[I_2^{(2)} + I_{-2}^{(2)} + \sqrt{\frac{2}{3}}I_0^{(2)}\right], && \boldsymbol{I}_{23} = \frac{i}{2}\left[I_1^{(2)} + I_{-1}^{(2)}\right],
\end{aligned} \tag{C.3}$$

$$\boldsymbol{I}_{33} = \sqrt{\frac{2}{3}} I_0^{(2)}, \qquad \boldsymbol{I}_{31} = -\frac{1}{2}\left[I_1^{(2)} - I_{-1}^{(2)}\right].$$

Furthermore, we list the results for the coefficients C_i and the dependency of the parameters Ω_i of Sec. 4.5.2 on the Luttinger parameters. The coefficients read

$$\begin{aligned}
C_1 &= \Xi\left(2\gamma_1'^2 + 4\gamma_2^2 - 3\gamma_3^2 + 6\gamma_1'\gamma_2 + 6\gamma_2\gamma_3 + 3\gamma_1'\gamma_3\right), \\
C_2 &= 6\Xi\left(2\gamma_2^2 - 3\gamma_3^2 + 2\gamma_1'\gamma_2 + 3\gamma_2\gamma_3\right), \\
C_5 &= 12\Xi\left(\gamma_2\gamma_3 + \gamma_1'\gamma_3\right), \\
C_3 &= C_4 = C_6 = 0,
\end{aligned} \tag{C.4}$$

with

$$\Xi = \frac{m_0}{\hbar m_\mathrm{e}}\left[\left(\gamma_1' - 2\gamma_2\right)\left(\gamma_1' + 4\gamma_2\right)\left(2\gamma_1' + 2\gamma_2 + 3\gamma_3\right) - 27\gamma_1'\gamma_3^2\right]^{-1}. \tag{C.5}$$

The parameters Ω_i are given by

$$\begin{aligned}
\frac{\Omega_1}{k_0^2} &= \frac{\hbar^2}{2m_\mathrm{e}} - \frac{\hbar^3}{m_\mathrm{e}}C_1 + \frac{\hbar^4\gamma_1'}{18m_0}\left(9C_1^2 + 2C_2^2 + 3C_5^2\right) \\
&\quad - \frac{\hbar^4\gamma_2}{18m_0}\left(24C_1C_2 - 4C_2^2 - 3C_5^2\right) - \frac{\hbar^4\gamma_3}{12m_0}C_5\left(24C_1 - 4C_2 - 3C_5\right),
\end{aligned} \tag{C.6a}$$

$$\begin{aligned}
\frac{\Omega_3}{k_0^2} &= \frac{\hbar^3}{3m_\mathrm{e}}C_2 - \frac{\hbar^4\gamma_1'}{72m_0}\left(24C_1C_2 - 4C_2^2 - 3C_5^2\right) \\
&\quad + \frac{\hbar^4\gamma_2}{3m_0}\left(3C_1^2 - 2C_1C_2 + C_2^2 - C_5^2\right) - \frac{\hbar^4\gamma_3}{24m_0}C_5\left(12C_1 - 2C_2 + 3C_5\right),
\end{aligned} \tag{C.6b}$$

$$\begin{aligned}
\frac{\Omega_5}{k_0^2} &= \frac{\hbar^3}{m_\mathrm{e}}C_5 - \frac{\hbar^4\gamma_1'}{24m_0}C_5\left(24C_1 - 4C_2 - 3C_5\right) - \frac{\hbar^4\gamma_2}{12m_0}\left(12C_1C_5 - 2C_2C_5 + 3C_5^2\right) \\
&\quad + \frac{\hbar^4\gamma_3}{24m_0}\left(72C_1^2 - 24C_1C_2 - 36C_1C_5 - 16C_2^2 - 12C_2C_5 + 27C_5^2\right).
\end{aligned} \tag{C.6c}$$

C.2 $\boldsymbol{p}^4$-Terms

As has already been stated in Sec. 6.1.1, the terms of the fourth power of $\boldsymbol{p}$ span a fifteen dimensional space with the basis functions

$$p_i^4, \quad p_i^3 p_j, \quad p_i^2 p_j^2, \quad p_i p_j p_k^2, \tag{C.7}$$

with $i, j, k \in \{1, 2, 3\}$ and $i \neq j \neq k \neq i$. The six linear combinations of p^4 terms (including the quasi-spin I), which transform according to Γ_1^+ [90] read in terms of irreducible tensors

$$\begin{aligned} &(\mathrm{I}): \quad p^4, && (\mathrm{IV}): \quad p^2 \left[P^{(2)} \times I^{(2)}\right]^{(4)} \left(\Gamma_1^+\right), \\ &(\mathrm{II}): \quad P^{(4)} \left(\Gamma_1^+\right), && (\mathrm{V}): \quad \left[P^{(4)} \times I^{(2)}\right]^{(4)} \left(\Gamma_1^+\right), \\ &(\mathrm{III}): \quad p^2 \left(P^{(2)} \cdot I^{(2)}\right), && (\mathrm{VI}): \quad \left[P^{(4)} \times I^{(2)}\right]^{(6)} \left(\Gamma_1^+\right), \end{aligned} \tag{C.8}$$

with

$$T^{(4)} \left(\Gamma_1^+\right) = \sqrt{\frac{5}{24}} \sum_{k=\pm 4} T_k^{(4)} + \sqrt{\frac{7}{12}} T_0^{(4)}, \tag{C.9a}$$

and

$$T^{(6)} \left(\Gamma_1^+\right) = -\frac{\sqrt{7}}{4} \sum_{k=\pm 4} T_k^{(6)} + \frac{1}{\sqrt{8}} T_0^{(6)}. \tag{C.9b}$$

One can choose appropriate linear combinations of the states (I)-(VI):

$$\frac{1}{5}(\mathrm{I}) - \frac{1}{3\sqrt{30}}(\mathrm{II}) = \left[p_1^2 p_2^2 + \text{c.p.}\right], \tag{C.10a}$$

$$\frac{2}{3}\hbar^2(\mathrm{I}) + \frac{2}{45}(\mathrm{III}) + \frac{1}{18}\sqrt{\frac{24}{5}}(\mathrm{IV}) = \boldsymbol{p}^2 \left[p_1^2 \boldsymbol{I}_1^2 + \text{c.p.}\right], \tag{C.10b}$$

$$\frac{1}{30}(\mathrm{III}) - \frac{1}{36}\sqrt{\frac{24}{5}}(\mathrm{IV}) = \boldsymbol{p}^2 \left[p_1 p_2 \left\{\boldsymbol{I}_1,\, \boldsymbol{I}_2\right\} + \text{c.p.}\right], \tag{C.10c}$$

$$\frac{6}{5}\hbar^2(\mathrm{I}) - \frac{8}{9\sqrt{30}}\hbar^2(\mathrm{II}) - \frac{4}{27}\sqrt{\frac{7}{11}}(\mathrm{V}) + \frac{1}{9}\sqrt{\frac{14}{33}}(\mathrm{VI}) = \left[\left(p_1^4 + 6 p_2^2 p_3^2\right) \boldsymbol{I}_1^2 + \text{c.p.}\right], \tag{C.10d}$$

$$-\frac{1}{18}\sqrt{\frac{7}{11}}(\mathrm{V}) - \frac{1}{9}\sqrt{\frac{14}{33}}(\mathrm{IV}) = \left[\left(p_1^2 + p_2^2 - 6 p_3^2\right) p_1 p_2 \left\{\boldsymbol{I}_1,\, \boldsymbol{I}_2\right\} + \text{c.p.}\right], \tag{C.10e}$$

with $\{a, b\} = \frac{1}{2}(ab + ba)$ and c.p. denoting cyclic permutation. These linear combinations enter the generalized expressions of the kinetic energy of the hole and the electron in Sec. 6.1.1.

D

Hamiltonians

Here we give the expressions for the Hamiltonian of the exciton in external magnetic fields $\boldsymbol{B}$ or with a finite momentum of the center of mass $\hbar\boldsymbol{K}$.

D.1

In external magnetic fields

Here we give the Hamiltonian of Eq. (7.25) and describe the rotation necessary to make the quantization axis coincide with the direction of the magnetic field. Let us write the Hamiltonian (7.25) in the form

$$H = E_{\mathrm{g}} - \frac{e^2}{4\pi\varepsilon_0\varepsilon}\frac{1}{r} + \frac{2}{3}\Delta\left(1 + \frac{1}{\hbar^2}\boldsymbol{I}\cdot\boldsymbol{S}_{\mathrm{h}}\right) + H_0 + (eB)H_1 + (eB)^2H_2 - e\boldsymbol{F}\cdot\boldsymbol{r} \tag{D.1}$$

with $B = |\boldsymbol{B}|$. Using $\hat{B}_i = B_i/B$ with the components B_i of $\boldsymbol{B}$, the terms H_0, H_1, and H_2 are given by

$$\begin{aligned} H_0 = {} & \frac{1}{2m_0}\left(\gamma_1' + 4\gamma_2\right)\boldsymbol{p}^2 + \frac{1}{\hbar^2 m_0}\left(\eta_1 + 2\eta_2\right)\left(\boldsymbol{I}\cdot\boldsymbol{S}_{\mathrm{h}}\right)\boldsymbol{p}^2 \\ & - \frac{3\gamma_2}{\hbar^2 m_0}\left[\boldsymbol{I}_1^2 p_1^2 + \mathrm{c.p.}\right] - \frac{6\eta_2}{\hbar^2 m_0}\left[\boldsymbol{I}_1\boldsymbol{S}_{\mathrm{h}1}p_1^2 + \mathrm{c.p.}\right] \\ & - \frac{6\gamma_3}{\hbar^2 m_0}\left[\left\{\boldsymbol{I}_1,\, \boldsymbol{I}_2\right\}p_1p_2 + \mathrm{c.p.}\right] - \frac{6\eta_3}{\hbar^2 m_0}\left[\left(\boldsymbol{I}_1\boldsymbol{S}_{\mathrm{h}2} + \boldsymbol{I}_2\boldsymbol{S}_{\mathrm{h}1}\right)p_1p_2 + \mathrm{c.p.}\right], \end{aligned} \tag{D.2a}$$

$$\begin{aligned} H_1 = {} & \frac{1}{2m_0}\left(\frac{2m_0}{m_{\mathrm{e}}} - \gamma_1' + 4\gamma_2\right)\hat{\boldsymbol{B}}\cdot\boldsymbol{L} - \frac{1}{\hbar^2 m_0}\left(\eta_1 + 2\eta_2\right)\left(\boldsymbol{I}\cdot\boldsymbol{S}_{\mathrm{h}}\right)\hat{\boldsymbol{B}}\cdot\boldsymbol{L} \\ & + \frac{1}{2m_0}\left[g_c\boldsymbol{S}_{\mathrm{e}} + \left(3\kappa + \frac{g_s}{2}\right)\boldsymbol{I} - g_s\boldsymbol{S}_{\mathrm{h}}\right]\cdot\hat{\boldsymbol{B}} \end{aligned}$$

$$+\frac{3\gamma_2}{\hbar^2 m_0}\left[\boldsymbol{I}_1^2\left(\hat{B}_2 r_3 p_1-\hat{B}_3 r_2 p_1\right)+\text{c.p.}\right]+\frac{6\eta_2}{\hbar^2 m_0}\left[\boldsymbol{I}_1\boldsymbol{S}_{\text{h}1}\left(\hat{B}_2 r_3 p_1-\hat{B}_3 r_2 p_1\right)+\text{c.p.}\right]$$

$$+\frac{3\gamma_3}{\hbar^2 m_0}\left[\{\boldsymbol{I}_1,\,\boldsymbol{I}_2\}\left(\hat{B}_2 r_3 p_2-\hat{B}_1 r_3 p_1+\hat{B}_3 r_1 p_1-\hat{B}_3 r_2 p_2\right)+\text{c.p.}\right]$$

$$+\frac{3\eta_3}{\hbar^2 m_0}\left[\left(\boldsymbol{I}_1\boldsymbol{S}_{\text{h}2}+\boldsymbol{I}_2\boldsymbol{S}_{\text{h}1}\right)\left(\hat{B}_2 r_3 p_2-\hat{B}_1 r_3 p_1+\hat{B}_3 r_1 p_1-\hat{B}_3 r_2 p_2\right)+\text{c.p.}\right], \tag{D.2b}$$

$$H_2=\frac{1}{8m_0}\left(\gamma_1'+4\gamma_2\right)\left[\hat{\boldsymbol{B}}^2\boldsymbol{r}^2-\left(\hat{\boldsymbol{B}}\cdot\boldsymbol{r}\right)^2\right]+\frac{1}{4\hbar^2 m_0}\left(\eta_1+2\eta_2\right)\left(\boldsymbol{I}\cdot\boldsymbol{S}_{\text{h}}\right)\left[\hat{\boldsymbol{B}}^2\boldsymbol{r}^2-\left(\hat{\boldsymbol{B}}\cdot\boldsymbol{r}\right)^2\right]$$

$$-\frac{3\gamma_2}{4\hbar^2 m_0}\left[\boldsymbol{I}_1^2\left(\hat{B}_2 r_3-\hat{B}_3 r_2\right)^2+\text{c.p.}\right]-\frac{3\eta_2}{2\hbar^2 m_0}\left[\boldsymbol{I}_1\boldsymbol{S}_{\text{h}1}\left(\hat{B}_2 r_3-\hat{B}_3 r_2\right)^2+\text{c.p.}\right]$$

$$-\frac{3\gamma_3}{2\hbar^2 m_0}\left[\{\boldsymbol{I}_1,\,\boldsymbol{I}_2\}\left(\hat{B}_2 r_3-\hat{B}_3 r_2\right)\left(\hat{B}_3 r_1-\hat{B}_1 r_3\right)+\text{c.p.}\right]$$

$$-\frac{3\eta_3}{2\hbar^2 m_0}\left[\left(\boldsymbol{I}_1\boldsymbol{S}_{\text{h}2}+\boldsymbol{I}_2\boldsymbol{S}_{\text{h}1}\right)\left(\hat{B}_2 r_3-\hat{B}_3 r_2\right)\left(\hat{B}_3 r_1-\hat{B}_1 r_3\right)+\text{c.p.}\right]. \tag{D.2c}$$

In the calculations of Chapter 8 we express the magnetic field in spherical coordinates. For the different orientations of the magnetic field we rotate the coordinate system by

$$\boldsymbol{R}=\begin{pmatrix}\cos\varphi\cos\vartheta & \sin\varphi\cos\vartheta & -\sin\vartheta\\ -\sin\varphi & \cos\varphi & 0\\ \cos\varphi\sin\vartheta & \sin\varphi\sin\vartheta & \cos\vartheta\end{pmatrix}, \tag{D.3}$$

i.e., we replace $\boldsymbol{x}\to\boldsymbol{x}'=\boldsymbol{R}^{\mathrm{T}}\boldsymbol{x}$ with $\boldsymbol{x}\in\{\boldsymbol{r},\,\boldsymbol{p},\,\boldsymbol{L},\,\boldsymbol{I},\,\boldsymbol{S}\}$ to make the quantization axis coincide with the direction of the magnetic field [248, 281]. Finally we express the Hamiltonian in terms of irreducible tensors.

In Chapter 7 we treat the cases that the magnetic field is oriented along the [001], [110] or [111] direction [79, 248, 281]. For these cases we now give the Hamiltonian in terms of irreducible tensors. Here we rotated the coordinate system by the Euler angles $(\alpha,\,\beta,\,\gamma)=(\pi,\,\pi/2,\,\pi/4)$ for $\boldsymbol{B}\parallel[110]$ and by $(\alpha,\,\beta,\,\gamma)=\big(0,\,\arccos(1/\sqrt{3}),\,\pi/4\big)$ for $\boldsymbol{B}\parallel[111]$.

The first-order and second-order tensor operators used in the following correspond, as in Ref. [281], to the vector operators $\boldsymbol{r}$, $\boldsymbol{L}=\boldsymbol{r}\times\boldsymbol{p}$, $\boldsymbol{I}$, $\boldsymbol{S}_{\text{e/h}}$ and to the second-rank Cartesian operators

$$I_{mn} = 3\{I_m,\,I_n\}-\delta_{mn}I^2, \tag{D.4a}$$

$$P_{mn} = 3\{p_m,\,p_n\}-\delta_{mn}p^2, \tag{D.4b}$$

$$-iM_{mn} = 3\{r_m,\,p_n\}-\delta_{mn}\boldsymbol{r}\boldsymbol{p}, \tag{D.4c}$$

$$X_{mn} = 3\{r_m,\,r_n\}-\delta_{mn}r^2, \tag{D.4d}$$

respectively. The operator $D_k^{(2)}$ and the coefficients γ_1', μ', δ' ν, and τ are given by Eqs. (4.12) and (4.13), respectively.

D.1.1 Magnetic field in [001] direction

$$H_0 = \frac{\gamma_1'}{2\hbar^2 m_0} \left\{ \hbar^2 p^2 - \frac{\mu'}{3} \left(P^{(2)} \cdot I^{(2)} \right) + \frac{\delta'}{3} \left(\sum_{k=\pm 4} \left[P^{(2)} \times I^{(2)} \right]^{(4)}_{k} + \frac{\sqrt{70}}{5} \left[P^{(2)} \times I^{(2)} \right]^{(4)}_{0} \right) \right\}$$

$$+ \frac{3\eta_1}{\hbar^2 m_0} \left\{ \frac{1}{3} p^2 \left(I^{(1)} \cdot S^{(1)}_{\mathrm{h}} \right) - \frac{\nu}{3} \left(P^{(2)} \cdot D^{(2)} \right) \right.$$

$$\left. + \frac{\tau}{3} \left(\sum_{k=\pm 4} \left[P^{(2)} \times D^{(2)} \right]^{(4)}_{k} + \frac{\sqrt{70}}{5} \left[P^{(2)} \times D^{(2)} \right]^{(4)}_{0} \right) \right\}, \tag{D.5a}$$

$$H_1 = \frac{1}{m_{\mathrm{e}}} L^{(1)}_0 + \frac{\mu_{\mathrm{B}}}{e\hbar} \left(g_c S^{(1)}_{\mathrm{e}\,0} - g_s S^{(1)}_{\mathrm{h}\,0} + \left(3\kappa + \frac{1}{2} g_s \right) I^{(1)}_0 \right)$$

$$+ \frac{\gamma_1'}{2\hbar^2 m_0} \left\{ -\hbar^2 L^{(1)}_0 + \frac{\delta'}{3} \left(\left[M^{(2)} \times I^{(2)} \right]^{(4)}_{-4} - \left[M^{(2)} \times I^{(2)} \right]^{(4)}_{4} \right) \right.$$

$$+ \sqrt{\frac{2}{5}} \delta' \left(\left[L^{(1)} \times I^{(2)} \right]^{(3)}_{0} - \frac{1}{3} \left[M^{(2)} \times I^{(2)} \right]^{(3)}_{0} \right)$$

$$\left. + \sqrt{\frac{5}{12}} \mu' \left(\left[L^{(1)} \times I^{(2)} \right]^{(1)}_{0} + \sqrt{\frac{2}{3}} \left[M^{(2)} \times I^{(2)} \right]^{(1)}_{0} \right) \right\}$$

$$+ \frac{3\eta_1}{\hbar^2 m_0} \left\{ -\frac{1}{3} L^{(1)}_0 \left(I^{(1)} \cdot S^{(1)}_{\mathrm{h}} \right) + \frac{\tau}{3} \left(\left[M^{(2)} \times D^{(2)} \right]^{(4)}_{-4} - \left[M^{(2)} \times D^{(2)} \right]^{(4)}_{4} \right) \right.$$

$$+ \sqrt{\frac{2}{5}} \tau \left(\left[L^{(1)} \times D^{(2)} \right]^{(3)}_{0} - \frac{1}{3} \left[M^{(2)} \times D^{(2)} \right]^{(3)}_{0} \right)$$

$$\left. + \sqrt{\frac{5}{12}} \nu \left(\left[L^{(1)} \times D^{(2)} \right]^{(1)}_{0} + \sqrt{\frac{2}{3}} \left[M^{(2)} \times D^{(2)} \right]^{(1)}_{0} \right) \right\}, \tag{D.5b}$$

$$H_2 = \frac{\gamma_1'}{24\hbar^2 m_0} \left\{ \hbar^2 \left(2r^2 - \sqrt{\frac{2}{3}} X^{(2)}_0 \right) + \sqrt{\frac{2}{3}} \left(\mu' - \frac{6}{5} \delta' \right) r^2 I^{(2)}_0 \right.$$

$$- \delta' \left(\sum_{k=\pm 4} \left[X^{(2)} \times I^{(2)} \right]^{(4)}_{k} - \frac{2}{\sqrt{70}} \left[X^{(2)} \times I^{(2)} \right]^{(4)}_{0} \right)$$

$$+\frac{\sqrt{14}}{3}\left(\mu'-\frac{12}{35}\delta'\right)\left[X^{(2)}\times I^{(2)}\right]_0^{(2)}+\frac{\mu'}{3}\left(X^{(2)}\cdot I^{(2)}\right)\Bigg\}$$

$$+\frac{\eta_1}{4\hbar^2 m_0}\left\{\frac{1}{3}\left(2r^2-\sqrt{\frac{2}{3}}X_0^{(2)}\right)\left(I^{(1)}\cdot S_{\mathrm{h}}^{(1)}\right)+\sqrt{\frac{2}{3}}\left(\nu-\frac{6}{5}\tau\right)r^2 D_0^{(2)}\right.$$

$$-\tau\left(\sum_{k=\pm4}\left[X^{(2)}\times D^{(2)}\right]_k^{(4)}-\frac{2}{\sqrt{70}}\left[X^{(2)}\times D^{(2)}\right]_0^{(4)}\right)$$

$$\left.+\frac{\sqrt{14}}{3}\left(\nu-\frac{12}{35}\tau\right)\left[X^{(2)}\times D^{(2)}\right]_0^{(2)}+\frac{\nu}{3}\left(X^{(2)}\cdot D^{(2)}\right)\right\}. \tag{D.5c}$$

D.1.2 Magnetic field in [110] direction

$$H_0=\frac{\gamma_1^{'}}{2\hbar^2 m_0}\left\{\hbar^2 p^2-\frac{\mu^{'}}{3}\left(P^{(2)}\cdot I^{(2)}\right)+\frac{\delta^{'}}{4}\left(\sum_{k=\pm4}\left[P^{(2)}\times I^{(2)}\right]_k^{(4)}\right)\right.$$

$$\left.-\frac{\sqrt{7}}{6}\delta'\left(\sum_{k=\pm2}\left[P^{(2)}\times I^{(2)}\right]_2^{(4)}+\sqrt{\frac{1}{10}}\left[P^{(2)}\times I^{(2)}\right]_0^{(4)}\right)\right\}$$

$$+\frac{3\eta_1}{\hbar^2 m_0}\left\{\frac{1}{3}p^2\left(I^{(1)}\cdot S_{\mathrm{h}}^{(1)}\right)-\frac{\nu}{3}\left(P^{(2)}\cdot D^{(2)}\right)+\frac{\tau}{4}\left(\sum_{k=\pm4}\left[P^{(2)}\times D^{(2)}\right]_k^{(4)}\right)\right.$$

$$\left.-\frac{\sqrt{7}}{6}\tau\left(\sum_{k=\pm2}\left[P^{(2)}\times D^{(2)}\right]_k^{(4)}+\sqrt{\frac{1}{10}}\left[P^{(2)}\times D^{(2)}\right]_0^{(4)}\right)\right\}, \tag{D.6a}$$

$$H_1=\frac{1}{m_{\mathrm{e}}}L_0^{(1)}+\frac{\mu_{\mathrm{B}}}{e\hbar}\left(g_c S_{\mathrm{e}\,0}^{(1)}-g_s S_{\mathrm{h}\,0}^{(1)}+\left(3\kappa+\frac{1}{2}g_s\right)I_0^{(1)}\right)$$

$$+\frac{\gamma_1^{'}}{2\hbar^2 m_0}\left\{-\hbar^2 L_0^{(1)}-\frac{\delta^{'}}{16}\left(\sum_{k=\pm4}k\left[M^{(2)}\times I^{(2)}\right]_k^{(4)}\right)\right.$$

$$+\frac{\sqrt{7}}{24}\delta'\left(\sum_{k=\pm2}k\left[M^{(2)}\times I^{(2)}\right]_k^{(4)}\right)$$

$$
+\frac{1}{4\sqrt{3}}\delta'\left(\sum_{k=\pm 2}\left[M^{(2)}\times I^{(2)}\right]^{(3)}_{k}+\sqrt{\frac{2}{15}}\left[M^{(2)}\times I^{(2)}\right]^{(3)}_{0}\right)
$$

$$
-\frac{\sqrt{3}}{4}\delta'\left(\sum_{k=\pm 2}\left[L^{(1)}\times I^{(2)}\right]^{(3)}_{k}+\sqrt{\frac{2}{15}}\left[L^{(1)}\times I^{(2)}\right]^{(3)}_{0}\right)
$$

$$
+\frac{1}{2}\sqrt{\frac{5}{3}}\mu'\left(\left[L^{(1)}\times I^{(2)}\right]^{(1)}_{0}+\sqrt{\frac{2}{3}}\left[M^{(2)}\times I^{(2)}\right]^{(1)}_{0}\right)\Bigg\}
$$

$$
+\frac{3\eta_1}{\hbar^2 m_0}\Bigg\{-\frac{1}{3}L^{(1)}_{0}\left(I^{(1)}\cdot S^{(1)}_{\mathrm{h}}\right)-\frac{\tau}{16}\left(\sum_{k=\pm 4}k\left[M^{(2)}\times D^{(2)}\right]^{(4)}_{k}\right)
$$

$$
+\frac{\sqrt{7}}{24}\tau\left(\sum_{k=\pm 2}k\left[M^{(2)}\times D^{(2)}\right]^{(4)}_{k}\right)
$$

$$
+\frac{1}{4\sqrt{3}}\tau\left(\sum_{k=\pm 2}\left[M^{(2)}\times D^{(2)}\right]^{(3)}_{k}+\sqrt{\frac{2}{15}}\left[M^{(2)}\times D^{(2)}\right]^{(3)}_{0}\right)
$$

$$
-\frac{\sqrt{3}}{4}\tau\left(\sum_{k=\pm 2}\left[L^{(1)}\times D^{(2)}\right]^{(3)}_{k}+\sqrt{\frac{2}{15}}\left[L^{(1)}\times D^{(2)}\right]^{(3)}_{0}\right)
$$

$$
+\frac{1}{2}\sqrt{\frac{5}{3}}\nu\left(\left[L^{(1)}\times D^{(2)}\right]^{(1)}_{0}+\sqrt{\frac{2}{3}}\left[M^{(2)}\times D^{(2)}\right]^{(1)}_{0}\right)\Bigg\}, \tag{D.6b}
$$

$$
H_2=\frac{\gamma_1'}{24\hbar^2 m_0}\Bigg\{\hbar^2\left(2r^2-\sqrt{\frac{2}{3}}X^{(2)}_{0}\right)+\frac{\delta'}{\sqrt{21}}\left(\sum_{k=\pm 2}\left[X^{(2)}\times I^{(2)}\right]^{(2)}_{k}\right)
$$

$$
+\sqrt{\frac{2}{3}}\left(\mu'+\frac{3}{10}\delta'\right)r^2 I^{(2)}_{0}+\frac{\delta'}{2}r^2\left(I^{(2)}_{2}+I^{(2)}_{-2}\right)
$$

$$
-\frac{3}{4}\delta'\left(\sum_{k=\pm 4}\left[X^{(2)}\times I^{(2)}\right]^{(4)}_{k}+\frac{1}{3}\sqrt{\frac{2}{35}}\left[X^{(2)}\times I^{(2)}\right]^{(4)}_{0}\right)
$$

$$+\frac{\delta'}{2\sqrt{7}}\left(\sum_{k=\pm 2}\left[X^{(2)}\times I^{(2)}\right]^{(4)}_{k}\right)+\frac{\delta'}{2\sqrt{3}}\left(\sum_{k=\pm 2}k\left[X^{(2)}\times I^{(2)}\right]^{(3)}_{k}\right)$$

$$+\frac{2}{3}\sqrt{\frac{7}{2}}\left(\mu'+\frac{3}{35}\delta'\right)\left[X^{(2)}\times I^{(2)}\right]^{(2)}_{0}+\frac{\mu'}{3}\left(X^{(2)}\cdot I^{(2)}\right)\Bigg\}$$

$$+\frac{\eta_1}{4\hbar^2 m_0}\Bigg\{\frac{1}{3}\left(2r^2-\sqrt{\frac{2}{3}}X^{(2)}_0\right)\left(I^{(1)}\cdot S^{(1)}_{\mathrm{h}}\right)+\frac{\tau}{\sqrt{21}}\left(\sum_{k=\pm 2}\left[X^{(2)}\times D^{(2)}\right]^{(2)}_{k}\right)$$

$$+\sqrt{\frac{2}{3}}\left(\nu+\frac{3}{10}\tau\right)r^2 D^{(2)}_0+\frac{\tau}{2}r^2\left(D^{(2)}_2+D^{(2)}_{-2}\right)$$

$$-\frac{3}{4}\tau\left(\sum_{k=\pm 4}\left[X^{(2)}\times D^{(2)}\right]^{(4)}_{k}+\frac{1}{3}\sqrt{\frac{2}{35}}\left[X^{(2)}\times D^{(2)}\right]^{(4)}_{0}\right)$$

$$+\frac{\tau}{2\sqrt{7}}\left(\sum_{k=\pm 2}\left[X^{(2)}\times D^{(2)}\right]^{(4)}_{k}\right)+\frac{\tau}{2\sqrt{3}}\left(\sum_{k=\pm 2}k\left[X^{(2)}\times D^{(2)}\right]^{(3)}_{k}\right)$$

$$+\frac{2}{3}\sqrt{\frac{7}{2}}\left(\nu+\frac{3}{35}\tau\right)\left[X^{(2)}\times D^{(2)}\right]^{(2)}_{0}+\frac{1}{3}\nu\left(X^{(2)}\cdot D^{(2)}\right)\Bigg\}. \tag{D.6c}$$

D.1.3 Magnetic field in [111] direction

$$H_0=\frac{\gamma_1'}{2\hbar^2 m_0}\Bigg\{\hbar^2 p^2-\frac{\mu'}{3}\left(P^{(2)}\cdot I^{(2)}\right)$$

$$+\frac{4}{27}\delta'\left(\sum_{k=\pm 3}k\left[P^{(2)}\times I^{(2)}\right]^{(4)}_{k}-3\sqrt{\frac{7}{10}}\left[P^{(2)}\times I^{(2)}\right]^{(4)}_{0}\right)\Bigg\}$$

$$+\frac{3\eta_1}{\hbar^2 m_0}\Bigg\{\frac{1}{3}p^2\left(I^{(1)}\cdot S^{(1)}_{\mathrm{h}}\right)-\frac{\nu}{3}\left(P^{(2)}\cdot D^{(2)}\right)$$

$$+\frac{4}{27}\tau\left(\sum_{k=\pm 3}k\left[P^{(2)}\times D^{(2)}\right]^{(4)}_{k}-3\sqrt{\frac{7}{10}}\left[P^{(2)}\times D^{(2)}\right]^{(4)}_{0}\right)\Bigg\}, \tag{D.7a}$$

$$
\begin{aligned}
H_1 = {} & \frac{1}{m_{\mathrm{e}}} L_0^{(1)} + \frac{\mu_{\mathrm{B}}}{e\hbar}\left(g_c S_{\mathrm{e}\,0}^{(1)} - g_s S_{\mathrm{h}\,0}^{(1)} + \left(3\kappa + \frac{1}{2} g_s\right) I_0^{(1)}\right) \\
& + \frac{\gamma_1^{'}}{2\hbar^2 m_0}\left\{ -\hbar^2 L_0^{(1)} - \frac{\delta^{'}}{3}\left(\sum_{k=\pm 3}\left[M^{(2)} \times I^{(2)}\right]_k^{(4)}\right)\right. \\
& \qquad - \frac{\delta^{'}}{27}\left(\sum_{k=\pm 3} k\left[M^{(2)} \times I^{(2)}\right]_k^{(3)} - 6\sqrt{\frac{2}{5}}\left[M^{(2)} \times I^{(2)}\right]_0^{(3)}\right) \\
& \qquad + \frac{\delta^{'}}{9}\left(\sum_{k=\pm 3} k\left[L^{(1)} \times I^{(2)}\right]_k^{(3)} - 6\sqrt{\frac{2}{5}}\left[L^{(1)} \times I^{(2)}\right]_0^{(3)}\right) \\
& \qquad \left. + \frac{1}{2}\sqrt{\frac{5}{3}}\mu^{'}\left(\left[L^{(1)} \times I^{(2)}\right]_0^{(1)} + \sqrt{\frac{2}{3}}\left[M^{(2)} \times I^{(2)}\right]_0^{(1)}\right)\right\} \\
& + \frac{3\eta_1}{\hbar^2 m_0}\left\{ -\frac{1}{3} L_0^{(1)}\left(I^{(1)} \cdot S_{\mathrm{h}}^{(1)}\right) - \frac{\tau}{3}\left(\sum_{k=\pm 3}\left[M^{(2)} \times D^{(2)}\right]_k^{(4)}\right)\right. \\
& \qquad - \frac{\tau}{27}\left(\sum_{k=\pm 3} k\left[M^{(2)} \times D^{(2)}\right]_k^{(3)} - 6\sqrt{\frac{2}{5}}\left[M^{(2)} \times D^{(2)}\right]_0^{(3)}\right) \\
& \qquad + \frac{\tau}{9}\left(\sum_{k=\pm 3} k\left[L^{(1)} \times D^{(2)}\right]_k^{(3)} - 6\sqrt{\frac{2}{5}}\left[L^{(1)} \times D^{(2)}\right]_0^{(3)}\right) \\
& \qquad \left. + \frac{1}{2}\sqrt{\frac{5}{3}}\nu\left(\left[L^{(1)} \times D^{(2)}\right]_0^{(1)} + \sqrt{\frac{2}{3}}\left[M^{(2)} \times D^{(2)}\right]_0^{(1)}\right)\right\},
\end{aligned}
\tag{D.7b}
$$

$$
\begin{aligned}
H_2 = {} & \frac{\gamma_1^{'}}{24\hbar^2 m_0}\left\{ \hbar^2\left(2r^2 - \sqrt{\frac{2}{3}} X_0^{(2)}\right) + \sqrt{\frac{2}{3}}\left(\mu^{'} + \frac{4}{5}\delta^{'}\right) r^2 I_0^{(2)}\right. \\
& \qquad + \frac{2}{3}\delta^{'}\left(-\frac{1}{3}\sum_{k=\pm 3} k\left[X^{(2)} \times I^{(2)}\right]_k^{(4)} - \sqrt{\frac{2}{35}}\left[X^{(2)} \times I^{(2)}\right]_0^{(4)}\right) \\
& \qquad - \frac{2}{3}\delta^{'}\sum_{k=\pm 3}\left[X^{(2)} \times I^{(2)}\right]_k^{(3)} + \frac{2}{3}\sqrt{\frac{7}{2}}\left(\mu^{'} + \frac{8}{35}\delta^{'}\right)\left[X^{(2)} \times I^{(2)}\right]_0^{(2)}
\end{aligned}
$$

$$
\begin{aligned}
&+\frac{\mu'}{3}\left(X^{(2)}\cdot I^{(2)}\right)\Big\}\\
&+\frac{\eta_1}{4\hbar^2 m_0}\left\{\frac{1}{3}\left(2r^2-\sqrt{\frac{2}{3}}X_0^{(2)}\right)\left(I^{(1)}\cdot S_{\mathrm{h}}^{(1)}\right)+\sqrt{\frac{2}{3}}\left(\nu+\frac{4}{5}\tau\right)r^2 D_0^{(2)}\right.\\
&+\frac{2}{3}\tau\left(-\frac{1}{3}\sum_{k=\pm 3}k\left[X^{(2)}\times I^{(2)}\right]_k^{(4)}-\sqrt{\frac{2}{35}}\left[X^{(2)}\times D^{(2)}\right]_0^{(4)}\right)\\
&-\frac{2}{3}\tau\sum_{k=\pm 3}\left[X^{(2)}\times I^{(2)}\right]_k^{(3)}+\frac{2}{3}\sqrt{\frac{7}{2}}\left(\nu+\frac{8}{35}\tau\right)\left[X^{(2)}\times D^{(2)}\right]_0^{(2)}\\
&\left.+\frac{\nu}{3}\left(X^{(2)}\cdot D^{(2)}\right)\right\}.
\end{aligned}
\tag{D.7c}
$$

D.2 Finite momentum $\hbar\boldsymbol{K}$

In this section we give the expressions for H_0, H_1 and H_2 of the Hamiltonian (9.5) in terms of irreducible tensors for the case that the wave vector $\boldsymbol{K}$ is oriented in [001], [110] or [111] direction [79, 248, 281]. Note that we rotate the coordinate system to make the quantization axis or z axis coincide with the direction of $\boldsymbol{K}$. Hence, we rotate the coordinate system by the Euler angles $(\alpha,\,\beta,\,\gamma)=(\pi,\,\pi/2,\,\pi/4)$ for $\boldsymbol{K}\parallel[110]$ and by $(\alpha,\,\beta,\,\gamma)=\left(0,\,\arccos(1/\sqrt{3}),\,\pi/4\right)$ for $\boldsymbol{K}\parallel[111]$.

D.2.1 Wave vector in [001] direction

$$
\begin{aligned}
H_0 = E_{\mathrm{g}} &- \frac{e^2}{4\pi\varepsilon_0\varepsilon}\frac{1}{r}-\frac{e^2}{4\pi\varepsilon_0 r}\left[\frac{1}{2\varepsilon_1^*}\left(e^{-r/\rho_{\mathrm{h1}}}+e^{-r/\rho_{\mathrm{e1}}}\right)+\frac{1}{2\varepsilon_2^*}\left(e^{-r/\rho_{\mathrm{h2}}}+e^{-r/\rho_{\mathrm{e2}}}\right)\right]\\
&+\frac{2}{3}\Delta\left(1+\frac{1}{\hbar^2}I^{(1)}\cdot S_{\mathrm{h}}^{(1)}\right)+\left[-V_0+J_0\left(\frac{1}{4}-\frac{1}{\hbar^2}S_{\mathrm{e}}^{(1)}\cdot S_{\mathrm{h}}^{(1)}\right)\right]V_{\mathrm{uc}}\delta(\boldsymbol{r})\\
&+\frac{\gamma_1'}{2\hbar^2 m_0}\left\{\hbar^2 p^2-\frac{\mu'}{3}\left(P^{(2)}\cdot I^{(2)}\right)\right.\\
&\left.+\frac{\delta'}{3}\left(\sum_{k=\pm 4}\left[P^{(2)}\times I^{(2)}\right]_k^{(4)}+\frac{\sqrt{70}}{5}\left[P^{(2)}\times I^{(2)}\right]_0^{(4)}\right)\right\}
\end{aligned}
$$

$$+\frac{3\eta_1}{\hbar^2 m_0}\left\{\frac{1}{3}p^2\left(I^{(1)}\cdot S_{\mathrm{h}}^{(1)}\right)-\frac{\nu}{3}\left(P^{(2)}\cdot D^{(2)}\right)\right.$$

$$\left.+\frac{\tau}{3}\left(\sum_{k=\pm 4}\left[P^{(2)}\times D^{(2)}\right]_k^{(4)}+\frac{\sqrt{70}}{5}\left[P^{(2)}\times D^{(2)}\right]_0^{(4)}\right)\right\}, \tag{D.8a}$$

$$H_1=\frac{1}{2\hbar^2 m_{\mathrm{e}}}\left\{-2\sqrt{\frac{5}{3}}\mu'\left[P^{(1)}\times I^{(2)}\right]_0^{(1)}-4\sqrt{\frac{2}{5}}\delta'\left[P^{(1)}\times I^{(2)}\right]_0^{(3)}\right\}$$

$$+\frac{3\eta_1}{\gamma_1'\hbar^2 m_{\mathrm{e}}}\left\{-\frac{2}{3}P_0^{(1)}\left(I^{(1)}\cdot S_{\mathrm{h}}^{(1)}\right)-2\sqrt{\frac{5}{3}}\nu\left[P^{(1)}\times D^{(2)}\right]_0^{(1)}-4\sqrt{\frac{2}{5}}\tau\left[P^{(1)}\times D^{(2)}\right]_0^{(3)}\right\}, \tag{D.8b}$$

$$H_2=\frac{\gamma_1' m_{\mathrm{e}}-m_0}{2\gamma_1' m_{\mathrm{e}}^2}+\frac{m_0}{2\gamma_1'\hbar^2 m_{\mathrm{e}}^2}\left\{\left(-\sqrt{\frac{2}{3}}\mu'+\frac{2}{5}\sqrt{6}\delta'\right)I_0^{(2)}\right\}$$

$$+\frac{3\eta_1 m_0}{\gamma_1'^2\hbar^2 m_{\mathrm{e}}^2}\left\{\frac{1}{3}\left(I^{(1)}\cdot S_{\mathrm{h}}^{(1)}\right)+\left(-\sqrt{\frac{2}{3}}\nu+\frac{2}{5}\sqrt{6}\tau\right)D_0^{(2)}\right\}. \tag{D.8c}$$

D.2.2 Wave vector in [110] direction

$$H_0=E_{\mathrm{g}}-\frac{e^2}{4\pi\varepsilon_0\varepsilon}\frac{1}{r}-\frac{e^2}{4\pi\varepsilon_0 r}\left[\frac{1}{2\varepsilon_1^*}\left(e^{-r/\rho_{\mathrm{h}1}}+e^{-r/\rho_{\mathrm{e}1}}\right)+\frac{1}{2\varepsilon_2^*}\left(e^{-r/\rho_{\mathrm{h}2}}+e^{-r/\rho_{\mathrm{e}2}}\right)\right]$$

$$+\frac{2}{3}\Delta\left(1+\frac{1}{\hbar^2}I^{(1)}\cdot S_{\mathrm{h}}^{(1)}\right)+\left[-V_0+J_0\left(\frac{1}{4}-\frac{1}{\hbar^2}S_{\mathrm{e}}^{(1)}\cdot S_{\mathrm{h}}^{(1)}\right)\right]V_{\mathrm{uc}}\delta(\boldsymbol{r})$$

$$+\frac{\gamma_1'}{2\hbar^2 m_0}\left\{\hbar^2 p^2-\frac{\mu'}{3}\left(P^{(2)}\cdot I^{(2)}\right)+\frac{\delta'}{4}\left(\sum_{k=\pm 4}\left[P^{(2)}\times I^{(2)}\right]_k^{(4)}\right)\right.$$

$$\left.-\frac{\sqrt{7}}{6}\delta'\left(\sum_{k=\pm 2}\left[P^{(2)}\times I^{(2)}\right]_2^{(4)}+\sqrt{\frac{1}{10}}\left[P^{(2)}\times I^{(2)}\right]_0^{(4)}\right)\right\}$$

$$+\frac{3\eta_1}{\hbar^2 m_0}\left\{\frac{1}{3}p^2\left(I^{(1)}\cdot S_{\mathrm{h}}^{(1)}\right)-\frac{\nu}{3}\left(P^{(2)}\cdot D^{(2)}\right)+\frac{\tau}{4}\left(\sum_{k=\pm 4}\left[P^{(2)}\times D^{(2)}\right]_k^{(4)}\right)\right.$$

$$-\frac{\sqrt{7}}{6}\tau\left(\sum_{k=\pm 2}\left[P^{(2)}\times D^{(2)}\right]^{(4)}_{k}+\sqrt{\frac{1}{10}}\left[P^{(2)}\times D^{(2)}\right]^{(4)}_{0}\right)\Bigg\}, \tag{D.9a}$$

$$H_1=\frac{1}{2\hbar^2 m_\mathrm{e}}\Bigg\{-2\sqrt{\frac{5}{3}}\mu'\left[P^{(1)}\times I^{(2)}\right]^{(1)}_{0}$$

$$+\sqrt{3}\delta'\left(\sum_{k=\pm 2}\left[P^{(1)}\times I^{(2)}\right]^{(3)}_{k}+\sqrt{\frac{2}{15}}\left[P^{(1)}\times I^{(2)}\right]^{(3)}_{0}\right)\Bigg\}$$

$$+\frac{3\eta_1}{\gamma_1'\hbar^2 m_\mathrm{e}}\Bigg\{-\frac{2}{3}P^{(1)}_{0}\left(I^{(1)}\cdot S^{(1)}_\mathrm{h}\right)-2\sqrt{\frac{5}{3}}\nu\left[P^{(1)}\times D^{(2)}\right]^{(1)}_{0}$$

$$+\sqrt{3}\tau\left(\sum_{k=\pm 2}\left[P^{(1)}\times D^{(2)}\right]^{(3)}_{k}+\sqrt{\frac{2}{15}}\left[P^{(1)}\times D^{(2)}\right]^{(3)}_{0}\right)\Bigg\}, \tag{D.9b}$$

$$H_2=\frac{\gamma_1' m_\mathrm{e}-m_0}{2\gamma_1' m_\mathrm{e}^2}+\frac{m_0}{2\gamma_1'\hbar^2 m_\mathrm{e}^2}\left\{-\frac{1}{2}\delta'\left(I^{(2)}_{-2}+I^{(2)}_{2}\right)+\left(-\sqrt{\frac{2}{3}}\mu'-\frac{1}{5}\sqrt{\frac{3}{2}}\delta'\right)I^{(2)}_{0}\right\}$$

$$+\frac{3\eta_1 m_0}{\gamma_1'^2\hbar^2 m_\mathrm{e}^2}\left\{\frac{1}{3}\left(I^{(1)}\cdot S^{(1)}_\mathrm{h}\right)-\frac{1}{2}\tau\left(D^{(2)}_{-2}+D^{(2)}_{2}\right)+\left(-\sqrt{\frac{2}{3}}\nu-\frac{1}{5}\sqrt{\frac{3}{2}}\tau\right)D^{(2)}_{0}\right\}. \tag{D.9c}$$

D.2.3 Wave vector in [111] direction

$$H_0=E_\mathrm{g}-\frac{e^2}{4\pi\varepsilon_0\varepsilon}\frac{1}{r}-\frac{e^2}{4\pi\varepsilon_0 r}\left[\frac{1}{2\varepsilon_1^*}\left(e^{-r/\rho_\mathrm{h1}}+e^{-r/\rho_\mathrm{e1}}\right)+\frac{1}{2\varepsilon_2^*}\left(e^{-r/\rho_\mathrm{h2}}+e^{-r/\rho_\mathrm{e2}}\right)\right]$$

$$+\frac{2}{3}\Delta\left(1+\frac{1}{\hbar^2}I^{(1)}\cdot S^{(1)}_\mathrm{h}\right)+\left[-V_0+J_0\left(\frac{1}{4}-\frac{1}{\hbar^2}S^{(1)}_\mathrm{e}\cdot S^{(1)}_\mathrm{h}\right)\right]V_\mathrm{uc}\delta(\boldsymbol{r})$$

$$+\frac{\gamma_1'}{2\hbar^2 m_0}\Bigg\{\hbar^2 p^2-\frac{\mu'}{3}\left(P^{(2)}\cdot I^{(2)}\right)$$

$$+\frac{4}{27}\delta'\left(\sum_{k=\pm 3}k\left[P^{(2)}\times I^{(2)}\right]^{(4)}_{k}-3\sqrt{\frac{7}{10}}\left[P^{(2)}\times I^{(2)}\right]^{(4)}_{0}\right)\Bigg\}$$

$$+\frac{3\eta_1}{\hbar^2 m_0}\left\{\frac{1}{3}p^2\left(I^{(1)}\cdot S_\mathrm{h}^{(1)}\right)-\frac{\nu}{3}\left(P^{(2)}\cdot D^{(2)}\right)\right.$$

$$\left.+\frac{4}{27}\tau\left(\sum_{k=\pm 3}k\left[P^{(2)}\times D^{(2)}\right]_3^{(4)}-3\sqrt{\frac{7}{10}}\left[P^{(2)}\times D^{(2)}\right]_0^{(4)}\right)\right\}, \tag{D.10a}$$

$$H_1=\frac{1}{2\hbar^2 m_\mathrm{e}}\left\{-2\sqrt{\frac{5}{3}}\mu'\left[P^{(1)}\times I^{(2)}\right]_0^{(1)}\right.$$

$$\left.-\frac{4}{9}\delta'\left(\sum_{k=\pm 3}k\left[P^{(1)}\times I^{(2)}\right]_k^{(3)}-6\sqrt{\frac{2}{5}}\left[P^{(1)}\times I^{(2)}\right]_0^{(3)}\right)\right\}$$

$$+\frac{3\eta_1}{\gamma_1'\hbar^2 m_\mathrm{e}}\left\{-\frac{2}{3}P_0^{(1)}\left(I^{(1)}\cdot S_\mathrm{h}^{(1)}\right)-2\sqrt{\frac{5}{3}}\nu\left[P^{(1)}\times D^{(2)}\right]_0^{(1)}\right.$$

$$\left.-\frac{4}{9}\tau\left(\sum_{k=\pm 3}k\left[P^{(1)}\times D^{(2)}\right]_k^{(3)}-6\sqrt{\frac{2}{5}}\left[P^{(1)}\times D^{(2)}\right]_0^{(3)}\right)\right\}, \tag{D.10b}$$

$$H_2=\frac{\gamma_1' m_\mathrm{e}-m_0}{2\gamma_1' m_\mathrm{e}^2}+\frac{m_0}{2\gamma_1'\hbar^2 m_\mathrm{e}^2}\left\{-\sqrt{\frac{2}{3}}\left(\mu'+\frac{4}{5}\delta'\right)I_0^{(2)}\right\}$$

$$+\frac{3\eta_1 m_0}{\gamma_1'^2\hbar^2 m_\mathrm{e}^2}\left\{\frac{1}{3}\left(I^{(1)}\cdot S_\mathrm{h}^{(1)}\right)-\sqrt{\frac{2}{3}}\left(\nu+\frac{4}{5}\tau\right)D_0^{(2)}\right\}. \tag{D.10c}$$

E Recursion relations of the Coulomb-Sturmian functions

In this section we give all important recursion relations of the Coulomb-Sturmian functions based on the calculations in Ref. [446]. In this regard, we also give the recursion relations needed if external magnetic or electric fields are present. The Coulomb-Sturmian functions read

$$\phi_{N,L,M}\left(\boldsymbol{r}\right) = U_{NL}\left(\rho\right) Y_{LM}\left(\Omega\right) = N_{NL}\left(2\rho\right)^{L} e^{-\rho} L_{N}^{2L+1}\left(2\rho\right) Y_{LM}\left(\Omega\right) \tag{E.1}$$

with $\rho = r/\alpha$, a normalization factor

$$N_{NL} = \frac{2}{\sqrt{\alpha^3}} \left[\frac{N!}{(N+2L+1)!\,(N+L+1)} \right]^{\frac{1}{2}}, \tag{E.2}$$

the associated Laguerre polynomials $L_n^m\left(x\right)$, and an arbitrary scaling parameter α. The radial functions obey the orthogonality relation

$$\int_0^\infty \mathrm{d}r\; r U_{N'L}\left(r\right) U_{NL}\left(r\right) = \frac{1}{\alpha\left(N+L+1\right)} \delta_{NN'}. \tag{E.3}$$

For the recursion relations we set $\alpha = 1$ and omit the dependency of the functions $\phi_{N,L,M}$ on $\boldsymbol{r}$. Coefficients in these relations will be given, e.g., in the form $\left(R_1\right)_{NL}^{j}$, which means that they are functions of j, n, and L, etc. The vectors $\hat{n}$ and $\nabla^{\hat{n}}$ are defined as in Ref. [446].

$$\hat{n}_3 \phi_{N,L,M} = \sum_{j=\pm 1} \left(N_1\right)_{LM}^{j} U_{NL} Y_{L+jM} \tag{E.4}$$

$$\left(N_1\right)_{LM}^{j} = \delta_{1j} \left\{ \left[\frac{(L+M+1)\,(L-M+1)}{(2L+1)\,(2L+3)} \right]^{\frac{1}{2}} \right\} + \delta_{-1j} \left\{ \left[\frac{(L+M)\,(L-M)}{(2L+1)\,(2L-1)} \right]^{\frac{1}{2}} \right\} \tag{E.5}$$

$$\nabla_3^{\hat{n}} \phi_{N,L,M} = \sum_{j=\pm 1} \left(D_1\right)_{LM}^{j} U_{NL} Y_{L+jM} \tag{E.6}$$

$$(D_1)^{j}_{LM} = \delta_{1j}\left\{-L\,(N_1)^{1}_{LM}\right\} + \delta_{-1j}\left\{(L+1)\,(N_1)^{-1}_{LM}\right\} \tag{E.7}$$

$$r\phi_{N,L,M} = \sum_{j=-1}^{1} (R_1)^{j}_{NL}\,\phi_{N+j,L,M} \tag{E.8}$$

$$\begin{aligned}(R_1)^{j}_{NL} &= \delta_{1j}\left\{-\frac{1}{2}\left[(N+1)\,(N+L+2)\right]^{\frac{1}{2}}\left[\frac{(N+2L+2)}{(N+L+1)}\right]^{\frac{1}{2}}\right\}\\ &+ \delta_{0j}\left\{N+L+1\right\} + \delta_{-1j}\left\{-\frac{1}{2}\left[(N)\,(N+L)\right]^{\frac{1}{2}}\left[\frac{(N+2L+1)}{(N+L+1)}\right]^{\frac{1}{2}}\right\}\end{aligned} \tag{E.9}$$

$$r\frac{\partial}{\partial r}\phi_{N,L,M} = \sum_{j=-1}^{-1} (RP_1)^{j}_{NL}\,\phi_{N+j,L,M} \tag{E.10}$$

$$(RP_1)^{j}_{NL} = \delta_{-1j}\left\{(R_1)^{-1}_{NL}\right\} + \delta_{0j}\left\{-1\right\} + \delta_{1j}\left\{-\,(R_1)^{1}_{NL}\right\} \tag{E.11}$$

$$r\phi_{N,L,M} = \sum_{j=-2}^{0} (L_1)^{j\,1}_{NL}\,\phi_{N+j,L+1,M} = \sum_{j=0}^{2} (L_1)^{j\,-1}_{NL}\,\phi_{N+j,L-1,M} \tag{E.12}$$

$$\begin{aligned}(L_1)^{j\,k}_{NL} &= \delta_{2j}\delta_{-1k}\left\{\frac{1}{2}\left[(N+2)\,(N+1)\right]^{\frac{1}{2}}\left[\frac{(N+L+2)}{(N+L+1)}\right]^{\frac{1}{2}}\right\}\\ &+ \delta_{1j}\delta_{-1k}\left\{-\left[(N+1)\,(N+2L+1)\right]^{\frac{1}{2}}\right\}\\ &+ \delta_{0j}\delta_{-1k}\left\{\frac{1}{2}\left[(N+2L)\,(N+2L+1)\right]^{\frac{1}{2}}\left[\frac{(N+L)}{(N+L+1)}\right]^{\frac{1}{2}}\right\}\\ &+ \delta_{0j}\delta_{1k}\left\{\frac{1}{2}\left[(N+2L+2)\,(N+2L+3)\right]^{\frac{1}{2}}\left[\frac{(N+L+2)}{(N+L+1)}\right]^{\frac{1}{2}}\right\}\\ &+ \delta_{-1j}\delta_{1k}\left\{-\left[(N)\,(N+2L+2)\right]^{\frac{1}{2}}\right\}\end{aligned}$$

$$+\,\delta_{-2j}\delta_{1k}\left\{\frac{1}{2}\left[(N)\,(N-1)\right]^{\frac{1}{2}}\left[\frac{(N+L)}{(N+L+1)}\right]^{\frac{1}{2}}\right\} \tag{E.13}$$

With these relations we calculate combined formulas:

$$r^2\phi_{N,L,M} = \sum_{j=-2}^{2} \left(R_2\right)^{j}_{NL}\,\phi_{N+j,L,M} \tag{E.14}$$

$$\left(R_2\right)^{j}_{NL} = \sum_{w=j-1}^{j+1} \left(R_1\right)^{w}_{NL}\left(R_1\right)^{j-w}_{N+w\,L} \tag{E.15}$$

$$r^3\phi_{N,L,M} = \sum_{j=-3}^{3} \left(R_3\right)^{j}_{NL}\,\phi_{N+j,L,M} \tag{E.16}$$

$$\left(R_3\right)^{j}_{NL} = \sum_{w=j-1}^{j+1} \left(R_2\right)^{w}_{NL}\left(R_1\right)^{j-w}_{N+w\,L} \tag{E.17}$$

$$r\hat{n}_3\phi_{N,L,M} = \sum_{k=\pm1}\ \sum_{j=-1-k}^{1-k} \left(LN_1\right)^{j\,k}_{NLM}\,\phi_{N+j,L+k,M} \tag{E.18}$$

$$\left(LN_1\right)^{j\,k}_{NLM} = \left(L_1\right)^{j\,k}_{NL}\left(N_1\right)^{k}_{LM} \tag{E.19}$$

$$r^2\hat{n}_3\phi_{N,L,M} = \sum_{k=\pm1}\ \sum_{j=-2-k}^{2-k} \left(RLN_1\right)^{j\,k}_{NLM}\,\phi_{N+j,L+k,M} \tag{E.20}$$

$$\left(RLN_1\right)^{j\,k}_{NLM} = \sum_{w=j-1}^{j+1} \left(LN_1\right)^{w\,k}_{NLM}\left(R_1\right)^{j-w}_{N+w\,L+k} \tag{E.21}$$

$$r^2\hat{n}_3^2\phi_{N,L,M} = \sum_{k=0,\pm2}\ \sum_{j=-2-k}^{2-k} \left(LN_2\right)^{j\,k}_{NLM}\,\phi_{N+j,L+k,M} \tag{E.22}$$

$$\left(LN_2\right)^{j\,k}_{NLM} = \sum_{v=\pm1}\ \sum_{w=j-1-v}^{j+1-v} \left(LN_1\right)^{w\,k+v}_{NLM}\left(LN_1\right)^{j-w\,-v}_{N+w\,L+k+v\,M} \tag{E.23}$$

$$r^3 \hat{n}_3^2 \phi_{N,L,M} = \sum_{k=0,\pm 2} \sum_{j=-3-k}^{3-k} (R_1 L N_2)^{j\,k}_{NLM} \, \phi_{N+j,L+k,M} \tag{E.24}$$

$$(R_1 L N_2)^{j\,k}_{NLM} = \sum_{w=j-1}^{j+1} (L N_2)^{w\,k}_{NLM} \, (R_1)^{j-w}_{N+w\,L+k} \tag{E.25}$$

$$r^2 \frac{\partial}{\partial r} \phi_{N,L,M} = \sum_{j=-2}^{2} (R_2 P_1)^{j}_{NL} \, \phi_{N+j,L,M} \tag{E.26}$$

$$(R_2 P_1)^{j}_{NL} = \sum_{w=j-1}^{j+1} (R P_1)^{w}_{NL} \, (R_1)^{j-w}_{N+w\,L} \tag{E.27}$$

$$r^3 \frac{\partial}{\partial r} \phi_{N,L,M} = \sum_{j=-3}^{3} (R_3 P_1)^{j}_{NL} \, \phi_{N+j,L,M} \tag{E.28}$$

$$(R_3 P_1)^{j}_{NL} = \sum_{w=j-1}^{j+1} (R_2 P_1)^{w}_{NL} \, (R_1)^{j-w}_{N+w\,L} \tag{E.29}$$

F Matrix elements and reduced matrix elements

F.1 Matrix elements

In this section we give all matrix elements of the terms of the Hamiltonians used in this thesis in the basis of Eq. (4.22) in Hartree units using the formalism of irreducible tensors [248]. We use the abbreviation

$$\tilde{\delta}_{\Pi\Pi'} = \delta_{LL'}\delta_{JJ'}\delta_{FF'}\delta_{F_tF_t'}\delta_{M_{F_t}M_{F_t}'} \tag{F.1}$$

in the following. The functions of the form $(R_1)^j_{NL}$ are taken from the recursion relations of the Coulomb-Sturmian functions in Appendix E. The value of the integral $I_{N'\,L';N\,L}$ is given in Appendix F.2.

Note that in Eq. (F.8) the order of the quantum numbers in the rows of the $9j$-symbol is given by relations in Refs. [248, 302] and differs from Eq. (14) of the Supplementary Material of Ref. [36] or Eq. (A2) of Ref. [78]. This odd permutation of rows changes the sign of the sign of the $9j$-symbol by [248]

$$(-1)^{L'+L+2+J'+J+2+F'+F+4}. \tag{F.2}$$

So there is change in the sign of the $9j$-symbol, e.g., for $L = L' = 3$, $J = 1/2$, $J' = 3/2$ and $F = F' = 5/2$ (cf. Eq. (15a) of the Supplementary Material of Ref. [36]), which is important for the evaluation in Sec. 4.5.1.

$$\left\langle \Pi' \left| r^{-1} \right| \Pi \right\rangle = \tilde{\delta}_{\Pi\Pi'}\delta_{NN'}\left[N + L + 1\right]^{-1} \tag{F.3}$$

$$\left\langle \Pi' \left| 1 \right| \Pi \right\rangle = \tilde{\delta}_{\Pi\Pi'} \sum_{j=-1}^{1} (R_1)^j_{NL} \left[N + L + j + 1\right]^{-1} \delta_{N',N+j} \tag{F.4}$$

$$\left\langle \Pi' \left| p^2 \right| \Pi \right\rangle = 2\tilde{\delta}_{\Pi\Pi'}\delta_{NN'} - \tilde{\delta}_{\Pi\Pi'} \sum_{j=-1}^{1} (R_1)^j_{NL} \left[N + L + j + 1\right]^{-1} \delta_{N',N+j} \tag{F.5}$$

$$\left\langle \Pi' \left| 1 + I^{(1)} \cdot S_{\mathrm{h}}^{(1)} \right| \Pi \right\rangle = \tilde{\delta}_{\Pi\Pi'} \left(\frac{1}{2} J \left(J+1 \right) - \frac{3}{8} \right)$$

$$\times \sum_{j=-1}^{1} \left(R_1 \right)_{NL}^{j} \left[N + L + j + 1 \right]^{-1} \delta_{N', N+j} \tag{F.6}$$

$$\left\langle \Pi' \left| P^{(2)} \cdot I^{(2)} \right| \Pi \right\rangle = \sqrt{5} \left\langle \Pi' \left| \left[P^{(2)} \times I^{(2)} \right]_{0}^{(0)} \right| \Pi \right\rangle \tag{F.7}$$

$$\left\langle \Pi' \left| \left[P^{(2)} \times I^{(2)} \right]_{q}^{(K)} \right| \Pi \right\rangle = 3\sqrt{5} \left(-1 \right)^{F_t' + F_t - M_{F_t}' + F' + J + K} \left\langle N' \, L' \left\| P^{(2)} \right\| N \, L \right\rangle$$

$$\times \left[\left(2F_t + 1 \right) \left(2F_t' + 1 \right) \left(2F + 1 \right) \left(2F' + 1 \right) \right]^{\frac{1}{2}}$$

$$\times \left[\left(2K + 1 \right) \left(2J + 1 \right) \left(2J' + 1 \right) \right]^{\frac{1}{2}} \begin{pmatrix} F_t' & K & F_t \\ -M_{F_t}' & q & M_{F_t} \end{pmatrix}$$

$$\times \begin{Bmatrix} F' & F_t' & \frac{1}{2} \\ F_t & F & K \end{Bmatrix} \begin{Bmatrix} 1 & J' & \frac{1}{2} \\ J & 1 & 2 \end{Bmatrix} \begin{Bmatrix} L' & L & 2 \\ J' & J & 2 \\ F' & F & K \end{Bmatrix} \tag{F.8}$$

$$\left\langle \Pi' \left| p^2 \left(I^{(1)} \cdot S_{\mathrm{h}}^{(1)} \right) \right| \Pi \right\rangle = \frac{1}{2} \left(J \left(J+1 \right) - \frac{11}{4} \right) \left\langle \Pi' \left| p^2 \right| \Pi \right\rangle \tag{F.9}$$

$$\left\langle \Pi' \left| P^{(2)} \cdot D^{(2)} \right| \Pi \right\rangle = \sqrt{5} \left\langle \Pi' \left| \left[P^{(2)} \times D^{(2)} \right]_{0}^{(0)} \right| \Pi \right\rangle \tag{F.10}$$

$$\left\langle \Pi' \left| \left[P^{(2)} \times D^{(2)} \right]_{q}^{(K)} \right| \Pi \right\rangle = 3\sqrt{5} \left(-1 \right)^{F_t' + F_t - M_{F_t}' + F' + K + \frac{1}{2}} \left\langle N \, L' \left\| P^{(2)} \right\| N \, L \right\rangle$$

$$\times \left[(2F_t + 1)(2F_t' + 1)(2F + 1)(2F' + 1) \right]^{\frac{1}{2}}$$

$$\times \left[(2K + 1)(2J + 1)(2J' + 1) \right]^{\frac{1}{2}} \begin{pmatrix} F_t' & K & F_t \\ -M_{F_t}' & q & M_{F_t} \end{pmatrix}$$

$$\times \begin{Bmatrix} F' & F_t' & \frac{1}{2} \\ F_t & F & K \end{Bmatrix} \begin{Bmatrix} L' & L & 2 \\ J' & J & 2 \\ F' & F & K \end{Bmatrix} \begin{Bmatrix} 1 & 1 & 1 \\ \frac{1}{2} & \frac{1}{2} & 1 \\ J' & J & 2 \end{Bmatrix} \tag{F.11}$$

$$\begin{aligned}\left\langle \Pi' \left|\delta\left(\boldsymbol{r}\right)\right| \Pi\right\rangle &= \delta_{L'0}\delta_{L0}\delta_{JJ'}\delta_{F_tF_t'}\delta_{M_{F_t}M'_{F_t}}\,\frac{1}{\pi}\left(-1\right)^{F_t+F'+F+J+\frac{1}{2}}\\ &\times\ \left[\left(2F_t+1\right)\left(2F+1\right)\left(2F'+1\right)\right]^{\frac{1}{2}}\\ &\times \begin{Bmatrix} F' & F_t & \frac{1}{2}\\ F_t & F & 0\end{Bmatrix}\begin{Bmatrix} 0 & F' & J\\ F & 0 & 0\end{Bmatrix}\end{aligned}\tag{F.12}$$

$$\begin{aligned}\left\langle \Pi' \left|\boldsymbol{S}_{\mathrm{e}}\cdot\boldsymbol{S}_{\mathrm{h}}\,\delta\left(\boldsymbol{r}\right)\right| \Pi\right\rangle &= \delta_{L'0}\delta_{L0}\delta_{F_tF_t'}\delta_{M_{F_t}M'_{F_t}}\,\frac{3}{2\pi}\left(-1\right)^{F_t+F'+F+J+J'}\\ &\times\ \left[\left(2F+1\right)\left(2F'+1\right)\left(2J+1\right)\left(2J'+1\right)\right]^{\frac{1}{2}}\\ &\times \begin{Bmatrix} F' & F & 1\\ \frac{1}{2} & \frac{1}{2} & F_t\end{Bmatrix}\begin{Bmatrix} F & F' & 1\\ J' & J & 0\end{Bmatrix}\begin{Bmatrix} \frac{1}{2} & J' & 1\\ J & \frac{1}{2} & 1\end{Bmatrix}\end{aligned}\tag{F.13}$$

$$\begin{aligned}\left\langle \Pi' \left|\frac{1}{r}e^{-r/\rho}\right| \Pi\right\rangle &= \delta_{LL'}\delta_{JJ'}\delta_{F_tF_t'}\delta_{M_{F_t}M'_{F_t}}\,\frac{1}{4}N^{(1)}_{N'L}N^{(1)}_{NL}\\ &\times \sum_{k=0}^{N'}\sum_{j=0}^{N}\left(-1\right)^{k+j}\binom{N'+2L+1}{N'-k}\binom{N+2L+1}{N-j}\\ &\times \frac{\left(2L+k+j+1\right)!}{k!\,j!}\left[\frac{2\rho}{1+2\rho}\right]^{\left(2+2L+k+j\right)}\end{aligned}\tag{F.14}$$

$$\left\langle \Pi' \left|r^2\right| \Pi\right\rangle = \tilde{\delta}_{\Pi\Pi'}\sum_{j=-3}^{3}\left(R_3\right)^{j}_{NL}\left[N+L+j+1\right]^{-1}\delta_{N',N+j}\tag{F.15}$$

$$\begin{aligned}\left\langle \Pi' \left|r^2 I^{(2)}_q\right| \Pi\right\rangle &= \delta_{LL'}3\sqrt{5}\left(-1\right)^{F_t'+F_t-M'_{F_t}+2F'+L+2J}\\ &\times\ \left[\left(2F_t+1\right)\left(2F_t'+1\right)\left(2F+1\right)\left(2F'+1\right)\right]^{\frac{1}{2}}\\ &\times\ \left[\left(2J+1\right)\left(2J'+1\right)\right]^{\frac{1}{2}}\begin{pmatrix} F_t' & 2 & F_t\\ -M'_{F_t} & q & M_{F_t}\end{pmatrix}\\ &\times \begin{Bmatrix} F' & F_t' & \frac{1}{2}\\ F_t & F & 2\end{Bmatrix}\begin{Bmatrix} J' & F' & L\\ F & J & 2\end{Bmatrix}\begin{Bmatrix} 1 & J' & \frac{1}{2}\\ J & 1 & 2\end{Bmatrix}\end{aligned}$$

$$\times \sum_{j=-3}^{3} \left(R_3\right)^{j}_{NL} \left[N+L+j+1\right]^{-1} \delta_{N',N+j} \tag{F.16}$$

$$\begin{aligned}
\left\langle \Pi' \left| X^{(2)}_{q} \right| \Pi \right\rangle &= \delta_{JJ'} \left(-1\right)^{F'_t+F_t-M'_{F_t}+F'+F+L'+J+\frac{1}{2}} \left\langle N'\,L' \left\| X^{(2)} \right\| N\,L \right\rangle \\
&\times \left[\left(2F_t+1\right)\left(2F'_t+1\right)\left(2F+1\right)\left(2F'+1\right)\right]^{\frac{1}{2}} \\
&\times \begin{pmatrix} F'_t & 2 & F_t \\ -M'_{F_t} & q & M_{F_t} \end{pmatrix} \begin{Bmatrix} F' & F'_t & \frac{1}{2} \\ F_t & F & 2 \end{Bmatrix} \begin{Bmatrix} L' & F' & J \\ F & L & 2 \end{Bmatrix}
\end{aligned} \tag{F.17}$$

$$\begin{aligned}
\left\langle \Pi' \left| S^{(1)}_{\mathrm{e}\,0} \right| \Pi \right\rangle &= \delta_{LL'}\delta_{JJ'}\delta_{FF'}\delta_{M_{F_t}M'_{F_t}} \sqrt{\frac{3}{2}} \left(-1\right)^{2F'_t-M_{F_t}+F+\frac{3}{2}} \\
&\times \left[\left(2F_t+1\right)\left(2F'_t+1\right)\right]^{\frac{1}{2}} \begin{pmatrix} F'_t & 1 & F_t \\ -M_{F_t} & 0 & M_{F_t} \end{pmatrix} \\
&\times \begin{Bmatrix} \frac{1}{2} & F'_t & F \\ F_t & \frac{1}{2} & 1 \end{Bmatrix} \sum_{j=-1}^{1} \left(R_1\right)^{j}_{NL} \left[N+L+j+1\right]^{-1} \delta_{N',N+j}
\end{aligned} \tag{F.18}$$

$$\begin{aligned}
\left\langle \Pi' \left| S^{(1)}_{\mathrm{h}\,0} \right| \Pi \right\rangle &= \delta_{LL'}\delta_{M_{F_t}M'_{F_t}} \sqrt{\frac{3}{2}} \left(-1\right)^{F'_t+F_t-M_{F_t}+2F'+L+J+J'+1} \\
&\times \left[\left(2F_t+1\right)\left(2F'_t+1\right)\left(2F+1\right)\left(2F'+1\right)\right]^{\frac{1}{2}} \\
&\times \left[\left(2J+1\right)\left(2J'+1\right)\right]^{\frac{1}{2}} \begin{pmatrix} F'_t & 1 & F_t \\ -M_{F_t} & 0 & M_{F_t} \end{pmatrix} \\
&\times \begin{Bmatrix} F' & F'_t & \frac{1}{2} \\ F_t & F & 1 \end{Bmatrix} \begin{Bmatrix} J' & F' & L \\ F & J & 1 \end{Bmatrix} \begin{Bmatrix} \frac{1}{2} & J' & 1 \\ J & \frac{1}{2} & 1 \end{Bmatrix} \\
&\times \sum_{j=-1}^{1} \left(R_1\right)^{j}_{NL} \left[N+L+j+1\right]^{-1} \delta_{N',N+j}
\end{aligned} \tag{F.19}$$

$$\left\langle \Pi' \left| L^{(1)}_{0} \right| \Pi \right\rangle = \delta_{LL'}\delta_{JJ'}\delta_{M_{F_t}M'_{F_t}} \left(-1\right)^{F'_t+F_t-M_{F_t}+F+F'+L+J+\frac{1}{2}}$$

$$\times\ \left[(2F_t+1)\left(2F_t'+1\right)(2F+1)\left(2F'+1\right)\right]^{\frac{1}{2}}$$

$$\times\ \left[L(L+1)(2L+1)\right]^{\frac{1}{2}}\begin{pmatrix} F_t' & 1 & F_t \\ -M_{F_t} & 0 & M_{F_t}\end{pmatrix}$$

$$\times\left\{\begin{matrix} F' & F_t' & \frac{1}{2} \\ F_t & F & 1\end{matrix}\right\}\left\{\begin{matrix} L & F' & J \\ F & L & 1\end{matrix}\right\}$$

$$\times\sum_{j=-1}^{1}(R_1)^j_{NL}\left[N+L+j+1\right]^{-1}\delta_{N',N+j} \tag{F.20}$$

$$\left\langle\Pi'\left|I_0^{(1)}\right|\Pi\right\rangle=\delta_{LL'}\delta_{M_{F_t}M_{F_t}'}\sqrt{6}\,(-1)^{F_t'+F_t-M_{F_t}+2F'+L+2J+1}$$

$$\times\ \left[(2F_t+1)\left(2F_t'+1\right)(2F+1)\left(2F'+1\right)\right]^{\frac{1}{2}}$$

$$\times\ \left[(2J+1)\left(2J'+1\right)\right]^{\frac{1}{2}}\begin{pmatrix} F_t' & 1 & F_t \\ -M_{F_t} & 0 & M_{F_t}\end{pmatrix}$$

$$\times\left\{\begin{matrix} F' & F_t' & \frac{1}{2} \\ F_t & F & 1\end{matrix}\right\}\left\{\begin{matrix} J' & F' & L \\ F & J & 1\end{matrix}\right\}\left\{\begin{matrix} 1 & J' & \frac{1}{2} \\ J & 1 & 1\end{matrix}\right\}$$

$$\times\sum_{j=-1}^{1}(R_1)^j_{NL}\left[N+L+j+1\right]^{-1}\delta_{N',N+j} \tag{F.21}$$

$$\left\langle\Pi'\left|X^{(2)}\cdot I^{(2)}\right|\Pi\right\rangle=\sqrt{5}\left[X^{(2)}\times I^{(2)}\right]^{(0)}_0 \tag{F.22}$$

$$\left\langle\Pi'\left|\left[M^{(2)}\times I^{(2)}\right]^{(K)}_q\right|\Pi\right\rangle=3\sqrt{5}\,(-1)^{F_t'+F_t-M_{F_t}'+F'+J+K}\left\langle N'\,L'\left\|M^{(2)}\right\|N\,L\right\rangle$$

$$\times\ \left[(2F_t+1)\left(2F_t'+1\right)(2F+1)\left(2F'+1\right)\right]^{\frac{1}{2}}$$

$$\times\ \left[(2K+1)(2J+1)\left(2J'+1\right)\right]^{\frac{1}{2}}\begin{pmatrix} F_t' & K & F_t \\ -M_{F_t}' & q & M_{F_t}\end{pmatrix}$$

$$\times \begin{Bmatrix} F' & F'_t & \frac{1}{2} \\ F_t & F & K \end{Bmatrix} \begin{Bmatrix} 1 & J' & \frac{1}{2} \\ J & 1 & 2 \end{Bmatrix} \begin{Bmatrix} L' & L & 2 \\ J' & J & 2 \\ F' & F & K \end{Bmatrix} \tag{F.23}$$

$$\left\langle \Pi' \left| \left[L^{(1)} \times I^{(2)} \right]^{(K)}_{q} \right| \Pi \right\rangle = \delta_{LL'} 3\sqrt{5} \, (-1)^{F'_t + F_t - M'_{F_t} + F' + J + K} \left[L \, (L+1) \, (2L+1) \right]^{\frac{1}{2}}$$

$$\times \; \left[(2F_t + 1) \left(2F'_t + 1 \right) (2F + 1) \left(2F' + 1 \right) \right]^{\frac{1}{2}}$$

$$\times \; \left[(2K + 1) \, (2J + 1) \left(2J' + 1 \right) \right]^{\frac{1}{2}} \begin{pmatrix} F'_t & K & F_t \\ -M'_{F_t} & q & M_{F_t} \end{pmatrix}$$

$$\times \begin{Bmatrix} F' & F'_t & \frac{1}{2} \\ F_t & F & K \end{Bmatrix} \begin{Bmatrix} 1 & J' & \frac{1}{2} \\ J & 1 & 2 \end{Bmatrix} \begin{Bmatrix} L' & L & 1 \\ J' & J & 2 \\ F' & F & K \end{Bmatrix}$$

$$\times \sum_{j=-1}^{1} (R_1)^{j}_{NL} \left[N + L + j + 1 \right]^{-1} \delta_{N',N+j} \tag{F.24}$$

$$\left\langle \Pi' \left| \left[X^{(2)} \times I^{(2)} \right]^{(K)}_{q} \right| \Pi \right\rangle = 3\sqrt{5} \, (-1)^{F'_t + F_t - M'_{F_t} + F' + J + K} \left\langle N' \, L' \left\| X^{(2)} \right\| N \, L \right\rangle$$

$$\times \; \left[(2F_t + 1) \left(2F'_t + 1 \right) (2F + 1) \left(2F' + 1 \right) \right]^{\frac{1}{2}}$$

$$\times \; \left[(2K + 1) \, (2J + 1) \left(2J' + 1 \right) \right]^{\frac{1}{2}} \begin{pmatrix} F'_t & K & F_t \\ -M'_{F_t} & q & M_{F_t} \end{pmatrix}$$

$$\times \begin{Bmatrix} F' & F'_t & \frac{1}{2} \\ F_t & F & K \end{Bmatrix} \begin{Bmatrix} 1 & J' & \frac{1}{2} \\ J & 1 & 2 \end{Bmatrix} \begin{Bmatrix} L' & L & 2 \\ J' & J & 2 \\ F' & F & K \end{Bmatrix} \tag{F.25}$$

$$\left\langle \Pi' \left| L^{(1)}_{0} \left(I^{(1)} \cdot S^{(1)}_{\mathrm{h}} \right) \right| \Pi \right\rangle = \frac{1}{2} \left(J \, (J+1) - \frac{11}{4} \right) \left\langle \Pi' \left| L^{(1)}_{0} \right| \Pi \right\rangle \tag{F.26}$$

$$\left\langle \Pi' \left| r^{2} \left(I^{(1)} \cdot S^{(1)}_{\mathrm{h}} \right) \right| \Pi \right\rangle = \frac{1}{2} \left(J \, (J+1) - \frac{11}{4} \right) \left\langle \Pi' \left| r^{2} \right| \Pi \right\rangle \tag{F.27}$$

$$\left\langle \Pi' \left| X_q^{(2)} \left(I^{(1)} \cdot S_{\mathrm{h}}^{(1)} \right) \right| \Pi \right\rangle = \frac{1}{2} \left(J\,(J+1) - \frac{11}{4} \right) \left\langle \Pi' \left| X_q^{(2)} \right| \Pi \right\rangle \tag{F.28}$$

$$\begin{aligned}
\left\langle \Pi' \left| r^2 D_q^{(2)} \right| \Pi \right\rangle &= \delta_{LL'} 3\sqrt{5}\,(-1)^{F'_t+F_t-M'_{F_t}+2F'+L+J+\frac{1}{2}} \\
&\times \left[(2F_t+1)(2F'_t+1)(2F+1)(2F'+1)\right]^{\frac{1}{2}} \\
&\times \left[(2J+1)(2J'+1)\right]^{\frac{1}{2}} \begin{pmatrix} F'_t & 2 & F_t \\ -M'_{F_t} & q & M_{F_t} \end{pmatrix} \\
&\times \begin{Bmatrix} F' & F'_t & \frac{1}{2} \\ F_t & F & 2 \end{Bmatrix} \begin{Bmatrix} J' & F' & L \\ F & J & 2 \end{Bmatrix} \begin{Bmatrix} 1 & 1 & 1 \\ \frac{1}{2}, & \frac{1}{2} & 1 \\ J' & J & 2 \end{Bmatrix} \\
&\times \sum_{j=-3}^{3} (R_3)_{NL}^{j} \left[N+L+j+1\right]^{-1} \delta_{N',N+j}
\end{aligned} \tag{F.29}$$

$$\left\langle \Pi' \left| X^{(2)} \cdot D^{(2)} \right| \Pi \right\rangle = \sqrt{5} \left\langle \Pi' \left| \left[X^{(2)} \times D^{(2)} \right]_0^{(0)} \right| \Pi \right\rangle \tag{F.30}$$

$$\begin{aligned}
\left\langle \Pi' \left| \left[X^{(2)} \times D^{(2)} \right]_q^{(K)} \right| \Pi \right\rangle &= 3\sqrt{5}\,(-1)^{F'_t+F_t-M'_{F_t}+F'+K+\frac{1}{2}} \left\langle N'\,L' \left\| X^{(2)} \right\| N\,L \right\rangle \\
&\times \left[(2F_t+1)(2F'_t+1)(2F+1)(2F'+1)\right]^{\frac{1}{2}} \\
&\times \left[(2K+1)(2J+1)(2J'+1)\right]^{\frac{1}{2}} \begin{pmatrix} F'_t & K & F_t \\ -M'_{F_t} & q & M_{F_t} \end{pmatrix} \\
&\times \begin{Bmatrix} F' & F'_t & \frac{1}{2} \\ F_t & F & K \end{Bmatrix} \begin{Bmatrix} L' & L & 2 \\ J' & J & 2 \\ F' & F & K \end{Bmatrix} \begin{Bmatrix} 1 & 1 & 1 \\ \frac{1}{2} & \frac{1}{2} & 1 \\ J' & J & 2 \end{Bmatrix}
\end{aligned} \tag{F.31}$$

$$\begin{aligned}
\left\langle \Pi' \left| \left[M^{(2)} \times D^{(2)} \right]_q^{(K)} \right| \Pi \right\rangle &= 3\sqrt{5}\,(-1)^{F'_t+F_t-M'_{F_t}+F'+K+\frac{1}{2}} \left\langle N'\,L' \left\| M^{(2)} \right\| N\,L \right\rangle \\
&\times \left[(2F_t+1)(2F'_t+1)(2F+1)(2F'+1)\right]^{\frac{1}{2}}
\end{aligned}$$

$$\times \left[(2K+1)(2J+1)(2J'+1)\right]^{\frac{1}{2}} \begin{pmatrix} F_t' & K & F_t \\ -M_{F_t}' & q & M_{F_t} \end{pmatrix}$$

$$\times \begin{Bmatrix} F' & F_t' & \frac{1}{2} \\ F_t & F & K \end{Bmatrix} \begin{Bmatrix} L' & L & 2 \\ J' & J & 2 \\ F' & F & K \end{Bmatrix} \begin{Bmatrix} 1 & 1 & 1 \\ \frac{1}{2} & \frac{1}{2} & 1 \\ J' & J & 2 \end{Bmatrix} \tag{F.32}$$

$$\left\langle \Pi' \middle| \left[L^{(1)} \times D^{(2)}\right]_q^{(K)} \middle| \Pi \right\rangle = \delta_{LL'} 3\sqrt{5}\,(-1)^{F_t'+F_t-M_{F_t}'+F'+K+\frac{1}{2}} \left[L(L+1)(2L+1)\right]^{\frac{1}{2}}$$

$$\times \left[(2F_t+1)(2F_t'+1)(2F+1)(2F'+1)\right]^{\frac{1}{2}}$$

$$\times \left[(2K+1)(2J+1)(2J'+1)\right]^{\frac{1}{2}} \begin{pmatrix} F_t' & K & F_t \\ -M_{F_t}' & q & M_{F_t} \end{pmatrix}$$

$$\times \begin{Bmatrix} F' & F_t' & \frac{1}{2} \\ F_t & F & K \end{Bmatrix} \begin{Bmatrix} L' & L & 2 \\ J' & J & 2 \\ F' & F & K \end{Bmatrix} \begin{Bmatrix} 1 & 1 & 1 \\ \frac{1}{2} & \frac{1}{2} & 1 \\ J' & J & 2 \end{Bmatrix}$$

$$\times \sum_{j=-1}^{1} (R_1)_{NL}^{j} \left[N+L+j+1\right]^{-1} \delta_{N',N+j} \tag{F.33}$$

$$\left\langle \Pi' \middle| I_q^{(2)} \middle| \Pi \right\rangle = \delta_{LL'} 3\sqrt{5}\,(-1)^{F_t'+F_t-M_{F_t}'+2F'+2J+L}$$

$$\times \left[(2F_t+1)\left(2F_t'+1\right)(2F+1)\left(2F'+1\right)\right]^{\frac{1}{2}}$$

$$\times \left[(2J+1)\left(2J'+1\right)\right]^{\frac{1}{2}} \begin{pmatrix} F_t' & 2 & F_t \\ -M_{F_t}' & q & M_{F_t} \end{pmatrix}$$

$$\times \begin{Bmatrix} F' & F_t' & \frac{1}{2} \\ F_t & F & 2 \end{Bmatrix} \begin{Bmatrix} J' & F' & L \\ F & J & 2 \end{Bmatrix} \begin{Bmatrix} 1 & J' & \frac{1}{2} \\ J & 1 & 2 \end{Bmatrix}$$

$$\times \sum_{j=-1}^{1} (R_1)_{NL}^{j} \left[N+L+j+1\right]^{-1} \delta_{N',N+j} \tag{F.34}$$

$$\left\langle \Pi' \middle| D_q^{(2)} \middle| \Pi \right\rangle = \delta_{LL'} 3\sqrt{5}\,(-1)^{F_t'+F_t-M_{F_t}'+2F'+L+J+\frac{1}{2}}$$

$$\times \left[(2F_t+1)\left(2F_t'+1\right)(2F+1)\left(2F'+1\right)\right]^{\frac{1}{2}}$$

$$\times \left[(2J+1)\left(2J'+1\right)\right]^{\frac{1}{2}} \begin{pmatrix} F_t' & 2 & F_t \\ -M_{F_t}' & q & M_{F_t} \end{pmatrix}$$

$$\times \begin{Bmatrix} F' & F_t' & \frac{1}{2} \\ F_t & F & 2 \end{Bmatrix} \begin{Bmatrix} J' & F' & L \\ F & J & 2 \end{Bmatrix} \begin{Bmatrix} 1 & 1 & 1 \\ \frac{1}{2} & \frac{1}{2} & 1 \\ J' & J & 2 \end{Bmatrix}$$

$$\times \sum_{j=-1}^{1} (R_1)_{NL}^{j} \left[N+L+j+1\right]^{-1} \delta_{N',N+j} \tag{F.35}$$

$$\left\langle \Pi' \left| \left(I^{(1)} \cdot S_{\mathrm{h}}^{(1)} \right) \right| \Pi \right\rangle = \delta_{LL'} \delta_{M_{F_t} M_{F_t}'} \delta_{F_t F_t'} 3\sqrt{3} \, (-1)^{F_t+2F'+L+J+\frac{3}{2}}$$

$$\times \left[(2F_t+1)(2F+1)\left(2F'+1\right)(2J+1)\left(2J'+1\right)\right]^{\frac{1}{2}}$$

$$\times \begin{Bmatrix} F' & F_t & \frac{1}{2} \\ F_t & F & 0 \end{Bmatrix} \begin{Bmatrix} J' & F' & L \\ F & J & 0 \end{Bmatrix} \begin{Bmatrix} 1 & 1 & 1 \\ \frac{1}{2} & \frac{1}{2} & 1 \\ J' & J & 0 \end{Bmatrix}$$

$$\times \sum_{j=-1}^{1} (R_1)_{NL}^{j} \left[N+L+j+1\right]^{-1} \delta_{N',N+j} \tag{F.36}$$

$$\left\langle \Pi' \left| \left[P^{(1)} \times I^{(2)} \right]_q^{(K)} \right| \Pi \right\rangle = 3\sqrt{5} \, (-1)^{F_t'+F_t-M_{F_t}'+F'+J+K} \left\langle N' \, L' \left\| P^{(1)} \right\| N \, L \right\rangle$$

$$\times \left[(2F_t+1)\left(2F_t'+1\right)(2F+1)\left(2F'+1\right)\right]^{\frac{1}{2}}$$

$$\times \left[(2J+1)\left(2J'+1\right)(2K+1)\right]^{\frac{1}{2}} \begin{pmatrix} F_t' & K & F_t \\ -M_{F_t}' & q & M_{F_t} \end{pmatrix}$$

$$\times \begin{Bmatrix} F' & F_t' & \frac{1}{2} \\ F_t & F & K \end{Bmatrix} \begin{Bmatrix} L' & L & 1 \\ J' & J & 2 \\ F' & F & K \end{Bmatrix} \begin{Bmatrix} 1 & J' & \frac{1}{2} \\ J & 1 & 2 \end{Bmatrix} \tag{F.37}$$

$$\begin{aligned}\left\langle \Pi' \left| \left[P^{(1)} \times D^{(2)} \right]^{(K)}_q \right| \Pi \right\rangle &= 3\sqrt{5}\,(-1)^{F'_t+F_t-M'_{F_t}+F'+\frac{1}{2}+K} \left\langle N'\,L' \left\| P^{(1)} \right\| N\,L \right\rangle \\ &\times \left[(2F_t+1)\left(2F'_t+1\right)(2F+1)\left(2F'+1\right) \right]^{\frac{1}{2}} \\ &\times \left[(2J+1)\left(2J'+1\right)(2K+1) \right]^{\frac{1}{2}} \begin{pmatrix} F'_t & K & F_t \\ -M'_{F_t} & q & M_{F_t} \end{pmatrix} \\ &\times \begin{Bmatrix} F' & F'_t & \frac{1}{2} \\ F_t & F & K \end{Bmatrix} \begin{Bmatrix} L' & L & 1 \\ J' & J & 2 \\ F' & F & K \end{Bmatrix} \begin{Bmatrix} 1 & 1 & 1 \\ \frac{1}{2} & \frac{1}{2} & 1 \\ J' & J & 2 \end{Bmatrix} \end{aligned} \tag{F.38}$$

$$\begin{aligned}\left\langle \Pi' \left| P^{(1)}_0 \left(I^{(1)} \cdot S^{(1)}_{\mathrm{h}} \right) \right| \Pi \right\rangle &= \delta_{M_{F_t} M'_{F_t}}\, 9\,(-1)^{F'_t+F_t-M_{F_t}+F'+\frac{1}{2}} \left\langle N'\,L' \left\| P^{(1)} \right\| N\,L \right\rangle \\ &\times \left[(2F_t+1)\left(2F'_t+1\right)(2F+1)\left(2F'+1\right) \right]^{\frac{1}{2}} \\ &\times \left[(2J+1)\left(2J'+1\right) \right]^{\frac{1}{2}} \begin{pmatrix} F'_t & 1 & F_t \\ -M_{F_t} & 0 & M_{F_t} \end{pmatrix} \\ &\times \begin{Bmatrix} F' & F'_t & \frac{1}{2} \\ F_t & F & 1 \end{Bmatrix} \begin{Bmatrix} L' & L & 1 \\ J' & J & 0 \\ F' & F & 1 \end{Bmatrix} \begin{Bmatrix} 1 & 1 & 1 \\ \frac{1}{2} & \frac{1}{2} & 1 \\ J' & J & 0 \end{Bmatrix} \end{aligned} \tag{F.39}$$

F.2 Reduced matrix elements

We now give the values of the reduced matrix elements of the form $\left\langle N'\,L' \left\| P^{(2)} \right\| N\,L \right\rangle$. We use the abbreviation $I_{N'\,L';N\,L}$ for the integral

$$\begin{aligned} I_{N'\,L';N\,L} &= \int_0^\infty \mathrm{d}r\, U_{N'L'}(r)\, U_{NL}(r) \\ &= 2\left[\frac{N'!N!\,(N'+2L'+1)!\,(N+2L+1)!}{(N'+L'+1)\,(N+L+1)} \right]^{\frac{1}{2}} \\ &\quad \times \sum_{k=0}^{N'} \sum_{j=0}^{N} \frac{(k+j+L+L')!}{k!j!\,(N'-k)!\,(N-j)!} \, \frac{(-1)^{k+j}}{(k+2L'+1)!\,(j+2L+1)!} \end{aligned} \tag{F.40}$$

with $\alpha = 1$. The functions of the form $(R_1)^j_{NL}$ are taken from the recursion relations of the Coulomb-Sturmian functions in Appendix E.

$$
\begin{aligned}
\left\langle N'\,L' \left\| P^{(2)} \right\| N\,L \right\rangle &= \delta_{L',L+2}\,\frac{3}{2}\left[\frac{(2L+4)\,(2L+2)}{(2L+3)}\right]^{\frac{1}{2}} \\
&\quad \times \left[\sum_{j=-2}^{2}\Big(-\left(R_2\right)^{j}_{NL}-\delta_{j0}L\,(2L+3)\Big)\,I_{N'\,L+2;\,N+j\,L}\right. \\
&\qquad \left.+\sum_{j=-1}^{1}\Big((2L+3)\left(RP_1\right)^{j}_{NL}+2\,(N+L+1)\left(R_1\right)^{j}_{NL}\Big)\,I_{N'\,L+2;\,N+j\,L}\right] \\
&\quad + \delta_{L',L}\,\left(-\sqrt{3}\right)\left[\frac{L\,(2L+1)\,(2L+2)}{(2L+3)\,(2L-1)}\right]^{\frac{1}{2}} \\
&\quad \times \left[2\delta_{NN'}-\sum_{j=-1}^{1}\left(R_1\right)^{j}_{NL}\left[N+L+j+1\right]^{-1}\delta_{N',N+j}\right] \\
&\quad + \delta_{L',L-2}\,\frac{3}{2}\left[\frac{(2L)\,(2L-2)}{(2L-1)}\right]^{\frac{1}{2}} \\
&\quad \times \left[\sum_{j=-2}^{2}\Big(-\left(R_2\right)^{j}_{NL}+\delta_{j0}\left(1-L-2L^2\right)\Big)\,I_{N'\,L-2;\,N+j\,L}\right. \\
&\qquad \left.+\sum_{j=-1}^{1}\Big((1-2L)\left(RP_1\right)^{j}_{NL}+2\,(N+L+1)\left(R_1\right)^{j}_{NL}\Big)\,I_{N'\,L-2;\,N+j\,L}\right]
\end{aligned}
\tag{F.41}
$$

$$
\begin{aligned}
\left\langle N'\,L' \left\| X^{(2)} \right\| N\,L \right\rangle &= \delta_{L',L+2}\,\frac{3}{2}\,\frac{1}{(L+1)\,(L+2)}\left[\prod_{j=1}^{5}(2L+j)\right]^{\frac{1}{2}} \\
&\quad \times \left[\sum_{j=-5}^{1}\frac{\left(R_1LN_2\right)^{j\,2}_{NL0}}{(N+L+j+3)}\,\delta_{N',N+j}\right] \\
&\quad + \delta_{L',L}\,\left(-\sqrt{\frac{3}{8}}\right)\frac{1}{L\,(L+1)}\left[\prod_{j=-1}^{3}(2L+j)\right]^{\frac{1}{2}}
\end{aligned}
$$

$$
\begin{aligned}
&\times \left[\sum_{j=-3}^{3} \frac{3\,(R_1 L N_2)^{j\,0}_{NL0} - (R_3)^{j}_{NL}}{(N+L+j+1)}\, \delta_{N',N+j} \right] \\
&+ \delta_{L',L-2}\, \frac{3}{2}\, \frac{1}{L\,(L-1)} \left[\prod_{j=-3}^{1} (2L+j) \right]^{\frac{1}{2}} \\
&\times \left[\sum_{j=-1}^{5} \frac{(R_1 L N_2)^{j\,-2}_{NL0}}{(N+L+j-1)}\, \delta_{N',N+j} \right]
\end{aligned}
\tag{F.42}
$$

$$
\begin{aligned}
\left\langle N'\,L' \left\| M^{(2)} \right\| N\,L \right\rangle &= \delta_{L',L+2}\, \frac{3}{2} \left[\frac{(2L+4)\,(2L+2)}{(2L+3)} \right]^{\frac{1}{2}} \\
&\times \left[\sum_{j=-3}^{3} (R_3 P_1)^{j}_{NL}\, I_{N'\,L+2;\,N+j\,L} + \sum_{j=-2}^{2} \Big(-L\,(R_2)^{j}_{NL} \Big)\, I_{N'\,L+2;\,N+j\,L} \right] \\
&+ \delta_{L',L} \left(-\frac{\sqrt{3}}{2} \right) \left[\frac{L\,(2L+1)\,(2L+2)}{(2L+3)\,(2L-1)} \right]^{\frac{1}{2}} \\
&\times \left[\sum_{j=-2}^{2} \frac{2\,(R_2 P_1)^{j}_{NL}}{(N+L+j+1)}\, \delta_{N',N+j} + \sum_{j=-1}^{1} \frac{3\,(R_1)^{j}_{NL}}{(N+L+j+1)}\, \delta_{N',N+j} \right] \\
&+ \delta_{L',L-2}\, \frac{3}{2} \left[\frac{(2L)\,(2L-2)}{(2L-1)} \right]^{\frac{1}{2}} \\
&\times \left[\sum_{j=-3}^{3} (R_3 P_1)^{j}_{NL}\, I_{N'\,L-2;\,N+j\,L} + \sum_{j=-2}^{2} (L+1)\,(R_2)^{j}_{NL}\, I_{N'\,L-2;\,N+j\,L} \right]
\end{aligned}
\tag{F.43}
$$

$$
\left\langle N'\,L' \left\| P^{(1)} \right\| N\,L \right\rangle = \delta_{L',L+1}\, (-i) \left[\frac{(2L+3)\,(2L+1)}{L+1} \right]^{\frac{1}{2}} \left[\sum_{j=-1}^{1} \sum_{k=-2}^{0} (L_1)^{k,1}_{N',L+1} \right.
$$

$$\times \left\{ (RP_1)^{j}_{N,L}\,(N_1)^{1}_{L,0} + \delta_{0j}\,(D_1)^{1}_{L,0} \right\} I_{N'+k\,L+2;\,N+j\,L} \Bigg]$$

$$+\,\delta_{L',L-1}\;(+i)\left[\frac{(2L+1)\,(2L-1)}{L}\right]^{\frac{1}{2}} \Bigg[\sum_{j=-1}^{1}\sum_{k=-2}^{0} (L_1)^{k,1}_{N+j,L}$$

$$\times \left\{ (RP_1)^{j}_{N,L}\,(N_1)^{-1}_{L,0} + \delta_{0j}\,(D_1)^{-1}_{L,0} \right\} I_{N'\,L-1;\,N+j+k\,L+1} \Bigg] \tag{F.44}$$

$$\left\langle N'\,L' \left\| R^{(1)} \right\| N\,L \right\rangle = \delta_{L',L+1}\left[\frac{(2L+3)\,(2L+2)\,(2L+1)}{2\,(L+1)}\right]^{\frac{1}{2}}\left[\sum_{j=-3}^{1}\frac{(LN_1)^{j\,1}_{NL0}}{(N+L+j+2)}\,\delta_{N',N+j}\right]$$

$$-\,\delta_{L',L-1}\left[\frac{(2L+1)\,(2L)\,(2L-1)}{2L}\right]^{\frac{1}{2}}\left[\sum_{j=-1}^{3}\frac{(LN_1)^{j\,-1}_{NL0}}{(N+L+j)}\,\delta_{N',N+j}\right] \tag{F.45}$$

Bibliography

[1] J. A. Frenkel. On the transformation of light into heat in solids. I. *Phys. Rev.* 37, 17 (1931).

[2] J. A. Frenkel. On the transformation of light into heat in solids. II. *Phys. Rev.* 37, 1276 (1931).

[3] J. A. Frenkel. On the absorption of light and the trapping of electrons and positive holes in crystalline dielectrics. *Phys. Z. Sowjetunion* 9, 533 (1936).

[4] R. Peierls. Zur Theorie der Absorptionsspektren fester Körper. *Annalen der Physik* 405, 905 (1932).

[5] G. H. Wannier. The structure of electronic excitation levels in insulating crystals. *Phys. Rev.* 52, 191 (1937).

[6] E. F. Gross and I. A. Karryjew. The optical spectrum of the exciton. *Dokl. Akad. Nauk. SSSR* 84, 471 (1952).

[7] R. S. Knox. *Theory of excitons*, volume 5 of *Solid State Physics Supplement*. Academic, New York (1963).

[8] M. Baldo and V. Stojanović. Optical switching: Excitonic interconnects. *Nature Photon* 3, 558 (2009).

[9] N. F. Mott. Conduction in polar crystals. II. The conduction band and ultra-violet absorption of alkali-halide crystals. *Trans. Faraday Soc.* 34, 500 (1938).

[10] C. G. Kuper and G. D. Whitefield (editors). *Polarons and Excitons.* Oliver and Boyd, Edinburgh (1963).

[11] R. S. Knox and D. I. Dexter. *Excitons.* Wiley, New York (1981).

[12] C. F. Klingshirn. *Semiconductor Optics.* Springer, Berlin, third edition (2007).

[13] M. A. Lampert. Mobile and immobile effective-mass-particle complexes in nonmetallic solids. *Phys. Rev. Lett.* 1, 450 (1958).

[14] S. A. Moskalenko. The theory of Mott exciton in alkali-halide crystals. *Opt. Spektrosk.* 5, 147 (1958).

[15] C. Klingshirn and H. Haug. Optical properties of highly excited direct gap semiconductors. *Phys. Rep.* 70, 315 (1981).

[16] E. L. Rashba and M. D. Sturge. *Excitons.* North-Holland, Amsterdam (1982).

[17] B. Hönerlage, R. Lévy, J. B. Grun, C. Klingshirn, and K. Bohnert. The dispersion of excitons, polaritons and biexcitons in direct-gap semiconductors. *Phys. Rep.* 124, 161 (1985).

[18] K. F. Mak, K. He, C. Lee, G. H. Lee, J. Hone, T. F. Heinz, and J. Shan. Tightly bound trions in monolayer MoS_2. *Nature Mater.* 12, 207 (2013).

[19] A. G. Steele, W. G. McMullan, and M. L. W. Thewalt. Discovery of polyexcitons. *Phys. Rev. Lett.* 59, 2899 (1987).

[20] R. Hull, C. Jagadish, R. M. Osgood Jr., J. Parisi, Z. Wang, and H. Warlimont (editors). *Zinc Oxide: From Fundamental Properties Towards Novel Applications*, volume 120 of *Springer Series in Materials Science.* Springer, Berlin (2010).

[21] A. Imamoğlu, R. J. Ram, S. Pau, and Y. Yamamoto. Nonequilibrium condensates and lasers without inversion: Exciton-polariton lasers. *Phys. Rev. A* 53, 4250 (1996).

[22] A. Kavokin and G. Malpuech. *Cavity Polaritons.* Elsevier, Amsterdam (2003).

[23] L. V. Butov. Solid-state physics: A polariton laser. *Nature* 447, 540 (2007).

[24] Christian Schneider, A. Rahimi-Iman, N. Young Kim, J. Fischer, I. G. Savenko, M. Amthor, M. Lermer, A. Wolf, L. Worschech, V. D. Kulakovskii, I. A. Shelykh, M. Kamp, S. Reitzenstein, A. Forchel, and Y. Yamamoto S. Höfling. An electrically pumped polariton laser. *Nature* 497, 348 (2013).

[25] H. Stolz, R. Schwartz, F. Kieseling, S. Som, M. Kaupsch, S. Sobkowiak, D. Semkat, N. Naka, T. Koch, and H. Fehske. Condensation of excitons in Cu_2O at ultracold temperatures: Experiment and theory. *New J. Phys.* 14, 105007 (2012).

[26] J. M. Blatt, K. W. Boer, and W. Brandt. Bose–Einstein condensation of excitons. *Phys. Rev.* 126, 1691 (1962).

[27] S. A. Moskalenko. Reversible optico-hydrodynamic phenomena in a nonideal exciton gas. *Sov. Phys. Solid State* 4, 199 (1962).

[28] L. V. Keldysh and A. N. Kozlov. Collective properties of excitons in semiconductors. *Sov. Phys. JETP-USSR* 27, 521 (1968).

[29] J. D. Plumhof, T. Stöferle, L. Mai, U. Scherf, and R. F. Mahrt. Room-temperature Bose–Einstein condensation of cavity exciton–polaritons in a polymer. *Nature Mat.* 13, 247 (2014).

[30] T. Kazimierczuk, D. Fröhlich, S. Scheel, H. Stolz, and M. Bayer. Giant Rydberg excitons in the copper oxide Cu_2O. *Nature* 514, 343 (2014).

[31] M. Aßmann, J. Thewes, D. Fröhlich, and M. Bayer. Quantum chaos and breaking of antiunitary symmetries in Rydberg excitons. *Nature Mater.* 15, 741 (2016).

[32] M. Freitag, J. Heckötter, M. Bayer, and M. Aßmann. The role of phonons in the quantum chaos of Rydberg excitons. *Phys. Rev. B* 95, 155204 (2017).

[33] F. Schweiner, J. Main, and G. Wunner. Linewidths in excitonic absorption spectra of cuprous oxide. *Phys. Rev. B* 93, 085203 (2016).

[34] P. Grünwald, M. Aßmann, J. Heckötter, D. Fröhlich, M. Bayer, H. Stolz, and S. Scheel. Signatures of quantum coherence in Rydberg excitons. *Phys. Rev. Lett.* 117, 133003 (2016).

[35] M. Feldmaier, J. Main, F. Schweiner, H. Cartarius, and G. Wunner. Rydberg systems in parallel electric and magnetic fields: an improved method for finding exceptional points. *J. Phys. B: At. Mol. Opt. Phys.* 49, 144002 (2016).

[36] J. Thewes, J. Heckötter, T. Kazimierczuk, M. Aßmann, D. Fröhlich, M. Bayer, M. A. Semina, and M. M. Glazov. Observation of high angular momentum excitons in cuprous oxide. *Phys. Rev. Lett.* 115, 027402 (2015). And Supplementary Material.

[37] F. Schöne, S. O. Krüger, P. Grünwald, H. Stolz, S. Scheel, M. Aßmann, J. Heckötter, J. Thewes, D. Fröhlich, and M. Bayer. Deviations of the exciton level spectrum in Cu_2O from the hydrogen series. *Phys. Rev. B* 93, 075203 (2016).

[38] F. Schweiner, J. Main, M. Feldmaier, G. Wunner, and Ch. Uihlein. Impact of the valence band structure of Cu_2O on excitonic spectra. *Phys. Rev. B* 93, 195203 (2016).

[39] F. Schweiner, J. Main, G. Wunner, M. Freitag, J. Heckötter, Ch. Uihlein, M. Aßmann, D. Fröhlich, and M. Bayer. Magnetoexcitons in cuprous oxide. *Phys. Rev. B* 95, 035202 (2017).

[40] F. Schweiner, J. Main, and G. Wunner. Magnetoexcitons break antiunitary symmetries. *Phys. Rev. Lett.* 118, 046401 (2017).

[41] J. Heckötter, M. Freitag, D. Fröhlich, M. Aßmann, M. Bayer, M. A. Semina, and M. M. Glazov. High resolution study of the yellow excitons in Cu_2O subject to an electric field. *Phys. Rev. B* 95, 035210 (2017).

[42] S. Zielińska-Raczyńska, D. Ziemkiewicz, and G. Czajkowski. Magnetooptical properties of Rydberg excitons: center-of-mass quantization approach. *Phys. Rev. B* 95, 075204 (2017).

[43] F. Schweiner, J. Main, G. Wunner, and Ch. Uihlein. K dependent exchange interaction of the $1S$ exciton in Cu_2O. *Phys. Rev. B* 94, 115201 (2016).

[44] S. Zielińska-Raczyńska, G. Czajkowski, and D. Ziemkiewicz. Optical properties of Rydberg excitons and polaritons. *Phys. Rev. B* 93, 075206 (2016).

[45] S. Zielińska-Raczyńska, D. Ziemkiewicz, and G. Czajkowski. Electro-optical properties of Rydberg excitons. *Phys. Rev. B* 94, 045205 (2016).

[46] F. Schweiner, J. Main, G. Wunner, and Ch. Uihlein. The even exciton series in Cu_2O. *Phys. Rev. B* 95, 195201 (2017).

[47] F. Schweiner, J. Main, and G. Wunner. GOE-GUE-Poisson transitions in the nearest neighbor spacing distribution of magnetoexcitons. *Phys. Rev. E* 95, 062205 (2017).

[48] F. Schweiner, P. Rommel, J. Main, and G. Wunner. Exciton-phonon interaction breaking all antiunitary symmetries in external magnetic fields. *Phys. Rev. B* 96, 035207 (2017).

[49] F. Schweiner, J. Ertl, J. Main, G. Wunner, and Ch. Uihlein. Exciton-polaritons in cuprous oxide: Theory and comparison with experiment. *Phys. Rev. B* 96, 245202 (2017).

[50] F. Schweiner, J. Laturner, J. Main, and G. Wunner. Crossover between the Gaussian orthogonal ensemble, the Gaussian unitary ensemble, and Poissonian statistics. *Phys. Rev. E* 96, 052217 (2017).

[51] F. Schöne, H. Stolz, and N. Naka. Phonon-assisted absorption of excitons in Cu_2O. *Phys. Rev. B* 96, 115207 (2017).

[52] M. Kurz, P. Grünwald, and S. Scheel. Excitonic giant-dipole potentials in cuprous oxide. *Phys. Rev. B* 95, 245205 (2017).

[53] D. Semkat, S. Sobkowiak, F. Schöne, H. Stolz, Th. Koch, and H. Fehske. Multicomponent exciton gas in cuprous oxide: cooling behavior and the role of Auger decay. *J. Phys. B: At. Mol. Opt. Phys.* 50, 204001 (2017).

[54] T. Stielow, S. Scheel, and M. Kurz. A Green's function approach to giant-dipole systems. *arXiv:1705.10527* (2017).

[55] J. Heckötter, M. Freitag, D. Fröhlich, M. Aßmann, M. Bayer, M. A. Semina, and M. M. Glazov. Scaling laws of Rydberg excitons. *Phys. Rev. B* 96, 125142 (2017).

[56] J. Heckötter, M. Freitag, D. Fröhlich, M. Aßmann, M. Bayer, P. Grünwald, F. Schöne, D. Semkat, H. Stolz, and S. Scheel. Rydberg excitons in the presence of an ultralow-density electron-hole plasma. *arXiv:1709.00891* (2017).

[57] S. O. Krüger and S. Scheel. Waveguides for Rydberg excitons in Cu_2O from strain traps. *arXiv:1711.06639* (2017).

[58] M. Saffman, T. G. Walker, and K. Mølmer. Quantum information with Rydberg atoms. *Rev. Mod. Phys.* 82, 2313 (2010).

[59] J. B. Balewski, A. T. Krupp, A. Gaj, D. Peter, H. P. Büchler, R. Löw, S. Hofferberth, and T. Pfau. Coupling a single electron to a Bose-Einstein condensate. *Nature* 502, 664 (2013).

[60] S. Höfling and A. Kavokin. Solid-state physics: A historic experiment redesigned. *Nature* 514, 313 (2014).

[61] R. Huber, B. A. Schmid, Y. R. Shen, D. S. Chemla, and R. A. Kaindl. Stimulated terahertz emission form intraexcitonic transitions in Cu_2O. *Phys. Rev. Lett.* 96, 017402 (2006).

[62] R. J. Elliott. Intensity of optical absorption by excitons. *Phys. Rev.* 108, 1384 (1957).

[63] G. Dresselhaus. Effective mass approximation for excitons. *J. Phys. Chem. Solids* 1, 14 (1956).

[64] S. Nikitine. Experimental investigations of exciton spectra in ionic crystals. *Phil. Mag.* 4, 1 (1959).

[65] S. Nikitine. Exciton spectra in semiconductors and ionic compounds. In *Progress in Semiconductors*, edited by A. F. Gibson, R. E. Burgess, and F. A. Kröger, volume 6, p. 233. Wiley, New York (1962).

[66] E. F. Gross. Spektr vozbuždenija ėksitonov v tverdom tele. *Izv. Akad. Nauk. SSSR, Ser. Fiz.* 20, 89 (1956).

[67] E. F. Gross. Optical spectrum of excitons in the crystal lattice. *Il Nuovo Cimento Suppl.* 3, 672 (1956).

[68] E. F. Gross. Excitons and their motion in crystal lattices. *Sov. Phys. Usp.* 5, 195 (1962).

[69] M. Ueta. Survey of experiments on the exciton. *Prog. Theor. Phys. Suppl.* 12, 40 (1959).

[70] T. P. McLean. The absorption edge spectrum of semiconductors. In *Progress in Semiconductors*, edited by A. F. Gibson, volume 5, p. 54. Wiley, New York (1961).

[71] V. T. Agekyan. Spectroscopic properties of semiconductor crystals with direct forbidden energy gap. *phys. stat. sol. (a)* 43, 11 (1977).

[72] Ch. Uihlein, D. Fröhlich, and R. Kenklies. Investigation of exciton fine structure in Cu_2O. *Phys. Rev. B* 23, 2731 (1981).

[73] Y. Toyozawa. Theory of line-shapes of the exciton absorption bands. *Prog. Theor. Phys.* 20, 53 (1958).

[74] Y. Toyozawa. Interband effect of lattice vibrations in the exciton absorption spectra. *J. Phys. Chem. Solids* 25, 59 (1964).

[75] Y. Toyozawa. Further contribution to the theory of the line-shape of the exciton absorption band. *Prog. Theor. Phys.* 27, 89 (1962).

[76] Y. Toyozawa. On the dynamical behavior of an exciton. *Suppl. Prog. Theor. Phys.* 12, 111 (1959).

[77] A. Baldereschi and N. O. Lipari. Energy levels of direct excitons in semiconductors with degenerate bands. *Phys. Rev. B* 3, 439 (1971).

[78] A. Baldereschi and N. O. Lipari. Cubic contributions to the spherical model of shallow acceptor states. *Phys. Rev. B* 9, 1525 (1974).

[79] A. Baldereschi and N. O. Lipari. Spherical model of shallow acceptor states in semiconductors. *Phys. Rev. B* 8, 2697 (1973).

[80] N. O. Lipari and M. Altarelli. Theory of indirect excitons in semiconductors. *Phys. Rev. B* 15, 4883 (1977).

[81] M. Altarelli and N. O. Lipari. Exciton dispersion in semiconductors with degenerate bands. *Phys. Rev. B* 15, 4898 (1977).

[82] G. Dasbach, D. Fröhlich, H. Stolz, R. Klieber, D. Suter, and M. Bayer. Wave-vector-dependent exciton exchange interaction. *Phys. Rev. Lett.* 91, 107401 (2003).

[83] G. Dasbach, D. Fröhlich, R. Klieber, D. Suter, M. Bayer, and H. Stolz. Wave-vector-dependent exchange interaction and its relevance for the effective exciton mass in Cu_2O. *Phys. Rev. B* 70, 045206 (2004).

[84] G. Dasbach, D. Fröhlich, H. Stolz, R. Klieber, D. Suter, and M. Bayer. Anisotropic effective exciton mass in Cu_2O. *phys. stat. sol (c)* 2, 886 (2005).

[85] U. Rössler. *Solid State Theory.* Springer, Berlin, second edition (2009).

[86] S. Hunklinger. *Festkörperphysik.* Oldenbourg, München (2007).

[87] M. Jörger. *Terahertzspektroskopie an* Cu_2O*: Intraexzitonische und phononische Übergänge.* Ph.D. thesis, Universität Karlsruhe (2004).

[88] Ch. Kittel. *Introduction to Solid State Physics.* Wiley, New York, 7th edition (1996).

[89] G. F. Koster. Space Groups and their Representations. In *Solid State Physics*, edited by F. Seitz and D. Turnbull, volume 5, pp. 173–256. Academic Press, New York (1957).

[90] G. F. Koster, J. O. Dimmock, R. G. Wheeler, and H. Statz. *Properties of the Thirty-Two Point Groups.* M.I.T. Press, Cambridge, MA (1963).

[91] W. Ludwig and L. Falter. *Symmetries in Physics: Group Theory Applied to Physical Problems*, volume 64 of *Springer Series in Solid State Sciences.* Springer, Berlin (1988).

[92] G. Burns and A. M. Glazer. *Space Groups for Solid State Scientists.* Academic Press, Boston, second edition (1990).

[93] R. von Baltz. Dielectric Description of Semiconductors: From Maxwell- to Semiconductor-Bloch-Equations. In *Ultrafast Dynamics of Quantum Systems: Physical Processes and Spectroscopic Techniques*, edited by B. Di Bartolo, volume 372 of *NATO ASI Ser. B*, pp. 323–356. Plenum Press, New York (1998).

[94] O. Madelung. *Introduction to Solid-State Theory*, volume 2 of *Springer Series in Solid-State Sciences.* Springer, Berlin (1996).

[95] W. Nolting. *Grundkurs Theoretische Physik 3: Elektrodynamik.* Springer, Berlin, 8th edition (2007).

[96] C. Hamaguchi. *Basic Semiconductor Physics.* Springer, Berlin (2001).

[97] O. Madelung and U. Rössler (editors). *Landolt-Börnstein*, volume 17 a to i, 22 a and b, 41 A to D of *New Series, Group III.* Springer, Berlin (1982-2001).

[98] D. J. Thouless. *Quantum Mechanics of Many-Body Systems.* Academic Press, New York (1961).

[99] D. Pines (editor). *The Many-Body Problem.* Benjamin, New York (1961).

[100] R. Kubo and T. Nagamiya. *Solid State Physics.* McGraw-Hill, New York (1969).

[101] J. M. Ziman. *Principles of the Theory of Solids.* Cambridge University Press, Cambridge (1969).

[102] W. Ludwig. *Festkörperphysik.* Akademische Verlagsgesellschaft, Wiesbaden, second edition (1978).

[103] H. Jones. *The Theory of Brillouin Zones and Electronic Structure in Crystals.* North-Holland, Amsterdam (1975).

[104] P. Fulde. *Electron Correlations in Molecules*, volume 100 of *Springer Series in Solid State Sciences.* Springer, Berlin, third edition (1995).

[105] A. C. Hewson. *The Kondo Problem to Heavy Fermions.* Cambridge Studies in Magnetism. Cambridge University Press, Cambridge (1993).

[106] W. Jones and N. H. March. *Theoretical Solid State Physics, Vol. 1: Perfect Lattice in Equilibrium, Vol. 2: Non-Equilibrium and Disorder.* Wiley, London (1973).

[107] R. M. Dreizler and E. K. Gross. *Density Functional Theory: An Approach to the Quantum Many-Body Problem.* Springer, Berlin (1990).

[108] M. Levy. Universal variational functionals of electron densities, first-order density matrices, and natural spin-orbitals and solution of the v-representability problem. *Proc. Natl. Acad. Sci. USA* 76, 6062 (1979).

[109] H. Eschrig. *The Fundamentals of Density Functional Theory.* Teubner Verlagsgesellschaft, Stuttgart (1996).

[110] G. F. Guiliani and G. Vignale. *Quantum Theory of the Electron Liquid.* Cambridge University Press, New York (2005).

[111] P. Hohenberg and W. Kohn. Inhomogeneous electron gas. *Phys. Rev.* 136B, 864 (1964).

[112] W. Kohn and L. J. Sham. Self-consistent equations including exchange and correlation effects. *Phys. Rev.* 140A, 1133 (1965).

[113] W. A. Harrison. *Pseudopotentials in the Theory of Metals.* W. A. Benjamin, New York (1966).

[114] M. L. Cohen and V. Heine. The Fitting of Pseudopotentrials to Experimental Data and Their Subsequent Application. In *Solid State Physics*, edited by H. Ehrenreich, F. Seitz, and D. Turnbull, volume 24, pp. 37–248. Academic, New York (1970).

[115] D. Vanderbilt. Soft self-consistent pseudopotentials in a generalized eigenvalue formalism. *Phys. Rev. B* 41, 7892 (1990).

[116] N. Troullier and J. L. Martins. Efficient pseudopotentials for plane-wave calculations. *Phys. Rev. B* 43, 1993 (1991).

[117] A. Sommerfeld. Zur Elektronentheorie der Metalle auf Grund der Fermi'schen Statistik. *Z. Physik* 47, 1 (1928).

[118] A. H. Wilson. The theory of electronic semi-conductors. *Proc. Roy. Soc. A* 113, 458 (1931).

[119] C. Skierbiszewski, P. Perlin, P. Wisniewski, W. Knap, T. Suski, W. Walukiewicz, W. Shan, K. M. Yu, J. W. Ager, E. E. Haller, J. F. Geisz, and J. M. Olson. Large, nitrogen-induced increase of the electron effective mass in $\mathrm{In_yGa_{1-y}N_xAs_{1-x}}$. *Appl. Phys. Lett.* 76, 2409 (2000).

[120] E. O. Kane. The $\mathrm{k} \cdot \mathrm{p}$ Method. In *Semiconductors and Semimetals*, edited by R. K. Willardson and A. C. Beer, volume 1, pp. 75–101. Academic, New York (1966).

[121] W. Shockley. Energy band structures in semiconductors. *Phys. Rev.* 78, 173 (1950).

[122] E. O. Kane. Band structure of indium antimonide. *J. Phys. Chem. Solids* 1, 249 (1957).

[123] J. S. Blakemore. *Semiconductor Statistics.* Dover Publication, Dover (1987).

[124] B. D. Malone and M. L. Cohen. Quasiparticle semiconductor band structures including spin–orbit interactions. *J. Phys.: Condens. Matter* 25, 105503 (2013).

[125] R. J. Elliott. Theory of the effect of spin-orbit coupling on magnetic resonance in some semiconductors. *Phys. Rev.* 96, 266 (1954).

[126] J. M. Luttinger. Quantum theory of cyclotron resonance in semiconductors: General theory. *Phys. Rev.* 102, 1030 (1956).

[127] Y. Toyozawa. *Optical processes in solids.* Cambridge University Press, Cambridge (2003).

[128] O. Schütz and J. Treusch. Summability of the perturbation series of excitonic exchange, CuCl as an example. *Solid State Commun.* 13, 1155 (1973).

[129] P. Y. Yu and M. Cardona. *Fundamentals of Semiconductors.* Springer, Berlin, third edition (2005).

[130] W. Schäfer and M. Wegener. *Semiconductor Optics and Transport Phenomena.* Springer, Berlin (2002).

[131] Y. Toyozawa. *Optical Processes in Solids.* Cambridge University Press, Cambridge (2003).

[132] E. Rebhan. *Theoretische Physik: Relativistische Quantenmechanik, Quantenfeldtheorie und Elementarteilchentheorie.* Springer, Berlin (2010).

[133] F. Wooten. *Optical Properties of Solids.* Academic Press, New York (1972).

[134] H. Kuzmany. *Festkörperspektroskopie.* Springer, Berlin (1990).

[135] W. Greiner. *Theoretische Physik*, volume 1-10. Verlag Harri Deutsch, Frankfurt (1985).

[136] P. Meystre and M. Sargent III. *Elements of Quantum Optics.* Springer, Berlin, second edition (1992).

[137] I. Abraham and J. A. Levenson. Quantum Noise in Parametric Amplification. In *Nonlinear Spectroscopy of Solids: Advances and Application*, edited by B. Di Bartolo, volume 339 of *NATO ASI Ser. B*, pp. 251–287. Plenum Press, New York (1994).

[138] B. Bowlby. Definition of Coherence. In *Nonlinear Spectroscopy of Solids: Advances and Application*, edited by B. Di Bartolo, volume 339 of *NATO ASI Ser. B*, pp. 385–394. Plenum Press, New York (1994).

[139] H. Haug and S. W. Koch. *Quantum Theory of the Optical and Electronic Properties of Semiconductors.* World Scientific, Singapore, fifth edition (2009).

[140] W. C. Tait and R. L. Weiher. Contributions of scattering of polaritons by phonons to emission of radiation by solids. *Phys. Rev.* 178, 1404 (1969).

[141] J. J. Hopfield. Theory of the contibution of excitons to the complex dielectric constant of crystals. *Phys. Rev.* 112, 1555 (1958).

[142] N. Peyghambarian, S. W. Koch, and A. Mysyrowicz. *Introduction to Semiconductor Optics.* Prentice Hall, Englewood Cliffs (1993).

[143] C. I. Ivanov, H. Barentzen, and M. D. Girardeau. On the theory of dense exciton systems. *Physica A* 140, 612 (1987).

[144] M. Kira, F. Jahnke, S. W. Koch, J. D. Berger, D. V. Wick, T. R. Nelson Jr., G. Khitrova, and H. M. Gibbs. Quantum theory of nonlinear semiconductor microcavity luminescence explaining "boser" experiments. *Phys. Rev. Lett.* 79, 5170 (1997).

[145] M. Combescot and O. Betbeder-Matibet. Scattering rates and lifetime of exact and boson excitons. *Phys. Rev. Lett.* 93, 016403 (2004).

[146] H. Haug and E. Hanamura. Condensation effects of excitons. *Phys. Rep.* 33C, 209 (1977).

[147] L. Hrivnák. Die mittlere freie Weglänge von Exzitonen in Gegenwart von Dislokationen. *Czech. J. Phys.* 7, 390 (1957).

[148] Z. S. Kachlivskii. Scattering of a nonlocalized exciton at F-centers. *Soviet Phys. Solid State* 3, 361 (1961).

[149] Z. S. Kachlivskii. The classic scattering of a nonlocalized exciton by impurity centers. *Soviet Phys. Solid State* 3, 1554 (1962).

[150] Z. S. Kachlivskii. Elastic scattering of a nonlocalized exciton on U-centers. *Soviet Phys. Solid State* 3, 2091 (1962).

[151] Z. S. Kachlivskii. Scattering of free excitons by lattice defects of a molecular crystal. *Soviet Phys. Solid State* 3, 733 (1961).

[152] A. Mysyrowicz, D. Hulin, and E. Hanamura. Femtosecond Spectroscopy of Highly Excited Cu_2O. In *Ultrafast Phenomena VII*, edited by C. B. Harris, E. P. Ippen, G. A. Mourou, and A. H. Zewail, volume 53 of *Springer Series in Chemical Physics*, pp. 244–246. Springer, Berlin (1990).

[153] D. W. Snoke, D. Braun, and M. Cardona. Carrier thermalization in Cu_2O: Phonon emission by excitons. *Phys. Rev. B* 44, 2991 (1991).

[154] H. J. G. Meyer F. A. Kröger. The edge emission of ZnS, CdS and ZnO and its relation to the lattice vibrations of these solids. *Physica* 20, 1149 (1954).

[155] F. Seitz. Color centers in alkali halide crystals. II. *Rev. Mod. Phys.* 26, 7 (1954).

[156] P. R. Markworth, R. P. H. Chang, Y. Sun, G. K. Wong, and J. B. Ketterson. Epitaxial stabilization of orthorhombic cuprous oxide films on MgO(110). *J. Mat. Res.* 16, 914 (2001).

[157] K. Kawaguchi, R. Kita, M. Nishiyama, and T. Morishita. Molecular beam epitaxy growth of CuO and Cu_2O films with controlling the oxygen content by the flux ratio of Cu/O+. *J. Cryst. Growth* 143, 221 (1994).

[158] M. Göppert. *Infrarotspektroskopie an* CdS/ZnSe-*Heterostrukturen und am Volumenhalbleiter* Cu_2O. Ph.D. thesis, Universität Karlsruhe (2000).

[159] M. Ivanda, D. Waasmaier, A. Endriss, J. Ihringer, A. Kirfel, and W. Kiefer. Low-temperature anomalies of Cuprite observed by Raman spectroscopy and X-ray powder diffraction. *Journal of Raman Spectroscopy* 28, 487 (1997).

[160] A. Jolk. *Spektroskopische Untersuchungen an* Cu_2O. Diplomarbeit, Universität Karlsruhe (1997).

[161] P. Dawson, M. Hargreave, and G. Wilkinson. The dielectric and lattice vibration spectrum of cuprous oxide. *J. Phys. Chem. Solids* 34, 2201 (1973).

[162] G. M. Kavoulakis, Y.-C. Chang, and G. Baym. Fine structure of excitons in Cu_2O. *Phys. Rev. B* 55, 7593 (1997).

[163] G. Dasbach. *Spectroscopy of Polaritonic Excitations in Semiconductors.* Ph.D. thesis, Technische Universität Dortmund (2003).

[164] E. F. Gross and N. A. Karryev. Pogloshchenie sveta kristallom zakisi medi v infrakrasnoi i vidimoi chasti spektra. *Dokl. Akad. Nauk SSSR* 84, 261 (1952).

[165] M. Hayashi and K. Katsuki. Absorption spectrum of cuprous oxide. *J. Phys. Soc. Jpn.* 5, 381 (1950).

[166] M. Hayashi and K. Katsuki. Hydrogen-like absorption spectrum of cuprous oxide. *J. Phys. Soc. Jpn.* 7, 599 (1952).

[167] S. Nikitine. Excitons. In *Optical Properties of Solids*, edited by S. Nudelman and S. S. Mitra, pp. 197–238. Springer Science and Business Media, New York (1969).

[168] J. Robertson. Electronic structure and x-ray near-edge core spectra of Cu_2O. *Phys. Rev. B* 28, 3378 (1983).

[169] A. Abragam and B. Bleaney. *Electron Paramagnetic Resonance of Transition Ions.* Clarendon Press, Oxford (1970).

[170] C.J. Ballhausen. *Introduction to Liegand Field Theory.* McGraw-Hill Series in Advanced Chemistry. McGraw-Hill Book Company Inc., New York (1962).

[171] R. J. Elliott. Symmetry of excitons in Cu_2O. *Phys. Rev.* 124, 340 (1961).

[172] L. Kleinman and K. Mednick. Self-consistent energy bands of Cu_2O. *Phys. Rev. B* 21, 1549 (1980).

[173] J. Heckötter. *Stark-Effekt-Messungen an Rydberg Exzitonen in* Cu_2O. Master's thesis, Technische Universität Dortmund (2015).

[174] T. F. Gallagher. Rydberg atoms. *Rep. Prog. Phys.* 51, 143 (1988).

[175] G. Kuwabara, M. Tanaka, and H. Fukutani. Optical absorption due to paraexciton of Cu_2O. *Solid State Commun.* 21, 599 (1977).

[176] P. D. Bloch and C. Schwab. Direct evidence for phonon-assisted transitions to the 1s paraexciton level of the yellow exciton series in Cu_2O. *Phys. Rev. Lett.* 41, 514 (1978).

[177] L. Hanke, D. Fröhlich, A. L. Ivanov, P. B. Littlewood, and H. Stolz. LA Phonoritons in Cu_2O. *Phys. Rev. Lett.* 83, 4365 (1999).

[178] D. Fröhlich, A. Kulik, B. Uebbing, A. Mysyrowicz, V. Langer, H. Stolz, and W. von der Osten. Coherent propagation and quantum beats of quadrupole polaritons in Cu_2O. *Phys. Rev. Lett.* 67, 2343 (1991).

[179] D. Fröhlich, G. Dasbach, G. Baldassarri, Höger von Högersthal, M. Bayer, R. Klieber, D. Suter, and H. Stolz. High resolution spectroscopy of yellow 1s excitons in Cu_2O. *Solid State Commun.* 134, 139 (2005).

[180] D. Fröhlich, J. Brandt, C. Sandfort, M. Bayer, and H. Stolz. High resolution spectroscopy of excitons. *phys. stat. sol. (b)* 243, 2367 (2006).

[181] Y. Masumoto, Y. Unuma, Y. Tanaka, and S. Shionoya. Picosecond time of flight measurements of excitonic polariton in CuCl. *J. Phys. Soc. Jpn.* 47, 1844 (1979).

[182] J. Weiner, N. Caswell, P. Yu, and A. Mysyrowicz. Ortho to para-exciton conversion in Cu_2O: A subnanosecond time-resolved photoluminescence study. *Solid State Commun.* 46, 105 (1983).

[183] S. Denev and D. Snoke. Stress dependence of relaxation processes in Cu_2O. *Phys. Rev. B* 65, 085211 (2002).

[184] A. Jolk, M. Jörger, and C. Klingshirn. Exciton lifetime, Auger recombination, and exciton transport by calibrated differential absorption spectroscopy in Cu_2O. *Phys. Rev. B* 65, 245209 (2002).

[185] D. Snoke, D. Trauernicht, and J. Wolfe. Mechanism of orthoexciton-to-paraexciton conversion in Cu_2O. *Phys. Rev. B* 41, 5266 (1989).

[186] M. Jörger, M. Schmidt, A. Jolk, and R. Westphäling C. Klingshirn. Absolute external photoluminescence quantum efficiency of the $1s$-orthoexciton in Cu_2O. *Phys. Rev. B* 64, 113204 (2001).

[187] F. Kreingold and V. Makarov. Effect of the paraexciton level on the temperature dependence of exciton luminescence in a cuprous oxide crystal. *Sov. Phys. Solid State* 15, 105 (1973).

[188] F. Bassani and M. Rovere. Biexciton binding energy in Cu_2O. *Solid State Commun.* 19, 887 (1976).

[189] E. Fortin, S. Fafard, and A. Mysyrowicz. Exciton transport in Cu_2O: Evidence for excitonic superfluidity? *Phys. Rev. Lett.* 70, 3951 (1993).

[190] S. A. Moskalenko and D. W. Snoke. *Bose-Einstein Condensation of Excitons and Biexcitons.* Cambridge University Press, Cambridge (2000).

[191] D. Hulin, A. Mysyrowicz, and C. Benoât à la Guillaume. Evidence for Bose-Einstein statistics in an exciton gas. *Phys. Rev. Lett.* 45, 1970 (1980).

[192] D. Snoke, J. P. Wolfe, and A. Mysyrowicz. Quantum saturation of a Bose gas: Excitons in Cu_2O. *Phys. Rev. Lett.* 59, 827 (1987).

[193] D. W. Snoke, J. P. Wolfe, and A. Mysyrowicz. Evidence for Bose-Einstein condensation of a two-component exciton gas. *Phys. Rev. Lett.* 64, 2543 (1990).

[194] D. Snoke, J. Wolfe, and A. Mysyrowicz. Evidence for Bose-Einstein condensation of excitons in Cu_2O. *Phys. Rev. B* 41, 11171 (1990).

[195] J. L. Lin and J. P. Wolfe. Bose-Einstein condensation of paraexcitons in stressed Cu_2O. *Phys. Rev. Lett.* 71, 1222 (1993).

[196] A. Griffin, D. Snoke, and S. Stringari. *Bose-Einstein Condensation.* Cambridge University Press, Cambridge (1995).

[197] K. E. O'Hara, L. Ó Súilleabháin, and J. P. Wolfe. Strong nonradiative recombination of excitons in Cu_2O and its impact on Bose-Einstein statistics. *Phys. Rev. B* 60, 10565 (1999).

[198] N. Naka and N. Nagasawa. Optical tracking of high-density cooled excitons in potential traps in Cu_2O. *phys. stat. sol. (b)* 238, 397 (2003).

[199] D. P. Trauernicht, J. P. Wolfe, and A. Mysyrowicz. Thermodynamics of strain-confined paraexcitons in Cu_2O. *Phys. Rev. B* 34, 2561 (1986).

[200] W. Ketterle. Experimental studies of Bose-Einstein condensation. *Physics Today* 52, (12) 30 (1999).

[201] J. J. Baumberg, P. G. Savvidis, R. M. Stevenson, A. I. Tartakovskii, M. S. Skolnick, D. M. Whittaker, and J. S. Roberts. Parametric oscillation in a vertical microcavity: A polariton condensate or micro-optical parametric oscillation. *Phys. Rev. B* 62, R16247 (2000).

[202] D. Porras, C. Ciuti, J. J. Baumberg, and C. Tejedor. Polariton dynamics and Bose-Einstein condensation in semiconductor microcavities. *Phys. Rev. B* 66, 085304 (2002).

[203] L. V. Butov, A. L. Ivanov, A. Imamoglu, P. B. Littlewood, A. A. Shashkin, V. T. Dolgopolov, K. L. Campman, and A. C. Gossard. Stimulated scattering of indirect excitons in coupled quantum wells: signature of a degenerate Bose-gas of excitons. *Phys. Rev. Lett.* 86, 5606 (2001).

[204] L. Hanke, D. Fröhlich, A. L. Ivanov, P. B. Littlewood, and H. Stolz. Spectroscopy of LA-phonoritons in Cu_2O. *phys. stat. sol. (b)* 221, 287 (2000).

[205] A. Jolk and C. F. Klingshirn. Linear and Nonlinear excitonic absorption and photoluminescence spectra in Cu_2O: line shape analysis and exciton drift. *phys. stat. sol. (b)* 206, 841 (1998).

[206] J. W. Hodby, T. E. Jenkins, C. Schwab, H. Tamura, and D. Trivich. Cyclotron resonance of electrons and of holes in cuprous oxide Cu_2O. *J. Phys. C: Solid State Phys.* 9, 1429 (1976).

[207] S. L. Artyukhin. *Frustrated magnets: non-collinear spin textures, excitations and dynamics.* Ph.D. thesis, Rijksuniversiteit Groningen (2012).

[208] H. E. Swanson and R. K. Fuyat. Standard X-ray diffraction powder patterns. *NBS Circular* 539, II:23 (1953).

[209] T. Ohyama, T. Ogawa, and H. Nakata. Determination of deformation-potential constants of Cu_2O by microwave cyclotron resonance. *Phys. Rev. B* 56, 3871 (1997).

[210] K. Shindo, T. Goto, and T. Anzai. Exciton-LO phonon scattering in Cu_2O. *J. Phys. Soc. Jpn.* 36, 753 (1974).

[211] H. Haken. *Quantum Field Theory of Solids.* North-Holland, Amsterdam, second edition (1983).

[212] S. Nakajima, Y. Toyozawa, and R. Abe. *The Physics of Elementary Excitations*, volume 12 of *Springer Series in Solid State Sciences.* Springer, Berlin (1980).

[213] P. Vogl. The Electron–Phonon Interaction in Semiconductors. In *Physics of Nonlinear Transport in Semiconductors*, edited by D. K. Ferry, J. R. Barker, and C. Jacoboni, volume 52 of *NATO ASI Series B: Physics*, pp. 75–115. Plenum Press, New York (1980).

[214] U. Rössler. Energy bands of hexagonal II-VI semiconductors. *Phys. Rev.* 184, 733 (1969).

[215] M. L. Cohen and J. R. Chelikowsky. Nonlocal pseudopotential calculations for the electronic structure of eleven diamond and zinc-blende semiconductors. *Phys. Rev. B* 14, 556 (1976).

[216] J. Pollmann and H. Büttner. Effective Hamiltonians and bindings energies of Wannier excitons in polar semiconductors. *Phys. Rev. B* 16, 4480 (1977).

[217] H.-R. Trebin. Exciton-phonon interaction in the degenerate band case. *phys. stat. sol (b)* 92, 601 (1979).

[218] M. Matsuura and H. Büttner. Exciton polaron with the arbitrary exciton-phonon coupling. *Solid State Commun.* 36, 81 (1980).

[219] B. Pertzsch and U. Rössler. Polarons and Wannier excitons in polar crystals. *phys. stat. sol. (b)* 101, 197 (1980).

[220] Y. Toyozawa. Theory of the electronic polaron and ionization of a trapped electron by an exciton. *Prog. Theor. Phys.* 12, 422 (1954).

[221] J. Bardeen and W. Shockley. Deformation potentials and mobilities in non-polar crystals. *Phys. Rev.* 80, 72 (1950).

[222] H. Fröhlich, H. Pelzer, and S. Zienau. Properties of slow electrons in polar materials. *Phil. Mag.* 41, 221 (1950).

[223] H. Fröhlich. On the theory of superconductivity: The one-dimensional case. *Proc. Roy. Soc. A* 223, 296 (1954).

[224] H. Haken. Über den Einfluß von Gitterschwingungen auf Energie und Lebensdauer des Excitons. *Z. Physik* 155, 223 (1959).

[225] A. V. Tulub. The mean free path of an exciton in a polar crystal. *Soviet Phys. JETP* 9, 1325 (1959).

[226] Ch. Kittel. *Quantum Theory of Solids.* Wiley, New York (1963).

[227] J. T. Devreese and F. Peeters (editors). *Polarons and Excitons in Polar Semiconductors and Ionic Crystals*, volume 108 of *NATO ASI Ser. B.* Plenum Press, New York (1984).

[228] L. Reggiani (editor). *Hot Electron Transport in Semiconductors*, volume 58 of *Topics in Applied Physics.* Springer, Berlin (1985).

[229] J. Shah (editor). *Hot Carriers in Semiconductors.* Pergamon, Oxford (1988).

[230] J. Shah (editor). *Hot Carriers in Semiconductor Nanostructures.* Academic, Boston (1992).

[231] J. Shah. *Ultrafast Spectroscopy of Semiconductors and Semiconductor Nanostructures*, volume 115 of *Springer Series in Solid State Sciences.* Springer, Berlin (1997).

[232] G. Mahan. *Many-particle physics.* Kluwer Academic/Plenum Publ., New York, third edition (2002).

[233] K. Seeger. *Semiconductor Physics*, volume 40 of *Springer Series in Solid State Sciences.* Springer, Berlin, 8th edition (2002).

[234] V. L. Bonch-Bruevich and S. G. Kalashnikov. *Halbleiterphysik.* VEB Deutscher Verlag der Wissenschaften, Berlin (1982).

[235] M. Lundstrom. *Fundamentals of Carrier Transport.* Cambridge University Press, Cambridge, second edition (2000).

[236] O. Madelung. *Festkörpertheorie.* Springer, Berlin (1972).

[237] D. Fröhlich, E. Mohler, and P. Wiesner. Observation of Exciton Polariton Dispersion in CuCl. *Phys. Rev. Lett.* 26, 554 (1971).

[238] D. Fröhlich. Aspects of nonlinear spectroscopy. *Festkörperprobleme / Adv. Solid State Phys.* 21, 363 (1981).

[239] R. G. Ulbrich. Optical Properties and Charge Transport. In *Electronic Structure and Properties of Semiconductors*, edited by R. W. Cahn, P. Haasen, E. J. Kramer, and W. Schröter, volume 4 of *Materials Science and Technology*, pp. 65–104. Wiley-VCH, Weinheim (1991).

[240] L. van Hove. Energy corrections and persistent perturbation effects in continuous spectra. *Physica* 21, 901 (1955).

[241] P. Rommel. *Modell mit Mastergleichung zur Beschreibung der Exziton-Phonon-Wechselwirkung in* Cu_2O. Master's thesis, Universität Stuttgart (2017).

[242] H. Fröhlich. Electrons in lattice fields. *Advances in Physics* 3, 325 (1954).

[243] T. Ueno. On the contour of absorption lines in Cu_2O. *J. Phys. Soc. Jpn.* 26, 438 (1969).

[244] F. Urbach. The long-wavelength edge of photographic sensitivity and of the electronic absorption of solids. *Phys. Rev.* 92, 1324 (1953).

[245] M. V. Kurik. Urbach rule. *phys. stat. sol. (a)* 8, 9 (1971).

[246] A. S. Davydov. Theory of Urbach's rule. *phys. stat. sol.* 27, 51 (1968).

[247] A. Messiah. *Quantenmechanik 1.* Walter de Gruyter, Berlin (1976).

[248] A. R. Edmonds. *Angular momentum in quantum mechanics.* Princeton University Press, Princeton (1960).

[249] J. J. Hopfield. On the energy dependence of the absorption constant and photoconductivity near a direct band gap. *J. Phys. Chem. Solids* 22, 63 (1961).

[250] L. Zverev, M. Noskov, and M. Shur. Concerning the contour of exciton absorption bands in cuprous oxide. *Soviet Phys. Solid State* 2, 2357 (1961).

[251] J. Grun and S. Nikitine. Étude de la forme des raies des séries jaune et verte de la cuprite. *J. Phys. France* 24, 355 (1963).

[252] A. Radkowsky. Temperature dependence of electron energy levels in solids. *Phys. Rev.* 73, 749 (1948).

[253] H. Y. Fan. Temperature dependence of the energy gap in semiconductors. *Phys. Rev.* 82, 900 (1951).

[254] S. Nikitine, G. Perny, and M. Sieskind. *Compt. Rend. Acad. Sci.* 238, 1987 (1954).

[255] S. Rudin, T. L. Reinecke, and B. Segall. Temperature-dependent exciton linewidths in semiconductors. *Phys. Rev. B* 42, 11218 (1990).

[256] S. Nikitine, J. B. Grun, and M. Sieskind. Étude spectrophotométrique de la série jaune de Cu_2O aux basses températures. *J. Phys. Chem. Solids* 17, 292 (1961).

[257] S. Nikitine and R. Reiss. Spectroscopie de reflexion et reflexion selective des halogenures cuivreux aux basses temperatures. *J. Phys. Chem. Solids* 16, 237 (1960).

[258] P. Y. Yu and Y. R. Shen. Resonance Raman studies in Cu_2O. I. The phonon-assisted 1s yellow excitonic absorption edge. *Phys. Rev. B* 12, 1377 (1975).

[259] K. Huang. The long wave modes of the Cu_2O lattice. *Zeitschrift für Physik* 171, 213 (1963).

[260] C. Carabatos. Lattice Vibrations of Cu_2O at the long wave limit. *phys. stat. sol. (b)* 37, 773 (1970).

[261] C. Carabatos and B. Prevot. Rigid ion model lattice dynamics of cuprite (Cu_2O). *phys. stat. sol. (b)* 44, 701 (1971).

[262] M. M. Beg and S. M. Shapiro. Study of phonon dispersion relations in cuprous oxide by inelastic neutron scattering. *Phys. Rev. B* 13, 1728 (1976).

[263] U. Fano. Effects of configuration interaction on intensities and phase shifts. *Phys. Rev.* 124, 1866 (1961).

[264] K. Hannewald, S. Glutsch, and F. Bechstedt. Spontaneous Emission from Semiconductors After Ultrafast Pulse Excitation: Theory and Simulation. In *Ultrafast Dynamical Processes in Semiconductors*, edited by K.-T. Tsen, volume 92 of *Topics in Applied Physics*, pp. 139–192. Springer, Berlin (2004).

[265] V. T. Agekyan, B. S. Monozon, and I. P. Shiryapov. The fine structure of Wannier-Mott excitons in a cubic crystal and its behaviour in an electric field. *phys. stat. sol. (b)* 66, 359 (1974).

[266] S. Rudin and T. L. Reinecke. Effects of exciton–acoustic-phonon scattering on optical line shapes and exciton dephasing in semiconductors and semiconductor quantum wells. *Phys. Rev. B* 66, 085314 (2002).

[267] M. A. Kanehisa. Exciton dispersion in degenerate bands. *Physica B+C* 117-118, 275 (1983).

[268] V. F. Gantmakher and Y. B. Levinson. *Carrier Scattering in Metals and Semiconductors*, volume 19. North-Holland, Amsterdam (1987).

[269] J. Hallberg and R. C. Hanson. The elastic constants of cuprous oxide. *phys. stat. sol. (b)* 42, 305 (1970).

[270] J. I. Jang and J. P. Wolfe. Relaxation of stress-split orthoexcitons in Cu_2O. *Phys. Rev. B* 73, 075207 (2006).

[271] J. C. Merle, S. Nikitine, and H. Haken. Temperature dependence of the 1S line of the yellow series of Cu_2O. *phys. stat. sol. (b)* 61, 229 (1974).

[272] A. C. Mitchell and M. W. Zemansky. *Resonance Radiation and Excited Atoms.* Cambridge University Press, Cambridge (1971).

[273] J. P. Dahl and A. C. Switzendick. Energy bands in cuprous oxide. *J. Phys. Chem. Solids* 27, 931 (1966).

[274] V. M. Agranovich and Yu. V. Konobeev. Contribution to the exciton absorption band edge theory. *Soviet Phys. Solid State* 3, 260 (1961).

[275] M. L. Cohen and T. K. Bergstresser. Band Structures and Pseudopotential Form Factors for Fourteen Semiconductors of the Diamond and Zinc-blende Structures. *Phys. Rev.* 141, 789 (1966).

[276] N. O. Lipari. The effective-mass theory in real semiconductors: Excitons and impurities in diamond and zincblende lattices. *Il Nuovo Cimento B* 23, 51 (1974).

[277] H. J. Mattausch and Ch. Uihlein. Fine Structure of P excitons in CuBr. *phys. stat. sol (b)* 96, 189 (1979).

[278] F. Schweiner, J. Main, G. Wunner, and Ch. Uihlein. Exciton-polaritons in cuprous oxide: I. Theory. *Phys. Rev. B* (2017). Submitted.

[279] M. French, R. Schwartz, H. Stolz, and R. Redmer. Electronic band structure of Cu_2O by spin density functional theory. *J. Phys.: Condens. Matter* 21, 015502 (2009).

[280] J. M. Luttinger and W. Kohn. Motion of electrons and holes in perturbed periodic fields. *Phys. Rev.* 97, 869 (1955).

[281] J. Broeckx. Acceptor excitation spectra in germanium in a uniform magnetic field. *Phys. Rev. B* 43, 9643 (1991).

[282] L. C. Andreani. Exciton-polaritons in bulk semiconductors and in confined electron and photon systems. In *Strong Light-Matter Coupling: From Atoms to Solid-State Systems*, edited by A. Auffèves, D. Gerace, M. Richard, S. Portolan, M. F. Santos, L. C. Kwek, and Ch. Miniatura, pp. 37–82. World Scientific, Singapore (2014).

[283] M. A. Caprio, P. Maris, and J. P. Vary. Coulomb-Sturmian basis for the nuclear many-body problem. *Phys. Rev. C* 86, 034312 (2012).

[284] E. Anderson, Z. Bai, C. Bischof, S. Blackford, J. Demmel, J. Dongarra, J. Du Croz, A. Greenbaum, S. Hammarling, A. McKenney, and D. Sorensen. *LAPACK Users' Guide*. Society for Industrial and Applied Mathematics, Philadelphia, PA, third edition (1999).

[285] R. J. Elliott and R. Loudon. Theory of fine structure on the absorption edge in semiconductors. *J. Phys. Chem. Solids* 8, 382 (1959).

[286] J. C. Merle, C. Wecker, A. Daunois, J. L. Deiss, and S. Nikitine. Modulated exciton absorption on Cu_2O in magnetic or parallel electric and magnetic fields. *Surface Science* 37, 347 (1973).

[287] M. Inoue and Y. Toyozawa. Two-photon absorption and energy band structure. *J. Phys. Soc. Jpn.* 20, 363 (1965).

[288] T. R. Bader and A. Gold. Polarization dependence of two-photon absorption in solids. *Phys. Rev.* 171, 997 (1968).

[289] M. M. Denisov and V. P. Makarov. Polarization dependence of the two-photon absorption coefficient in crystals. *J. Phys. C* 5, 2651 (1972).

[290] J. J. Hopfield and D. G. Thomas. Fine structure and magneto-optic effects in the exciton spectrum of cadmium sulfide. *Phys. Rev.* 122, 35 (1961).

[291] E. F. Gross and B. S. Razbirin. Fine structure of exciton absorption lines of CdS monocrystals. *Sov. Phys. Solid State* 4, 146 (1962).

[292] N. F. Mott and H. S. W. Massey. *The Theory of Atomic Collisions*. The International Series of Monographs on Physics. Oxford University Press, London, third edition (1965).

[293] H. A. Bethe and E. E. Salpeter. *Quantum Mechanics of One- and Two-Electron Atoms*. Plenum Press, New York, first edition (1977).

[294] T. Timusk. Far-infrared absorption study of exciton ionization in germanium. *Phys. Rev. B* 13, 3511 (1976).

[295] T. Timusk, H. Navarro, N. O. Lipari, and M. Altarelli. Far-infrared absorption by excitons in silicon. *Solid State Commun.* 25, 217 (1978).

[296] D. Labrie, M. L. W. Thewalt, I. J. Booth, and G. Kirczenow. Detailed ground- and excited-state spectroscopy of indirect free excitons. *Phys. Rev. Lett.* 61, 1882 (1988).

[297] M. Jörger, E. Tsitsishvili, T. Fleck, and C. Klingshirn. Infrared absorption by excitons in Cu_2O. *phys. stat. sol. (b)* 238, 470 (2003).

[298] M. Jörger, T. Fleck, and C. Klingshirn. 1s→2p terahertz transitions of the 1s paraexciton in Cu_2O. *J. Luminesc.* 112, 21 (2005).

[299] M. Kuwata-Gonokami, M. Kubouchi, R. Shimano, and A. Mysyrowic. Time-resolved excitonic Lyman spectroscopy of Cu_2O. *J. Phys. Soc. Jpn.* 73, 1065 (2004).

[300] M. Kuwata-Gonokami. Observation of ortho and para-excitons by time-resolved excitonic Lyman spectroscopy. *Solid State Commun.* 134, 127 (2005).

[301] C. Klingshirn, M. Jörger, T. Fleck, and A. Jolk. Exciton transport in Cu_2O, exciton detection by field ionization in a Schottky barrier and intraexcitonic transitions. *Solid State Commun.* 134, 155 (2005).

[302] J. W. Cederberg. Application of Racah algebra to molecular point groups. *Am. J. Phys.* 40, 159 (1972).

[303] K. Cho. Unified theory of symmetry-breaking effects on excitons in cubic and wurtzite structures. *Phys. Rev. B* 14, 4463 (1976).

[304] U. Rössler and H.-R. Trebin. Exchange and polaron corrections for excitons in the degenerate-band case. *Phys. Rev. B* 23, 1961 (1981).

[305] G. L. Bir and G. E. Pikus. *Symmetry and Strain Induced Effects in Semiconductors.* Wiley, New York (1974).

[306] M. Bayer, G. Ortner, O. Stern, A. Kuther, A. A. Gorbunov, A. Forchel, P. Hawrylak, S. Fafard, K. Hinzer, T. L. Reinecke, S. N. Walck, J. P. Reithmaier, F. Klopf, and F. Schäfer. Fine structure of neutral and charged excitons in self-assembled In(Ga)As/(Al)GaAs quantum dots. *Phys. Rev. B* 65, 195315 (2002).

[307] E. L. Ivchenko and G. E. Pikus. *Superlattices and Other Heterostructures.* Springer, Berlin (1995).

[308] W. R. Heller and A. Marcus. A note on the propagation of excitation in an idealized crystal. *Phys. Rev.* 84, 809 (1951).

[309] M. M. Denisov and V. P. Makarov. Longitudinal and transverse excitons in semiconductors. *phys. stat. sol. (b)* 56, 9 (1973).

[310] O. Schütz and J. Treusch. Summability of the perturbation series of excitonic exchange, CuCl as an example. *Solid State Commun.* 13, 1155 (1973).

[311] M. Born and K. Huang. *Dynamical Theory of Crystal Lattices.* Oxford University Press, London (1954).

[312] J. J. Hopfield and D. G. Thomas. On some observable properties of longitudinal excitons. *Phys. Chem. Solids* 12, 276 (1960).

[313] L. P. Bouckaert, R. Smoluchowski, and E. Wigner. Theory of Brillouin zones and symmetry properties of wave functions in crystals. *Phys. Rev.* 50, 58 (1936).

[314] G. F. Koster. Space groups and their representations. *Solid State Phys.* 5, 173 (1957).

[315] V. A. Kiselev and A. G. Zhilich. Exchange and exchange-deformation splitting of exciton levels in a cuprous oxide crystal. *Sov. Phys. Solid State* 13, 2008 (1972).

[316] G. E. Pikus and G. L. Bir. Exchange interaction in excitons in semiconductors. *Sov. Phys. JETP* 33, 108 (1971).

[317] D. Fröhlich, R. Kenklies, Ch. Uihlein, and C. Schwab. Assignment of the even-parity excitons in Cu_2O. *Phys. Rev. Lett.* 43, 1260 (1979).

[318] K. Suzuki and J. C. Hensel. Quantum resonances in the valence bands of germanium. I. Theoretical considerations. *Phys. Rev. B* 9, 4184 (1974).

[319] Y. Toyozawa and J. Hermanson. Exciton-phonon bound state: A new quasiparticle. *Phys. Rev. Lett.* 21, 1637 (1968).

[320] L. Kalok and J. Treusch. A note concerning the exciton-phonon-bound state. *phys. stat. sol. (b)* 52, K125 (1972).

[321] M. Betz, G. Göger, A. Leitenstorfer, R. Zimmermann, M. Bichler, W. Wegscheider, and G. Abstreiter. Femtosecond optical response of exciton–LO phonon quasiparticles in GaAs. *phys. stat. sol. (b)* 231, 181 (2002).

[322] H. Haken. Die Theorie des Exzitons im festen Körper. *Fortschr. Physik* 6, 271 (1958).

[323] H. Haken. Zur Quantentheorie des Mehrelektronensystems im schwingenden Gitter. Teil 1. *Z. Phys.* 146, 527 (1956).

[324] H. Haken. Kopplung nichtrelativistischer Teilchen in einem quantisierten Feld. Teil 1. Das Exziton im schwingenden, polaren Kristall. *Il Nuovo Cimento* 3, 1230 (1956).

[325] H. Haken. Der heutige Stand der Exzitonen-Forschung in Halbleitern. In *Halbleiterprobleme IV*, edited by W. Schottky, pp. 1–48. Vieweg, Berlin (1957).

[326] H. Haken and W. Schottky. Die Behandlung des Exzitons nach der Vielelektronentheorie. *Z. Phys. Chem.* 16, 218 (1958).

[327] E. Menéndez-Proupin, C. L Beltrán Rios, and P. Wahnón. Nonhdrogenic exciton spectrum in perovskite $CH_3NH_3PbI_3$. *Phys. Status Solidi RRL* 9, 559 (2015).

[328] H.-R. Trebin and U. Rössler. Polarons in the degenerate-band case. *phys. stat. sol. (b)* 70, 717 (1975).

[329] K. K. Bajaj. Effect of the electron-phonon interaction on the binding energy of a Wannier exciton in a polarizable medium. *Solid State Commun.* 15, 1221 (1974).

[330] J. Pollmann and H. Büttner. Upper bounds for the ground-state energy of the exciton-phonon system. *Solid State Commun.* 17, 1171 (1975).

[331] S. Bednarek, J. Adamowski, and M. Suffczyński. Effective Hamiltonian for few-particle systems in polar semiconductors. *Solid State Commun.* 21, 1 (1977).

[332] J. Hermanson. Exciton and impurity states in rare-gas solids. *Phys. Rev.* 150, 660 (1966).

[333] V. T. Agekyan an Yu. A. Stepanov. Exchange-strain splitting of the S exciton levels in cuprous oxide. *Sov. Phys. Solid State* 17, 1041 (1975).

[334] A. G. Zhilich, J. Halpern, and B. P. Zakharchenya. Magnetoabsorption oscillations and the Zeeman effect of excitons for forbidden interband transitions in Cu_2O crystals. *Phys. Rev.* 188, 1294 (1969).

[335] D. Fishman. *Excitons in cuprous oxide.* Ph.D. thesis, Rijksuniversiteit Groningen (2008).

[336] E. F. Gross, B. P. Zakharchenya, and L. M. Kanskaya. Investigation of the Stark exciton effect in oriented monocrystals of copper oxide. *Sov. Phys. Solid State* 3, 706 (1961).

[337] R. G. Waters, F. H. Pollak, R. H. Bruce, and H. Z. Cummins. Effects of uniaxial stress on excitons in Cu_2O. *Phys. Rev. B* 21, 1665 (1980).

[338] H.-R. Trebin, H. Z. Cummins, and J. L. Birman. Excitons in cuprous oxide under uniaxial stress. *Phys. Rev. B* 23, 597 (1981).

[339] E. F. Gross, A. A. Kaplianskii, and V. T. Agekyan. Effect of directed deformations on the spectra of direct and indirect excitation of the exciton ground state in Cu_2O. *Sov. Phys. Solid State* 4, 744 (1962).

[340] E. F. Gross, A. A. Kaplianskii, V. T. Agekyan, and D. S. Bulyanitsa. Polarization of the yellow exciton series in the spectrum of Cu_2O under crystal deformation. *Sov. Phys. Solid State* 4, 1219 (1962).

[341] E. F. Gross and A. A. Kaplianskii. The quadrupole absorption coefficient and the optical lifetime of the ground state of excitons in a crystal of Cu_2O. *Sov. Phys. Dokl.* 6, 592 (1962).

[342] N. Naka and N. Nagasawa. Nonlinear paraexciton kinetics in a potential trap in Cu_2O under two-photon resonance excitation. *Phys. Rev. B* 65, 245203 (2002).

[343] E. U. Condon and G. H. Shortley. *The Theory of Atomic Spectra.* Cambridge University Press, Cambridge (1970).

[344] J. W. Allen. Effect of electric fields on hydrogen-like excitons. *Nature* 187, 51 (1960).

[345] E. F. Gross, B. P. Zakharchenya, and N. M. Reinov. Exhibition of the Stark and Zeeman effects by excitons in cuprous oxide crystal. *Dokl. Akad. Nauk SSSR* 97, 57, 221 (1954).

[346] D. G. Thomas and J. J. Hopfield. Direct observation of exciton motion in CdS. *Phys. Rev. Lett.* 5, 505 (1960).

[347] D. G. Thomas and J. J. Hopfield. A magneto-stark effect and exciton motion in CdS. *Phys. Rev.* 124, 657 (1961).

[348] H. Ruder, G. Wunner, H. Herold, and F. Geyer. *Atoms in Strong Magnetic Fields.* Springer, Heidelberg (1994).

[349] R. J. Elliott and R. Loudon. Theory of the absorption edge in semiconductors in a high magnetic field. *J. Phys. Chem. Solids* 15, 196 (1960).

[350] R. J. Elliott and R. Loudon. Theory of fine structure on the absorption edge in semiconductors. *J. Phys. Chem. Solids* 8, 382 (1959).

[351] K. Cho (editor). *Exciton*, volume 14 of *Topics Curr. Phys.* Springer, Berlin (1979).

[352] M. Cardona. *Modulation Spectroscopy.* Academic, New York (1969).

[353] B. O. Seraphin (editor). *Modulation Spectroscopy.* North-Holland, Amsterdam (1973).

[354] G. J. Goldsmith. Modulation Spectroscopy Revisited. In *Frontiers of Optical Spectroscopy*, edited by O. Forte B. Di Bartolo, volume 168 of *NATO ASI Ser. II*, pp. 669–685. Kluwer Academic Publishers, Dordrecht (2005).

[355] P. Schmelcher and L. S. Cederbaum. Regularity and chaos in the center of mass motion of the hydrogen atom in a magnetic field. *Z. Phys. D* 24, 311 (1992).

[356] P. Schmelcher and L. S. Cederbaum. Intermittent chaos in Hamiltonian systems: The three-dimensional hydrogen atom in magnetic fields. *Phys. Rev. A* 47, 2634 (1993).

[357] M. Altarelli and N. O. Lipari. Perturbation-theory investigation of the exciton ground state of cubic semiconductors in a magnetic field. *Phys. Rev. B* 7, 3798 (1973).

[358] M. Altarelli and N. O. Lipari. Exciton states of semiconductors in a high magnetic field. *Phys. Rev. B* 9, 1733 (1974).

[359] Y. Chen, B. Gil, H. Mathieu, and J. P. Lascaray. Exciton-polaritons in InP: Magnetoreflectance investigation. *Phys. Rev. B* 36, 1510 (1987).

[360] R. J. Elliott, T. P. McLean, and G. G. MacFarlane. Theory of the effect of a magnetic field on the absorption edge in semiconductors. *Proc. Phys. Soc.* 72, 553 (1958).

[361] J. Fuchs, J. Main, H. Cartarius, and G. Wunner. Harmonic inversion analysis of exceptional points in resonance spectra. *J. Phys. A: Math. Theor.* 47, 125304 (2014).

[362] J. Main, P. A. Dando, Dž. Belkić, and H. S. Taylor. Decimation and harmonic inversion of periodic orbit signals. *J. Phys. A: Math. Gen.* 33, 1247 (2000).

[363] M. M. Glazov. Private communications.

[364] F. Haake. *Quantum Signatures of Chaos.* Springer Series in Synergetics. Springer, Heidelberg, third edition (2010).

[365] H.-J. Stöckmann. *Quantum Chaos: An Introduction.* Cambridge University Press, Cambridge (1999).

[366] O. Bohigas, M. J. Giannoni, and C. Schmit. Characterization of chaotic quantum spectra and universality of level fluctuation laws. *Phys. Rev. Lett.* 52, 1 (1984).

[367] M. L. Mehta. *Random Matrices.* Elsevier, Amsterdam, third edition (2004).

[368] C. E. Porter (editor). *Statistical Theory of Spectra.* Academic Press, New York (1965).

[369] J. Rao and K. T. Taylor. The closed orbits and the photo-excitation scaled spectrum of the hydrogen atom in crossed fields. *J. Phys. B: At. Mol. Opt. Phys.* 35, 2627 (2002).

[370] S. Schierenberg, F. Bruckmann, and T. Wettig. Wigner surmise for mixed smmetry classes in random matrix theory. *Phys. Rev. E* 85, 061130 (2012).

[371] G. Lenz and F. Haake. Reliability of small matrices for large spectra with nonuniversal fluctuations. *Phys. Rev. Lett.* 67, 1 (1991).

[372] A. Pandey. Statistical properties of many-particle spectra III. Ergodic behavoir in random matrix ensembles. *Ann. Phys.* 119, 170 (1979).

[373] G. E. Mitchell, A. Richter, and H. A. Weidenmüller. Random matrices and chaos in nuclear physics: nuclear reactions. *Rev. Mod. Phys.* 82, 2845 (2010).

[374] T. A. Brody, J. Flores, J. B. French, P. A. Mello, A. Pandey, and S. S. M. Wong. Random-matrix physics: spectrum and strength fluctuations. *Rev. Mod. Phys.* 53, 385 (1981).

[375] N. Rosenzweig and C. E. Porter. Repulsion of energy levels in complex atomic spectra. *Phys. Rev.* 120, 1698 (1960).

[376] H. S. Camarda and P. D. Georgopulos. Statistical behavior of atomic energy levels: agreement with random-matrix theory. *Phys. Rev. Lett.* 50, 492 (1983).

[377] H.-J. Stöckmann and J. Stein. Quantum chaos in billiards studied by microwave absorption. *Phys. Rev. Lett.* 64, 2215 (1990).

[378] H. Alt, H.-D. Gräf, H. L. Harney, R. Hofferbert, H. Lengeler, A. Richter, P. Schardt, and H. A. Weidenmüller. Gaussian orthogonal ensemble statistics in a microwave stadium billiard with chaotic dynamics: Porter-Thomas distribution and algebraic decay of time correlations. *Phys. Rev. Lett.* 74, 62 (1995).

[379] H. Alt, H.-D. Gräf, R. Hofferbert, C. Rangacharyulu, H. Rehfeld, A. Richter, P. Schardt, and A. Wirzba. Chaotic dynamics in a three-dimensional superconducting microwave billiard. *Phys. Rev. E* 54, 2303 (1996).

[380] Th. Zimmermann, H. Köppel, L. S. Cederbaum, G. Persch, and W. Demtröder. Confirmation of random-matrix fluctuations in molecular spectra. *Phys. Rev. Lett.* 61, 3 (1988).

[381] W. Zhou, Z. Chen, B. Zhang, C. H. Yu, W. Lu, and S. C. Shen. Magnetic field control of the quantum chaotic dynamics of hydrogen analogs in an anisotropic crystal field. *Phys. Rev. Lett.* 105, 024101 (2010).

[382] L. Vina, M. Potemski, and W. Wang. Signatures of quantum chaos in the magneto-excitonic spectrum of qunatum wells. *Phys.-Usp.* 41, 153 (1998).

[383] H. Held, J. Schlichter, G. Raithel, and H. Walther. Observation of level statistics and Heisenberg-time orbits in diamagnetic Rydberg spectra. *Europhys. Lett.* 43, 392 (1998).

[384] A. Frisch, M. Mark, K. Aikawa, F. Ferlaino, J. L. Bohn, C. Makrides, A. Petrov, and S. Kotochigova. Quantum chaos in ultracold collisions of gas-phase erbium atoms. *Nature* 507, 475 (2014).

[385] D. Wintgen and H. Friedrich. Classical and quantum-mechanical transition between regularity and irregularity in a Hamiltonian system. *Phys. Rev. A* 35, 1464(R) (1987).

[386] H. Friedrich and D. Wintgen. The hydrogen atom in a uniform magnetic field - an example of chaos. *Phys. Rep.* 183, 37 (1989).

[387] M. V. Berry and M. Tabor. Level clustering in the regular spectrum. *Proc. Roy. Soc. London A* 356, 375 (1977).

[388] P. So, S. M. Anlage, E. Ott, and R. N. Oerter. Wave chaos experiments with and without time reversal symmetry: GUE and GOE statistics. *Phys. Rev. Lett.* 74, 2662 (1995).

[389] K. Sacha, J. Zakrzewski, and D. Delande. Chaotic Rydberg atoms with broken time-reversal symmetry. *Phys. Rev. Lett.* 83, 2922 (1999).

[390] P. Shukla and A. Pandey. The effect of symmetry-breaking in 'chaotic' spectral correlations. *Nonlinearity* 10, 979 (1997).

[391] H. Haake, M. Kuś, and R. Scharf. Classical and quantum chaos for a kicked top. *Z. Phys. B* 65, 381 (1987).

[392] P. Shukla. Level statistics of Anderson model of disordered systems: connection to Brownian ensembles. *J. Phys. Condens. Matter* 17, 1653 (2005).

[393] F. J. Dyson. A Brownian motion model for the eigenvalues of a random matrix. *J. Math. Phys.* 3, 1191 (1962).

[394] U. Stoffregen, J. Stein, H.-J. Stöckmann, M. Kuś, and F. Haake. Microwave billards with broken time reversal symmetry. *Phys. Rev. Lett.* 74, 2666 (1995).

[395] L. A. Ponomarenko, F. Schedin, M. I. Katsnelson, R. Yang, E. W. Hill, K. S. Novoselov, and A. K. Geim. Chaotic Dirac billiard in graphene quantum dots. *Science* 320, 356 (2008).

[396] S.-H. Chung, A. Gokirmak, D.-H. Wu, J. S. A. Bridgewater, E. Ott, T. M. Antonsen, and S. M. Anlage. Measurement of wave chaotic eigenfunctions in the time-reversal symmetry-breaking crossover regime. *Phys. Rev. Lett.* 85, 2482 (2000).

[397] D. Wintgen. Connection between long-range correlations in quantum spectra and classical periodic orbits. *Phys. Rev. Lett.* 58, 1589 (1987).

[398] E. P. Wigner. Results and theory of resonance absoprtion. In *Conference on neutron physics by time-of-flight*, edited by R. C. Block, W. M. Good, J. A. Harvey, H. W. Schmitt, and G. T. Trammell, volume 2309 of *Oak Ridge National Laboratory Report*, pp. 59–70. Union Carbide Nuclear Company, Oak Ridge, Tennessee (1957).

[399] H. Harada and H. Hasegawa. Correspondence between classical and quantum chaos for hydrogen in a uniform magnetic field. *J. Phys. A* 16, L259 (1983).

[400] H. Hasegawa, S. Adachi, and A. Harada. On the scaling properties of the energy spectrum of hydrogen in a uniform magnetic field. *J. Phys. A: Math. Gen.* 16, L503 (1983).

[401] A. Messiah. *Quantum Mechanics 2*. North-Holland, Amsterdam (1969).

[402] S. Keppeler. *Spinning Particles - Semiclassics and Spectral Statistics*. Springer, Berlin (2003).

[403] J.-B. Grosa, O. Legranda, F. Mortessagnea, E. Richalotb, and K. Selemanib. Universal behaviour of a wave chaos based electromagnetic reverberation chamber. *Wave Motion* 51, 664 (2014).

[404] P. Kunstman, K. Życzkowski, and J. Zakrzewski. Nonuniversality in level dynamics. *Phys. Rev. E* 55, 2446 (1997).

[405] M. V. Berry and M. Robnik. Semiclassical level spacings when regular and chaotic orbits coexist. *J. Phys. A* 17, 2413 (1984).

[406] T. A. Brody. A statistical measure for the repulsion of energy levels. *Lett. Nuovo Cimento* 7, 482 (1973).

[407] E. Caurier, B. Grammaticos, and A. Ramani. Level repulsion near integrability: a random matrix analogy. *J. Phys. A* 23, 4903 (1990).

[408] H. Hasegawa, H. J. Mikeska, and H. Frahm. Stochastic formulation of energy-level statistics. *Phys. Rev. A* 38, 395 (1988).

[409] F. Izrailev. Simple models of quantum chaos: spectrum and eigenfunctions. *Phys. Rep.* 196, 299 (1990).

[410] M. Abramowitz and I. A. Stegun. *Handbook of Mathematical Functions*. Dover Publ., New York (1964).

[411] I. S. Gradshteyn and I. M. Ryzhik. *Tables of Integrals, Series, and Products*. Academic Press, Burlington, MA, 7th edition (2007).

[412] J. Laturner. Parameterabhängigkeit des Quantenchaos bei Rydberg-Exzitonen im Magnetfeld (2017).

[413] U. Fano. Atomic theory of electromagnetic interactions in dense materials. *Phys. Rev.* 103, 1202 (1956).

[414] V. M. Agranovich. Dispersion of electromagnetic waves in crystals. *Sov. Phys. JETP* 10, 307 (1960).

[415] J. J. Hopfield. Theory of the contribution of excitons to the complex dielectric constant of crystals. *Phys. Rev.* 112, 1555 (1958).

[416] J. J. Hopfield and D. G. Thomas. Theoretical and experimental effects of spatial dispersion on the optical properties of crystals. *Phys. Rev.* 132, 563 (1963).

[417] J. Brandmüller R. Claus, L. Merten. *Light Scattering by Phonon Polaritons*, volume 75 of *Springer Tracts Mod. Phys.* Springer, Berlin (1975).

[418] V. M. Agranovich and V. L. Ginzburg. *Crystal Optics with Spatial Dispersion, and Excitons*, volume 42 of *Springer Series in Solid State Sciences.* Springer, Berlin, second edition (1984).

[419] C. Klingshirn. Some Selected Aspects of Light-Matter Interaction in Solids. In *Ultrafast Dynamics of Quantum Systems: Physical Processes and Spectroscopic Techniques*, edited by B. Di Bartolo, volume 372 of *NATO ASI Ser. B*, pp. 143–211. Plenum Press, New York (1998).

[420] J. Mund, D. Yakovlev, D. Fröhlich, and M. Bayer (2017). To be published.

[421] J. Schmutzler, D. Fröhlich, and M. Bayer. Signatures of coherent propagation of blue polaritons in Cu_2O. *Phys. Rev. B* 87, 245202 (2013).

[422] J. Schmutzler. *Spectroscopy of exciton-polaritons in* Cu_2O *and GaAs-based microcavities.* Ph.D. thesis, Technische Universität Dortmund (2014).

[423] N. N. Bogolyubov. On a new method in the theory of superconductivity. *Nuovo Cimento* 7, 794 (1958).

[424] N. N. Bogolyubov. On the theory of superfluidity. *J. Phys. USSR* 11, 23 (1947).

[425] C. Mavroyannis. Scattering of electromagnetic waves in molecular crystals. *J. Math. Phys.* 8, 1515 (1967).

[426] E. T. Jaynes and F. W. Cummings. Comparison of quantum and semiclassical radiation theories with application to the beam maser. *Proceedings of the IEEE* 51, 89 (1963).

[427] N. J. Stor, I. Slapničar, and J. L. Barlow. Accurate eigenvalue decomposition of real symmetric matrices and applications. *Lin. Alg. Appl.* 464, 62 (2015).

[428] C. F. Borges and W. B. Gragg. A parallel divide and conquer algorithm for the generalized real symmetric definite tridiagonal eigenproblem. In *Numerical Linear Algebra and Scientific Computing*, edited by L. Reichel, A. Ruttan, and R. S. Varga, pp. 11–29. de Gruyter, Berlin (1993).

[429] D. P. O'Leary and G. W. Stewart. Computing the eigenvalues and eigenvectors of symmetric arrowhead matrices. *J. Comput. Phys.* 90, 497 (1990).

[430] W. C. Tait. Quantum theory of a basic light-matter interaction. *Phys. Rev. B* 5, 648 (1972).

[431] I. I. Rabi. On the process of space quantization. *Phys. Rev.* 49, 324 (1936).

[432] V. A. Kiselev, B. S. Razbirin, and I. N. Uraltsev. Additional waves and Fabry-Perot interference of photoexcitons (polaritons) in thin II–VI crystals. *phys. stat. sol. (b)* 72, 161 (1975).

[433] D. D. Sell, S. E. Stokowski, R. Dingle, and J. V. DiLorenzo. Polariton reflectance and photoluminescence in high-purity GaAs. *Phys. Rev. B* 7, 4568 (1973).

[434] D. Fröhlich. Two- and three-photon spectroscopy of solids. In *Nonlinear Spectroscopy of Solids:Advances and Applications*, edited by B. Di Bartolo and B. Bowlby, volume 339 of *NATO ASI Ser. B*, pp. 289–326. Plenum Press, New York (1994).

[435] D. Fröhlich, St. Kirchhoff, P. Köhler, and W. Nieswand. Three-photon difference-frequency spectroscopy of polaritons in alkali halides. *Phys. Rev. B* 40, 1976 (1989).

[436] L. C. Andreani. Optical Transitions, Excitons, and Polaritons in Bulk and Low-Dimensional Semiconductor Structures. In *Confined Electrons and Photons*, edited by C. Weisbuch E. Burstein, volume 340 of *NATO ASI Series*, pp. 57–112. Plenum Press, New York (1995).

[437] J. Ertl. Polaritontransformation der gelben Magnetoexzitonen in Kupferoxydul (2017).

[438] P. Y. Yu and Y. R. Shen. Study of dispersive Raman modes in Cu_2O by resonant Raman scattering. *Phys. Rev. Lett.* 32, 939 (1974).

[439] S. I. Pekar. The theory of electromagnetic waves in a crystal in which excitons are produced. *Soviet Phys. JETP* 6, 785 (1958).

[440] F. Schweiner, J. Ertl, J. Main, G. Wunner, and Ch. Uihlein. Exciton-polaritons in cuprous oxide: II. Dispersion results and comparison with experiment. *Phys. Rev. B* (2017). Submitted.

[441] J. Luft. *Closed-Orbit Theorie für Magnetoexzitonen in Kupferoxydul.* Master's thesis, Universität Stuttgart (2018).

[442] A. Matzkin, P. A. Dando, and T. S. Monteiro. Closed-orbit theory for molecules in fields. *Phys. Rev. A* 66, 013410 (2002).

[443] F. Schweiner, J. Main, H. Cartarius, and G. Wunner. Classical dynamics and localization of resonances in the high-energy region of the hydrogen atom in crossed fields. *Phys. Rev. E* 91, 012915 (2015).

[444] H. Cartarius, J. Main, and G. Wunner. Exceptional points in atomic spectra. *Phys. Rev. Lett.* 99, 173003 (2007).

[445] P. J. Mohr and B. N. Taylor. CODATA recommended values of the fundamental physical constants: 2002. *Rev. Mod. Phys.* 77, 1 (2005).

[446] J. Zamastil, F. Vinette, and M. Šimánek. Calculation of atomic integrals using commutation relations. *Phys. Rev. A* 75, 022506 (2007).

Zusammenfassung in deutscher Sprache

Seit der theoretischen Formulierung ihrer Existenz durch Frenkel [1–3], Peierls [4], und Wannier [5] in den 30er Jahren, jedoch spätestens seit Ihrer experimentellen Entdeckung in Kupferoxydul (Cu_2O) durch Gross and Karryjew im Jahre 1952 [6], sind Exzitonen als Quanten der fundamentalen optischen Anregungen sowohl in Halbleitern wie auch in Isolatoren im sichtbaren und ultravioletten Spektralbereich von großem physikalischen Interesse. Die Einzigartigkeit der Exzitonen zeigt sich in der Tatsache, dass sie gebundene Zustände darstellen, welche sich über eine riesige Anzahl an Gitter-Elementarzellen ausdehenen, sich dabei jedoch koherent durch den Kristall bewegen können [7].

Exzitonen setzen sich aus einem positiv geladenen Loch im Valenzband und einem negativ geladenen Elektron im Leitungsband des Kristalls zusammen. In Abhängigkeit des Abstandes der beiden Teilchen unterscheidet man hierbei zwischen Frenkel- und (Mott-)Wannier-Exzitonen [5, 9]. Im Falle von Frenkel-Exzitonen ist die Bindungsenergie zwischen Elektron und Loch sehr stark ($\sim 1\,\mathrm{eV}$) und beide Quasiteilchen befinden sich im Bereich eines Atoms des Festkörpers. Im Gegensatz dazu erstreckt sich die Wellenfunktion von Wannier-Exzitonen über eine sehr große Anzahl an Elementarzellen, wobei die Bindungsenergie deutlich kleiner ist ($\sim 1 - 100\,\mathrm{meV}$). Diese Exzitonen können in einer sehr einfachen Näherung als das Analogon des Wasserstoffatoms in der Festkörperphysik betrachtet werden. Die zugehörige wasserstoffähnliche Schrödingergleichung ist die Wannier-Gleichung [7, 10, 11]. Wir beschränken uns in dieser Arbeit auf Wannier-Exzitonen, da sie die typischen Exzitonen in Halbleitern sind. Frenkel-Exzitonen können hingegen in Isolatoren und Molekülkristallen gefunden werden.

Ein kürzlich durchgeführtes Experiment, in dem die sogannte gelbe Exzitonserie von Kupferoxydul bis zu einer Hauptquantenzahl von $n = 25$ beobachtet werden konnte [30], ließ den Exzitonen in dreidimensionalen Halbleitern neue Aufmerksamkeit zukommen. Die Entdeckungen in dieser herausragenden Arbeit eröffneten das Forschungsgebiet der Rydberg-Exzitonen, auf welchem in den vergangenen drei Jahren nun eine beachtliche Anzahl experimenteller wie theoretischer Arbeiten erschienen sind [30, 31, 33–57]. Das sehr weite Forschungsfeld der Exzitonen verheißt eine ganze Reihe möglicher technischer Anwendungen, unter anderem in der Informationstechnik wie auch in der Optoelektronik [8]. Durch ein präzises Bewegen von Rydberg-Exzitonen in Kristallen mithilfe mikroskopischer Potentiallandschaften und gleichzeitige Beobachtung ihrer Wechselwirkungen mit anderen Anregungen des Festkörpers verspricht man sich zudem ganz neuartige Erkenntnisse in der Festkörperphysik [30]. Rydbergatome, wie dann vielleicht auch Rydberg-Exzitonen, zeigen weiterhin eine Vielzahl interessanter Phänomene, wie starke Dipolwechselwirkungen und lange Lebenszeiten angeregter Zustände. Diese lassen sich möglicherweise für Quanten-Informationstechnologien verwenden [58]. In der Arbeit zu Rydberg-Exzitonen [30] wurde ein Dipol-Blockadeeffekt beobachtet, welcher die Anregung eines weiteren Exzitons in der direkten Umgebung eines bereits vorhandenen Exzitons verhindert. Dieser könnte sich eigenen, um mesoskopische logische Bauelemente oder optische Schalter zu konstruieren [60]. Vor diesem Hintergrund möglicher Anwendungen ist es unumgänglich, die Theorie der Exzitonen in Halbleitern wie $\mathrm{Cu_2O}$ genau zu verstehen.

Die wichtigsten Eigenschaften von $\mathrm{Cu_2O}$, die dieses Material zu einem der am meisten untersuchten Halbleiter auf dem Gebiet der Exzitonen machen, sind die große Exziton-Bindungsenergie von $R_{\mathrm{exc}} \approx 86\,\mathrm{meV}$ [37] sowie ein nichtenetartetes oberstes Valenzband, welches das einfache Wasserstoffmodell für die gelbe Exzitonserie in einigen Fällen rechtfertigt. In der vorliegenden Arbeit werden vor allem Korrekturen zu diesem einfachen Wasserstoffmodell eingeführt und diskutiert, um experimentelle Spektren quantitativ möglichst genau zu beschrieben. Weitere Schwerpunkte dieser Arbeit stellen Wechselwirkungen der Exzitonen mit Phononen und Photonen sowie Spektren in äußeren Magnetfeldern dar.

Grundlagen der Theorie Eine der wichtigsten Näherungen in der Festkörperphysik ist die Born-Oppenheimer-Näherung, welche im Abschnitt 2.1.3 angesprochen wird. Sie besagt, dass sich die Valenzelektronen aufgrund ihrer deutlich geringeren Masse praktisch instantan einer beliebigen Anordnung der Atomrümpfe anpassen können. Dies ermöglicht es, die Bewegung der Valenzelektronen und der Atomrümpfe zunächst getrennt zu behandeln.

Obwohl man sich in der Festkörperphyik mit einer riesigen Anzahl an Teilchen in der Größenordnung von 10^{23} konfrontiert sieht, gelingt es oft, elementaren Anregungen einen „Ein-Teilchen-Charakter“ zuzuweisen. Die Dynamik der Atomrümpfe beziehungsweise des Kristallgitters führt im Abschnitt 2.2 auf das Konzept der Phononen. Nach einer harmonischen Näherung für die Gitterbewegung und eine Transformation auf Normalkoordinaten ergeben sich die Phononen im Rahmen der zweiten Quantisierung als die elementaren quantisierten Anregungen des Gitters. Hierbei unterscheidet man akustische und optische Phononen, je nachdem, ob die Atomrümpfe gleich- oder gegenphasig zueinander ausgelenkt werden (siehe Abb. 2.6).

Im Falle der Elektronendynamik spielen Energiebänder sowie das Bloch-Theorem eine entscheidende Rolle. Ein recht anschauliches Modell ist hierbei das LCAO-Modell, welches im Abschnitt 2.3.5 angesprochen wird. Man nimmt an, dass sich bei der Annäherung zunächst isolierter Atome Linearkombinationen von Atomorbitalen ausbilden, welche schließlich, wie in Abb. 2.10 gezeigt, auf Energiebänder führen. Diese Bänder werden nach aufsteigender Energie mit Elektronen „gefüllt“. Ist dabei ein Band vollständig mit Elektronen besetzt (Valenzband) und besteht zum nächsthöheren, leeren Band (Leitungsband) eine Energielücke von $\lesssim 4\,\mathrm{eV}$, so spricht man von einem Halbleiter. Bei der Bestimmung der Elektronwellenfunktionen findet das Bloch-Theorem seine Anwendung (siehe Abs. 2.1.1 und 2.3.3). Da das Gitter der Atomrümpfe periodisch aufgebaut ist, lässt sich die Wellenfunktion als das Produkt einer ebenen Welle und einer gitterperiodischen Funktion schreiben. Die Blochfunktionen bilden eine vollständige Basis, deren Eigenschaften vielfach in dieser Arbeit ausgenutzt werden. Trotz der großen Anzahl an Elektronen im Halbleiter gelingt es, zu einer Ein-Teilchen-Beschreibung zu gelangen, wobei der Einfluss der anderen Elektronen auf ein bestimmtes Elektron durch das Einführen einer effektive Masse berücksichtigt wird (siehe Abs. 2.3.7). Aus diesem Grunde spricht man auch von Quasiteilchen.

Wird ein Elektron aus dem voll besetzten Valenzband in das leere Leitungsband angeregt, behandelt man das nun fehlende Elektron im Valenzband als positiv geladenenes Quasiteilchen, als sogenanntes Loch, welches mit dem Elektron wechselwirkt. Diese Wechselwirkung wird über eine mit der Dielektrizitätskonstante abgeschirmte Coulomb-Wechselwirkung genähert. Nimmt man zudem an, dass sowohl Leitungs- als auch Valenzband ideal parabolisch sind, führt dies auf den Hamiltonoperator (2.197) der Exzitonen im Wasserstoffmodell. Eine detaillierte Herleitung dieses Operators wird in Abschnitt 2.5.2 präsentiert. Nun muss allerdings beachtet werden, dass Exzitonen komplizierte Vielteilchenzustände des Festkörpers sind und dass aus diesem Grunde das Wasserstoffmodell nur eine sehr begrenzte Gültigkeit besitzt [61]. Dies umfasst sowohl Korrekturen aufgrund der tatsächlichen Bandstruktur, der Austauschwechselwirkung zwischen Elektron und Loch sowie des geringen Abstandes zwischen Elektron und Loch im Exziton-Grundzustand als auch die Berücksichtigung von Wechselwirkungen mit anderen Quasiteilchen wie Phononen oder Photonen. Auf diese Korrekturen wird in der vorliegenden Arbeit im Detail eingegangen.

Linienbreiten in Absorptionsspektren Das Absorptionsspektrum der Rydberg-Exzitonen in Abb. 2.15 zeigt charaktersitische asymmetrische Lorentzkurven. Einer der Hauptgründe für eine Verschiebung und asymmetrische Verbreiterung der Exziton-Absorptionslinien ist, neben dem Effekt von Unreinheiten im Kristall, die Exziton-Phonon-Wechselwirkung.

Phononen beeinflussen das elektronische System, wie im Abschnitt 3.1.1 beschrieben, auf unterschiedliche Weise. Akustische Phononen führen zu einer Streckung oder Stauschung des Gitters, welche sich auf die Bänder und folglich auf die Elektronenzustände auswirkt. Optische Phononen verurachen in ionischen Kristallen hingegen eine Polarisation, mit der die Elektronen wechselwirken. Die Phononen beeinflussen somit die einzelnen Bestandteile des Exzitons, d.h. das Elektron und das Loch, und damit das Exziton selbst. Mithilfe der Exziton-Wellenfunktion lässt sich die Exziton-Phonon-Wechselwirkung in zweiter Quantisierung in besonders kompakter Form schreiben, wie man anhand von Gleichung (3.59) sieht. Bei der Wechselwirkung spielen dann die effektiven Ladungen q_e und q_h der Quasiteilchen eine entscheidende Rolle, deren Bestimmung einen wesentlichen Teil der Berechnungen für Kupferoxydul im Abschnitt 3.2 einnimmt.

Die theoretische Beschreibung, wie sich die Exziton-Phonon-Wechselwirkung auf das Absorptionsspektrum auswirkt, gelang Y. Toyozawa in den späten 50er und frühen 60er Jahren [73–76]. Das wesentliche Ergebnis seiner Arbeit ist die Formel (3.78) für den Absorptionskoeffizienten in Abhängigkeit der Frequenz des Lichtes, welche eine Überlagerung asymmetrischer Lorentzkurven darstellt.

In der vorliegenden Arbeit werden die Linienbreiten und Verschiebungen für Kupferoxydul, wie in Abschnitt 3.2.1 beschrieben, ausgewertet. Bei der Betrachtung beider Größen fällt auf, dass der Beitrag akustischer Phononen vernachlässigbar klein ist, während optische Phononen eine entscheidende Rolle spielen. Ein wichtige Bedeutung haben auch die sogenannten „Central-Cell Corrections“ oder „Zentralzellen-Korrekturen“, welche aufgrund des winzigen Radius des Exziton-Grundzustandes notwendig werden. Hiermit gelingt es, die experimentellen Linienbreiten innerhalb derselben Größenordnung theoretisch zu berechnen, was eine deutliche Verbesserung im Vergleich zu früheren Arbeiten darstellt [73, 210]. Korrekturterme höherer Ordnung in den Formeln für die Linienbreiten und Verschiebungen sowie eine Kopplung der betrachteten Exzitonzustände an das Kontinuum der freien Elektronen und Löcher können vernachlässigt werden. In Abschnitt 3.3.2 findet sich eine ausführliche Diskussion möglicher Effekte, welche die verbleibende Abweichung zwischen Theorie und Experiment erklären könnten. Diese umfassen unter anderem die Verwendung des einfachen Wasserstoffmodells, die Vernachlässigung des Phononenuntergrundes, auf dem die Absorptionslinien im Experiment liegen, sowie Verunreinigungen und Störungen des Gitters.

Einfluss der Valenzbandstruktur Eines der beeindruckendsten experimentellen Ergebnisse für Cu_2O ist die Beobachtung von F-Exzitonen, d.h. Exzitonen mit Drehimpuls $L = 3$, sowie deren Feinstrukturaufspaltung bei einer genaueren Betrachtung des Exziton-Absorptionsspektrums [36]. Beide Beobachtungen lassen sich nicht mit dem einfachen Wasserstoffmodell der Exzitonen erklären. Betrachtet man die jeweils drei obersten Valenzbänder und niedrigsten Leitungsbänder von Kupferoxydul, so ergeben sich, wie in Abb. 2.14 dargestellt, zunächst vier Exzitonserien, die nach der Farbe des Lichtes benannt wurden, mit dem sie angeregt werden können. Man sieht hier bereits, dass in Cu_2O entartete Bänder auftreten und dass der Abstand zwischen den Valenzbändern, der sich aufgrund der Spin-Bahn-Wechselwirkung ergibt, in der Größenordung der Exziton-Rydbergenergie liegt. Folglich kann die Näherung des Wasserstoffmodells, dass die Bänder ideal parabolisch und nichtentartet sind, nicht verwendet werden, und es ist nötig, die volle Valenzbandstruktur in einer quantitativen Theorie der Exzitonen in Cu_2O zu berücksichtigen.

In der theoretischen Beschreibung der Valenzbandstruktur nach Luttinger [126] wird das zunächst als dreifach entartet angenommene Valenzband über einen Quasi-Spin $I = 1$ beschrieben, welcher eine Abstraktion für die drei zugrundeliegenden Blochfunktionen ist. Die Spin-Bahn-Wechselwirkung zwischen dem Quasi-Spin und dem Spin des Lochs führt dann zur Aufspaltung der Valenzbänder. Im allgemeinen Fall ist die kinetische Energie des Lochs in einem kubischen Halbleiter über den Luttinger-Hamiltonoperator (4.6) gegeben, in dem die Luttinger-Parameter γ_i die effektive Masse des Lochs sowie die Aufspaltung und kubische Verformung der Bänder angeben. Im Abschitt 4.2 wird der Hamiltonoperator des Exzitons mit der vollen kinetischen Energie des Lochs (4.6) eingeführt. Die kubische Valenzbandstruktur führt, wie im Abschnitt 4.1 ausführlich diskutiert, zu einer Kopplung zwischen der Relativbewegung von Elektron und Loch mit den orbitalen Blochfunktionen, welche im Wasserstoffmodell nicht auftritt. Die sich ergebende Symmetrieerniedrigung macht sich direkt im Exzitonspektrum als Feinstrukturaufspaltung bemerkbar. Der Einfluss kubischer Valenzbandstrukturen auf Exzitonspektren wurde erstmals von Altarelli, Baldereschi and Lipari in den 70er Jahren für jene Halbleiter wie Galluimarsenid untersucht, bei denen bereits das oberste Valenzband entartet ist [77–81].

Der Hamiltonoperator des Exzitons kann mithilfe des Formalismus der irreduziblen Tensoren [79, 248, 281] umgeschrieben werden und ist in Gleichung (4.10) angegeben. Zur Lösung der zugehörigen Schrödingergleichung wird eine vollständige Basis verwendet. Der Aufbau dieser Basis ist im Detail im Abschnitt 4.3 beschrieben. Für den sphärischen Anteil der Basis muss berücksichtigt werden, dass der Hamiltonooperator verschiedene Drehimpule und Spins miteinander koppelt. So werden zunächst der Quasi-Spin I und der Lochspin S_h zum Gesamtlochspin $J = I + S_\mathrm{h}$ gekoppelt, bevor dieser dann mit dem Drehimpuls L der Relativbewegung des Exzitons zum Gesamtdrehimpuls $F = L + J$ gekoppelt wird. Zur Vollständigkeit wird der Elektronenspin S_e ebenfalls in der Basis berücksichtigt. Der radiale Anteil der Basis wird mithilfe der Coulomb-Sturmschen Funktionen (4.21) beschrieben. Der Ansatz (4.23) für die Wellenfunktion des Exzitons führt schließlich auf ein verallgemeinertes Eigenwertproblem, welches mithilfe einer geeigneten LAPACK-Routine numerisch gelöst wird.

Die Lösungsmethode mit einer vollständigen Basis erlaubt es nicht nur die Energien der Exzitonenzustände für beliebige direkte Halbleiter mit kubischer Valenzbandstruktur zu bestimmen sondern auch deren Oszillatorstärken. Die Formeln für Dipol- und Quadrupoloszillatorstärken werden ausführlich in Abschnitt 4.4 hergeleitet. Bei der Berechnung der Oszillatorstärken spielen dabei folgende drei Punkte eine entscheidende Rolle: (i) Dipolübergänge sind aufgrund derselben Parität von Leitungs- und Valenzband in Cu_2O paritätsverboten. Folglich ist das Übergangsmatrixelement proportional zum Gradienten der Wellenfunktion am Ursprung und der Exzitonzustand muss eine Komponente mit $L = 1$ besitzen. Bei Quadrupolübergängen hängt das Übergangsmatrixelement vom Wert der Wellenfunktion am Ursprung ab und der Exzitonzustand muss hier eine Komponente mit $L = 0$ aufweisen. (ii) Dipol- und Quadrupoloperator ändern den Gesamtspin $S = S_\mathrm{e} + S_\mathrm{h}$ nicht, weshalb der Exzitonzustand eine Komponente mit $S = 0$ besitzen muss. (iii) Die Gesamtsymmetrie der Exzitonwellenfunktion muss identisch zur Symmetrie Γ_4^- des Dipoloperators bzw. zur Symmetrie Γ_5^+ des Quadrupoloperators sein. Da Kupferoxydul kubische Symmetrie besitzt, lassen sich alle Symmetrien im System mithilfe der irreduziblen Darstellungen der kubischen Gruppe O_h ausdrücken [12, 90, 169, 170].

Im Abschnitt 4.5.1 wird die Feinstrukturauspaltung der Exzitonen in $\mathrm{Cu_2O}$ mit Gesamtdrehimpuls $F = 5/2$ und $F = 7/2$ untersucht und mit experimentellen sowie theoretischen Ergebnissen aus Ref. [36] vergleichen. Es kann gezeigt werden, dass mehrere Kombinationen der Luttinger-Parameter γ_i existieren, für welche dieselbe Aufspaltung erhalten wird. Da die Luttinger-Parameter jedoch untrennbar mit der Bandstruktur zusammenhängen, dürfen diese nicht einfach wie in vorangegangenen Arbeiten [36, 72] durch Anpassung an Exzitonspektren bestimmt werden, sondern müssen wie in Ref. [37] geschehen, durch einen Fit an die Valenzbänder festgelegt werden. Speziell für die Ref. [37] erhaltenen Werte der Luttinger-Parameter lässt sich ebenfalls eine gute Übereinstimmung mit den experimentellen Spektren nicht nur bezüglich der Energie sondern auch bezüglich der Oszillatorstärken erhalten.

In früheren Arbeiten zu Exzitonen [82–84] wurde eine Aufspaltung des $1S$ Ortho-Exzitons, d.h. des quadrupolerlaubten Anteils des Exziton-Grundzustandes, beobachtet und im Rahmen einer Austauschwechselwirkung erklärt, welche vom Schwerpunktimpuls $\hbar K$ des Exzitons abhängt. Berücksichtigt man jedoch im Hamiltonoperator mit der kubischen Valenzbandstruktur auch den Schwerpunktimpuls des Exzitons, so ergeben sich Operatoren von derselben Form wie in [82–84]. Man vergleiche hierzu die Gleichungen (4.81) und (4.88) im Abschnitt 4.5.2. Diese Operatoren, welche die richtungsabhängige Dispersion des Exzitons beschreiben, hängen von den Luttinger-Parametern ab. Es kann gezeigt werden, dass sie von der korrekten Größenordnung sind, um die K-abhängige Aufspaltung des Grundzustandes zu beschreiben. Daher wird gefolgert, dass die Dispersion und nicht die Austauschwechselwirkung Ursache der beobachteten Aufspaltung ist.

K-abhängige Austauschwechselwirkung Im Rahmen der Behandlung der Austauschwechselwirkung für $\mathrm{Cu_2O}$ werden üblicherweise nur die führenden Terme behandelt. Da nun zwar gezeigt werden konnte, dass sich die in [82–84] beobachtete Aufspaltung des $1S$ Ortho-Exzitons über die Dispersion und die kubische Valenzbandstruktur erklären lässt, sich ein Beitrag höherer Terme der Austauschwechselwirkung, wie in [82–84] vermutet, jedoch nicht von Vornherein ausschließen lässt, verdienen diese Terme eine genauere Betrachtung. Die einzige uns bekannte Arbeit zu dieser Thematik von Kavoulakis *et al.* [162] geht hierfür nicht weit genug, weshalb wir die Austauschwechselwirkung umfassend behandeln.

Die Austauschwechselwirkung zwischen zwei Exziton-Zuständen ist in der allgemeinen Form durch Gleichung (5.2) gegeben und lässt sich, wie in Abschnitt 5.1.2 gezeigt, am geeignetsten in der Fourierdarstellung behandeln. In dieser Darstellung zerfällt die Austauschwechselwirkung in einen analytischen und einen nichtanalytischen Teil. Der Name des nichtanalytischen Teiles beruht auf der Tatsache, dass dieser zwar von der Richtung des Schwerpunktimpulses $\hbar\boldsymbol{K}$, jedoch nicht von dessen Betrag abhängt. Mittels der sogenannten $\boldsymbol{k}\cdot\boldsymbol{p}$-Störungstheorie, bei welcher der gitterperiodische Anteil der Blochfunktionen für kleine Wellenvektoren entwickelt wird [siehe Gl. (5.20)], lassen sich Terme beliebiger Ordnung in der analytischen und nichtanalytischen Austauschwechselwirkung erhalten. Dabei zeigt sich, dass das Auftreten einer K-abhängigen Austauschwechselwirkung der S-Exzitonen, d.h. der Exzitonen mit Drehimpuls $L = 0$, untrennbar mit einem Auftreten einer

K-unabhängigen Austauschwechselwirkung der P- und D-Exzitonen verknüpft ist, welche jedoch bisher noch nie nachgewiesen wurde.

Im Abschnitt 5.3 wird die Größenordnung der höheren Terme der Austauschwechselwirkung abgeschätzt. Hierbei wird verwendet, dass der führende Term der analytischen Austauschwechselwirkung zu einer Aufspaltung des Exziton-Grundzusandes in einen Ortho- und einen Para-Anteil mit einer Energiedifferenz von 12 meV führt. Der nächsthöhere Term ist fünf Größenordnungen kleiner und damit zu klein, um die in [82–84] beobachtete Aufspaltung des $1S$ Ortho-Exzitons zu erklären. Die nichtanalytische Austauschwechselwirkung, deren führender Term in Cu_2O aus Paritätsgründen verschwindet, ist nochmals um zwei Größenordnungen kleiner. Jedoch kann gezeigt werden, dass aufgrund der Form der höheren Terme der nichtanalytischen Austauschwechselwirkung transversale und longitudinale Exzitonzustände, d.h. jene Zustände, deren Dipolmoment senkrecht oder parallel zum Vektor $\boldsymbol{K}$ steht, prinzipiell gemischt werden.

Gerade Exzitonserie In Kupferoxydul ist die Parität eine gute Quantenzahl, weshalb das Exzitonsprektrum in zwei Teile zerfällt: in die dipolaktiven Zustände negativer Parität mit ungeradem Drehimpuls, welche in Ein-Photonen-Spektroskopie beobachtet werden, und die dipolverbotenen Zustände positiver Parität mit geradem Drehimpuls, welche in Zwei-Photonen-Spektroskopie beobachtet werden. Die ungerade Serie wurde bereits im Rahmen der Auswirkungen der Valenzbandstruktur eingehend untersucht. Bei der Behandlung der geraden Exzitonserie bedarf es weiterer Korrekturterme im Hamiltonoperator aufgrund der sehr kleinen Radii der Exziton-Grundzustände der gelben und grünen Serie, für welche die Annahmen des Wannier-Modells nicht mehr gelten. Diese als „Central-Cell Corrections“ oder „Zentralzellen-Korrekturen“ bekannten Korrekturen wurden erstmals von Kavoulakis *et al.* [162], jedoch nicht im Zusammenhang mit der kubischen Valenzbandstruktur, für Cu_2O betrachtet. Sie umfassen (i) eine reduzierte Abschirmung der Coulomb-Wechselwirkung aufgrund einer frequenz- und wellenvektorabhängigen Dielektrizitätskonstante bei kleinen Abständen zwischen Elektron und Loch, (ii) höhere Terme in der Austauschwechselwirkung sowie (iii) Terme vierter Ordnung in den Impulsen in den kinetischen Energien von Elektron und Loch. Im Rahmen der ausführlichen Diskussion der Korrekturen im Abschnitt 6.1 stellt sich heraus, dass nur Effekte bezüglich der Dielektrizitätskonstante berücksichtigt werden müssen. Die zugehörigen Korrekturpotentiale sind das sogenannte Haken-Potential (6.6) oder Pollmann-Büttner-Potential sowie ein deltaförmiges Potential (6.15), welches von Kavoulakis *et al.* [162] hergeleitet wurde.

Im Abschnitt 6.2 wird der Einfluss der Korrekturterme auf das Exzitonspektrum untersucht. Da die $1S$-Exziton-Zustände aufgrund der Valenzbandstruktur an alle anderen Zustände positiver Parität gekoppelt sind, wirken sich die Korrekturen auf die gesamte gerade Serie aus. Ein spezieller Fall ist dabei der Grundzustand der grünen Serie, welcher aufgrund der Korrekturen im Bereich des gelben $2S$-Zustandes liegt. Zwischen beiden Zuständen kommt es zu einer starken Wechselwirkung, wodurch in der Folge die Oszillatorstärke des $2S$-Zustandes deutlich abnimmt.

Als einzige freie Parameter werden der Koeffizient der analytischen Austauschwechselwirkung sowie der Koeffizient des deltaförmigen Potentials bestimmt. Dabei kann gezeigt werden, dass beide Parameter nahezu unabhängig bestimmt werden können, weshalb das Ergebnis eindeutig ist. Bezüglich der Exzitonenergien als auch der Oszillatorstärken lässt sich eine sehr gute Übereinstimmung mit experimentellen Werten erreichen, welche in den Tabellen 6.2 und 6.3 aufgeführt sind. Da die Zentralzellen-Korrekturen die ungerade Exzitonserie nicht beeinflussen, ermöglicht der volle Hamiltonoperator (4.7) mit den Korrekturen (6.17a) eine konsistente theoretische Beschreibung der kompletten gelben und grünen Serie.

Magnetoexzitonen Die für Kupferoxydul beobachtete Feinstrukturaufspaltung in Exzitonenspektren zeigte bereits, dass es zwingend erforderlich ist, die kubische Valenzbandstruktur in der Theorie der Exzitonen zu berücksichtigen. Dies ist umso wichtiger im Falle von Magnetoexzitonen, d.h. von Exzitonen in äußeren Magnetfeldern, weil die Felder die Symmetrie im System noch weiter erniedrigen. Da der Exzitonradius sehr viel größer als der Bohrradius des Wasserstoffatoms ist, wirken sich Magnetfelder deutlich stärker auf Exzitonspektren aus. Dadurch kann im Gegensatz zum Wasserstoffatom der sogenannte Bereich „hoher Magnetfeldstärken“ bereits bei Laborfeldstärken erreicht werden.

Im Abschnitt 7.1 wird zunächst gezeigt, dass sich äußere Felder über die minimale Substitution in die Wannier-Gleichung integrieren lassen. Dies nicht selbstverständlich, da sich die Wannier-Gleichung selbst über Näherungen aus einem Vielteilchenproblem herleitet. Im Magnetfeld ergibt sich die Besonderheit, dass nicht mehr der Gesamtimpuls sondern ein sogenannter Pseudo- oder verallgemeiner Impuls (7.18) erhalten ist. Folglich wird dieser bei der Betrachtung der Relativbewegung des Exzitons auf Null gesetzt. Der Hamiltonoperator der Magnetoexzitonen in $\mathrm{Cu_2O}$ wir kurz im Abschnitt 7.2 besprochen. Neben der Tatsache, dass das Magnetfeld B über die minimale Substitution in die Terme für die kinetische Energie von Elektron und Loch eingeht, wodurch sich aufgrund der Valenzbandstruktur sehr komplizierte Ausdrücke ergeben, muss auch berücksichtigt werden, dass die Spins im System an das Magnetfeld koppeln. Der Operator H_B (7.26), welcher diese Kopplung beschreibt, erhält einen bis dato für $\mathrm{Cu_2O}$ unbekannten Materialparameter: den vierten Luttinger-Parameter κ.

Die Schrödingergleichung der Magnetoexzitonen wird wieder mit der bereits beschriebenen vollständigen Basis gelöst. Bei der Berechnung der Oszillatorstärken muss nun darauf geachtet werden, wie das Magnetfeld die Symmetrie im System bricht. Im Falle der drei betrachteten Magnetfeldrichtungen entlang [001], [110] und [111] erniedrigt sich die Symmetrie O_h auf $C_{4\mathrm{h}}$, $C_{2\mathrm{h}}$ oder $C_{3\mathrm{i}}$. Die irreduziblen Darstellungen dieser Gruppen lassen sich bestimmten Polarisationen des Lichtes zuordnen. Während im Falle eines Magnetfeldes in [001]- und [111]-Richtung links- und rechtszirkular polarisiertes Licht mit unterschiedlichen irreduziblen Darstellungen verknüpft sind und sich folglich unterschiedliche Exzitonenzustände anregen lassen, gehören die beiden Polarisationen bei einem Magnetfeld in [110]-Richtung zu derselben irreduziblen Darstellung. Folglich lassen sich mit links- oder rechtszirkular polarisiertem Licht prinzipiell alle dipolerlaubten Exzitonzustände anregen. Im Gegensatz zu den anderen Richtungen sind die Exzitonzustände hier, wie in Abschnitt 7.3.2 beschrieben, mit einer elliptischen Polarisation verknüpft.

Da die theoretischen Ergebnisse zu Magnetoexzitonen werden mit experimentellen Daten der Gruppe von M. Bayer, D. Fröhlich und M. Aßmann der TU Dortmund verglichen. Eine eine kurze Beschreibung der Experimente findet sich in Ref. [39]. Für die Vergleiche mit theoretischen Ergebnissen werden immer die zweiten Ableitungen der experimentellen Spektren bezüglich der Energie berechnet, da hierdurch Intensitätsunterschiede verringert und schwächere Strukturen stärker hervorgehoben werden.

Mittels gruppentheoretischer Überlegungen zu Beginn von Abschnitt 7.4 wird gezeigt, dass sich die Anzahl dipolerlaubter Zustände in Abhängigkeit der Magnetfeldrichtung (und der Hauptquantenzahl) unterscheidet. Für das Magnetfeld in [001]-Richtung erhält man 6 bzw. 20 Zustände für die Hauptquantenzahlen $n = 2, 3$ bzw. $n = 4, 5$. Entsprechend erhält man für die [110]-Richtung 6 bzw. 20 und für die [111]-Richtung 8 bzw. 26 Zustände. Einen übersichtlichen Vergleich theoretischer und experimenteller Ergebnisse für die Exzitonzustände mit den Hauptquantenzahlen $n = 3$ bis $n = 7$ zeigt die Abbildung 7.1. Man sieht deutlich die schnelle Zunahme der Anzahl der beobachteten Linien mit der Hauptquantenzahl n sowie die Aufspaltung zwischen P, F und H-Exzitonen bei $B = 0$. Weiterhin fällt die deutliche Krümmung der Exzitonlinien und die Zunahme der Oszillatorstärke bei den F- und H-Exzitonen mit steigender Magnetfeldstärke auf.

Bei der theoretischen Berechnung der Exzitonenergien wird der unbekannte vierte Luttinger-Parameter zunächst variiert. Über den Vergleich mit den experimentellen Ergebnissen kann dann der optimale Wert zu $\kappa = -0.5 \pm 0.1$ bestimmt werden. Die sehr gute Übereinstmmung zwischen Theorie und Experiment zeigen die Abbildungen 7.2 bis 7.5. Die aus den Absorptionsspektren ausgelesenen Positionen der Exzitonzustände wurden dort mit blauen Dreiecken dargestellt und über die theoretischen Ergebnisse gelegt. Die Abbildung 7.4 zeigt die Elliptizität der Exzitonzustände für den Fall eines Magnetfeldes in [110]-Richtung.

Die Ergebnisse können noch auf zwei andere Weisen bestätigt werden: Bei der Methode der harmonischen Inversion [361, 362] wird das experimentelle Spektrum für einen festen Wert der Magnetfeldstärke fouriertransformiert und als Summe von Lorentzfunktionen ausgedrückt. Dadurch lassen sich die Positionen, Amplituden und Breiten zugrundeliegender Resonanzen bestimmen. Der Vergleich der so bestimmten Amplituden mit den theoretischen Werten für die Oszillatorstärken in der Abbildung 7.5 zeigt eine sehr gute Übereinstimmung. Abschließend wird der Wert von κ über die Theorie von Luttinger bestimmt, nach welcher der vierte Luttinger-Parameter von den ersten drei abhängt. Eine Abschätzung mittels gruppentheoretischer Überlegungen ergibt $\kappa \approx -0.7$ und somit eine vernünftige Übereinstimmung mit dem zuvor ermittelten Wert. Die sich ergebende Abweichung lässt sich durch Näherungen im Rahmen der Abschätzung erklären.

Niveaustatistik der Magnetoexzitonen Da die klassische Beschreibung von Chaos über Trajektorien und positive Lyapunov-Exponenten in der Quantenmechanik nicht anwendbar ist, stellte sich lange die Frage, wie sich klassisches Chaos in quantenmechanischen Spektren manifestiert. Die Bohigas-Giannoni-Schmit-Vermutung [366] besagt, dass solche Quantensysteme mithilfe der „Random Matrix Theory“ oder der „Theorie der Zufallsmatrizen“ [367, 368] beschrieben werden können und sich folglich irreguläres klassisches Verhalten in den statistischen Eigenschaften des zugehörigen Quantensystems widerspiegelt. Da in der Theorie der Zufallsmatrizen der Hamiltonoperator durch eine Zufallsmatrix mit geeigneten Symmetrien ersetzt wird, um die statistischen Eigenschaften des Eigenwertspektrums zu untersuchen [370], spielen nur universelle Größen des betrachteten physikalischen Systems eine entscheidende Rolle. Die genauen dynamischen Eigenschaften sind hierbei irrelavant.

Alle Systeme, deren Hamiltonoperatoren im Falle der klassischen Dynamik zu globalem Chaos führen, lassen sich drei Universalitätsklassen zuordnen. Zu welcher dieser Klassen ein System gehört, wird von den verbleibenden Symmetrien im System bestimmt. Die meisten physikalischen Systeme sind invariant unter Zeitumkehr oder weisen zumindest eine antiunitäre Symmetrie auf und zeigen damit die Statistik eines Gauß'schen orthogonalen Ensembles (GOE). Beispiele für die anderen Universalitätsklassen sind weitaus schwieriger zu finden, da Systeme ohne jegliche antiunitäre Symmetrie [Gauß'sches unitäres Ensemble (GUE)] oder Systeme mit Zeitumkehr-Invarianz und Kramer's-Entartung, aber ohne jegliche geometrische Symmetrie [Gauß'sches symplektisches Ensemble (GSE)] gefunden werden müssen [364]. Selbst eines der wichtigsten Systeme für die Untersuchung von Quantenchaos, das Wasserstoffatom in gekreuzten elektrischen und magnetischen Feldern, besitzt immer noch eine verbleibende antiunitäre Symmetrie und zeigt folglich nur GOE-Statistik [364].

Umso erstaunlicher ist daher die kürzliche Beobachtung von GUE-Statistik bei Magnetoexzitonen in Kupferoxydul [31, 32], wo doch Exzitonen als das Wasserstoff-Analogon des Festkörpers angesehen werden. Im Kapitel 8 wird der Ursache dieses Symmetriebruchs nachgegangen, wobei die kubische Valenzbandstruktur eine entscheidende Rolle spielt.

Im Abschnitt 8.1 wird zunächst ein vereinfachtes Modell für Exzitonen in Cu_2O vorgestellt, bei dem die Spin-Bahn-Wechselwirkung sowie die Kopplung der Spins an das Magnetfeld vernachlässigt werden. Beide Terme besitzen sphärische Symmetrie und spielen daher für die Statistik keine Rolle. Durch das Vernachlässigen des Elektron- und Lochspins ist die Basis zur Lösung der Schrödingergleichung viel kleiner, wodurch auch Exzitonzustände zu hohen Hauptquantenzahlen bei fest vorgegebenem Computerspeicher noch numerisch berechnet werden können.

Die Schrödingergleichung kann für konstante Feldstärken, aber auch für konstante skalierte Energien gelöst werden. Die Methode der konstanten skalierten Energien $\hat{E}$ ist aus der Atomphysik bekannt (siehe Abschnitt 8.1.2). Hierbei werden die Größen im System gemäß Gl. (8.9) mit einem magnetfeldabhängigen Parameter γ skaliert. Die Schrödingergleichung lässt sich dann mit der bekannten vollständigen Basis wieder auf ein Eigenwertproblem (8.13) umschreiben, bei dem die skalierten Energien als Eigenwerte auftreten.

Im Abschnitt 8.2.1 wird analytisch gezeigt, dass der Hamiltonoperator des Exzitons alle antiunitären Symmetrien bricht. Wie bereits erwähnt, zeigt das Wasserstoffatom in äußeren Feldern noch eine verbleibende antiunitäre Symmetrie: Zeitumkehr mit anschließender Spiegelung an jener Ebene, welche von den beiden Feldern aufgespannt wird. Im Falle des Exzitons muss die kubische Struktur des Festkörpers oder die kubische Valenzbandstruktur berücksichtigt werden. Fällt die Ebene der äußeren Felder nicht mit einer Symmetrieebene des Gitters zusammen oder liegt das Magnetfeld im Falle eines verschwindenden elektrschen Feldes in keiner dieser Symmetrieebenen, so überführt die vom Wasserstoffatom bekannte Spiegelung das Gitter nicht in sich selbst. Folglich bricht das Exziton diese Symmetrie für fast alle Feldkonfigurationen. Dies ist der erste Nachweis, dass in einem räumlich homogenen System alle antiunitären Symmetrien gebrochen werden.

Der numerische Nachweis der GUE-Statistik erfolgt in Abschnitt 8.2.2. Hierbei wird das Eigenwertspektrum mit der Methode der vollständigen Basis bestimmt und anschließend entfaltet, um das Verhalten der nicht-universellen spektralen Dichte von den universellen spektralen Fluktuationen zu trennen. Die sich ergebende Niveaustatistik oder kumulative Verteilungsfunktion (8.24) wird mit den bekannten Formeln für Poisson, GOE- oder GUE-Statistik verglichen. Befindet sich das Magnetfeld in einer Symmetriebene des Gitters oder wird der Koeffizient δ' der kubischen Terme im Hamiltonoperator auf Null gesetzt, so zeigt sich wie erwartet GOE-Statistik, anderenfalls GUE-Statistik (siehe Abbildungen 8.1 und 8.2). Von der Atomphysik ist zudem bekannt, dass sich für kleine skalierte Energien reguläres klassisches Verhalten ergibt und damit das quantenmechanische Spektrum Poisson-Statistik zeigt.

Das Auftreten aller drei Statistiken in Abhängigkeit der Systemparameter erlaubt es nun auch, Übergänge zwischen diesen zu untersuchen. Dies ist nach unserem besten Wissen bisher nur bei zwei anderen Systemen möglich gewesen: dem sogenannten „Kicked Top“ [391] und dem Anderson-Modell [392]. Während der Kicked Top jedoch ein zeitabhängiges System ist, welches mit Floquet-Theorie behandelt werden muss, und das Anderson-Modell lediglich ein Modellsystem für ein d-dimensionales ungeordnetes Gitter ist, stellen Magnetoexzitonen ein realistisches physikalisches System dar. Insbesondere lassen sich die Parameter wie die sklaierte Energie und der Winkel des Magnetfeldes, welche die Übergänge zwischen den Statistiken beschreiben, auch experimentell variieren.

Im Abschnitt 8.3 werden die Übergänge zwischen den Statistiken untersucht. Hierbei werden die theoretischen Ergebnisse mit den Formeln aus der Theorie der Zufallsmatrizen für diese Übergänge verglichen. Da für das Wasserstoffatom der Übergang Poisson → GOE schon detailliert untersucht wurde [385], liegt in dieser Arbeit der Schwerpunkt auf dem Übergang GOE → GUE in Abhängigkeit der Orientierung des Magnetfeldes zum Gitter sowie auf dem Übergang Poisson → GUE in Abhängigkeit der skalierten Energie. In beiden Fällen zeigen sich sehr gute Übereinstimmungen mit den Formeln aus der Theorie der Zufallsmatrizen, wie man den Abbildungen 8.4 und 8.6 entnehmen kann.

Die Beobachtungen von M. Aßmann *et al.* [31, 32] zeigen, dass GUE-Statistik selbst dann auftritt, wenn das Magnetfeld in einer Hochsymmetrierichtung des Gitters liegt. Dies lässt sich nicht mehr allein mit der kubischen Valenzbanstruktur erklären. M. Aßmann *et al.* [31, 32] hatten zunächst vermutet, dass das Brechen aller antiunitären Symmetrien über die Exziton-Phonon-Wechselwirkung zu erklären sei. Aus diesem Grunde wird die Auswirkung der Exziton-Phonon-Wechselwirkung auf die Niveaustatistik im Abschnitt 8.4 für den Fall eines in einer Symmetrieebene liegenden Magnetfeldes untersucht. Es zeigt sich, dass der Wechselwirkungsoperator (8.32) von der Schwerpunktkoordinate $\boldsymbol{R}$ des Exzitons abhängt.Folglich ist der Pseudoimpuls keine Erhaltungsgröße mehr und kann nicht wie bisher auf Null gesetzt werden. Aus der Atomphysik ist bekannt, dass die Schwerpunktbewegung in einem Magnetfeld zu einem Bewegungs-Stark-Effekt (8.33) führt. Da sich das Gesamtsystem mit kubischer Valenzbandstruktur, endlichem Schwerpunktimpuls $\hbar K$ und Phononen numerisch (noch) nicht lösen lässt, müssen ein paar Vereinfachungen vorgenommen werden. Wir nehmen an, dass sich das phononische System im thermischen Gleichgewicht befindet und sich somit der mittlere Wert von K über die Temperatur mittels Gl. (8.35) bestimmt. Dieser Wert von K geht dann in den Bewegungs-Stark-Effekt ein, wobei nur der führende Term dieses Effekts berücksichtigt wird. Die Orientierung des entsprechenden Bewegung-Stark-Feldes [siehe Gln. (8.33) und (8.34)] wird als isotrop angenommen. Es zeigt sich, dass sich bei einer Mittelung über alle diese Orientierungen die Exzitonzustände energetisch verschieben und sich somit Auswirkungen auf die Niveaustatistik ergeben. Dieser Nachweis erfolgte in Abb. 8.11 auch mit dem vollständigen Modell für Kupferoxydul, in dem die Spins von Elektron und Loch berücksichtigt werden. Somit wurde bestätigt, dass die Exziton-Phonon-Wechselwirkung, welche zu einem endlichen Schwerpunktimpuls und damit in einem Magnetfeld zu einem Bewegungs-Stark-Effekt führt, zusammen mit der kubischen Valenzbandstruktur alle antiunitären Symmetrien bricht - und das unabhängig von der Orientierung des Magnetfeldes. Man beachte jedoch, dass die Exziton-Phonon-Wechselwirkung allein den beobachteten Symmetriebruch nicht erklären kann. Die kubische Valenzbandstruktur muss in jedem Falle berücksichtigt werden.

Exziton-Polaritonen Die Beobachtung von Rydberg-Exzitonen in Kupferoxydul wirft unausweichlich die Frage auf, ob diese Quasiteilchen im Rahmen eines Multi-Polariton-Konzeptes beschrieben werden müssen, da Exzitonen und Photonen im Festkörper immer zu Polaritonen gekoppelt werden. Im Vergleich zu Atomen ergibt sich bei Festkörpern ein fundamentaler Unterschied bezüglich der Kopplung an Licht. Man könnte annehmen, dass sich die Absorption von Licht über die Anregung eines Exzitons bei gleichzeitigem Verschwinden eines Photons beschreiben lässt. Nun sind jedoch Anregungen im Festkörper immer mit einer Polarisation verknüpft. Da eine oszillierende Polarisation wiederum eine elektromagnetische Welle emittiert, die auf die einfallende Welle rückwirkt, ergibt sich ein Wechselspiel zwischen Licht und Materie. Befindet sich die Frequenz des Lichtes in der Nähe der Resonanzfrequenz einer Anregung, kommt es einer starken Kopplung und anomaler Dispersion. Exzitonen und Photonen können daher nicht als gute Eigenzustände angesehen werden. Stattdessen wird das Polariton als neues Quasiteilchen eingeführt, welches das Quant der gemischten Zustände aus Polarisation und elektromagnetischer Welle darstellt.

Bei der Betrachtung der Polaritonen spielt der Schwerpunktimpuls der Exzitonen eine entscheidende Rolle. Daher wird in Abschnitt 9.1 der Exziton-Hamiltonoperator, der bereits die Valenzbandstruktur, die Zentralzellen-Korrekturen und die Austauschwechselwirkung enthält, für einen nichtverschwindenden Schwerpunktimpuls $\hbar K$ betrachtet. Die zugehörige Schrödingergleichung wird anschließend wieder mittels der bereits bekannten vollständigen Basis gelöst. Wie im Falle der Magnetoexzitonen muss auch hier für die Berechnung der Oszillatorstärken die Symmetrieerniedrigung – diesmal durch den endlichen K-Vektor – berücksichtigt werden. Dies geschieht in Abschnitt 9.2.

Die quantenmechanische Beschreibung der Polaritonen, welche zunächst von Hopfield, Fano, und Agranovich [141, 413, 414] entwickelt wurde, erfolgt in der Regel im Formalismus der zweiten Quantisierung. Die Gleichung (9.25) im Abschnitt 9.3.1 beschreibt hierbei die Wechselwirkung zwischen Exzitonen und Photonen. Der Hamiltonoperator lässt sich mithilfe der sogenannten Hopfield-Transformation [141, 413] diagonalisieren, wodurch sofort die Polaritondispersion erhalten wird. Für verschwindenden Lichtwellenvektor kommt es zu einer energetischen Aufspaltung zwischen longitudinalen und transversalen Moden (LT-Aufspaltung). Eine wichtige Tatsache ist, dass die Größe der LT-Aufspaltung exakt identisch zur Größe der nichtanalytischen Austauschwechselwirkung bei verschwindendem Wellenvektor ist. Dadurch besitzen longitudinale und transversale Zustände wieder dieselbe Energie, was aus Gründen der Symmetrie auch erforderlich ist. Folglich muss bei einer Beschreibung der Polaritonen immer auch die nichtanalytische Austauschwechselwirkung berücksichtigt werden.

Nach der allgemeinen Lösung wird in Abschnitt 9.3.2 die Drehwellennäherung beschrieben, bei der Einflüsse von schnell rotierenden Termen im System vernachlässigt werden. Der sich ergebende Jaynes-Cummings-Hamiltonoperator [426] lässt sich leicht auf einen Eigenwertproblem umschreiben. Das dies, wie in Abschnitt 9.3.3 gezeigt, auch für die nichtanalytische Austauschwechselwirkung möglich ist, erhält man so ein Eigenwertproblem, in welches die K-abhängigen Energien sowie Oszillatorstärken der Exzitonen eingehen und welches als Lösung die Polaritondispersionen liefert. Der Abschnitt 9.3.4 beschäftigt sich mit der Beobachtbarkeit von Polaritoneffekten im Experiment und diskutiert die von Tait in Ref. [430] aufgestellten Kriterien. Um Polaritonen beobachten zu können muss entweder in nichtlinearen optischen Experimenten wie der Zweiphotonenabsorption ein kohärenter Energieübertrag zwischen Exziton und Photon stattfinden oder in Absorptionsexperimenten die mittlere freie Weglänge des Exzitons sehr viel größer als die Wellenlänge des Lichtes sein. Mittels dieser Kriterien kann im Abschnitt 9.5 gezeigt werden, dass Polaritoneffekte in Absorptionsspektren von Kupferoxydul für Exzitonen mit einer Hauptquantenzahl $n \geq 2$ nicht beobachtbar sind.

Für den Exziton-Grundzustand, dessen Polaritoneigenschaften trotz der sehr kleinen Quadrupoloszillatorstärke experimentell bereits mehrfach nachgewiesen werden konnten [178–180], wird in Abschnitt 9.4 ein 5×5-Matrixmodell aufgestellt, welches eine sehr einfache Berechnung der Polaritondispersion für beliebige Orientierungen des Schwerpunktimpulses ermöglicht.

Im Falle der Exzitonen mit Hauptquantenzahlen $n \geq 5$ ist der Einfluss der Valenzbandstruktur, der Zentralzellen-Korrekturen und der Austauschwechselwirkung klein. Folglich wird die Dispersion der zugehörigen Exziton-Polaritonen im Abschnitt 9.5 mit dem Wasserstoffmodell bestimmt. Hierbei zeigt sich bereits eine starke Durchmischung der Exzitonzustände verschiedener Hauptquantenzahl in der Nähe der Exziton-Photon-Resonanz aufgrund der Exziton-Photon-Wechselwirkung. Folglich müssen Rydberg-Polaritonen immer über ein Multi-Polaritonkonzept beschrieben werden. Eine unabhängige Behandlung der Polaritonen zu verschiedener Hauptquantenzahl würde zu falschen Ergebnissen führen.

Für die Exzitonen mit kleinen Hauptquantenzahlen müssen alle oben genannten Korrekturen berücksichtigt werden. Eine Betrachtung der zugehörigen Polaritondispersionen erfolgt im Abschnitt 9.6. Um quantitativ korrekte Ergebnisse zu erhalten, müssen jedoch hier zunächst die absoluten Größen der Oszillatorstärken und der nichtanalytischen Austauschwechselwirkung bestimmt werden. Die in dieser Arbeit vorgestellte Methode zur Berechnung der Oszillatorstärken liefert zunächst nur relative Oszillatorstärken. Folglich wird der theoretisch berechnete Wert für die Oszillatorstärke des $1S$ Ortho-Exzitons mit dem experimentell bestimmten Wert verglichen, um einen entsprechender Skalierungsfaktor η zu bestimmen und absolute Oszillatorstärken zu erhalten [siehe Gl. (9.74)]. Die Größe der nichtanalytischen Austauschwechselwirkung ergibt sich dadurch, dass die durch sie hervorgerufene LT-Aufspaltung bei $K = 0$ identisch sein muss mit der Aufspaltung durch die Exziton-Photon-Wechselwirkung. Mit der Kenntnis der erforderlichen Größen ist dann möglich, innerhalb der Drehwellennäherung die Polariton-Dispersionen zu berechnen. Diese sind für die verschiedenen Orientierungen [001], [110], und [111] von $\boldsymbol{K}$ und die verschiedenen Licht-Polarisationen in den Abbildungen 9.4 bis 9.7 dargestellt. In den Teilbildern (a) dieser Abbildungen ist dabei das Exzitonspektrum gezeigt, wobei die Zustände mit der in Kapitel 6 eingeführten Nomenklatur bezeichnet werden. In den Polaritondispersionen, welche in den Teilbildern (b) gezeigt werden, fallen vor allem die starken vermiedenen Kreuzungen für die P-Exzitonen auf, die sich aufgrund ihrer hohen Oszillatorstärke ergeben. Diese starken vermiedenen Kreuzungen verschieben sehr deutlich die Postionen der anderen schwächeren vermiedenen Kreuzungen der S-, D- und F-Exzitonen. Der Photon-Anteil der Polaritonen in den Teilbildern (c) weist wieder auf eine starke Durchmischung der Exzitonzustände hin.

Im Falle des $1S$ Ortho-Exzitons wird in Abschnitt 9.7.1 zunächst noch einmal dessen K-abhängige Aufspaltung untersucht. Im Gegensatz zu Kapitel 4 wird hier nicht mit Störungstheorie gearbeitet, sondern der vollständige Hamiltonoperator inklusive Zentralzellen-Korrekturen diagonalisiert. Beim Vergleich der Ergebnisse für die Parameter Δ_i, welche diese Aufspaltung beschreiben, mit den experimentellen Ergebnissen zeigt sich eine relativ gute Übereinstimmung (siehe Tabelle 9.2). Dabei muss allerdings beachtet werden, dass in den experimentellen Spektren der Wert von K unscharf ist und damit die Auswertung der experimentellen Ergebnisse in der in [82–84] vorgenommenen Art und Weise eigentlich unkorrekt ist.

Mittels der nun bekannten Parameter Δ_i ist es in Abschnitt 9.7.2 über das 5×5-Matrixmodell möglich, die Dispersion des $1S$ Orto-Exziton-Polaritons für beliebige Orientierungen von $\boldsymbol{K}$ zu bestimmen. Weiterhin kann aus der Steigung der Dispersionskurve die Gruppengeschwindigkeit v_{g} dieses Quasiteilchens ermittelt werden. Die Vergleiche mit den Ergebnissen für v_{g} sowie mit experimentellen Transmissionsspektren zeigen eine qualitativ sehr gute Übereinstimmung. Die beobachteten Abweichungen lassen sich über im Kristall vorhandene Verspannungen erklären, welche sich auf die experimentellen Exzitonspektren auswirken, jedoch in der Theorie nicht berücksichtigt wurden.

Fazit und Ausblick In der vorliegenden Dissertation wurden Korrekturen zum wasserstoffartigen Hamiltonoperator der Exzitonen in Kupferoxydul untersucht. Zunächst konnte mithilfe der Theorie von Y. Toyozawa das Absorptionsspektrum der Exzitonen berechnet werden. Die durch die Exziton-Phonon-Wechselwirkung hervorgerufenen Linienbreiten wurden innerhalb derselben Größenordnung wie die experimentell beobachteten Linienbreiten bestimmt. Die Ursache für verbleibende Unterschiede zwischen Theorie und Experiment wurden ausführlich diskutiert. Als wichtige Korrektur zum Exziton-Hamiltonoperator stellte sich die kubische Valenzbandstruktur heraus. Nur mit dieser gelingt es, eine experimentell beobachtete Feinstrukturaufspaltung zu erklären. Zur Lösung der zugehörigen Schrödingergleichung wurde eine vollständige Basis eingeführt, welche es auch erlaubt, Dipol- und Quadrupoloszillatorstärken zu berechnen. Weiterhin wurde gezeigt, dass eine Aufspaltung des $1S$-Ortho-Exzitons mit der durch die kubische Valenzbandstruktur verursachten anisotropen Dispersion zu erklären ist. Der Einfluss einer hier im Detail diskutierten K-abhängigen Austauschwechselwirkung auf diese Aufspaltung konnte als verschwindend klein identifiziert werden. Bei der Behandlung der Exziton-Zustände mit geradem Drehimpuls müssen neben der Valenzbandstruktur auch die Zentralzellen-Korrekturen berücksichtigt werden. Bei der Diskussion dieser Korrekturen konnte gezeigt werden, dass nur die Frequenz- und Wellenvektorabhängigkeit der Dielektrizitätskonstante von Bedeutung sind. Nach der Bestimmung der zwei Parameter J_0 und V_0 durch Vergleich mit experimentellen Ergebnissen ist es nun möglich, die gesamte gelbe wie grüne Exzitonserie mit einem konsistenten theoretisches Modell zu beschreiben. Hierdurch wird die Enführung von Quantendefekten, wie in einigen Arbeiten zu Kupferoxydul geschehen [37, 41], überflüssig.

Die Theorie wurde anschließend für den Fall äußerer Magnetfelder erweitert. Vergleiche mit experimentellen Spektren zeigten sehr gute Übereinstimmung sowohl bezüglich der Energien als auch der Oszillatorstärken der Exzitonen und erlaubten die Bestimmung des vierten Luttinger-Parameters κ. Zudem konnte eine Abhängigkeit der Spektren von der Richtung des Magnetfeldes nachgewiesen werden, welche beim Wasserstoffatom in äußeren Feldern nicht vorhanden ist. Die Exzitonspektren im Magnetfeld zeigen weiterhin typische Niveaustatistiken. Allein das Vorhandensein der kubischen Valenzbandstruktur reicht aus, dass für nahezu alle Magnetfeldrichtungen alle antiunitären Symmetrien im System gebrochen werden. Folglich konnte der erste Nachweis für eine räumlich homogenes System erbracht werden, in dem antiunitären Symmetrien gebrochen sind. Da das Aufreten der typischen Niveaustatistiken von den Systemparametern abhängt, konnten die Übergänge zwischen Poisson-, GOE- und GUE-Statistik theoretisch untersucht werden. Hierbei ergab sich eine sehr gute Übereinstimmung mit den Formeln aus der Theorie der Zufallsmatrizen. Durch die gleichzeitige Veränderung zweier Systemparameter ist es prinzipiell auch möglich, beliebige Übergänge im Dreieck Poisson-GOE-GUE-Statistik untersuchen. Dies ist jüngst geschehen [50, 412]. Für alle zuvor nicht behandelten Fälle eines Magnetfeldes in einer der Symmetrieebenen des Gitters ergab sich unter gleichzeitiger Berücksichtigung der Exziton-Phonon-Wechselwirkung ebenfalls GUE-Statistik. Die Wechselwikrung führt hierbei zu einem endlichen Schwerpunktimpuls und damit zu einem Bewegungs-Stark-Effekt im Magnetfeld, welcher die Niveaustatistik beeinflusst. Damit wurde das Auftreten von GUE-Statistik für alle Magnetfeldorientierungen erklärt.

Da Exzitonen und Photonen im Festkörper aufgrund ihrer gegenseitigen Wechselwirkung immer zu Exziton-Polaritonen gekoppelt sind, wurde abschließend deren Dispersion und Beobachtbarkeit untersucht. Es zeigte sich, dass die Dispersion sehr komplex ist und sich nur im Rahmen eines Multi-Polariton-Konzeptes beschreiben lässt. Speziell für die Exziton-Zustände mit Hauptquantenzahl $n \leq 4$ wurden die Valenzbandstruktur, die Zentralzellen-Korrekturen und die Austauschwechselwirkung berücksichtigt. Dabei konnte die K-abhängige Aufspaltung des $1S$ Ortho-Exzitons nochmals quantitativ korrekt untersucht werden. Die Anwendung der Kriterien von Tait zur Beobachtbarkeit von Polaritoneffekten ergab, dass sich diese in Absorptionsspektren für alle Exzitonen mit Hauptquantenzahlen $n \geq 2$ vernachlässigen lassen. Für den Exziton-Grundzustand, bei welchem Polaritoneffekte bereits experimentell nachgewiesen wurden, konnte ein 5×5-Matrixmodell aufgestellt werden, das die Berechnung der zugehörigen Polariton-Dispersion für alle Richtung von $\boldsymbol{K}$ zulässt. Die Vergleiche der Ergebnisse für das $1S$-Ortho-Exziton-Polariton mit experimentellen Resultaten zeigten gute Übereinstimmungen.

Das Forschungsgebiet der Rydberg-Exzitonen ist bei weitem noch nicht erschöpft. Bereits die in dieser Arbeit vorgestellten Themengebiete lassen weitere Untersuchungen zu. So ist es zum Beispiel möglich, mithilfe der Resultate für die Exziton-Polaritonen unter der Annahme Pekarscher Randbedingungen und der Anwendung der Fresnel-Formeln Transmissionsspektren zu berechnen [439]. Dies könnte zu einem tiefergehenden Verständnis der Form der Absorptionslinien in experimentellen Spektren beitragen. Im Zusammenhang mit der kubischen Valenzbandstruktur ergibt sich die Frage, welche Eigenschaften das zugehörige klassische System aufweist [441]. Hier ist eine Untersuchung im Rahmen der „Closed-Orbit Theory“ oder „Theorie der geschlossenen Bahnen“ möglich, um einen Zusammenhang zwischen „klassischen“ Exzitonenbahnen und experimentellen Spektren herzustellen [442].

Neben einer Betrachtung der Exzitonen im reinen Magnetfeld wäre auch eine theoretische Behandlung in kombinierten elektrischen und magnetischen Feldern sehr interessant. Hierbei erlaubt die Methode der komplexen Rotation [35, 443] eine Untersuchung der Resonanzen im System. Für das Wasserstoffatom in parallelen oder gekreuzten Feldern konnte dabei bereits die Existenz sogenannter „Exceptional Points“ oder „Ausnahmepunkte“ theoretisch nachgewiesen werden [35, 444]. Diese Punkte liegen jedoch in Feldstärkenbereichen, die experimentell (noch) nicht zugänglich sind. Aufgrund der kleineren Rydberg-Energie der Exzitonen wäre ein experimenteller Nachweis dieser Punkte durch die so erforderlichen niedrigeren Feldstärken bei Kupferoxydul möglich.

Frank Stefan Schweiner

Persönliche Daten

Geburtsdatum	07.09.1989
Geburtsort	Böblingen

Sprachen

Deutsch	Muttersprache
Englisch	fließend
Französisch	mittlere Kenntnisse
Latein	kleines Latinum

Schulausbildung

09/96 - 07/00	**Grundschule**, *Grafenau-Döffingen*.
09/00 - 06/09	**Stiftsgymnasium**, *Sindelfingen*, Allgemeinbildendes Abitur. Abschluss Abitur am 23.06.2009, Note: 1.0

Studium

10/09 - 10/12	**Bachelorstudiengang Physik**, *Universität Stuttgart*. Abschluss Bachelor of Science am 10.10.2012, Note: 1.0 mit Auszeichnung
04/12 – 08/12	**Bachelorarbeit**, *Behandlung der linearisierten Gilbert-Gleichung mit der Greenschen Funktion*, unter der Betreuung von Prof. Dr. Manfred Fähnle, Max-Planck-Institut für Intelligente Systeme, Stuttgart.
10/12 - 09/14	**Masterstudiengang Physik**, *Universität Stuttgart*. Abschluss Master of Science am 10.09.2014, Note: 1.0 mit Auszeichnung
10/13 – 09/14	**Masterarbeit**, *Klassische Dynamik und Lokalisierung von Resonanzen in der Umgebung des Stark-Sattelpunktes beim Wasserstoffatom in gekreuzten elektrischen und magnetischen Feldern*, unter der Betreuung von Apl. Prof. Dr. Jörg Main, 1. Institut für Theoretische Physik, Universität Stuttgart.
10/14 - 12/17	**Promotion**, *Theory of Excitons in Cuprous Oxide*, unter der Betreuung von Apl. Prof. Dr. Jörg Main, 1. Institut für Theoretische Physik, Universität Stuttgart. Abschluss Dr. rer. nat.

Berufliche und wissenschaftliche Tätigkeiten

10/11 - 09/14	**Studentische Hilfskraft**, *Fachbereich Mathematik, Universität Stuttgart*, Betreuung diverser Übungsgruppen zur Höheren Mathematik.
10/14 - heute	**Wissenschaftlicher Mitarbeiter**, *1. Institut für Theoretische Physik, Universität Stuttgart*, Betreuung diverser Übungsgruppen zur theoretischen Physik und Experimentalphysik. Betreuung von Bachelor- und Masterarbeiten.

Stipendien und Preise

2009	**Ferry Porsche Preis**, für herausragende Leistungen in den Fächern Mathematik und Physik/Technik.
2009	**DPG-Buchpreis**, als Anerkennung für hervorragende Leistungen im Fach Physik.
2009 - heute	**Online-Stipendium von e-fellows.net**, aufgrund hervorragender Leistungen.
2015	**Artur-Fischer-Preis**, für hervorragende Studienleistungen bei kurzer Studiendauer im Studiengang Physik.
2017	**Stipendium nach dem Landesgraduiertenförderungsgesetz (LGFG)**, zur Förderung des hochqualifizierten wissenschaftlichen Nachwuchses.

Wissenschaftliche Fachvorträge

17. 04. 2014	**Observation of a stability island in the high energy ($E > 0$) region of the hydrogen atom in crossed electric and magnetic fields**, *Humboldt-Universität zu Berlin*, Frühjahrstagung der Deutschen Physikalischen Gesellschaft.
23. 03. 2015	**Exciton-phonon coupling in external fields**, *Universität Heidelberg*, Frühjahrstagung der Deutschen Physikalischen Gesellschaft.
16. 12. 2015	**Excitons in an external magnetic field**, *Technische Universität Dortmund*, Institut für Experimentelle Physik 2.
29. 02. 2016	**Excitonic spectra in high external fields**, *Universität Hannover*, Frühjahrstagung der Deutschen Physikalischen Gesellschaft.
10. 10. 2016	**Excitonic spectra in high external fields**, *Dortmund*, 13th International Workshop on Nonlinear Optics and Excitation Kinetics in Semiconductors.
07. 03. 2017	**Magnetoexcitons in cuprous oxide**, *Universität Mainz*, Frühjahrstagung der Deutschen Physikalischen Gesellschaft.
26. 05. 2017	**Theory of excitons in cuprous oxide**, *Ioffe Institut, St. Petersburg, Russland*, Workshop on Rydberg excitons in semiconductors.

Wissenschaftliche Veröffentlichungen

- **Construction of tensorial Green's functions for the linearized Gilbert equation for magnetization dynamics**, F. Schweiner, M. Fähnle, IEEE Trans. Magn. **49**, 2936 (2013).
- **Classical dynamics and localization of resonances in the high energy region of the crossed fields hydrogen atom**, F. Schweiner, J. Main, H. Cartarius, G. Wunner, Phys. Rev. E **91**, 012915 (2015).
- **Linewidths in excitonic absorption spectra of cuprous oxide**, F. Schweiner, J. Main, G. Wunner, Phys. Rev. B **93**, 085203 (2016).
- **Impact of the valence band structure of $\mathbf{Cu_2O}$ on excitonic spectra**, F. Schweiner, J. Main, M. Feldmaier, G. Wunner, Ch. Uihlein, Phys. Rev. B **93**, 195203 (2016).
- **Rydberg systems in parallel electric and magnetic fields: an improved method for finding exceptional points**, M. Feldmaier, J. Main, F. Schweiner, H. Cartarius, G. Wunner, J. Phys. B: At. Mol. Opt. Phys. **49**, 144002 (2016).
- **$\boldsymbol{K}$ dependent exchange interaction of the 1$\boldsymbol{S}$ exciton in $\mathbf{Cu_2O}$**, F. Schweiner, J. Main, G. Wunner, Ch. Uihlein, Phys. Rev. B **94**, 115201 (2016).
- **Magnetoexcitons in cuprous oxide**, F. Schweiner, J. Main, G. Wunner, M. Freitag, J. Heckötter, Ch. Uihlein, M. Aßmann, D. Fröhlich, M. Bayer, Phys. Rev. B **95**, 035202 (2017).
- **Magnetoexcitons break antiunitary symmetries**, F. Schweiner, J. Main, G. Wunner, Phys. Rev. Lett. **118**, 046401 (2017).
- **Even exciton series in $\mathbf{Cu_2O}$**, F. Schweiner, J. Main, G. Wunner, Ch. Uihlein, Phys. Rev. B **95**, 195201 (2017).
- **GOE-GUE-Poisson transitions in the nearest neighbor spacing distribution of magnetoexcitons**, F. Schweiner, J. Main, G. Wunner, Phys. Rev. E **95**, 062205 (2017).
- **Exciton-phonon interaction breaking all antiunitary symmetries in external magnetic fields**, F. Schweiner, P. Rommel, J. Main, G. Wunner, Phys. Rev. B **96**, 035207 (2017).
- **Crossover between the Gaussian orthogonal ensemble, the Gaussian unitary ensemble, and Poissonian statistics**, F. Schweiner, J. Laturner, J. Main, G. Wunner, Phys. Rev. E **96**, 052217 (2017).
- **Exciton-polaritons in cuprous oxide: Theory and comparison with experiment**, F. Schweiner, J. Ertl, J. Main, G. Wunner, Ch. Uihlein **96**, Phys. Rev. B, 245202 (2017).

Danksagung

An dieser Stelle möchte ich mich bei allen bedanken, die zum Gelingen der vorliegenden Dissertation beigetragen haben. Mein besonderer Dank gilt:

- Herrn Prof. Dr. Jörg Main für die Möglichkeit, dieses interessante Thema zu bearbeiten, die hervorragende Betreuung, die Freiheiten bei der Wahl der zu untersuchenden Fragestellungen und die Übernahme des Hauptberichtes. Weiterhin für die gemeinsamen Urlaube, die die letzten Jahre zu einer besonderen Zeit gemacht haben.
- Frau Prof. Dr. Maria Daghofer für die Übernahme des Mitberichtes.
- Herrn Prof. Dr. Manfred Bayer für die Übernahme des Mitberichtes.
- Herrn Prof. Dr. Peter Michler für die Übernahme des Prüfungsvorsitzes.
- Herrn Prof. Dr. Günter Wunner für die freundliche Aufnahme am 1. Institut für Theoretische Physik und das Interesse an der Arbeit.
- Herrn Prof. Dr. Manfred Bayer und Herrn Prof. Dr. Dietmar Fröhlich für die sehr gute Zusammenarbeit, die Bereitstellung experimenteller Ergebnisse, ohne die diese Arbeit in der vorliegenden Form nicht möglich gewesen wäre, die Hilfe bei Fragen zur Literatur und Theorie der Exzitonen sowie für die Einladungen auf Konferenzen in Dortmund und St. Petersburg.
- Herrn Dr. Christoph Uihlein für die ausführlichen und hilfreichen Gespräche, die zu einem tieferen Verständnis der Theorie der Exzitonen geführt haben. Ohne ihn wäre diese Arbeit in der vorliegenden Form ebenfalls nicht möglich gewesen.
- Herrn Priv.-Doz. Dr. Holger Cartarius und Herrn Dr. Robin Gutöhrlein für die Unterstützung bei Fragen zur Programmierung sowie für die ausgezeichnete Systemadministration. Herrn Priv.-Doz. Dr. Holger Cartarius danke ich weiterhin für die hilfreiche Unterstützung bei jeglichen Fragen physikalischer oder mathematischer Natur, auf die man sich jederzeit verlassen konnte.
- Herrn Dr. Marc Aßmann, Herrn M. Sc. Julian Heckötter und Herrn M. Sc. Marcel Freitag für die sehr gute Zusammenarbeit, die Bereitstellung experimenteller Ergebnisse und die interessanten Gespräche.

- Herrn Dr. Mikhail Glazov für die hilfreichen Gespräche zur Theorie der Exzitonen und zur Gruppentheorie in der Festkörperphysik.
- Herrn M. Sc. Matthias Feldmaier für die gute Büroatmosphäre, die sehr gute Zusammenarbeit sowie die gegenseitige Unterstützung.
- Herrn M. Sc. Patric Rommel, Herrn B. Sc. Jan Ertl, Frau B. Sc. Jeanine Laturner und Herrn B. Sc. Jonathan Luft für die gute und erfolgreiche Zusammenarbeit auf dem Gebiet der Exzitonen in Kupferoxydul.
- Allen weiteren Mitarbeiter des 1. Instituts für Theoretische Physik für das gute Arbeitsklima und dafür, dass sie dieses Institut zu etwas ganz Besonderem gemacht haben. Ich bin mir sicher, dass mir die Gespräche in der Kaffeerunde fehlen werden.
- Dem Land Baden-Württemberg und der Universität Stuttgart für die Gewährung des Promotionsstipendiums nach dem Landesgraduiertenförderungsgesetz.
- Meinen Eltern für die Unterstützung während des gesamten Physikstudiums und der Promotionsarbeit.

Ehrenwörtliche Erklärung

Ich erkläre, dass ich diese Dissertation, abgesehen von den ausdrücklich bezeichneten Hilfsmitteln, selbständig verfasst habe.

Stuttgart, den 29. September 2017 *Frank Stefan Schweiner*